

**POST-RIFT GEOLOGY OF THE JEANNE D'ARC BASIN, WITH A
FOCUS ON THE ARCHITECTURE AND EVOLUTION OF EARLY
PALEOGENE SUBMARINE FANS, AND INSIGHTS FROM MODERN
DEEP-WATER SYSTEMS**

by

Mark E. Deptuck

Submitted in partial fulfillment of the requirements
for the degree of Doctor of Philosophy

at

Dalhousie University
Halifax, Nova Scotia
September 2003

© Copyright by Mark E. Deptuck, 2003

DALHOUSIE UNIVERSITY

DATE: May 2003

AUTHOR: Mark E. Deptuck

TITLE: Post-rift geology of the Jeanne d'Arc Basin, with a focus on the architecture and evolution of Early Paleogene submarine fans, and insights from modern deep-water systems

DEPARTMENT OR SCHOOL: Earth Sciences

DEGREE: Ph.D. CONVOCATION: Spring YEAR: 2004

Permission is herewith granted to Dalhousie University to circulate and to have copied for non-commercial purposes, at its discretion, the above title upon the request of individuals or institutions.

Signature of Author

The author reserves other publication rights, and neither the thesis nor extensive extracts from it may be printed or otherwise reproduced without the author's written permission.

The author attests that permission has been obtained for the use of any copyrighted material appearing in the thesis (other than the brief excerpts requiring only proper acknowledgement in scholarly writing), and that all such use is clearly acknowledged.

To my father, the first geologist I ever knew
- with love and admiration -

*Standing on the outskirts of a vast ancient Ocean
Seeking truth where none was sought before
Through shifting shorelines and scouring seascapes
History deposited in deep shades of Blue
Though not present to see,
The rocks are my eyes
And if I can learn to speak their language,
They will tell me time's tales of an ever-changing Sea*

TABLE OF CONTENTS

TABLE OF CONTENTS.....	v
LIST OF FIGURES.....	xiii
ABSTRACT.....	xxiii
LIST OF ABBREVIATIONS.....	xxiv
ACKNOWLEDGMENTS.....	xxvi
Chapter 1 - Introduction	1
1.1 General statement.....	1
1.1.1 Jeanne d’Arc Basin	1
1.1.2 Architecture of small sandy fans.....	2
1.1.3 Channel-belt architecture and evolution	3
1.2 Primary research objectives	5
1.3 Organization of dissertation.....	6
1.4 Explanation of lead authors contributions to each paper	7
1.4.1 Chapter 3.....	7
1.4.2 Chapter 4.....	8
1.4.3 Chapter 5.....	9
1.4.4 Chapter 6.....	10
Chapter 2 - Methods and background.....	11
2.1 Marine reflection seismic data	11
2.1.1 Resolution	12
Vertical resolution.....	13
Horizontal resolution	14
2.2 3-D seismic data.....	15
2.2.1 Methods for viewing 3-D seismic data	17
Volume visualization	19
2.2.2 Seismic attributes	21
Reflection amplitude and strength	21
Coherence	21
Dip and azimuth.....	22

2.3	Time-structure and time-thickness (isochron)	22
2.4	Seismic interpretation software.....	25
2.4.1	Schlumberger GeoQuest software package	25
	IESX.....	28
	Basemap Plus	29
	Geoviz.....	29
2.5	Seismic stratigraphy.....	31
2.5.1	Seismic facies analysis.....	31
2.6	Borehole data	34
2.6.1	Gamma ray.....	34
2.6.2	Sonic	36
2.6.3	Density	36
2.6.4	Resistivity	37
2.6.5	Conventional cores, sidewall cores, and drill cuttings.....	38
2.6.6	Checkshot surveys and synthetic seismograms	38
2.7	Microfossil data	39
2.7.1	Paleoenvironment interpretations	40
2.8	Submarine fans - models and classification.....	41
2.8.1	Upper, middle, and lower fan models.....	42
2.8.2	Efficient versus inefficient systems	43
2.8.3	Types I, II, and III fans	45
2.8.4	Classification according to tectonic setting	47
2.8.5	Classification according to grain size and feeder system	48
2.8.6	Elemental approach.....	50
2.9	Sediment gravity flows and their deposits.....	53
2.9.1	Turbidity currents and turbidites.....	55
	Bouma sequence (“classic turbidites”)	56
	Lowe sequence (high-density turbidites).....	58
2.10	Use of modern submarine fan analogues	60
2.11	Submarine fans in the context of sequence stratigraphy.....	62
2.11.1	Lowstand systems tract.....	63

2.12	General rift-drift processes	64
2.12.1	Syn-rift (rift phase, rift-valley)	67
2.12.2	Post-rift (syn-drift, drift phase).....	67
2.13	Jeanne d’Arc Basin - regional setting and basin structure.....	69
2.13.1	Rift - drift history in the Jeanne d’Arc Basin.....	74

Chapter 3 - Revised Upper Cretaceous and Lower Paleogene Lithostratigraphy and Depositional history of the Jeanne d’Arc Basin* 78

3.1	Introduction.....	78
3.1.1	Scope.....	78
3.1.2	Data and approach.....	79
3.2	Lithostratigraphic classification.....	80
3.2.1	Dawson Canyon Formation	80
	Petrel Member (formalized by Jansa and Wade, 1975b).....	83
	Red Island Member (new)	84
	Otter Bay Member (formalized)	84
	Bay Bulls Member (new).....	90
	Fox Harbour Member (formalized)	90
3.2.2	Wyandot Formation	91
3.2.3	Banquereau Formation.....	94
	Avondale Member (new)	95
	Tilton Member (renamed, formalized)	95
	South Mara Member (range restricted, formalized)	97
3.3	Seismic stratigraphy, unconformities and depositional settings.....	98
3.3.1	Petrel, Otter Bay, and Red Island members.....	98
3.3.2	Otter Bay Unconformity	101
3.3.3	Late Cretaceous submarine fans	101
3.3.4	Bay Bulls and Fox Harbour members.....	106
3.3.5	Wyandot Formation	106
3.3.6	Fox Harbour Unconformity	107
3.3.7	Avondale and Tilton members.....	108

3.3.8	South Mara Unconformity	111
3.3.9	South Mara Member	114
3.4	Southern Jeanne d'Arc Basin.....	115
3.5	Discussion.....	117
3.6	Summary of key points	120

Chapter 4 - Post-rift evolution of the Jeanne d'Arc Basin and northeastern Grand Banks: transition from a confined rift basin to an unconfined passive-margin shelf and slope	122
4.1 Introduction.....	122
4.1.1 Basin setting at the end of the Cretaceous	122
4.1.2 Scope.....	125
4.1.3 Data and methodology	125
4.2 Post-rift lithostratigraphy	127
4.3 Broad-scale basin evolution and variations in long-term sedimentation rates ...	129
4.3.1 Stage 1 - Late Cretaceous to earliest Eocene	129
Lithostratigraphy and seismic stratigraphy	133
Stage 1 sedimentation rates.....	133
4.3.2 Stage 2 - Early to Middle Eocene	140
Lithostratigraphy and seismic stratigraphy	140
Stage 2 sedimentation rates.....	144
4.3.3 Stage 3 - late Middle Eocene to Late Miocene	144
Lithostratigraphy and seismic stratigraphy	145
Stage 3 sedimentation rates.....	146
4.3.4 Stage 4 - Latest Miocene to Quaternary	147
Lithostratigraphy and seismic stratigraphy	148
Stage 4 sedimentation rates.....	149
4.4 Ocean circulation - past and present	149
4.4.1 Ocean current indicators - stages 1 to 4	150
Stage 1.....	150
Stage 2.....	155

Stages 3 and 4	159
4.5 Discussion	160
4.5.1 Changing basin structure and margin evolution - stages 1 to 4	161
4.5.2 Stage 1 influx of clastics from the west	165
4.5.3 Linking ocean current indicators to past ocean circulation	168
Currents passing through the JDB (stages 1 and 2)	168
Currents passing through the Flemish Pass (stages 3 and 4)	173
4.6 Summary of key points	174

Chapter 5 - Early Paleogene (Danian to Ypresian) submarine fans in the Jeanne d’Arc Basin: architecture, evolution and insight from modern Fans off Eastern

Corsica	177
5.1 Introduction	177
5.1.1 Early Paleogene submarine fans in the Jeanne d’Arc Basin (JDB)	179
5.1.2 Scope	182
5.1.3 Jeanne d’Arc Basin data set	183
5.2 Early Paleogene submarine fan complexes	184
5.3 Mara fan complex	188
5.3.1 Early to Middle Paleocene (Danian to Selandian) (T1 to T10)	188
Hibernia and Rankin canyons	192
Mara fan-valley	196
Avondale mounds	200
Basin plain	204
5.3.2 Late Paleocene (Thanetian) to earliest Eocene (early Ypresian)	204
Avondale Canyon	206
Slope gullies	210
South Mara mounds	210
5.3.3 Early Eocene (Ypresian) (T15 to T25)	212
Fan delta	215
5.4 Insight from modern fans off the eastern margin of Corsica	215
5.4.1 Regional setting	217

5.4.2	Data set.....	218
5.4.3	General fan architecture.....	218
5.4.4	East Corsica lobes - potential mound forming elements?.....	222
	Proximal-inefficient lobes (PILs)	222
	Channel-termination lobes (CTLs)	233
5.5	Discussion.....	235
5.5.1	Origin of mounds in the Jeanne d'Arc Basin.....	235
	Compacted channel-termination lobes.....	236
	Compacted proximal-inefficient lobes.....	238
	Compaction-inverted channels.....	238
5.5.2	Reservoir potential of PILs and CTLs	239
5.5.3	Why does submarine fan style change in the JDB?.....	241
5.6	Summary of key points	242

Chapter 6 - Insight into channel-belt architecture and evolution from much larger systems	245	
6.1	Introduction.....	245
6.2	Indus Fan - Arabian Sea.....	246
6.2.1	Seismic data set.....	247
6.2.2	Channel-levee complex C	247
	Channel-levee system stacking architecture	250
6.2.3	Architecture of individual channel-levee systems	253
	Erosional fairway element	253
	Outer levee element	258
	Inner levee element.....	259
	Channel and channel-fill elements (HARs)	259
	Mass transport deposits.....	262
6.2.4	Temporal relationship between inner and outer levees.....	263
6.3	Benin-major CLS	265
6.3.1	Data and methodology	265
6.3.2	General channel-levee architecture.....	269

6.3.3	Evolution of the channel-belt.....	270
	Incision.....	270
	Fill - Phase 1	271
	Fill - Phase 2	273
	Transition - Phase 2 to Phase 3.....	275
	Fill - Phase 3	275
6.3.4	Outer levee deposition	282
6.4	Discussion.....	282
6.4.1	Upper fan avulsions	282
6.4.2	Origin of “terrace” forming elements	287
6.4.3	Lithological composition of inner levees.....	289
6.4.4	HARs - Indus Fan and Benin-major	291
6.4.5	Relationship between channel migration and inner levee deposition.....	291
6.4.6	Why does sinuosity increase through time?.....	293
6.4.7	Scaled comparisons with other systems.....	299
6.4.8	Linking seismic- and outcrop-scale observations.....	307
6.4.9	General changes in flow character through time – Benin-major	309
6.4.10	Architectural variability	312
6.5	Summary of key points	315
Chapter 7 - contributions and future work		318
7.1	Lithostratigraphy and basin evolution	318
7.2	Early Paleogene submarine fans and modern analogues	321
7.3	Submarine channel-belt architecture and evolution.....	323
7.4	Suggestions for future research.....	324
References.....		327
Appendix I		353
Appendix II.....		361
Appendix III.....		364

Appendix IV..... 367

LIST OF FIGURES

	Page
Figure 2.1	Summary of 3-D seismic display methods. 16
Figure 2.2	Comparison of 3-D time-slices from amplitude data and coherence data. 18
Figure 2.3	Example of a sculpted 3-D seismic volume and corresponding interval with transparency added to highlight higher positive amplitudes. 20
Figure 2.4	Examples of coherence time-slices from the Jeanne d'Arc Basin, showing channels, faults, and a gas anomaly. 23
Figure 2.5	Fence diagrams illustrating the process of interpreting and gridding a seismic horizon from 2-D seismic-reflection profiles. 24
Figure 2.6	Example of a) gridded time-structure map draped by structure contours, b) time-thickness map showing elongate lens, and c) corresponding sculpted 3-D seismic reflection volume. 26
Figure 2.7	Three block images generated in GeoViz, showing integration of amplitude volume, volume sculpting along a horizon, and horizontal coherence time slices. 30
Figure 2.8	Figure illustrating principles of seismic stratigraphy a) bounding discontinuities, b) seismic facies, and c) reflection configurations, used in this study. 32
Figure 2.9	Schematic diagram showing potential gamma ray response from different submarine fan settings. 35
Figure 2.10	Variable coarse-grained deposits capable of generating a “blocky” gamma ray response. 35
Figure 2.11	Upper, middle, and lower fan model from Normark (1978). 44
Figure 2.12	Fan model from Walker (1978) showing inferred lithofacies character in specific fan settings. 44
Figure 2.13	Type I, II, and III fans from Mutti (1985). 46
Figure 2.14	Active-margin fan versus mature passive-margin fan (Shanmugam and Moiola, 1991). 46

Figure 2.15	Mounded stratal geometry in immature passive-margin or active-margin fans versus sheeted stratal geometry in mature passive-margin fans.	49
Figure 2.16	Model for proximal to distal trends in elongate mounds on the Frigg Fan, North Sea.	49
Figure 2.17	Twelve fan models based on the character of the feeder systems (single, multiple, or line source) and grain-size (mud-rich, sand/mud-rich, sand-rich, gravel-rich).	51
Figure 2.18	Block diagram illustrating primary architectural elements in submarine fan systems (canyon, channels, levees, lobes, mass transport deposits, slump scarps).	54
Figure 2.19	Potential channel stacking patterns.	54
Figure 2.20	Initiation mechanisms for flows and potential evolutionary paths resulting in debris flow, high-density turbidity current, or low-density turbidity current.	57
Figure 2.21	Classic Bouma turbidite from low-density turbidity current, and corresponding ideal Lowe turbidite from high-density turbidity current.	57
Figure 2.22	Schematic drawing of a surge-type high-density turbidity current, with corresponding velocity and concentration profiles through the flow.	59
Figure 2.23	Schematic structural cross-section through an Atlantic-type passive margin, with synrift ("rift valley stage) and post-rift (post-breakup progradation) deposits shown, separated by a break-up unconformity.	66
Figure 2.24	Schematic cartoon showing the evolution of an Atlantic-type rifted continental margin. On the right are examples of margins representative of each stage (from Keen and Beaumont, 1990).	68
Figure 2.25	a) Structure map based on regional seismic data showing major faults and location of salt. b) Regional map showing location of basins and their relationship to the magnetic anomalies to the east.	70
Figure 2.26	Basemap of Jeanne d'Arc Basin and surrounding areas, showing basement highs and faults that offset Upper Cretaceous and younger strata. Wells are numbered.	72

Figure 2.27	Four diagrams illustrating various stages in the evolution of the northern Atlantic Ocean.	76
Figure 3.1	Map of the Jeanne d’Arc Basin (JDB) showing the main structural elements of the basin, including faults that extend into the Upper Cretaceous succession.	81
Figure 3.2	Generalized litho-chronostratigraphic chart for the Upper Cretaceous and the lower part of the Paleogene stratigraphic succession in the Jeanne d’Arc Basin (modified from Sinclair, 1987).	82
Figure 3.3	Lithostratigraphic correlation of the Petrel, Otter Bay, Fox Harbour, Red Island, and Bay Bulls members (Mb) of the Dawson Canyon Formation, and the Tilton and South Mara members (Mb) of the Banquereau Formation along the western margin of the basin.	85
Figure 3.4	South-to-north lithostratigraphic correlation of wells located east of the latest Cretaceous offlap break.	86
Figure 3.5	Lithostratigraphic correlation near Terra Nova.	87
Figure 3.6	South (left) to North (right) lithostratigraphic correlation showing the increase in thickness of Upper Cretaceous strata in the northern Jeanne d’Arc Basin.	88
Figure 3.7	Schematic diagram illustrating the inferred stratigraphic relationships between the different members and formations identified in this and previous studies.	89
Figure 3.8	Contoured isopach map of the Petrel Member (modified from Shimeld et al., 2000), showing the erosional features inferred to have developed during the Otter Bay unconformity. b) Time-structured map of the K1 marker.	92
Figure 3.9	Uninterpreted and interpreted west-east seismic profile across the central Jeanne d’Arc Basin, near Hibernia (line 83-5052).	99
Figure 3.10	Line drawings of Upper Cretaceous seismic facies observed in the Jeanne d’Arc Basin.	102
Figure 3.11	Perspective view of the K1 marker time-structure map from the Terra Nova 3-D seismic survey.	105
Figure 3.12	Time-structure map on the T1 marker, following the base of	

	erosional features where the marker is truncated.	109
Figure 3.13	Line drawings of lower Paleogene seismic facies observed in the Jeanne d'Arc Basin.	112
Figure 3.14	Depth converted, shaded relief perspective image of the Hibernia Canyon mapped along the erosional base of the canyon and along the T1 marker, viewed from the southeast.	116
Figure 4.1	Plate reconstruction at 65 Ma (modified from Ocean Drilling Stratigraphic network - from Hay et al., 1999 - ODSN web page).	123
Figure 4.2	Basemap of Jeanne d'Arc Basin and surrounding areas, showing basement highs and faults that offset the K1 marker or younger strata.	124
Figure 4.3	Upper Cretaceous and Tertiary lithostratigraphic chart (with new units marked with asterisk).	126
Figure 4.4	Regional west to east seismic profile (line 5072) across northern Jeanne d'Arc Basin, with tie to Hibernia o-35 (projected), Hibernia B-08, and Botwood G-89 (projected).	130
Figure 4.5	a) Time-thickness map between K1 and T40 seismic markers. b) Time-thickness map between T40 and T100 seismic markers.	131
Figure 4.6	Regional west to east seismic profile (line 5000) across southern Jeanne d'Arc Basin, with ties to Egret N-46 (projected, Terra Nova K-18, Terra Nova C-09, and Voyager J-18).	132
Figure 4.7	Perspective views (birds's eye view looking toward the northwest) of 5 regional time-structure maps through the Jeanne d'Arc Basin and across the Flemish Pass region (see Figure 4.1 for location).	134
Figure 4.8	a) Time-structure map of the T1-marker (base of the Tertiary). b) Time-thickness map of Upper Cretaceous strata (K1 to T1).	138
Figure 4.9	Schematic illustration showing the spatial changes in sedimentation rates in different basin locations during stages 1 through 4.	139
Figure 4.10	Time-thickness maps of a) marine unit 2a, b) marine unit 2b, c) marine unit 2c.	141
Figure 4.11	West to east profiles across a) northern and b) central Jeanne d'Arc Basin, showing stage 1 (K1 to T20) and stage 2 (T20 to T40)	

	deposits.	152
Figure 4.12	West to East seismic profiles across the Flemish Pass.	156
Figure 4.13	Basemap of study area showing the location of ocean current indicators like scours, sediment waves and drifts.	157
Figure 4.14	North (left) to South (right) profiles along the axis of the Flemish Pass.	158
Figure 4.15	Profile across the Cormorant Arch, showing up-warped Otter Bay clinoforms.	163
Figure 4.16	Schematic cartoon showing the inferred surface current flow direction during the Latest Cretaceous to Early Eocene.	169
Figure 4.17	Upper Cretaceous and Tertiary lithostratigraphic chart, with corresponding seismic markers defined in this study, and equivalent markers (A*, Ac, Au) in the western North Atlantic indicated (from the Tucholke and Mountain, 1979).	170
Figure 5.1	Plate reconstruction for 65 Ma, showing locations of known Paleocene and Early Eocene submarine fans.	178
Figure 5.2	a) Scaled comparison of fan outlines within the outline of the largest known fan, Bengal. Note that the Mara, Thorvald and Trinity fan complexes are from the Jeanne d'Arc Basin. b) Scaled comparison of small modern fans from various locations and ancient fans from the Jeanne d'Arc Basin and the North Sea.	180
Figure 5.3	a) Basemap of the Jeanne d'Arc Basin showing location of 2-D and 3-D seismic data. Also shown are three time-thickness maps of the mounded seismic facies recognized in the basin. Each time-thickness map represents the total thickness of mounded seismic facies within each submarine fan complex, including both Paleocene and lower-most Eocene strata. Contour interval is 25 ms. From northwest to southeast they are named the Thorvald, Mara, and Trinity complexes. b) Basemap showing location of Paleocene to early Ypresian erosional features and mounds mapped in this study.	185
Figure 5.4	Schematic cartoons summarizing stratal architecture from seismic-reflection profiles along four west to east tranverses across the basin, ordered from north (a) to south (d). Each traverse summarizes observations from several profiles. Regions from which profiles were taken is shown in Figure 5.3a.	187

Figure 5.5	Series of line-drawings from proximal to distal profiles roughly perpendicular to the Mara fan complex.	189
Figure 5.6	a) 3-D seismic profile and b) line drawing through Avondale A-46, across the most expanded Paleocene section in the basin.	190
Figure 5.7	a) Multi-panel seismic profile (2-D and 3-D) and b) line drawing across western margin of basin and down axis of the Mara fan-valley and younger Avondale Canyon above it.	191
Figure 5.8	Perspective view of the T1 marker in the JDB, as viewed from the east. Note prominent canyons eroding the shelf and slope along the western margin (top). Inset shows close-up of the Mara fan-valley at the T1 marker, from 3-D seismic data.	193
Figure 5.9	Horizon slices at a) the T1 marker and b) 128 ms below T1 marker (mapped horizontally above canyon-fill, not along erosive base as in Figure 3.14) showing planform character near the brim of the canyon (a) and near its erosive base (b).	195
Figure 5.10	a) Contoured dip map and b) line drawing of the T1-marker showing the Mara fan-valley and sinuous thalweg channels at its erosive base.	197
Figure 5.11	Shaded perspective view of the T1 seismic marker (time-structure map - viewed from the north).	199
Figure 5.12	Basemap of the JDB showing a time-thickness map of the Avondale mounds (T1 to T10) above a mosaic of horizon coherence-slices showing Early Paleocene feeder systems.	201
Figure 5.13	a) Multipanel display through South Mara C-13, North Ben Nevis P-93, and North Ben Nevis M-61. Gamma ray curves shown. b) West to East 2-D seismic profile across mounded region on Mara fan complex.	203
Figure 5.14	Basemap of the JDB showing a mosaic of horizon slices at different levels above the T1 seismic marker, illustrating different erosion features (gullies) and mounded regions in the basin, associated with the South Mara mounds.	205
Figure 5.15	Horizon slice 104 ms above the T1 marker (mapped horizontally above canyon-fill) crossing Upper Paleocene deposits on the shelf and slope.	207

Figure 5.16	Time-thickness map of South Mara mounds between the T10 and T15/T20 seismic markers.	208
Figure 5.17	a) Line drawing schematic of South Mara mounds and gullies from a series of coherence horizon-slices. b) Coherence horizon slice through South Mara mounds 1 and 2, showing linear curvi-linear channels.	209
Figure 5.18	a) Gridded time-structure map with lighting effects - the earliest Eocene unconformity in the Jeanne d'Arc Basin. b) Time-thickness map (thickest area in red) showing elongated lens isolated through volume sculpting along horizons above and below it (c). d) Close-up of three of the segments in (c). d) sculpted volume with transparency affects to highlight interpreted fan delta.	213
Figure 5.19	Series of 3-D seismic-reflection profiles showing general uparching along the axis of the basin of the occurrence of prominent scours at the T1 and T20 seismic markers (dashed line).	214
Figure 5.20	Basemap of East Corsica showing location of submarine fans mapped from Hunttec DTS profiles. Isobaths are from a combination of Stanley et al. (1980), Bellaiche et al. (1994), and Pichevin (2000).	216
Figure 5.21	Series of line drawings from Hunttec DTS profiles across the shelf and slope of the East Corsican margin.	220
Figure 5.22	a) Schematic drawing of the Pineto gully and lobe based on a series of Hunttec DTS profiles, offshore Corsica. b) Chart showing the abrupt down slope increase and then decrease in maximum thickness of the Pineto lobe. c) Profile f across the Pineto lobe showing the chaotic, high-backscatter acoustic response characteristic of sands.	223
Figure 5.23	Hunttec DTS profile across the proximal North Golo lobe that fills the last remaining relief of the North Golo channel-levee system.	225
Figure 5.24	Hunttec DTS profile across the proximal Biguglia lobe, eroded by the St. Damiano channel. Note the multiple, small stacked sand lenses.	226
Figure 5.25	Hunttec DTS profile across a small, proximal lobe (proximal Biguglia lobe).	227
Figure 5.26	Hunttec DTS profile across the distal end of one of the proximal Biguglia lobes, just down-dip from Figure 2.25.	228

Figure 5.27	Line drawing from a Hunttec DTS profile across several stacked channel-termination lobes (CTLs) on the floor of the Corsican Trough. Figure and lobe location shown on Figure 5.20.	229
Figure 5.28	a) Line drawing from a Hunttec DTS profile down the length axis of the South Golo composite mid-fan lobe.	230
Figure 6.1	Indus upper fan with location of 2-D seismic data, channel-levee systems (CLSs) C1, C2, C3, and figure locations.	248
Figure 6.2	Regional profile located roughly perpendicular to orientation of several stacked channel systems on the upper Indus Fan.	249
Figure 6.3	Three traverses roughly perpendicular to CLC C showing the distribution of different seismic facies representing outer levees (blue and green), inner levees (white), HARs (dark grey), mass transport deposits (orange), and sheet-like deposits at base of complex (canyon initiation deposits - yellow).	251
Figure 6.4	Block diagram illustrating the three dimensional relationship between CLSs C1, C2, and C3 on the Indus Fan.	252
Figure 6.5	a) Uninterpreted and b) interpreted seismic profile across CLS C1 showing the first-order architectural elements (erosional fairway, inner levees, outer levees, and various types of HARs corresponding to channel deposits).	254
Figure 6.6	a) Uninterpreted and interpreted b) black and white and c) colour seismic profile across CLS C2 showing the principal architectural components identified in CLSs in this study.	255
Figure 6.7	a) Interpreted seismic profile traversing perpendicular to CLS C3, and roughly down the axis of CLS C2, showing a complicated “cactus-like” HARs. b) Interpreted seismic profile oblique to CLS C2, showing multiple phases of inner levee growth. c) Interpreted seismic profile across CLS C3 showing a rather complex channel-belt architecture.	256
Figure 6.8	Seismic profiles illustrating different characteristics of HARs on Indus Fan.	261
Figure 6.9	Regional location map of Niger Delta, and the Benin-major channel-belt located on the western slope (inset shows close-up).	266

Figure 6.10	a) Contoured dip map from the erosive base of the Benin-major CLS, mapped along the base of the outer levees that flank the system. b) Contoured dip map from the modern sea floor.	267
Figure 6.11	Interpreted seismic profiles across Benin-major.	268
Figure 6.12	Generalized schematic drawing showing the incision (a-b) and the three-phase fill history (c-e) of the Benin-major channel-levee system.	272
Figure 6.13	Dip map of the base of incision of the erosional fairway at Benin-major.	274
Figure 6.14	Series of uninterpreted dissemblance horizon-slices flattened on the seafloor with the corresponding line drawings at a) 312 ms (phase 1), b) 232 ms (phase 2), c) 156 ms (phase 3), and d) 73 ms (phase 3) below the sea floor.	276
Figure 6.15	Drawing showing the planform geometry of the stacked channel-axis deposits (HARs) every 36 to 40 ms below the sea floor (from seafloor-flattened dissemblance slices).	278
Figure 6.16	a) Channel-centerline plots every 8ms showing three phases of channel deposit evolution at Benin-major. b) Graph showing the change in sinuosity and number of channel-bends from the base of the Benin-major CLS to the modern sea floor.	280
Figure 6.17	Dissemblance horizon-slice at 76 ms below the flattened sea floor horizon.	281
Figure 6.18	Series of block diagrams illustrating the initiation of a new channel-levee complex and two subsequent upper fan avulsions.	284
Figure 6.19	Scales of observation in deep-water systems and a schematic model illustrating how submarine channels migrate at Benin-major.	294
Figure 6.20	a) Perspective view from the southeast of the Benin-major erosional fairway and several stacked channel-forms mapped within the channel-belt. b) Planview close-up of late-stage channel-forms showing abrupt channel-straightening and the development of three meander cut-offs. c) Amplitude extraction from an 80 ms window near the base of the system (equivalent to Phase 1 and 2 channels) showing the sinuous character of stacked channel-forms prior to the channel-straightening shown in (b). d) Close-up perspective view of stacked channels showing down-system translation and cross-channel stepwise migration of successive channel-forms.	295

- Figure 6.21** Seismic profile down the axis of the Benin-major CLS showing stepwise down system translation in successive channel-forms. 297
- Figure 6.22** a) Scaled comparison of three cross-sections through channel-levee systems, showing the range of dimensions from small systems like Einstein (Gulf of Mexico), to very large systems like CLS C2 on the Indus Fan. b) Scaled comparison of selected channel-belt planforms, from small systems like South Golo (offshore east Corsican margin) and Einstein (Gulf of Mexico), to large systems like the modern Indus, Zaire, Amazon and Rhone. 300
- Figure 6.23** Dip map scaled comparisons of entrenched meandering channels at the erosive base of a) Benin-major and b) Benin-minor, West Africa, and c) the Mara fan-valley, Jeanne d’Arc Basin, offshore Newfoundland. 302
- Figure 6.24** Line drawing scaled comparisons of HARs from a) CLS C2 (Indus Fan), b) Benin-major (Niger Delta slope), c) a deeper CLS located below CLS C1 (Indus Fan), d) South Golo CLS (offshore East Corsica), and e) a line drawing of the “Solitary” channel (SE Spain - drawing based on photo mosaic in Figure 6.20). 303
- Figure 6.25** a) Uninterpreted and b) interpreted photo mosaic of the “Solitary” channel, in SE Spain (Site 2 of Cronin, 1995). 305
- Figure 6.26** Schematic illustration showing the change in cross-sectional geometry of the Benin-major CLS during a) Phase 2, b) Phase 2, and c) Phase 3. 310

ABSTRACT

The Jeanne d'Arc Basin (**JDB**) is a relatively small passive-margin rift basin that underlies the northeastern part of the present day Grand Banks of Newfoundland. Up to 4 km of Upper Cretaceous and Tertiary strata were deposited in or above the basin and are generally believed to record the post-rift history of the region (i.e. after active sea floor spreading began in surrounding oceanic basins). The interval has, until now, remained poorly studied despite the plethora of well and seismic data in the region. This thesis aims to 1) improve the understanding of the post-rift succession in the JDB, 2) determine the architecture and growth patterns of early Tertiary submarine fans in the JDB, and draw comparisons with both modern and ancient analogues, and 3) investigate the architecture and evolution of sinuous submarine channels in the JDB and other locations around the world.

The primary JDB data set consists of a regional grid of 2-D seismic lines (20 300 line kilometers, covering 40 720 km²), several 3-D seismic volumes (covering 1800 km²), and 84 industry wells. Key seismic markers correlated across the JDB and Flemish Pass, combined with well ties, were used to establish a regional framework for the post-rift history of the northeastern part of the Grand Banks. The succession has been divided into four stages, each defined according to its depositional setting and basin structure and relief. The study area evolved from a confined rift basin (i.e. the JDB - stages 1 and 2) to the unconfined Grand Banks shelf and slope located along the present margin (stages 3 and 4). A formal lithostratigraphic classification scheme is proposed for Upper Cretaceous and Tertiary strata in the JDB, and formal definitions are provided for four members of the Dawson Canyon Formation and five members of the Banquereau Formation.

In the Late Cretaceous through Middle Eocene (early-Bartonian) the JDB formed a depression bounded by basement highs along its southern, eastern and western margins. The depression was filled by a combination of prograding clastics from the west, submarine fans in basinal areas, pelagic drape, and sediment transported by ocean currents. Broad scours, sediment drifts, and sediment waves provide evidence for ocean currents that periodically swept through the JDB, starting at the end of the Cretaceous and continuing until the basin filled in the Middle Eocene. After the Middle Eocene, ocean currents were largely diverted towards the Flemish Pass region by the broad proto-Grand Banks shelf. Sparse wells combined with 2-D and 3D seismic data were used to study the architecture and evolution of small, sand-prone early Tertiary submarine fans. The fans consist of complex mounded seismic facies located at the mouths of sinuous to straight submarine channels of various dimensions.

Modern analogues were used to classify mounds in the JDB and to understand the distribution, and pre-compaction geometry and dimensions of potential mound-forming elements like channels and lobes. Both 2-D and 3-D seismic data from much larger submarine channel-belts off West Africa and in the Arabian Sea were used to study how channels evolve within the confines of channel-belts, and their intimate relationship with inner levees. Temporal changes in channel stacking architecture and planform geometry provide important insights into reservoir architecture in channel-belts that range over an order of magnitude in size, and provide information about temporal changes in the size and erosiveness of flows passing through channel-levee systems.

LIST OF ABBREVIATIONS

AAPG	American Association of Petroleum Geologists
ASAP	Automatic Seismic Area Picker
CLC	Channel-levee Complex
CLS	Channel-levee System
C-NOPB	Canada-Newfoundland Offshore Petroleum Board
C-P HARs	Continuous - Parallel High Amplitude Reflections
CTLs	Channel-termination lobes
D-C HARs	Discontinuous - Chaotic High Amplitude Reflections
DSDP	Deep Sea Drilling Project
DTS	Deep-Tow Seismic
<i>f</i>	frequency
GCSSEPM	Gulf Coast Section Society for Sedimentary Geology
GSC	Geological Survey of Canada
GSI	Geophysical Service Incorporated
HARP	High Amplitude Reflection Package (channel-avulsion lobe)
HARs	High Amplitude Reflections (channel-axis deposits)
IL	Inner Levee
JDB	Jeanne d'Arc Basin
K-T	Cretaceous - Tertiary (boundary)
K1 to K10	Upper Cretaceous seismic markers
Ma	Million years ago
Mb	Member

ms	milliseconds (two-way travel time)
MTD	Mass Transport Deposit
m.y.	million years
ODP	Ocean Drilling Program
OL	Outer Levee
PILs	Proximal-inefficient lobes
r	radius of Fresnel zone
R	Reflection coefficient
s	seconds (two-way travel time)
SGI	Silicon Graphics Interface
T1 to T100	Tertiary seismic markers
TWT	Two-way travel time
v	velocity
v.e.	vertical exaggeration
v.r.	vertical resolution
VSP	Vertical Seismic Profile
w	width of the Fresnel zone
Z	Acoustic impedance
z	reflector depth
λ	wavelength
3-D	Three-dimensional
2-D	Two-dimensional

ACKNOWLEDGMENTS

Financial support for this project was provided by two Natural Sciences and Engineering Research Council (NSERC) of Canada post-graduate scholarships (A and B), a Natural Resources Canada Supplemental Scholarship, a Fred A. Dix AAPG Grant-in-Aid, and four months of funding from David Piper's NSERC grant. Contributions of data and logistical support came from many sources including the Geological Survey of Canada (Atlantic) and several oil companies (listed below), to whom I am indebted. This project began with very little digital seismic data, and in-kind contributions of several multi-million dollar data-sets (both 2-D and 3-D) by several generous oil companies facilitated this project. These companies therefore made a significant contribution to this project.

My deepest appreciation goes to David Piper for leading by example, exemplifying integrity, and allowing me the freedom to explore ideas that had only a slim hope of making it into this thesis. My appreciation also goes to my other committee members, Andrew MacRae, Martin Gibling, and Patrick Ryall, for their guidance and patience as this project evolved.

The Geological Survey of Canada (Atlantic), at the Bedford Institute of Oceanography, provided me with a great learning environment and a place to hang my hat. Thanks for your hospitality. I am especially grateful to Arthur Jackson, Al Grant, Graham Williams, Rob Fensome, Phil Moir, Don McAlpine, Mark Williamson, John Shimeld, Frank Thomas, Chris Jauer, and Hans Wielens; I learned something from each of you. My appreciation also goes to the Turbidite Research Team at Shell, and in particular Gary Steffens, Carlos Pirmez, Brad Prather, and Jeremy Willson for making my stay in Houston enjoyable, and for challenging my ideas and providing me with new ones. A special thanks to Miriam Barber for logistical help and your friendship.

Thanks to my office mates Thian Hundert and Jon Mackie for tolerating my coffee-bingeing ways and for some great conversations (and not always about geology!). Thanks also to the Grad House crew (Gavin Manson, Dorthe Moller-Hansen, Duncan Johannessen, Eugene MacDonald, Elisabeth Levac, Jenn Russel-Houston, and Mark Ferguson) for introducing me to Scotch and for never forgetting one slip of the tongue (I guess I will always be the Greek 'Goddess' of Love).

To my parents, thank-you for teaching me what limestone was when I was 5, and for showing me how to work hard to achieve my goals. Most importantly, to my wife, Denise, thank-you for your patience and love, and for teaching me that there is more to life than hard work (now that I've finished, maybe we can both start enjoying life!).

Additional chapter acknowledgments

Chapter 3

Thanks to G. Manson for reviewing an earlier version of the manuscript, A. Jackson for logistical assistance, and B. Prather and J. Waldron for helpful discussions. The Hibernia Management and Development Company and Petro-Canada are acknowledged for providing the 3-D seismic data over the Hibernia and Terra Nova oil

fields, respectively. CanStrat Ltd. supplied the digital data necessary to generate the stratigraphic columns. The Canada-Newfoundland Offshore Petroleum Board is thanked for allowing me to conduct sampling in St. John's, Newfoundland. Rick Hiscott, John Hogg, and Iain Sinclair are thanked for their insightful reviews, which improved the manuscript.

Chapter 4

Digital 2-D seismic data were provided in kind by the Ex-Parex Group (this project began with paper copies of your data; the digital data made a world of difference!). I am grateful to the companies of the ex-Parex Group for their interest in, and support of, this research. Without it chapter 4 would not have been possible.

Chapter 5

Many thanks to Chevron Canada Resources, Mobil Oil Canada (now ExxonMobil), Petro-Canada, Husky Oil, Norsk Hydro Canada Oil & Gas, Mosbacher Operating Ltd., Murphy Oil Company, and the Hibernia Management and Development Company for providing the 3-D seismic data used in Chapter 5 and for supporting this research. Special thanks to Ivan Sereda, Bob Leatherbarrow, and Sarah Saltzer at Chevron Canada Resources for helping me get access to the data and for covering tape copying charges.

Chapter 6

Mike Stovall, Peter Swinburn, and Andre Coffa provided help in the early stages of the project, Patrick McVeigh is thanked for logistical assistance, and Brad Prather, Ciaran O'Byrne, Jeremy Willson, Charlie Winker, and Craig Shipp are thanked for helpful discussions. Gary Steffens, Carlos Pirmez, and Mark Barton (co-authors on the M&PG paper that formed part of Chapter 6) are gratefully acknowledged for their contributions and insight that significantly improved the final product. Tim McHargue, David Jennette and Ven Kolla are thanked for their thoughtful reviews, which improved the manuscript. Shell International E&P, Shell Pakistan, ExxonMobil and the Nigerian National Petroleum Company are thanked for permission to publish these results.

CHAPTER 1 - INTRODUCTION

1.1 General statement

1.1.1 *Jeanne d'Arc Basin*

The Jeanne d'Arc Basin (**JDB**) contains up to 4 km of Upper Cretaceous and Tertiary strata, an interval that has been poorly studied in most offshore areas of Eastern Canada. The Upper Cretaceous and Tertiary interval in the JDB is commonly grouped into a post-rift succession (deposited as the margin thermally subsided after sea floor spreading began in surrounding areas), but little effort has been made to understand the stratigraphic evolution of the basin fill or the post-rift structural evolution of the margin. Moreover, the lack of a formalized stratigraphic framework for the post-rift succession has created confusion and has led to the inconsistent use of informal nomenclature (e.g. "South Mara member", Sinclair, 1988; "South Mara unit", McAlpine, 1990; "South Mara formation", Deptuck, 1998). As well as creating problems within the basin, the lack of a formalized nomenclature has made it difficult to draw comparisons with surrounding areas. As hydrocarbon exploration moves into deeper water, a clearer understanding of the post-rift interval in the JDB, where abundant data is available, is needed to provide a link to the geology in deeper-water areas, where virtually no well data exist.

Industry needs commonly motivate research in offshore areas of Eastern Canada, and the general perception that Upper Cretaceous and Tertiary strata have limited economic potential is largely responsible for the lack of detailed study of these rocks. Limited structural deformation, lack of significant discoveries, and in some areas shallow burial depths, all contribute to this perception. However, hydrocarbon discoveries, though sub-economic, have been made in lower Tertiary submarine fan reservoirs in the basin, a play that has proven to be prolific in the North Sea (e.g. Heritier et al., 1979; McGovney and Radovich, 1985; Timbrell, 1993), but is poorly understood in the JDB and surrounding areas. With 84 exploration and delineation wells drilled in the study area to date, the JDB is the best-sampled offshore area on the East Coast of North America, north of Sable Island (Scotian Shelf). The large number of wells, combined with widespread digital 2-D and 3-D reflection seismic data (made available by several oil companies for this study), provide a unique opportunity for both regional studies of

lithostratigraphy, depositional settings, and basin evolution, and detailed studies of submarine fan architecture and evolution.

Unlike the continental margins along much of Eastern North America (e.g. New Jersey, Nova Scotia, southern Grand Banks, and Labrador margins) where the post-rift phase is broadly characterized by a seaward-thickening wedge extending from a hinge-zone to the shelf-break, above a break-up unconformity (see Falvey, 1974; Jansa and Wade, 1975b; Grant, 1975; Keen et al., 1987; MacLean and Wade, 1992; Poag, 1992), early post-rift deposits in the JDB were confined within a prominent funnel-shaped depression flanked by basement highs to the south, east, and west. How did a negative-relief depression evolve into what is now a broad flat-lying shelf? When did the depression fill and how did the depositional setting change as it filled? What role did turbidites and contourites play?

The modern Grand Banks are situated at the intersection of the south-flowing Labrador Current and the north-flowing Gulf Stream (Gradstein and Srivastava, 1980). Substantial geological evidence, particularly on the Blake Plateau (e.g. Pinet et al., 1981; Pinet and Popenoe, 1985; Tucholke and Mountain, 1986; Dillon and Popenoe, 1988), and to a lesser extent as far north as the Orphan Knoll (e.g. Gradstein et al., 1990), suggests that an ancestral Gulf Stream was active throughout the Tertiary (though the inception of the Labrador Current at times diverted it from the Grand Banks). Results from ocean circulation models based on paleogeography and paleobiogeography support this finding (e.g. Berggren and Hollister, 1974; Haq, 1984; Barron and Peterson, 1991). What clues are there for past ocean current activity in the JDB or Flemish Pass? Were current indicators generated by the proto-Gulf Stream or proto-Labrador Current or another, deeper current? What was the paleoceanography and paleogeography of the region and how did it change through time? The answers to these questions provide insight into the post-rift evolution of passive margins, and help to understand how a passive-margin shelf is constructed in a geologically complex region.

1.1.2 Architecture of small sandy fans

Recognition of small, sand-prone submarine fans in the JDB, combined with the availability of large 3-D seismic surveys covering them from the shelf to the basin floor,

provides an ideal opportunity to investigate their three-dimensional architecture and evolution. The spatial density of 3-D seismic data (< 25 m), combined with advances in computer-based visualization and interpretation methods, allows deeply buried systems to be studied at a level of detail previously unattainable. What kinds of submarine fans were deposited in the basin and when? How did their architecture change as the basin evolved? What insight do modern analogues provide about the processes responsible for their deposition?

Comparisons to similar-sized modern submarine fans off Eastern Corsica and California (see Normark et al., 1998; Piper et al., 1999; Gervais et al., in press) allow insight into sand body geometry, dimensions, and distribution. Through combined use of 3-D seismic data from deeply buried fans, and high-resolution seismic data from modern fans, a detailed account of the types of sand-prone architectural elements is provided in this study. What are the important sandy architectural elements? Are the dimensions of lobes in the modern systems sufficient to produce mounds like those observed in deeply buried fans in the JDB? Are there other mechanisms for mound formation in the JDB? What role does compaction play?

Detailed study of small, sand-prone submarine fans not only provides information about reservoir architecture in the JDB, but also provides a basis for evaluating submarine fans in surrounding areas, where deep-water systems are increasingly becoming primary hydrocarbon targets. It also provides vital information about how such systems are constructed, and highlights important similarities and differences between Quaternary and early Paleogene examples. Such comparisons provide an improved understanding of the expression of architectural elements at different seismic resolutions, and provides a general understanding of gravity flow products and processes in small, sandy fans.

1.1.3 Channel-belt architecture and evolution

Identification of sinuous channels in the JDB (Deptuck, 2000) and offshore Eastern Corsica (Gervais et al., 2003) led to an investigation in this study of submarine channel-belts in other settings, including offshore West Africa and the Arabian Sea. Channel-belts flanked by outer levees (together forming channel-levee systems) act as

important conduits through which clastic sediment is transported into the deep sea, and they provide confining and sorting mechanisms that allow sand to reach the basin plain. They form important repositories for coarse-grained sediment deposited along channel-axes (Bouma et al., 1985; Manley et al., 1997) and for fine-grained sands and silts deposited on levees (Hiscott et al., 1997; Piper and Deptuck, 1997). In the past, seismic studies of channel-levee systems (both shallow and in the deep subsurface) were hindered by problems related to poor data-quality or insufficient thickness to reveal detailed internal architecture (the latter being the case for the early Paleogene submarine channels in the JDB). These issues hamper the study of channel evolution and in particular make it difficult to assess how submarine channels migrate through time and the importance of point bars and inner levees. Such limitations thwart efforts to understand flow processes responsible for the formation of sinuous channels and related architectural elements.

The potential of channel-levee systems as hydrocarbon reservoirs makes them attractive targets for petroleum companies, and has led to the acquisition of excellent-quality seismic data-sets (both 2-D and 3-D) along continental margins around the world. Significant improvements in data quality, and increasing availability of 3-D seismic data (particularly from shallow systems where resolution is optimal), now make detailed studies of channel-levee systems possible and timely. Two excellent-quality data-sets above channel-levee systems in the Arabian Sea (2-D) and Gulf of Guinea (3-D) were available for this study. Though these systems are much larger and formed in a different setting than those in the JDB, their study provides insight into the reservoir architecture in systems that are simply too small and deeply buried to adequately image using conventional 3-D seismic data. Superb 2-D and 3-D seismic resolution, combined with the large size of architectural components and their shallow burial depths, provides an ideal opportunity for detailed investigation.

The ability to recreate sea floor surfaces (time-lines) at multiple levels allows for the temporal evolution of channel-belts to be recreated. This study investigates how an aggrading submarine channel evolves through time, including changes in its planform geometry (e.g. sinuosity, number of channel-bends), width, depth, and gradients. Various aspects of the architecture, such as the height of levee crests above the channel thalweg, are used to constrain flow thickness, and more importantly, to constrain flow thickness as

it evolves through time. What are the important architectural elements of channel-levee systems? What are the similarities in architecture between channel-belts in small fans and much larger fans? How do submarine channels evolve through time? This aspect of the dissertation provides perspective that helps to understand the global context of submarine fans in the JDB. Moreover, this work provides detailed information about potential reservoir architecture in channel-belts within submarine fans around the world, and provides information about the evolution of channel-levee systems from their inception to abandonment.

1.2 Primary research objectives

The primary objectives of this research project are:

- 1) To improve the understanding of the post-rift geological history of the northeastern Grand Banks margin (including such things as evolving basin structure, stratigraphy, depositional settings, paleoceanography).
- 2) To formally define a lithostratigraphic framework for Upper Cretaceous and Tertiary strata in the JDB.
- 3) To develop a detailed understanding of the 3-D architecture and evolution of Late Cretaceous and early Tertiary submarine fans in the JDB (by examining the spatial and temporal distribution of architectural elements) and to understand their regional context.
- 4) To develop a better understanding of the sub-seismic-scale architecture of sand bodies in the JDB through the use of modern analogues off eastern Corsica, and comparisons to previous work in the Santa Monica Basin. To develop a qualitative and quantitative understanding of the variability in sand body geometry and distribution in small sand-prone submarine fans.
- 5) To investigate the architecture and evolution of sinuous submarine channels in the large systems on the Western Niger Delta slope and in the Arabian Sea, and to compare

the results to smaller systems, like those in the JDB and offshore Eastern Corsica. To use this information to define and refine a consistent suite of architectural elements for channel-levee systems.

Meeting the objectives of this study will provide a much sharper understanding of the post-rift geologic history in the JDB, and will substantially improve the understanding of submarine fans in the basin. Beyond the JDB, this study has practical relevance because submarine channels and lobes have become primary targets for hydrocarbon exploration. Detailed study of small sandy fans and large channel-levee systems provides insight into sediment gravity flow processes active in a broad range of deep-water systems and the range of products they generate (i.e. architectural elements).

1.3 Organization of dissertation

Chapter 2 explains the methods used in this study, and presents background information on seismic methods, rifting processes, submarine fan classification and architectural element analysis, and the use of various kinds of analogues. A detailed explanation of the approach to seismic interpretation (both 2-D and 3-D), seismic stratigraphy, and seismic interpretation software is provided. This section also covers material on well data, including an explanation of the different well logs, mud logs, and biostratigraphic interpretations used. An introduction to the structure and tectonic history of the JDB is provided at the end of Chapter 2.

The body of the dissertation consists of four chapters written as self-contained papers. Chapter 3 presents a lithostratigraphic classification scheme for the Upper Cretaceous and lower Paleogene interval in the JDB. The chapter also incorporates interpretations from a regional grid of 2-D seismic reflection lines and two smaller 3-D seismic surveys. Seismic data combined with well data were used to interpret the Late Cretaceous and early Paleogene basin evolution. Chapter 4 describes the broad-scale Late Cretaceous and Tertiary evolution of the northeastern Grand Banks, and presents a framework that subdivides the post-rift succession into four stages that track the transition from a confined basin to the broad passive-margin shelf and slope that now exist along the margin. This chapter discusses the influence of ocean currents and

provides links between basin evolution and sea floor spreading history in surrounding oceanic basins. Chapter 5 is focused on the latter part of stage 1 of the framework presented in Chapter 4 (Paleocene to Ypressian), and describes the architecture and evolution of small sand-prone submarine fans in the basin, using 3-D seismic and well data. Comparisons are made to modern submarine fans located off Eastern Corsica, where sand body geometry has been investigated in detail using ultra-high frequency single channel seismic data. A classification for mounds in the JDB is provided. Chapter 6 explores the detailed architecture of channel-belts in large deep-water systems located in the Arabian Sea (offshore Pakistan) and in the Gulf of Guinea (West Africa), and draws comparisons with smaller systems like those described in Chapter 5.

The dissertation ends with Chapter 7, which provides a summary of the previous chapters and describes the principal conclusions and contributions of this study, as well as identifying future work and unresolved issues.

1.4 Explanation of lead authors contributions to each paper

Each of the four main chapters (3 to 6) has been written as a self-contained paper, though some introductory material was consolidated and moved to Chapter 2 (e.g. JDB structure and tectonic evolution). Chapters 3 and 6 have been accepted for publication in refereed journals, but some additional material has been added for this thesis. Chapters 4 and 5 have not yet been submitted. Because there have been intellectual (and other) contributions from several individuals during the preparation of this thesis, each paper has one or more co-authors. I wrote all of the chapters in this thesis, but as noted below, specific information was provided to me by co-authors. In addition, discussion with co-authors and others helped to develop some of the ideas presented.

1.4.1 Chapter 3

Chapter 3 will be published in Septembers issue of the American Association of Petroleum Geologists Bulletin (Deptuck et al., 2003a). The title of the article is “Revised Upper Cretaceous and lower Paleogene lithostratigraphy and depositional history of the Jeanne d’Arc Basin, offshore Newfoundland, Canada”. The co-authors are Mark Deptuck (MED), Andrew MacRae, John Shimeld, Graham Williams, and Rob Fensome.

Graham Williams and Rob Fensome conducted most of the biostratigraphic work that forms the temporal framework for the revised nomenclature. Figures 3.8a, 3.11, and 3.14 were originally conceived by John Shimeld and Andrew MacRae, and figures 3.8b and 3.12 were originally generated for a B.Sc. Honours thesis by Deptuck (1998). All other work, unless otherwise stated in Chapter 3, was conducted by MED, including conceiving and developing the overall stratigraphic synthesis and writing the manuscript.

My contributions include all seismic interpretation (the data at that time was available only on paper), mapping of seismic facies, correlation between well data and seismic data, lithostratigraphic correlations/interpretations, and formal definitions for lithostratigraphic units. Three available cores (with a total length of 20.4 m) were examined and photographed by MED at the Canada-Newfoundland Offshore Petroleum Board in St. John's, Newfoundland. Unwashed cuttings samples were collected from Cormorant N-83 and Mara E-30 (a total of 145, 25 g samples) and sidewall core samples were collected from Port au Port J-97 (total of 41, 5 g samples). The samples were processed for palynology slides by Bernard Crilley and interpreted by Graham Williams (GSC Atlantic). While in St. John's, several other sidewall core samples were examined for ground truthing of lithological units. Additional methods employed by MED, and the rationale behind them, are provided in section 3.1.2.

1.4.2 Chapter 4

Chapter 4 has not yet been submitted for publication, and the content of the chapter is likely to change prior to submittal. The contributors to this chapter are MED, Graham Williams and Rob Fensome. Most of the age control was provided through biostratigraphic interpretations made by Graham Williams and Rob Fensome (as in Chapter 3). 2-D seismic data were provided in-kind by the ex-Parex Group through an agreement with the GSC (Atlantic), and Arthur Jackson loaded the data into GeoQuest software on UNIX/Silicon Graphics workstations. All other work, unless otherwise stated in Chapter 4, was conducted by MED.

I was responsible for synthesizing the ideas presented in this paper, and in particular establishing the regional framework and links between the evolution of the JDB and Flemish Pass. Additional technical work included the mapping of more than 30

regional and local seismic horizons (this time from digital 2-D seismic data), mapping of seismic facies (including erosional and depositional features), and identifying and correlating faults in the post-rift succession. My contributions also included loading of digital well log data, correlation between seismic horizons and well data, calculation of sedimentation rates, and the generation of time-structure and time-thickness maps (including data gridding and contouring using GeoQuest software). Additional methods employed by MED, and the rationale behind them, are provided in section 4.1.3.

1.4.3 Chapter 5

Chapter 5 has not yet been submitted for publication, and the content of the chapter is likely to change prior to submittal. The contributors to this chapter are MED and David Piper. Permission to use several 3-D seismic volumes was sought by MED in 1999 and was granted by all the oil companies that owned the data at that time (including Chevron Canada Resources, Mobil Oil Canada (now Exxon Mobil), Husky Oil, Norsk Hydro Canada Oil & Gas, Mosbacher Operating Ltd., Murphy Oil Company, Petro-Canada, and the Hibernia Management and Development Company). Chevron provided MED with copies of the 3-D seismic volumes on Exabyte tapes and Arthur Jackson loaded the data into GeoQuest software on UNIX/Silicon Graphics workstations. Data from modern analogues, and some previous published and unpublished interpretations of those modern analogues, were provided by David Piper (GSC Atlantic - referenced accordingly in the text). David Piper designed and managed the field programs that collected the modern analogue data. All other work, unless otherwise stated in Chapter 5, was conducted by MED.

Digital Hunttec DTS reflection profiles from offshore eastern Corsica were loaded into GeoQuest by MED (with the assistance of Arthur Jackson - a process that took 2 months). Paper copies of Hunttec data were also interpreted. In the JDB, vertical profiles, time-slices, and horizon-slices (parallel to mapped horizons), in combination with several other approaches, were used to interpret 1800 km² of 3-D seismic data. These methods are described in detail in Chapter 2.

1.4.4 Chapter 6

Chapter 6 has been submitted and accepted for publication in the *Journal of Marine and Petroleum Geology* (Deptuck et al., in press). The title of the article is “Architecture and evolution of upper fan channel-belts on the Niger Delta slope and in the Arabian Sea”. The co-authors are MED, Gary Steffens, Mark Barton, and Carlos Pirmez. Access to the 2-D and 3-D seismic data-sets used in Chapter 6 was provided by Shell International Exploration and Production. I developed the concepts in the paper based largely on my own interpretative work, but discussions with the three co-authors sharpened many of the concepts presented. Mark Barton conceived the idea for Figure 6.20 and provided the photo mosaic. He, along with Gary Steffens and Carlos Pirmez, provided many of the interpretations for the “Solitary Channel” (the remaining interpretations for the outcrop were based on published articles, referenced accordingly). All mapping was done by MED, and several of the approaches used in Chapter 5 (and described in Chapter 2) were also used in Chapter 6. Additional methods employed by MED, and the rationale behind them, are provided in section 6.3.1.

CHAPTER 2 - METHODS AND BACKGROUND

2.1 Marine reflection seismic data

The primary tool used in this study is reflection seismic data. The method for collecting reflection seismic data in marine settings involves triggering an acoustic pulse (sound source - many different kinds) near the sea surface, which propagates through the water column and into the subsurface. Part of the acoustic pulse reflects or echoes off the sea floor as well as other subsurface interfaces. The arrival time of the “echoes” is recorded by hydrophones towed behind the vessel, just below the sea surface. Such data provide a cross-sectional *representation* of the subsurface, based on reflected acoustic energy from subsurface stratal interfaces, in units of two-way travel time.

Acoustic energy is reflected at the boundaries between strata of varying acoustic impedance (Z , the product of bulk density and seismic velocity - Kearey and Brooks, 1991). In general, the harder the rock the greater its acoustic impedance (Kearey and Brooks, 1991). The magnitude of the change in acoustic impedance between two stratigraphic units determines the strength or amplitude of the reflection. The ratio between the reflected and transmitted waves is the reflection coefficient (R) (North, 1985). In addition to the amplitude of the reflection coefficient, equation (2.1) determines the polarity of the reflection coefficient, based on whether the seismic pulse passes from higher to lower impedance strata or vice versa (on its way down). Therefore if a low impedance layer (e.g. shale) overlies a high impedance layer (e.g. limestone), a positive reflection coefficient is generated; if the deeper layer has lower impedance, a negative reflection coefficient is generated.

$$(2.1) \quad R = \frac{Z_{\text{layer 2}} - Z_{\text{layer 1}}}{Z_{\text{layer 2}} + Z_{\text{layer 1}}}$$

An individual seismic trace (wiggle plot) represents a time-series (in units of two-way travel time - TWTT) of reflection returns from subsurface interfaces, convolved with the input sound source, and recorded by hydrophones towed behind the vessel. The reflected returns decrease in amplitude with increasing depth due to spherical spreading

and absorption of the sound source. In single-channel data, each hydrophone within an array samples a different location on the sea floor, and the outputs of individual hydrophones are summed (Kearey and Brooks, 1991). In multi-channel seismic data, several traces are collected for a given “point” (a common-depth point or common mid point), but at varying offsets from the acoustic source. The hydrophone closest to the source (i.e. shortest offset) receives the reflection in a shorter period of time because of the shorter ray path. Since the distance from the source to the hydrophones increases for successive traces (with respect to a single mid-point), a process called normal moveout is required to correct for the effect of increasing offset distances. The normal moveout correction effectively shifts the offset of all traces in the common mid point gather to zero, by applying an appropriate velocity (Yilmaz, 1987). Once the variations in offset are accounted for, the traces are “stacked” to reinforce primary reflections and to attenuate incoherent noise (Kearey and Brooks, 1991). This procedure significantly improves the signal to noise ratio (Yilmaz, 1987). The normal moveout correction also provides important information about subsurface velocities (the “stacking velocity” or “normal moveout velocity”).

2.1.1 Resolution

It is important to understand the limitations of the seismic tools used for subsurface studies. By varying the frequency content of the sound source, a wide range of resolution is possible, and likewise different seismic devices have widely varying capabilities. Frequencies absent from the input sound source, will also be absent from the resulting seismic trace, and therefore the sound source is very important (Mosher and Simpkin, 1999). Higher resolution data can provide very detailed information at nearly the bed-scale (Piper et al., 1999), but the sound source has limited penetration due to the lack of lower frequencies and consequently only shallow strata are well imaged (typically less than 75 m). Huntec Deep-Tow Seismic (DTS) is an example of such data, with a boomer source that has a bandwidth of 500 to 6000 Hz (Mosher and Simpkin, 1999). In contrast, conventional industry 2-D and 3-D seismic data use an airgun source with the dominant frequency range between 30 and 60 Hz. Such data have lower vertical resolution (6-20

m) but are capable of imaging deeply buried systems. Therefore, there is a trade-off between resolution and acoustic penetration.

Resolution refers to the minimum separation of two objects such that they can be distinguished as two separate entities rather than one (Sheriff and Geldart, 1995). In an earlier publication, Sheriff (1985) described resolution as the ability to tell that more than one feature is contributing to an observed effect. Resolution is commonly described in both the vertical sense and the horizontal sense.

Vertical resolution

The vertical resolution of seismic data used in this study varies from less than 0.5 m to greater than 10 m. Vertical resolution (also known as temporal resolution) is a measure of the ability to distinguish individual closely spaced reflectors, and, as discussed earlier, depends strongly on the frequency content of the acoustic source (Kearey and Brooks, 1991). The vertical resolution is typically taken as $\frac{1}{4}$ the dominant wavelength of the acoustic source (Yilmaz, 1987). However, a bed that is significantly thinner than $\frac{1}{4}$ wavelength (e.g. $\frac{1}{20}^{\text{th}}$ or $\frac{1}{30}^{\text{th}}$ the dominant wavelength) can still produce a reflection, but the bed thickness cannot be determined from the wave shape (i.e. a reflection is not generated from the base and top of the bed - Yilmaz, 1987; Sheriff and Geldart, 1995). The vertical resolution (*v.r.*) can be calculated using equation (2.2b)

$$(2.2a) \quad \lambda = v/f$$

$$(2.2b) \quad v.r. = (v/f) / 4$$

where v is the velocity and f is the dominant frequency (Yilmaz, 1987). For example, if the dominant frequency is 60 Hz, and the velocity is 2000 m/s, the dominant wavelength would be about 33 m (from equation 2.2a), with a vertical resolution $\frac{1}{4}$ this value (just over 8 m - according to equation 2.2b).

Vertical resolution can be improved by increasing the dominant frequency of the input source and decreasing unwanted noise (Yilmaz, 1987). Two types of waveform manipulation are commonly used. The first is referred to as filtering, and involves applying a low-cut and/or high-cut filter to the data during or after acquisition (i.e.

bandpass filter - cutting the lowest and the highest undesired frequencies). Ship noise, for example, can be removed in this manner (Kearey and Brooks, 1991). The second kind of waveform manipulation is referred to as inverse-filtering or deconvolution, and is the principal post-acquisition tool for improving vertical resolution (Brown, 1996). Deconvolution is used to remove unwanted noise that has the same frequency content as the primary reflections (and hence cannot be removed with frequency filters - Kearey and Brooks, 1991). It results in a shortening or compression of the input seismic wavelet and can also attenuate noise from multiples (Yilmaz, 1987; Kearey and Brooks, 1991).

Horizontal resolution

Horizontal resolution (also known as spatial or lateral resolution) refers to the ability to distinguish between features that are displaced horizontally with respect to one another (Sheriff, 1985). The horizontal resolution in unmigrated seismic data depends closely on the size of the Fresnel zone, a circular *area* on a reflector from which a reflection is generated (Sheriff and Geldart, 1995). The width of the Fresnel zone depends on the dominant wavelength (and hence frequency - f) of the sound source, the distance from the source to the reflector (z), and the velocity (v) above the reflector (Yilmaz, 1987). The Fresnel zone gets larger with increasing depth due to spherical divergence of the wavefront and attenuation of higher frequencies. Consequently, the horizontal resolution deteriorates with depth (Kearey and Brooks, 1991). For unmigrated seismic data the radius of the Fresnel zone (r) can be determined from equation (2.3) or (2.4) (2.3 and 2.4 are different forms of the same equation).

$$(2.3) \quad r = (z\lambda/2)^{1/2} = (v/2) (t/f)^{1/2} \text{ (Yilmaz, 1987)}$$

$$(2.4) \quad 2r = w = (2z \lambda)^{1/2} \text{ (Kearey and Brooks, 1991)}$$

where t is the two-way travel time to the reflector, λ is the wavelength (in metres), and w is the Fresnel zone width. For example, with a 40 m wavelength (50 Hz frequency at 2000 m/s; see equation 2.2a), a reflector that is 1000 m from the source will have a Fresnel zone that is 282 m wide ($r = 141$ m). Because reflections are generated from an

area rather than a single point in the subsurface, out-of-plane noise is common in unmigrated data.

Migration is the principal tool for improving horizontal resolution (Brown, 1996). Migration can be thought of as collapsing the Fresnel zone (Sheriff and Geldart, 1995); it focuses energy spread out over the Fresnel zone, collapses diffractions, and repositions reflections from dipping strata into their correct subsurface positions (Brown, 1996; Yilmaz, 1987). The horizontal resolution of migrated seismic data is approximately equivalent to the dominant wavelength of the source. Migration for 3-D seismic data collapses the Fresnel zone in three dimensions, significantly improving horizontal resolution and reducing out-of-plane effects (as opposed to collapsing the Fresnel zone into a single plane, as in 2-D seismic data). For 3-D seismic data, the horizontal resolution is ideally equivalent to the bin spacing, typically 25 m x 25 m or 12.5 m x 25 m (discussed in more detail below - Figure 2.1e).

2.2 3-D seismic data

Marine 3-D seismic data are acquired by ships that tow airgun arrays and hydrophones back and forth across a survey area, shooting closely spaced parallel to sub-parallel lines, typically less than 50 m apart (Yilmaz, 1987; Hart, 1999). The in-line direction is parallel to the ship tracks, whereas the cross-line direction is perpendicular to the ship tracks (yielding in-lines and cross-lines - see Figure 2.1a). Rather than traces collected as common mid-point gathers, as in 2-D multi-channel seismic data (described earlier), 3-D seismic data consist of traces collected as common-cell gathers, that are stacked into bins (Yilmaz, 1987). **Bin** size, either square or rectangular, is largely determined by the acquisition configuration (e.g. distance between the sources and hydrophones - Hart, 1999), and all traces that lie within a given bin area are stacked into a common-cell gather (a process called binning - Yilmaz, 1987). Typically bins are sampled vertically at either 2 or 4 ms (two-way travel time). Each vertical sample, combined with the horizontal bin area, defines a cube corresponding to a voxel (Figure 2.1e). Each **voxel** has a single amplitude value associated with it (Hart, 1999). The 3-D seismic surveys used in this study have bins that range in dimension from 25 m x 25 m to 12.5 m x 25 m, sampled at 4 ms.

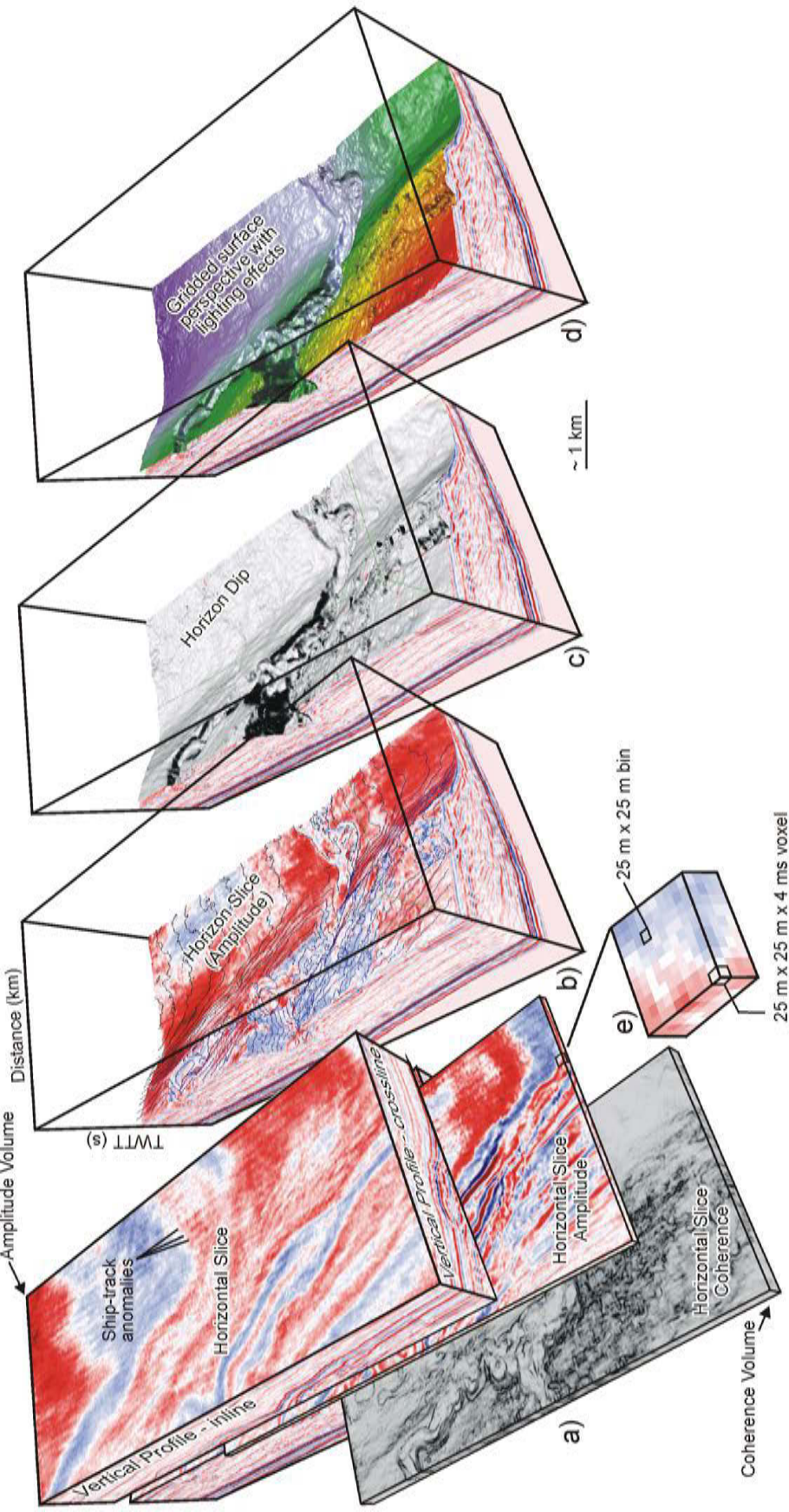


Figure 2.1. Images summarizing various methods for viewing 3-D seismic data. a) Vertical seismic-reflection profiles, time-slices (through both an amplitude and coherence volume). b) Perspective view of horizon-slice (amplitude) extraction along mapped horizon). c) Perspective view of dip magnitude. d) Perspective view of time-structure map with lighting effects. e) Close-up showing individual 25 m x 25 m bins sampled at 4 ms (voxel). On vertical sections, red represents positive and blue represents negative amplitude polarity.

Because data points are collected in three dimensions, migration is also carried out in three dimensions. 3-D migration minimizes out-of-plane effects (e.g. sideswipe), thereby increasing resolution and the general accuracy of profiles (as representations of true vertical cross-sections - Hart, 1999).

2.2.1 Methods for viewing 3-D seismic data

Because 3-D seismic surveys consist of a volume of data, various methods allow the interpreter to “slice” through the volume and extract specific information from an otherwise vast quantity of data. Several approaches were exploited in this study to enhance interpretations. In many cases specific strategies were developed to investigate different aspects of deep-water depositional systems. The most common methods for viewing 3-D seismic data include vertical seismic sections, time-slices, and horizon slices.

A vertical **seismic section** can be taken in any orientation (parallel to inlines or cross lines, diagonally, or multi-panel displays - Figure 2.1). Such sections provide cross-sectional information about the subsurface. Vertical sections were used to determine the external morphology and internal seismic character (otherwise known as “seismic facies”) of marginal marine and deep-water architectural elements. In many cases, features that are too subtle to identify in vertical sections are well-imaged using horizontally oriented sections known as **time-slices** (parallel to a given two-way travel time, or depth, if the volume has been depth converted). For example, channels (both sinuous and straight) can often be identified and mapped from time-slices (e.g. Figure 2.2). In this study, horizontal time-slices were used to characterize the planform geometry of architectural elements by examining the data for patterns in the amplitude or coherence distribution (both attributes discussed later). Figure 2.2 shows two examples of time-slices from amplitude data and equivalent slices from coherence data. Observations of channel width, length, and sinuosity as well as the lateral extent of lobes were all made, at least in part, from time-slices.

More complicated slices are also feasible, and in many cases necessary. For instance, whereas horizontal time-slices work well in areas where seismic reflections are flat-lying, in areas where seismic reflections are dipping or offset by faults, a given time-

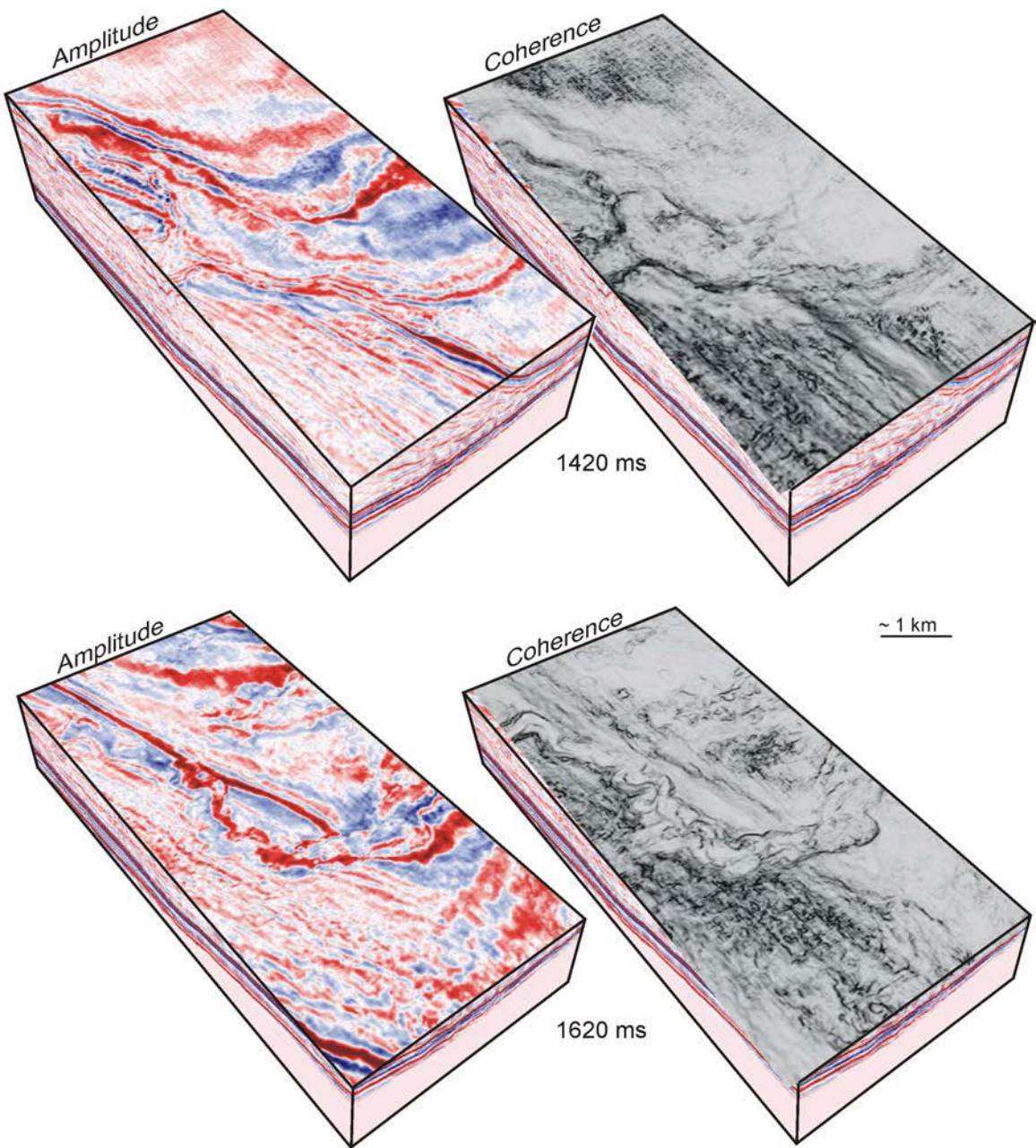


Figure 2.2. 3-D images comparing time-slices from amplitude (left) and coherence (right) volumes. Note the improved imaging of the channel in the coherence volume (lower left).

slice will cross strata of significantly different ages (i.e. cross geologic time-lines). If this situation is undesirable, a seismic horizon can be interpreted and flattened (shifted back to horizontal). Horizontal slices through the flattened data volume, and parallel to the interpreted horizon, may then be extracted and examined in a similar fashion as horizontal time-slices. The result are known as **horizon-slices** (Brown, 1996), which allow the interpreter to cut the volume parallel to a mapped horizon, and therefore sample strata of approximately the same age. Figure 2.1b is an example of a horizon slice, showing the amplitude distribution at the T1 seismic marker (see Chapter 3) draped by structural contours. Horizon-slices are very useful for showing the planform geometry of features like channels and faults. Commonly a smoothing filter is applied to the traveltime of the horizon before the amplitude extraction to remove local irregularities in the horizon interpretation.

Volume visualization

Aside from surface-based interpretations (described above), 3-D seismic data can be visualized in three-dimensional space by applying various levels of transparency (Kidd, 1999). Transparency effects can be applied to the entire volume or a subset of the volume, and to specific ranges of amplitudes or other attributes. The process of isolating a specific subset of a 3-D seismic volume is referred to as **volume sculpting** in this study, and two approaches can be used. First, a volume subset can be generated by choosing a narrow range of two-way travel time, a process referred to as time-windowed sculpting. A narrower range of in-lines and cross-lines can also be applied, thereby defining a smaller area. In flat-lying strata, transparency effects can be applied to the time-windowed sculpted volume to evaluate specific stratigraphic features that may have a distinct amplitude expression (Kidd, 1999).

The second approach to volume sculpting involves using two interpreted horizons to bracket a specific subset of the volume. This horizon-keyed approach is useful in areas where strata are not flat-lying. In Figure 2.3, interpreted horizons above and below a seismically defined lens-shaped unit were used to sculpt the volume. This process removes all extraneous data above and below the lens, and allows for volume transparency effects to be applied without interference (Kidd, 1999). This approach can

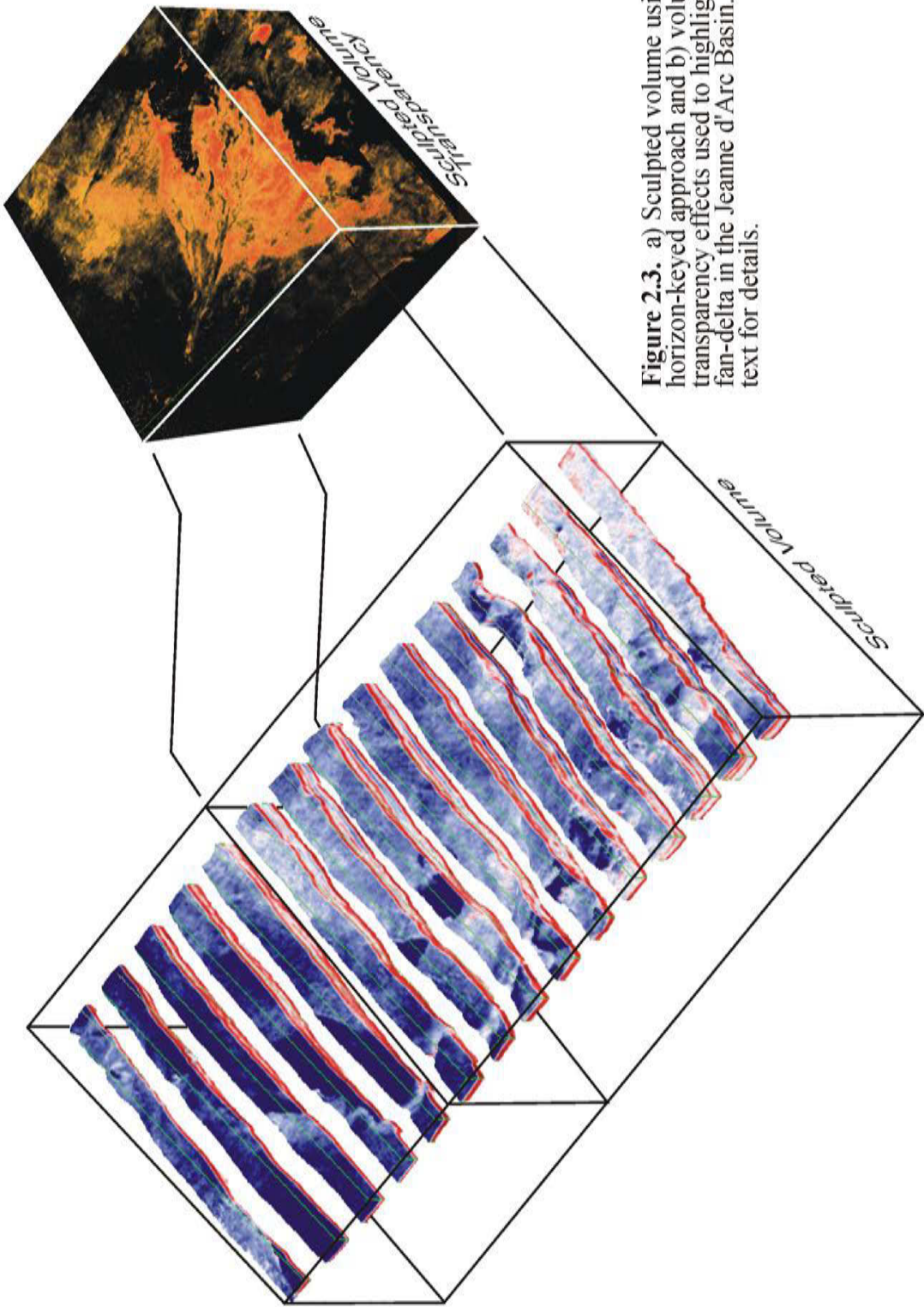


Figure 2.3. a) Sculpted volume using horizon-keyed approach and b) volume transparency effects used to highlight a fan-delta in the Jeanne d'Arc Basin. See text for details.

sometimes be useful for imaging stratigraphic features like the interpreted fan delta in Figure 2.3. More importantly, time-windowed and horizon-keyed volume sculpting isolates specific portions of the data volume, from which various other seismic attributes can be extracted (e.g. maximum positive amplitude, maximum absolute amplitude, time-thickness maps, etc. - see below).

2.2.2 Seismic attributes

A seismic attribute is a derivation of the basic seismic measurements: time, amplitude, frequency, and attenuation (Brown, 1996). As discussed above, attributes can be extracted along a horizon or from within a pre-defined window. The attributes most commonly used in this study include reflection amplitude, reflection strength (magnitude), coherence, dip, azimuth, and two-way travel time (both time-thickness and time-structure - discussed in the following section).

Reflection amplitude and strength

Reflection amplitude is the most widely used attribute for vertical, horizontal, and horizon-parallel slices (Brown, 1996). As discussed earlier, it is a measure of the strength and polarity (either negative or positive) of a reflection, and depends on the contrasts in acoustic impedance between overlying and underlying lithological units. The amplitude attribute is non-unique, and therefore different geologic situations can generate similar amplitudes. Amplitude in multi-channel seismic data is most strongly influenced by contrasts in porosity, bed thickness, and fluid content (Mitchum et al., 1977b).

Reflection strength (also known as magnitude) is similar to amplitude, but has no phase information associated with it. Instead, reflection strength is plotted independent of polarity. In this way reflection magnitude can be regarded as the absolute value of amplitude. It is particularly useful for viewing digital Huntec DTS data.

Coherence

Next to amplitude data, the most commonly used attribute in this study is coherence (also known as variance, dissemblance, semblance, and continuity). The coherence attribute is calculated from the amplitude volume, and is a measure of the

amount of similarity between a seismic trace and surrounding traces within a predefined time window (Hart, 2000). The coherence algorithm provides a measure of reflection continuity using a cross-correlation calculation (Brown, 1996). If a wavelet is strongly similar to neighbouring wavelets, a high coherence value is calculated (Hart, 2000). If, on the other hand, the wavelet is dissimilar to its neighbours as would be the case near a fault offset or where a reflection is truncated by a channel, a low coherence value is calculated. In most cases, much of the seismic volume consists of relatively coherent data, and hence incoherent features like faults and channel-margins are well imaged and relatively simple to identify. Figure 2.4 is an example of a horizontal slice through a coherence volume in the Jeanne d’Arc Basin showing the edges of a prominent amplitude anomaly interpreted to delineate a region of shallow gas (764 ms TWT below the surface). Figure 2.5 is a horizon-slice 20 ms above the K1 marker in the Jeanne d’Arc Basin (smoothed - approximately a 90 Ma marker), showing several other features commonly well imaged on coherence data (including channels and faults).

Dip and azimuth

Dip is a time-derived attribute that shows variations in the *amount* of dip on an interpreted seismic horizon (Brown, 1996). Dip maps are useful because they highlight regions on a surface where dips are steeper, for example along the margins of a channel (Figure 2.1c). They are also useful for highlighting faults without the need for lighting effects. Typically a grey-scale colour bar is used, and darker shades correspond to steeper dips (a convention used throughout this thesis). Azimuth maps, on the other hand, show in which *direction* an interpreted seismic horizon is dipping (as opposed to the magnitude of the dip). Individual colours on the colour bar correspond to a specific dip orientation.

2.3 Time-structure and time-thickness (isochron)

Time-structure maps are used throughout this thesis, and represent the structure of a seismic horizon in units of two-way travel time (TWT). Both regional and local seismic horizons were mapped from both 2-D and 3-D seismic data using GeoQuest software (described below). Mapped 2-D seismic horizons were correlated using “cross-over”

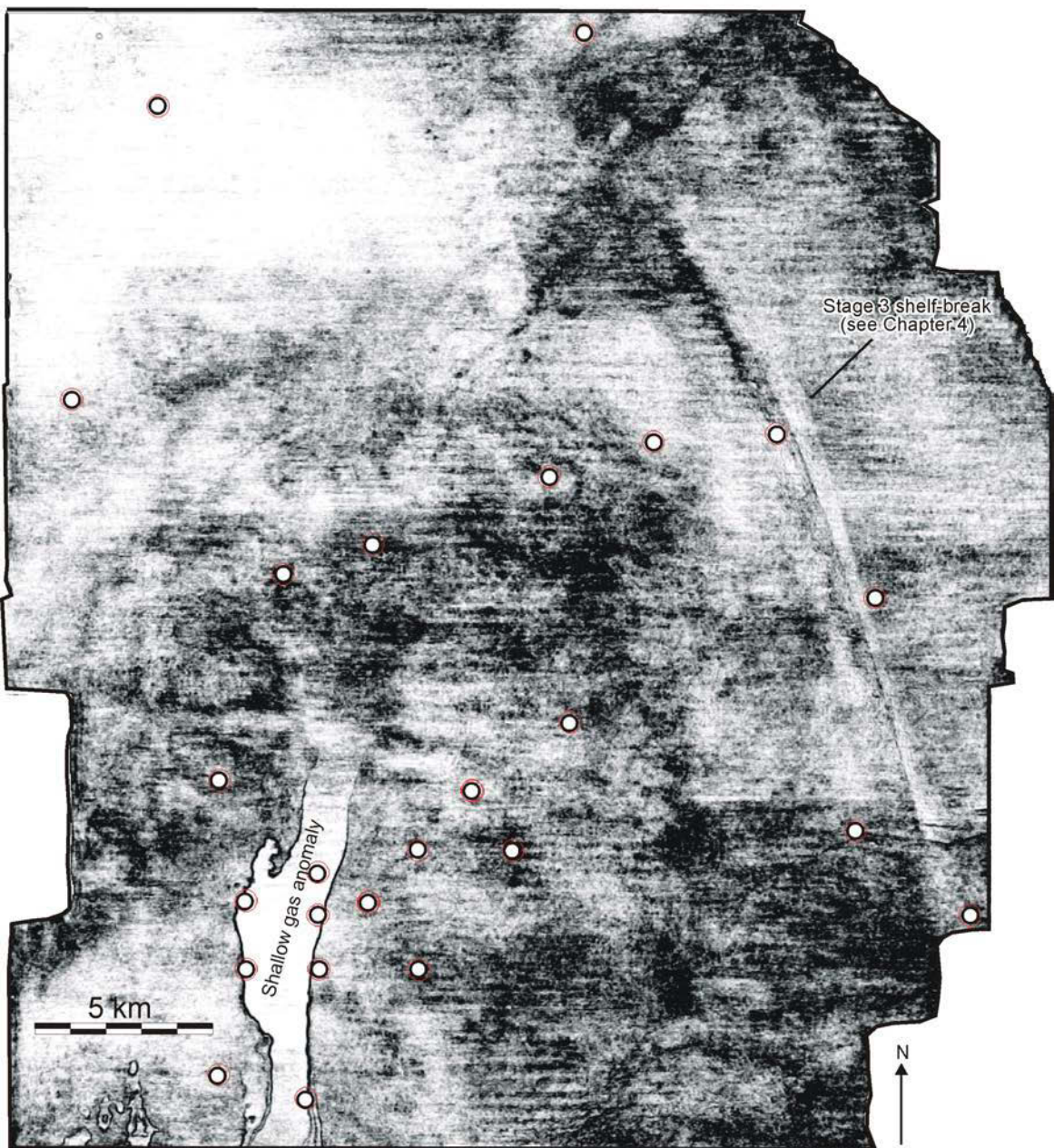


Figure 2.4. Coherence time-slice - 764 ms below sea floor marker (T100). Note the sharp definition of an interpreted shallow gas anomaly. This feature appears as a very high-amplitude and continuous anomaly in the amplitude volume. Also note the linear feature to the northeast that corresponds to a subtle Late Eocene shelf break.

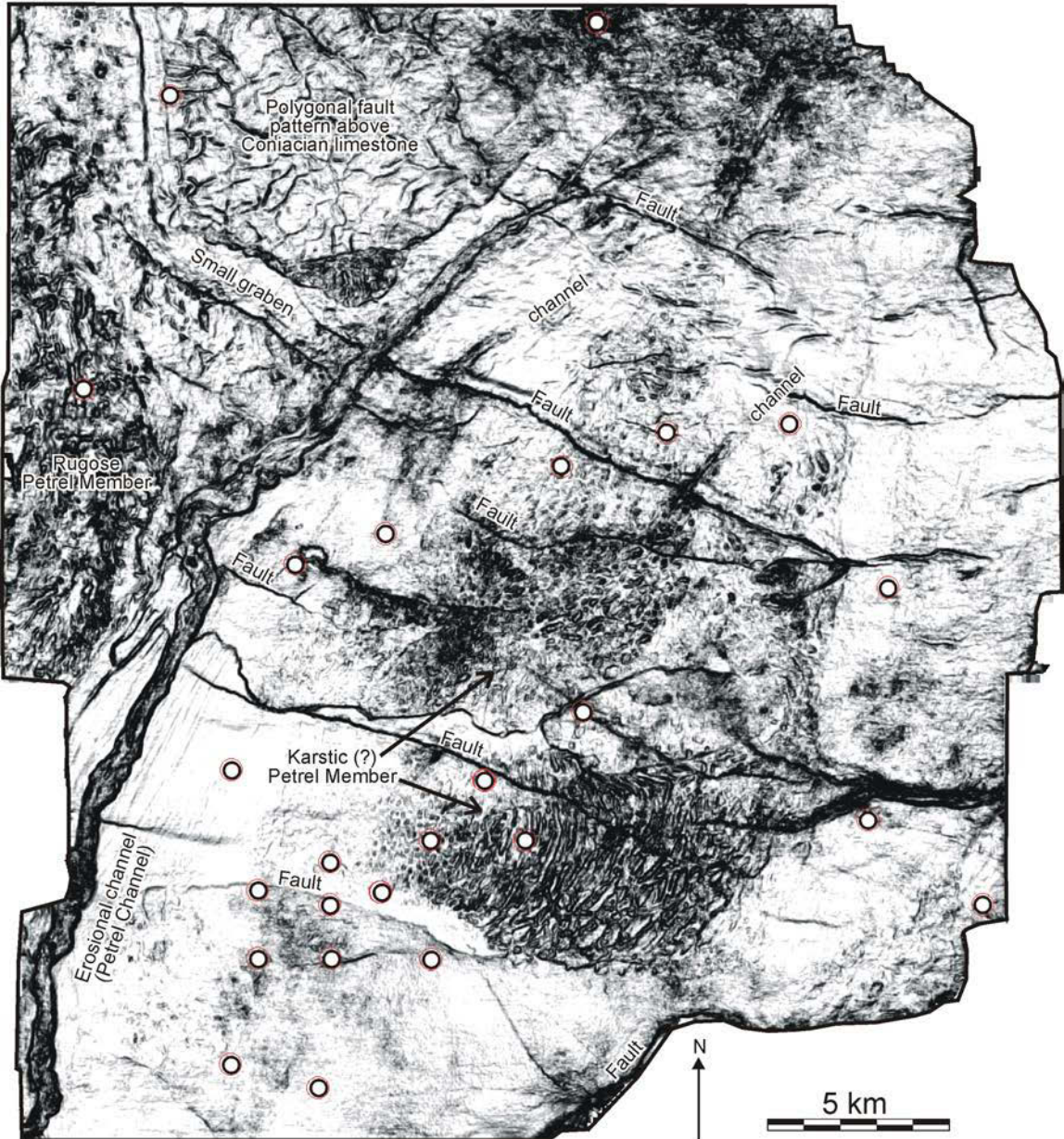


Figure 2.5. Coherence horizon-slice - 20 ms above smoothed K1 marker (see Chapters 3-5). NW to SE trending normal faults are prominent at this level, though offsets are commonly less than 100 m. Note the prominent north to northeast trending Petrel Channel and two smaller channels to the east (slightly shallower and hence not fully imaged by this slice). Note also the peculiar region near the center of the figure interpreted as submarine karst (see Chapter 5).

points (see fence diagram in Figure 2.6a), and fault polygons were traced above fault offsets to allow for better recognition during gridding. After the horizon was mapped across the survey area (e.g. Figure 2.6b), the data were gridded with a 400 m grid spacing and contours based on the gridded data were overlain on the surface (Figure 2.6c).

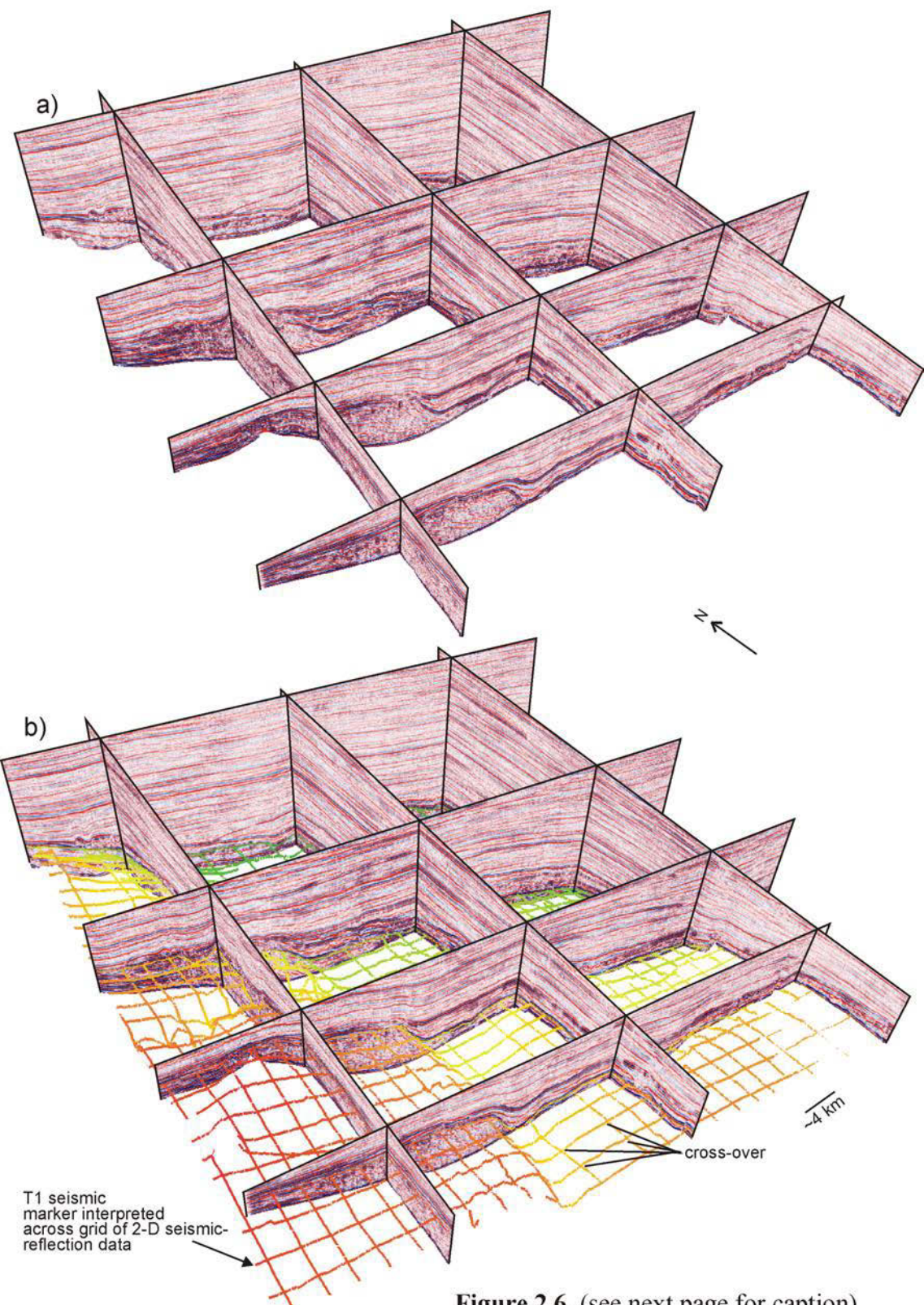
The procedure for horizon interpretation from 3-D seismic is somewhat different. A grid of lines, typically every 10 or 20 in-lines and cross-lines, was mapped, and an autopicker was used cautiously to fill in gaps (see next section for more details on this procedure). Fault polygons were not necessary for 3-D seismic horizons due to the spatial density of interpretation points. Gridding was carried out at 25 to 50 m spacing and typically produced similar results as the original horizon interpretation (but did fill in minor gaps). In some cases, interpreted 2-D and 3-D seismic horizons were merged into one by overlaying the 2-D with the 3-D gridded surfaces (see Chapter 5).

Isopach maps show, by means of contour lines, the distribution of thickness of a specified mapping unit. Isochron maps, herein referred to as time-thickness maps, are similar but rather than showing thickness in depth, they show the distribution of thickness in units of two-way travel time (with the true depth dependent on the velocity of the time-thickness interval, i.e. the interval velocity). Several of these maps were generated to illustrate changes in sediment depocenters (regions of maximum sediment accumulation) or the general planform thickness character of various depositional elements. Time-thickness maps are generated by subtracting a shallower horizon from a deeper horizon. The remainder corresponds to the time-thickness of the interval between the two horizons. Similar to time-structure maps, time-thickness maps can be gridded and overlain by contours.

2.4 Seismic interpretation software

2.4.1 Schlumberger GeoQuest software package

The primary seismic interpretation software used in this study is Schlumberger's GeoQuest software package, consisting of three primary modules: Basemap Plus, IESX, and Geoviz. The Geological Survey of Canada (Atlantic) holds two 2-D and one 3-D license for the GeoQuest software package, and interpretation was done using Sun and Silicon Graphics Interface (SGI) workstations, also owned by the GSC (Atlantic). In



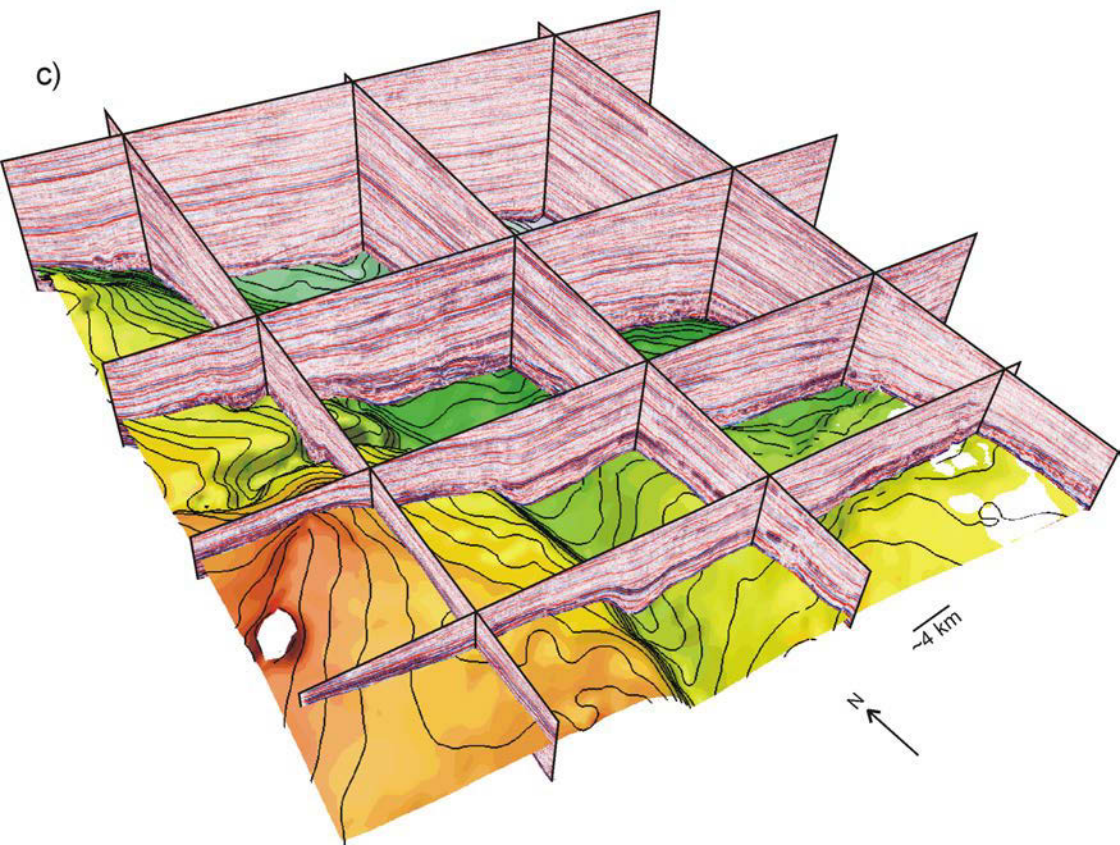


Figure 2.6. a) Fence diagram with profiles from the Jeanne d'Arc Basin, clipped below the K1 marker. b) T1 seismic marker interpreted from grid of 2-D seismic data. c) 400 m x 400 m interpolated grid of the T1 seismic marker shown in (b), generated in Geoquest IESX and BasemapPlus.

addition, GeoQuest provided a temporary license for their variance module, which I used to extract the variance (coherence) attribute from available 3-D seismic volumes.

IESX

GeoQuest's IESX module was used to interpret horizons and faults from both 2-D and 3-D seismic data sets. IESX allows the integration of petrophysical well logs (tied to seismic-reflection profiles using checkshot surveys, described later) and provides a variety of options to improve interpretation efficiency. Horizon interpretation was done using a combination of manual picking (snapped to a selected horizon), autotracking (automatically tracks a horizon along a given seismic profile), and autopicking (automatically tracks a horizon over a given area, based on a grid of interpreted seed points).

Autotracking involves selecting a seed point on a given horizon, followed by the selection of the autotracker option (either via a pulldown menu or a short-cut key). The software uses a search window and operator length that are either preset (i.e. the default setting) or manually set, combined with the seed point, to follow the desired horizon as far as possible within the visible IESX window. This procedure can significantly increase the pace of interpretation, but is only useful for high continuity reflections. If the reflection is low amplitude and/or low continuity the autotracker either terminates (e.g. at a fault) or mistracks the horizon (i.e. jumps to another, more continuous reflection). Autotracked horizons were manually checked during the interpretation process and re-tracked or manually picked where necessary.

Autopicking, using the Automatic Seismic Area Picker (ASAP), is similar to autotracking, but is strictly used during 3-D seismic interpretation to fill in gaps in a horizon after a minimum grid has first been interpreted. The interpreted grid (e.g. every tenth inline and crossline - roughly 250 x 250 m grid) provides the seed points that guide the autopicker. The required seed point density (i.e. the interpreted grid), however, was sometimes much greater, and depended on the complexity of the interpreted horizon and its regional continuity. This process worked well for high continuity/high amplitude/high frequency reflections, but failed under some circumstances. For example, ASAP could not be used to interpret the erosive base of canyons/channels because such surfaces are

commonly discontinuous and of variable amplitude. Manual picking was required in such situations, and in all cases the autopicked horizons were carefully checked and re-picked manually where necessary, sometimes across every inline or crossline.

These techniques increase the efficiency of interpretation, particularly with the enormous amount of data contained in 3-D seismic volumes, but at all times they were carefully monitored for quality-control.

Basemap Plus

Basemap Plus is a GeoQuest module that allows all project data to be displayed in a single window (planview), including wells, seismic line/volume location, cartography (e.g. latitude and longitude coordinates), and culture data (like coastlines, isobaths, or manually added outlines). In addition, the software is used to display horizon interpretations, updated in real-time, as the seismic profile is interpreted in the IESX window. Basemap Plus allows various attribute maps associated with interpreted horizons to be displayed, including two-way travel time, amplitude, dip magnitude and azimuth (see previous section). This module was also used to generate time-thickness maps (by subtracting two horizons from one another), and to grid and contour interpreted horizons. Gridding parameters were selected based on data-coverage (400 m with 2-D seismic-reflection profile coverage and 25 - 50 m with 3-D seismic coverage).

Geoviz

Geoviz is a GeoQuest module that is fully linked to GeoQuest IESX and Basemap Plus. It is used for three-dimensional visualization of 2-D/3-D seismic and well data, as well as interpreted horizons and faults. Figure 2.7 shows a series of three-dimensional block diagrams generated in Geoviz. These diagrams illustrate the integration of a sculpted amplitude volume, vertical sections, and coherence time-slices. The software allows the user to sculpt 3-D seismic data, add transparency effects, and extract amplitudes (voxel picks). The software also allows for the display of gridded seismic horizons that can be draped by various seismic attributes (like extracted amplitudes from overlying or underlying horizon-windowed intervals). The surfaces can be rotated in three dimensions and lighting effects to create shadows can be used to enhance subtle

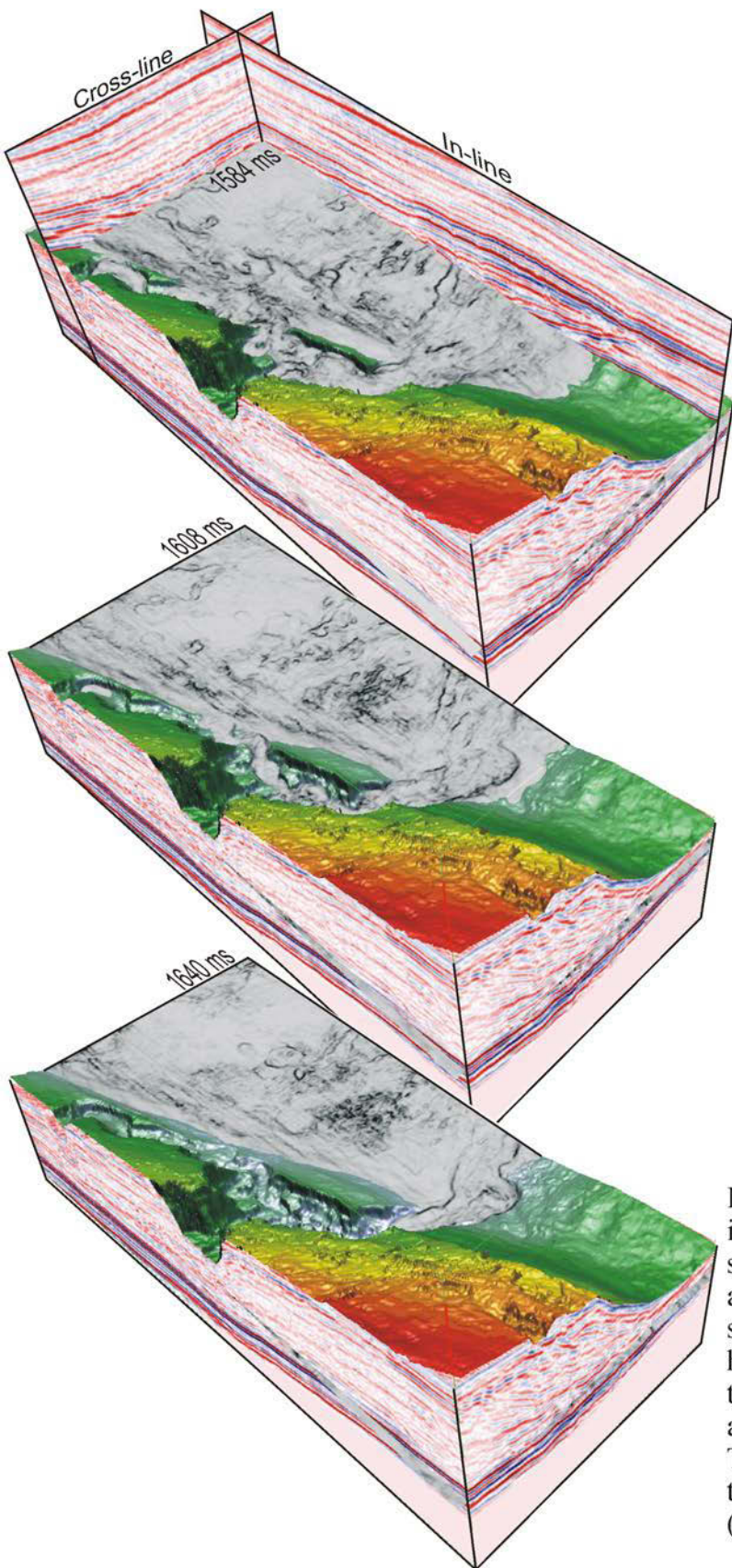


Figure 2.7. Three block images generated in GeoViz, showing integration of an amplitude volume, volume sculpting along a gridded horizon, and time-slices through a coherence volume at three different depths (in TWT). Top image shows two vertical seismic sections (an in-line and cross-line).

features (like the canyon surface shown in Figure 2.7). The texture of 3-D seismic surfaces can also be modified to the desired settings (varying the glossiness or granularity of the surface).

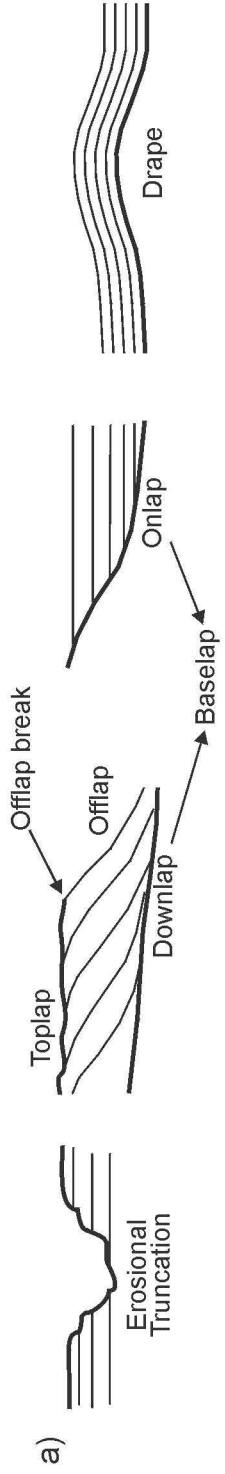
2.5 Seismic stratigraphy

Seismic stratigraphy is the “study of stratigraphy and depositional facies as interpreted from seismic data” (Mitchum et al., 1977b; page 117). It involves the recognition of patterns (seismic facies) and requires an ability to identify important surfaces (bounding discontinuities). Recognition of reflection termination patterns like onlap, downlap, toplap, and erosional truncation (Figure 2.8a) are critical for the identification of important surfaces that are necessary for subdividing the seismically imaged stratigraphic record. Erosional truncation of the topsets and onlap onto the slope, for example, are the most common criteria used for the identification of regional unconformities on seismic-reflection profiles (sequence boundaries - as defined by Mitchum et al., 1977a,b).

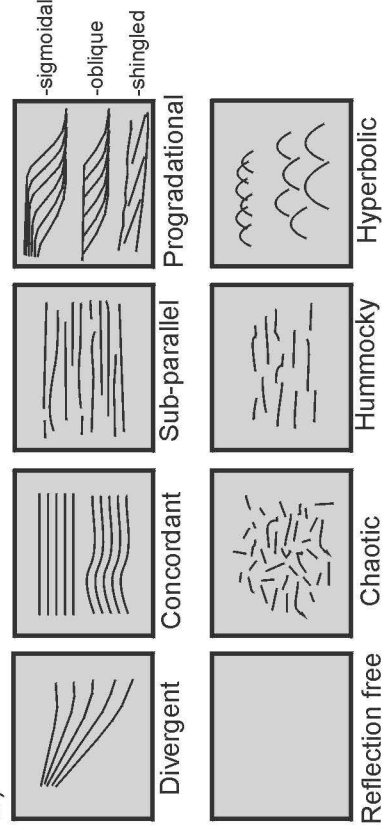
Reflection termination patterns combined with reflection configurations (Figure 2.8b) were used to identify where the shelf, shelf-break, slope and basin floor were located at various times in the Jeanne d’Arc Basin and to identify important bounding discontinuities (particularly for Upper Cretaceous and lower Paleogene strata). At a more detailed scale, the principles of seismic facies analysis were used to identify depositional and erosional elements, and their distribution was used to interpret the evolution of depositional systems (from shelf-slope systems and submarine fans to channel-levee systems).

2.5.1 Seismic facies analysis

Reflection configurations (Figure 2.8b) and seismic facies (Figure 2.8c) for conventional multi-channel seismic-reflection profiles are described following the definitions provided by Mitchum et al. (1977b), Sangree and Widmier (1977, 1979), Roksandic (1978, 1985) and Mitchum (1985). Seismic facies analysis involves “the delineation and interpretation of reflection geometry, continuity, amplitude, frequency, and interval velocity, as well as the external form and three-dimensional associations of

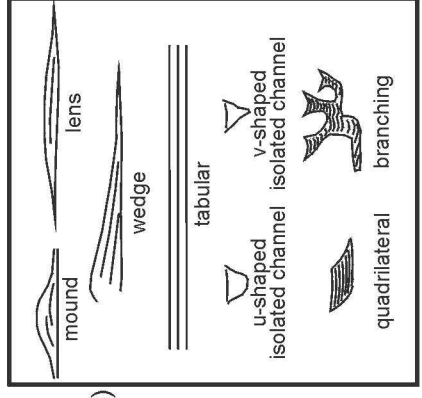


b) Reflection configurations



c) Seismic facies

- 1. Internal seismic character**
 - frequency (low, moderate, high)
 - amplitude (low, moderate, high)
 - continuity (continuous, discontinuous)
- 2. Cross-sectional external form**
 - mound
 - lens
 - wedge
 - tabular
 - u-shaped
 - isolated channel
 - v-shaped
 - branching
 - quadrilateral
 - parallelogram



3. Planform geometry (descriptors)

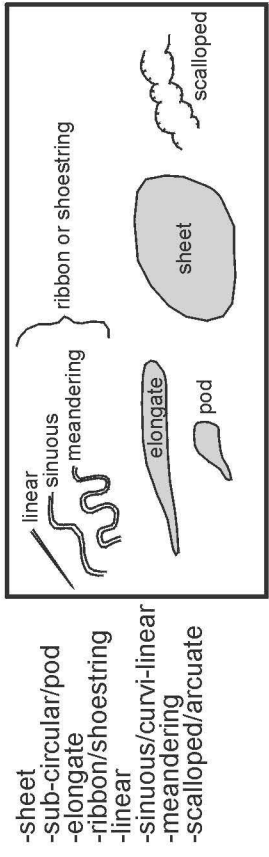


Figure 2.8. Seismic stratigraphy - see text for details.

groups of reflections” (Sangree and Widmier, 1977, p. 165). Aside from “interval velocity” (which Sangree and Widmier, 1977 and 1979 do not use despite their definition), the principles for seismic facies analysis presented by Sangree and Widmier (1977) and Mitchum et al. (1977b) were used throughout this study. Seismic facies analysis is used to determine the relative age and geometry of depositional units, and to interpret their lithology, depositional environments and processes, and sediment transport direction (Roksandic, 1978). Abrupt changes in interval velocities (based on stacking velocities) could be used in some cases (e.g. for identifying a carbonate reef or an unconformity lacking truncation or angular discordance), but well data in this study were found to be more useful in this regard.

Reflection continuity is interpreted to closely correspond to the continuity of strata, and reflection amplitude indicates contrasts in lithology and/or the reflector spacing (Mitchum et al., 1977b). Reflection frequency for the most part is related to the seismic tool (frequency content of the sound source - as discussed earlier), but is also related to reflector spacing, bed thickness, fluid content (Mitchum et al., 1977b) and abruptness of impedance contrasts.

Reflection geometry may be described as parallel (concordant), sub-parallel, divergent, progradational, reflection-free, wavy, chaotic, hummocky, or contorted (Figure 2.8b). Progradational seismic facies can be further subdivided into shingled, oblique, or sigmoidal (Figure 2.8b). Commonly, reflection configurations can vary depending on the orientation of the profile. For example, prominent progradation may be observed on dip-parallel sections, but concordant reflection patterns may be observed on strike-parallel sections, with little evidence for progradation. Therefore, the three-dimensional character of deposits is important to consider. The external morphology of seismic “packages” may be described as a sheet, lens, mound, wedge, or drape (Mitchum et al., 1977b), and additional qualifiers like elongate or sub-circular are commonly used in this study (e.g. elongate mounds) (Figure 2.8b).

2.6 Borehole data

2.6.1 *Gamma ray*

Gamma ray logs measure the natural radioactivity of the sediment penetrated by the borehole. Gamma ray intensities are expressed in American Petroleum Institute units (API - Rider, 1991), and low API values are to the left throughout the thesis. Natural gamma emissions are usually much higher in shale than in sandstone and limestone. For this reason, the gamma ray log is often used to distinguish shale from non-shale and thus acts somewhat as a lithology indicator. Shales often have higher gamma values because they usually contain a high proportion of clay minerals, which have an affinity for elements with radioactive isotopes (uranium, potassium, thorium). Conversely, quartz-rich sands, as might be expected within a submarine channel, usually show very low gamma values (e.g. Figure 2.9).

In this study, gamma ray logs were used for correlation and interpretation purposes. Combined with lithological data (from cuttings and sidewall cores, where available), they were used to identify vertical grain-size trends in well logs, which can sometimes be diagnostic of specific depositional settings. Funnel-shaped curves are commonly diagnostic of upward-coarsening grain-size trends, whereas bell-shaped curves are commonly diagnostic of upward-fining trends. Galloway and Hobday (1996) also proposed various gamma ray log patterns for submarine fan deposits (Figure 2.9), with a blocky character corresponding to channel fill sands. Shanmugam et al. (1995), however, cautioned that when interpreting depositional process from gamma ray logs, additional information is required to constrain interpretations because a similar gamma ray response can be generated by different deposits (e.g. debrites, turbidites, slumps - see Figure 2.10). Caution is also required in interpreting sands that contain a high proportion of feldspars or mica grains, since these may be radioactive due to their potassium content (Rider, 1991). Similarly, pelagic carbonate units commonly generate a very low gamma ray response, and hence based on gamma ray alone can look similar to sandstone units. In lower Paleogene rocks in the Jeanne d'Arc Basin, some finer-grained intervals also generate a low gamma ray response, ranging from bell-shaped to blocky, believed to be caused by their high siliceous content.

a) Sediment Source

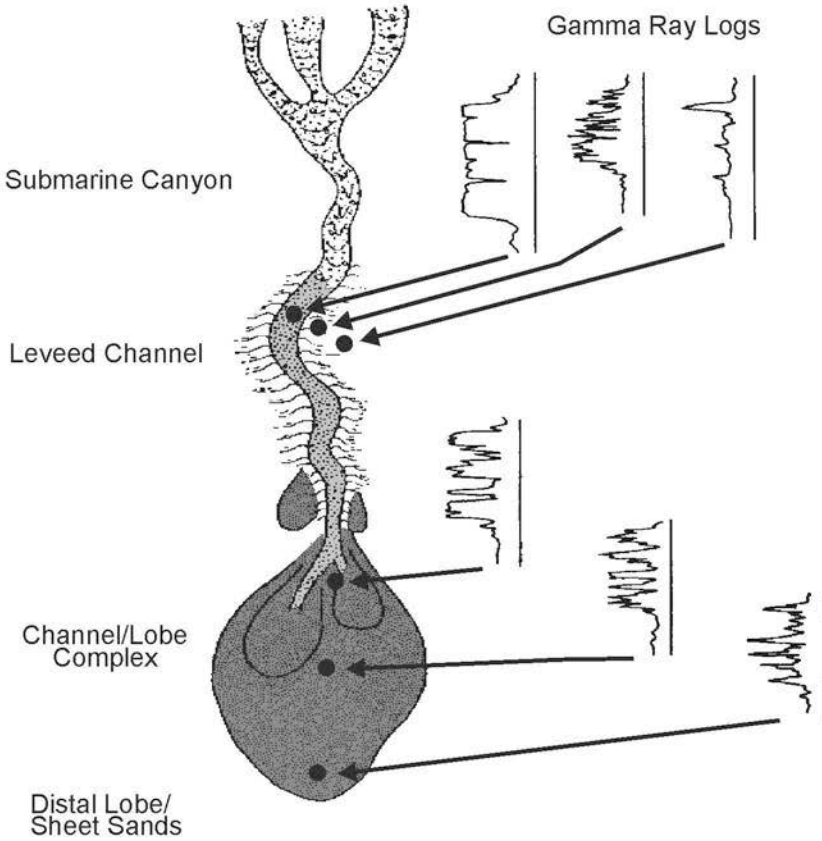


Figure 2.9. Schematic diagram illustrating potential gamma ray responses from different reaches of a submarine fan (adapted from Galloway and Hobday, 1996).

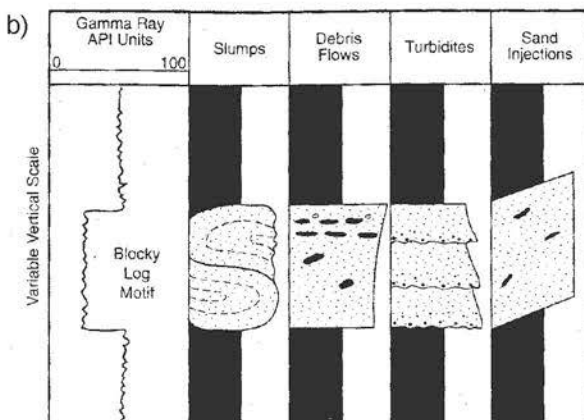


Figure 2.10. Schematic diagram illustrating the various sandy sedimentary facies that can produce a "blocky" gamma ray response (from Shanmugam et al., 1995).

2.6.2 *Sonic*

Sonic (acoustic) logging devices measure the acoustic interval transit time (in microseconds per metre) of rocks penetrated in the borehole (Rider, 1991). The sonic log is a measure of the amount of time required for a sound pulse to travel from an emitter at one end of a sonde (borehole tool), into the borehole, then into the formation, and finally back to receivers located at the other end of the sonde (Sheriff, 1989; Rider, 1991). The greater the interval transit time the slower the formation interval velocity (i.e. the interval transit time is the inverse of velocity).

The interval transit time of a rock is closely related to its texture and more specifically its porosity (Rider, 1991). It is equal to the sum of time a sound wave spends in the matrix of the rock and the fluid of a rock. As you increase the porosity, the interval transit time increases (velocity decreases) because the sound wave spends a greater proportion of its time within lower velocity fluids. For example, sandstone, which is usually quite porous, commonly has a lower velocity (higher interval transit time) than carbonate units. In normal pressure gradients, velocity increases with depth (and porosity decreases). Sonic logs were used for correlation and to generate synthetic seismograms.

2.6.3 *Density*

Density logging devices measure the combined (bulk) density of the matrix and pore fluids of rocks penetrated in the borehole (Rider, 1991). The logging tool operates by bombarding a formation with gamma rays emitted from a source and measuring the attenuation of the gamma rays as they are received at the detector (Rider, 1991). The amount of gamma ray attenuation (via Compton scattering) is directly related to the electron density of the formation being tested (matrix and pore fluids) which, in turn, is a close approximation to the formations actual density (Sheriff, 1989; Rider, 1991). The greater the electron density, the greater the attenuation of the gamma rays. In dense formations, gamma ray attenuation is high and few reach the detector, whereas the reverse is true for lower density formations (Rider, 1991). Under normal pressure regimes, shale density increases with depth, and thus the density log will read progressively higher values with increasing depth.

Density logs were used to generate synthetic seismograms and to a lesser extent for correlation.

2.6.4 Resistivity

Resistivity logging devices measure the electrical resistivity of formations penetrated in the borehole (Rider, 1991). Electrical resistivity (expressed in units of ohms/m²/m) is the inverse of conductivity and is a measure of a rock's ability to impede the flow of an electrical current (Rider, 1991). The total resistivity of a rock (matrix and pore fluids) is dictated by (1) the resistivity of the pore fluids and (2) the formation factor (described below).

The salinity of the pore fluids has the strongest impact on the total resistivity of a sedimentary rock. For instance, porous and permeable rocks filled with highly saline formation waters will register low resistivity values, as electrical currents are easily carried by free ions through the pores. Conversely, rocks with pore fluids consisting of hydrocarbons, which are insulators and do not transmit electrical currents, will register high resistivity values.

In addition to pore fluid salinity, the volume and connectivity of the pore spaces also influences the total resistivity of the rock (Rider, 1991). The percent volume of the pores and their connectivity is quantified into a number called the formation factor. In a porous rock with a high formation factor (i.e. a rock with poorly connected pore spaces), electrical currents are impeded because the ions have difficulty being transmitted from pore to pore. Similarly, compacted shales have a higher resistivity than non-compacted shales because of poorly connected pore spaces (higher formation factors) and lower porosity for saline fluids to reside. In porous rocks, low resistivity generally means water saturation whereas high resistivity generally means hydrocarbon saturation (Goetz and Nutt, 1997). Low porosity and permeability rocks generally produce a high resistivity response, because the matrix acts as an insulator.

Resistivity logs were used solely for correlation purposes in this study.

2.6.5 *Conventional cores, sidewall cores, and drill cuttings*

Collection of conventional cores is expensive and hence is usually only done within proven hydrocarbon-bearing reservoir intervals. For this reason, only three conventional cores were collected in the Upper Cretaceous and Tertiary interval in the Jeanne d'Arc Basin, with a total recovered length of just 20.4 m. Far more common are sidewall cores, which consist of small plugs/samples of rock taken from the walls of the borehole. Sidewall core samples are collected either by firing a hollow, cylindrical bullet at the borehole wall, or by drilling directly into it (Goetz and Nutt, 1997).

Drill cuttings are collected and logged in most eastern Canadian offshore wells. Cuttings rise to the surface with drilling fluid, where a drill-site geologist analyzes them and records their lithology against depth. The lithological data presented in this study have been plotted using both grain size and lithological information extracted from digital Canstrat logs using in-house software at the GSC Atlantic (Lithoplot3 by Andrew MacRae). Where available, sidewall cores were used to verify lithological information recorded on the Canstrat logs.

2.6.6 *Checkshot surveys and synthetic seismograms*

The velocities derived from checkshot surveys were used to convert borehole depths into time. These surveys form the primary basis for well ties in the study area, and permitted direct comparison between the seismic facies and lithofacies penetrated in the borehole. Checkshot surveys are collected by lowering a receiver (or series of receivers) into the borehole, and clamping it to the borehole walls at known depths (Hardage, 1985). A sound source is emitted from a surface vessel, and up going and down going reflection are recorded within the borehole receivers (Hardage, 1985). The amount of time required for a sound pulse to travel from the vessel to the known depth in the borehole provides a time - depth pair. A series of time - depth pairs allows changes in velocity through the stratigraphic column to be calculated, and allows depth in the borehole to be converted to units of two-way travel time. Well to seismic ties using velocity information derived from checkshot surveys were generally very good, producing consistent and predictable results.

Synthetic seismograms are sometimes necessary to clarify which lithological

interfaces in wells are responsible for the seismic reflections on seismic data (though this can sometimes be done in a qualitative way by examining the acoustic velocity or density logs). They are used to correlate lithological observations from wells to seismic data. To generate a synthetic seismogram, borehole velocity information (from sonic logs) and density information (from density logs) is converted into acoustic impedance data (velocity x density). From these data, reflection coefficients (impedance contrasts between adjacent layers) are calculated and convolved with an appropriate input seismic signal (e.g. Ricker wavelet, or one extracted from the seismic data) to generate the synthetic seismogram. The synthetic log, now in time (not depth), can be compared directly to the seismic data. One problem encountered using such a technique is the lack of sonic and density log data in the shallow parts of most wells (e.g. shallower than 400 - 600 m), requiring the velocity of this interval to be estimated.

2.7 Microfossil data

Biostratigraphy is the process of dividing and correlating the stratigraphic record based on the types, ages, and abundance of fossils. Age control for this study was derived primarily from palynology (spores, pollen, dinoflagellates, acritarchs - see Owens, 1981) interpretations done by Rob Fensome and Graham Williams at the Geological Survey of Canada on Avondale A-46, South Mara C-13, Mara M-54, North Ben Nevis M-61, Terra Nova K-18, Cormorant N-83, Port au Port J-97, Rankin M-36, Hibernia C-96, Hibernia B-08, and Hibernia O-35. See Appendix Ia for a summary of these biostratigraphic interpretations. Sampling for these wells was typically from a combination of sidewall cores and cuttings samples. The sampling interval typically ranged from 4 to 8 samples (cuttings and sidewall cores combined) in a 100 m interval. In ideal circumstances (i.e. if distinctive zonal assemblages are present in the samples and caving is minimal), the precision can be as high (+/- 15 m), but is probably more commonly on the order of +/- 30 m, depending on the study interval.

Additional age control was provided by both micropaleontology (forams, radiolarians, diatoms, silicoflagellates) and palynology interpretations conducted by other workers for Thorvald P-24 (Thomas, 1994; Chevron Canada Resources, 1992), Whiterose L-61 (Bujak Davies Group, 1989), West Ben Nevis B-75 (Petro-Canada,

1985), Ben Nevis I-45 (Bujak Davies Group, 1987; Associated Biostratigraphic Consultants, 1991), Hebron I-13 (Bujak Davies Group, 1987), North Ben Nevis P-93 (Bujak Davies Group, 1987), Springdale M-29 (Nova/Husky Research Corporation, 1989), Voyager J-18 (Bujak Davies Group, 1987), Gabriel C-60 (Bujak Davies Group, 1987), Botwood G-89 (Mobil et al., 1992), Adolphus D-50 (Doeven, 1983), Dominion O-23 (Bujak Davies Group, 1989), and North Trinity H-71 (Associated Biostratigraphic Consultants, 1991). See Appendix Ib for a summary of these biostratigraphic interpretations.

Where available, the age designations of Williams and Fensome were preferred over most others. A detailed micropaleontology study on Adolphus D-50 by Doeven (1983) was also used because of the high-density of samples examined. All biostratigraphic interpretations (both palynology and micropaleontology) are available in the BASIN database at the GSC Atlantic, or through the Canada-Newfoundland Offshore Petroleum Board (C-NOPB).

2.7.1 Paleoenvironment interpretations

Reports by Thomas (1994, 1995) were used in this study to provide constraints on paleo-water depths. Thomas (1994) used the ratio of planktic to benthic foraminifers, combined with the identification of certain benthic species and assemblages of species to interpret paleo-water depths in several wells in the JDB. The proportion of planktic species tends to decrease significantly at shallow water depths and correspondingly the proportion of benthic species increases (Thomas, pers. comm., 2003). Some complications can arise in very deep water, below the carbonate compensation depth, because carbonate dissolution will remove some species. However, water depths were not great enough in the study area for this to have been a problem.

Benthic foraminiferal assemblages can be used as indicators of water depth based on the assumption that some species consistently inhabit(ed) deeper-water areas whereas others inhabit(ed) shallow-water areas (Van der Zwaan et al., 1999). These interpretations, however, are not without uncertainty. As Van der Zwaan et al. (1999) have pointed out, benthic foraminiferal distribution patterns are strongly linked to the availability of oxygen and food (organic flux), and weakly linked to water temperature

and salinity. Drawing relationships between benthic foraminiferal distribution and paleoenvironment can therefore be tenuous. Predicting paleo-water depths can also be difficult because isobathyal species (i.e. species that exist at only one water depth or a small range of water depths) are rare (Van der Zwaan et al., 1999).

The use of planktic to benthic foraminifer ratios, however, as employed by Thomas (1994, 1995), can significantly improve the results (Van der Zwann et al., 1999). The number of planktic species shows a generally increasing trend with increasing water depths (Van der Zwaan et al., 1990). Paleo-bathymetric interpretations from Thomas (1994, 1995) were used in conjunction with other information based on seismic stratigraphic interpretations, to constrain water depths (e.g. height of the shelf-break above the toe-of-slope).

2.8 Submarine fans - models and classification

Submarine fans are morphological features on the slope, rise and/or abyssal plain which result from the accumulation of terrigenous and marine sediment in a deep marine setting, typically at the mouths of slope-incised canyons. Submarine fans show a great deal of architectural variability and a tremendous range of size (e.g. the 70 km² Crati fan, Ricci Lucchi, 1985, versus the 2 800 000 km² Bengal fan, Emmel and Curray, 1985). They form on both active and passive margins, in relatively shallow (< 800 m) to very deep water (> 3000 m) settings (marine and lacustrine), and are preserved at the sea floor, in the subsurface, and in outcrops where ancient successions have been exposed. Submarine fans typically consist of a canyon that incises the slope (perhaps extending headward onto the shelf), leveed channels extending from the mouth of the canyon, and lobes extending from the mouth of the channels (e.g. Figure 2.9). Sediment gravity flows are considered the most important process for transporting and depositing sediment on submarine fans (Shanmugam and Moiola, 1988).

Over the past 30 years, several models have been proposed to explain the variability in fan geometry and evolution. Below is a short summary of the progression of such models.

2.8.1 *Upper, middle, and lower fan models*

Normark (1970, 1978) suggested that fans could be divided into three reaches: an upper fan, middle fan, and lower fan (Figure 2.11). The characteristics of each division were based on generalities drawn from several fans that had been studied at that time, many of which were from California Continental Borderland basins (e.g. La Jolla, San Lucas). Normark (1970) described the ideal fan shape as radial, but cautioned that the symmetrical form would only develop if deposits were randomly distributed through geologic time. Walker (1978) used a combination of Normark's (1970) model for modern fans and Mutti and Ricci Lucchi's (1972) facies model for ancient fans to generate a generic model for submarine fans (Figure 2.12). His model is a distillation of features observed in many different and quite varying fan systems observed in outcrop and on the modern sea floor. He linked a lithofacies classification scheme to a morphological model and identified several different lithofacies types (described below).

The **upper fan** consists of a leveed fan-valley at the mouth of the canyon (Figures 2.11, 2.12). Normark (1970) studied the La Jolla fan and identified a sinuous thalweg channel within a relatively straight fan-valley, flanked by low relief levees (less than 10 m thick). He interpreted the sinuous channel to form from erosion into horizontally bedded strata, and used the La Jolla fan-valley as an end-member for erosional channels. Flat terraces within the fan-valley, and in particular on the inside bend of meanders, combined with low levee relief, were key criteria for the interpretation that fan-valley relief developed principally from vertical incision. The terraces were interpreted to develop from more resistive layers during incision. As will be discussed in Chapter 6, the terraces may be more indicative of inner levees formed from under-fit flows (*sensu* Piper et al., 1999) within the erosional fairway, rather than episodes of vertical channel incision. Normark (1970) described depositional channels as those bordered by levees with valley floors built above the level of the surrounding sea floor. He cautioned that depositional and erosional channels represent end-members of a gradational series, and that any channel could show both erosional and depositional characteristics. The coarsest upper fan sediment is located on the floor of the fan valley, interpreted to consist of conglomeratic turbidites, with adjacent levees consisting of thin-

bedded silty or muddy turbidites, perhaps with interbeds of fine-grained sandy turbidites (Walker, 1978; Normark, 1978 - Figure 2.12).

The **middle fan** consists of a channeled suprafan lobe, a convex-upward bulge located at the mouth of the leveed fan-valley (Figures 2.11, 2.12). Normark (1970) originally described the suprafan lobe as a “small delta or fanlike deposit probably formed as turbidity currents dissipate after leaving the confinement of the leveed valley”. The upper suprafan consists of a succession of coarsening-upward and thickening-upward sandy turbidites, cut by numerous unleveed ephemeral distributary channels and scours (Normark, 1978). Sands become less common distally, and distributary channels terminate on the middle suprafan. The lower suprafan (e.g. at Navy fan) consists of thickening- and coarsening-upward sands in non-channeled lobes (Normark, 1978). The thickening- and coarsening-upward vertical succession was envisioned to represent the progradation of a suprafan lobe, from a distal lobe setting at the base, to a channeled proximal suprafan lobe at the top (similar to a prograding delta, with distal prodelta sediment at the base to coarser-grained delta platform sediment at the top) (Walker, 1978; Normark, 1978). Walker (1978) interpreted massive sandstone to pebbly sandstone turbidites to dominate the upper suprafan lobe. Massive sandstones may consist of several amalgamated events, and may also contain fluid escape features like vertical tubes and dish structures. Classic “Bouma-type” turbidites dominate the lower suprafan lobe and the lower fan, passing distally into finer-grained and thinner facies of the basin plain. Normark has since recanted the term “suprafan”, citing its obsolescence, and suggesting instead that it be described in terms of channel, lobe, and scour architectural elements (Normark, 1991 - an approach described later).

The **lower fan** consists of flat-lying non-channeled, unconfined sediment (or ponded sediment in a confined basin), and may be very difficult to distinguish from basin plain deposits (Normark, 1978).

2.8.2 *Efficient versus inefficient systems*

Mutti (1979) proposed a general fan model based on the efficiency of sand transport in flows. He described sand-rich flows as poorly efficient, with most sand deposited abruptly near the mouth of the feeder channel. Fans fed by poorly efficient

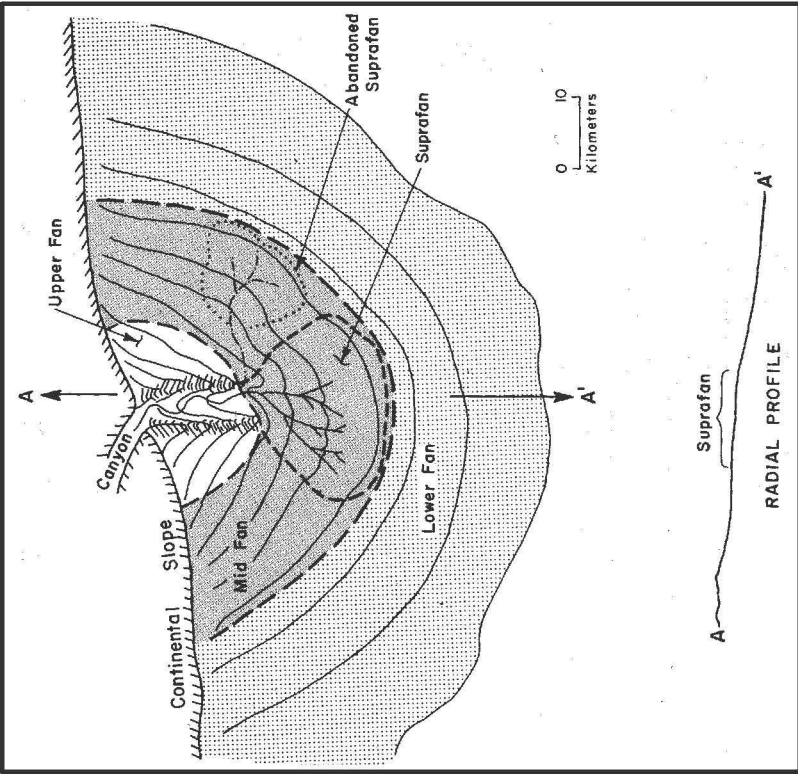


Figure 2.11. Upper, middle, and lower fan model from Normark (1978).

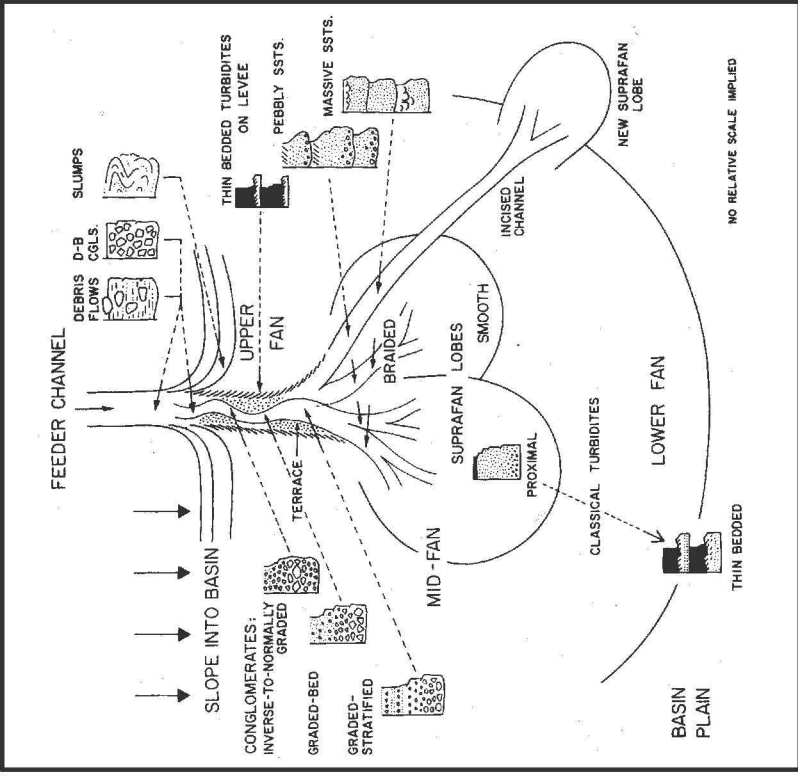


Figure 2.12. Fan model from Walker (1978), incorporating lithofacies units for specific fan settings.

flows are smaller and sandier, and are typically fed by canyons that head in a relatively well-sorted sediment source region like a beach or high energy coast. Mutti (1979) described mud-rich flows as efficient because they are capable of transporting sand long distances. Fans dominated by highly efficient flows are large and muddy, and are typically fed by mixed-load deltaic systems. According to Mutti (1979) and Mutti and Normark (1987), lobes in such systems tend to be detached from the channel mouth.

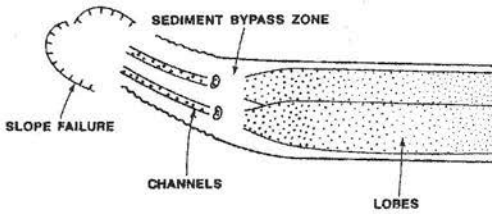
There is some criticism of this approach because many fans contain deposits from flows with widely varying transport efficiencies (Shanmugam and Muiola, 1988). The terms efficient and inefficient are commonly used in a general sense when describing specific flows or deposits, but rarely is this terminology applied to an entire fan system.

2.8.3 *Types I, II, and III fans*

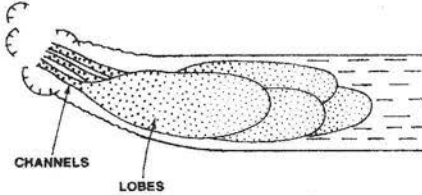
Based principally on outcrop studies, Mutti (1985a) described three main types of fan systems that differed mainly in terms of where sand was deposited within the system (Type I, II, and III). Each type forms an end-member of a continuous series, controlled by the volume of flows and their mud content (which he, in turn, proposed was strongly influenced by sea level position). He suggested that sand deposition within channels was enhanced as flow size decreased, whereas very large flows would be prone to deposit thick-bedded sand lobes distally. All systems are characterized by channel-fill deposits proximally, replaced by non-channelized sand bodies or basinal mudstones in the down current direction (Mutti, 1985a).

Mutti described **type I** systems as those where most sands are deposited on the outer fan (a physiographic region that according to Normark, 1978 and Walker, 1978 corresponds to the middle fan in their models - similar to suprafan lobes). Sands are deposited as laterally continuous, tabular, non-channelized bodies forming elongated lobes (Figure 2.13). Type I fans are essentially “highly efficient” fans (Mutti, 1979). Distally, the thick sands grade into finer-grained lobe-fringe deposits. Proximally, type I systems are characterized by sediment bypass and prominent erosional features (e.g. canyons). Mutti suggested that the lobes in such systems are essentially detached, and that the age of sediment filling the feeder channels post-dates deposition of the sand-prone lobes.

TYPE I: CHANNELS WITH DETACHED LOBES



TYPE II: CHANNELS WITH ATTACHED LOBES



TYPE III: CHANNEL-LEVEE COMPLEX WITHOUT LOBES

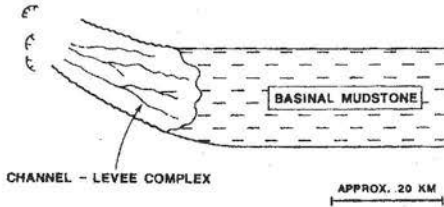
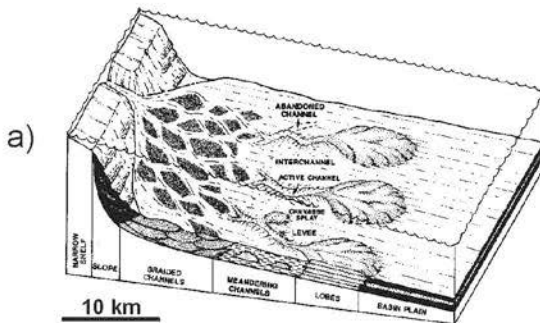
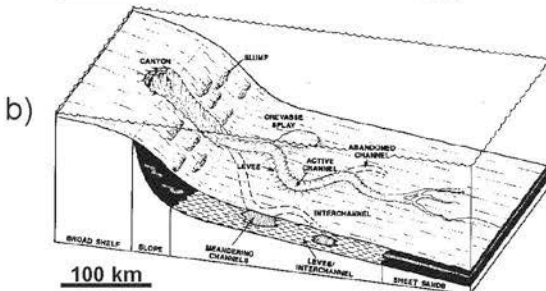


Figure 2.13. Type I, II, and III systems (modified from Mutti, 1985 by Shanmugam and Muiola, 1991).



Active-margin fans

- high gradient
- low sinuosity channels
- high sand:mud ratios
- small "sandy" fans
- channel-mouth lobes



Mature passive-margin fans

- low gradient
- high sinuosity channels with levees
- low sand:mud ratios
- large "muddy" fans
- channel-levee systems

Figure 2.14. Block diagrams illustrating active-margin submarine fan model with prominent channel-mouth lobes and mature passive-margin submarine fan with sheet sands (modified from Shanmugam and Muiola, 1991).

Type II systems are those where most sands are deposited at the lower reaches of channels and at the channel mouth (Mutti, 1985a). Extensively channeled bodies grade down system into coarse-grained lobes that are attached both laterally and vertically to channel deposits (Figure 2.13). Mutti considered such systems “poorly efficient” (Mutti, 1979). **Type III** systems contain sand that is restricted to channels on the proximal part of the fan. The channels are enclosed in, and grade laterally into, mud-prone facies (either levees or basin plain), without significant sandy lobe deposition at their termination (Mutti, 1985a). He compared type III systems to fans with large channel-levee systems fed by major deltas, like the Amazon fan.

Mutti (1985a) suggested that a given system could evolve from a type I system to a type II and eventually into a type III systems in response to rising sea level. In his model, type I lobes would develop during falling sea level and are associated with large, sand-prone flows. In contrast, as sea level rises, flow size decreases, eventually leading to type III channel-levee systems developed during a highstand in sea level.

2.8.4 *Classification according to tectonic setting*

Many workers have broadly subdivided fans according to tectonic setting, classifying them as either active- or passive-margin fans (Figure 2.14). Shanmugam and Muiola (1988) proposed a classification that included four tectonic settings: active margin fans (Pacific type), mature passive-margin fans (Atlantic type), immature passive-margin fans (North Sea type), and mixed-setting fans.

Active-margin fans and **immature passive-margin fans** are small, high gradient fans with high sand-to-mud ratios, low-sinuosity channels, and well-developed lobes (or mounds - Figures 2.14a, 2.15a, 2.16). They commonly develop in basins bordered by narrow shelves with a proximal sediment source region. Examples of active-margin fans include several examples on the west coast of the United States (e.g. Navy, La Jolla, Hueneme, Monterey). Examples of immature passive-margin fans include most of the Paleocene and Eocene fans in the North Sea, like Frigg and Balder (Figure 2.16), as well as fans of similar age in the Jeanne d’Arc Basin (see Chapters 3 and 5).

Mature passive-margin fans are large, low gradient fans with low sand-to-mud ratios, sinuous channels, and sheet sands, rather than lobes, in the lower fan (Figures

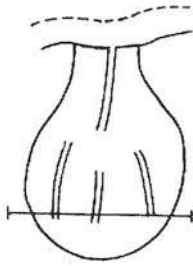
2.14b, 2.15b). Examples include the Mississippi, Amazon, and Laurentian fans. They commonly develop in basins bordered by wide shelves with a distal sediment source region. **Mixed-setting fans** are considered those that show attributes of both passive and active margin fans. For example, the Indus and Bengal fans are considered mixed-setting fans because they are bordered by both passive and active margins.

The similar descriptions for active-margin and immature passive-margin fans raises questions about the need for separate categories. Such a classification is valuable in that it recognizes the importance of tectonic setting and basin structure, but such a classification does not adequately consider other variables that influence fan architecture (e.g. characteristics of the sediment source area, dominant trigger for flows, and sediment dispersal - Piper and Normark, 2001). In addition, many passive-margin fans (e.g. on the Niger Delta slope) have been influenced by tectonic processes, either through active extensional faulting, compressional fold-and-thrust belts, or salt and shale diapirism, so although they may not be located along convergent margins, they may still be tectonically active. Still, such a classification is an improvement over single, all-encompassing models.

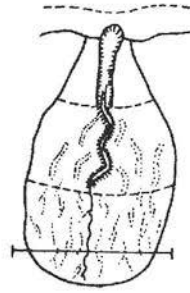
2.8.5 *Classification according to grain size and feeder system*

Reading and Richards (1994) developed a classification scheme for submarine fans based on their grain size and the type of feeder system. They split fans into three categories: those with a single point source (i.e. one canyon), those with multiple point sources, and those with a line source. They further subdivided each category into four according to whether the fans were mud-rich, mud/sand-rich, sand-rich, or gravel-rich, yielding a total of 12 different fan types (Figure 2.17). They noted that a continuum is present between the various types, and cautioned that some ancient fans may appear to have been fed by multiple sources but at shorter time-frames may consist of only one point source that has shifted through time.

At one end of the spectrum mud-rich systems are commonly large, elongate, have low gradients and well developed channel-levee systems, infrequent but efficient flows, and are fed by large delta systems, which in turn are supplied by large source regions. Mud-rich point source systems include the Mississippi (Bouma et al., 1985), Amazon



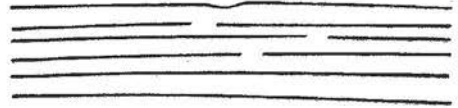
IMMATURE PASSIVE MARGIN
ACTIVE MARGIN



MATURE PASSIVE MARGIN



MOUNDED
BIDIRECTIONAL DOWNLAP
(SARG AND SKJOLD, 1982;
MITCHUM, 1985)



SHEET
CONTINUOUS, PARALLEL

Figure 2.15. Immature passive-margin and active-margin fans, commonly characterized by well developed lobes, sometimes expressed as mounds like those in the Frigg Fan in the North Sea (below) and in the Paleocene in the Jeanne d'Arc Basin (see Chapters 3 and 5). Passive margin fans characterized by sheet deposits, rather than mounds (from Shanmugam and Moiola, 1988).

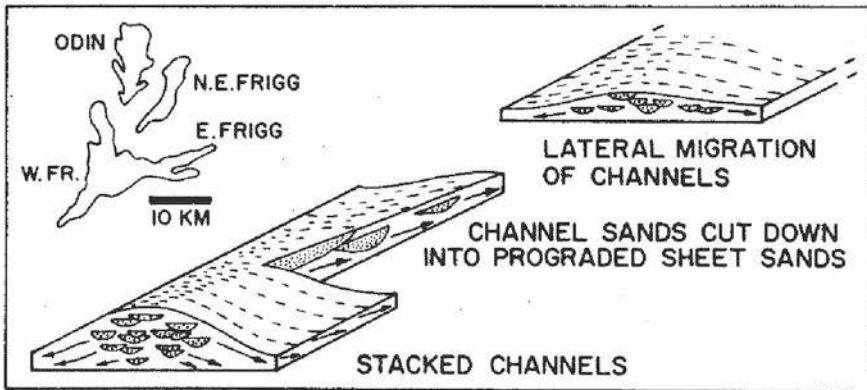


Figure 2.16. Model for proximal to distal trends in mounded seismic facies on the Frigg Fan in the North Sea, calibrated with wells (from McGovney and Radovich, 1985).

(Damuth and Flood, 1985), Indus (McHargue and Webb, 1986; Kolla and Coumes, 1987), Bengal (Emmel and Curray, 1985), and Laurentian (Piper et al., 1985) fans, among others. At the other end of the spectrum, gravel-rich systems are much smaller, have high gradients and ephemeral channels, and have small proximal source regions. Gravel-rich systems include fan deltas in the Gulf of Corinth (Piper et al., 1990; Piper and Normark, 2001).

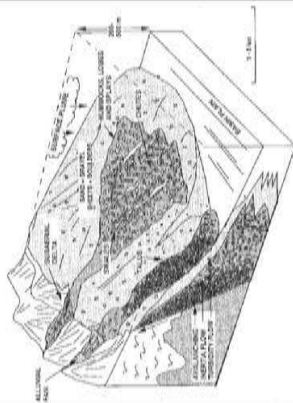
Most of the submarine fans in the Jeanne d'Arc Basin fall into the category of point-source to multiple-source mud/sand-rich to sand-rich fans (bold boxes in Figure 2.17). According to the classification of Reading and Richards (1994), point-source sand/mud-rich fans include La Jolla (Shepard and Buffington, 1968; Shepard et al., 1969; Piper, 1970), Navy (Piper and Normark, 1983), Delgada (Normark et al., 1985), and Rhone (Bellaiche et al., 1984), whereas sand-rich fans include some of the early Tertiary fans in the North Sea including Frigg (Heritier et al., 1979; McGovney and Radovich, 1985), Balder (Sarg and Skjold, 1982; Timbrell, 1993), and Gryphon (Newman et al., 1993) (see Chapter 5).

Single point-source mud/sand-rich fans correspond well to the models proposed by Normark (1978) and Walker (1978), based largely on fans off California. They are typically medium to small in size, consist of a leveed channel that feeds a lobe (in the sense of Normark, 1970), and are fed by mixed-load deltas or by sediment transported parallel to the shore and intercepted by canyons incised back onto the shelf (Reading and Richards, 1994). Lobe switching is accomplished through successive channel avulsions and in deeply buried fans, lobes may be expressed as mounds on multi-channel seismic (e.g. channeled lobe - Figure 2.16). Sand-rich fans are characterized by a more radial geometry than mud/sand-rich fans, have a sediment source region characterized by a sand-rich shelf, with sediment supplied to canyons by littoral drift cells or failure of sandy shelf sediment (Reading and Richards, 1994). Low efficiency flows (in the sense of Mutti, 1979) deposit thick massive sands in a suprafan lobe at the termination of the feeder channel.

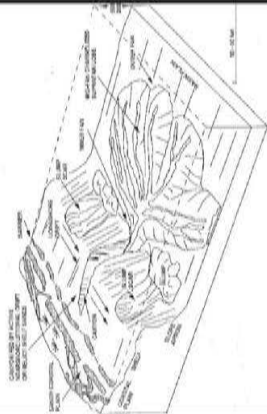
2.8.6 *Elemental approach*

Miall (1985) suggested that fluvial stratigraphic successions could be divided into

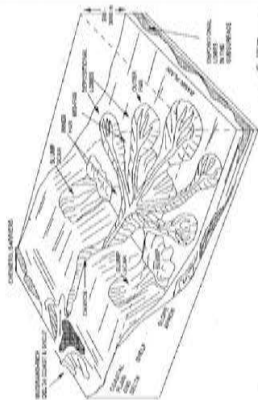
Gravel-rich



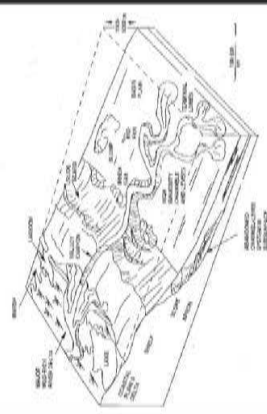
Sand-rich



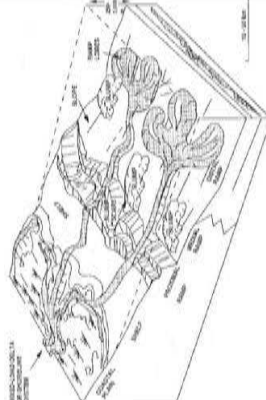
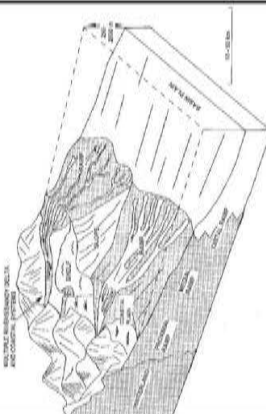
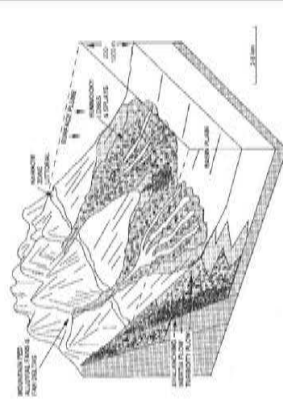
Sand/Mud-rich



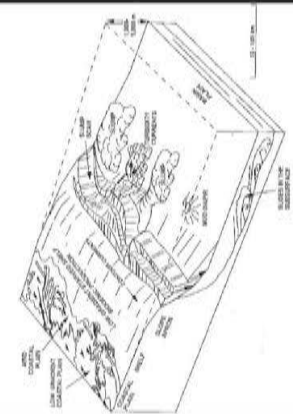
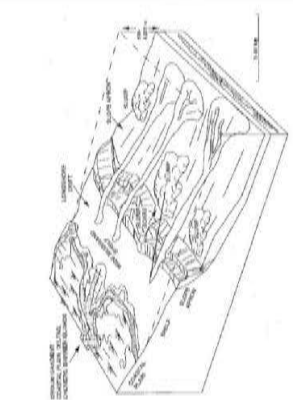
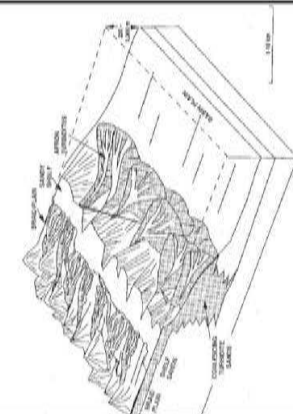
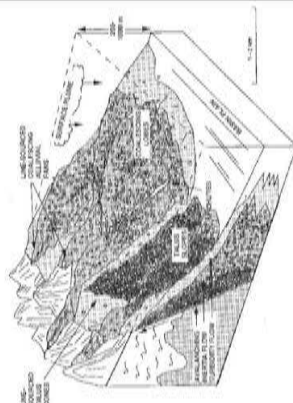
Mud-rich



Point Source



Multiple Source



Line Source

Figure 2.17. Fan models based on the character of the feeder system and grain-size (from Reading and Richards, 1994).

architectural elements of various scales, each separated by bounding surfaces, also of various scales. He defined an architectural element as “a lithosome characterized by its geometry, facies composition, and scale” and “the depositional product of a particular process or suite of processes occurring within a depositional system”. In other words, an architectural element is a three-dimensional sedimentary body that has a distinctive external geometry and internal lithofacies assemblage (Miall, 1985), that formed as a result of predictable depositional and/or erosional processes.

Because deep-sea fan models based on facies assemblages, sea-level, and tectonic classification are inadequate for predicting the distribution and character of reservoir rocks in the diverse range of submarine fans (Piper and Normark, 2001), recent work has moved towards characterizing individual turbidite systems in detail by examining their constituent architectural elements (e.g. channels, levees, lobes - Figure 2.18) and sub-elements (e.g. scours, bedforms, thalweg-fill features, etceteras - Clark and Pickering 1996a, 1996b). The elemental approach was first applied to submarine fan stratigraphic successions by Mutti and Normark (1987, 1991), Normark et al. (1993), and Pickering et al. (1995). According to Clark and Pickering (1996a), the philosophy of the elemental approach is “...not concerned with comparing fan systems, but rather concentrates on describing the architectural elements within deep-water systems. Comparisons can then be made between similar architectural elements, or suites of elements”. According to Walker (1990) the “description of architectural elements embodies the search for the basic building blocks of sedimentology, world-wide, Archean to Recent”.

The strength of identifying various architectural elements is that each element can be placed into context with others believed to be genetically related in other fan systems (Walker, 1990), allowing for direct comparison. Rather than developing models for entire systems, models for each component (architectural element) of a system can be devised. This approach should lead to predictive capabilities within specific elements. If the precise chronostratigraphic framework of elements can be unraveled (i.e. identification of time-equivalent elements), the different growth stages of submarine fans can also be studied (e.g. see Chapter 6 for the growth stages of a submarine channel-levee system) and the influence of sea level and other controls can be evaluated. From a practical point of view, primary architectural elements can often be recognized on

seismic reflection profiles (for larger systems in particular), so most seismic interpreters can identify architectural elements like channels, levees, and lobes.

The organization of common elements within different fans should provide a means for fan classification, and allows for comparison between modern and ancient systems (Mutti and Normark, 1987). The distribution and character of architectural elements can vary from one system to another. Submarine channels in particular evolve such that their morphology reflects the cumulative effects of many flows, and hence submarine channel architecture can be used to predict the average behavior of sediment gravity flows (Normark and Piper, 1991; Skene, 1998). In aggradational channels, the average character of sediment gravity flows through time may be predicted based on changes in channel morphology through time. Figure 2.19 illustrates some of the different channel stacking patterns that may be observed, discussed at length in Chapter 6. Overall, the reservoir quality of a submarine fan (i.e. the lateral continuity and vertical connectivity of potential hydrocarbon-bearing reservoir rocks) is dictated by the lithology, thickness, continuity, and porosity of its architectural elements (Shanmugam and Moiola 1988), each of which can be influenced by several factors including sediment source characteristics, element stacking patterns (e.g. vertical, laterally offset), and bounding surfaces (erosional versus drape) between elements.

The elemental approach is used throughout this dissertation. Mutti and Normark (1987, 1991) recognized five basic elements that can be recognized in most turbidite systems: canyons, channels, overbank deposits (levees), lobes, and channel-lobe transitions (Figure 2.18). Normark et al. (1993) added slump scarps and mass movement deposits to this list. Several additional elements are identified in this study, including gullies and several kinds of mounded lobes in Chapters 5, and inner levees and erosional fairways in Chapter 6.

2.9 Sediment gravity flows and their deposits

Middleton and Hampton (1973) defined a sediment gravity flow as “a general term for sediment or sediment-fluid mixtures under the action of gravity”, and recognized four categories in subaqueous settings defined according to the dominant sediment support mechanism: turbidity currents, fluidized flows, grain flows and debris flows (Figure

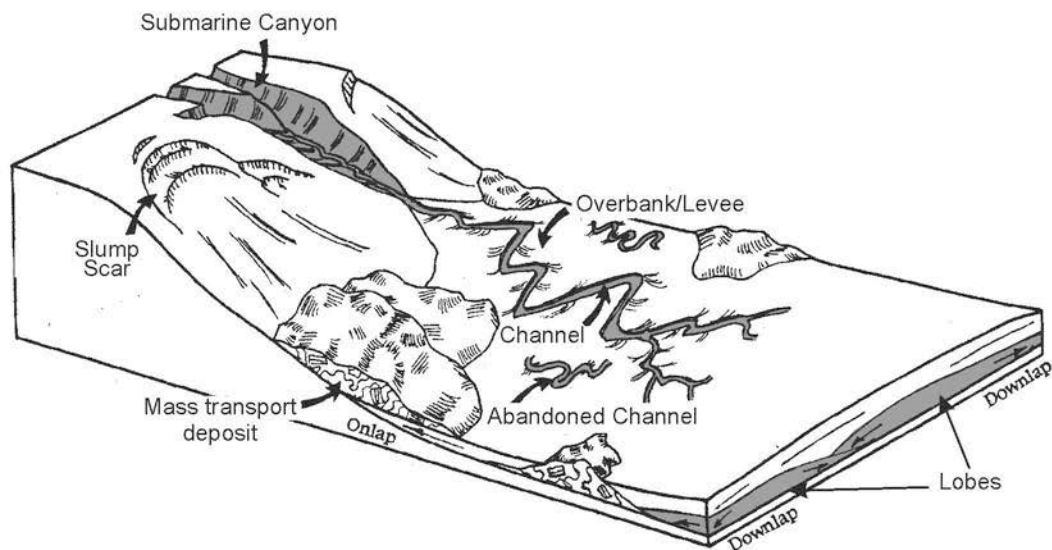


Figure 2.18. Block diagram illustrating primary architectural elements in submarine fan systems (modified from Normark et al., 1993).

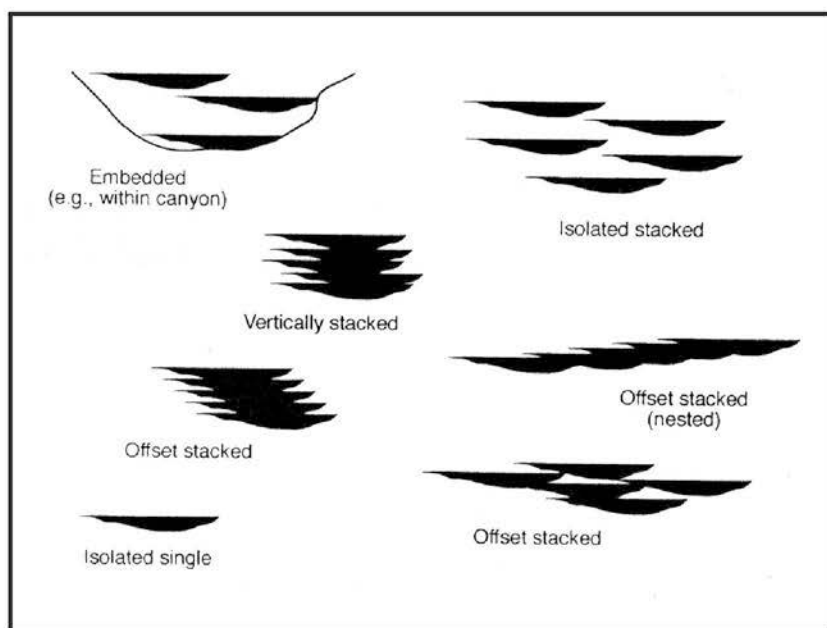


Figure 2.19. Channel stacking patterns (from Pickering et al., 1995).

2.20). In turbidity currents, turbulence is the primary sediment support mechanism. In fluidized flows and grain flows, fluid escape and grain interactions, respectively, are the primary sediment support mechanisms. In debris flows, larger grains are supported by a matrix of finer sediment. Only turbidity currents and debris flows appear to be volumetrically important in submarine settings, and are discussed further below.

Lowe (1982) evaluated sediment gravity flows in terms of end-member depositional processes and flow rheology (plastic versus fluid), in addition to the dominant sediment support mechanisms proposed by Middleton and Hampton (1973). Deposition from a decelerating fluidal flow like turbidity currents occurs progressively through the accumulation of individual particles either through bed load (traction sedimentation) or from suspended load (suspended sedimentation) (Lowe, 1982). Deposition from plastic flows like debris flows occurs as the “shear stress drops below the yield strength of the moving material”, resulting in “freezing” of the flow en masse due to frictional grain resistance (frictional freezing) or cohesive grain interactions (cohesive freezing) (Lowe, 1982).

2.9.1 Turbidity currents and turbidites

The term turbidity current was first introduced by Johnson (1938) and later Kuenen (1957) applied the term “turbidite” to deposits from turbidity currents. Saltation via hydraulic lift and grain impact, and traction via dragging and rolling particles (bedload) may operate in a turbidity current, but the dominant sediment support mechanism is the upward component of fluid turbulence, causing suspension (Middleton and Hampton, 1973). Most flows are believed to show an upward decrease in grain-size, concentration, and velocity, though frictional drag creates a velocity minimum at the base of the flow (Normark and Piper, 1991). Lowe (1982) considered two principal types of turbidity currents: those with a low concentration (or density) of mainly fine-grained sediment (clay to medium grained sand), and those with a high concentration (or density) and a significant population of coarser-grained sediment (sand to small and large pebbles, and even cobbles). High-density turbidity currents are considered those with greater than 20 - 30 percent grain concentration (Lowe, 1982).

Turbidity currents can be initiated by several mechanisms, including prodelta or basin slope failures triggered by earthquakes or sediment loading, storm surges, and direct river input at times of flooding (Normark and Piper, 1991; Piper and Normark, 2001). The duration, volume, sediment concentration, grain-size distribution, velocity, and thickness of flows can vary significantly (Normark and Piper, 1991). Large muddy flows are generally believed to be thick and slow moving (e.g. 1 m/s), whereas large sandy flows are believed to be thinner, more erosive, and faster moving (e.g. 15 m/s) (Normark and Piper, 1991).

Bouma sequence (“classic turbidites”)

Bouma (1962) proposed a vertical facies model for turbidites that has become known as the Bouma sequence, consisting of five divisions (Ta through Te - Figure 2.21a). With the exception of massive sands deposited in the Ta division (see below), Lowe (1982) considered Bouma-division turbidites as those deposited from low-density turbidity currents. Classic Bouma turbidites, as defined by Walker (1978), consist of a suite of characteristics which include sharp-based beds commonly with sole marks (e.g. flutes, scours), overall graded bedding with massive beds at the base and horizontal lamination and ripple cross-lamination higher up, and a bedding regularity that can be traced for long distances without appreciable change in thickness.

The Bouma sequence develops during the passage of a single flow, with each division deposited under different flow regimes during the passage of the head, body and tail of the flow (Walker, 1978; Komar, 1985). Grains deposited from suspension accumulate gradually to form a bed, with the Bouma sequence forming from both a decrease in flow intensity and rate of deposition, as well as an increase in traction through time (Middleton and Hampton, 1973).

The Ta division consists of massive to normally graded sandstone deposited at the base of the Bouma Sequence. The base of the Ta division is sharp, commonly erosive with sole-markings, overlain by massive sandstone deposited rapidly from suspension. The rapid rate of deposition precludes traction deposition (Middleton and Hampton, 1973). Water-escape features like pipes and dish-structures develop because of rapid deposition, and may contribute to the massive character. The Tb division consists of

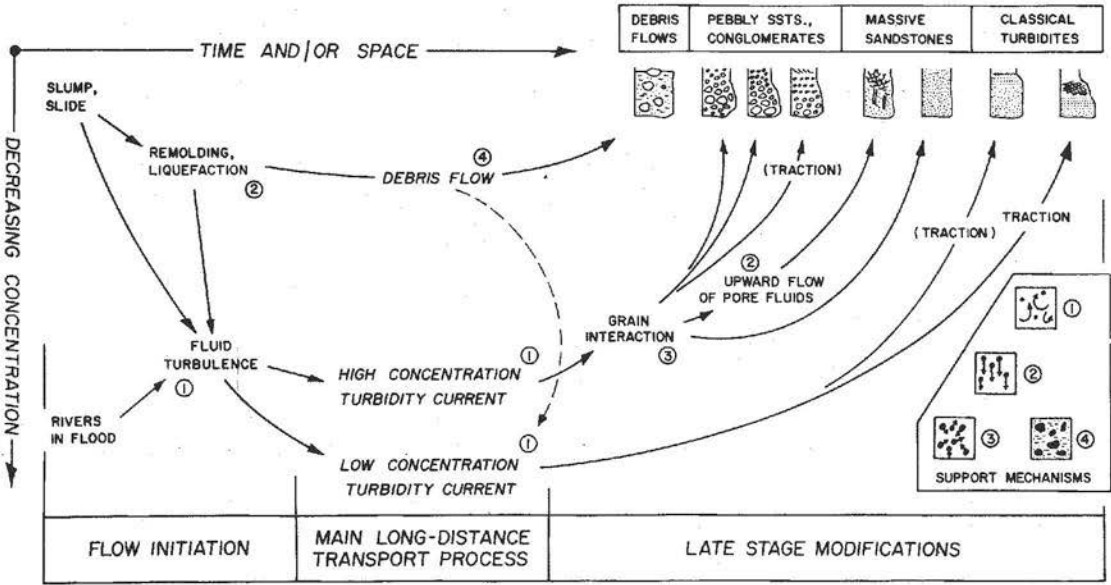


Figure 2.20. Initiation mechanisms for flows (left - slump, slide or river input) with possible evolutionary paths with time and distance. Resulting deposits are shown in upper right (and illustrated on Figure 2.12). Grain support mechanisms shown in lower right (1, fluid turbulence; 2, liquifaction; 3, grain collision; 4, matrix strength). From Walker (1978).

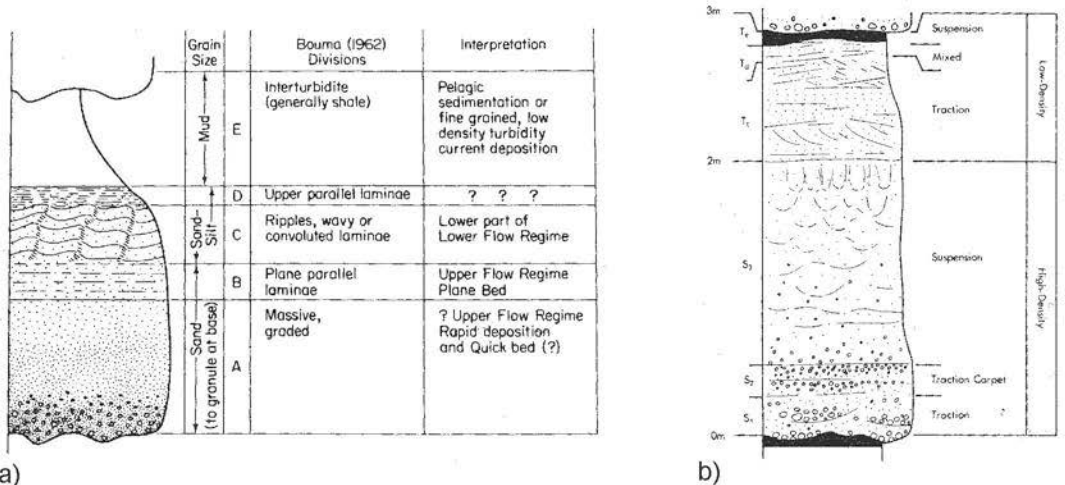


Figure 2.21. a) A "classic" turbidite with corresponding Bouma divisions (from Middleton and Hampton, 1973, after Bouma, 1962). b) The "Low" sequence for high-density sandy turbidity currents (from Lowe, 1982).

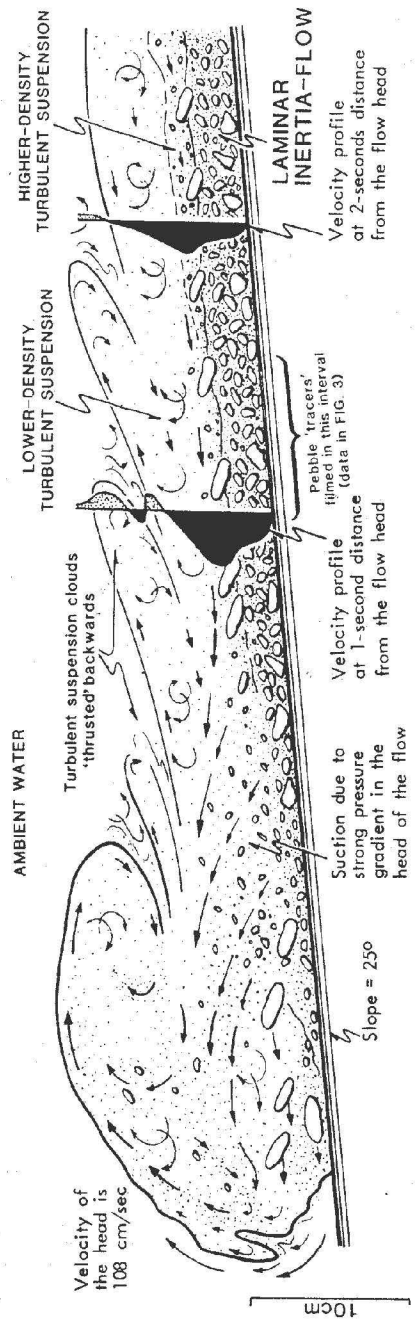
parallel laminated sandstones with parting lineations (on bedding planes), interpreted to have been deposited during upper flow regime conditions which may have eroded previously deposited Ta sands. The Tc division consists of ripple cross-laminated sandstone, probably formed during reworking of underlying Tb deposits or during continued deposition from the waning flow (lower flow velocities). Both the Tb and Tc deposits can undergo traction during bedload transport (Lowe, 1982). The Td division consists of horizontally laminated mudstone and siltstone that can be difficult to distinguish from the overlying pelagic mudstone of the Te division. The Td division represents finer-grained sediment deposited under reduced flow velocities from the tail of the turbidity current (see below for flow structure).

Lowe sequence (high-density turbidites)

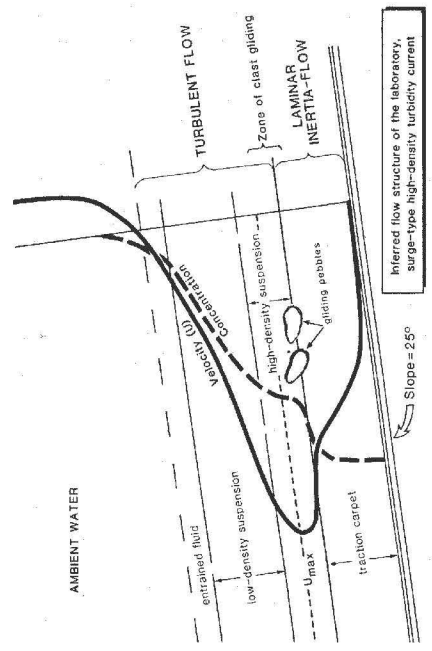
Lowe (1982) proposed a vertical facies model for deposits from high-density turbidity currents that can be thought of as a subdivision of the Bouma Ta division (Figure 2.21b). Figure 2.22a illustrates the probable flow structure of a high-density sediment gravity flow. The Lowe sequence begins with a traction sedimentation stage (S1 - laminated, cross-laminated, and scoured sandstone to pebble conglomerates), followed by a traction-carpet stage (S2 - inversely graded sand to granule layers formed in a highly concentrated layer dominated by dispersive pressure and grain collisions rather than turbulence), and ending with a suspension sedimentation stage (S3 - rapid deposition resulting in a massive bed with fluid escape structures - similar to the Ta Bouma division). The S1-S3 divisions are commonly overlain by deposits from the lower-density part of the flow, corresponding closely to the Bouma Tb to Te divisions (Figure 2.21b). For flows with a significant component of gravel, Lowe (1982) added an R2 to R3 division at the base of the sequence in Figure 2.21b, with gravel deposited as a highly concentrated traction-carpet (R2 - inversely graded gravel layer) or abruptly from suspension (R3 - graded gravel layer) in proximal settings early in the flows evolution.

Through flume experiments, Postma et al. (1988) studied the character of high-density turbulent flows. They identified a basal highly concentrated layer consisting of pebbly sand, referred to as an “inertia-flow layer”. It was interpreted as a laminar (non-turbulent) layer that formed from the partial settling of sediment particles at the initiation

HIGH-DENSITY TURBULENT FLOW



a)



b)

Figure 2.22. a) Drawing of a high-density surge-type sediment gravity flow with a lower high-concentration, coarse-grained non-turbulent layer and an overlying lower concentration fully turbulent suspension. Between the two is an interval interpreted as a turbulent high-density suspension. b) Schematic diagram illustrating the concentration and velocity gradient of a surge-type, high-density flow. Note that the flow concentration is greatest near the base of the flow, within the inertia flow layer, whereas flow velocity reaches a maximum (U_{max}) above the base of the flow due to frictional drag (from Postma et al., 1988).

of the flow. Turbulence in the inertia-flow layer is suppressed due to the high grain concentration, which is above the Bagnold limit (9 percent sediment concentration) and hence grain-to-grain interactions are important in transport (Bagnold, 1962). The layer formed as a result of bed-load transport and is considered a traction carpet (Postma et al., 1988 - see Sohn, 1997). A faster-moving high-density turbulent sandy suspension cloud was identified above the inertia-flow layer, and a fully turbulent low-density suspension cloud developed above this (Figure 2.22a - Postma et al., 1988). Sohn (1997) indicated that the highly concentrated bedload layer (traction carpet) is driven by the turbulence of the overlying flow, and deposition occurs gradually rather than by en masse freezing as suggested by Shanmugam (1996), who promoted the idea that traction carpets are sandy debris flows.

2.10 Use of modern submarine fan analogues

Several different kinds of modern analogues are used to understand the early Paleogene submarine fans in the JDB in this study. An ideal modern analogue is one that has a similar architectural style (configuration of architectural elements) as the ancient system, has elements that are dimensionally and lithologically similar, and has undergone a similar long-term and short-term depositional history. Finally, there must be some advantage gained by using the modern analogue, for example improved resolution or sampling (e.g. cores). Submarine fan analogues that fit all of these criteria rarely exist. Analogues that fit some of these criteria and not others can still be very useful. It is important then to define the different types of analogues and how each is used in this study to better understand early Paleogene submarine fans in the JDB.

The ancient submarine fans in the JDB (50 to 65 million year old) were studied using 3-D seismic data and industry exploration and delineation wells. Quaternary submarine fans in the Corsican Trough (offshore Eastern Corsica) and in the Santa Monica Basin (offshore California) represent *scaled-geometric analogues*. Similarities in gradients, basin size, shape, and water depths, sediment grade and architectural elements make the Quaternary submarine fans useful scaled-geometric analogues. Ultra-high resolution shallow penetrating seismic-reflection profiles for these systems provide

bed-scale details about the dimensions, geometry, and distribution of channels and lobes, and hence therein lies the advantage gained by using these analogues.

These systems, however, form very poor *temporal analogues* because their long-term depositional histories are significantly different from the fans in the JDB. Temporal analogues represent systems that have undergone a similar depositional/tectonic history, including such things as recurrence rates of flows, long-term sedimentation rates, and frequency of channel avulsions. The long-term sedimentation rates and frequency of sea level fluctuations appear to be vastly different between the early Paleogene fans in the JDB and the Quaternary analogues in the Santa Monica and Golo basins. As a result the long-term evolution of the systems will be different. The closest temporal analogues to the fans in the JDB are Paleogene fans in the North Sea (which have been studied in detail by others, and hence do form useful ancient analogues - see Chapter 5).

Non-scaled-geometric analogues are also used in this study. They represent systems that show similar architectural styles, but the dimension or scale of the systems are much different. As an example, a sinuous submarine channel is recognized in the JDB, but because the dimensions of the channel are small, its detailed architecture and evolution cannot be determined using the conventional 3-D seismic data available in this study. Much larger sinuous channels, however, contain architectural components that are big enough to be imaged using conventional 2-D or 3-D seismic data. Therefore larger systems may provide insight into the formation of sinuous channels in smaller systems. The primary assumption here is that the processes responsible for forming sinuous channels are the same regardless of scale, and that the dimensional differences reflect changes in the magnitude of the processes (e.g. the size of the gravity flows) only. This assumption is supported by recent work conducted by Skene (1998) who examined the dimensions of several submarine channels around the world and found that in general channel dimensions scale with the size of flows (i.e. large channels form from large flows, small channels form from small flows). In this study, this assumption can be further tested by comparing the geometry of small sinuous channels off Corsica, where high resolution data are available, to much larger systems, where high resolution data are not required. The architectural styles compare well.

2.11 Submarine fans in the context of sequence stratigraphy

Sequence stratigraphy is the study of seismic architecture and stratal packages and their relation to relative sea level history (with relative sea level dictated by a combination of subsidence rate, eustatic sea level fluctuations, and the rate of sediment supply). The approach is used to divide the stratigraphic record into genetically related packages using chronostratigraphically important surfaces like unconformities (the “Exxon approach”), identified using a combination of seismic, well log, biostratigraphic, and lithostratigraphic data. As defined in AAPG Memoir 26 (see Mitchum et al., 1977a), a **depositional sequence** (or “sequence” for short) is a relatively conformable succession of genetically related strata bounded above and below by unconformities and their correlative conformities. A sequence represents strata deposited during a single relative sea level cycle, and according to the Exxon approach, a sequence begins and ends with a relative sea level fall that result in widespread unconformities (i.e. sequence boundaries - Mitchum et al., 1977a; Posamentier and Vail, 1988).

Sequence stratigraphy has two main components. The first deals with the response of sedimentary systems, and their resulting seismic architectures, to fluctuations in relative sea level. The second component deals with global correlation of sequences recorded in the stratigraphic record that may develop as a result of the effects of global eustatic sea level fluctuations predominating over tectonic or sedimentation effects (Haq et al., 1987). The validity of global correlation of sequences and sequence boundaries that supposedly result from global sea level fluctuations is a hot topic for debate (e.g. Cloetingh, 1988; Miall, 1992). Even widespread recognition of sequences along, for example, the eastern margin of North America is not sufficient to demonstrate global significance, for very broad, continent-scale interplate stresses could generate widespread regressions and transgressions in the geologic record (Cloetingh, 1988). On the other hand, correlation of sea level changes with oxygen isotopes indicates that global sea level fluctuations, particularly in the post Oligocene time period, may be real (Abreu and Haddad, 1998).

In contrast to the validity of global sequence correlation, the response of depositional systems to fluctuating relative sea level, at least in marginal-marine settings, is generally agreed on. The primary control on sand body character in such settings is the

fluvial response to changes in accommodation (space for sediment to accumulate). A sequence can be subdivided into several component systems tracts, each corresponding to sediment deposited during a specific segment of a single cycle of the relative sea level curve, occupying a specific position within a sequence (Posamentier and Vail, 1988). According to the Exxon approach, sediment supply is generally assumed to be reasonably constant, and therefore eustatic sea level fluctuations combined with subsidence are assumed to be responsible for relative sea level fluctuations.

A sequence begins with a fall in relative sea level. If the fall is abrupt (i.e. outpaces subsidence) and is of sufficient magnitude, the shelf will be exposed and a subaerial unconformity will be generated. This situation results in the formation of a type 1 sequence boundary, accompanied by fluvial incision and deposition of a **lowstand systems tract** seaward of the shelf break (above the slope and basin floor). If the rate of sea level fall does not exceed subsidence, then a type 2 sequence boundary is generated and a **shelf-margin systems tract** is deposited rather than a lowstand systems tract. The type 2 sequence boundary is characterized by little, if any, fluvial incision (Posamentier and Vail, 1988). The rising segment of a relative sea level cycle corresponds to a **transgressive systems tract**, during which the rate of shelf accommodation generation exceeds sediment input, and fluvial systems may get trapped on the inner shelf or in estuaries, and may backstep landward (Posamentier and Vail, 1988). As the rate of sea level rise slows towards the end of the cycle, sediment supply may once again outpace the formation of accommodation, resulting in progradation and the development of a **highstand systems tract**. Though progradation probably begins prior to the period of maximum flooding, the base of the highstand systems tract is commonly placed at the maximum flooding surface, which on seismic profiles corresponds to a downlap surface. The top of the highstand systems tract corresponds with the unconformity associated with the base of the subsequent sequence.

2.11.1 Lowstand systems tract

In sequence stratigraphic terms, submarine fans are considered part of the lowstand systems tract. In instances where there is a sudden loss of accommodation on the shelf (e.g. during a rapid eustatic sea level fall accompanied by exposure of the shelf -

i.e. a type 1 unconformity), rivers may incise the shelf with sand transported directly into basinal settings, effectively bypassing the shelf and slope. Based largely on evidence from the North Sea, Mitchum (1985), Posamentier and Vail (1988), and Posamentier et al. (1991) proposed a subdivision of the lowstand systems tract into two or three separate, temporally distinct members that are similar to the type I, II, and III fans of Mutti (1985a). The **lowstand fan** (or basin-floor fan) consists of mounded deposits on the basin floor that accumulated during rapid relative sea level fall as sediment bypassed the shelf and slope during canyon incision (Posamentier and Vail, 1988). The lowstand fan consists of the coarse-grained clastics deposited on the basin floor during the initiation, and subsequent continuation, of a relative sea level fall, when accommodation was not available on the shelf. Posamentier and Vail (1988) suggested that fans deposited during this time had the highest sand:mud ratios.

The lowstand systems tract model of Mitchum (1985), Posamentier and Vail (1988), and Posamentier et al. (1991) also predicts that channel-levee deposits will dominate when the rate of sea level fall slows towards the maximum regression and slowly rises during the initial segment of the subsequent sea level rise. During this time the regressive **lowstand wedge** forms, consisting of more proximal muddy “slope fans” dominated by overbank/levee deposits. During deposition of the lowstand wedge, stream incision ceases, canyons are backfilled, and sand:mud ratios decrease (Posamentier and Vail, 1988). The lowstand wedge can be further subdivided into an early part characterized by muddy channel-levee systems (“slope fans”), with mud inferred to originate from slumping of the unstable muddy canyon walls, and a later part characterized by deltaic progradation above leveed channels (Posamentier and Vail, 1988). Chapter 5 describes the applicability of sequence stratigraphic models for submarine fans in the Jeanne d’Arc Basin.

2.12 General rift-drift processes

Atlantic-type (also known as aseismic, passive, or divergent) continental margins develop by rifting and subsequent break-up of continental margins (Falvey, 1974; Bally, 1983). The term “rifting” refers to the general process of continental break-up and separation, and includes extension (resulting in horizontal displacement of continental

crust via listric faults), vertical tectonics (resulting in uplift and subsidence of the crust), and sea floor spreading (resulting in the emplacement of oceanic crust) (Falvey, 1974; McKenzie, 1978; Falvey and Middleton, 1981; Bally, 1983). Unlike oceanic crust, where vertical movements can be explained by heating (thermal expansion and uplift) and cooling (thermal contraction and subsidence) of the crust, there is less agreement on the mechanisms for vertical movements in continental crust and for crustal thinning (Falvey, 1974; McKenzie, 1978). Heating of the continental crust would result in uplift (doming), but as the thermal anomaly decays, the uplifted crust would subside back to its original level rather than forming a basin. McKenzie (1978) pointed out that models based on thermal anomalies alone could not thin the crust, and hence there is a “space problem”.

Falvey (1974) argued that crustal thinning is accomplished by erosion after a thermal anomaly in the upper mantle has caused “doming” of the continental crust (up to 2 km of denudation). Collapse of the dome and thermal contraction result in subsidence and formation of a rift-valley (grabens and half-grabens). Subsidence is accommodated in part by deep crustal metamorphism causing a decrease in crustal volume and increase in crustal density. In contrast, McKenzie (1978) argued that abrupt stretching of the crust causes extension, and listric faulting causes crustal thinning. In turn, passive upwelling of hot asthenosphere (without necessitating a thermal anomaly) causes thermal expansion and uplift followed later by subsidence due to thermal contraction. In this case, the rift-valley is formed by the listric faulting.

Two distinct types of uplift associated with rifting have been identified, resulting in the formation of prominent “rift-onset” and “break-up” unconformities (Falvey, 1974 - discussed in more detail below - see Figure 2.23). Identification of these unconformities allows the continental stratigraphic succession to be subdivided into pre-rift, syn-rift and post-rift successions (Figure 2.24). A more detailed discussion of the syn-rift and post-rift phases of Atlantic-type margins is provided below. Detailed explanation of the geodynamics involved in various rift-drift models, however, is beyond the scope of this thesis and the interested reader is directed to Keen and Beaumont (1990) for an excellent account.

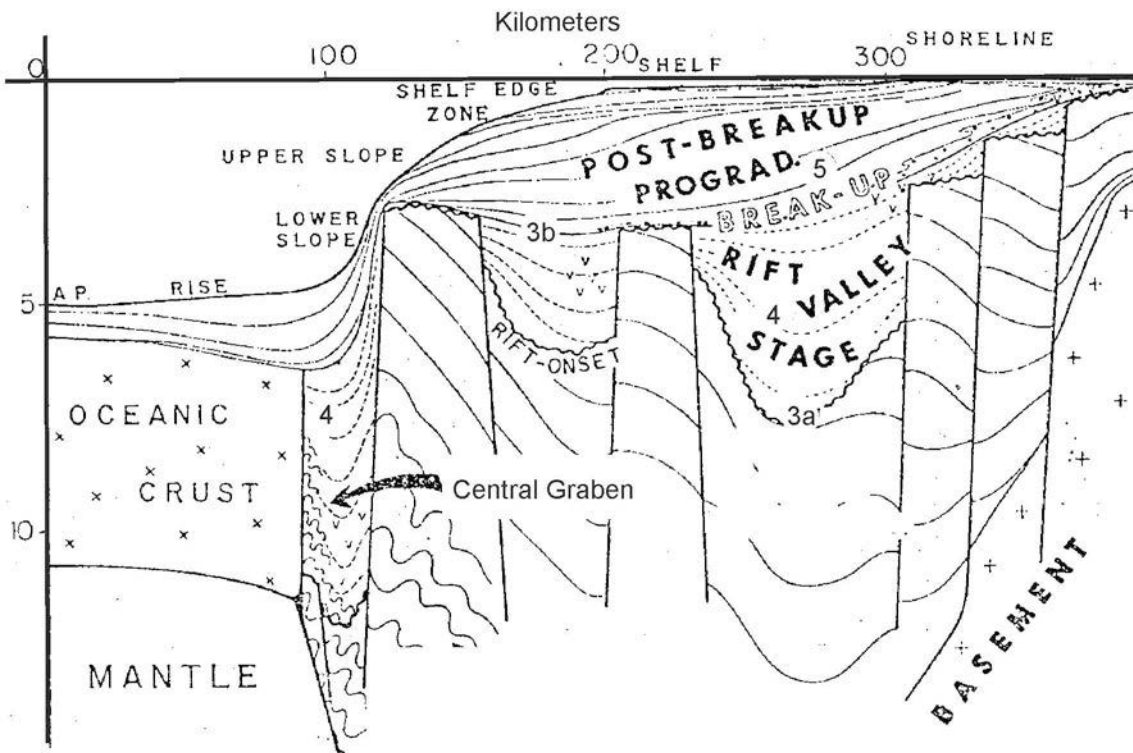


Figure 2.23. Schematic structural cross-section of an Atlantic-type margin, showing rift-valley (syn-rift - 4) strata bounded below by a rift-onset unconformity (3a) and above by a break-up unconformity (3b). Note the syn-rift volcanics and volcanics (v) near the break-up unconformity (and correlative conformity). The post-rift (drift) succession (5) consists initially of widespread transgressive deposits followed by regression of a seaward thickening wedge as the rate of post-rift subsidence decreases (modified from Falvey, 1974).

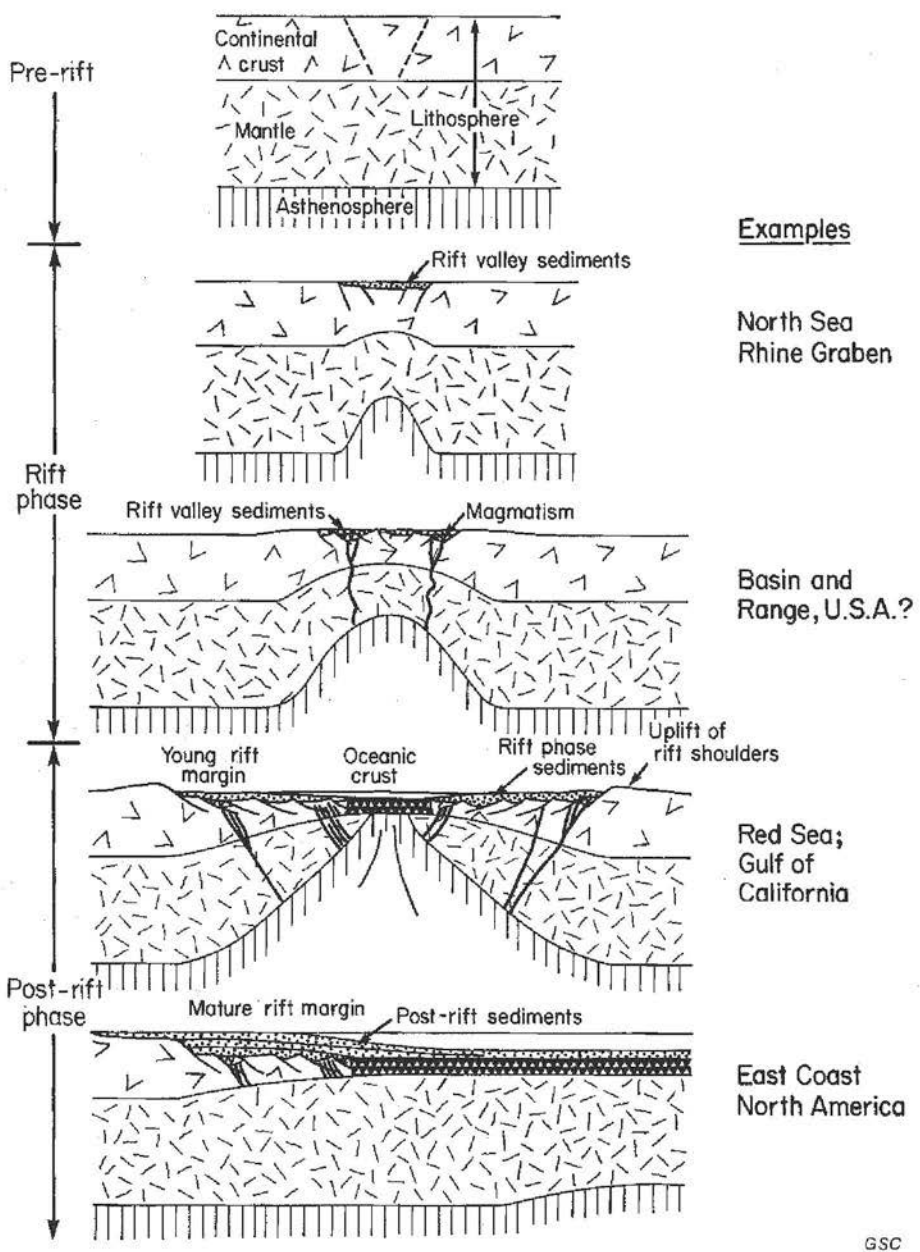
2.12.1 *Syn-rift (rift phase, rift-valley)*

The rift phase develops before the final break-up between plates, a period commonly believed to be tectonically active (Keen and Beaumont, 1990 - Figure 2.24). The onset of rifting is caused by lithospheric thinning that can result from a number of processes, including crustal extension and/or erosion (other processes are highlighted by Keen and Beaumont, 1990). Rift phase deposits (i.e. fill of rift-valley) are bounded above and below by angular unconformities (rift-onset and break-up unconformities - Falvey, 1974 - Figure 2.23). Doming or arching in response to thermal expansion of the continental crust, as much as 50 million years before actual continental break-up, results in substantial erosion and the formation of a rift-onset unconformity (Falvey, 1974).

Subsidence combined with collapse of the up-arched crust results in the development of a rift-valley (graben or half-graben) that forms in response to listric faulting and extension (McKenzie, 1978; Bally, 1983) and/or crustal metamorphism (Falvey, 1974; Falvey and Middleton, 1981). Other models predict that a rift-valley forms and only the margins or shoulders of the rift-valley are uplifted. Keen and Beaumont (1990) suggested that the footwall of a normal fault would be uplifted proportional to the amount of subsidence of the hanging wall because the fault effectively unloads the hanging wall, causing an isostatic adjustment. Uplift, then, could take place along the faulted margins or shoulders of the rift-valley, the timing of which would be contemporaneous with, or post-date, the initiation of rifting. Drainage can be away from or towards a central rift-valley (or both), and depositional environments within the rift-valley are typically terrestrial to shallow-marine (consisting of continental and deltaic facies), commonly accompanied by igneous activity (Falvey, 1974; Sinclair, 1988; Pe-Piper et al., 1990).

2.12.2 *Post-rift (syn-drift, drift phase)*

The transition from syn-rift to post-rift is reportedly marked by a change in depositional environments, from non-marine or shallow-marine deposits, to deeper water more open marine deposits (Falvey and Middleton, 1981). This transition is sometimes accompanied by a “break-up” unconformity (Falvey, 1974; Keen and Beaumont, 1990), which forms in response to convective upwelling of the asthenosphere and a second



GSC

Figure 2.24. Schematic cartoon showing the evolution of an Atlantic-type rifted continental margin. On the right are examples of margins representative of each stage (from Keen and Beaumont, 1990).

period of thermal expansion, as well as isostatic rebound due to significant strain and decoupling of tectonic plates (Falvey, 1974). The result is a “short, sharp period of emergence” and it is more localized than the rift-onset unconformity and difficult to define towards the center of the basin (Falvey, 1974).

The drift phase starts as the continental plates have completely separated and oceanic crust is emplaced between them (i.e. the start of sea floor spreading - Figure 2.24). Geothermal gradients progressively decrease as the spreading center moves away from the edge of the rifted continental margin, and lithospheric cooling and contraction results in rapid subsidence (Falvey, 1974; Falvey and Middleton, 1981; Bally, 1983; Keen and Beaumont, 1990). The rates of subsidence typically decrease exponentially after the onset of drifting (Bally, 1983), though Keen and Beaumont (1990) and Royden and Keen (1980) described an initial increase in rate of subsidence for the first 60 m.y. after break-up, followed by exponential decrease thereafter for the Labrador and Scotian margins. Post-rift subsidence can also result from salt withdrawal, sediment compaction, and in response to sediment loading. Rapid marine transgression is inferred to take place in response to post-rift subsidence. A broad shelf develops and as the rate of subsidence decreases exponentially, sediment supply out-paces accommodation and a thick regressive wedge develops, causing the outbuilding of the shelf and slope (Falvey, 1974 - Figures 2.23, 2.24).

The onset of drifting can be dated by determining the age of the first magnetic anomaly, corresponding to the oldest oceanic crust adjacent to continental crust (Bally, 1983). Corresponding to the youngest oceanic crust, a period of erosion on continental crust results in the formation of a “break-up” unconformity (Falvey, 1974; Bally, 1983).

2.13 Jeanne d’Arc Basin - regional setting and basin structure

The Jeanne d’Arc Basin (**JDB**) is a small passive-margin rift basin that underlies what is now the northeastern part of the Grand Banks of Newfoundland, offshore eastern Canada (Figures 2.25). It forms one of several interconnected Mesozoic-Cenozoic depocenters that developed along the western margin of the North Atlantic Ocean during a complicated rift-drift history (Tankard and Welsink 1987; Sinclair, 1988; Ziegler, 1989; Schlische, 1993). The JDB - the deepest of these basins - formed a trough-shaped

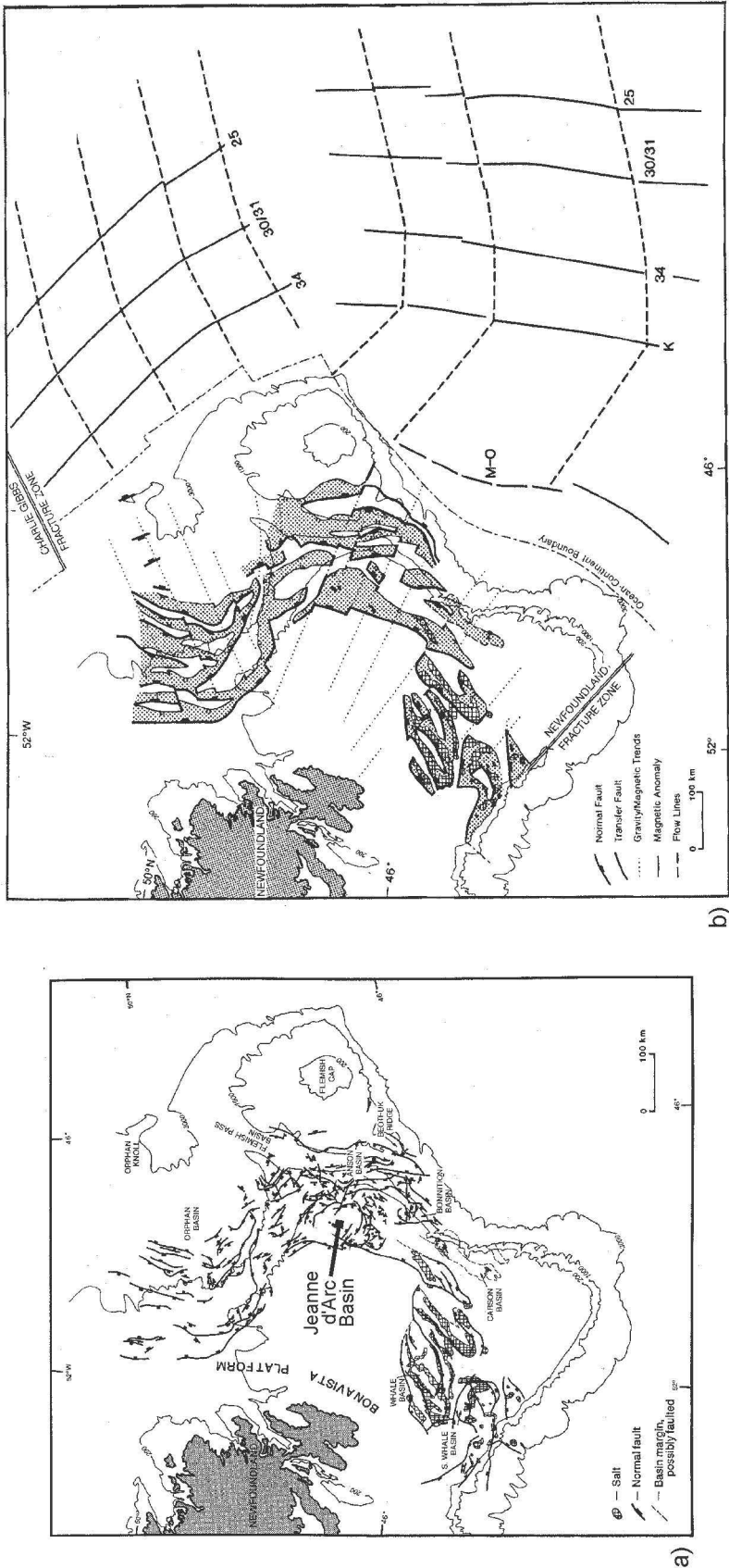


Figure 2.25. a) Structure map based on regional seismic data showing major faults and location of salt. b) Regional map showing location of basins and their relationship to the magnetic anomalies to the east (based on a number of datasets including gravity, magnetic and reflection seismic). Ocean-continent boundary is indicated and dashed lines represent flow lines, showing the trend of plate motion during sea floor spreading (from Welsink et al., 1989). Magnetic anomalies and flow lines are from Srivastava and Tapscott (1986).

depression until about the Middle Eocene, located approximately 300 km east-southeast of St. John's, Newfoundland. After the Middle Eocene, the relief of the basin was filled (see Chapter 4). The basin covers an area greater than 10 000 km², with a maximum thickness of more than 20 km of Mesozoic and Cenozoic strata (Enachescu, 1987; de Voogd et al., 1990).

The Murre and Mercury faults form the western boundary of the basin, separating a relatively stable continental platform (Bonavista Platform) to the west from a subsiding depocenter to the east (Figure 2.26). Paleozoic rocks of the Bonavista Platform are overlain by a thin veneer of Upper Cretaceous and Tertiary sediment (Sinclair et al., 1992). The Voyager Fault System, located along the Outer Ridge Complex (also known as the Central Ridge), forms the eastern boundary of the basin. The JDB is further subdivided on either side of the Egret fault into a northern segment and a southern segment (Figure 2.26). North of the Egret fault, Upper Cretaceous and Tertiary strata thicken significantly across the Trans-Basin Fault Trend, a zone of sub-parallel, northwest-trending normal faults (Sinclair et al., 1992). South of the Egret fault, the basin underwent little subsidence, and hence the stratigraphic succession is much thinner.

Salt diapirism in the Adolphus region, as well as along the western margin of the basin (Egret region), also played an important role in modifying the basin structure and deforming Upper Cretaceous and Tertiary strata (McAlpine, 1990). Two additional anticlinal structures deform Upper Cretaceous and lower Tertiary strata in the basin, though the mechanism for deformation is less clear. The first is located in a relatively narrow region just south of the Egret fault, near Cormorant N-83, and is referred to as the Cormorant arch (Figures 2.26 - described as the "Cormorant anticline" by Sinclair, 1995). The second is located near the Terra Nova wells, and is referred to as the Terra Nova arch (Figures 2.26 - name from Sinclair, 1995). Both structures were attributed to basin inversion (i.e. uplift as a result of transpressional or compressional stresses - Ziegler, 1988) by Sinclair (1995), who interpreted the structures to have formed from transpressional (oblique-slip) movement during mid Aptian to late Albian NE-SW extension along pre-existing NE-SW oriented normal faults (which formed from NW-SE extension during early rifting). Though he interpreted the structures as inactive in the

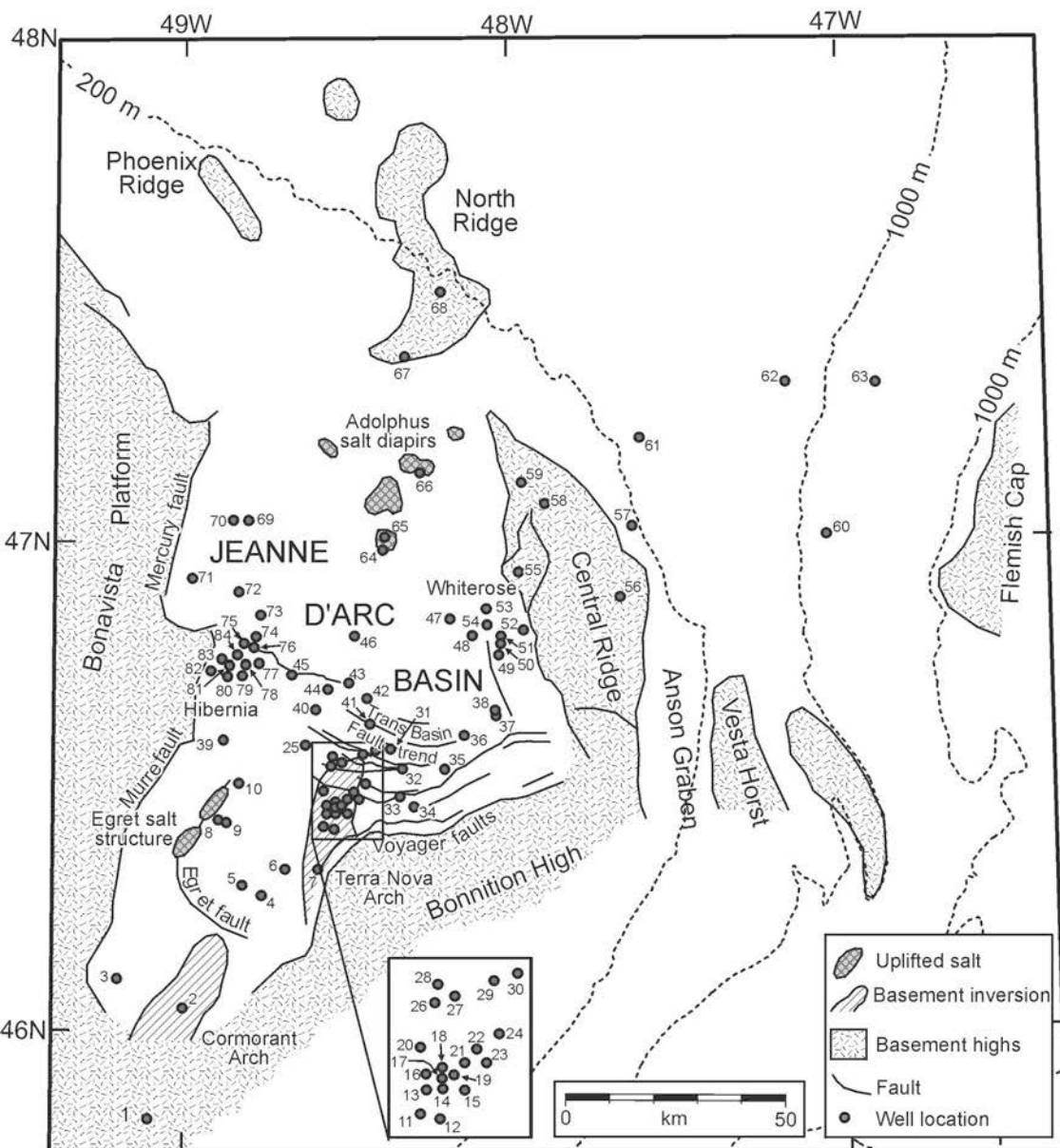


Figure 2.26. Basemap of Jeanne d'Arc Basin and surrounding areas, showing basement highs and faults that offset Upper Cretaceous and younger strata. Wells are numbered (see next page for the well names corresponding to the numbers). See text for details.

Figure 2.26. Continued. WELLS: **1** Spoonbill C-30; **2** Cormorant N-83; **3** Murre G-67; **4** Port au Port J-97; **5** Riverhead N-18; **6** Gambo N-70; **7** South Brook N-30; **8** Egret N-46; **9** Egret K-36; **10** East Rankin H-21; **11** King's Cove A-26; **12** Beothuk M-05; **13** Terra Nova K-17; **14** Terra Nova K-07; **15** Terra Nova I-97; **16** Terra Nova K-18; **17** Terra Nova K-08; **18** Terra Nova C-09; **19** Terra Nova L-98; **20** Brent's Cove I-30; **21** Terra Nova H-99; **21** Terra Nova G-90; **23** Terra Nova E-79; **24** North Trinity H-71; **25** Avondale A-46; **26** Hebron I-13; **27** Hebron D-94; **28** Hebron M-04; **29** West Ben Nevis B-75; **30** Ben Nevis L-55; **31** Ben Nevis I-45; **32** West Bonne Bay C-23; **33** Springdale M-29; **34** Voyager J-18; **35** Bonne Bay C-73; **36** Fortune G-57; **37** Archer K-19; **38** Amethyst F-20; **39** Rankin M-36; **40** Mara E-30; **41** Cape Race N-68; **42** North Ben Nevis M-61; **43** North Ben Nevis P-93; **44** South Mara C-13; **45** Mara M-54; **46** Botwood G-89; **47** Whiterose L-61; **48** Whiterose J-49; **49** Whiterose A-17; **50** Whiterose L-08; **51** Whiterose E-09; **52** Whiterose A-90; **53** Whiterose N-22; **54** Whiterose N-30; **55** Trave E-87; **56** Golconda C-64; **57** Panther P-52; **58** South Merasheen K-55; **59** South Tempest G-88; **60** Kyle L-11; **61** North Dana I-43; **62** Lancaster F-70; **63** Gabriel C-60; **64** Adolphus D-50; **65** Adolphus 2k-41; **66** Conquest K-09; **67** Dominion O-23; **68** Bonanza M-71; **69** Flying Foam I-13; **70** West Flying Foam L-23; **71** Mercury K76; **72** Thorvald P-24; **73** Nautilus C-92; **74** South Nautilus H-09; **75** Hibernia K-18; **76** Hibernia B-08; **77** Hibernia C-96; **78** Hibernia P-15; **79** Hibernia K-14; **80** Hibernia J-34; **81** Hibernia O-35; **82** Hibernia G-55; **83** Hibernia I-46; **84** Hibernia B-27.

Late Cretaceous and Tertiary, both structures clearly deform Upper Cretaceous and lower Tertiary strata in the basin (discussed in more detail in Chapter 4).

2.13.1 Rift - drift history in the Jeanne d'Arc Basin

Opening of the central North Atlantic around the Grand Banks progressed from south to north, with regional trends in magnetic anomalies and fracture zones reflecting changes in the orientation of spreading around the broad Grand Banks peninsula (Welsink et al., 1989; Srivastava et al., 1990 - Figure 2.25b). The proximity of the JDB to four rift - drift margins (Scotian Margin/Northern Africa; Western Grand Banks/Iberia; Northeast Newfoundland Shelf/Europe; Labrador/Greenland) made it susceptible to periods of uplift and subsidence in the immediate and neighboring regions during the fragmentation of Pangea. Two major transform faults, located to the south (Azores/Newfoundland Fracture Zone) and north (Charlie Gibbs Fracture Zone) of the basin (Figure 2.25b), also played an important role in the basin evolution, forming strike-slip margins that accommodated plate motion during sea floor spreading (Enachescu, 1987; Tankard and Welsink, 1987; Sinclair, 1988; McAlpine, 1990).

Because of its complex surroundings and the multiple plate tectonic events affecting it, rifting along the Grand Banks margin lasted for much longer (upwards of 90 - 100 m.y.) than most margins with simpler configurations (e.g. the Scotian Margin where rifting lasted 40 to 60 m.y.) (Keen et al., 1987; Keen and Beaumont, 1990). Tectonostratigraphic interpretations for the JDB have been published by Amoco and Imperial (1973a), Jansa and Wade (1975 a, b), Keen et al. (1987, 1990), Enachescu (1987), Tankard and Welsink (1987), Sinclair (1988, 1993), Tankard et al. (1989), Grant and McAlpine (1990), Edwards (1990), and Driscoll et al. (1995). The JDB is believed to have experienced two (Jansa and Wade, 1975; Hubbard et al., 1985; McAlpine, 1990) or three (Enachescu, 1987; Sinclair, 1988, 1993) periods of rifting during the Late Triassic to mid-Cretaceous, followed by a post-rift phase starting in the Late Cretaceous.

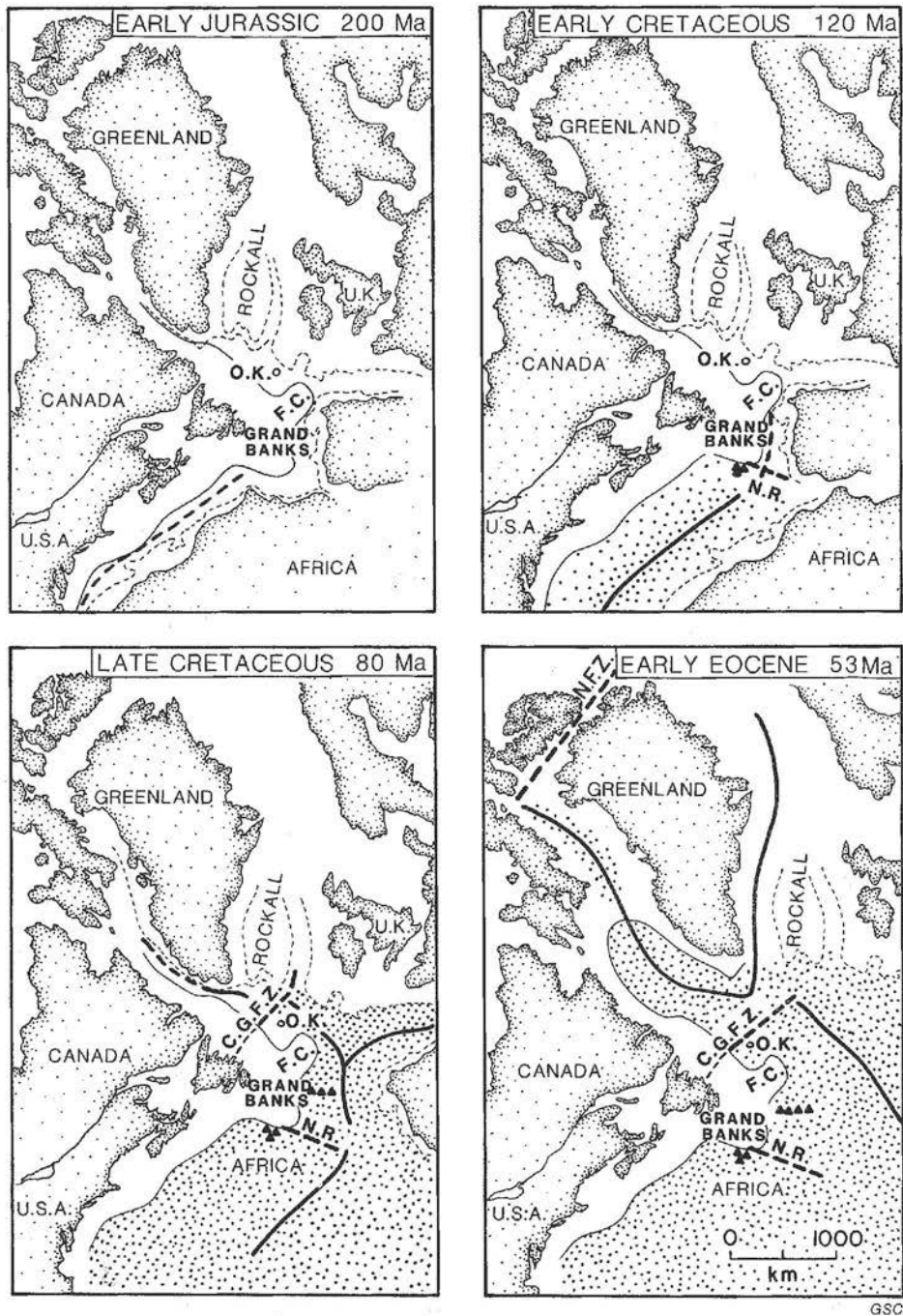
The first period of rifting is generally agreed to be Late Triassic to Early Jurassic, and is associated with the separation of the Scotian Margin and northwestern Africa, and a contemporaneous failed-rift margin between the Grand Banks and Iberia (Sinclair,

1988; McAlpine, 1990). There is less agreement on the second and third periods of rifting (which are sometimes grouped into one) that ultimately led to a complex decoupling between the Grand Banks and Iberia, and the Northeast Newfoundland Shelf and Europe. The timing is generally believed to be latest Jurassic to mid-Cretaceous, with some workers suggesting a period of late Valanginian to Hauterivian quiescence prior to the separation of the Northeast Newfoundland Shelf from Europe (e.g. Sinclair, 1988).

Basin deformation was prevalent during periods of rifting, with extension creating prominent growth faults and rollover anticlines (Tankard and Welsink, 1987; Sinclair, 1988, 1993; McAlpine, 1990). As with other basins around the circum North Atlantic Ocean, episodes of rift-related uplift south of the JDB triggered widespread erosion and the transport of large quantities of coarse-grained clastic sediment to the north. The JDB is perhaps best known for its hydrocarbon production from Lower to mid-Cretaceous reservoirs in the large Hibernia and Terra Nova oil fields, which were deposited during formation of the Avalon Uplift, a broad up-arched region south of the basin interpreted to have formed as rifting resumed between the Grand Banks and Iberia (Jansa and Wade, 1975a; Enachescu, 1987; Sinclair, 1988).

Widespread erosion of the Avalon Uplift led to the development of a prominent peneplain surface south of the basin that is easily recognized on seismic-reflection profiles (the Avalon Unconformity - Jansa and Wade, 1975a). The peneplain surface represents the merger of several unconformities that have been correlated north into several separate unconformities within the fill of the JDB (Driscoll et al., 1995). The Avalon unconformity above basement highs surrounding the JDB, therefore, probably represents both rift-onset and a break-up unconformity, whereas within the expanded section in the JDB, individual unconformities may have been initiated by rift-onset, break-up, or other controls like eustatic sea level.

In contrast to the rift phase, the post-rift phase is generally believed to be associated with the onset of thermal subsidence, perhaps preceded by uplift and the formation of a 'break-up' unconformity (Falvey, 1974; Keen et al., 1990; Keen and Beaumont, 1990). Off eastern Canada, sea floor spreading propagated northwards through time, beginning in the Early to Middle Jurassic along the Scotian Margin (Jansa



GSC

Figure 2.27. Four diagrams illustrating various stages in the evolution of the northern Atlantic Ocean. Densely stippled areas represent oceanic crust. Dashed lines represent fracture zones and bold continuous lines represent active spreading centers (mid-ocean ridge). O.K. Orphan Knoll; F.C. Flemish Cap; N.R. Newfoundland Fracture Zone; C.G.F.Z. Charlie Gibbs Fracture Zone. Triangles are seamounts (from Keen and Beaumont, 1990).

and Wade, 1975b), Early to Middle Cretaceous between Iberia and the Grand Banks (Jansa and Wade, 1975b; Sinclair 1988), Late Cretaceous (Roest and Srivastava, 1989) or Early Paleocene (Chalmers et al., 1993) in the Labrador Sea, and Late Paleocene to Early Eocene in the northern Labrador Sea, Baffin Bay, and Norwegian Sea (Gradstein et al., 1990). Therefore the timing of drift-related subsidence and age of youngest oceanic crust varies, but generally becomes younger towards the north.

By the Late Cretaceous, sea floor spreading was under way to the south, east, and northeast of the Grand Banks (Figure 2.27). Hence, Upper Cretaceous and Tertiary strata in the JDB are commonly believed to have accumulated along a passively subsiding margin (Hubbard et al., 1985; Enachescu, 1987; Sinclair, 1988; de Silva, 1993), as the distance to the mid-ocean ridge progressively increased and the lithosphere underwent thermal contraction (see Keen and Beaumont, 1990 for a more detailed discussion about this process). Most workers interpret the post-rift phase in the JDB to have begun in the Late Cretaceous. Drawing a sharp boundary between the final syn-rift and post-rift phases in the basin, however, may not be straight forward because sea floor spreading did not commence north of the Charlie Gibbs Fracture Zone until the Late Cretaceous (Roest and Srivastava, 1989) or Paleocene (Chalmers et al., 1993), and continent-to-continent transform motion is believed to have persisted just north of the JDB until the early Tertiary (Keen et al., 1987). This raises questions about whether post-rift strata in the JDB record any evidence for rejuvenated rifting and sea floor spreading north of this important transform margin, an idea explored in more detail in Chapter 4, and implied by Grant et al. (1988) and McAlpine (1990) who identified a Late Cretaceous to Early Eocene “transition to drift” phase that preceded their post-rift phase.

CHAPTER 3 - REVISED UPPER CRETACEOUS AND LOWER PALEOGENE LITHOSTRATIGRAPHY AND DEPOSITIONAL HISTORY OF THE JEANNE D'ARC BASIN*

* AAPG © 2003 - reprinted by permission of the AAPG whose permission is required for further use (see Appendix IV).

3.1 Introduction

3.1.1 Scope

In the Late Cretaceous and early Paleogene, the JDB formed an elongated depression, where sediment accumulated in and along the margins of a shallow shelf sea. The basin contains an interesting arrangement of Coniacian to Ypresian shelf and slope progradational units that were widely correlated across the western basin margin, and submarine fans that were mapped on the slope and basin floor. Until now, few published attempts had been made to unravel the complex pattern sandstone, shale, and chalk deposition in the basin. While Lower Cretaceous and older strata in the JDB have been studied in detail by several workers (e.g. Arthur et al., 1982; Tankard and Welsink, 1987; Tankard et al., 1989, Hiscott et al., 1990; McAlpine, 1990; Sinclair, 1993, 1995; Fowler and McAlpine, 1995), Upper Cretaceous and lower Paleogene strata have received less attention, even though they are known to contain hydrocarbons, in some cases within excellent quality reservoirs (e.g. in South Mara C-13 with over 30 m of continuous sands with 30% average porosity - Taylor et al., 1992). Although hydrocarbon discoveries made within Upper Cretaceous and Paleogene strata are sub-economic, much of the interval remains untested, particularly in the northern parts of the basin.

The only formally defined stratigraphic units in the Upper Cretaceous through Paleogene succession in the JDB are the Dawson Canyon, Wyandot and Banquereau formations, and the Petrel Member of the Dawson Canyon Formation. These units were originally defined for Scotian Shelf rocks (McIver, 1972), but their use was later extended to the time-equivalent strata of the Grand Banks (e.g. by Amoco and Imperial, 1973a; Jansa and Wade, 1975a, b). Later workers (e.g. Boudreau et al., 1986; Sinclair,

1988; McAlpine, 1990; de Silva, 1993; Agrawal et al., 1995; Deptuck, 1998) used informal nomenclature to subdivide the Dawson Canyon, Wyandot, and Banquereau formations in the JDB. This nomenclature, however, has not been applied consistently (e.g. “South Mara member”, Sinclair, 1988; “South Mara unit”, McAlpine, 1990; “South Mara formation”, Deptuck, 1998) and thus a formally revised lithostratigraphic classification is proposed in this paper.

Shelf and slope systems correspond to both sandstone and shale units that stack in a generally regressive manner with intermittent periods of widespread shale blankets and distal chalk deposition. Submarine fans correspond to relatively thick sandstone intervals (30 to 65 m thick) that form mounds on the slope and basin floor. Significant variation in shelf and slope progradational styles are observed between the JDB proper and the southern JDB, and these variations are described in this chapter. Using a combination of seismic-reflection profiles and well data, a formal lithostratigraphic nomenclature for the Upper Cretaceous and lower Paleogene succession of the JDB is proposed. The resulting framework is used to interpret the depositional history of the basin.

3.1.2 Data and Approach

Data from 52 wells, including wireline logs, descriptions of drill cuttings and sidewall cores, and biostratigraphic interpretations, were used in this study (wells shown in Figure 3.1). I build on and, in some cases, modify the formal and informal nomenclature described and used by McIver (1972), Amoco and Imperial (1973a), Jansa and Wade (1975a, b), Boudreau et al. (1986), Sinclair (1988), Grant et al. (1988), McAlpine (1990), and de Silva (1993). Biostratigraphic interpretations used in this study were extracted from published and unpublished reports stored at the Canada-Newfoundland Offshore Petroleum Board and also available through the Marine Resources Geoscience Subdivision at the Geological Survey of Canada (Atlantic). The biostratigraphic interpretations from wells with good sample coverage (especially those with sidewall cores) are preferred over wells with poorer sample distribution for constraining stratigraphic ages. The biostratigraphic results from key wells can be found in Appendix Ia and Ib. Paleobathymetric data were extracted from a report by Thomas (1994), who used benthic foraminifera to reconstruct paleo-water depths in several wells.

Unless otherwise noted, all lithostratigraphic information presented in this study was obtained from paper and digital CanStrat Limited well log interpretations and from well history reports. Lithological and grain size data were plotted using in-house software and well data were tied to industry seismic-reflection data using vertical seismic profiles (checkshot surveys).

Paper copies of more than 100 migrated, 60-fold seismic-reflection lines (about 6800 line km), from a survey acquired by the Soquip/Parex Group (1983) at a line spacing ranging from 2 - 8 km (Figure 3.1 - CNOPB Project No. 8620-S14-8E), were used to identify and map erosional and depositional features and regional unconformities. In the northern and southern parts of the basin, where data coverage from the 1983 dataset is sparse, additional 2-D seismic data from various other public-domain surveys were used to verify interpretations. In addition to 2-D seismic profiles and well data, two 3-D seismic surveys were used, acquired over the Hibernia (covering 500 km²) and Terra Nova (covering 220 km²) oil fields (Mobil Oil Canada, 1991; Petro-Canada, 1984). These data provided a detailed view of two erosional features associated with the regional unconformities described in this paper.

3.2 Lithostratigraphic classification

3.2.1 Dawson Canyon Formation

The Dawson Canyon Formation (McIver, 1972) consists of a variety of sedimentary rocks, ranging from fine- and coarse-grained clastics to chalky carbonates (Figures 3.2, 3.3). On the Scotian Shelf, for which the formation was originally defined, its lower boundary is conformable and gradational and lies just below the Petrel Member (defined below). Its upper boundary is defined as the base of the nearly ubiquitous chalky Wyandot Formation (Jansa and Wade, 1975b). In the JDB, where the Wyandot Formation is only locally developed, the accepted convention is to place the upper boundary of the Dawson Canyon Formation at the top of the Fox Harbour Member (described later) which coincides with a prominent peak/spike on gamma ray curves (Figure 3.3b). Where the gamma ray spike is absent, the boundary is defined biostratigraphically as the Cretaceous-Tertiary boundary, which closely coincides with the top of the Wyandot Formation and/or the base of the Tilton and Avondale members

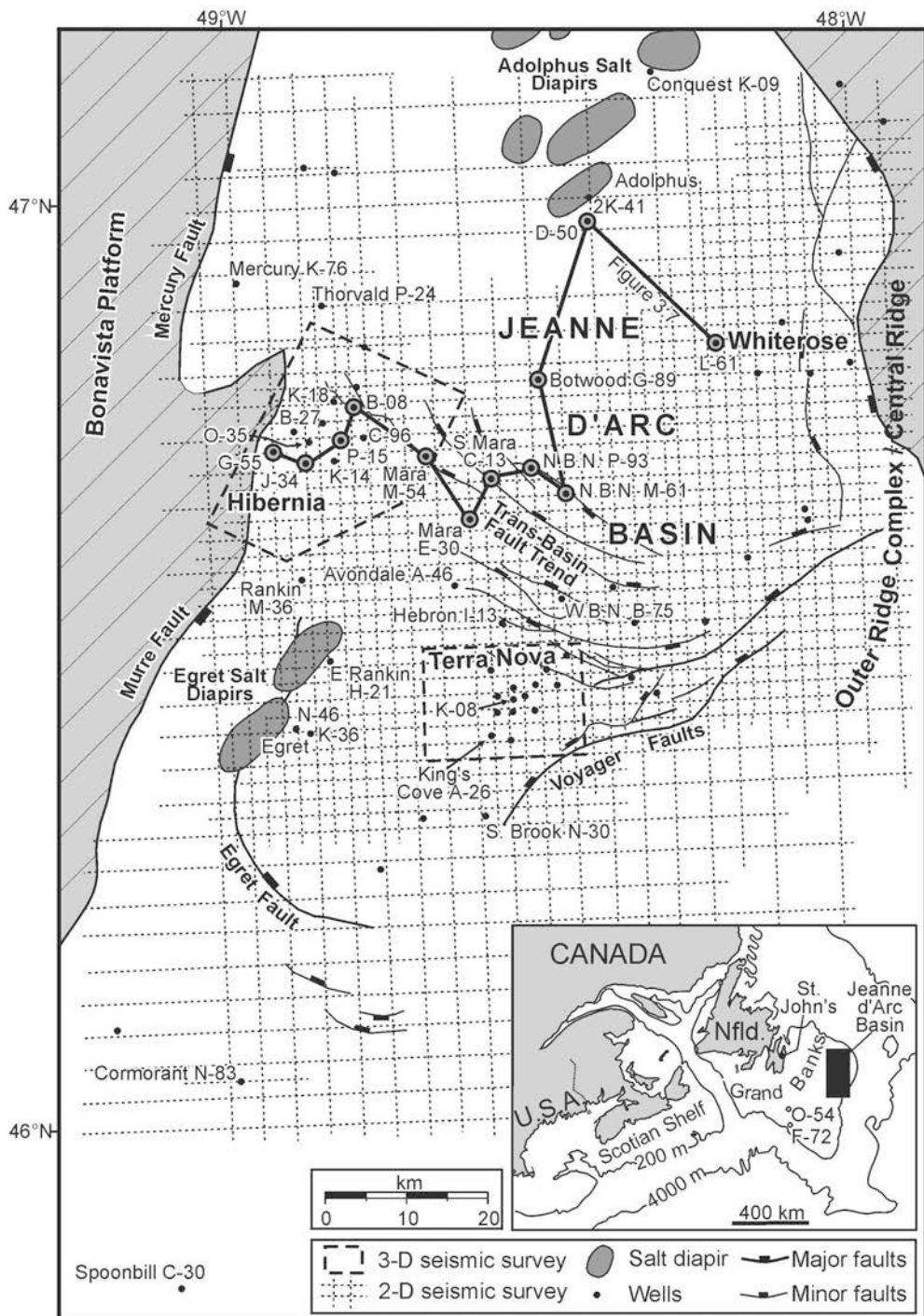


Figure 3.1. Map of the Jeanne d'Arc Basin showing main structural elements of the basin, including faults that extend into the Upper Cretaceous succession. Well locations also shown, with labels on the wells mentioned in the text and shown in other figures. Also shown is the grid of 2-D reflection seismic data used in this study (C-NOPB Project No. 8620-S14-8E) and the locations of the Hibernia and Terra Nova 3-D seismic surveys. N.B.N. = North Ben Nevis; W.B.N. = West Ben Nevis. Inset shows the location of eastern Canada and the Gannet O-54 and Gull F-72 well locations.

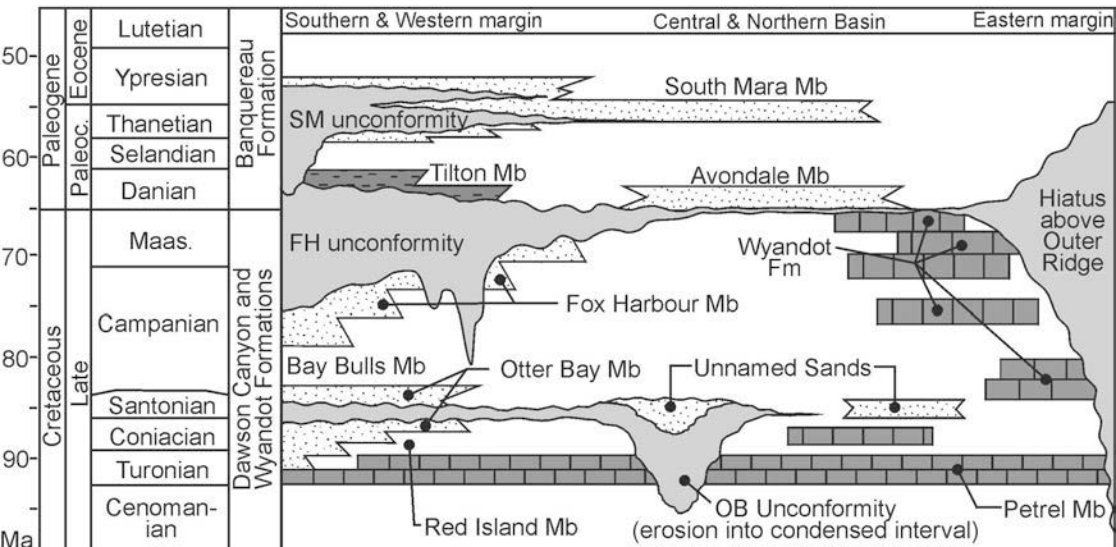


Figure 3.2. Generalized litho-chronostratigraphic chart for the Upper Cretaceous and the lower part of the Paleogene stratigraphic succession in the Jeanne d'Arc Basin (modified from Sinclair, 1987). Absolute ages on the timescale are from Gradstein et al. (1995) and Berggren et al. (1995). OB = Otter Bay; FH = Fox Harbour; SM = South Mara; Mb = Member; Fm = Formation.

(described later).

Following Boudreau et al. (1986), Sinclair (1988) and de Silva (1993), the Dawson Canyon Formation is subdivided into the Petrel, Otter Bay, and Fox Harbour members. Two new stratigraphic units are also defined: the Red Island and Bay Bulls members (Figures 3.2, 3.3, Table 3.1). The Otter Bay, Fox Harbour, Red Island, and Bay Bulls members are restricted to the western margin of the JDB. Except for the identification of the Petrel Member, the Dawson Canyon Formation is not subdivided farther east.

Petrel Member (formalized by Jansa and Wade, 1975b)

The Petrel Member (Figures 3.2-3.7) is a limestone unit located near the base of the Dawson Canyon Formation and is widely distributed on both the Scotian Margin and the Grand Banks. It was originally defined by Amoco and Imperial (1973a) as the “Petrel Limestone” and later formally defined as the “Petrel Member” by Jansa and Wade (1975b). Although Jansa and Wade (1975b) did not designate a type section for the Petrel Member, they did make reference to the Petrel Member in Gannet O-54 (Figure 3.1 inset). This well was subsequently used as a reference section for the Petrel Member by Williams et al. (1985). In this study, Gannet O-54 (1589.8 – 1664.8 m) is formally proposed as the type section for the Petrel Member.

The Petrel Member consists mostly of coccolith-rich microcrystalline limestone and marlstone, with glauconite throughout, and sand stringers developed locally (Shimeld et al., 2000). A 12.5 m core collected from the Petrel Member at Gull F-72, southwest of the JDB (Figure 3.1 inset), consists entirely of chalky well bioturbated limestone with foraminifera and fragments of pelecypods, and a porosity ranging from 13 to 23 % (Amoco and Imperial, 1973b).

Doeven (1983) calculated a 1 cm per thousand year sedimentation rate for the Petrel Member in Adolphus D-50 in the northern JDB (Figure 3.1). The member produces a low, commonly cylindrical (“blocky”) to symmetrical, gamma ray response (average of 48 API, Zehui Huang, pers comm., 1997) owing to its low clay content (Figures 3.3, 3.4). In some wells, it shows a gradual, upward-decreasing gamma ray response indicating a transition from calcareous shales or silts to cleaner limestones (e.g.

at North Ben Nevis P-93, 2328 – 2387 m) (Figure 3.4). The lower boundary of the Petrel Member is commonly gradual and in places difficult to identify where it overlies a clean sandstone unit. The upper boundary is usually sharply defined on gamma ray logs, marked by an abrupt transition from limestone to clastic sedimentary rocks.

The thickness of the Petrel Member is highly variable, ranging from 0 to over 100 m. Its thickness variation corresponds, at least in part, to the distribution of incised channels associated with an overlying unconformity. Where present, the channels have eroded the member, thus thinning or removing it (Figures 3.8a, b).

Red Island Member (new)

The Red Island Member (type section: Hibernia J-34, 1591 – 1713 m; Table 3.1) is a shale-prone unit found stratigraphically above the Petrel Member (Figure 3.3). It consists of grey mudstones and siltstones with minor sandstone stringers. The Red Island Member produces a higher gamma ray response than the underlying Petrel Member and overlying Otter Bay Member. In the type section, the Red Island Member sharply overlies the Petrel Member. In some wells, the Red Island Member contains abundant microfossils, large shell fragments, and detrital plant fragments. Sparse palynology samples indicate that the member was deposited during the Turonian to Santonian.

The contact between the Red Island and Otter Bay members varies from sharp to gradational. Where the Otter Bay Member is absent, the Red Island Member is in direct contact with the overlying Bay Bulls Member and, as a result, the two shale-prone units cannot be distinguished (e.g. at Hibernia B-08 - Figure 3.3). The easternmost limit of the Otter Bay Member, as used here, defines an arbitrary eastern limit for both the Red Island and Bay Bulls members (Figure 3.7).

Otter Bay Member (formalized)

The Otter Bay Member (type section: Hibernia J-34, 1482 - 1591 m; Table 3.1; Sinclair, 1988) is a sandstone unit located along the western margin of the basin. It consists of medium to very coarse-grained sandstones that show a regressive, upward-coarsening grain size trend and a funnel- to cylindrical-shaped gamma ray response. Near Hibernia (Figure 3.1) the Otter Bay Member is located stratigraphically above the

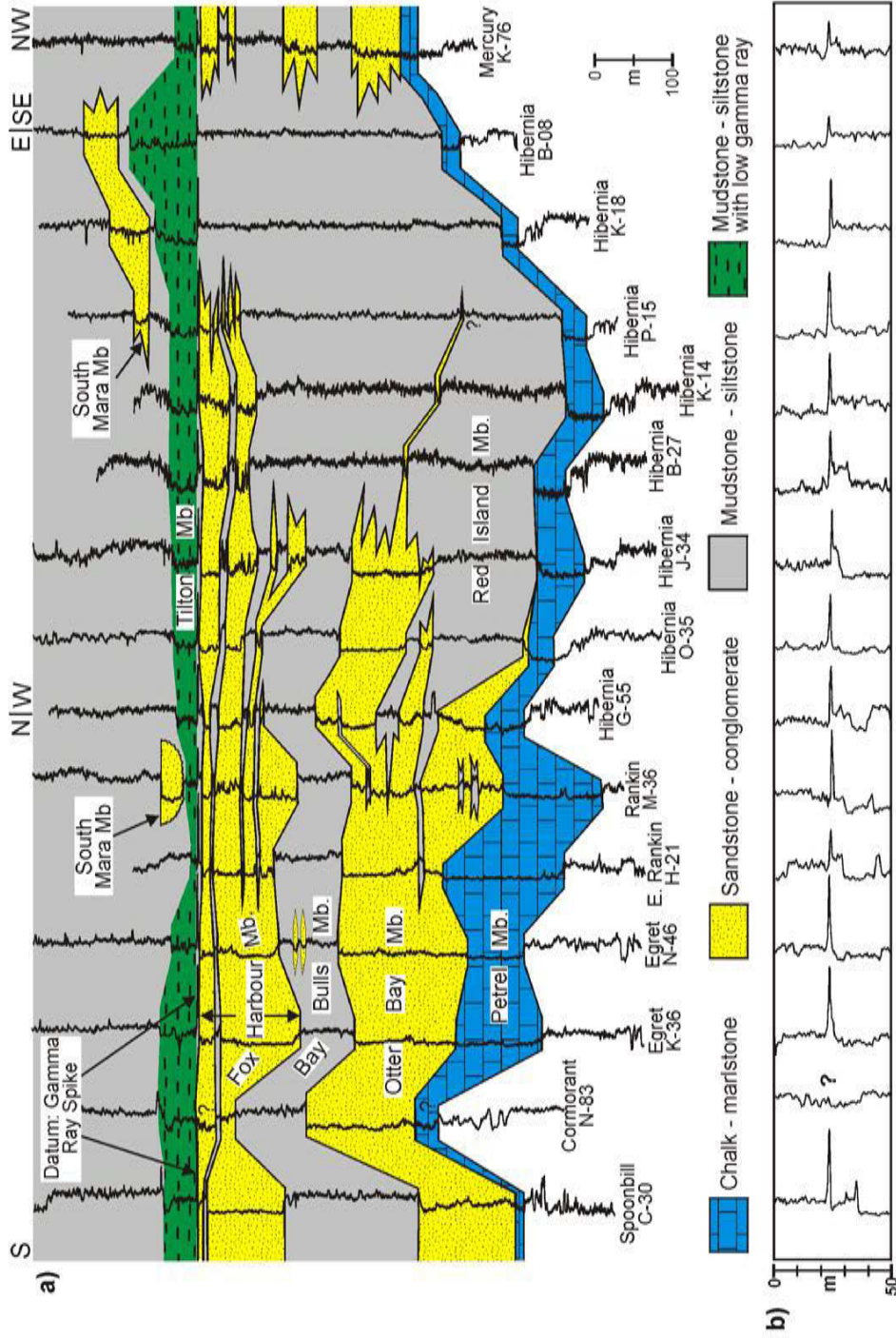


Figure 3.3. a) Lithostratigraphic correlation of the Petrel, Otter Bay, Fox Harbour, Red Island, and Bay Bulls members (Mb) of the Dawson Canyon Formation, and the Tilton and South Mara members (Mb) of the Banquereau Formation along the western margin of the basin. Datum is a prominent gamma ray spike which defines the top of the Fox Harbour Member. All wells are arranged from south to north (left to right) with Hibernia wells arranged from west to east (proximal to distal). See text for details. b) Close-up of gamma ray spike.

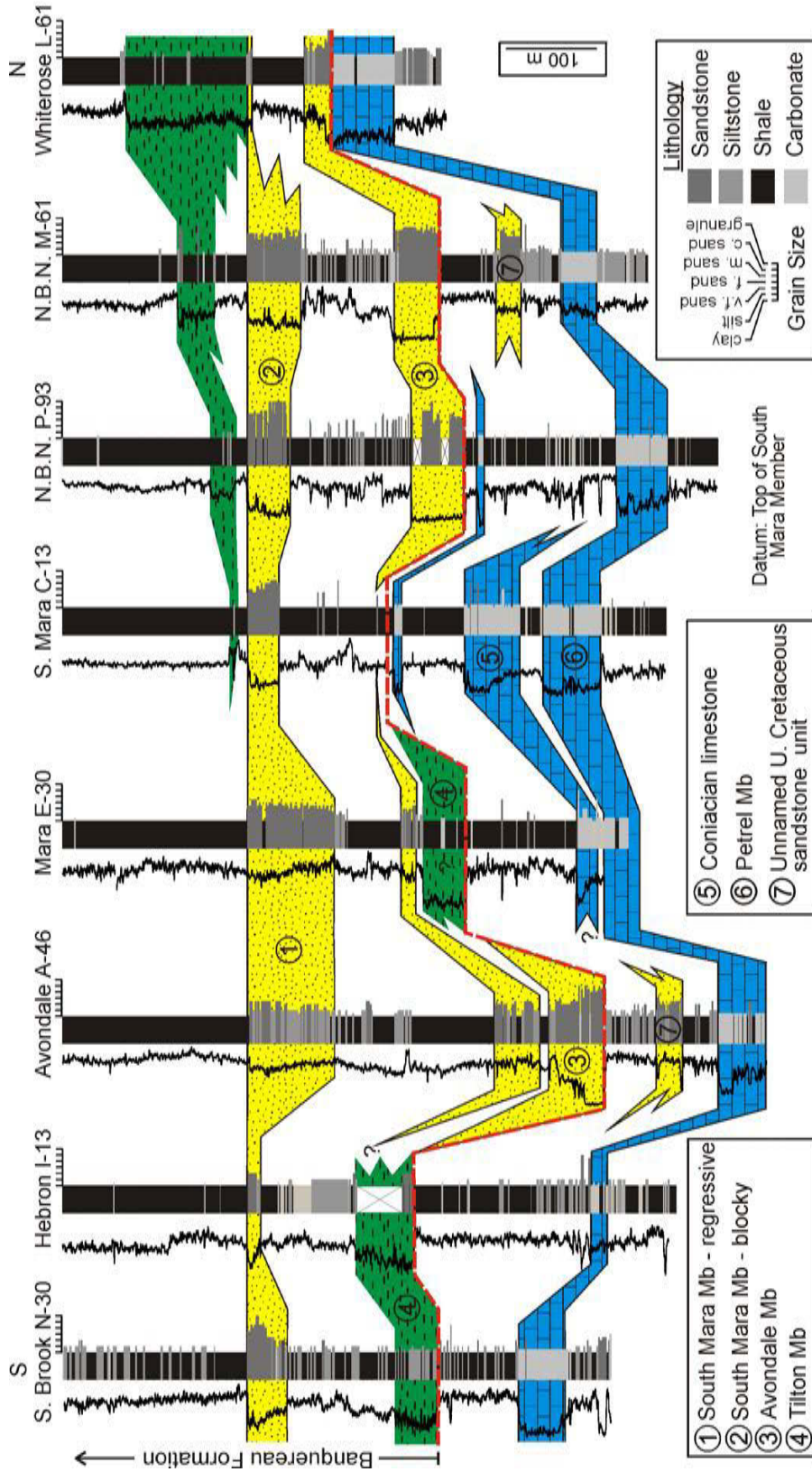


Figure 3.4. South-to-north lithostratigraphic correlation of wells located east of the latest Cretaceous offlap break (central and northern reaches of the basin - Figure 3.12b for location). Two lower Paleogene sandstone units, the Avondale and South Mara members, are widely correlatable. The exact stratigraphic relationship between the Avondale and Tilton members is uncertain. Avondale A-46 penetrates the thickest stratigraphic succession at the mouths of the Hibernia and Rankin canyons. Note also the unnamed Upper Cretaceous sands (probably Coniacian-Santonian) penetrated at Avondale A-46 and N.B.N. (North Ben Nevis) M-61. These sands were deposited seaward of the regressive Otter Bay Member, probably during the development of the Otter Bay unconformity. The orange dashed line is the Fox Harbour unconformity, and separates the Cretaceous and Tertiary stratigraphic successions.

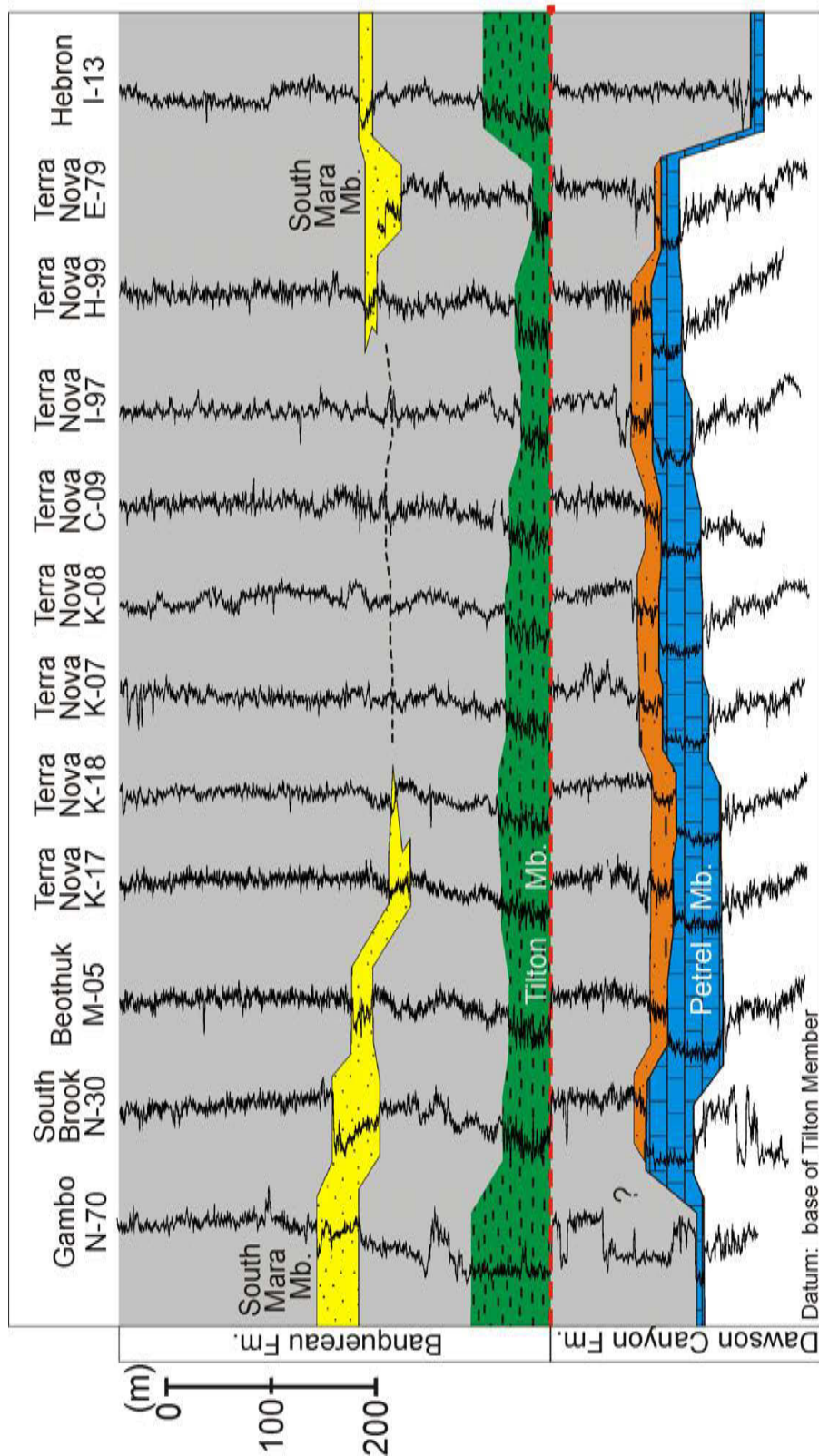


Figure 3.5. Lithostratigraphic correlation near Terra Nova.

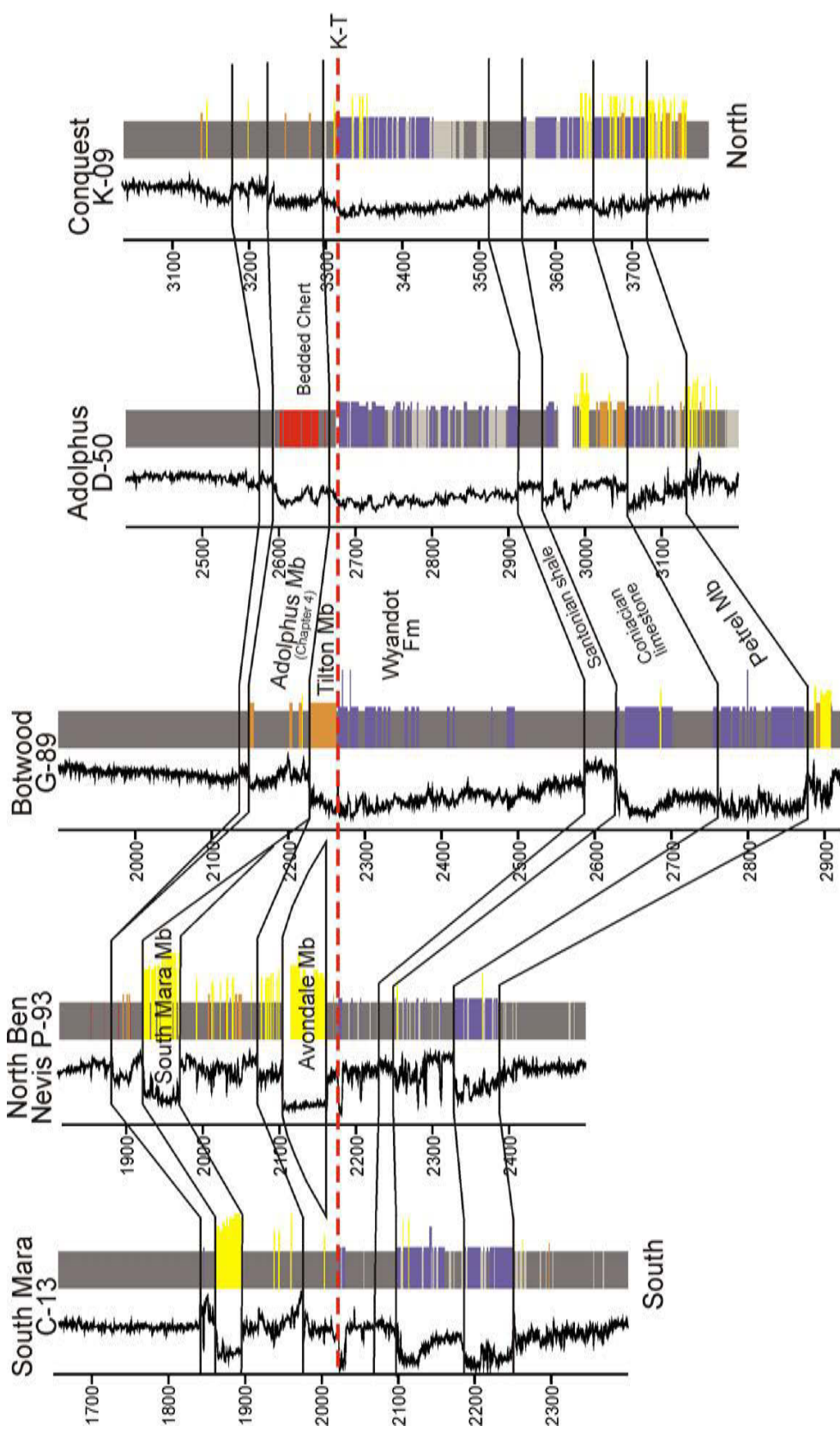


Figure 3.6. South (left) to north (right) lithostratigraphic correlation showing the increase in thickness of Upper Cretaceous strata in the northern Jeanne d’Arc Basin. Datum is the uppermost limestone (chalk) corresponding to the Wyandot Formation, closely approximating the K-T boundary. Note also the Coniacian limestone and widespread Santonian shale at the base of the Wyandot Formation. The Adolphus Member correlates above the Avondale and South Mara Members and consists of bedded chert at Adolphus D-50 (logged as shale or clay in other wells). See Figure 3.12a for location.

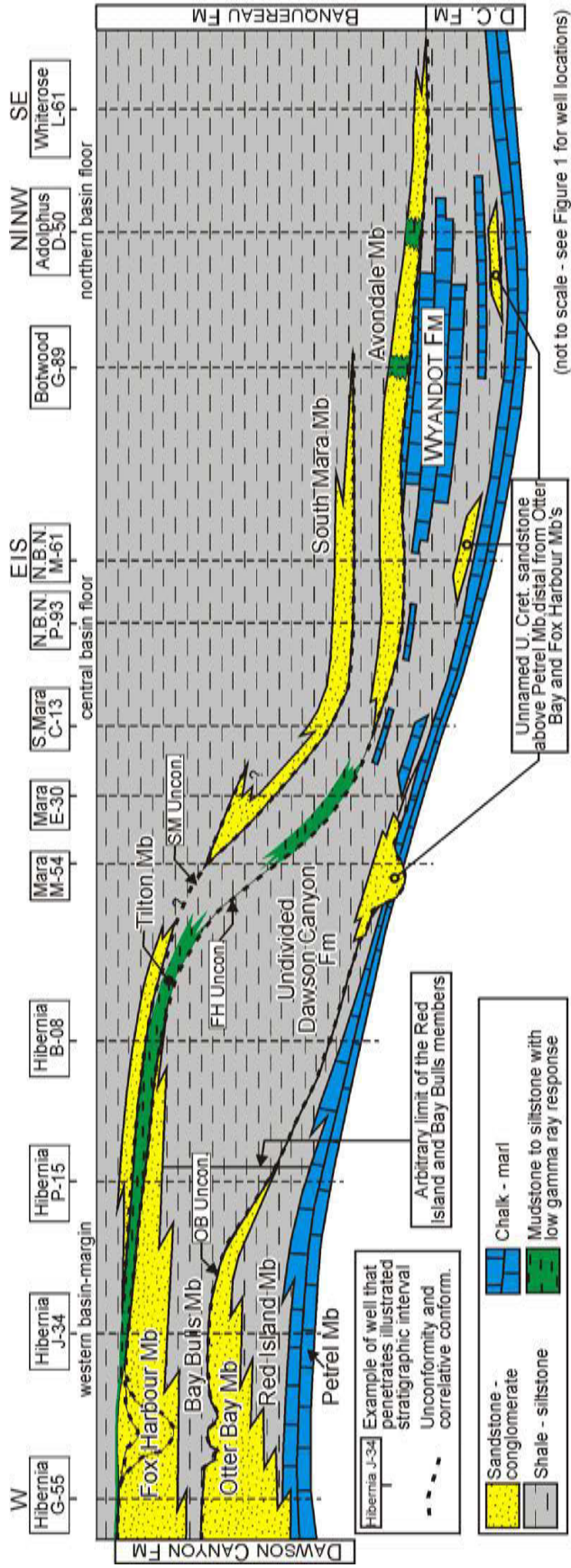


Figure 3.7. Schematic diagram illustrating the inferred stratigraphic relationships between the different members and formations identified in this and previous studies. Dashed lines are unconformities and their correlative conformities identified from wells and seismic ties. Note that the Otter Bay unconformity is located above the Otter Bay sands, and represents the probable stratigraphic situation in the southern parts of the basin where a prominent top lap surface is observed near Cormorant N-83. Near Hibernia, the Otter Bay unconformity may be located within or even below the sandstones of the Otter Bay Member. Similarly, the Fox Harbour unconformity is shown above the Fox Harbour sands, but in some areas the unconformity may be located within the upper parts of the Fox Harbour Member. This uncertainty is due to sparse palynology assemblages within the Fox Harbour and Otter Bay members. See text for details. N.B.N. = North Ben Nevis.

Red Island Member. South of Hibernia, where the Red Island Member is sometimes absent, the Otter Bay Member can directly overlies the Petrel Member (Figure 3.3). In the type section, the Otter Bay Member is Coniacian to earliest Campanian and consists of 60% sandstone and 10% granule conglomerate with a porosity ranging from 12 to more than 20%. Otter Bay sandstones commonly contain quartz and chert pebbles, shell debris, and glauconite. Grains are typically subrounded and poorly sorted. The sandstones pinch-out abruptly to the east (decreasing, for example, from 109 m thick at Hibernia J-34 to less than 15 m thick at Hibernia K-14, 3.3 km away), where they interfinger with the shale-prone Red Island Member (Figure 3.3). The lower boundary of the Otter Bay Member varies from sharp to gradational and its upper boundary with the Bay Bulls Member is usually sharply defined.

Bay Bulls Member (new)

The Bay Bulls Member (type section: Hibernia J-34, 1360 to 1482 m; Table 3.1) is a shale-prone unit found stratigraphically between the sand-prone Otter Bay and Fox Harbour members. It was originally described by de Silva (1993) as the siltstone and shale equivalent of the informal “Wyandot member” (discussed below). In the type section, the Bay Bulls Member is Campanian. It consists of grey glauconite-rich shale and siltstone, with rare sandstone stringers. It also contains scattered pyrite and traces of both siderite and plant remains.

The Bay Bulls Member was deposited with an abrupt contact above the Otter Bay Member and produces a relatively high gamma ray response. Its upper contact is gradational near Hibernia (e.g. at Hibernia J-34, Figure 3.3) and sharp farther south, where it passes abruptly up-section into fine- to very coarse-grained sandstone and pebble conglomerates of the Fox Harbour Member (e.g. at Rankin M-36, Figure 3.3). The member has been penetrated in every well along the western margin of the JDB and increases significantly in thickness to the east (e.g. 122 m at Hibernia J-34 and 225 m at Hibernia K-14).

Fox Harbour Member (formalized)

The Fox Harbour Member (type section: Hibernia J-34, 1286 – 1360 m; Table

3.1; Sinclair, 1988) is a sandstone unit located stratigraphically above the Bay Bulls Member. At the type section the member shows a well developed upward-coarsening regressive grain-size trend and consists of more than 50% sandstone and 15% granule to pebble conglomerates. Sandstones are composed primarily of quartz grains that are subrounded and poorly sorted. They are locally glauconite-rich and cherty, with sparse feldspar grains and occasional limestone stringers. In some wells (e.g. at Hibernia O-35) the Fox Harbour Member contains greater than 50% granules or larger grains and has a porosity that ranges from 12 to 20%. At the type section, the Fox Harbour member is Campanian. Some samples from the interval contain Early Paleocene palynomorph species interpreted to be contamination from cavings. A more reliable Campanian age is interpreted from palynology samples derived from sidewall cores at Hibernia O-35.

The lower boundary of the Fox Harbour Member is gradational near Hibernia and sharp farther south, near the Egret salt structure (Figure 3.3). The upper boundary is sharp, corresponding to a prominent gamma ray spike located above the regressive sandstones (Sinclair, 1988). The Fox Harbour Member shows an overall decrease in grain size and thickness to the east (e.g. 74 m at Hibernia J-34, 42 m at Hibernia P-15, less than 5 m at Hibernia C-96).

3.2.2 *Wyandot Formation*

The Wyandot Formation, consisting of pelagic coccolithic/foraminiferal chalks and marlstones, is widely distributed on the Scotian Shelf, but developed only locally in the JDB. The formation, originally termed the “Wyandot Chalk” by McIver (1972), was formally defined by Jansa and Wade (1975b), who described it as “a dominantly chalk formation with marl and calcareous shale interbeds”.

In the JDB, the Wyandot Formation is thickest to the north, near Botwood G-89, Adolphus D-50 and 2K-41, and Conquest K-09, an area outlined in Figure 3.8b. In this area, the formation is similar to the type section on the Scotian Margin. Gamma ray logs have an overall upward-decreasing character, corresponding to a basal marl and calcareous shale interval passing up-section into an interval of cleaner chalky limestones (e.g. at Adolphus D-50, 2674 - 2910 m). A Santonian shale unit (part of the Dawson Canyon Formation) commonly underlies the Wyandot Formation (e.g. at Adolphus D-50,

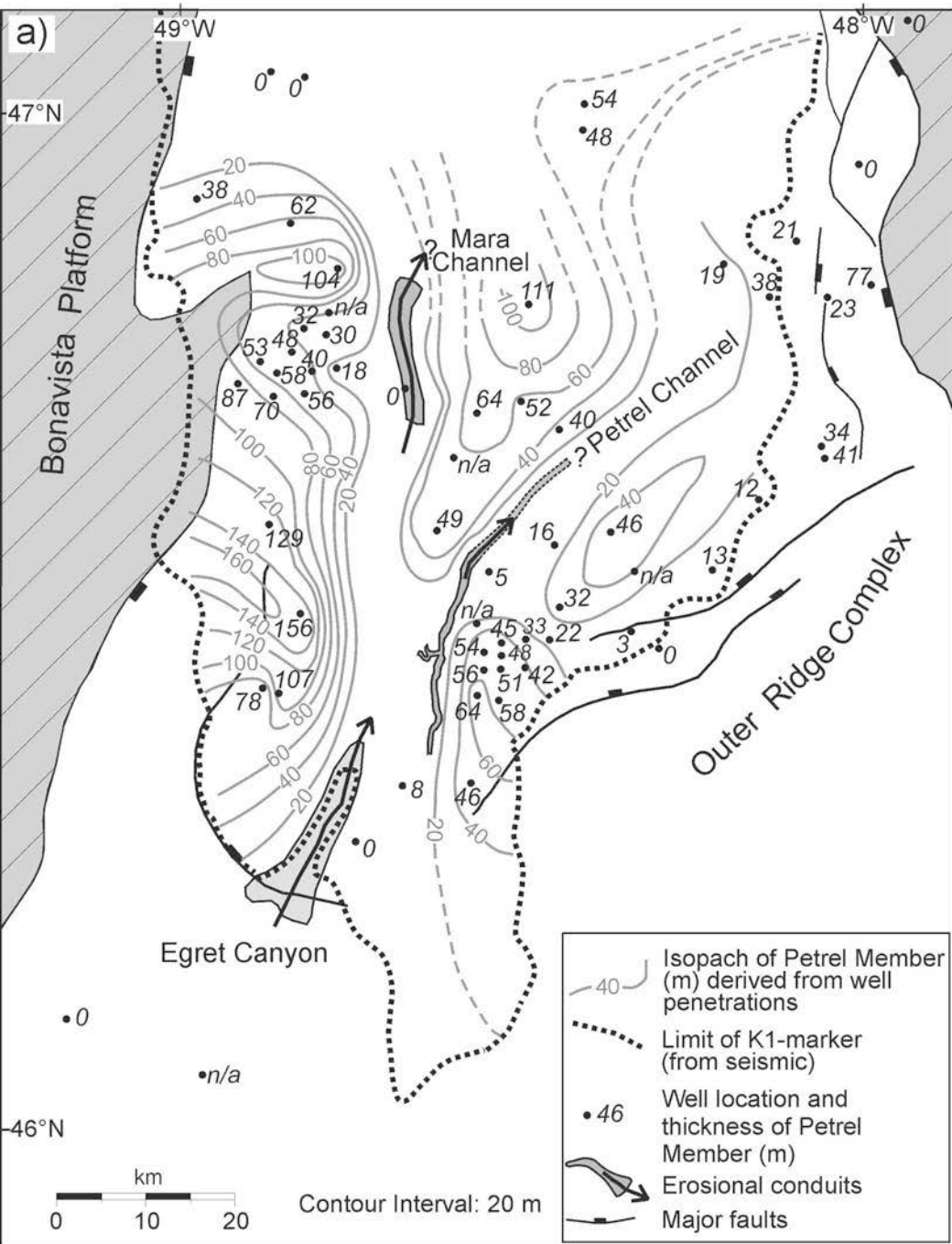


Figure 3.8. a) Contoured isopach map of the Petrel Member (modified from Shimeld et al., 2000), showing the erosional features inferred to have developed during the Otter Bay unconformity. Note the locations of the Egret Canyon and the Petrel and Mara channels indicating a dominantly northward sediment transport direction. Note also the correspondence between channel locations and the thickness distribution of the Petrel Member (see next page for additional caption)

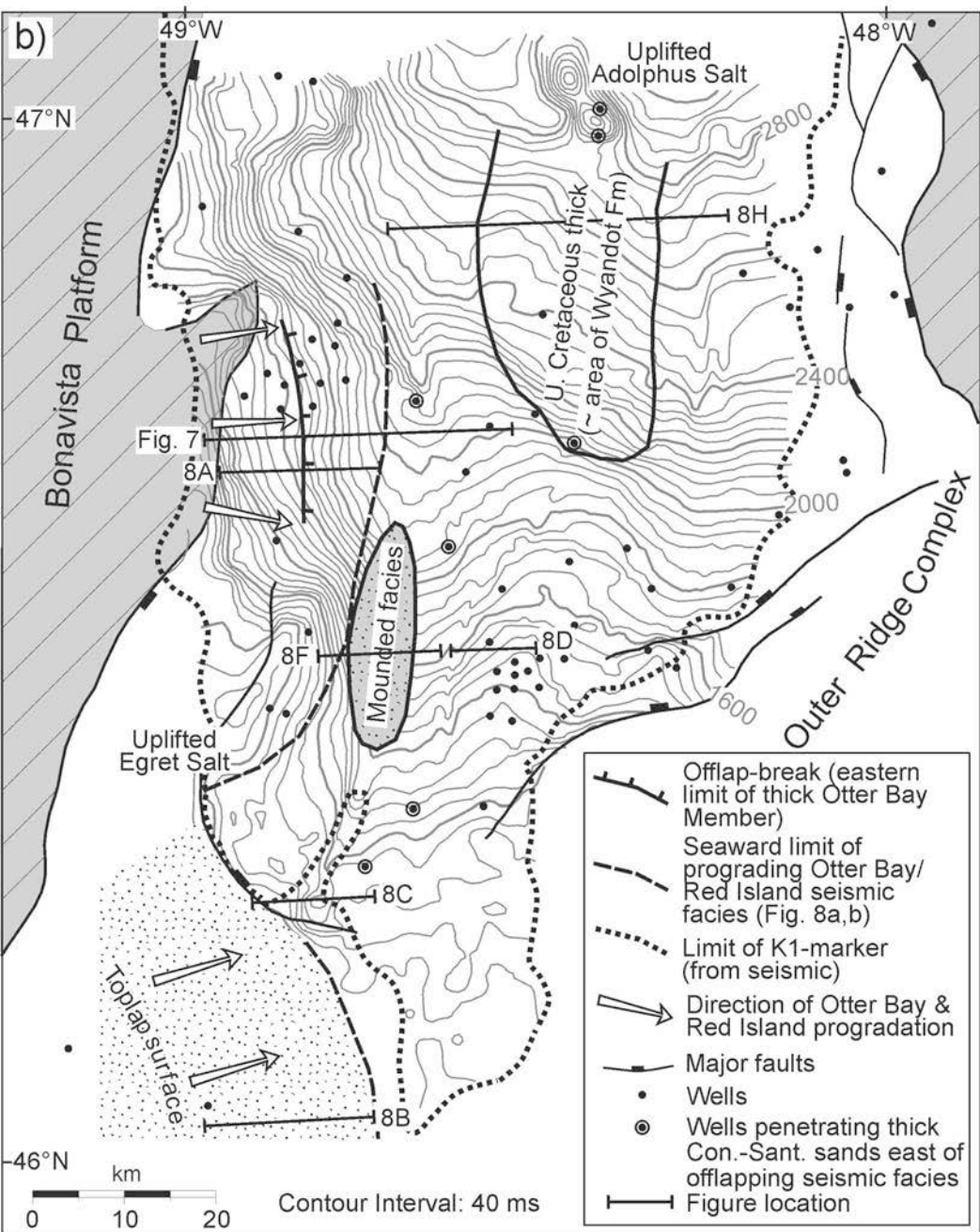


Figure 3.8. b) Time-structure map of the K1-marker. The Otter Bay unconformity correlates to a prominent toplap surface south of the Egret fault (stipple). Map shows the distribution of the mounded seismic facies at the mouth of the Egret Canyon, the thick Upper Cretaceous package developed north of the Trans-Basin Fault Trend (corresponding closely to distribution of the Wyandot Formation), and the maximum progradation of the Otter Bay Member and equivalent finer-grained sediments. Also shown is the location of the offlap break near Hibernia and the wells which penetrate Upper Cretaceous sandstones to the east of the progradational seismic facies (corresponding to the Otter Bay/Red Island members). The locations of line drawings in Figure 8 are indicated. Erosional and depositional limits of the K1-marker are from Edwards et al. (2000).

2910 - 2945 m - Doeven, 1983).

At Botwood G-89, the upper boundary of the formation is sharp and unconformable (2265 m). In other locations, the chalky limestone is overlain by a thin Maastrichtian shale (e.g. at Adolphus D-50, 2660 – 2674 m) which is in turn unconformably overlain by Danian shale (Doeven, 1983). A calculated sedimentation rate of 1.5 to 2.0 cm per thousand years led Doeven (1983) to suggest that late Santonian to middle Campanian chalk deposition at Adolphus D-50 took place in deeper water, farther off shore than correlative chalk on the Scotian Margin.

South of Botwood G-89, the Wyandot Formation is much thinner (e.g. at North Ben Nevis P-93, 2176 – 2184 m) or absent (e.g. at West Ben Nevis B-75). Some wells penetrate a relatively thick Coniacian limestone that could also be regarded as the Wyandot (e.g. at South Mara C-13, 2099-2156 m, shown in Figure 3.4) even though it appears to be older than the chalky limestone recognized elsewhere.

3.2.3 *Banquereau Formation*

The Banquereau Formation, formally defined by McIver (1972), consists generally of deep-neritic to bathyal shales with minor chalks, siliceous mudstones, and locally developed sandstone units (McAlpine, 1990). The formation extends for the entire Tertiary succession above the Wyandot Formation, and until now has never been formally subdivided.

In the JDB, an interval containing outer neritic to bathyal sandstone and siltstone is found stratigraphically above the Dawson Canyon and Wyandot formations, within the lower parts of the Banquereau Formation (Thomas, 1994). McAlpine (1990) designated this sandy interval, including intercalated shale-prone intervals, as the “South Mara unit”. In this study, two distinct sandstone units are recognized near or at the base of the Banquereau Formation (Figures 3.2, 3.4, 3.7). The lower sandstone unit is defined here as the Avondale Member and the upper sandstone unit is designated the South Mara Member, a formalization of the 31 m thick lower Tertiary sandstone unit originally described by Sinclair (1988) at South Mara C-13 (1864-1895 m).

In addition to the sandstone members, a siltstone and shale dominated unit found directly above the Dawson Canyon Formation is formally defined. This unit, herein

referred to as the Tilton Member of the Banquereau Formation, was originally described by the Canada-Newfoundland Offshore Petroleum Board (1998) as the “Paleocene Porcelaneous Mudstone”, but it appears to be more lithologically diverse than their informal nomenclature implies, and hence it is renamed here.

Avondale Member (new)

The Avondale Member (type section: Avondale A-46, 1760 – 1823 m; Table 3.2) consists of very fine- to coarse-grained sandstones that were deposited east of the thickest Upper Cretaceous deposits, unconformably above the Dawson Canyon Formation. Sidewall cores in Avondale A-46 indicate loosely consolidated fine- to very coarse-grained clean sandstones (Mobil et al., 1988). The sandstones are poorly to well sorted, with subangular to subrounded grains and traces of glauconite. Biostratigraphic analyses indicate that the Avondale Member is Danian at the type section (Table 3.2, Fensome, 1996). The Avondale Member is 61 m thick at North Ben Nevis P-93, where it consists of 70% sandstone with a 26% average porosity (Husky-Bow Valley et al., 1984). The member has been penetrated as far north as Whiterose L-61, where it consists of 31 m of medium- to well-sorted, very fine- to medium-grained sandstone. In some areas, the Avondale Member is laterally discontinuous, with thick sandstone pinching out or shaling out over relatively short distances. For example, it is 61 m thick at North Ben Nevis P-93 (2103 - 2164 m), but pinches out completely at South Mara C-13, less than 5 km away (Figure 3.4).

The Avondale Member usually produces a cylindrical (“blocky”) gamma ray response (Figure 3.4), although at the type section, where the member is 63 m thick, only the lower 25 m produces such a response. The lower boundary of the member is always sharp and unconformable, whereas the upper boundary can be gradational, as in the type section, or can be sharp, as at North Ben Nevis P-93.

Tilton Member (renamed, formalized)

The Tilton Member (type section: Hibernia O-35, 1277-1309 m, Table 3.2) is a grey to brown siltstone- and shale-dominated unit that produces a distinctive low, bell-shaped, and less commonly cylinder-shaped, gamma ray response (Figures 3.3, 3.4). At

Table 3.1. Summary of the members of the Dawson Canyon Formation in the Jeanne d'Arc Basin.

	Petrel Member	Red Island Member	Otter Bay Member	Bay Bulls Member	Fox Harbour Member
Proposed by:	Jansa & Wade (1975b); Type section not declared	This study	Boudreau et al. (1986), Sinclair (1988)	This study	Sinclair (1988)
Derivation of Name:	Small seabird	Red Island: located in Placentia Bay, Newfoundland	Otter Bay: located on the southern shore of Newfoundland	Bay Bulls: port community in Newfoundland	Fox Harbour: community in Newfoundland
Type Section:	Gannet O-54 (1589.8 – 1664.8 m) (proposed herein)	Hibernia J-34 (1591-1713 m)	Hibernia J-34 (1482-1591 m)	Hibernia J-34 (1360 – 1482 m)	Hibernia J-34 (1286 – 1360 m)
Dominant Lithology:	microcrystalline limestone	mudstone to siltstone	sandstone to conglomerate	mudstone to siltstone	sandstone to conglomerate
Age at type section:	Turonian	Turonian to Santonian	Coniacian to early Campanian	Campanian	Late Campanian

Table 3.2. Summary of the members in the lower part of the Banquereau Formation, Jeanne d'Arc Basin.

	Tilton Member	Avondale Member	South Mara Member
Proposed by:	This study	This study	Sinclair (1988)
Derivation of Name: (etymology)	Named after a port community in Newfoundland	Named after the type section in Avondale A-46 which was named after a port community in Newfoundland	Named after type section at South Mara C-13. "Mara" is Gaelic for "marine"
Type Section:	Hibernia O-35 (1277 – 1309 m)	Avondale A-46 (1760 – 1823 m)	South Mara C-13 (1862-1895 m)
Reference Section:	King's Cove A-26 (1169 – 1218 m)	North Ben Nevis P-93 (2103 – 2164 m)	Mara E-30 (1682 - 1775 m)
Dominant Lithology:	mudstone to siltstone	very fine to coarse-grained sandstone	very fine to coarse-grained sandstone
Age at type section:	Danian	Danian	Ypresian

the type section, the Tilton Member is Danian and is glauconitic and slightly dolomitic. The member is commonly siliceous and can contain foraminifera, shell fragments, and layers of chert (e.g. at King's Cove A-26, 1169-1218 m). The base of the Tilton Member closely corresponds to the beginning of a widespread Paleogene radiolarian event documented by Thomas (1995), which may account for the siliceous character of the unit. A 2.5 m core recovered at Hibernia C-96 (from the interval between 1670.0-1677.3 m) shows a well-indurated interval of grey siliceous shale with a 20 cm clean silica-cemented sandstone bed. At Mara E-30 (1874-1922 m) light to dark grey chert fragments are observed in cuttings samples. These fragments have a conchoidal fracture and exhibit microporosity, which is also observed in the core at Hibernia C-96.

The Tilton Member is best developed both along the western margin of the basin and farther south, near Terra Nova. On the western margin, the lower boundary of the Tilton Member is a prominent high gamma ray spike which also defines the top of the Fox Harbour Member (Figures 3.3a, b). The gamma spike ranges in magnitude from 260 API units at Egret K-36 (782 m) to 90 API units at Hibernia B-08 (1743 m), on average twice as high as the mean value in Upper Cretaceous shale. The origin of the spike is uncertain due to limited sampling and lack of spectral gamma ray measurements. The spike usually corresponds to a dark shale or siltstone and, in some wells, to a chert layer (e.g. at Mercury K-76, 1594 m and East Rankin H-21, 801 m). Near Terra Nova, where the gamma ray spike is absent, the Tilton Member sharply overlies higher gamma ray shales of the Dawson Canyon Formation. The upper boundary of the Tilton Member is usually gradational, although where it is unconformably overlain by sandstone along the western margin of the basin, the upper boundary can be sharp (e.g. at Rankin M-36, 1039 m).

Above the Tilton and Avondale members, and below the South Mara Member (described below), there is a relatively conformable succession of interbedded shale, siltstone, and rare sandstone, with a cumulative thickness that locally exceeds 130 m (e.g. at North Ben Nevis P-93, 1971 – 2103 m; Figure 3.4).

South Mara Member (range restricted, formalized)

The South Mara Member (type section: South Mara C-13, 1862-1895 m; Table

3.2) consists of fine- to very coarse-grained sandstone (sometimes unconsolidated sands) that lies unconformably to conformably above the shale-prone unit deposited above the Avondale or Tilton members. In the type section, the South Mara Member consists of 80% sandstone with quartz grains that are subrounded and well sorted to moderately well sorted (and commonly oil-stained). Glauconite (which locally makes up more than 40% of the sandstone) and quartz pebbles are also common.

At the type section, the South Mara Member is Ypresian and was deposited in upper bathyal water depths (Thomas, 1994, 1995). At South Brook N-30, the member is 43 m thick, and consists of light brown to greenish fine- to coarse-grained sandstone with occasional quartz and chert pebbles and minor conglomerate. At Mara E-30 (1682 - 1775 m; Figure 3.4) the member is 93 m thick and consists of a grey to green argillaceous sandstone (bordering on arenaceous shale near the base) with abundant glauconite. Here, and at Avondale A-46, the member contains carbonaceous plant remains. A short core recovered from Avondale A-46 (1464.5 to 1465.1 m) shows a light green, heavily bioturbated, fine-grained sandstone with a siderite nodule and a thin, well indurated chert layer (about 9 cm thick) near its base.

The South Mara Member can be further subdivided according to its gamma ray character. It produces a cylindrical gamma ray response in wells that penetrate it farthest to the north (e.g. at North Ben Nevis P-93, 1922-1970 m and the type section; Figure 3.4). Here, the member has sharp upper and lower boundaries. In other regions, the member produces a funnel-shaped gamma ray response with an upward-coarsening grain size trend (e.g. at South Brook N-30, 818 – 861 m). The regressive character is best developed adjacent to the latest Cretaceous shelf-slope system (near Avondale A-46 and Mara E-30) and further south near Terra Nova (e.g. at South Brook N-30). Here, the lower boundary of the member is gradational, and the upper boundary is sharply defined.

3.3 Seismic stratigraphy, unconformities and depositional settings

3.3.1 Petrel, Otter Bay, and Red Island members

The Petrel Member corresponds in most areas to a regional seismic event, referred to here as the K1-marker. This marker shows significant regional variability in amplitude and character, although it can still be widely mapped. Along the western basin margin,

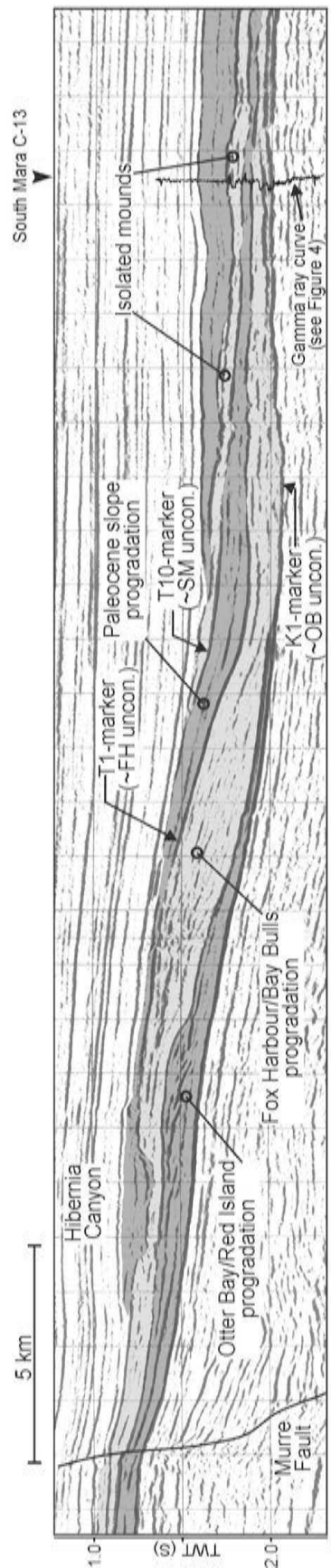
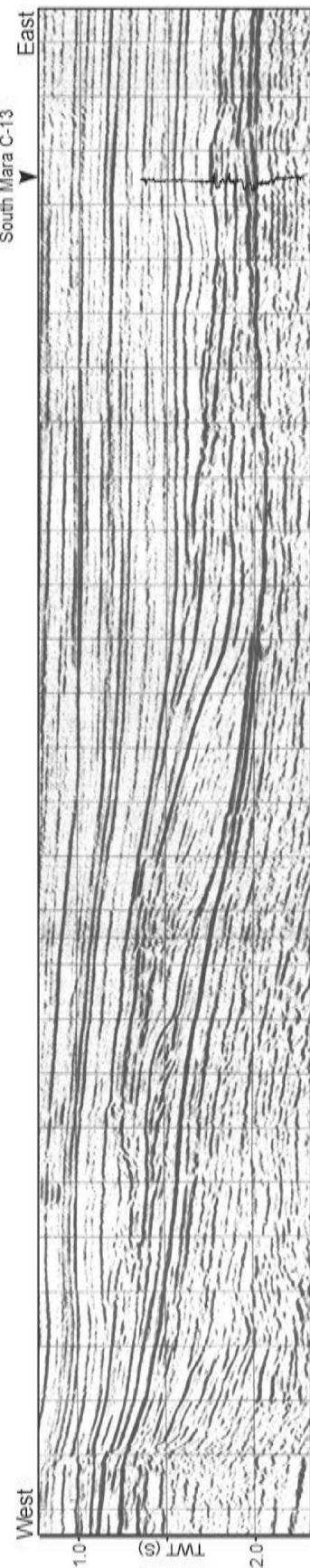


Figure 3.9. a) Uninterpreted and b) interpreted west-east seismic profile across the central Jeanne d'Arc Basin, near Hibernia (line 83-5052). Western portion of profile corresponds to the prograding Otter Bay and Fox Harbour members and their finer-grained equivalents. Note that the Hibernia Canyon incises the shelf in this region. See Figure 3.8b for location.

the K1-marker forms a prominent downlap surface for the overlying Otter Bay Member and the shale-prone laterally equivalent Red Island Member (e.g. Figures 3.9, 3.10a, b). The marker has been mapped west of the Murre fault where it corresponds to a clinoform of the early Otter Bay/Red Island progradational succession.

The Otter Bay and Red Island members are thickest in two areas: near Hibernia and south of the Egret fault. Near Hibernia, the Otter Bay and Red Island members correspond to a wedge-shaped seismic package that downlaps and merges with the K1-marker (Figures 3.9, 3.10a). Internally, this seismic unit consists of low-angle, shingled clinoforms that indicate an eastward sediment transport direction. Figure 3.8b shows the maximum limit to which the Otter Bay and Red Island seismic package can be recognized before it thins below seismic resolution and merges with the K1-marker. A poorly developed offlap break (Figures 3.8b, 3.10a) divides the Hibernia wells into two sets: a western group with thick Otter Bay sandstone, and an eastern group with much thinner or no sandstone (Figure 3.3).

South of the Egret fault, the Otter Bay and Red Island members produce a prominent shingled seismic pattern, with an east to northeast sediment transport direction indicated by the clinoforms (Figure 3.10b). The upper boundary of these clinoforms is a prominent erosional toplap surface lacking a discernible offlap break (Figure 3.10b).

Both near Hibernia and south of the Egret fault, seismic clinoforms have heights of less than 200 m, suggesting that the western and southern margins of the basin were relatively shallow. Paleobathymetric interpretations from benthic foraminifera provide corroborating evidence, suggesting outer neritic (100-200 m) to upper bathyal (200-600 m) water depths (Thomas, 1994).

Seismic architecture, together with paleobathymetric and well data, suggest a deltaic depositional setting for the Otter Bay and Red Island members (following de Silva, 1993). Deltas are interpreted to have prograded across a relatively shallow ramp-margin with clastic sediments derived from the Bonavista Platform (Sinclair, 1988) and south of the Egret fault. East of the Otter Bay and Red Island members, calcareous sediments continued to accumulate in areas far removed from clastic input (e.g. Coniacian limestones in South Mara C-13, 2099 – 2156 m; Thomas, 1994). Where preserved, the limestones generate a second, laterally restricted, high- amplitude seismic

event directly above the K1-marker (Figure 3.9, penetrated by South Mara C-13).

3.3.2 *Otter Bay Unconformity*

The prominent toplap surface observed above the Otter Bay Member south of the Egret fault (Figure 3.8b) corresponds to a sharp lithological boundary between Otter Bay sandstone and overlying Bay Bulls shale at Cormorant N-83 (Figures 3.1, 3.3). This toplap surface also shows evidence of channeling and the development of a canyon just north of the Egret fault, and is therefore interpreted as a regional unconformity, referred to herein as the Otter Bay unconformity.

Four types of evidence bracket the age of the Otter Bay unconformity. First, the Mara Channel, an erosional feature that is believed to have acted as a conduit for sediment transport during the development of the unconformity, has fill dated as Santonian in Mara M-54. Second, sediment above the prominent toplap surface (and above the Otter Bay Member) in the southern JDB is Santonian (e.g. at Cormorant N-83). Third, the Petrel Member, into which the Mara Channel, and several other erosional features are incised, underlies the unconformity and is Turonian. Fourth, Coniacian to Santonian sandstones were penetrated by several wells in the central parts of the basin. The sandstones are interpreted to have been transported into the basin during the development of the Otter Bay unconformity (e.g. at North Ben Nevis M-61, 2131–2162 m). Based on these lines of evidence, the unconformity developed in the Coniacian or Santonian.

3.3.3 *Late Cretaceous submarine fans*

North of the Egret fault, and east of the mapped limit of the Otter Bay/Red Island progradational seismic facies, the Otter Bay unconformity merges with the K1-marker, causing the two surfaces to be seismically indistinguishable. The contours of the K1-marker (Figure 3.8b) show three significant erosional features associated with the Otter Bay unconformity: the Egret Canyon, the Petrel Channel and the Mara Channel (Figure 3.8a). These erosional features are interpreted to have transported sediment from the subaerially exposed southern parts of the basin, towards deeper water to the north, where the K1-marker is overlain by concordant to subtly mounded seismic facies (Figure

Figure 3.10. Line drawings of Upper Cretaceous seismic facies observed in the Jeanne d'Arc Basin. Progradation of Otter Bay and Red Island members along western (a) and southern (b) margins of the basin. Note the prominent toplap surface (b) that corresponds to the Otter Bay (OB) unconformity. The Egret Canyon (c) and Petrel Channel (d) are erosional features related to the Otter Bay unconformity. Dip line (e) and strike-line (g) across prominently progradational shelf-slope system along the western margin of the basin, corresponding to the Fox Harbour and Bay Bulls members of the Dawson Canyon Formation. Note the mounded seismic facies underlying the clinofolds (f). The T1-marker is the seismic event that corresponds approximately to the Fox Harbour (FH) unconformity observed in wells. In the northern part of the basin, Upper Cretaceous sediment consisting of chalk, mudstone, and rare sandstone, form a depositional lens-shaped thick (h) eroded by two broad scours at the Fox Harbour unconformity. See Figures 3.8b and 3.12b for locations and text for details.

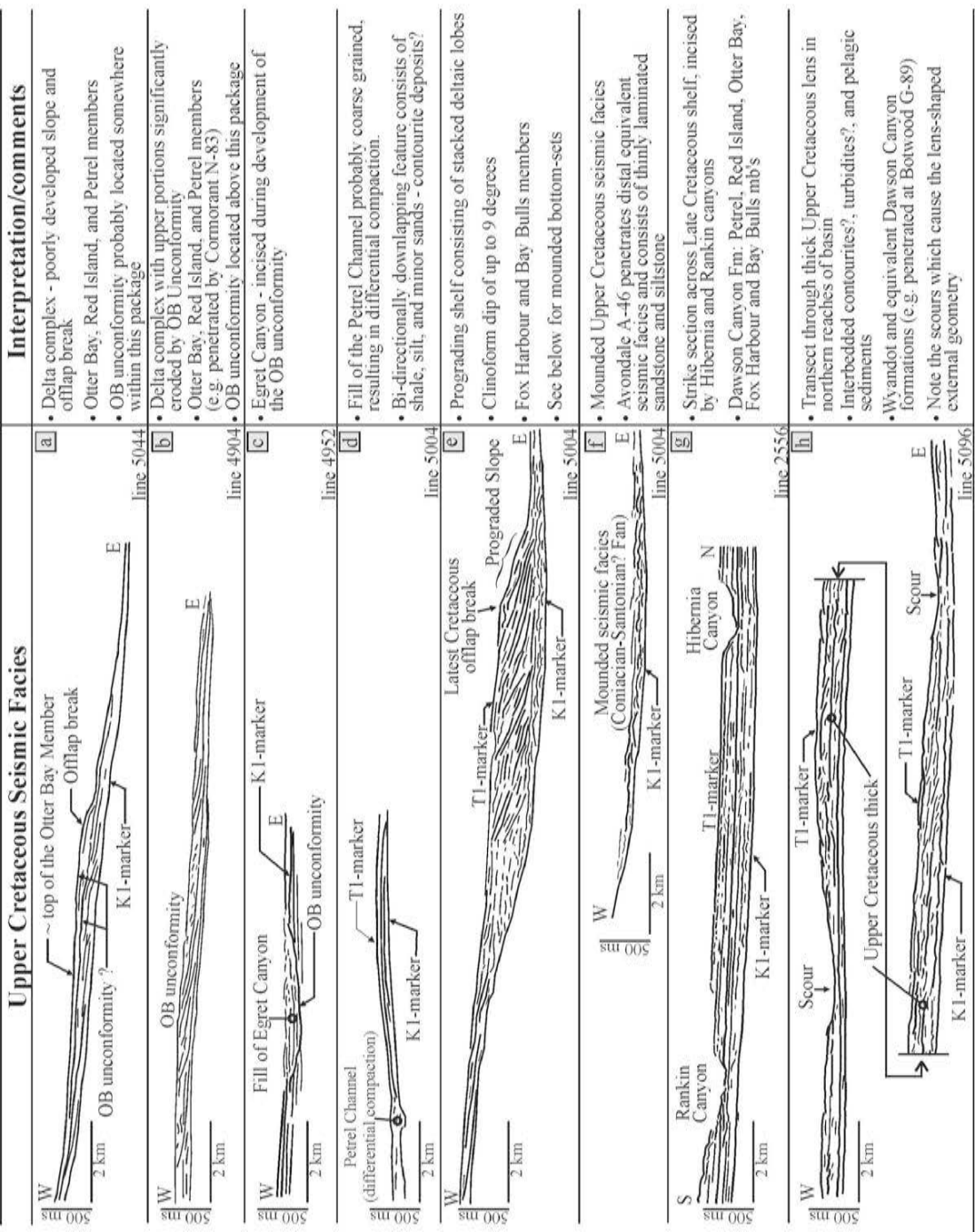


Figure 3.10. Continued (see previous page for caption)

3.10h). The Petrel and Mara channels are interpreted to have a submarine origin, although water depths are unlikely to have been greater than 400 m.

Based on 3-D seismic interpretations, the Petrel Channel is a narrow (0.4 to 1.5 km), low sinuosity, branching erosional channel, likely filled with coarser-grained clastic sediments that, after compaction, created the present-day positive relief now observed above the channel (Figures 3.10d, 3.11). The well rounded, medium- to coarse-grained quartz sandstone penetrated at North Ben Nevis M-61 (2131–2162 m; Figure 3.4) was probably transported through the Petrel Channel. Other Coniacian-Santonian sandstone units further north (e.g. Adolphus D-50, 2986 - 3004 m; Doeven, 1983) may have a similar origin. Mud logs at Mara M-54 indicate that the fill of the Mara Channel is composed of coarse-grained sandstone to granule and pebble conglomerate (2255 – 2312 m). The sequence at Mara M-54 also indicates that the Petrel Member is absent, presumably eroded away. The close correspondence between the location of erosional features and regions where the Petrel Member is thinned or absent (Figure 3.8a, b) suggests that the thickness distribution of the Petrel Member is largely the result of erosion/dissolution during the development of the Otter Bay unconformity.

Just north of the Egret Canyon, directly above the K1-marker, there is an elongated seismic package consisting of mounded, bi-directionally downlapping, and in places hummocky to contorted seismic facies (Figures 3.8b, 3.10f). A core retrieved from Avondale A-46 (1881-1899 m; Figure 3.4), a well penetrating the northernmost fringe of this feature, reveals Coniacian-Santonian thinly laminated sandstone, siltstone and shale interpreted as fine-grained turbidites (Mobil et al., 1988). The core also contains an interval of soft sediment deformation interpreted as a slump. The elongated seismic feature is interpreted as a small submarine fan that trends sub-parallel to the toe of the western Otter Bay/Red Island delta complex. The sediment source for this feature is unclear. Agrawal et al. (1995) suggested that the mounds were formed by sediment shed from the west during Late Cretaceous clinoform progradation. The similar orientations of the Egret Canyon and the elongated fan make it equally plausible that the Egret Canyon was the conduit for sediment forming these mounds.

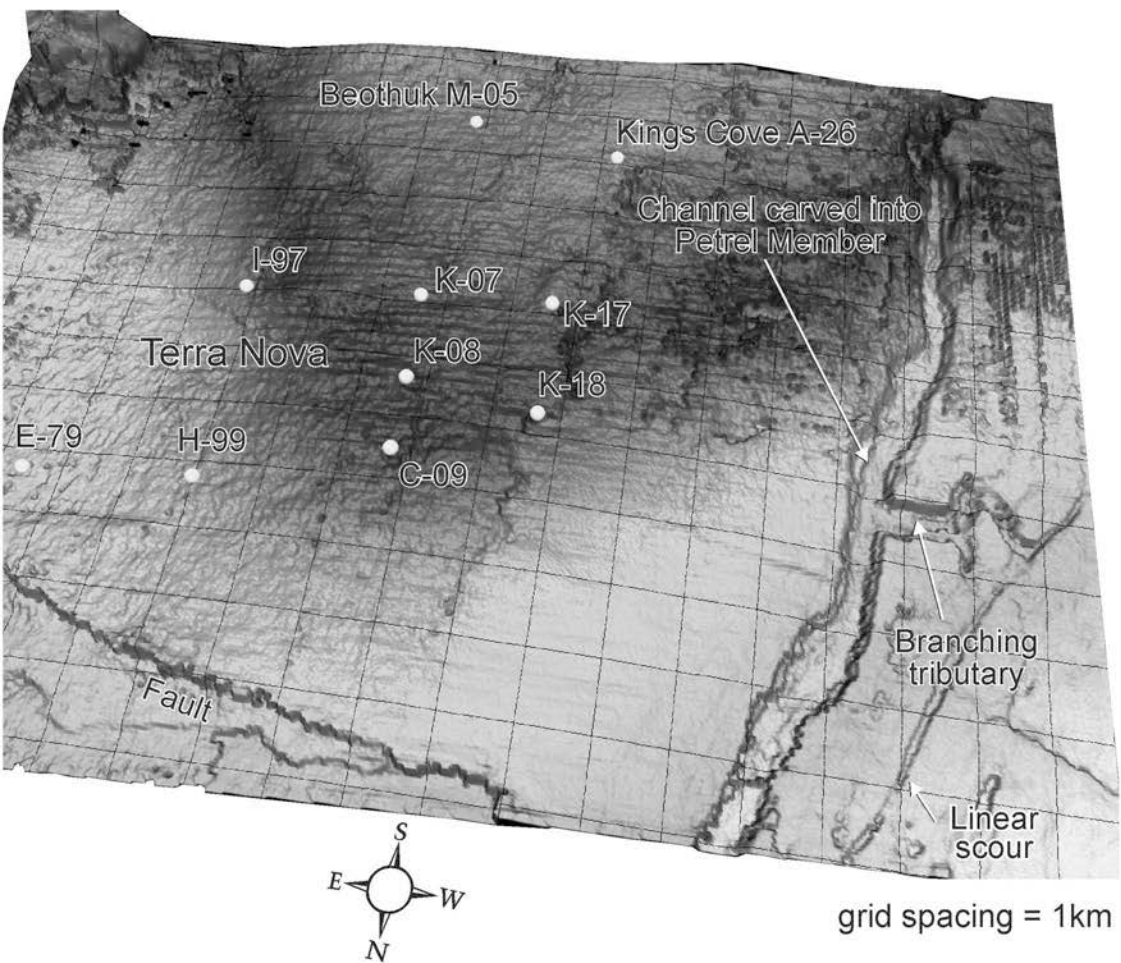


Figure 3.11. Perspective view of the K1 - marker time-structure map from the Terra Nova 3-D seismic survey. The marker was correlated to the base of the north-trending Petrel Channel. The Petrel Channel is interpreted as a submarine channel that eroded the Petrel Member during the development of the OB Unconformity (above the Otter Bay Member on the shelf). The conspicuous right-angle tributary probably indicates that small-scale faults or fractures influenced its orientation.

3.3.4 *Bay Bulls and Fox Harbour members*

Near Hibernia, the Bay Bulls Member ties to seismic events that onlap and/or drape the top of the Otter Bay/Red Island delta complex. Here, the member is interpreted to have been deposited during a period of marine flooding, blanketing the underlying Otter Bay delta plain. Where the diachronous Bay Bulls Member and undivided Dawson Canyon Formation thicken towards the east, seismic facies consist of moderately continuous, low to moderate amplitude, eastward-prograding oblique (Figure 3.10e) to sigmoidal (Figure 3.9) clinoforms. In contrast, the Fox Harbour Member corresponds to relatively continuous, medium amplitude reflections that form the topsets of the Bay Bulls equivalent offlapping seismic facies (Figure 3.10e).

This seismic architecture, combined with well data, indicates that the Fox Harbour Member was deposited on a sandy progradational deltaic platform or shelf, varying from low energy sedimentary regime to the north (sigmoidal clinoforms), to a higher energy sedimentary regime further south (oblique clinoforms) (see Mitchum et al., 1977b). During its progradation, deposition of the Bay Bulls Member and the distal undivided Dawson Canyon Formation continued seaward (to the east) in a marine prodeltaic/slope setting. The eastern limit of progradation is shown in Figure 3.12.

3.3.5 *Wyandot Formation*

The Wyandot Formation corresponds to seismic facies ranging from subtly mounded, discontinuous reflections with minor shingling, to continuous, moderately high amplitude reflections that stack sub-concordantly (Figure 3.10h). These seismic facies are located within a broad seismic package with a lens-shaped external geometry, restricted to the northern parts of the basin, where the Upper Cretaceous interval thickens significantly (Figure 3.8b). Wells that penetrate this region have the thickest Wyandot Formation. The lens-shaped external geometry results, at least in part, from two broad, north-trending erosional valleys or scours associated with the overlying Fox Harbour unconformity (described next). Similar erosional features above Upper Cretaceous and Danian chinks in the North Sea were interpreted to form from a mid-Paleocene drainage system (Clausen and Huuse, 1999).

Given that the water depths for the northern JDB were probably upper bathyal

during the deposition of the Wyandot Formation (Doeven, 1983), it is unlikely that this region was ever subaerially exposed, and therefore these features are interpreted to have a submarine origin. Erosion and/or dissolution from ocean currents, perhaps enhanced during or just prior to the development of the Fox Harbour unconformity on the shelf, is considered a plausible mechanism for the erosional scours in the JDB. Such a scenario may have developed during the re-organization of tectonic plates, as the British Isles decoupled from North America, and/or Greenland separated from Labrador, causing short-lived modification/intensification in ocean currents. Alternatively, these erosional scours may have developed during an early bypass phase of gravity currents, indicating that reservoir sands might have been transported quite far north in the JDB, where well control is poor.

3.3.6 *Fox Harbour Unconformity*

A significant stratigraphic gap that encompasses the entire Maastrichtian and upper Campanian is recognized near the top of the Fox Harbour Member along the western margin of the JDB (e.g. at Hibernia J-34 and Hibernia O-35). This gap, which represents about 12 million years, is referred to herein as the Fox Harbour unconformity, but has also been called the “base Tertiary unconformity” (e.g. Sinclair, 1988; de Silva, 1993). The Fox Harbour unconformity is commonly placed at a prominent gamma ray spike that is used to define the upper boundary of the Fox Harbour Member. Palynological studies based on both cuttings and sidewall cores at Hibernia J-34, O-35, P-15, and Rankin M-36 indicate that the actual unconformity may lie anywhere in the sandy interval between the gamma ray spike and up to 40 m below it (i.e. in the top 40 m of the Fox Harbour Member), a succession with a very diluted palynomorph assemblage. Further east, on the paleo-slope and basin floor, biostratigraphic data indicate that Danian strata overlie a Campanian or older Dawson Canyon Formation substrate (e.g. at Avondale A-46), with the Fox Harbour unconformity located between higher gamma ray muds below and a distinctive low gamma ray interval above. The overlying interval consists of strata varying from siliceous shale (e.g. at Mara E-30) and thick siltstone (e.g. at South Brook N-30) of the Tilton Member to sandstone of the Avondale Member (e.g. at Avondale A-46; Figure 3.4).

In the northern parts of the basin, the unconformity is less pronounced or absent, with Danian strata overlying Maastrichtian shales and/or chinks of the Wyandot Formation (e.g. Botwood G-89, Mobil et al., 1992). At Adolphus D-50, which has a high density of sidewall core samples, the lower half of the Danian (NP1 and NP2 zones - Martini, 1971) is missing (Doeven, 1983). This indicates that the Fox Harbour unconformity extends far out into the deeper parts of the basin, albeit with a much smaller stratigraphic gap (about 1 million years) than is present on the paleo-shelf.

On seismic profiles, the Fox Harbour unconformity corresponds approximately to a widespread, high amplitude seismic marker that defines the maximum progradational limit of the Late Cretaceous shelf-slope system (i.e. the toe of the final clinoform - Figures 3.10e, 3.12a). This seismic event, herein referred to as the T1-marker, records the beginning of a period in which most sediment bypassed the shelf and slope system (north of the Egret fault) and was deposited in basinal settings to the east and north.

3.3.7 *Avondale and Tilton members*

During the development of the Fox Harbour unconformity, little accommodation was available anywhere other than adjacent to the latest Cretaceous slope and on the basin floor. As a result, there was an eastward shift in the depocenter in the Paleocene, marked by seismic events that onlap the latest Cretaceous slope (Figures 3.13b, c). The Avondale and Tilton members were deposited above the Fox Harbour unconformity and correspond to seismic facies which overlie the T1-marker. Paleobathymetric interpretations indicate that Paleocene strata were deposited in upper bathyal water depths at South Mara C-13 and outer neritic or upper bathyal water depths at Terra Nova K-08 (Thomas, 1994).

At North Ben Nevis M-61 and P-93, the sandy Avondale Member is over 60 m thick and corresponds to mounded, discontinuous, sometimes bi-directionally downlapping seismic facies with variable amplitudes (Figures 3.13d, e). Combined with the deeper-water marine biota and basinal position of the Avondale Member, these seismic facies strongly suggest a submarine fan depositional setting (de Silva, 1993; Deptuck, 2000). Similar mounded seismic facies have been reported for submarine fans in the North Sea (e.g. Frigg Fan - McGovney and Radovich, 1985).

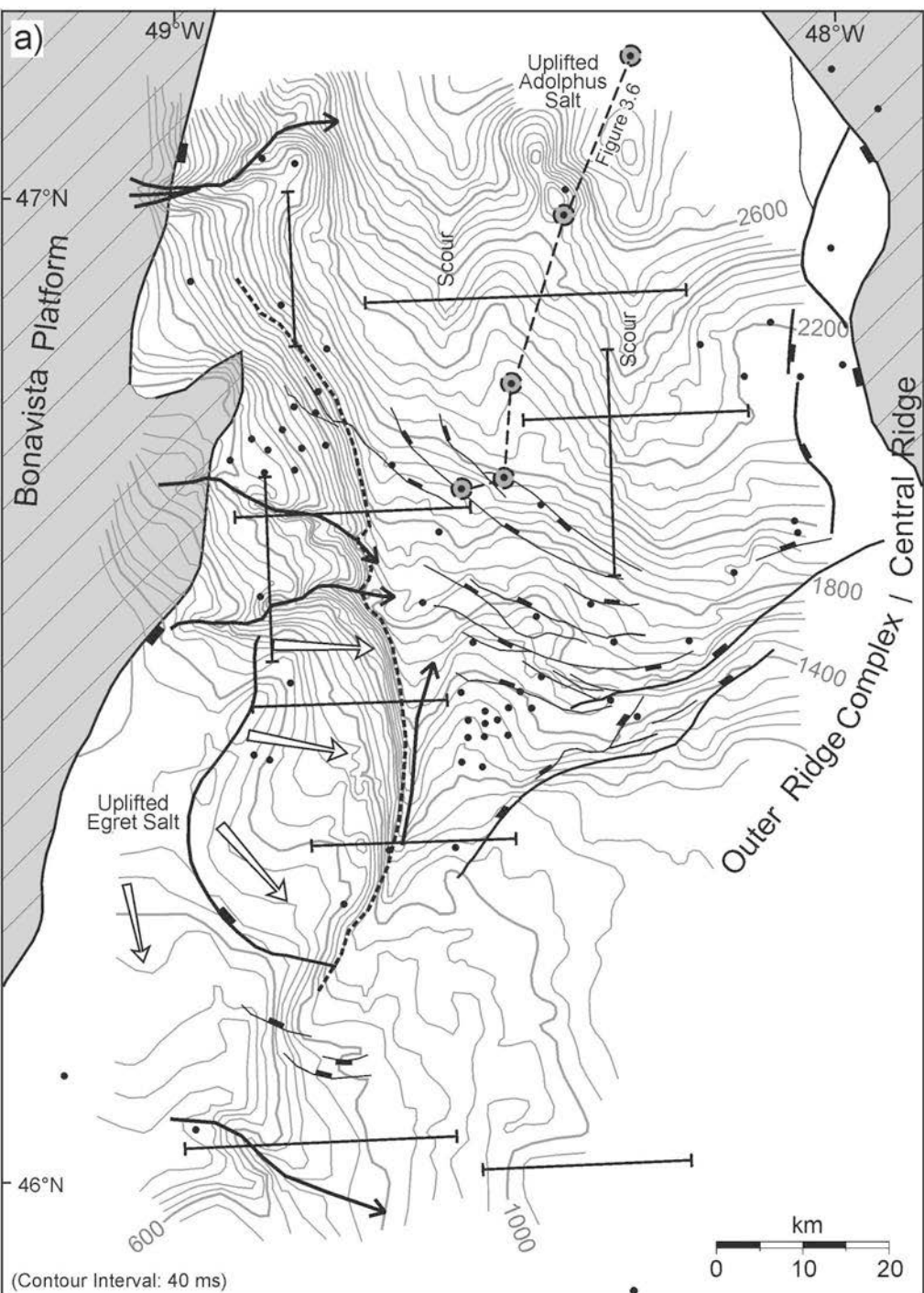


Figure 3.12. a) Time-structure map on the T1-marker, following the base of erosional features where the marker is truncated. The Flying Foam, Hibernia, and Rankin canyons as well as the western-most erosional feature in the southern Jeanne d'Arc Basin, incise the Upper Cretaceous deltaic platform (shelf) and slope. b) Seismic facies map showing the location of the main seismic units which overlie the T1-marker. Arrows indicate sediment transport directions. Also shown are the locations of mounded seismic facies on the basin floor and erosional features mapped in the southern reaches of the basin which incise Paleogene strata. The location of the Bonniton Canyon is from Parker (1999). See text for details and next page for legend.

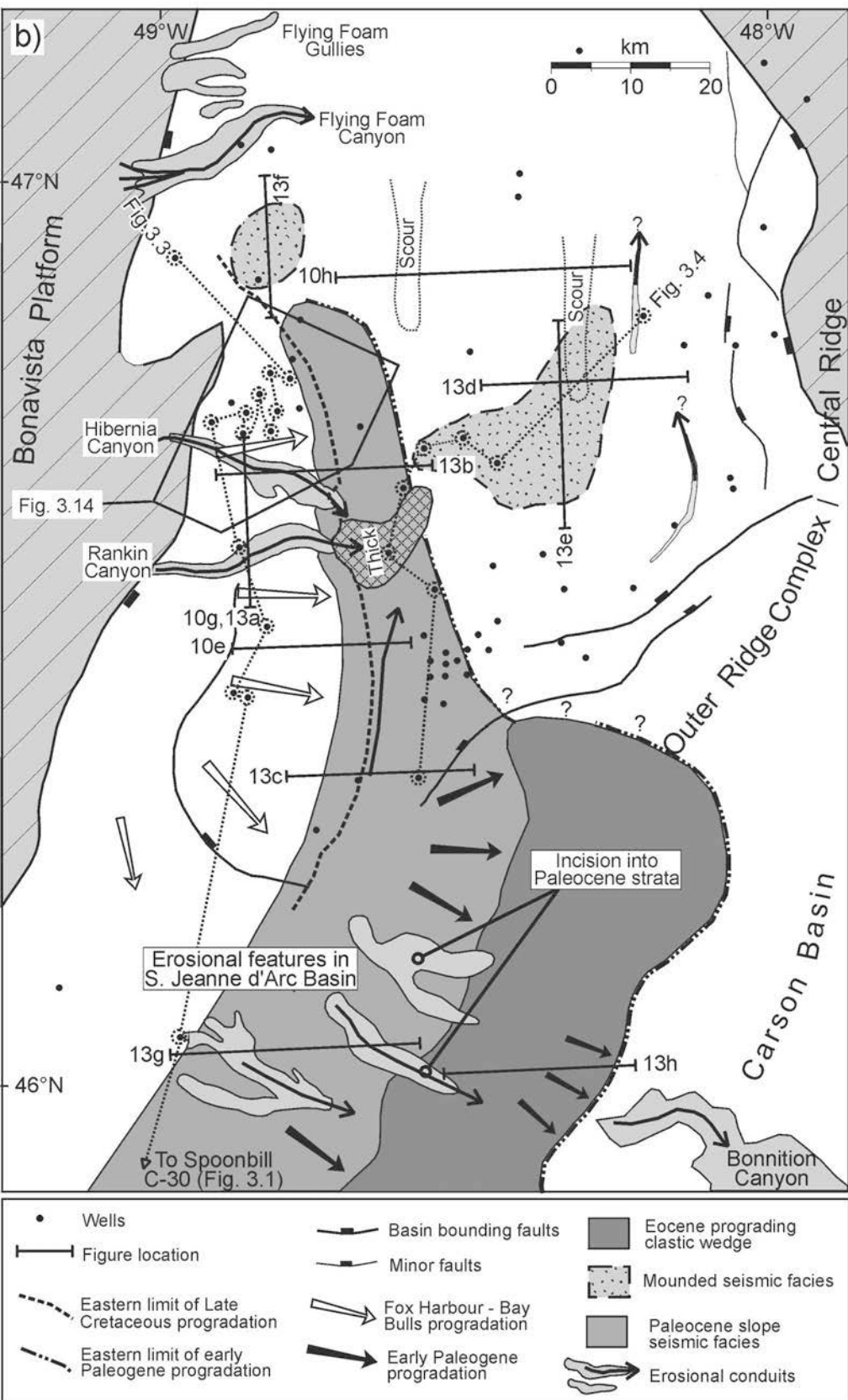


Figure 3.12 b). Continued (see previous page for caption).

The main conduits for sediment fed into Paleocene submarine fans in the JDB were the Hibernia and Rankin canyons (Sinclair, 1988; de Silva, 1993; Williamson et al., 1996). These east-trending canyons are incised into the Fox Harbour and Bay Bulls members, locally (on the shelf) cutting as deeply as the underlying Otter Bay Member (Figures 3.12a, b, 3.13a). The 150-220 m deep Hibernia Canyon varies in width from approximately 1.5 km on the shelf to greater than 5 km near the latest Cretaceous shelf-slope break (Figure 3.14). On vertical seismic profiles, the canyon is defined by the abrupt termination of strong, relatively continuous seismic horizons, including the T1-marker, and contains several cut-and-fill packages (Williamson et al., 1996; Friis, 1997), indicating that additional, smaller-scale unconformities are probably present in the Paleocene section.

Directly in front of the Hibernia and Rankin canyons (e.g. at Avondale A-46), the Avondale Member corresponds to discontinuous to continuous seismic facies located directly above the erosive T1-marker. These seismic facies pass laterally into mounded seismic facies that extend towards the northeast, filling a basin floor bathymetric low (Figure 3.12b). The mounded facies, in turn, pass laterally and distally into high amplitude, continuous seismic events which, based on Whiterose L-61, consist of very fine- to medium-grained, moderately well-sorted sandstone.

The Tilton Member corresponds to fairly continuous, low to moderate amplitude seismic horizons directly above the T1-marker. At Terra Nova, the member is located above a subtle baselap surface interpreted to correspond to the re-establishment of slope facies following the development of the Fox Harbour unconformity in the southern parts of the basin. In contrast, near Hibernia, the member corresponds to seismic facies that converge above the latest Cretaceous shelf, where the lower Paleogene interval is extremely condensed.

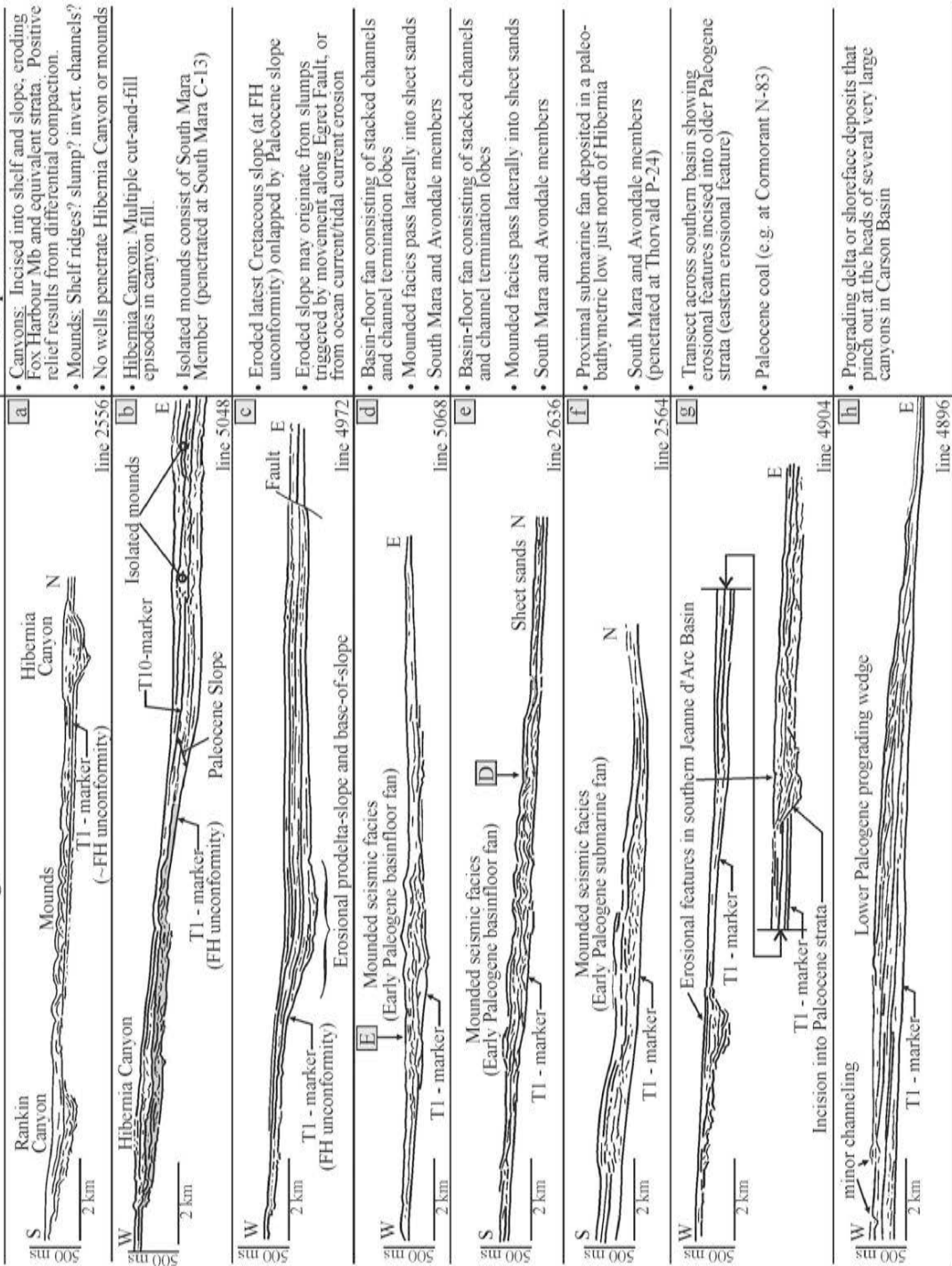
3.3.8 *South Mara Unconformity*

A second early Paleogene unconformity is recognized in the strata above the Avondale and Tilton members, referred to herein as the South Mara unconformity (Figure 3.2). Palynological data from sidewall cores at South Mara C-13 and cuttings at Avondale A-46 indicate that the South Mara unconformity is located at the base of the

Figure 3.13. Line drawings of lower Paleogene seismic facies observed in the Jeanne d'Arc Basin. a) Strike-line showing the erosive base and fill of the Rankin (left) and Hibernia (right) canyons incised into the Late Cretaceous shelf (shown in Figure 3.10g). Note the mounds between the two canyons of uncertain origin (large shelf-ridges?). b) Dip-line through the Hibernia Canyon fill and across slope, showing Paleocene slope deposits overlain by Early Eocene mounds. c) Dip-line showing the erosive character of the slope at the T1-marker overlapped by lower Paleogene strata. d) Strike-line and e) dip-line across prominently mounded seismic facies above the T1-marker in the central Jeanne d'Arc Basin. f) Mounded seismic facies observed just north of Hibernia. g) Probable incised valleys in the southern Jeanne d'Arc Basin that truncate Upper Cretaceous and lower Paleogene strata, including the T1-marker. h) Dip-line across lower Paleogene progradational seismic facies in the southern Jeanne d'Arc Basin. See figure 3.12 for line locations and text for details.

Lower Paleogene Seismic Facies

Interpretations/comments



- Canyons: Incised into shelf and slope, eroding Fox Harbour Mb and equivalent strata. Positive relief results from differential compaction.
- Mounds: Shelf ridges? slump? invert, channels? No wells penetrate Hibernia Canyon or mounds
- Hibernia Canyon: Multiple cut-and-fill episodes in canyon fill.
- Isolated mounds consist of South Mara Member (penetrated at South Mara C-13)
- Eroded latest Cretaceous slope (at FH unconformity) overlapped by Paleocene slope
- Eroded slope may originate from slumps triggered by movement along Egret Fault, or from ocean current/tidal current erosion
- Basin-floor fan consisting of stacked channels and channel termination lobes
- Mounded facies pass laterally into sheet sands
- South Mara and Avondale members
- Basin-floor fan consisting of stacked channels and channel termination lobes
- Mounded facies pass laterally into sheet sands
- South Mara and Avondale members
- Proximal submarine fan deposited in a paleobathymetric low just north of Hibernia
- South Mara and Avondale members (penetrated at Thorvald P-24)
- Transsect across southern basin showing erosional features incised into older Paleogene strata (eastern erosional feature)
- Paleocene coal (e.g. at Cormorant N-83)
- Prograding delta or shoreface deposits that pinch out at the heads of several very large canyons in Carson Basin

Figure 3.13. Continued (see previous page for caption)

Ypresian. Along the western margin of the basin, near Hibernia, there is a significant gap in the stratigraphic record. Palynological data from sidewall cores at Hibernia O-35 indicate that the Thanetian to Ypresian is absent or condensed below sampling resolution. Similarly, palynological data from cuttings at Hibernia P-15 indicate that the Thanetian is absent. On seismic profiles, the South Mara unconformity corresponds to a seismic marker referred to herein as the T10-marker. This marker forms the erosive top of a subtly prograding Paleocene slope succession and is overlain by mounded seismic facies associated with the South Mara Member (Figures 3.9, 3.12b).

3.3.9 *South Mara Member*

By the Early Eocene, strata deposited in front of the Hibernia and Rankin canyons formed a prominent, 400 m thick succession (Figure 3.12b) that, at Avondale A-46, consists of 34% sandstone, 24% siltstone, and 42% shale. The Avondale Member occupies the lower 63 m and the South Mara Member occupies the upper 90 m of this succession. The division of the South Mara Member into a funnel-shaped (regressive) unit and a cylinder-shaped (“blocky”) unit is made to distinguish the paleo-geographic setting at the end of the Paleocene and into the Eocene. At Avondale A-46, the regressive South Mara Member consists of subtly prograding seismic facies that, combined with lithologic evidence like carbonaceous plant remains, suggest that the regressive unit was deposited along the margins of the latest Paleocene to Ypresian basin in a delta platform or shelf depositional setting. In contrast, to the northeast of the regressive South Mara Member, the blocky South Mara Member was deposited on the slope and basin floor, above the T10-marker. Here, the member corresponds to isolated, in some places elongated mounds (Figures 3.9, 3.13b). The elongated mounds are interpreted as compaction-inverted submarine channels that formed as a result of differential compaction between coarse-grained channel-axis deposits and finer-grained levee or slope deposits outside the channel. Submarine fans deposited in the Early Eocene have a similar character to those deposited in the Early Paleocene (discussed in more detail in Chapter 5).

3.4 Southern Jeanne d'Arc Basin

In contrast to the western margin of the central JDB, where a prominent progradational latest Cretaceous slope is preserved, the slope south of the Egret fault is barely discernible. The change in slope geometry is shown in the contours of the T1-marker in Figure 3.12a. The lack of progradation suggests that fluvial systems, which prograded into the basin further north, were less active south of the Egret fault during the latter part of the Cretaceous. The presence of glauconite, mollusc shell fragments (gastropods, bivalves, and scaphopods), bryozoans and echinoid spines at Murre G-67, as well as inoceramids at Cormorant N-83, indicate that a marine environment continued at least through the deposition of the Bay Bulls Member.

The presence of coal stringers and wood fragments in Cormorant N-83, as well as glauconite and scaphopod shells indicates that a combination of terrestrial and marine conditions prevailed during the early part of the Paleogene in the southern JDB (see sample e in Appendix III). Paleocene and Eocene seismic facies subtly onlap uppermost Cretaceous strata to the west. To the east, seismic facies are shingled (prograding east) and form a southeast-prograding clastic wedge that extends onto the stable platform that separates the Carson Basin and JDB (Figure 3.12b). The upper surface of this prograding wedge shows both toplap and erosional truncation. In strike sections, this wedge has a lens-shaped external geometry, pinching-out to the north and south. In dip sections, this clastic wedge thickens toward the southeast, and distally downlaps onto the Outer Ridge Complex (Figure 3.12b, 3.13h) where it pinches out near the heads of several large early Paleogene submarine canyons incised into the western margin of the Carson Basin (Parker, 1999).

Several southeast-trending erosional features incise the progradational strata located in the southern JDB. The westernmost erosional feature (Figures 3.12b, 3.13g) incises Fox Harbour equivalent strata in a region where the lower Paleogene succession is extremely condensed. Farther east, where the lower Paleogene succession is thicker, erosional features truncate both the T1-marker and younger strata above it (Figures 3.12b, 3.13g), indicating that they were incised during the development of one or more younger unconformities, although well control to determine the age of the unconformity (ies) is not available.

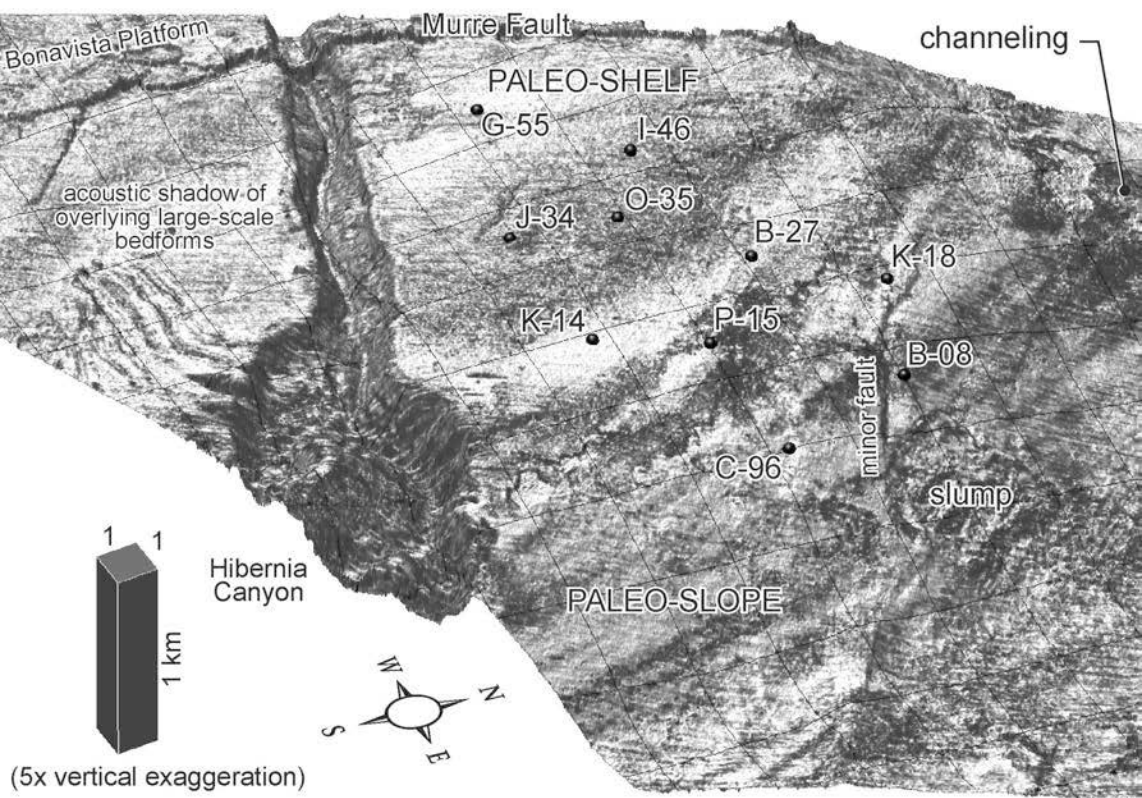


Figure 3.14. Depth converted, shaded relief perspective image of the Hibernia Canyon mapped along the erosional base of the canyon and along the T1-marker, viewed from the southeast. Note the prominent thalweg channel developed at the erosional base of the canyon and the erosional notches into the canyon walls, implying that sediment entered the canyon laterally either through shelf transport processes or through canyon wall slumping. 3-D seismic data courtesy of the Hibernia Management and Development Company Ltd (from John Shimeld, GSC Atlantic).

Most of the erosional features in the southern JDB are interpreted as incised valleys. These erosional features, and the prograding clastic wedge that they incise, are inferred to have transported clastic sediments into the heads of the large submarine canyons incised into the western margin of the Carson Basin. These canyons, in turn, are inferred to have fed sediment directly into submarine fans in the deeper reaches of the Carson Basin (Grant et al., 1988; Deptuck, 1998; Parker, 1999).

3.5 Discussion

During the Turonian, and perhaps the early Coniacian, chalks accumulated in the JDB and adjacent areas. As with other Upper Cretaceous chalk-rich units around the world, the Petrel Member has been interpreted as the product of pelagic carbonate sedimentation during a global second-order sea level highstand (Haq et al., 1987). The Petrel Member is a highly condensed unit deposited during a period of sediment starvation below storm base, in an outer shelf environment (Swift et al., 1974; Grant and McAlpine, 1990). Descriptions of cuttings and analyses from wireline data indicate that the Petrel Member becomes sandier towards the basin margins (Shimeld et al., 2000). This distribution suggests that, although the Petrel Member was deposited in deeper-water conditions, a clastic sediment source bordered the basin during its deposition. The clastic system appears to have been restricted to the Bonavista Platform and the area south of the Egret fault.

By the late Turonian or early Coniacian, the input of clastic sediments into the JDB increased and the Otter Bay Member (proximal, coarse-grained facies) and its lateral equivalent, the Red Island Member (distal, shale-prone facies), prograded from the west and southwest, downlapping onto the Petrel Member. Based on the height of the offlapping clinofolds, the Otter Bay Member prograded into a basin that was less than 200 m deep along its margins. During progradation along the western and southern margins, pelagic chalks continued to accumulate in more distal regions (e.g. Coniacian limestones in South Mara C-13). Such proximal sand - intermediate shale - distal chalk facies relationships have also been documented in studies of Upper Cretaceous outcrops in the Western Interior of the United States (e.g. Elder et al., 1994).

In the Coniacian or Santonian, progradation of the Otter Bay and equivalent Red Island Member ceased south of the Egret fault during the development of the Otter Bay unconformity. The Egret Canyon, the Petrel Channel, and the Mara Channel formed part of a network of submarine erosional features that transported clastic sediments north of the Trans-Basin Fault Trend. Otter Bay and Red Island progradation may have continued near Hibernia during or just after the development of this unconformity, but ceased completely when the margins of the basin were drowned and the shale-prone Bay Bulls Member was deposited in the Campanian, blanketing the former delta platform. During this period, the fluvial systems that were once the primary source of sediment for the Otter Bay Member moved inland, to the west of the Murre fault. As the coarser-grained fluvial sands of the Fox Harbour Member prograded seaward, beyond the Murre fault, deposition of the diachronous Bay Bulls Member also shifted to the east, where it formed a prominent slope.

Water depths at the base-of-slope were significantly deeper during the progradation of the Fox Harbour Member than they were during the progradation of the Otter Bay Member. Clinoform height indicates a basin margin that was 350 - 450 m deep (at the base of the prograding clinoforms, without correcting for compaction effects). The transition from a shallow shelf (estimated at less than 50 m deep at the slope break) to deeper basin occurred across a steep slope that dipped between 5 and 9 degrees (also not corrected for compaction). The increase in clinoform height, from less than 200 m in the Coniacian-Santonian, to more than 350 m in the Campanian-Maastrichtian, combined with the development of a prominent slope leading into the deeper basin, indicates a change from a shallow ramp-type margin to a deeper shelf-break margin (see Emery and Myers, 1996, p. 15). This transition also corresponds to a shift in the shelf-break of more than 10 km eastward. Northeast of the prograding Fox Harbour and equivalent strata, the deeper marine chalky Wyandot Formation accumulated in the northern parts of the basin, far removed from the input of most clastic sediment.

In the Early Paleocene, the latest Cretaceous shelf/delta platform provided little accommodation and, as a result, very little sediment accumulated above it. Instead, the depocenter shifted to the east, adjacent to the thickest Upper Cretaceous strata. The Hibernia and Rankin canyons provided a continuous land-to-deep-sea sediment transport

system, from a fluvial drainage system located on the Bonavista Platform, across the shelf, and into submarine fans, where the Avondale Member was deposited on the basin floor. The prominent slope that existed during this time was largely bypassed during the deposition of the Avondale Member. There is also evidence for northward sediment transport parallel to the slope, east of the Egret salt diapirs, where the T1-marker is erosive (Figure 3.13c).

Also in the Early Paleocene, the fine-grained Tilton Member was deposited in regions bordering the western and southern margins of the basin, above probable bathymetric highs (e.g. like the Late Cretaceous shelf and near Terra Nova). The onset of Tilton Member deposition closely corresponds to the initiation of a widespread radiolarian event in the JDB (Thomas, 1995), suggesting a change in ocean circulation at that time, perhaps accompanied by up-welling along the basin margins, as has been suggested in the North Sea (e.g. Mitlehner, 1996). The Tilton Member is interpreted to have formed during the initial flooding of the prominent Late Cretaceous shelf, that followed the development of the Fox Harbour unconformity. Such flooding conditions would have trapped fluvial systems back on the Bonavista Platform, allowing the accumulation of undiluted diatomaceous deposits (Sinclair, 1987). The member is interpreted as a dominantly pelagic unit that is slightly younger than the Avondale Member. Limitations on biostratigraphic resolution, however, prevent understanding the exact temporal relationship between the two members.

By the end of the Paleocene, the shelf-slope system along the western margin of the basin (north of the Egret fault) had once again prograded east, above proximal deposits of the Avondale and Tilton members (e.g. at Avondale A-46 and South Brook N-30, respectively). During this time the regressive South Mara Member accumulated along the margins of the basin and the blocky South Mara Member was deposited further east and northeast where accommodation existed above the latest Paleocene slope and basin floor. South of the Egret fault, where little accommodation was available, the lower Paleogene seismic architecture is dominantly progradational due to forced regression. The topsets of this regressive unit were probably subaerially exposed and more than 35 km of east-to-southeastward progradation occurred, extending the paleo-shoreline much farther east than it was, for example, near Hibernia (Figure 3.12b).

3.6 Summary of key points

1. Seven members of the Dawson Canyon and Banquereau formations are formally defined. The Red Island, Bay Bulls, and Avondale members are new units, while the Otter Bay, Fox Harbour, and South Mara members, which had already been introduced informally, are now formally defined. The Tilton Member, formerly the “porcelaneous mudstone” is renamed and formally defined.
2. Offlapping seismic facies, consisting of thick sandstone and laterally equivalent shale, formed along the western margin of the JDB during the Late Cretaceous. The Bonavista Platform and its hinterland were the primary source regions for these strata. Two main progradational pulses are recorded on both seismic and well data, corresponding to the Otter Bay and Fox Harbour members and their distally equivalent Red Island and Bay Bulls members. The seismic responses to these distinct progradational episodes are different, indicating a transition from a ramp-type margin to a shelf-break margin, caused by a deepening of the basin margins.
3. Seaward of the offlapping Late Cretaceous margin, equivalent sediments are condensed, dominated by shale of the undivided Dawson Canyon Formation and chalk of the Petrel Member and Wyandot Formation. Seaward of the Otter Bay and Fox Harbour members, relatively thick and locally developed, sandstone units are interbedded with the Dawson Canyon Formation. Sands were probably transported into the basin through north-trending erosional features during the development of the Otter Bay unconformity in the Coniacian or Santonian.
4. In the Early Paleocene, the main depocenter shifted from the western margin of the JDB to basinal areas further east where a succession of submarine fans was deposited (preserved in, for example, the South Mara and Avondale members). In the southern reaches of the basin, lower Paleogene strata prograded across a stable platform towards the western margin of the Carson Basin, marking a significant eastward shift in the inferred paleo-shoreline as compared to the central and northern reaches of the JDB.

5. At least three periods of widespread erosion are identified in the study interval, corresponding to the Otter Bay, Fox Harbour, and South Mara unconformities. These unconformities are estimated to have developed in the Coniacian-Santonian, Early Paleocene, and Early Eocene, respectively. The precise timing of these unconformities remains to be established and, based on the multiple cut-and-fill events within the Hibernia Canyon, there may be additional higher-order unconformities, particularly in the lower part of the Paleogene succession, that have not yet been identified biostratigraphically.

CHAPTER 4 - POST-RIFT EVOLUTION OF THE JEANNE D'ARC BASIN AND NORTHEASTERN GRAND BANKS: TRANSITION FROM A CONFINED RIFT BASIN TO AN UNCONFINED PASSIVE-MARGIN SHELF AND SLOPE

4.1 Introduction

4.1.1 Basin setting at the end of the Cretaceous

At the end of the Cretaceous, the JDB formed a depression that rimmed the northeastern margin of what is now the Grand Banks of Newfoundland (Figures 4.1, 4.2). It had a width that ranged from 50 to 90 km and a length of greater than 230 km, extending to the northern limit of the study area. The southern limit of the depression is well constrained because Upper Cretaceous and lower Tertiary strata thin significantly above the Bonniton High (a basement high located south of the basin - Figure 4.2). The northern limit of the depression is transitional with the Orphan Basin, and no thinning of stratigraphic units above basement highs is observed within the study area, implying that the basin was open to the north.

The eastern limit of the proto-Grand Banks shelf was located near the edge of the Bonavista Platform (except locally where Late Cretaceous progradation extended the shelf-edge up to 15 km further east), about 285 km from the Avalon Peninsula off easternmost Newfoundland (and more than 100 km west of the present position of the continental shelf-break). Several basement highs formed prominent bathymetric (perhaps topographic) features that influenced the distribution of Upper Cretaceous and lower Tertiary strata (Figure 4.2). These include the Central Ridge (also known as the Outer Ridge Complex, forming the eastern margin of the JDB), South Bank High (located south-southwest of the basin), and the Flemish Cap (located east of the basin).

South of the JDB, most of the interconnected rift basins that had been prevalent in the Mesozoic (e.g. Horseshoe, Whale) had little expression by the end of the Cretaceous and hence deposition was largely unconfined (see "base event" to sea floor isopach map of Grant and McAlpine, 1990 - their figure 6.16). In contrast, the JDB formed a prominent depression that confined depositional systems until the Middle Eocene (Bartonian).

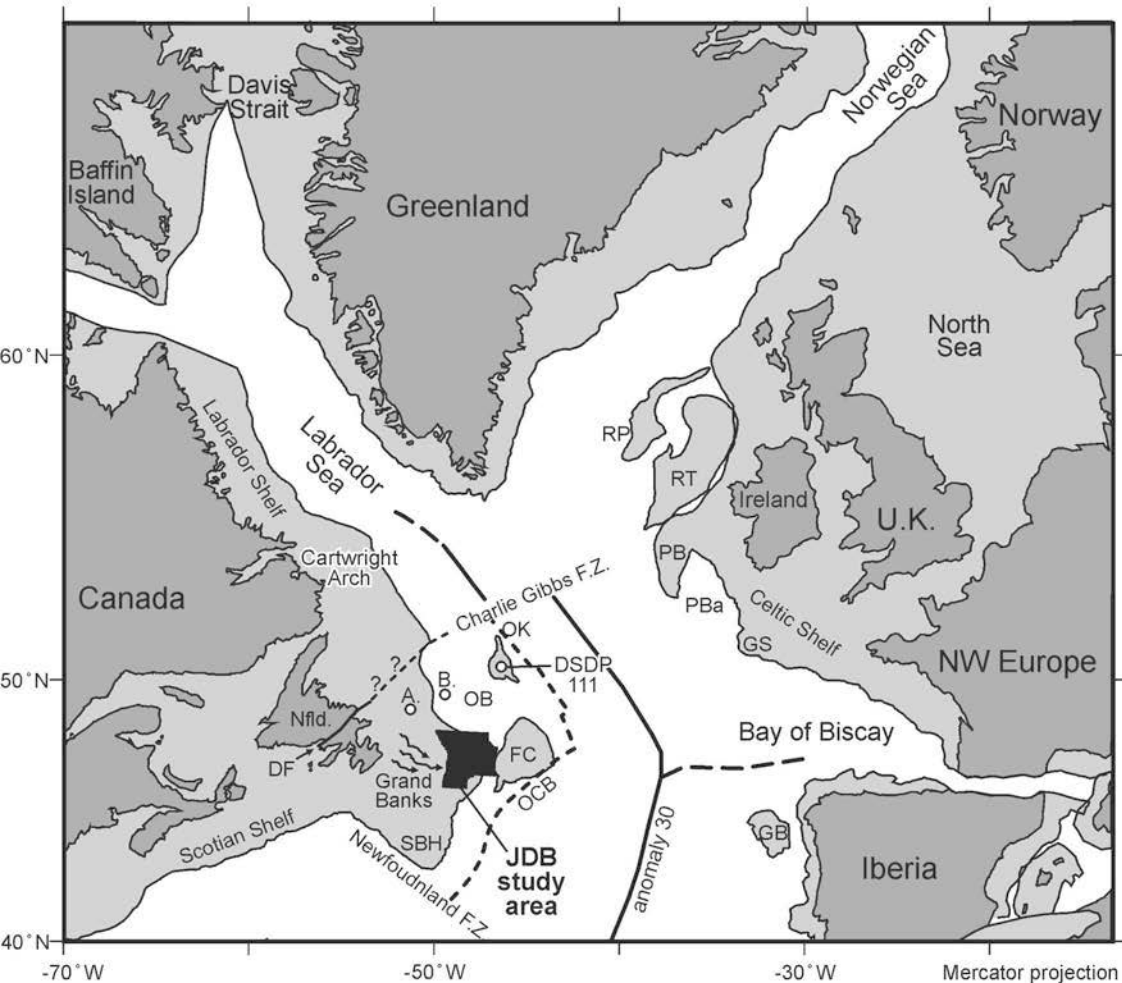


Figure 4.1. Plate reconstruction at 65 Ma (modified from Hay et al., 1999). The spreading center (bold line) corresponds approximately to magnetic anomaly 30 identified by Srivastava and Tapscott (1986). **SBH** South Bank High; **OB** Orphan Basin; **FC** Flemish Cap; **DF** Dover Fault; **FZ** Fracture Zone; **GB** Galicia Bank; **GS** Goban Spur; **PBa** Porcupine Basin; **PB** Porcupine Bank; **RT** Rockall Trough; **RP** Rockall Plateau; **OCB** Ocean-Continent Boundary. Arrows show direction of sediment input in the Late Cretaceous and early Paleogene. Location of Bonavista C-99 (A.) and Blue H-28 (B.) are shown.

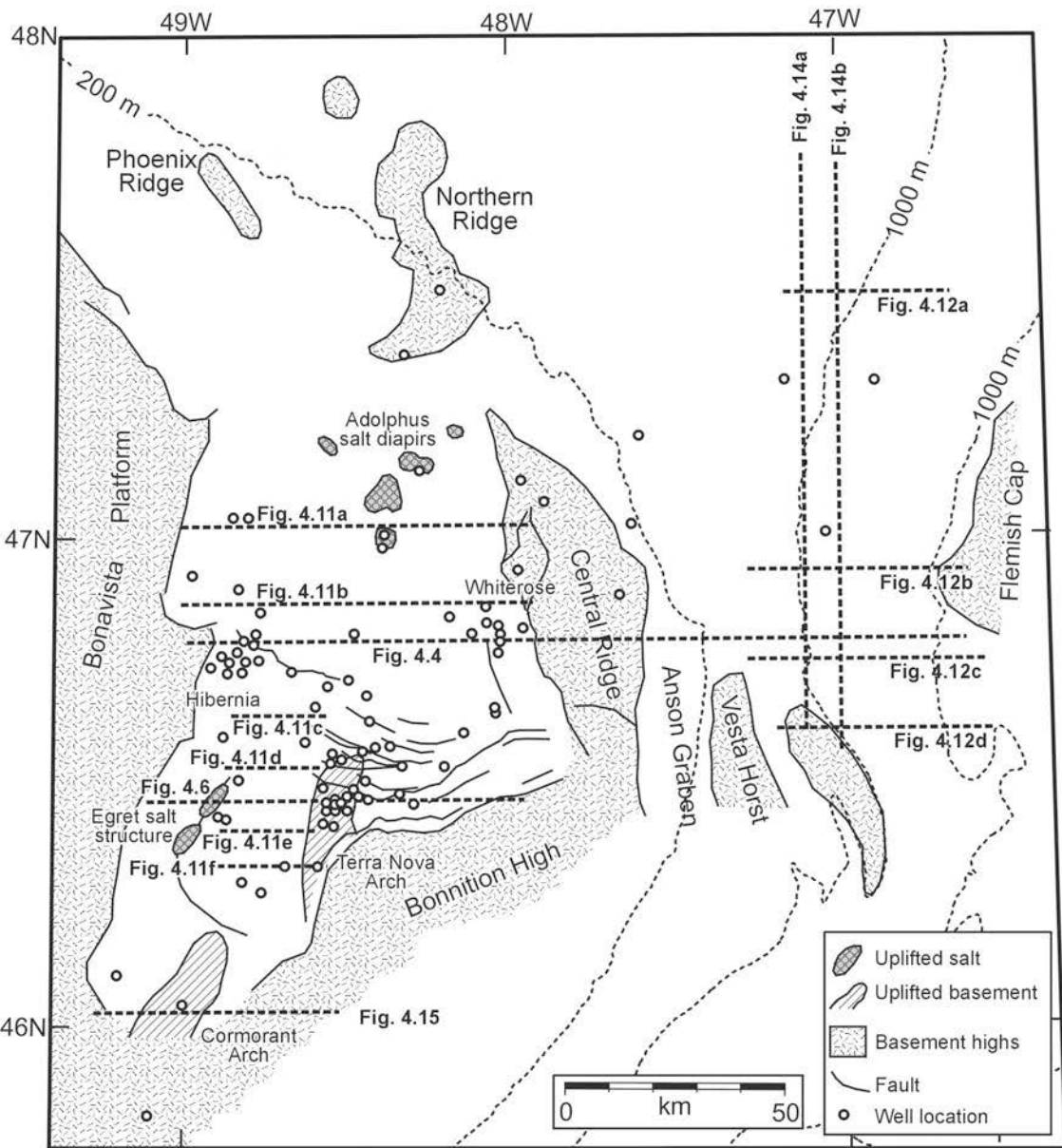


Figure 4.2. Basemap of Jeanne d'Arc Basin and surrounding areas, showing basement highs and faults that offset the K1 marker or younger strata. Figure locations are shown. Refer to Figure 2.26 for well names.

4.1.2 *Scope*

The primary objective of this chapter is to describe the broad-scale post-rift evolution of the JDB and surrounding areas, and to correlate that evolution to the regional sea floor spreading history established by previous workers. Regionally correlated seismic markers were used to generate time-structure and time-thickness maps across the study area. The results were used to examine the changes in the basin structure and depocenters through time. Based on the depositional setting and degree of confinement, a four - stage subdivision for the post-rift stratigraphic succession in the JDB and surrounding areas is proposed, and comparisons to the Orphan Basin and Labrador margin to the north are made (Figure 4.3b).

This study also describes the temporal and spatial distribution of bottom current indicators like sediment waves, scours, and sediment drifts. Combined with evidence from microfossil assemblages (from this study and previous studies), the bottom current indicators are used to infer temporal changes in ocean circulation in the study area. The results of this work provide insight into the paleo-geography and paleo-oceanography in the study area, and provide a framework for understanding the Upper Cretaceous and Tertiary evolution of the margin.

4.1.3 *Data and methodology*

The data set consists of a regional grid of digital 2-D seismic lines and data from all available exploration and delineation wells at the time of the study. Over 20 300 line km of migrated 60-fold 2-D seismic data, covering an area of 40 720 km² at a grid spacing ranging from 2 to 8 km, were available for this study. The seismic data set was collected and processed in 1983 by the Parex/Soquip Group (CNOPB Project No. 8620-S014-008E), and is of good quality in the Upper Cretaceous and younger interval across most the study area. Near the present-day shelf break and in the northern reaches of the study area, data quality is poorer, though key seismic markers could still be correlated through these regions.

A total of 84 wells from the JDB and Flemish Pass were used (Figure 4.2). Most wells that penetrate the Upper Cretaceous and Tertiary interval targeted deeper prospects

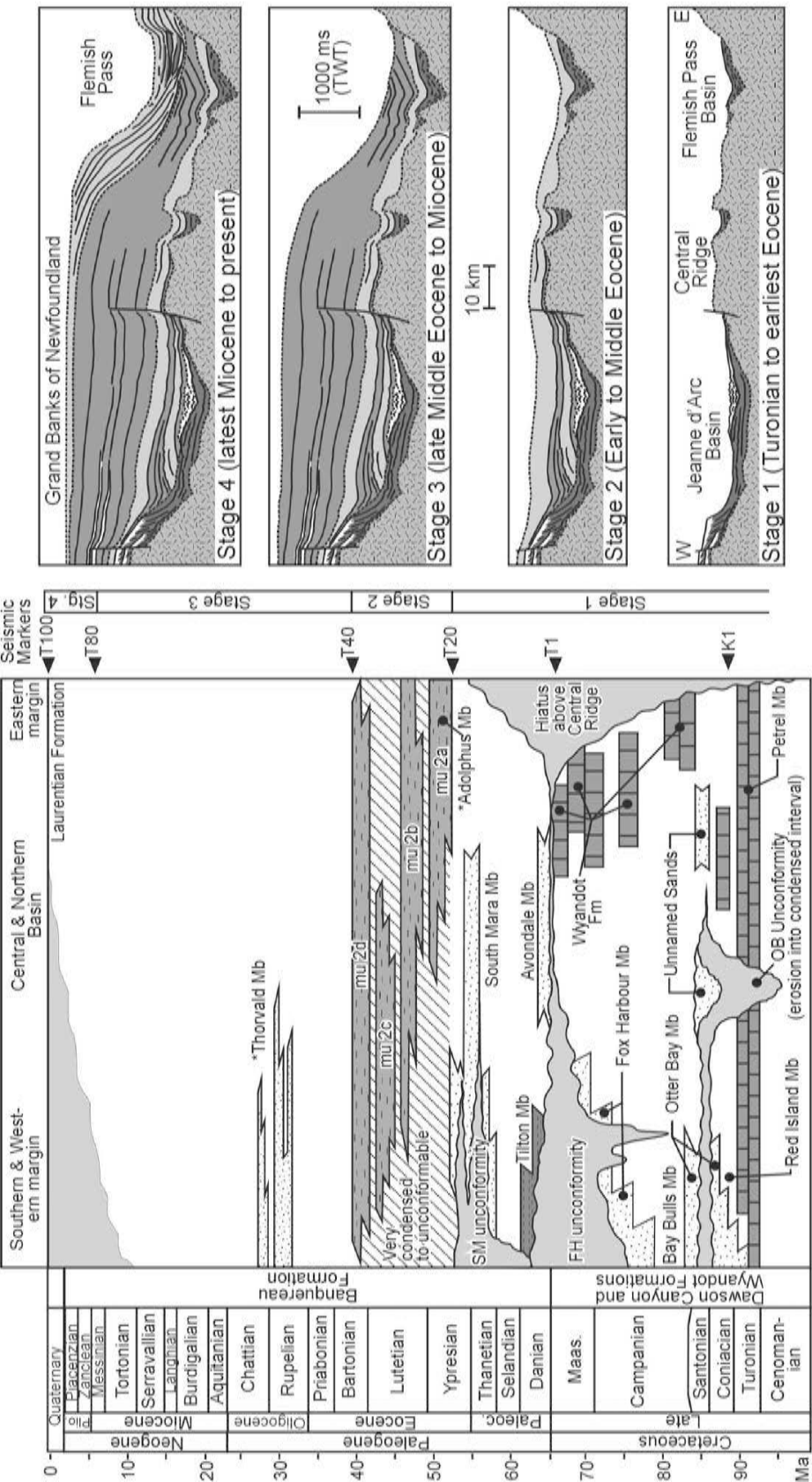


Figure 4.3. a) Upper Cretaceous and Tertiary lithostratigraphic chart (with new units defined in this chapter marked with asterisk *). Arrows indicate approximate age of key seismic markers mapped in this study. See Deptuck et al. (2003a) for details on Upper Cretaceous and lower Paleogene lithostratigraphy. b) A diagram illustrating the proposed four-stage subdivision of the post-rift stratigraphic succession in the Jeanne d'Arc Basin and adjacent Flemish Pass. Each stage defines a distinct period in the basins structural and deposition evolution, passing from a confined rift basin during stages 1 and 2, into an unconfined passive-margin shelf and slope in stages 3 and 4. Time-scale from Gradstein et al. (1995) and Berggren et al. (1995).

and therefore provide a somewhat random sampling of shallower strata. The gamma ray, sonic, density, and resistivity logs were most commonly used. Lithostratigraphic information was obtained from paper and digital Canstrat Limited well log interpretations and from mud logs and sidewall core descriptions in well history reports (unless otherwise stated). Wells were tied to seismic data using checkshot surveys and/or synthetic seismograms. Age control was provided by 10 key wells, highlighted on Figure 4.2 and summarized in Appendix Ia. Biostratigraphic interpretations for the key wells were carried out by Graham Williams and Rob Fensome (GSC Atlantic) over the past 7 years using both washed cuttings and sidewall cores. Samples were processed for palynology and, less commonly, micropaleontology slides. Age control for key seismic markers and stratigraphic units were fairly consistent in all 10 wells. The lithostratigraphic classification of Deptuck et al. (2003a, see Chapter 3) is used, with the addition of two new stratigraphic units in the Banquereau Formation in this chapter. All gridded surfaces and time-thickness maps are in units of two-way travel time, and were not depth-converted.

Calculated sedimentation rates are used in this paper to illustrate general trends in long-term sedimentation rates and the location of major depocenters. Compaction effects were not accounted for and thus resultant sedimentation rates are approximate, and should be considered minimum values (for deeper mud-prone strata, sedimentation rates could be underestimated by as much as 30 % - Van Hinte, 1978). One-dimensional modeling of compaction at Hibernia I-46 suggests that the Dawson Canyon Formation has undergone a 24 % reduction in thickness since its deposition (Williamson et al., 1996). Still, the measurements are sufficiently accurate to show general trends.

4.2 Post-rift lithostratigraphy

The earliest published Upper Cretaceous and Tertiary stratigraphic studies for the JDB were conducted by Amoco and Imperial (1973a) and Jansa and Wade (1975a, b), who extended the lithostratigraphic nomenclature, originally proposed for time-equivalent rocks on the Scotian Margin (McIver, 1972), to the JDB. The interval was subdivided into four formations: the Upper Cretaceous Dawson Canyon and Wyandot formations, the Tertiary Banquereau Formation, and the Quaternary Laurentian

Formation (Figure 4.3a). This work was followed by Boudreau et al. (1986), Sinclair (1988), and de Silva (1993) who informally designated several members of the Dawson Canyon and Banquereau formations. Their work was followed by Deptuck et al. (2003a) who defined a formal lithostratigraphic nomenclature for the Upper Cretaceous and Lower Paleogene interval in the basin. The lithostratigraphic framework is briefly described below, and discussed in more detail in Chapter 3.

The **Dawson Canyon Formation** consists of a combination of fine- to coarse-grained marginal marine to marine clastic sediments and marine pelagic carbonates that are exclusively Upper Cretaceous. The formation is subdivided into five members in the JDB (Figure 4.3a). The stratigraphically deepest is the chalky Petrel Member, which is overlain by fine to coarse-grained regressive sandstones of the Otter Bay and Fox Harbour members and their finer-grained equivalents the Red Island and Bay Bulls members (that prograded from the west - Deptuck et al. 2003a). As the western margin of the basin was dominated by clastic deposition, accumulations of chinks and marls of the **Wyandot Formation** dominated the northeastern parts of the basin. These chalk deposits can reach a thickness in excess of 400 m (e.g. at Botwood G-89, Figure 3.6 of Chapter 3), and indicate higher bioproductivity and/or low clastic input in the northern parts of the basin.

Above both the Dawson Canyon and Wyandot formations, the entire Cenozoic succession, with the exception of the Quaternary **Laurentian Formation** (defined by Jansa and Wade, 1975 and consisting of Quaternary pro-glacial sediment), has been designated the **Banquereau Formation** (McIver, 1972; Amoco and Imperial, 1973a; Jansa and Wade, 1975a, b). It consists mostly of muddy outer neritic to bathyal deposits, but also contains intervals of coarser-grained clastics deposited in shelf to submarine fan settings. The formation has been formally subdivided into five members in the JDB. The Avondale and South Mara members are coarser-grained units deposited near the base of the formation in the Paleocene to earliest Eocene. The Tilton Member is a finer-grained, siliceous unit that, despite its finer-grained lithology, generates a distinctive low gamma ray response (probably owing to its high silica and low detrital clay content - see Deptuck et al., 2003a). A second “low gamma ray” finer-grained unit is recognized above the South Mara Member and is here formally designated the Adolphus Member of the

Banquereau Formation (uppermost Thanetian to Ypresian - discussed later, see Appendix IIa for a formal definition and type section). Finally, an interval of Lower to Middle Oligocene (Graham Williams, pers. comm., 2003) coarser-grained clastics is recognized about mid-way through the mud-prone Banquereau Formation, and is here formally designated the Thorvald Member of the Banquereau Formation (discussed later - see Appendix IIb for a formal definition and type section).

4.3 Broad-scale basin evolution and variations in long-term sedimentation rates

Twelve regional seismic markers, representing important bounding discontinuities (displaying toplap, onlap, and/or erosional truncation), were identified and mapped in the JDB (Figures 4.3a, 4.4). Five of these surfaces (including the modern sea floor) were used to subdivide the post-rift stratigraphic succession into four stages, each representing a distinct period of basin structure, seismic facies, and depositional setting (Figure 4.3b). More than 4 km of post-rift strata were deposited in the study area through stages 1 to 4 (e.g. 3700 m at Conquest K-09, drilled on a basement high), ultimately building the broad shelf that now forms the Grand Banks of Newfoundland. The stages track the transition from a confined basin (stages 1 and 2 - Figure 4.5a) to an unconfined passive-margin shelf and slope system (stages 3 and 4 - Figure 4.5b).

4.3.1 Stage 1 - Late Cretaceous to earliest Eocene

Stage 1 strata were deposited in the Late Cretaceous through earliest Ypresian, and correspond to the Dawson Canyon to lowermost Banquereau formations (Figure 4.3a). During stage 1 significant quantities of sediment were supplied to the basin from the west in the form of eastward prograding deltas and basinal submarine fans (Figures 4.3b, 4.4, 4.6). The deltas stacked to create a narrow, linear prograding shelf and slope system that rimmed the western, and to some extent the southern, margin of the JDB (Figure 4.8b). Submarine fans stacked to generate mounded seismic facies on the slope and basin floor, fed by prominent canyons eroded into the shelf and slope along the western basin margin (Figures 4.7b, 4.8a).

Stage 1 is bracketed below by the K1 marker and above by the T20 marker (Figures 4.3, 4.4, 4.6). The K1 marker (Figures 4.3a, 4.7a) corresponds approximately to

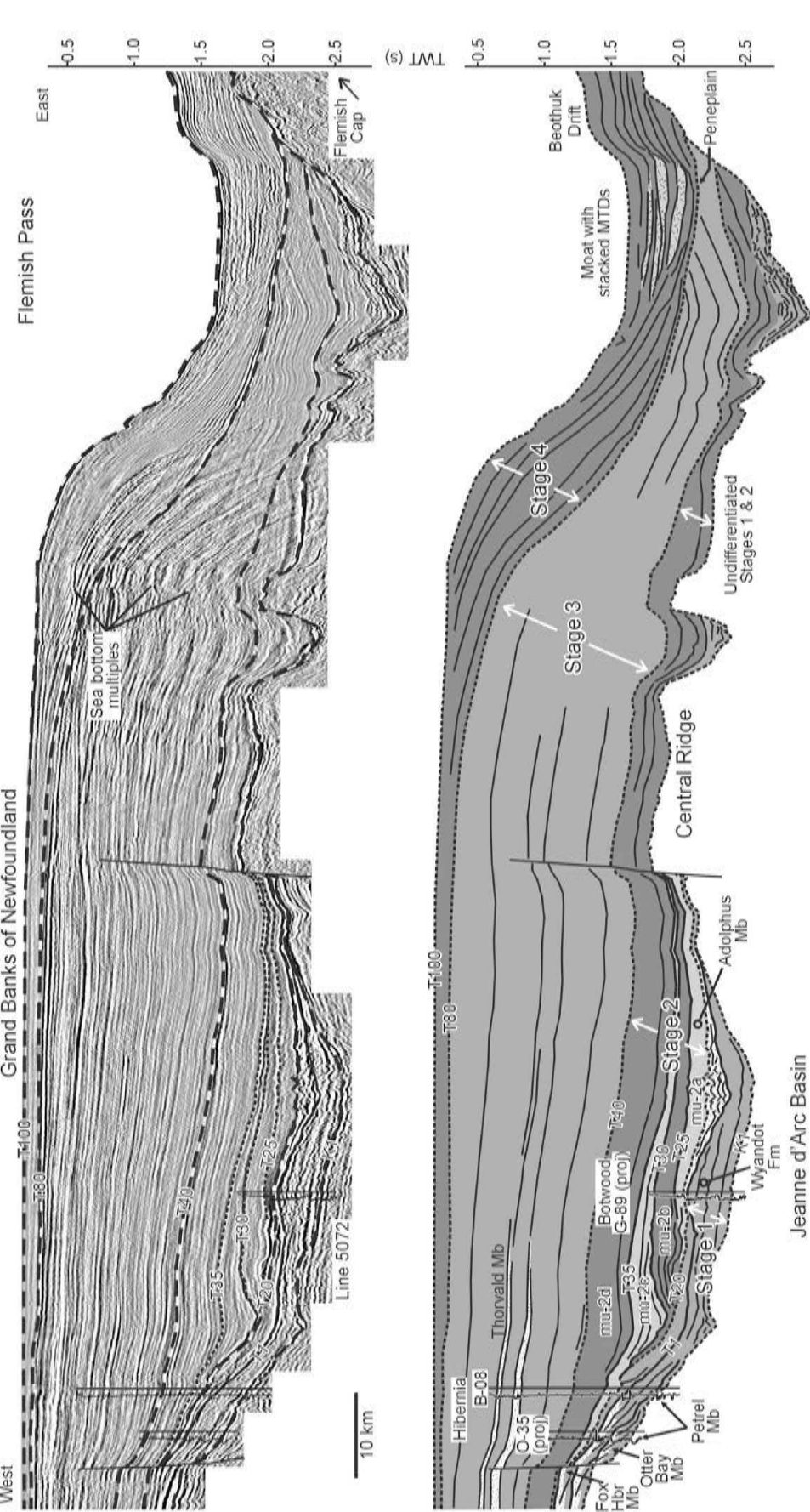


Figure 4.4. Regional west to east seismic profile (line 5072) across northern Jeanne d'Arc Basin, with tie to Hibernia O-35 (projected), Hibernia B-08, and Botwood G-89 (projected). Note the high amplitude character of the Oligocene Thorvald Member of the Banquereau Formation on the western side of the profile. Also note the tie between marine unit (m.u.) 2a and the Adolphus Member of the Banquereau Formation at Botwood G-89. Key seismic markers described in this chapter are indicated. MTD = mass transport deposit. Location shown in Figure 4.2.

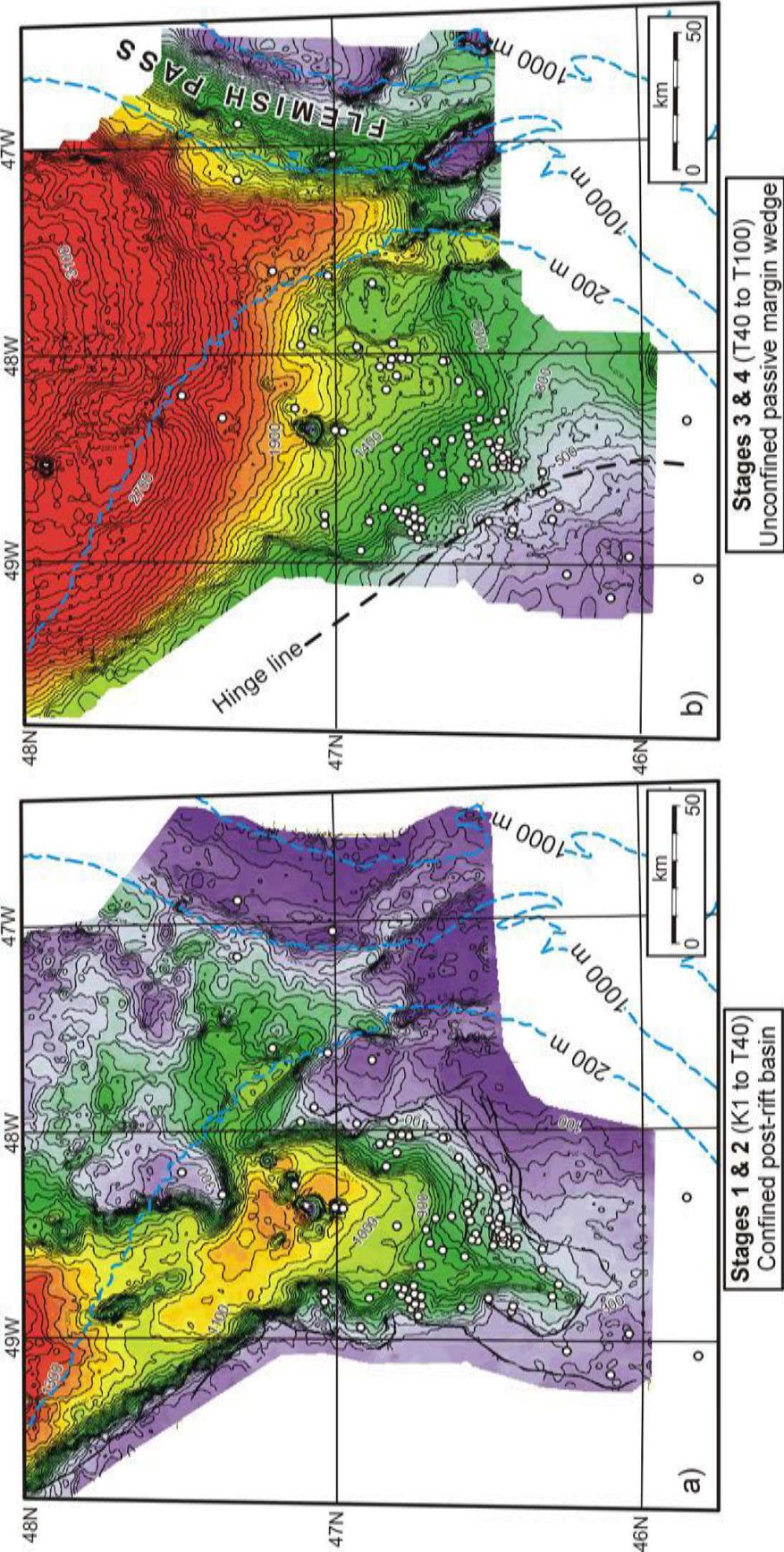


Figure 4.5. a) Time-thickness map between the K1 and T40 seismic markers. This interval corresponds to a confined basin stage, when deposits thinned significantly above basement highs (stages 1 and 2). b) Time-structure map between the T40 and the T100 (modern sea floor) markers. This interval corresponds to period when deposits accumulated above the Jeanne d'Arc Basin but were not constrained by the Central Ridge. Stage 3 and 4 deposits accumulated along an unconfined margin, in a broad seaward thickening progradational/aggradational wedge. Modern 200 m and 1000 m isobaths shown in blue. Time-thickness contour interval is 50 ms.

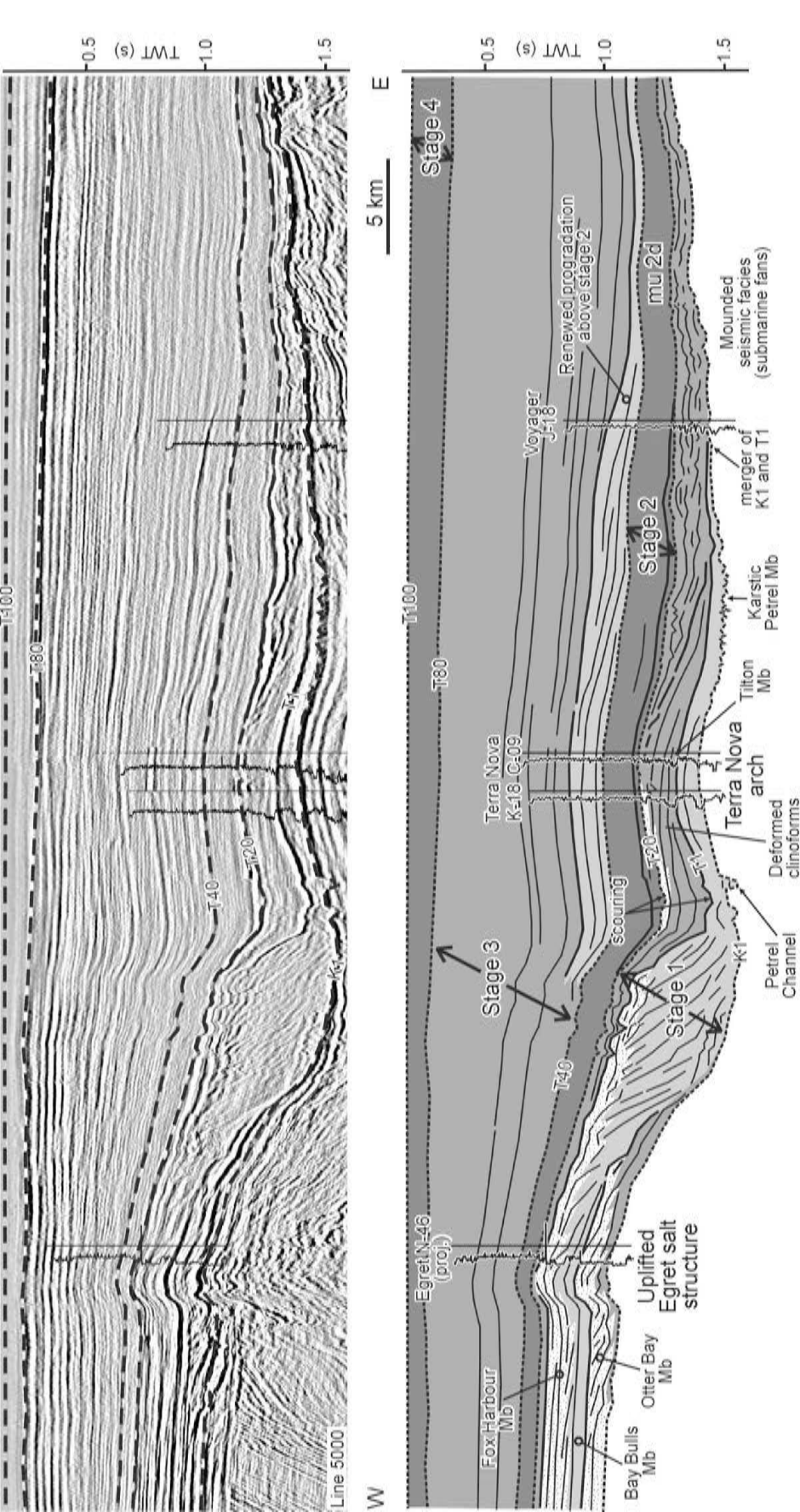


Figure 4.6. Regional west to east seismic profile (line 5000) across southern Jeanne d'Arc Basin, with ties to Egret N-46 (projected), Terra Nova K-18, Terra Nova C-09, and Voyager J-18. Note the mud-prone progradational unit above the T40 marker.

the top of the Turonian Petrel Member, a regional pelagic limestone marker deposited when long-term global sea level was high (Haq et al., 1987) and inundated much of the circum North Atlantic margins. For this study, the marker was merged with the basement highs that surround the basin in order to produce a regionally continuous surface. A time-structure map of the K1 marker illustrates the prominent basement highs that surrounded the basin in the Late Cretaceous (Figure 4.7a). The T20 marker is a composite seismic marker that forms the top of mounded seismic facies (associated with submarine fans on the basin floor) and forms a widespread onlap/downlap surface for overlying stage 2 deposits (Figure 4.3a). The marker lies within Ypresian strata.

Lithostratigraphy and seismic stratigraphy

During stage 1, the shelf was characterized by coarse-grained sediment of the Otter Bay, Fox Harbour, and regressive South Mara members (Figure 4.3a). The slope and basin floor were characterized by muddy marine deposits of the Dawson Canyon Formation, pelagic chinks of the Wyandot Formation, or siliceous to silt and shale deposits of the lowermost Banquereau Formation. Coarse-grained lithologies of the Avondale and South Mara members are typical of Paleocene and earliest Eocene submarine fans deposited on the basin floor. Stage 1 is also characterized by intermittent periods of extreme sediment starvation, when very little clastic sediment was supplied to the basin. The Petrel and Tilton members were probably deposited under such conditions.

A variety of seismic facies are recognized within the stage 1 interval, including shingled to oblique and sigmoidal clinoforms, corresponding to eastward building shelf-slope systems; mounds, corresponding to submarine fans; and regional draping reflections, corresponding to periods of pelagic accumulation. See Chapter 3 for a more detailed account of stage 1 lithostratigraphy and seismic stratigraphy.

Stage 1 sedimentation rates

Stage 1 deposits reach a maximum thickness of 700 m along the western margin of the basin, where prominent progradation is observed, and thin to less than 300 m in the central parts of the basin, east of the prograding shelf-slope systems (where submarine

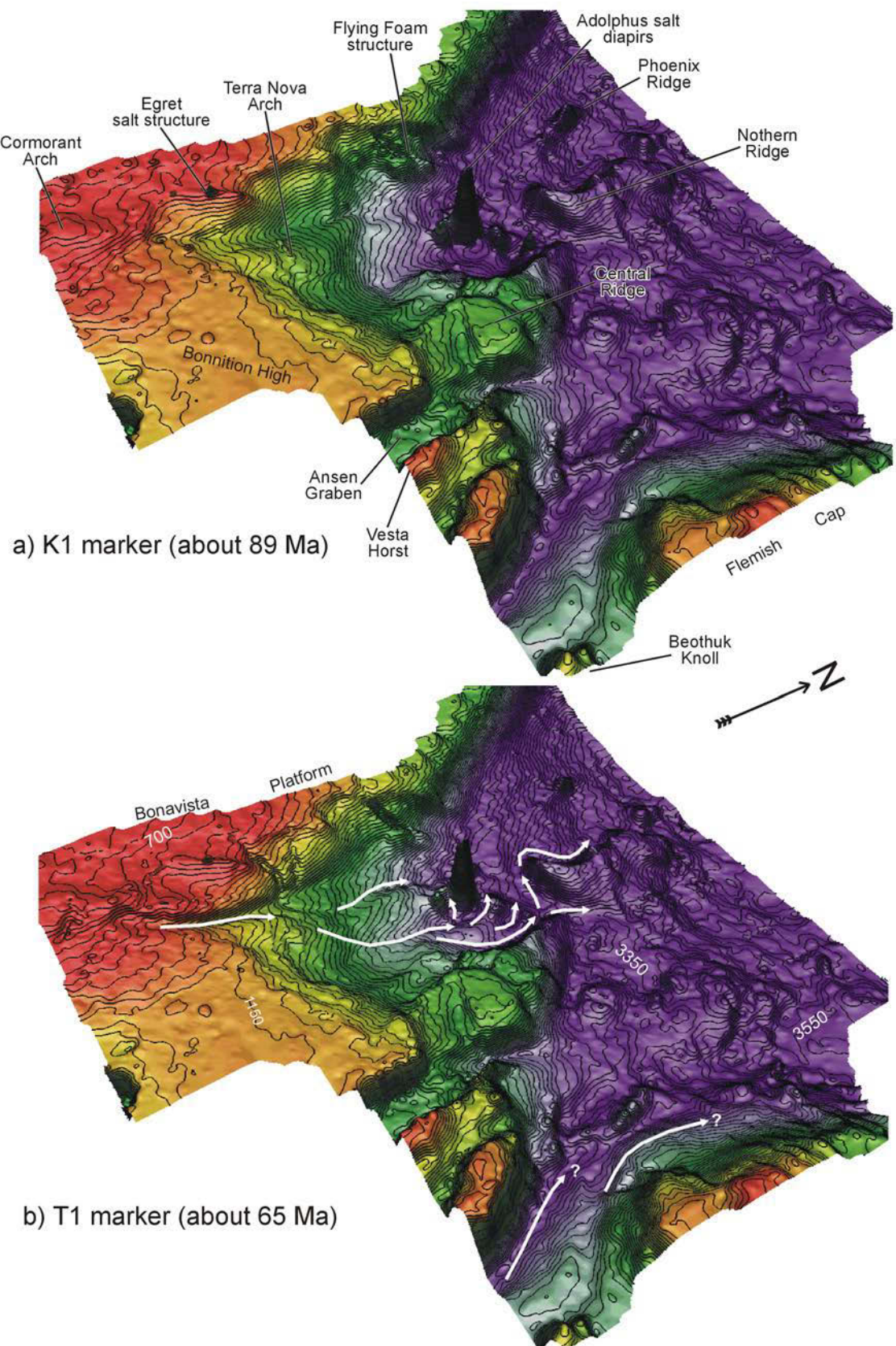


Figure 4.7. (caption located below Figure 4.7. e)

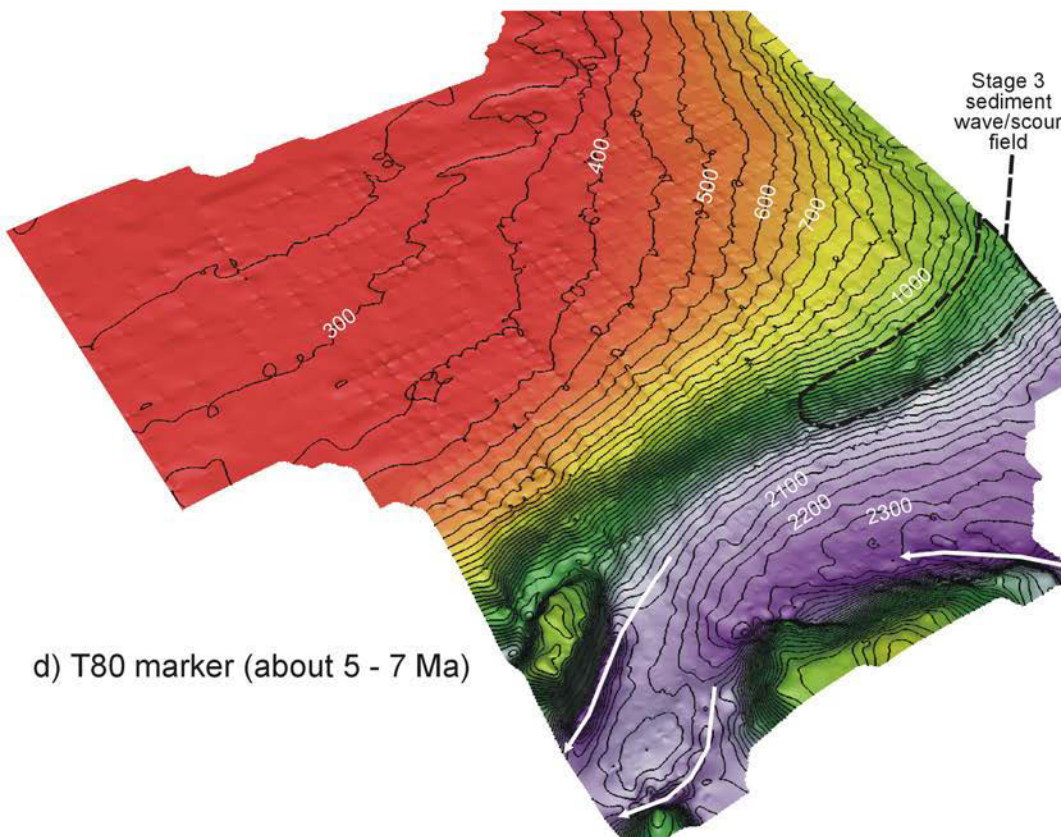
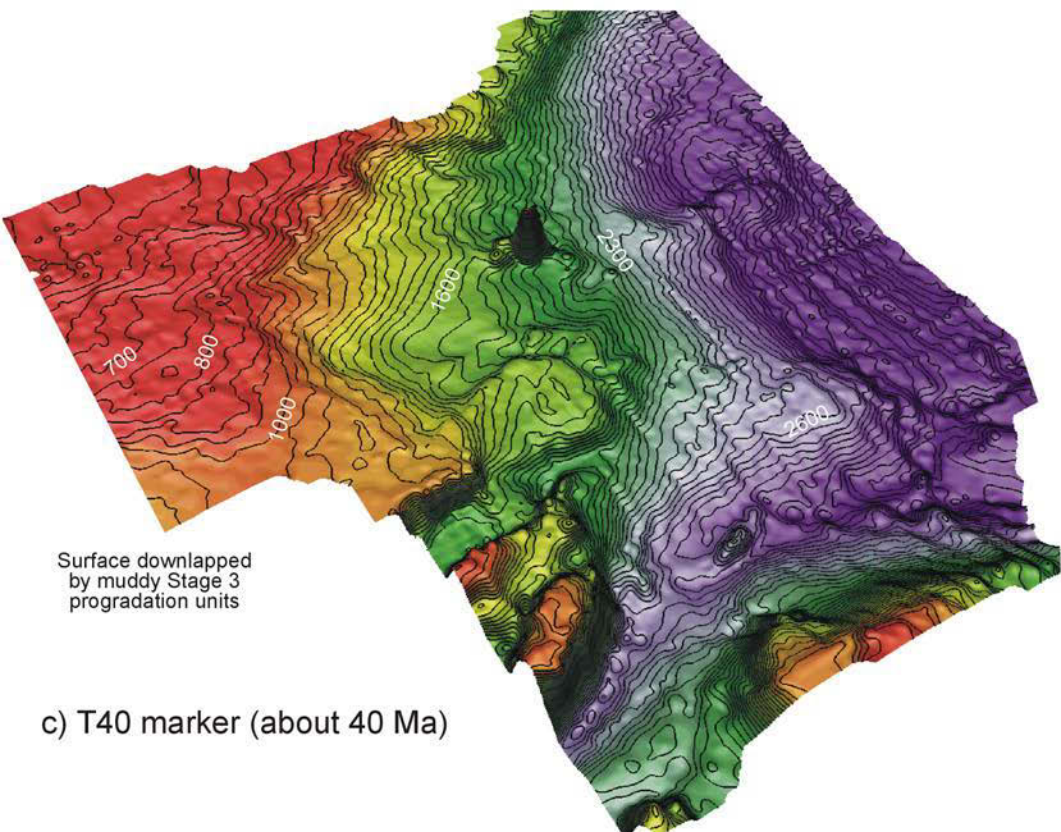


Figure 4.7. (continued - caption located below Figure 4.7. e)

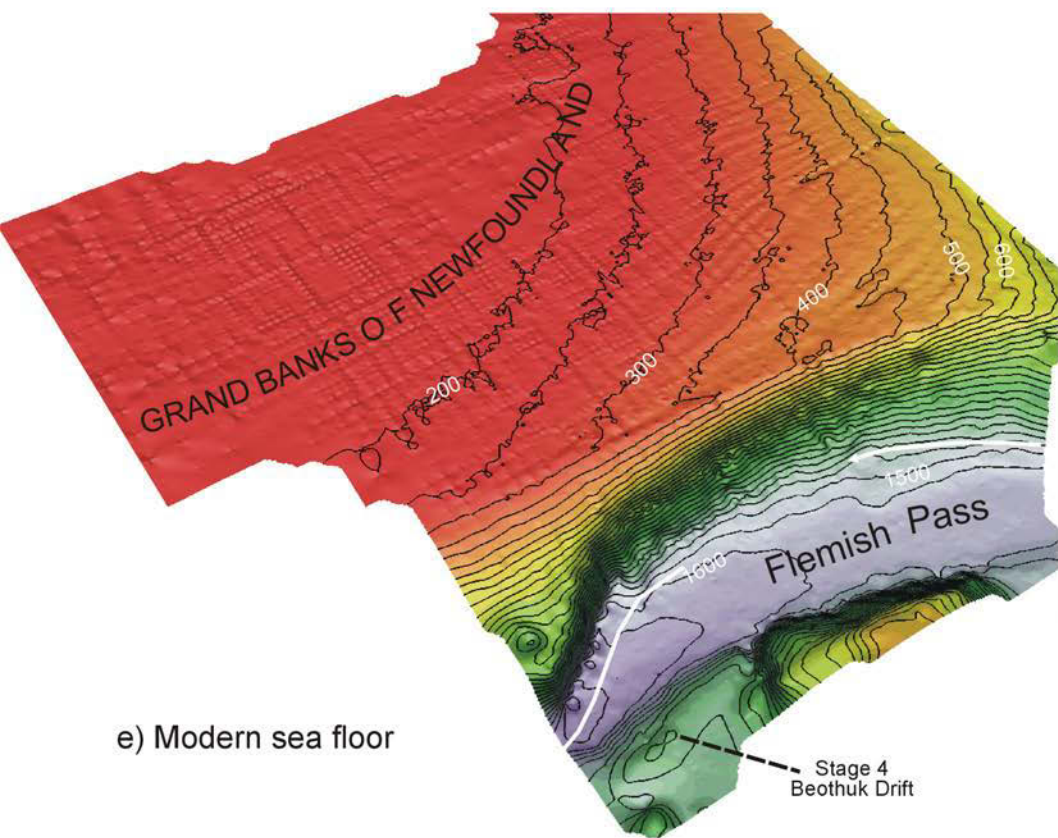


Figure 4.7. Continued. Perspective views (bird's eye view looking toward the northwest) of 5 regional time-structure maps through the Jeanne d'Arc Basin and across the Flemish Pass region (see Figure 4.1 for location). a) K1 marker, corresponding approximately to the top of the Turonian Petrel Member, and correlated above basement highs surrounding the basin. b) T1 marker, corresponding approximately to the boundary between Cretaceous and Tertiary strata. Blue arrows show the location of scours inferred to be caused by currents associated with circulation of the proto-Gulf Stream in the latest Cretaceous and/or earliest Tertiary. c) T40 marker, corresponding to the mid-Bartonian and defining the top of stage 2. d) T80 marker, corresponding to the Late Miocene (based on Gabriel C-60 in the Flemish Pass) and defining the top of stage 3. e) Modern sea floor. See text for details. Contour interval 50 ms (two-way travel time). Blue arrows in (d) and (e) indicate axis of scours inferred to have formed from circulation of the Labrador Current (Kennard et al., 1990).

fans are common). Stage 1 deposits are commonly less than 100 m thick above the Bonavista Platform and Central Ridge, indicating that basement highs played an important role in confining the distribution of sediment.

Despite the influx of clastics from the west, the long-term minimum (compacted) sediment accumulation rates during the Turonian to earliest Ypresian were low, at less than 2.0 cm/1000 years across much of the basin (Figure 4.9). When subdivided into Upper Cretaceous and lower Paleogene, the sedimentation rates are locally higher because in general, where Upper Cretaceous strata are thickest, lower Paleogene strata are thinnest (and vice versa). This is probably due to non-deposition above bathymetrically higher areas (like the thick prograded Late Cretaceous shelf-slope system - Figure 4.8b). Late Cretaceous accumulation rates vary from a maximum of 3.0 cm/1000 years along the western margin of the basin (e.g. near Hibernia), to less than 0.7 cm/1000 years in the central and southern parts of the basin (e.g. at North Ben Nevis P-93). Where the Wyandot Formation is thickest in the northern parts of the basin, sedimentation rates were as high as 2.0 cm/1000 years (Doeven, 1983).

The Paleocene to earliest Eocene accumulation rates were also quite variable, ranging from less than 0.8 cm/1000 years above the thickest part of the Late Cretaceous shelf, to as high as 3.5 cm/1000 years directly outboard of the Rankin and Hibernia canyons (e.g. at Avondale A-46), where progradational seismic facies are observed. In the central parts of the basin (e.g. at North Ben Nevis P-93, through both the Avondale and South Mara members), the long-term accumulation rates are 2.0 - 2.5 cm/1000 years.

Periods of sediment influx, via the progradation of shelf - slope systems and submarine fan deposition, were tempered by extended periods of sediment starvation in the basin. Combined with significant erosive gaps in the stratigraphic record (discussed in more detail later), sediment starvation contributed to the generally low long-term sedimentation rates during stage 1. If a 6 - 12 m.y. hiatus at the Fox Harbour unconformity is accounted for, long-term sedimentation rates increase to about 4.0 cm/1000 years. Estimated shorter-term sedimentation rates as high as 8 cm/1000 years could have been achieved along the western margin of the basin in the Campanian if the duration of significant hiatuses and highly condensed intervals are removed from the calculation.

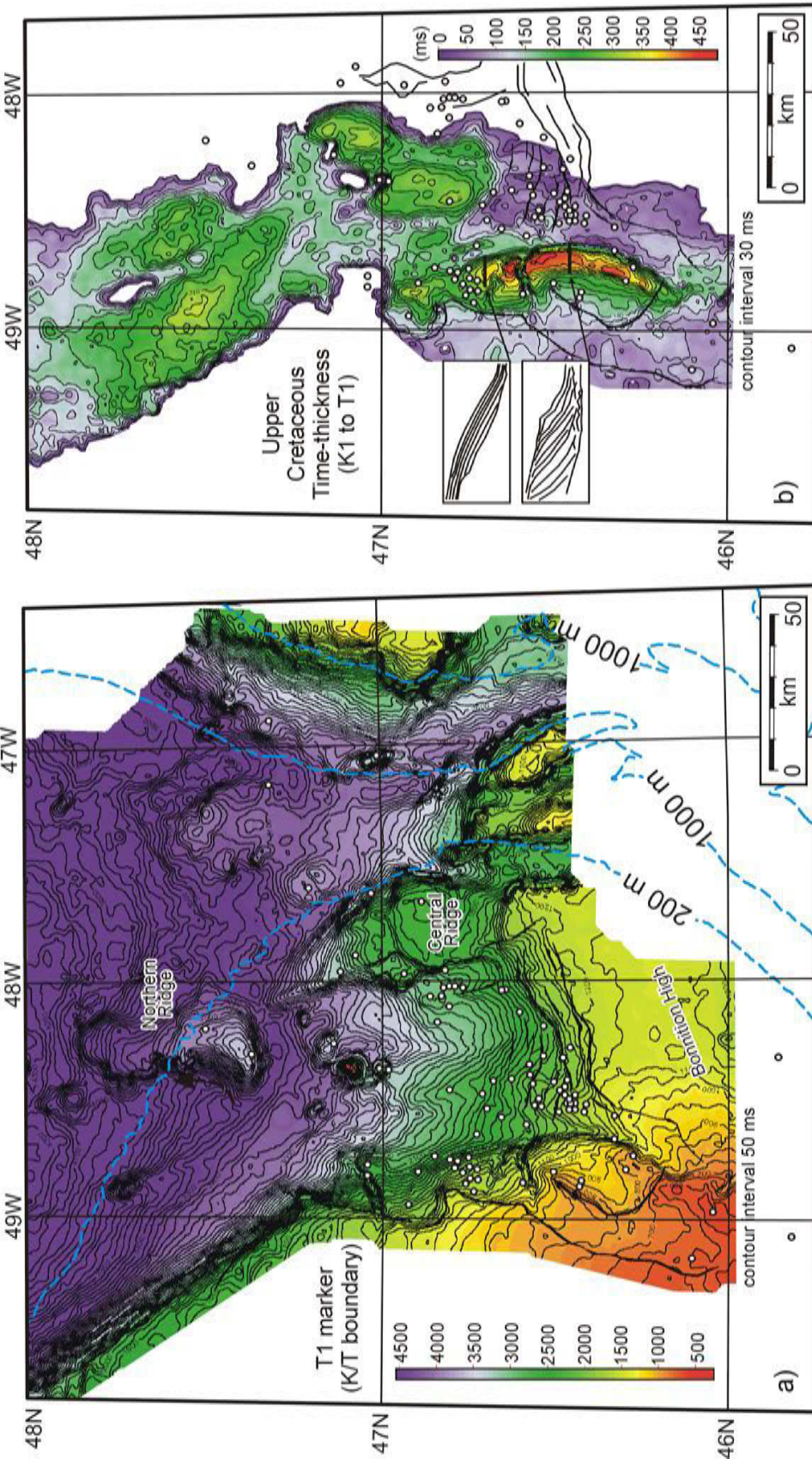


Figure 4.8. a) Time-structure map of the T1-marker (base of Tertiary). b) Stage 1 time-thickness map - Dawson Canyon and Wyandot formation interval (K1 to T1 markers). The broad "pods" in the northern parts of the basin are locations where the Wyandot Formation is best preserved. The "pods" were formed by a combination of erosion at the T1 marker, and local regions of increased basin floor sag. Note that much of the Upper Cretaceous succession has been removed (or was never deposited) in the southern parts of the study area.

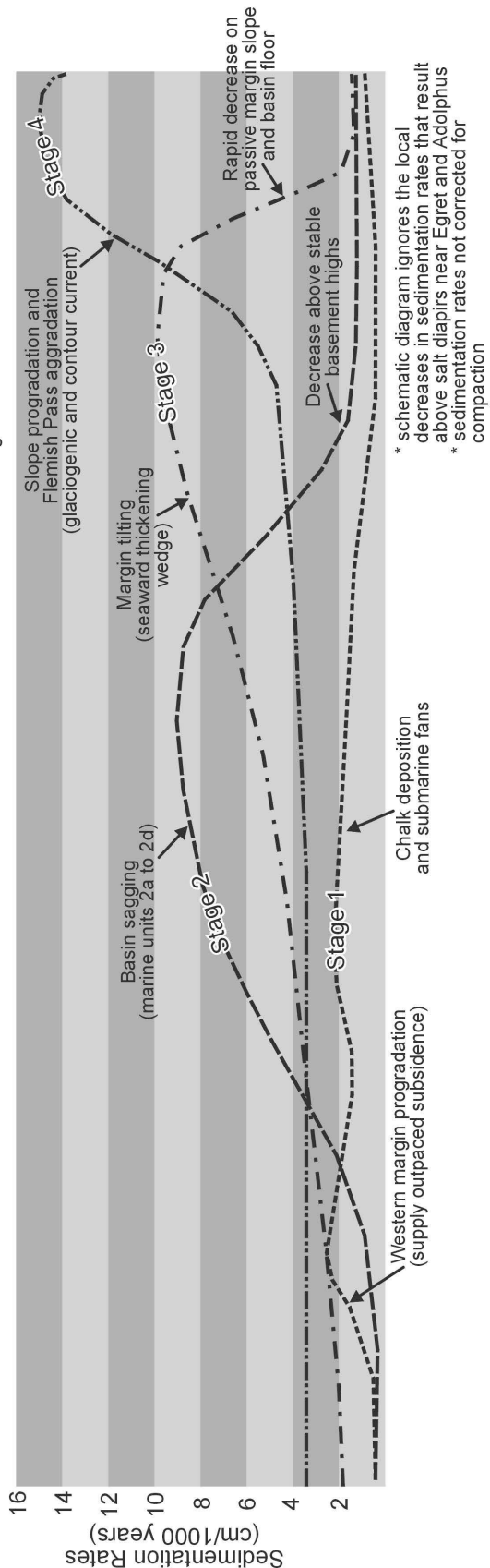


Figure 4.9. Schematic illustration showing the spatial changes in sedimentation rates in different basin locations during stages 1 through 4. Because sedimentation rates are long-term, and do not account for compaction effects, the rates are approximate, but are still useful for illustrating broad-scale changes in depositer changes during the post-rift evolution of the JDB. Note the shift in deposition from between basement highs during stage 2 to above basement highs during stage 3, as the entire margin tilted north and east of the hinge zone shown in Figure 4.5b.

4.3.2 *Stage 2 - Early to Middle Eocene*

Stage 2 strata were deposited in the Early to Middle Eocene (Ypresian to early Bartonian) within the Banquereau Formation (Figure 4.3a), and correspond to a profound change in depositional style in the JDB. The onset of stage 2 is marked by an abrupt termination of shelf - slope progradation and submarine fan deposition, replaced instead by the deposition of widespread fully marine shale units deposited in a confined basin.

Stage 2 is bracketed below by the T20 marker and above by the T40 marker (Figures 4.3a, 4.4, 4.6). The T20 marker, as described earlier, is a composite seismic marker that forms a widespread surface of onlap/downlap rather than an individual seismic reflection. Seismic facies on either side of the T20 are very different. The marker defines the top of mounded seismic facies associated with early Paleogene submarine fans and has been correlated above the sediment-starved shelf and slope. The surface is also characterized by scouring that locally erodes stage 1 deposits. The T40 marker is a regionally continuous seismic horizon that is downlapped (e.g. Figure 4.6) or overlain concordantly (e.g. Figure 4.4) by stage 3 deposits. It forms the first seismic marker above the T1 marker (approximately the K-T boundary) that can be mapped with confidence from the JDB, above the Central Ridge, and into the adjacent Flemish Pass, where it onlaps the western margin of the Flemish Cap (Figure 4.4). A time-structure map of the T40 marker shows that, by the end of stage 2, the depression between basement highs that surrounded the JDB had largely been filled in (Figure 4.7c).

Lithostratigraphy and seismic stratigraphy

The marine shales that progressively filled the basin during stage 2 can be subdivided into four seismically-defined units. From deepest to shallowest they are herein named 2a, 2b, 2c, and 2d (Figures 4.4, 4.10). Cumulatively, marine units 2a to 2d reach a maximum thickness of about 1000 m just north of the Adolphus salt diapirs, thinning to about 160 m thick near Terra Nova K-18. Poor data quality precluded mapping the marine units in the northern part of the data set, near the transition to the Orphan Basin.

Where penetrated by wells, the marine units consist dominantly of grey to brown shale and siltstone, and are difficult to distinguish from one another on the basis of

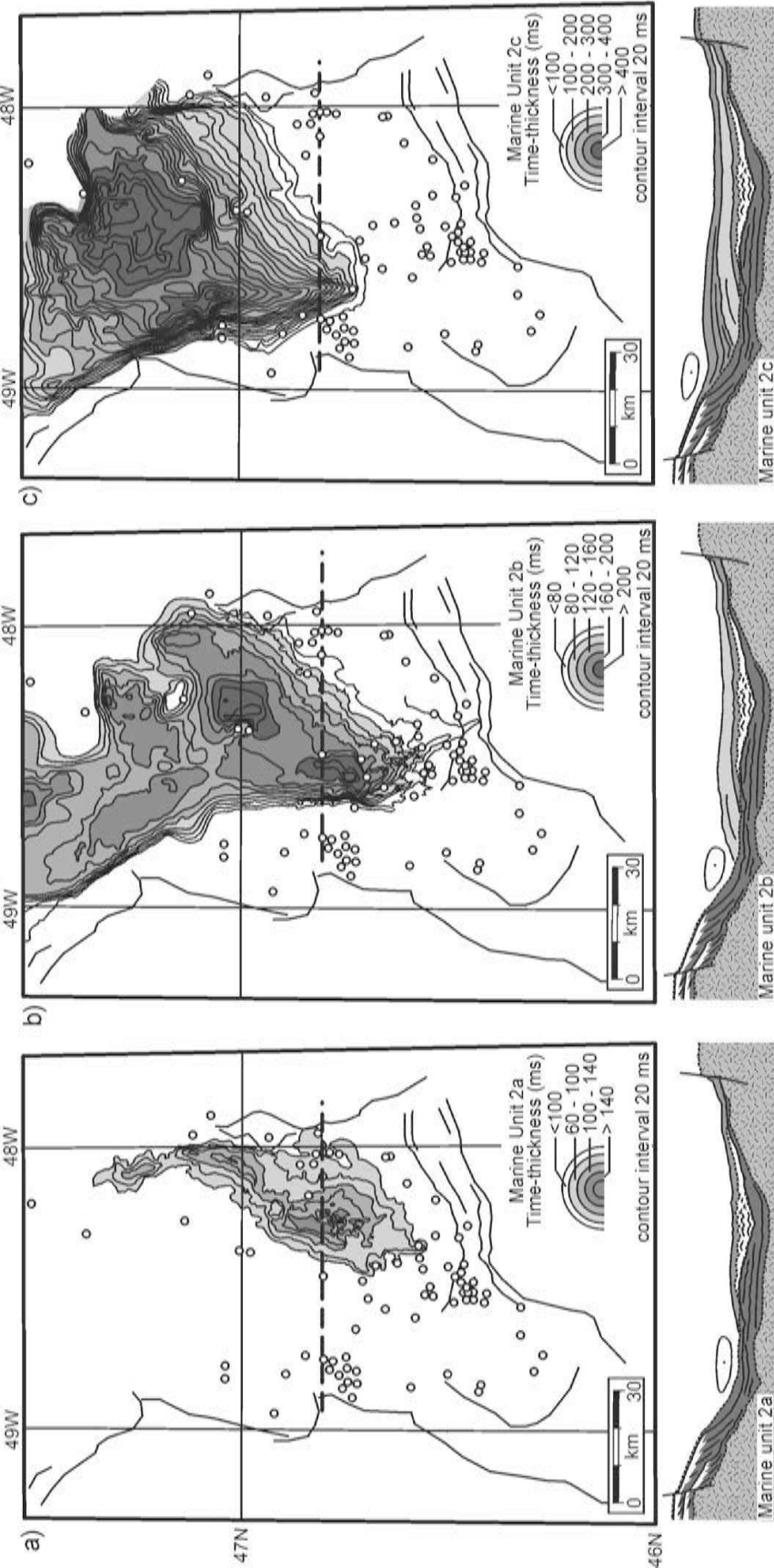


Figure 4.10. Time-thickness maps of a) marine unit 2a, b) marine unit 2b, c) marine unit 2c. Note the linear pinch out edge of each unit along the western margin of the basin. Contour interval is 20 ms (two-way time). Below each map is a cartoon illustrating the inferred depositional process for the marine units. Ellipse shows the inferred region of maximum current strength, corresponding to regions of non-deposition or scouring. Shale from marine units 2a to 2c accumulated adjacent to region of maximum current strength. The distribution of marine unit 2a (a) corresponds closely to the region of the thickest Adolphus Member of the Banquerey Formation.

lithology alone. Marine unit 2a, however, corresponds to the **Adolphus Member** of the Banquereau Formation, and can be distinguished by its low, blocky to serrated gamma ray response (Appendix IIa). The Adolphus Member is a dense, light to dark grey, slightly bentonitic and pyritic shale to siltstone unit. At Adolphus D-50, the member was logged as a bedded chert (see Figure 3.6, Chapter 3), whereas at Botwood G-89 it was identified as a shale deposited in middle to lower bathyal water depths (Frank Thomas, pers. comm., 1994). Its gamma ray character is distinctively low for a fine grained unit, and produces a similar response as the Lower Paleocene Tilton Member of the Banquereau Formation (Deptuck et al., 2003a). The API values are typically between 30 and 70, slightly higher than the typical response from the chalky Petrel Member, but lower than the average Banquereau Formation shale.

On seismic-reflection profiles, the top of marine unit 2a corresponds to the T25 seismic marker, which is commonly offset by small-scale or polygonal faults (Figures 4.11a, b). Similar “intraformational faulting” has been documented in Lower Eocene clays in the North Sea and was inferred to result from compaction effects rather than regional tectonic stresses (Henriet et al., 1988; Vanneste et al., 1995). Based on its age, the T25 marker corresponds approximately to the Ac seismic marker identified by Tucholke and Mountain (1979) further south in the Sohm and Hatteras abyssal plains. They correlated the Ac marker to the top of the Bermuda Rise Formation penetrated by several DSDP wells, a Lower Eocene sedimentary unit enriched in chert and biogenic silica (see Jansa et al., 1979).

In contrast to marine unit 2a, units 2b to 2d do not generate a low gamma ray response; instead they produce a moderately high gamma ray response typical of shale. In South Mara C-13, marine unit 2b consists of medium to dark grey/brown shale with pyritized worm burrows and occasional bivalves indicated in sidewall cores at 1650 and 1700 m.

Marine units 2a, 2b, and 2c thin and pinch-out below seismic resolution along the western, eastern, and southern basin margins, and are therefore inferred to have been deposited when the basin was still confined along three of its margins (Figure 4.10). Each marine unit is separated by a regionally continuous seismic marker that shows subtle onlap and/or downlap relationships, and local scouring. The seismic markers are

divergent (i.e. T25, T30, T35 - Figure 4.4), with increasing separation to the north and west. The western termination of each marine unit is distinctive. Deposits initially downlapped the toe-of-slope, and gradually onlapped the sediment starved western margin of the basin (Figures 4.4, 4.11a, b). In plan view, the pinch-out of marine units 2a, 2b, and 2c has a linear geometry, with an orientation that shifts from northeast (2a) to north (2b) (Figure 4.10). Marine unit 2a is thickest above a broad top-chalk scour located along the eastern basin floor, directly adjacent to the Central Ridge (Figure 4.10a). Successive marine units aggraded and built laterally towards the west, with deposits commonly thickest adjacent to the underlying marine unit. In this way the marine units gradually built toward the north and west as they filled the basin.

Marine unit 2d is considered transitional to the overlying “unconfined” stage 3 deposits. It thins above basement highs, but does not pinch out completely, and was the first unit deposited above the prominent Late Cretaceous shelf and Bonavista Platform since thin deposits of the Tilton and South Mara members. A hiatus, or highly condensed interval, should therefore be located at the base of marine unit 2d, above the Late Cretaceous shelf (where marine units 2a to 2c are condensed below seismic resolution). Marine unit 2d also drapes the southern part of the basin, extending beyond the southern termination of underlying marine units, with a thickness of about 120 m at Terra Nova K-18 (Figure 4.6). For comparison, marine units 2a to 2c have a cumulative thickness of less than 40 m at Terra Nova K-18. Deposition of marine unit 2d, therefore, corresponds to widespread deposition across much of the JDB, and above the basement highs that flank the basin, indicating that the entire study area was submerged. Interpreted bathyal water depths in Early to Middle Eocene strata above the Central Ridge at South Tempest G-88 and Trave E-87, and in the central parts of the basin at Botwood G-89, provides corroborating evidence that the basement highs and central basin floor were deeply submerged during stage 2 (Thomas, 1994, Frank Thomas pers. comm., 1994).

In the Flemish Pass, the T40 marker and underlying Early to Middle Eocene strata are penetrated at Gabriel C-60 and Lancaster G-70 (Figure 4.2) where the interval is dominantly shaly. Marine units 2a to 2d could not be identified in Flemish Pass.

Stage 2 sedimentation rates

Sedimentation rates during stage 2 are highly variable and depend on location (see Figure 4.9). Accumulation rates are lowest along the western, southern, and eastern flanks of the basin where the marine units are thinnest (highly condensed or absent). Stage 2 deposits at Terra Nova K-18, for example, have a long-term sedimentation rate of just 1.1 cm/1000 years. In contrast, at South Mara C-13 and Mara M-54, which penetrate over 500 m of stage 2 deposits, accumulation rates are between 3.5 and 5 cm/1000 years (Figure 4.9).

Botwood G-89, one of the only wells that penetrates all four marine units, penetrates more than 700 m of stage 2 deposits with accumulation rates between 5 and 6.5 cm/1000 years. Long-term accumulation rates of up to 9 cm/1000 years are estimated for the region north of the Adolphus salt diapirs and south of the Northern Ridge, where stage 2 deposits are as much as 1000 m thick (using an average acoustic velocity of 2000 m/s).

4.3.3 Stage 3 - late Middle Eocene to Late Miocene

Stage 3 strata of the Banquereau Formation were deposited in the late Middle Eocene (mid Bartonian) to Late Miocene (Figure 4.3a). Stage 3 is characterized by a period dominated by muddy shelf aggradation after most of the relief of the JDB had been filled in. A classic passive-margin shelf and slope system developed at this time (see Falvey, 1974 and Figure 2.23), and as the margin evolved through the Late Eocene to Miocene, the Grand Banks of Newfoundland began to take on a familiar form.

Stage 3 is bracketed below by the T40 marker and above by the T80 marker (Figure 4.3a). The T40 marker separates divergent reflections below (stage 2 marine units 2a to 2d) from relatively concordant, and locally downlapping, reflections above (Figure 4.4, 4.6). The T80 marker is a distinct regional seismic horizon that lies within 300 m of the sea floor on the Grand Banks, but underlies as much as 700 m of strata in the Flemish Pass. Where modern water depths are shallow, the T80 marker is commonly obscured by seafloor multiples. Stage 3 is considered a time of shelf-building. A time-structure map of the T80 marker strongly resembles the modern Grand Banks (Figure

4.7d). The broad shelf that developed between the T40 and T80 markers is considered the prototype of the modern Grand Banks.

Lithostratigraphy and seismic stratigraphy

Lithostratigraphically, stage 3 deposits consist dominantly of brown and grey neritic to bathyal shale and claystone of the Banquereau Formation, with scattered siltstone and rare marl and chalky limestone stringers. About mid-way through the Banquereau Formation, an interval of coarser-grained sediment (fine to very coarse sand and conglomerate) is recognized and formally designated the **Thorvald Member** of the Banquereau Formation (Appendix IIB). The Thorvald Member (identified informally as “Oligocene Sands” by the Canada-Newfoundland Offshore Petroleum Board, 1998) consists of two or three unconsolidated sand to conglomerate units separated by intervening Banquereau Formation shale. Each sand unit of the Thorvald Member produces a moderate to high amplitude, continuous seismic reflection, decreasing in amplitude to the east (interpreted to correspond to the eastward thinning of the member - observed in Figure 4.4). The Thorvald Member is interpreted as sandy inner shelf deposits that accumulated on the proto-Grand Banks. Interpretations from palynology samples at Hibernia C-96, P-15, and O-35 indicate that the member was deposited in the Early to Middle Oligocene (Graham Williams, pers. comm., 2003). In the northernmost study area, where the seismic data set is of poorest quality, there is some evidence for canyon incisions at a stratigraphically similar position to that of the Thorvald Member, though the correlation is tentative. It is possible that the sands were deposited during the period of mid-Oligocene lowered sea level identified by Haq et al. (1987), although this correlation is speculative with the available age precision.

Stage 3 deposits form a broad homocline, with strata generally dipping towards the northeast as sediment was loaded onto the margin. Increased subsidence and accommodation in the northeast part of the study area created a sedimentary wedge that thickens to the north and east, reaching its maximum thickness near the shelf-break of the T80 marker (Figure 4.7d). Minor thickness variations above the JDB suggest that low-relief saucer-shaped depressions may have been present on the shelf during stage 3, but otherwise the JDB had little expression. In stark contrast to stage 2, stage 3 stratigraphic

units show little thinning above basement highs, except along a hinge-zone (see Keen and Beaumont, 1990) located near the southern margin of the basin (Bonnition High, where most Tertiary stratigraphic units thin - Figure 4.5b).

Deposits above the T40 marker indicate the return to progradational seismic facies, once again building out from the west, above stage 2 deposits (downlapping the T40 marker). Where stage 2 deposits are thinned below seismic resolution, stage 3 muddy clinoforms prograded directly above stage 1 deposits (e.g. south of the Egret fault). In contrast to stage 1 progradation, stage 3 clinoforms are more subtle (low angle), cover broad areas, and consist dominantly of fine-grained lithologies (including the topsets - see well ties in Figure 4.6). Stage 3 progradation is best developed south of Terra Nova, and in the northernmost part of the study area, approaching the Orphan Basin.

By the Late Eocene the study area is interpreted to have formed a broad, unconfined, deeply submerged shelf. As the margin evolved, a true passive-margin shelf-break was established just west of the modern shelf-break. Poorer data quality in this region, however, prevents imaging the transition from shelf-perched progradation to passive-margin slope progradation. Aggradation and progradation of the muddy stage 3 slope built up the western margin of the Flemish Pass, and overlapped or downlapped the flank of the Flemish Cap. In the Flemish Pass, Lancaster C-70 and Gabriel C-60 penetrate stage 3 slope deposits and indicate a predominantly siltstone to shale succession with rare limestone stringers.

Stage 3 sedimentation rates

South of the Adolphus salt diapirs, the mid-Bartonian to Late Miocene long-term sedimentation rates decreased slightly in comparison to stage 2. At Mara M-54, South Mara C-13, and Botwood G-89, between 1100 and 1200 m of sediment were deposited during stage 3, accumulating at a rate of 3.2 to 3.8 cm/1000 years. In contrast to stage 2, the long-term sedimentation rates increased progressively north of the Adolphus area until the T80 shelf-break, seaward of which sedimentation rates decreased substantially (Figure 4.9). Stage 3 strata reach a maximum thickness of about 3200 m (assuming an average interval velocity of 2000 m/s) just west of the T80 shelf-break in the northeastern

corner of the study area where long-term sedimentation rates were as high as 9.5 cm/1000 years (Figure 4.9).

The thick shelf succession passes into a slope succession that flanks the western margin of the Flemish Pass and passes unconstricted to the north, towards the Orphan Basin. On the western margin of the Pass, stage 3 sedimentation rates decrease abruptly, corresponding to a thinning of the stratigraphic succession on the slope, east of the shelf-break. At Gabriel C-60, which samples a 600 m section of stage 3 muds, the long-term accumulation rate was 1.8 cm/1000 years, substantially slower than equivalent strata landward of the shelf-break.

4.3.4 Stage 4 - Latest Miocene to Quaternary

Stage 4 strata were deposited in the latest Miocene to recent (uppermost Banquereau Formation and Laurentian Formation - Figure 4.3). Significant sharpening of the shelf break took place during stage 4, and substantial deposits accumulated along the western margin and above the floor of Flemish Pass. In contrast, comparatively little sediment accumulated above the Grand Banks shelf during stage 4.

Stage 4 is bracketed below by the T80 marker and above by the modern sea floor (T100 marker). The T80 marker is a prominent surface of erosion in the Flemish Pass, and corresponds closely to the F' marker identified by Piper and Normark (1989) and an angular unconformity identified at the base of the Sackville Spur by Kennard et al. (1990). The Sackville Spur is a large, elongate sediment drift located northeast of the study area (discussed in more detail later - see also Kennard et al., 1990). The F' unconformity was inferred to have formed during a period of intensified bottom current erosion (Piper and Normark, 1989), and Kennard et al. (1990) linked it to the initiation of the south flowing Labrador Current in the Late Miocene (the timing of which is corroborated by evidence presented by Gradstein and Srivastava, 1980, and ties to Gabriel C-60). In this study, the T80 marker has been correlated to a prominent submarine peneplain surface across much of the southern Flemish Pass, and it is mapped laterally into prominent scours (Figures 4.7d, 4.12, 4.13). The modern sea floor in the study area is characterized by a broad submerged shelf, rimmed to the east by the Flemish

Pass and to the north by a scoured slope that extends into deep water of the Orphan Basin (just north of the study area, Figure 4.7e).

Lithostratigraphy and seismic stratigraphy

Little stratigraphic or age control is available from industry wells in the upper 400 m or so of strata above the Grand Banks shelf. Age control is, however, available for one well (Gabriel C-60) in Flemish Pass where the stage 4 interval thickens significantly. Stratigraphic control is provided by cuttings samples at Gabriel C-60, located in just over 1100 m of water on the western margin of the Pass. Additional stratigraphic control is provided by Lancaster F-70, Kyle L-11, and Baccalieu I-78, but biostratigraphic interpretations for these wells are not available at the relevant depths. All wells show an increase in unconsolidated coarse-grained material above the T80 marker. At Gabriel C-60 the sands are medium to coarse grained, poorly to moderately well sorted, and are argillaceous. They are interbedded with dark grey silty claystones.

On seismic-reflection profiles, stage 3 deposits are characterized by continuous seismic reflections that form sigmoidal clinofolds of a prograded slope. Slope clinofolds can be correlated back onto the Grand Banks shelf where they display toplap near the modern sea floor. In contrast to the slope, the floor of Flemish Pass is characterized by intervals of chaotic seismic facies, interleaved with continuous slope reflections. The chaotic units are interpreted as stacked mass transport deposits. In the early part of stage 4, the latest Miocene to Pliocene slope prograded east, and the Flemish Pass progressively narrowed. Basement highs located near the shelf-break were filled in and smoothed over (e.g. graben west of the Vesta Horst - compare Figures 4.7d and 4.7e). During the latter part of stage 4 the amount of slope progradation decreased and instead the floor of Flemish Pass underwent a period of rapid aggradation. Up to 700 m of sediment accumulated in the northeasternmost part of the study area in the latter part of stage 4 (since about the mid-Pliocene), interpreted to consist largely of stacked mass transport and contourite deposits (J. Mackie, pers. comm., 2003). Much of the sediment deposited during stage 4 is interpreted to be glaciogenic (see Piper and Normark, 1989).

Stage 4 sedimentation rates

The long-term sedimentation rates on the slope, and above the floor of Flemish Pass, were very high (Figure 4.9). At Gabriel C-60, which penetrates more than 700 m of stage 4 deposits on the floor of the Pass, the long-term sedimentation rates were as high as 14 cm/1000 years, a significant increase from any other time in the post-rift history of the study area (see Piper and Normark, 1989). Northeast of the study area, the Sackville Spur reaches a maximum thickness of 1200 m at its crest (Kennard et al., 1990) with a Pliocene to recent long-term sedimentation rate of more than 21 cm/1000 years.

4.4 Ocean circulation - past and present

Modern ocean circulation is driven by the prevailing winds as well as differences in sea water temperature and salinity, and it is influenced by sea floor bathymetry and deflection by the Coriolis force (Gradstein et al., 1990). Currents accelerate where bathymetric obstacles constrict them, and decelerate as they become unconstricted.

Maximum modern water depths in the study area are about 1100 m (on the floor of Flemish Pass), hence deep ocean circulation below this depth does not directly influence the sea floor in the study area. The modern sea floor is, however, directly influenced by the Labrador Current, a south-flowing cold water, low salinity surface current that has both a shelf component and a deeper upper slope component (down to depths of 960 m - Kennard et al., 1990). In addition, a deeper current, the Western Boundary Undercurrent, actively shapes the lower slope just north of the study area (Carter and Schafer, 1983). The Western Boundary Undercurrent is a south-flowing thermohaline (contour) current with a maximum current strength between 2600 and 2800 m depth (Kennard et al., 1990). Since the Late Miocene, the Labrador Current and Western Boundary Undercurrent have acted in tandem to mold the Sackville Spur (Kennard et al., 1990 - discussed later). The Western Boundary Undercurrent is also believed to have sculpted a broad moat along the northern and eastern margins of the Flemish Cap, in water depths of about 2550 m (Kennard et al., 1990).

A third current, the north-flowing Gulf Stream, is a warm-water surface current that is propelled out of the Gulf of Mexico through the gap between Florida, Cuba, and the Bahama Banks (the Straits of Florida), traveling northward along the East Coast of

North America. The current affects the seabed in water depths that exceed 500 m along the Blake Plateau (Pinet et al., 1981; McCave and Tucholke, 1986; Dillon and Popenoe, 1988) but further north travels above the much deeper Sohm Abyssal Plain (Laine and Hollister, 1981). Part of the current continues toward Iceland and the Arctic Ocean where it either cools and sinks, ultimately returning south via deeper thermohaline currents (e.g. the Western Boundary Undercurrent), or recirculates in a counterclockwise manner, joining the East Greenland Current, ultimately merging with the Labrador Current (see Laine and Hollister, 1981). The Gulf Stream is believed to have influenced the study area in the past (discussed in more detail below), but today is deflected from the east coast of Canada by the south-flowing Labrador Current (Berggren and Hollister, 1974; Gradstein and Srivastava, 1980).

4.4.1 Ocean current indicators - stages 1 to 4

A variety of morphological elements have been used as ocean current indicators, including scours, sediment waves and contourite drifts (e.g. Heezen and Hollister, 1964; Pinet et al., 1981; Kennett, 1982; Carter and Schafer, 1983; McCave and Tucholke, 1986; Kennard et al., 1990; Howe, 1996; Faugères et al., 1999; Hernandez-Molina et al., 2003). In this study, the distribution of broad scours, sediment waves, and contourite drifts was mapped throughout the study area (Figure 4.13). They are recognized as far back as the Cretaceous - Tertiary boundary, and are interpreted to have developed from the circulation of ocean currents. They imply that ocean currents periodically swept across the study area through stages 1 to 4, and at times played an important role both in supplying sediment to the margin (particularly during stage 2) and preventing sediment from accumulating (during stage 1, and locally during stage 2). The location and orientation of current indicators, as well as indirect evidence like microfossil assemblages, offer clues about the origin of the ocean currents and provide insight about post-rift paleoceanography along the margin.

Stage 1

The T1 marker, located mid-way through stage 1 deposits, appears to be widely unconformable, extending not only above the shelf, but also onto the slope and basin

floor, at least 350 m below the shelf-break. Here, prominent scours are observed in regions that could not have been subaerially exposed without an implausibly high relative sea level fall of at least 350 m across wide expanses of the basin (Figures 4.7b, 4.8, 4.11e, f). East of the Late Cretaceous shelf - slope system, the Cretaceous - Tertiary boundary is commonly sharp, corresponding to a change from pelagic carbonates, marls, or marine shales below (Dawson Canyon and Wyandot formations) to low gamma ray deposits of the coarse-grained Avondale Member (submarine fans) or finer-grained Tilton Member (marine siliceous unit) above (both members located at the base of the Banquereau Formation - Figure 4.3a, see chapter 3). Strata above and below the T1 marker were deposited in a marine setting (outer neritic to bathyal - Thomas, 1995), hence no stratigraphic evidence for subaerial exposure of the slope and basin floor has been identified. The observed erosion, therefore, is interpreted as a submarine unconformity.

The T1 marker is a widespread surface of erosion. Merger between the T1 reflection and underlying K1 reflection is observed in several locations, implying significant hiatuses on the basin floor and contributing to the low stage 1 long-term sedimentation rates. For example, the base of the latest Cretaceous slope on the western margin of the basin is highly erosive north of the Egret fault and south of Hibernia (Figure 4.11e, f). Merger of the T1 and K1 reflections demonstrates a hiatus of more than 25 m.y., with Lower Paleocene strata directly overlying Turonian chalks. Even in more northerly locations, where the Upper Cretaceous stratigraphic record is most complete (dominated by upper bathyal marine shales and pelagic carbonates), a hiatus of about 1 m.y. is present at the top of the Wyandot Formation in Adolphus D-50 (Doeven, 1983) and in Botwood G-89 the latest Maastrichtian is absent (Mobil et al., 1992). Broad scours erode the Wyandot chalk in the central and northern parts of the basin, where the formation is best preserved in broad pod-shaped lenses that can reach a thickness of 400 m at their apex (e.g. Botwood G-89 - Figures 4.8b, 4.11a, b, 4.13).

In some areas, erosion of the slope and basin floor is related to the incision of submarine channels that can be readily linked to prominent canyons along the western margin of the basin (e.g. the Hibernia and Rankin canyons - Figures 4.8a, b). Other scours like the top-chalk scours, however, are wider, trend parallel to the length-axis of the basin, and cannot be linked to submarine canyons. They are considered to be too long

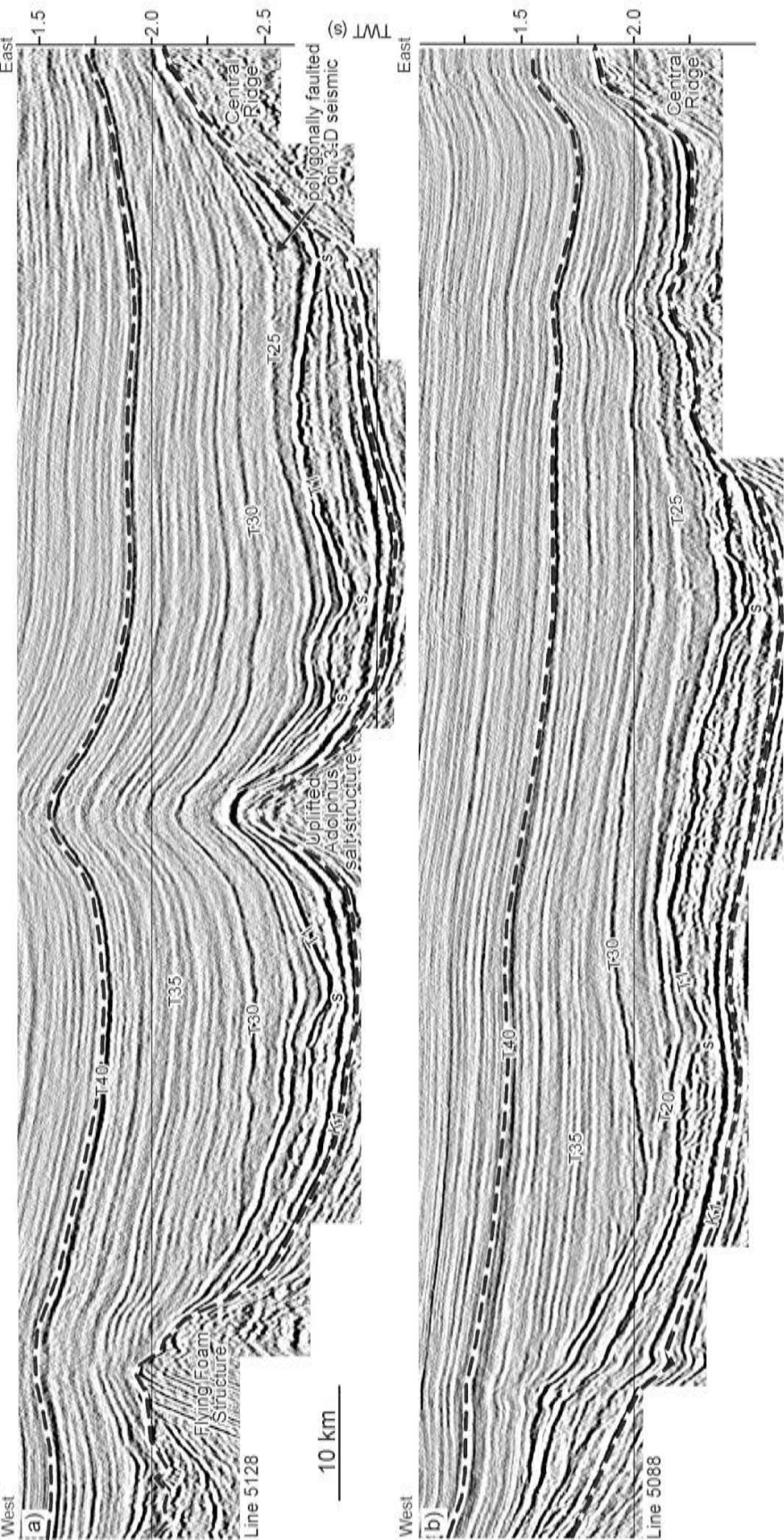


Figure 4.11. West to east profiles across a) northern and b) central Jeanne d'Arc Basin, showing stage 1 (K1 to T20) and stage 2 (T20 to T40) deposits. Note the scours (s = scour) that erode the Wyandot/Dawson Canyon formations near the K-T boundary (T1 marker). They are believed to have formed during the passage of erosive ocean currents that swept through the funnel-shaped basin in the latest Cretaceous and/or earliest Paleocene, and are perhaps associated with warm waters of the proto-Gulf Stream. Also note the western pinchout of the stage 2 marine units and the prominent thinning of stage 1 and 2 deposits above the western and eastern basin margins. See figure 4.2 for location.

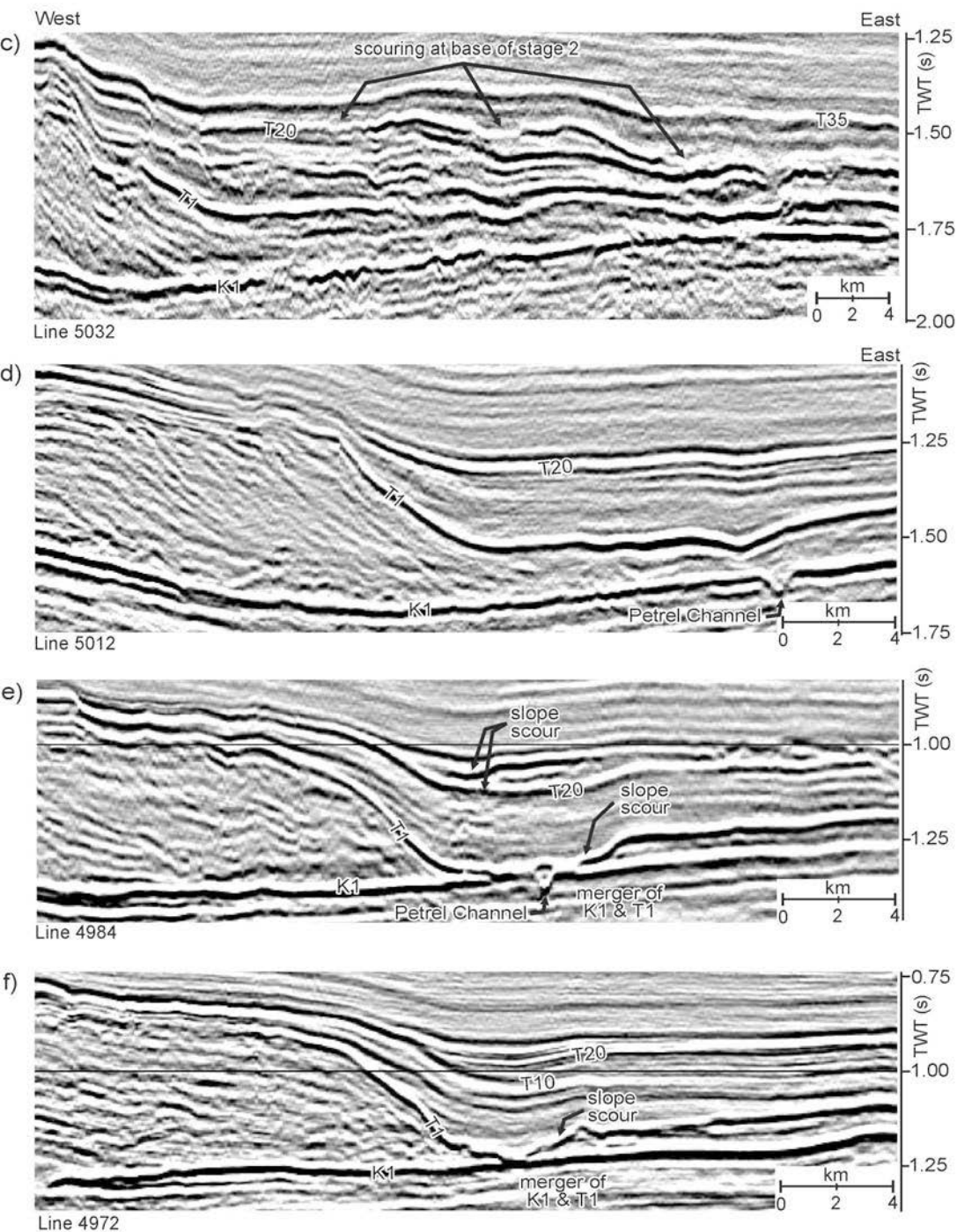


Figure 4.11. (continued) c) to f) show a series of west (left) to east (right) profiles across the erosive latest Cretaceous to earliest Paleocene slope. (c) is located furthest north and (f) is located furthest south. Note the prominent slope erosion in (e) and (f) causing the T1 seismic horizon to merge with the K1 seismic horizon, resulting in a substantial hiatus. See Figure 4.2 for location.

and broad (relative to the size of the shelf-slope depositional system) to have formed from turbidity currents or debris flows. They appear to be the marine equivalent of the Fox Harbour unconformity identified on the shelf, though deposition of submarine fans above the scours suggests that canyon incision on the shelf slightly post-dates the marine unconformity (Deptuck et al., 2003a). Scours have also been identified that erode the base of the Central Ridge and the Northern Ridge (e.g. Figure 4.13), hence erosion is not restricted to a calcareous substrate, and therefore did not form solely from carbonate dissolution.

Several mechanisms could have produced the submarine unconformity at the T1 horizon in the JDB, including tidal currents, wind-driven surface currents, or even a single catastrophic period of erosion associated with a tsunami from the K-T bolide impact (see Bralower et al., 1998; Norris et al., 2000; Klaus et al., 2000). Norris et al. (2000) interpreted the widespread A* seismic marker (Tucholke and Mountain, 1979; Jansa et al., 1979), which is time-equivalent to the T1 seismic marker in the JDB, to correspond to mass-flow deposits (allochthonous chalks) at the K-T boundary, triggered by the Chicxulub bolide impact on the Yucatan Peninsula. Norris et al. (2000) suggested that the 65 Ma bolide impact was responsible for slope instability and mass failure across extensive areas of the western North Atlantic, extending from Florida to the Grand Banks.

Since no core data exist across the K-T boundary in the JDB, this mechanism is difficult to evaluate. Given the large distance between the Yucatan Peninsula and the JDB, as well as “obstacles” like the Gulf of Mexico and Florida, it seems unlikely, however, that a tsunami would reach the JDB. Given also that there is considerable debate over the age of the mass transport deposits themselves (see Keller et al., 1993; Macleod et al., 2003), which Norris et al. (2000) and Klaus et al. (2000) interpret as synchronous with the bolide impact, a less exotic mechanism for the formation of T1 scours in the JDB is envisioned. The scours are interpreted to have formed either from tidal currents or from erosive ocean surface currents that flowed through the JDB at the end of the Cretaceous or earliest Paleocene. Based on anecdotal evidence presented in section 4.5.3, the latter mechanism is preferred. Relatively synchronous (within the limits of seismic resolution) and laterally extensive non-depositional to erosive

discontinuities, like the T1 marker, are relatively common in areas swept by strong ocean currents (Faugères et al., 1999).

In the Flemish Pass region, elongated lenticular deposits, characterized by moderate to high amplitude hummocky to mounded reflections, are recognized within a highly condensed stage 1 interval (Figures 4.12a, 4.13, 4.14b). No wells penetrate these deposits, but Gabriel C-60 penetrated Paleocene (?) chalks in the equivalent interval above a basement high adjacent to the elongated deposits (Bujak Davies Group, 1987). These deposits are therefore tentatively interpreted as chalks that were molded by stage 1 ocean currents.

Stage 2

Several depositional mechanisms have been considered for marine units 2a to 2d, and both structural and stratigraphic controls for their peculiar geometry have been evaluated. One interpretation is that their geometry reflects the subsidence history during stage 2, each unit forming in response to an abrupt pulse of basin sagging (hence creating the divergent reflections and discordances between units). Through subsidence, onlapping reflections would have been modified to downlapping reflections (e.g. marine unit 2b, Figure 4.10b). For this mechanism to be plausible, however, subsidence would have had to take place along narrow (less than 10 km) bands adjacent to the western basin margin, a scenario that is not believed to be possible without active strike-slip faults with a similar orientation, significant salt withdrawal, or other structural controls (none of which can account for the observed geometry of marine units 2a to 2d). Therefore a depositional control for the peculiar geometry of marine units 2a to 2d is preferred in this study.

Based on their geometry, fine grained lithology, and the recognition of linear scours, marine units 2a to 2d are interpreted as either hemipelagic deposits that were locally strongly influenced by ocean currents, or as contourites. They show a distinct linearity in thickness distribution, particularly where they pinch-out along the western margin of the basin, and are separated by major discontinuities (the T25, T30, T35, and T40 seismic horizons - Figures 4.4, 4.11a, b), interpreted to reflect changes in current strength and location. Regions with the most intense current strength correspond to areas

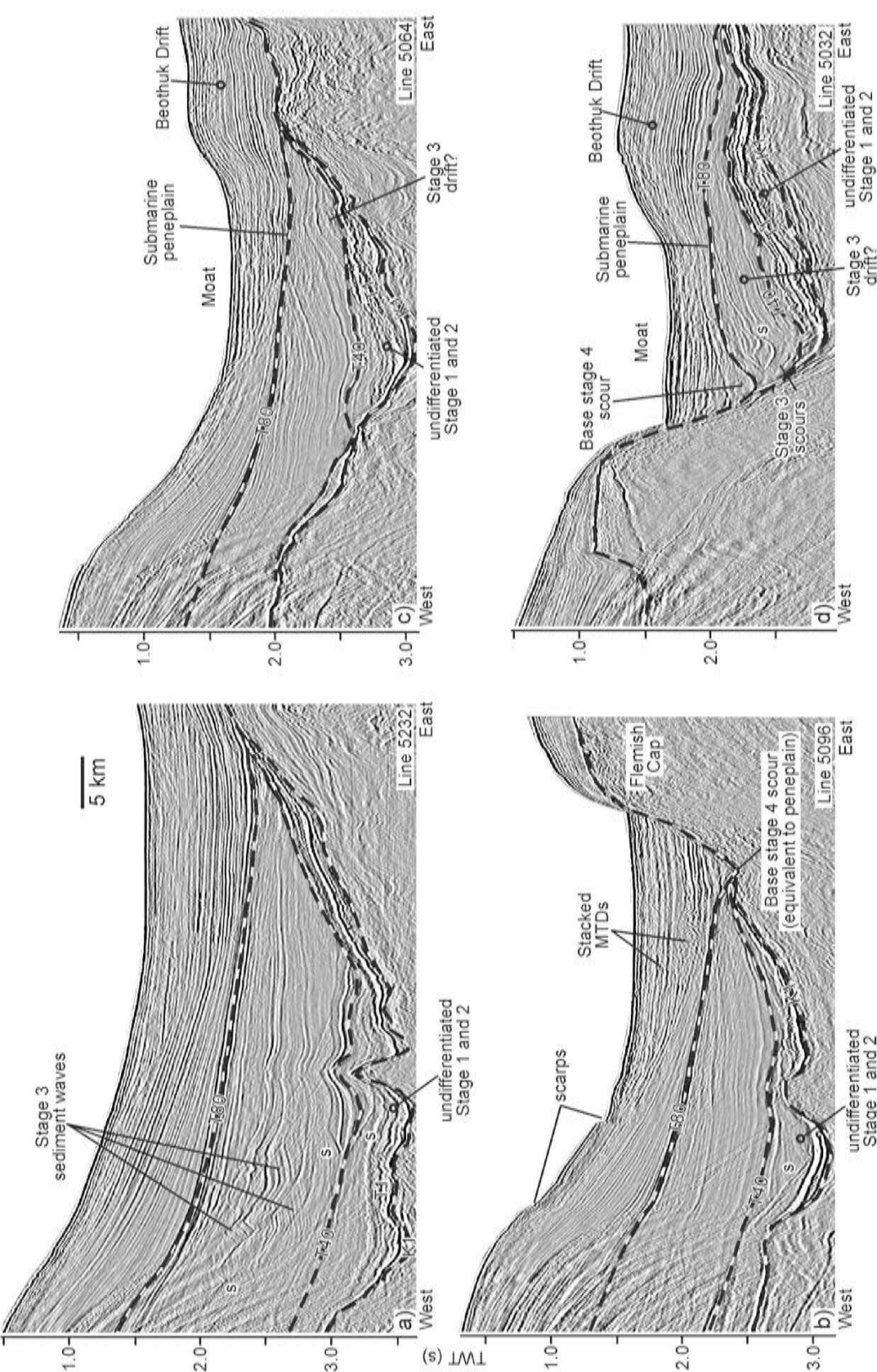


Figure 4.12. West to East seismic profiles across the Flemish Pass. a) b) c) d) See Figures 4.2 and 4.13 for location. MTD = mass transport deposit

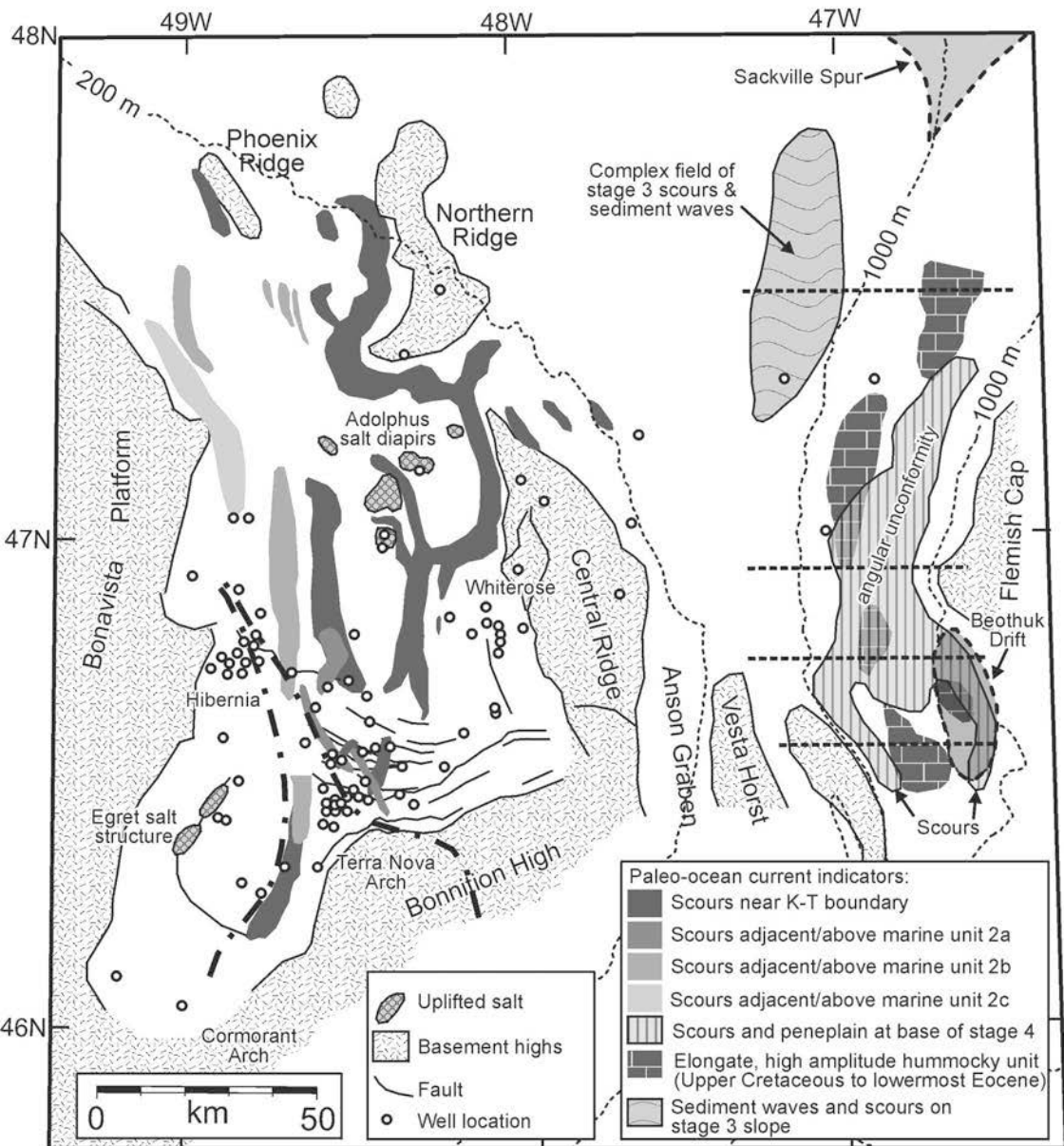


Figure 4.13. Basement of study area showing the location of ocean current indicators like scours, sediment waves and drifts. The shelf-breaks during the latest Cretaceous and early Ypresian are shown in bold dashed and dotted lines.

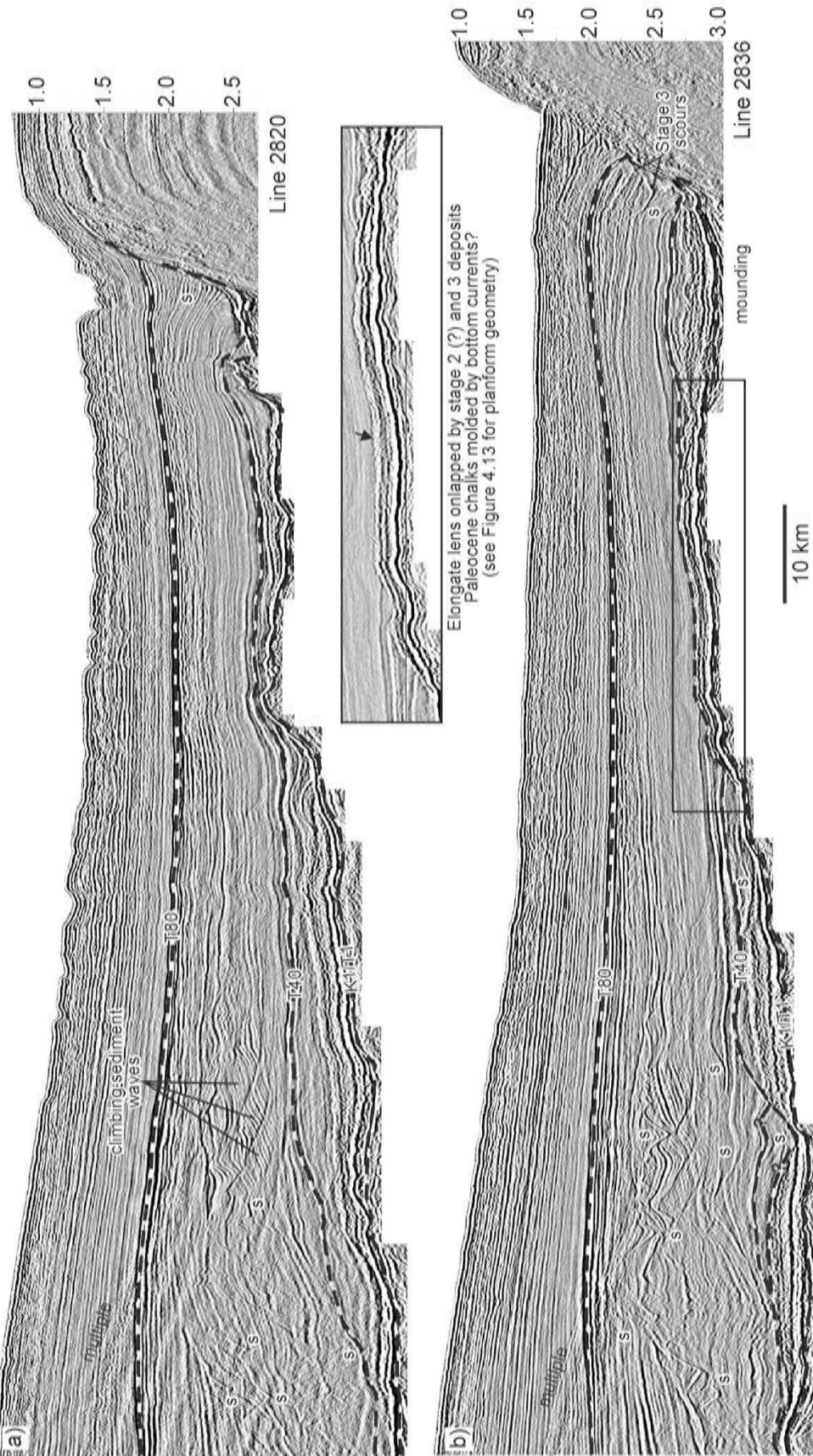


Figure 4.14. North (left) to South (right) profiles along the axis of the Flemish Pass. Stage 1 and 2 deposits are highly condensed within the Flemish Pass. Correlation of the T40 marker is difficult where scouring has removed part of the section. Above the T40 marker, stage 3 deposits show complex seismic facies interpreted as scours and climbing sediment waves formed in response to deeper currents (~1000 and 2200 m of water) that flowed along the stage 3 slope. s = scour. See Figure 4.2 for location.

of non-deposition or erosional scouring (sedimentation rates of less than 1 cm/1000 years), focused in a zone that progressively migrated up the western basin margin during stage 2 (Figures 4.10a-c).

The recognition of major discontinuities, a convex-upward lenticular geometry, and progradation/aggradation, are all characteristics outlined by Faugères et al. (1999) for the recognition of contourite drifts from seismic data. Based on their morphology, marine units 2a to 2d are interpreted as hybrids between confined drifts, developed in a narrow, elongated, structurally-controlled basin, and plastered drifts, formed from a migrating current above a basal erosive discontinuity (Faugères et al., 1999), in this case the T20 marker.

In the Flemish Pass, some scouring and possible small plastered drifts are recognized, but it is difficult to determine whether they formed during stage 2 or the overlying stage 3, because correlation of the T40 marker, particularly across scours, is difficult (e.g. Figure 4.14b).

Stages 3 and 4

By stages 3 and 4, the relief of the JDB had been filled in and no ocean current indicators are recognized above the basin. Instead, current indicators are recognized only in the Flemish Pass area, east of the filled JDB. A zone of complex seismic facies, interpreted as climbing sediment waves and erosive scours, is recognized on the stage 3 middle to lower slope (Figures 4.12a, 4.14). The sediment waves and complex scours are best developed near the northeast corner of the proto-Grand Banks, adjacent to and underlying the modern Flemish Pass (Figures 4.7d, 4.13). Seismic reflections can be correlated from this area to the south, into linear stage 3 scours located adjacent to a basement high near the southeastern corner of the study area (Figure 4.12d). These elements suggest that relatively deep contour currents swept across the middle to lower slope, outboard of the proto-Grand Banks shelf during the Middle Eocene to Miocene (between water depths of approximately 1000 and 2200 m).

The onset of stage 4 in Flemish Pass is marked by a significant unconformity (T80 marker), above which there is abundant evidence for contour-current-related deposition. The T80 marker peneplain surface correlates to the base of two linear erosive

scours that run parallel to the eastern and western margins of the Flemish Pass (Figures 4.7d, 4.12b, d, 4.13). The scours are interpreted as erosive moats that developed from bottom currents that were constricted by basement highs. The scours provide additional support for Piper and Normark's (1989) supposition that the unconformity formed from intense bottom currents. Comparison between the T80 and T100 time-structure maps in Figures 4.7d and 4.7e shows the infill of the graben east of the Vesta Horst and the formation of a confined contourite drift adjacent to the Flemish Cap (herein referred to as the Beothuk Drift - Figure 4.13). The Beothuk Drift, crossed by seismic profiles in Figures 4.12c and d, appears to be time-equivalent to the Sackville Spur, located northeast of the study area (see Kennard et al., 1990).

4.5 Discussion

Unlike the Scotian, the southern and southeastern Newfoundland, and the Labrador margins, where the post-rift succession is broadly characterized by a seaward-thickening wedge above a break-up unconformity (referred to as a "continental terrace wedge" by Tankard and Welsink, 1987 or a "continental terrace prism" by Balkwill, 1987), the JDB underwent a period of confined deposition (stages 1 and 2) during its early post-rift history, which delayed the development of a seaward-thickening wedge (stages 3 and 4) until the Middle Eocene.

In the Late Cretaceous to early Bartonian (stages 1 and 2), deposition in the JDB was confined along three margins (south, west, and east), with strata thinning significantly above basement highs, and little sediment accumulating in the Flemish Pass. The interval corresponds closely to McAlpine's (1990) depositional sequence 5, which he identified as the transition to drifting between Labrador and Greenland and Greenland and northern Europe. In the late Bartonian to Recent (stages 3 and 4), deposits were largely unconfined towards the north and east, accumulating in a seaward-thickening passive-margin shelf and slope setting, with significant quantities of sediment accumulating in Flemish Pass. Figure 4.9 schematically illustrates changes in sedimentation rates in the study area during stages 1 through 4 along a southwest to northeast transect across the basin. A prominent shift takes place between maximum stage 2 sedimentation rates where the depocenter is located *between basement highs* near

the Adolphus region, to maximum stage 3 sedimentation rates where the depocenter is located *above basement highs* further north and east.

4.5.1 *Changing basin structure and margin evolution - stages 1 to 4*

During **stage 1** the primary depocenters were located along the progradational western margin of the basin and near the Adolphus salt diapirs (where the Wyandot chinks and marls are at their greatest thickness - Figures 4.8b, 4.9). The rate of sediment supply temporarily outpaced subsidence during stage 1, at least along the western margin of the basin. Given that the overall sedimentation rates were fairly low during stage 1, the subsidence rates along the western margin must also have been low, otherwise the shelf-break could not have advanced. Geohistory analysis (see Van Hinte, 1978) on the Dominion O-23 well in the northern JDB, and on several other wells along the margin of the Orphan Basin and Labrador Shelf, indicate that basement subsidence was very slow during the Late Cretaceous, but increased abruptly at the end of the Cretaceous after sea floor spreading began in the Labrador Sea (Gradstein and Srivastava, 1980).

Much of the basin deformation that had been prevalent in the Early and mid Cretaceous stopped by the Late Cretaceous, a period commonly interpreted to correspond to the onset of passive-margin thermal subsidence in the JDB (Hubbard et al., 1985; Enachescu, 1987; Sinclair, 1988, 1995; de Silva, 1993). Still, some structural elements were active in the Late Cretaceous and early Paleogene, including normal faults (locally accompanied by growth on the down-thrown side) and local regions of up-arching related to salt tectonics, basin inversion and/or differential subsidence. Near the Egret and Adolphus wells (Figure 4.2) up-arching is related to latest Cretaceous and early Paleogene salt mobility (Figures 4.7a, 4.11). Salt-related uplift near the Egret wells appears to have diverted the path of the Rankin Canyon to the north and created a positive bathymetric feature that was overlapped by stage 2 strata. Coupled with motion along the Egret fault, salt-related uplift near Egret probably also played an important role in modifying the sediment delivery to the western margin of the basin in the earliest Paleogene. Scissor motion along the Egret Fault acted in tandem with salt uplift to divert river systems to the south where the most prominent early Paleogene progradation is observed, and to the north where the Rankin and Hibernia canyons are incised (Deptuck

et al., 2003a). The Adolphus salt diapirs, and one salt spine near the Egret wells, appear to have remained mobile for much of the Tertiary. The shallowest salt piercement in the Adolphus region forms a useful “metre-stick” for tracking the fill of the basin on successive surfaces in Figures 4.7a to 4.7d.

Other structural elements active during stage 1 are also recognized, though their effects appear to be minimal. For example, the Cormorant Arch just south of the Egret fault (Figures 4.2, 4.15) and the Terra Nova Arch near Terra Nova (Figure 4.6) form broad anticlines with clear deformation of stage 1 strata. The lack of thinning of progradational Otter Bay clinoforms in Figure 4.15 (and in time-thickness maps), combined with the up-warping of the prominent toplap surface (which would have originally been nearly flat-lying), clearly demonstrates post-Coniacian deformation after progradation of the Otter Bay Member.

During **stage 2**, the depocenter shifted principally to the Adolphus region. Progradation along the western margin of the basin abruptly stopped at the onset of stage 2, probably in response to a period of accelerated subsidence combined with a 2nd order increase in eustatic sea level that reportedly took place during the Early Eocene (see Figure 4.17 - Haq et al., 1987). At Cormorant N-83, the onset of stage 2 marks a change from shallow marine palynomorphs to deep-water (bathyal) conditions (Graham Williams, pers. comm., 2003). The Fox Harbour shelf, interpreted to have been nearly horizontal during the prominent stage 1 progradation, today dips up to 2 degrees towards the east, indicating that some basin sagging took place during stage 2 near Hibernia (see Figure 4.4). Such basin sagging is interpreted to be coincident with a period of accelerated subsidence in the Orphan Basin, which according to Keen et al. (1990) did not occur until the Early Eocene, at which point it was fairly rapid. Results from geohistory analysis show that by the Eocene, subsidence rates outpaced sediment supply in the northern JDB, Orphan Basin, and Labrador Margin, causing water depths in these regions to deepen (Gradstein and Srivastava, 1980).

Srivastava (1978) described a pronounced change in the direction of ocean spreading in the Labrador Sea in the Early Eocene, which could be related to a relaxation of plate stresses along the Charlie Gibbs Fracture Zone, leading to rapid subsidence in the Orphan Basin and northern JDB (Figure 4.17). Salt withdrawal near Adolphus could also

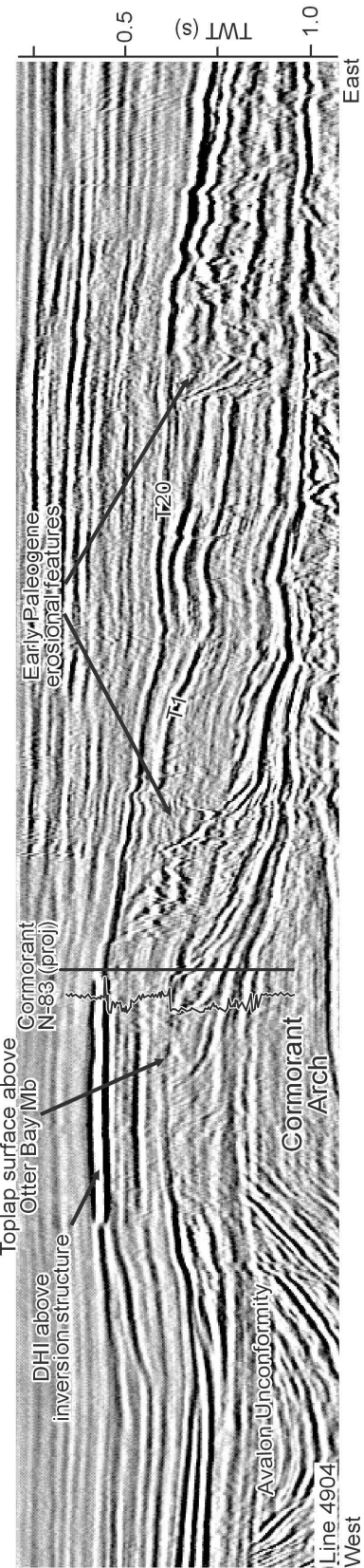


Figure 4.15. Profile across Cormorant Arch, showing up-warped Otter Bay clinoforms. Time-thickness maps of the clinoform interval show no thinning above the up-arched structure, indicating that up-arching post-dates Otter Bay progradation. See Figure 4.2 for location.

have accommodated some of the basin sagging, although the volume of salt withdrawn through diapirism is considered insufficient to account for the amount of subsidence. For the remainder of stage 2, the accommodation that developed between basement highs progressively filled with sediment believed to have been transported by ocean currents. It is not entirely clear whether deposits simply filled a pre-existing depression, or whether active basin sagging took place throughout stage 2.

The onset of **stage 3** marks a period of renewed shelf and slope progradation, and the development of a seaward-thickening wedge (referred to as a “continental terrace wedge” by Tankard and Welsink, 1987) after the relief of the JDB had largely been filled in. Regional subsidence is interpreted to have occurred gradually via margin tilting, in response to sediment loading, north and east of a hinge-line (Figure 4.5b), as an entirely constructional passive-margin shelf and slope system developed above the JDB. Basement highs north and east of the hinge-line subsided in pace with the seaward-thickening wedge.

Most accommodation was created by the northeastern plunge of the basin, and much of the study area was characterized by shelf aggradation during stage 3. Some progradation is observed where the stage 3 interval is condensed near Terra Nova (Figure 4.6), increasing south of the Egret fault. Most progradation, however, took place outside the study area further north, along the margin of the Orphan Basin and Labrador Sea (Balkwill, 1987, see also profiles in Grant, 1974). Balkwill (1987) suggested that the fine-grained clastics deposited in a seaward-prograding wedge along the Labrador Margin (similar to the stage 3 deposits in the JDB) were derived from widespread erosion of central Canada.

According to Haq et al. (1987), sea level was high during most of stage 3. Based on benthonic species, Thomas (1991) noted a progressive shallowing in the post-Late Eocene succession at Bonavista C-99, located on the margin of the Orphan Basin, and noted that this shallowing resulted from the progressive deltaic (or shelf) progradation. In contrast, Blue H-28 continued to show bathyal water depths, as this region corresponded to slope and basin floor settings throughout the Late Eocene to modern (Thomas, 1991). In a similar way, foraminiferal assemblages from wells on the northeastern Grand Banks located furthest west should show a pronounced shoaling

during stage 3 and 4. This shoaling would be delayed in wells located in regions where slope and basin floor deposition continued for a longer period of time, and in some wells continues today (e.g. Lancaster F-70, Gabriel C-60, Kyle L-11).

Little remaining bathymetric evidence for the JDB existed at the seafloor during stage 4.

4.5.2 Stage 1 influx of clastics from the west

The Late Cretaceous to earliest Eocene marks the first time that significant quantities of sediment were supplied to the JDB from the west. Prior to this, most clastics were supplied from the south (Sinclair, 1988). Therefore, there was roughly a 90 degree change in sediment transport direction from the mid to Late Cretaceous. Clastic sediment built into the basin during a series of third-order transgressive - regressive cycles, beginning in the Turonian - Coniacian from the west-southwest (early Otter Bay) and shifting entirely to the west by the Santonian (late Otter Bay). The most prominent progradation took place in the late Campanian as the Fox Harbour Member regressed more than 10 km into the basin. By the Paleocene, most eastward progradation shifted south of the Egret fault, building more than 35 km across the Boninition High until the earliest Eocene (regressive South Mara Member - Deptuck et al., 2003a).

What triggered the influx of clastic sediment from the west? This question is especially pertinent given that global sea level was high during much of stage 1 (Haq et al., 1987; Figure 4.17), and many locations around the world were characterized by pelagic chalk deposition, not clastic progradation. The Late Cretaceous in the North Sea, for example, is dominated by widespread pelagic chalk deposition, with prominent progradation of clastics only beginning in the mid-Paleocene, shortly after uplift of the Iceland Plume (White, 1989; White and Lovell, 1997; Nadin et al., 1997). Despite high global sea level (Haq et al., 1987) and supposed post-rift thermal subsidence during this period in the JDB (Enachescu, 1987; de Silva, 1993), sediment supply to the margin outpaced the creation of accommodation, at least intermittently.

Sinclair (1988) interpreted rapid post-rift thermal subsidence to have taken place in the Cenomanian to Turonian as chinks and marls were deposited in the basin. This was followed by progradation of the Otter Bay and Fox Harbour members during

exponential slowing of thermal subsidence (Sinclair, 1988). In contrast, de Silva (1993) interpreted the influx of clastics to correspond closely to stillstands in the Haq et al. (1987) eustatic sea level curve, when the rate of change of sea level was at a minimum (Figure 4.17). Though a stillstand and/or exponential decrease in subsidence can result in progradation of clastic sediment, these factors cannot account for the shift in drainage basin location. Other mechanisms must therefore be sought to account for shift in sediment source region.

Is there a relationship between the western influx of sediment into the JDB and the Coniacian to earliest Eocene sea floor spreading history adjacent to the Grand Banks? Models for rifting predict uplift and the development of a break-up unconformity at the onset of sea floor spreading (e.g. Falvey, 1974; Keen and Beaumont, 1990). For example, the final break-up between the Grand Banks and Iberia (south of the Flemish Cap) is commonly associated with the Avalon unconformity (Jansa and Wade, 1975b; Gradstein et al., 1990), a regional peneplain surface south of the JDB that passes to the north into several Early to mid Cretaceous unconformities. These unconformities were accompanied by the transport of large quantities of sediment into the basin from the south (approximately perpendicular to the Azores/Newfoundland transform margin; Sinclair, 1988; McAlpine, 1990).

As sea floor spreading propagated northward, however, potential effects of break-up unconformities associated with the separation of northeast Newfoundland margin from the Celtic margin and the Labrador shelf from West Greenland, on the JDB, have not been well documented. Final break-up between Orphan Knoll and Porcupine Bank was in the Santonian (Verhoef and Srivastava, 1989; Ziegler, 1989; Driscoll et al., 1995 - approximately magnetic anomaly 34 - Figure 4.17), and between Labrador and Greenland (north of the Charlie Gibbs Fracture Zone) in the latest Campanian - early Maastrichtian (70 Ma Srivastava and Tapscott, 1986), or as late as the Early Paleocene (Chalmers et al., 1993). Keen et al. (1990) described a mid-Late Cretaceous break-up unconformity in the Orphan Basin and along the Labrador margin, separating syn-rift and post-rift sediment. The development of this unconformity suggests that uplift took place along the Labrador margin just prior to sea floor spreading (Keen et al., 1990). Gradstein and Srivastava (1980) also reported an abrupt increase in sedimentation rates to more than 10 cm/1000

years along the Labrador Margin, and Balkwill et al. (1990) reported a “surge” of seaward prograding clastics in the Campanian.

The influx of clastics from the west in the JDB, then, could be related to break-up unconformities associated with the onset of sea floor spreading north of the Charlie Gibbs Fracture Zone. The timing of the break-up unconformity is roughly contemporaneous with the period of most prominent clastic influx into the JDB (Campanian Fox Harbour Member). Stage 1 progradational deposits in the JDB could have been supplied from uplifted areas to the northwest, associated with the final break-up between the Northeast Newfoundland and Celtic margins, or the Labrador and West Greenland margins. The coarse grade (coarse grained to granule sands) and immaturity (presence of feldspar) of clastics in the Otter Bay and Fox Harbour members suggest a relatively proximal hinterland (Friis, 1997; Deptuck et al., 2003a), and therefore supports this interpretation. If this scenario is correct, the JDB must have been sufficiently distal from the region of uplift to avoid significant deformation, but proximal enough to receive sediment shed from the uplifted region.

Tectonic plate reconstructions for the Late Cretaceous and earliest Paleogene indicate that the Charlie Gibbs Fracture Zone and its landward extension the Dover fault (Figure 1; Haworth and Lefort, 1979; Keen et al., 1990) were roughly normal to the direction of sediment transport into the JDB. An alternative interpretation, then, involves uplift west of the JDB caused by plate motion near the Charlie Gibbs Fracture Zone, perhaps extending onto Newfoundland near the Dover fault. Several mechanisms have been documented for uplift associated with transform margins (e.g. Ziegler, 1988; Vagnes, 1997; Lorenzo, 1997; Gadd and Scrutton, 1997; Lorenzo and Wessel, 1997; Mascle et al., 1997). Stresses exerted in response to differential rates of spreading on either side of the transform fault could have caused substantial strain (Ziegler, 1988), leading to deformation in this region just prior to plate separation. Other mechanisms involve the heating of continental crust as it is juxtaposed by a hot spreading center, causing thermal uplift (e.g. Lorenzo, 1997). Unfortunately, there is insufficient data to test these ideas.

Despite the coincidence in timing between the western influx of clastics and the resumption of rifting north of the Charlie Gibbs Fracture Zone, broader regional controls

cannot be discounted. Prograding Upper Cretaceous deltaic units have been documented south of the JDB, along the Scotian Shelf (e.g. Hardy, 1975; MacRae et al., 2002) and further south still along the northeastern U.S. margin (off New Jersey - Poag, 1992). Poag (1992) reported a significant increase in sedimentation rates starting in the Coniacian - Santonian and continuing through the Maastrichtian. Several large Coniacian - Santonian deltas developed on the continental shelf, and Poag (1992) linked their formation to renewed uplift of the New England Appalachian highlands (though little evidence and no mechanism for renewed uplift was provided). Recognition of equivalent progradation along the Scotian Shelf and eastern United States margin indicates that more regional (cratonic-scale) tectonic, sea level, and/or climatic processes could have been responsible for the establishing a western sediment source region adjacent to the JDB.

4.5.3 Linking ocean current indicators to past ocean circulation

The results of mapping current indicators during stages 1 to 4 suggest that ocean currents periodically swept through the JDB starting at the end of the Cretaceous and continued intermittently until the basin filled in the Middle Eocene. After the Middle Eocene, ocean current indicators are recognized only in the Flemish Pass region, presumably because currents were diverted to the east by the prominent Grand Banks shelf. Whether current indicators formed from surface or deep ocean circulation can be constrained to some extent in areas where physiographic features like shelf-breaks are present and where paleobathymetry data are available from foram studies (e.g. Thomas, 1994).

Currents passing through the JDB (stages 1 and 2)

The oldest current indicators recognized in the post-rift succession are scours located near the K - T boundary. They are inferred to have formed during a period of intensified surface currents when water depths were probably no greater than 400 to 600 m (e.g. upper bathyal above the Paleocene basin floor at South Mara C-13 - Thomas, 1994, and probably too deep for tidal current erosion). Based on the trend of most scours, the surface currents are inferred to have been oriented south to north, along the axis of the basin, but were locally diverted by basement highs like the Central and

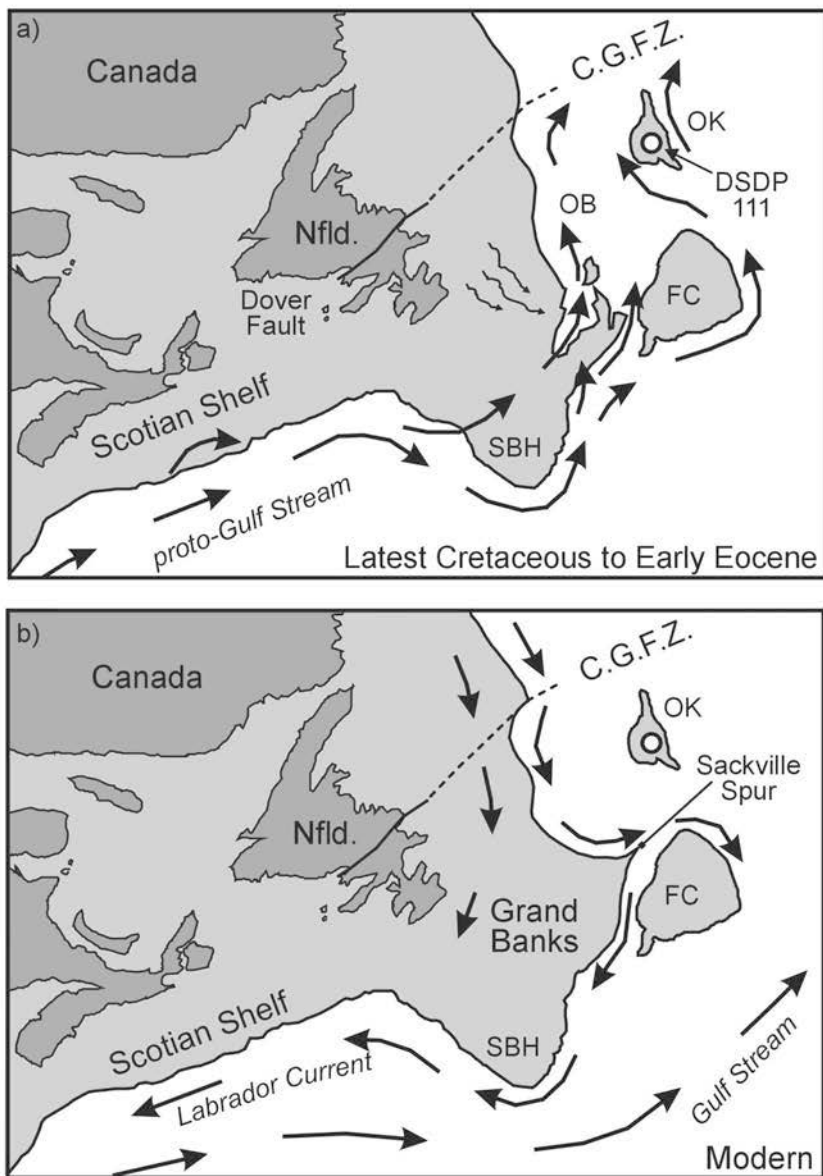


Figure 4.16. a) Schematic cartoon showing the inferred surface current flow direction during the Latest Cretaceous to Early Eocene. This current represents a proto-Gulf Stream. In the absence of a Labrador Current, the proto-Gulf Stream is interpreted to have been the most important surface current in the study area at this time. Smaller arrows show the direction of sediment input into the JDB during stage 1. b) Modern surface current circulation. Current arrows in part are from Berggren and Hollister (1974), Gradstein and Srivastava (1980), Haq (1984), Gradstein et al. (1990), and Barron and Peterson (1991). Diagram represents the generalized current patterns for periods of elevated sea level (when the shelves were submerged).

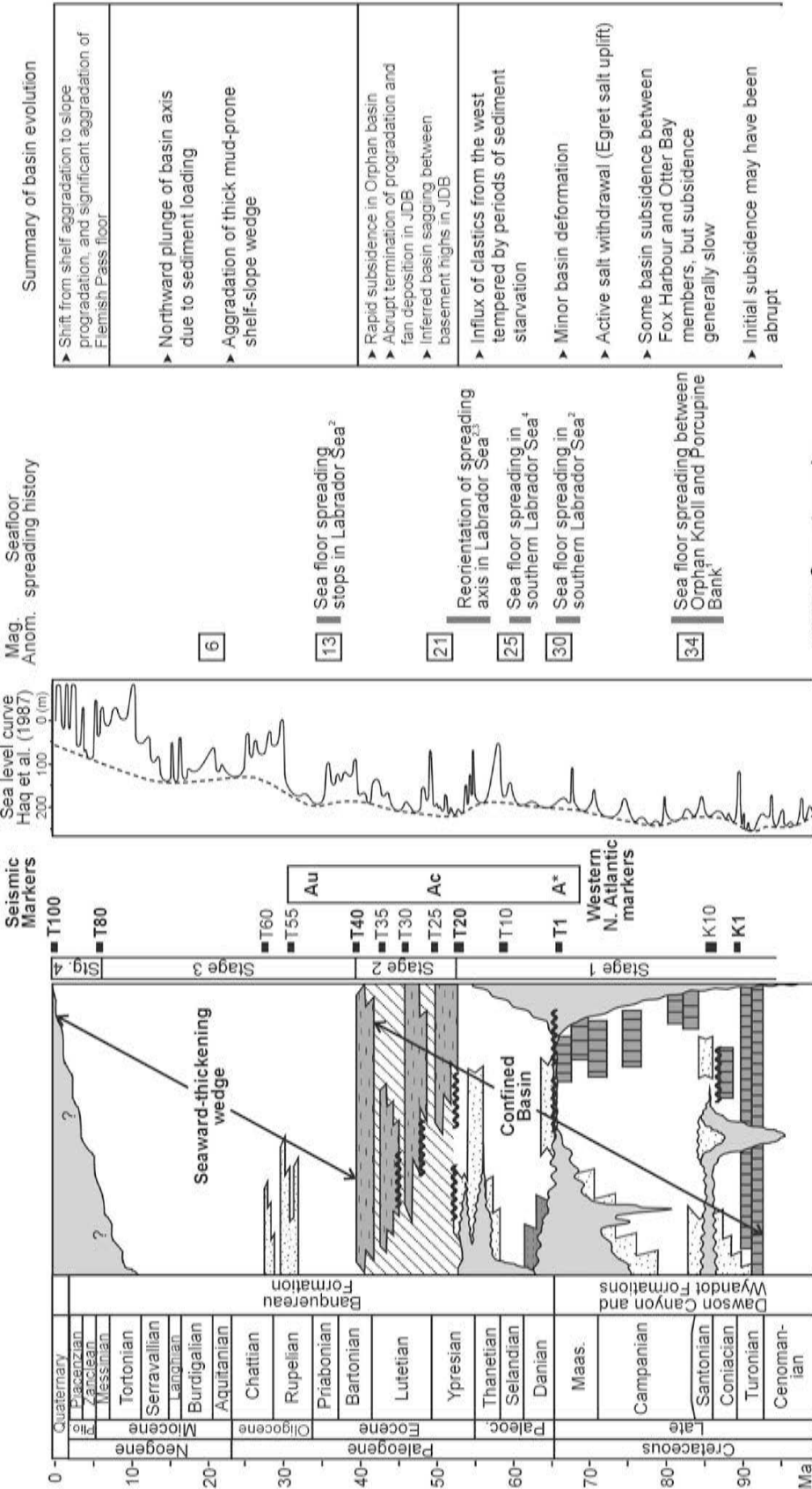


Figure 4.17. Upper Cretaceous and Tertiary lithostratigraphic chart, with corresponding seismic markers defined in this study, and equivalent markers (A*, Ac, Au) in the western North Atlantic indicated (from Tucholke and Mountain, 1979). Timing of magnetic anomalies is from Srivastava and Tapscott (1986). Sea level curve is from Haq et al. (1987). 1 = Verhoeff and Srivastava (1989); 2 = Srivastava and Tapscott (1986); 3 = Srivastava (1978); 4 = Chalmers and Laurson (1995). Time-scale from Gradstein et al. (1995) and Berggren et al. (1995).

Northern ridges. Several lines of evidence suggest a southern origin for these currents. Gradstein and Srivastava (1980) found tropical influences in Upper Cretaceous planktic foraminifer assemblages in strata at Orphan Knoll, north of the JDB (from DSDP Leg 12, Site 111). They interpreted these tropical influences to indicate the presence of a north-flowing proto-Gulf Stream (Figure 4.16a - see also Berggren and Hollister, 1974). In addition, warm water dinoflagellate species are abundant in uppermost Paleocene and Ypresian strata in the JDB (e.g. *Apectodinium homomorphum* - Bujak and Brinkhuis, 1998). Abundances in these species denote higher sea-surface temperatures, again suggesting a southern influence (Graham Williams, pers. comm. 2003).

The Gulf Stream was also an important current in other parts of the world in the latest Cretaceous and early Tertiary. Similar to the prominent north-trending scours that erode the Wyandot chinks in the JDB, top chalk erosion has also been documented along the Scotian Margin (mid-Campanian to Maastrichtian - MacRae et al., 2002) and as far south as the Blake Plateau (Paull and Dillon, 1980; Pinet et al., 1981). Evidence for scouring on the Blake Plateau was interpreted by Pinet et al. (1981) to mean that the Gulf Stream began to flow in the Late Paleocene, with sedimentation rates ranging from 2.1 to 2.4 cm/1000 years, on par with the long-term sedimentation rates in the JDB at this time. However, Dillon and Popenoe (1988) described a Late Cretaceous to Early Paleocene precursor to the Gulf Stream, the Suwanee Current, whose timing is more closely aligned with the scouring at the T1 marker observed in the JDB. The dominant water flow from the Gulf of Mexico and into the Atlantic at this time was across northern Florida and southern Georgia (the "Suwanee Strait"), rather than through the Straits of Florida (as it does today). Water was propelled through this strait creating an erosional to non-depositional hiatus and a 100 km wide channel, below which Maastrichtian strata are absent (Dillon and Popenoe, 1988), as they are absent across much of the JDB. Berggren and Hollister (1974) also reported high concentrations of warm-water planktic foraminifera from Alabama to New Jersey, which they used as evidence for a northward-flowing warm ocean current during the Maastrichtian.

These observations, combined with reports that the proto-Gulf Stream reached Baffin Bay as early as the Maastrichtian (Gradstein and Srivastava, 1980; Gradstein et al., 1990), suggest that the proto-Gulf Stream (or the Suwanee Current) was responsible for

the latest Cretaceous or earliest Paleocene scours in the JDB. In the absence of a south flowing proto-Labrador Current (which reportedly began in the Late Miocene - Kennard et al., 1990, see also Berggren and Hollister, 1974), the proto-Gulf Stream presumably would have hugged the western margin of the Atlantic (as depicted in Figure 4.16a). The positive relief of the South Bank High, combined with the sharp eastward bend of the southern Grand Banks margin, would have acted to deflect the deeper part of the north-flowing current to the east, with the remainder of the current forced to pass above the Grand Banks. The funnel-shaped JDB, in turn, would have formed a natural conduit for these currents until it was later filled with sediment. Preservation of Upper Cretaceous strata suggests that the surface currents were most erosive in the southern parts of the JDB, where a significant portion of the Upper Cretaceous stratigraphic record has been winnowed away (below the T1 seismic marker - Figure 2b). With increasing water depth to the north, the currents became less constricted and hence more Upper Cretaceous strata were preserved.

Periods of weak north-flowing surface currents are interpreted for the remainder of stage 1, during which time a Paleocene slope aggraded and prograded and Paleocene to earliest Eocene submarine fans were deposited. The onset of stage 2, however, is characterized by renewed scouring that locally eroded the Paleocene slope. The South Mara unconformity identified by Deptuck et al. (2003a) may be related, at least in part, to scouring associated with an intensification of surface currents. Scouring was diachronous during stage 2. Ocean currents of sufficient velocity to prevent fine-grained sediment from accumulating, are believed to have swept some parts of the basin at the same time that marine units 2a to 2d were deposited. The gradual onlap/downlap of stage 2 deposits onto the western basin margin represents a shift in the region of most intense ocean currents during the Ypresian to early Bartonian.

The thickest parts of each marine unit progressively built toward the north and west, suggesting that the currents originated from the south or southeast. However, stage 2 deposits at Terra Nova K-18 contain reworked material, including Carboniferous spores, Cretaceous dinocysts and spores, and Early to Middle Eocene dinocysts. Some of the reworked dinocysts are species known to occur in northern, high latitude areas (Graham Williams, pers. comm., 2003). This raises the possibility that ocean currents of

some sort (either surface or abyssal) originated from the north, rather than the south. Ocean circulation models generated by Barron and Peterson (1991) suggest that a proto-Labrador Current could have been active as early as 40 m.y. ago, which could be a potential source for reworked northern species. More work is required, however, before the origin of the reworked northern species can be understood with certainty.

Currents passing through the Flemish Pass (stages 3 and 4)

Low intensity surface currents may have continued to pass over the Grand Banks shelf during stage 3 (as they do on the modern shelf), but no direct current indicators are recognized in the multichannel reflection seismic data used in this region. The broad Grand Banks shelf is therefore interpreted to have deflected the most intense currents to the east, toward the Flemish Pass region, where there are abundant bottom current indicators. As described earlier, the field of sediment waves and complex scouring is found only between 1000 and 2200 m below the stage 3 shelf break. Hence, stage 3 current indicators are unlikely to have formed from wind-driven surface currents, and are interpreted instead to have formed from deep thermohaline circulation.

Recognition of moat and drift deposits along the northern and eastern Flemish Cap suggests that the Western Boundary Undercurrent was active throughout the Neogene (Kennard et al., 1990). In addition, erosion of the western Atlantic abyssal plain and rise, suggests that a precursor to the modern Western Boundary Undercurrent was active as early as the Late Eocene ("Au" horizon of Tucholke and Mountain, 1979; Gradstein et al., 1990). Hence the current indicators on the stage 3 slope may be evidence of a precursor to the Western Boundary Undercurrent. The Gulf Stream, however, which has been known to intermittently influence the sea floor at depths greater than 4000 m, cannot be completely ruled out (Hollister and McCave, 1984). Perhaps more importantly, the Gulf Stream has been known to interact with the Western Boundary Undercurrent, causing complex current-influenced deposits (McCave and Tucholke, 1986; Faugères et al., 1999).

The initiation of the south-flowing Labrador Current in the Late Miocene (Gradstein and Srivastava, 1980; Kennard et al., 1990), diverted the Gulf Stream away from the study area. Stage 4 was a time of progradation, as the shelf break rimming the

Grand Banks built towards the east (further constricting Flemish Pass), and aggradation, as the floor of the pass shoaled by as much as 700 m. The shallower water depths made it possible for the Labrador Current, in combination with the Western Boundary Undercurrent, to generate scours and drifts in the Flemish Pass and around the Flemish Cap (Kennard et al., 1990).

4.6 Summary of key points

1. A four-stage evolutionary framework is presented, tracking the transition from a confined passive-margin rift basin to an unconfined passive-margin shelf and slope. During stages 1 and 2 (Turonian to early Bartonian), the JDB formed a trough-shaped depression that appears to have been open to the north, toward the Orphan Basin. The distribution of stratigraphic units was largely controlled by basement highs on the western, eastern, and southern basin margins. Most stratigraphic units thin significantly above basement highs, indicating that the highs formed important bathymetric elements at the time. During stages 3 and 4 (late Bartonian to Recent) deposits were largely unconfined towards the north and east, accumulating in a passive-margin shelf and slope setting, with significant quantities of sediment accumulating in Flemish Pass.
2. An abrupt change in the sediment transport direction at the onset of stage 1 indicates a shift in sediment source regions, from just south of the JDB in the Early to mid Cretaceous, to west of the basin in the Late Cretaceous. The shift resulted in the influx of Upper Cretaceous to lowermost Eocene coarse clastics, starting in the Coniacian, peaking in the late Campanian, and abruptly diminishing by the Ypresian. The western source is inferred to be linked to renewed plate separation just north of or south of the Charlie Gibbs Fracture Zone, in response to a break-up unconformity during final separation of the Orphan Knoll and Porcupine Bank (84 Ma - Verhoef and Srivastava, 1989) or southern Labrador from western Greenland (68 Ma - Srivastava, 1978; or 61 Ma - Chalmers and Laurson, 1995). More regional controls like climate and continent-scale uplift, however, cannot be ruled out. As suggested by McAlpine (1990), the Late Cretaceous to earliest Eocene (stage 1) is a time of transition, with the interval probably

showing a stratigraphic response to plate separation further north, but undergoing minimal structural deformation from it.

3. The onset of rapid subsidence and/or a significant rise in sea level in the Ypresian (onset of stage 2 in this study) abruptly terminated the progradational stratigraphic response, coinciding with the deposition of the Ypresian Adolphus Member of the Banquereau Formation. Rapid subsidence in the Orphan Basin was contemporaneous with stage 2 deposits in the JDB, suggesting that the tectonic histories of both regions were closely linked (though the amount of subsidence in the JDB progressively diminished to the south, approaching the stable Bonniton High). Sagging of the basin floor took place between basement highs. An increase in sediment supply to the basin, via ocean currents, ultimately filled its remaining relief.

4. Much of the present-day northward tilt of the JDB appears to have formed during the deposition of stage 3 strata, which accumulated in a mud-dominated, seaward thickening wedge after the JDB relief had already filled. During stage 3, the entire margin (including basement highs) tilted along a curved hinge zone located across the southern part of the study area. Strata appear to have been deposited on a broad shelf similar to the modern Grand Banks, and sediment loading, as the shelf and slope system built upwards and northeastwards, appears to have been responsible for tilting the margin.

Starting in stage 3, water depths progressively shallowed across the Grand Banks, from bathyal in the Lutetian to shallow neritic by the time coarse-grained clastics of the Thorvald Member were deposited in the Early to Middle Oligocene. The dominance of muddy lithologies during much of stage 3 suggests that sediment was supplied from a relatively distal hinterland. Stage 4 marks an increase in progradational character of the slope in the study area, significant aggradation of the floor of Flemish Pass, and little aggradation of sediment above the shelf. This period also marks a significant increase in sedimentation rates and grain size, probably associated with the onset of glaciation in the northern hemisphere.

5. The recognition of bottom current indicators (e.g. scours, drifts, sediment waves) provides insight into ocean circulation during stages 1 to 4. The results suggest that ocean surface currents periodically swept through the JDB starting at the end of the Cretaceous and continuing until the basin filled in the Bartonian. After the Middle Eocene, ocean current indicators are recognized only in the Flemish Pass region, presumably because currents were diverted to the east by the proto-Grand Banks shelf. The increased depth of stage 3 current indicators in Flemish Pass suggests that deeper thermohaline currents were important.

Scours, believed to be associated with latest Maastrichtian to earliest Paleocene circulation of the proto-Gulf Stream, are most prominent at the T1 seismic marker, which prevented sediment from accumulating and produced a widespread submarine unconformity. The currents effectively “polished” the basin floor and margins. Sediment transported by ocean currents appears to have been an important process for filling the remaining relief of the basin during stage 2 (Early to Middle Eocene). Once filled, the JDB no longer acted as a conduit for currents. Instead the Flemish Pass region became the site of most prevalent currents during stages 3 and 4.

CHAPTER 5 - EARLY PALEOGENE (DANIAN TO YPRESIAN)
SUBMARINE FANS IN THE JEANNE D'ARC BASIN: ARCHITECTURE,
EVOLUTION AND INSIGHT FROM MODERN FANS OFF EASTERN
CORSICA

5.1 Introduction

Early Paleogene submarine fans are common in the relatively shallow shelf seas and deeper oceanic basins that rimmed the North Atlantic Ocean 50 to 65 million years ago (Figure 5.1). Paleocene and Early Eocene submarine fans have been reported in a wide variety of settings, including the North Sea (e.g. Heritier et al., 1979; Sarg and Skjold, 1982; McGovney and Radovich, 1985; Kulpecz and van Geuns, 1990; Timbrell, 1993; Jenssen et al., 1993; Newton and Flanagan, 1993; Shanmugam et al., 1995; Lonergan et al., 2000; Jennette et al., 2000; Duranti et al., 2002), offshore western Norway (Smith and Moller, in press), in the Faeroe-Shetland Basin (Mitchell et al., 1993; Ebdon et al., 1995), Porcupine Basin (Shannon, 1992), and southwestern Greenland (Chalmers et al., 1995). Uplift along the western margin of Greenland has exposed several latest Maastrichtian to Early Paleocene slope channels believed to have fed submarine fans offshore (Dam and Sonderholm, 1994, 1998), and collision between Iberia and Europe created the Pyrenees Mountains and exposed turbidites of the Eocene Hecho Group (Mutti, 1985b). Along the margin of Eastern Canada, Paleocene to Early Eocene submarine fans have been reported in offshore areas of Labrador (McWhae et al., 1980; Balkwill, 1987; Miller et al., 1988; Phil Moir pers. comm., 2003), in the Jeanne d'Arc Basin (Sinclair, 1988; de Silva, 1993; Williamson et al., 1996; Deptuck, 1998; Deptuck and Piper, 2003), and Carson Basin (Grant et al., 1988; Parker, 1999), and are probably present along the Scotian Margin where several buried canyons are recognized on the slope (Andrew MacRae and John Shimeld, pers. comm., 2003) (Figure 5.1).

Of these regions, early Paleogene submarine fans in the North Sea have undergone the most detailed study using cores, wireline logs, biostratigraphic interpretations, and seismic reflection profiles (e.g. Heritier et al., 1979; Sarg and Skjold, 1982; McGovney and Radovich, 1985; Timbrell, 1993; Jennette et al., 2000; Purvis et al., 2002, and many others mentioned above). Submarine fans like Frigg fan in the Viking

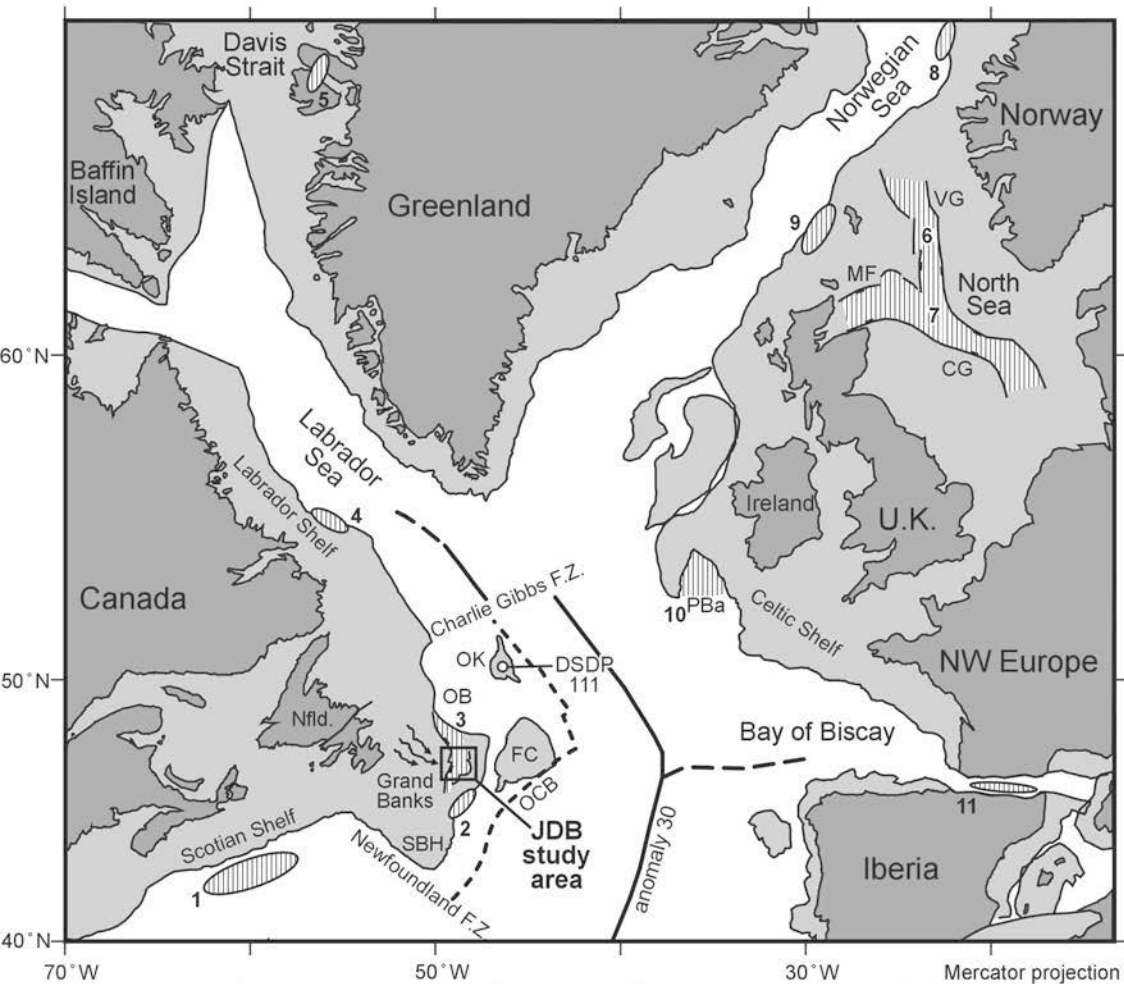


Figure 5.1. Plate reconstruction for 65 Ma (from Hay et al., 1999) showing locations of known Paleocene and Early Eocene submarine fans. **SBH** South Bank High; **OB** Orphan Basin; **FC** Flemish Cap; **FZ** Fracture Zone; **PBa** Porcupine Basin; **OCB** Ocean-Continent Boundary; **JDB** Jeanne d'Arc Basin; **MF** Morray Firth; **VG** Viking Graben; **CG** Central Graben. **1** Scotian Margin (A. MacRae and J. Shimeld, pers. comm., 2003); **2** Carson Basin (Grant et al., 1988; Parker, 1999); **3** Jeanne d'Arc Basin (Sinclair, 1988; de Silva, 1993; Williamson et al., 1996; Deptuck, 1998, 2000); **4** Labrador Margin (McWhae et al., 1980; Balkwill, 1987); **5** West Greenland (Dam and Sonderholm, 1994, 1998); **6** Viking Graben, North Sea (Frigg, Gryphon, Balder fans - Heritier et al., 1979; Sarg and Skjold, 1982; McGovney and Radovich, 1985; Timbrell, 1993); **7** Central Graben, North Sea (Andrew, Forties, Tay, Alba fans - Kulpecz and van Geuns, 1990; den Hartog Jager et al., 1993; Newton and Flanagan, 1993; Jennette et al., 2000); **8** Offshore Norway (Smith and Moller, in press); **9** Faeroe-Shetland Basin (Ebdon et al., 1995); **10** Porcupine Basin (Shannon, 1992; Shannon et al., 1993); **11** Hecho Group (Pyrenees Spain - Mutti, 1985). Arrows show sediment transport direction into JDB.

Graben (Ypresian - Heritier et al., 1979) and Forties fan in the Central Graben (Thanetian - Kulpecz and van Geuns, 1990), helped the North Sea become a prolific hydrocarbon province (see Figure 5.1 for location). Workers studying North Sea fans have documented the importance of mounded seismic facies as sand-prone hydrocarbon reservoirs (e.g. Heritier et al., 1979; McGovney and Radovich, 1985). The mounded expression of seismic facies was interpreted to originate from the depositional geometry of fan elements (e.g. channels, lobes), mildly to severely overprinted by compaction and other post-depositional effects (e.g. sandstone injection), resulting from their deep burial depths (e.g. Lonergan et al., 2000).

5.1.1 Early Paleogene submarine fans in the Jeanne d'Arc Basin (JDB)

Similar to the North Sea, the JDB contains seismically-detected mounded deposits interpreted as submarine fans. The fans accumulated in a confined passive-margin setting, within a relatively shallow depression surrounded by basement highs on three sides consisting of continental crust, rather than along the open margin of an oceanic basin (as is the case for the Scotian, Labrador, and Norwegian margins, as well as most modern passive-margin fans) or in a collisional setting (as is the case for the Hecho Group turbidites in Spain - Mutti, 1985b). Sediment was supplied to the basin from the west, and prominent progradation of sand-prone shelf and mud-prone slope deposits is recognized along the western basin margin. Submarine fans were deposited on the slope and basin floor, adjacent to the advancing shelf (Sinclair, 1988; de Silva, 1993; Deptuck, 2000; Deptuck et al., 2003a).

The dimensions of fans in the JDB are small compared to well known passive-margin fans like Amazon (offshore Brazil - Damuth and Flood, 1985), Mississippi (Gulf of Mexico - Bouma et al., 1985), Rhone (Mediterranean - Bellaiche et al., 1984), Bengal (offshore Bangladesh - Emmel and Curray, 1985), and Indus (offshore Pakistan - McHargue and Webb, 1986; Kolla and Coumes, 1987) (Figure 5.2a). Their dimensions, however, compare well to smaller fans deposited in relatively shallow, confined basins along the California Continental Borderland (e.g. Hueneme - Piper et al., 1999; Navy - Normark et al., 1979) and in the Mediterranean Sea (e.g. several fans off Eastern Corsica - Bellaiche et al., 1994, Gervais et al., in press; and Crati fan off southern Italy - Ricci

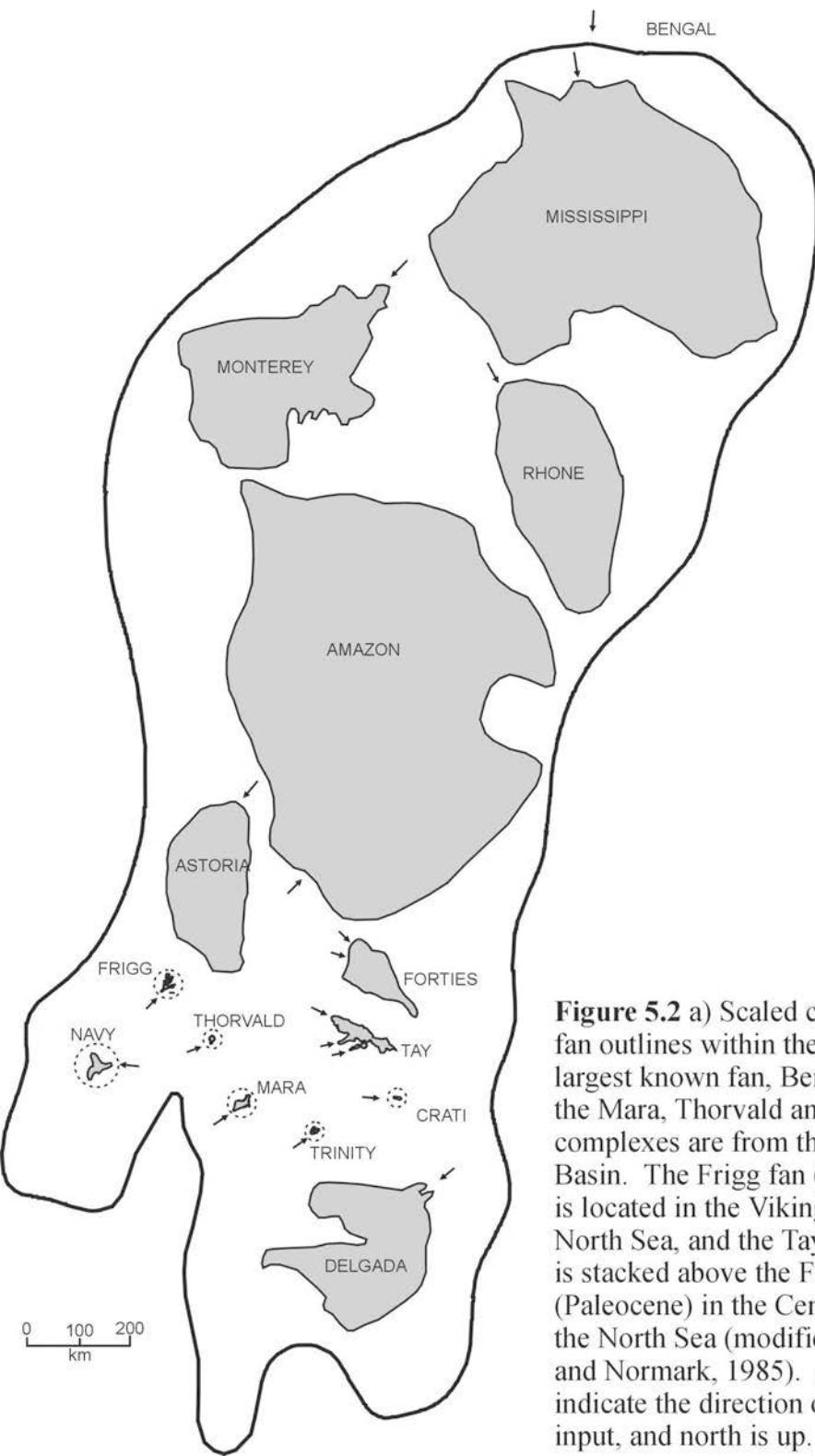


Figure 5.2 a) Scaled comparison of fan outlines within the outline of the largest known fan, Bengal. Note that the Mara, Thorvald and Trinity fan complexes are from the Jeanne d'Arc Basin. The Frigg fan (Early Eocene) is located in the Viking Graben of the North Sea, and the Tay fan (Eocene) is stacked above the Forties fan (Paleocene) in the Central Graben of the North Sea (modified from Barnes and Normark, 1985). Arrows indicate the direction of sediment input, and north is up.

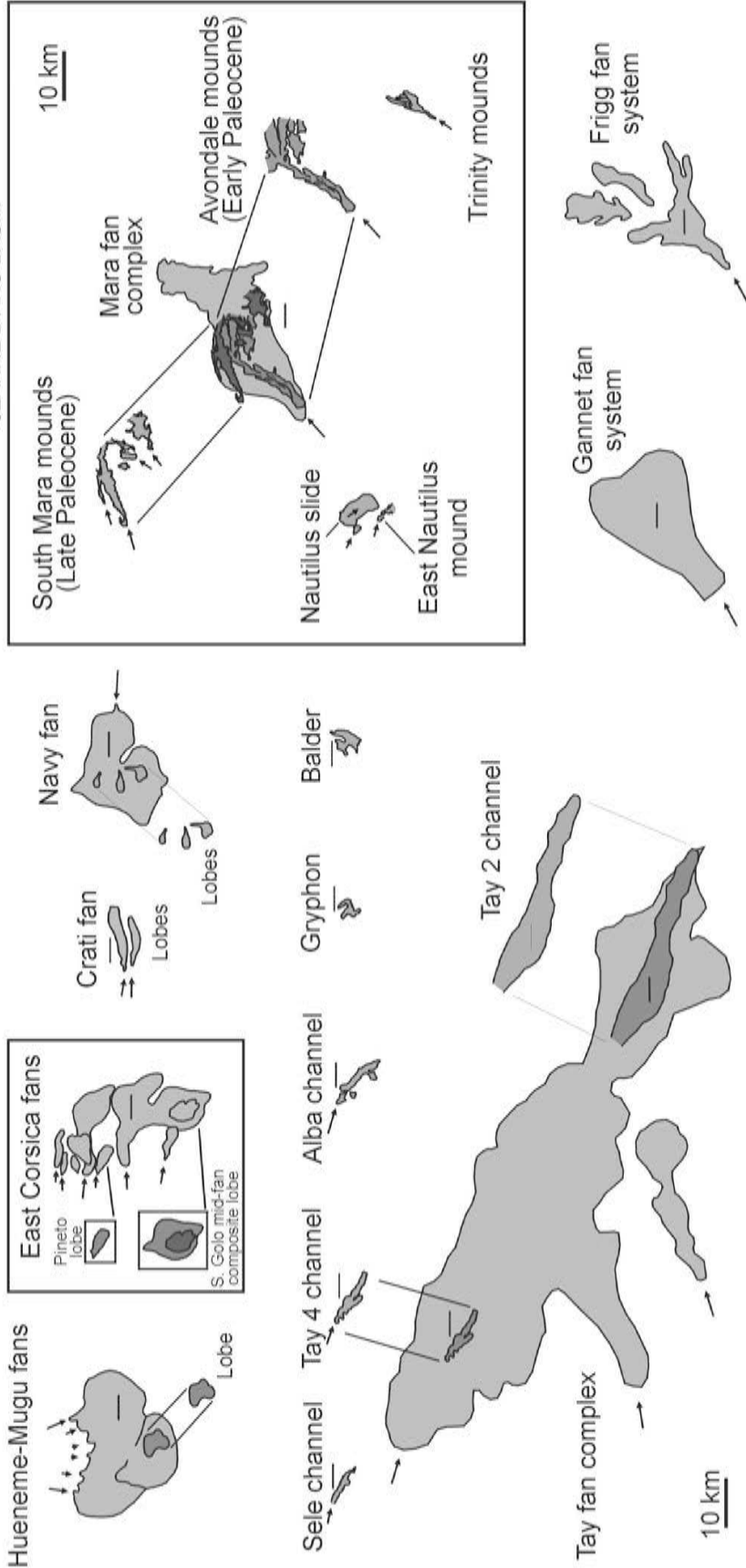


Figure 5.2. b) Scaled comparison of small modern fans from various locations and ancient fans from the Jeanne d'Arc Basin and the North Sea. Outlines for fans and mounded fan elements are from various literature sources: Hueneme-Mugu fan (Piper et al., 1999); Crati fan (Ricci Lucchi et al., 1985); Navy fan (Normark et al., 1979); East Corsica fans (this study and Gervais et al., in press); Tay fan complex, Sele channel, Tay 2 channel, Tay 4 channel, Tay 2 channel (Jennette et al., 2000); Gannet fan system (Kelpcz and Geuns, 1990); Frigg fan (McGovney and Radovich, 1985); Gryphon field (Purvis et al., 2002); Balder field (Jennsen et al., 1993); Alba channel (Newton and Flanagan, 1993). The South Mara, Avondale, Trinity, and East Nautilus mounds are based on 3-D seismic mapping. Mounds commonly extend beyond the limits of 3-D seismic data coverage, where only 2-D seismic coverage is available. Arrows indicate primary orientation of sediment input, where known. Short horizontal lines represent 5 km.

Lucchi et al., 1985). Their dimensions also compare well to many early Paleogene fans in the North Sea, like Frigg (Heritier et al., 1979), Gannet (Kelpecz and Geuns, 1990), Tay (Jennette et al., 2000), Gryphon (Purvis et al., 2002), and Balder (Jennsen et al., 1993). See Figure 5.2b for a scaled comparison of these fans.

Submarine fans in the JDB are now buried by 1000 m to more than 2200 m of strata. Their architecture is closely similar to fans in the North Sea, dominated by sub-circular to elongated mounds. Where penetrated by wells, the mounds are sand-prone, with very high net:gross sandstone to shale ratios. Hence, in terms of dimensions, age, lithology, burial depth and depositional setting, submarine fans in the JDB strongly resemble many of the early Paleogene submarine fans in the North Sea, and fit the criteria for “immature passive-margin fans” (North Sea-type) of Shanmugam and Moiola (1988) and point-source to multiple-source mud/sand-rich to sand-rich fans of Reading and Richards (1994).

5.1.2 *Scope*

Despite the abundance of studies done on North Sea fans, debate still exists over the origin of mounds in small deeply-buried fans, both in terms of depositional process (high-density turbidity currents versus sandy debris flows, Shanmugam, 1996) and the types of architectural elements they represent (e.g. lobes, inverted channels, or purely deformational features). Few attempts, however, have been made to rigorously compare mounded submarine fans in the North Sea with potential modern analogues. This is largely due to the lack of good-quality data for small modern sandy fans. Sand bodies in such systems have historically been difficult to image with conventional high-frequency seismic tools and most coring devices are incapable of penetrating thick sandy intervals (Mutti and Normark, 1987). Recently, the Hunttec deep-tow seismic (DTS) system has been used to collect ultra-high resolution (better than 0.5 m vertical resolution) seismic-reflection profiles above small sandy fans. Although acoustic penetration is commonly low, such profiles make it possible to image sand bodies within the upper 50 to 100 m of strata, including their stacking patterns and in some cases their internal stratal architecture (e.g. Piper et al., 1999; Piper and Normark, 2001, Pichevin, 2000). Comparisons between mounded seismic facies in deeply buried fans, and sand bodies in

modern fans, are now possible and timely. Such comparisons are necessary to understand the origin of mounds in deeply buried fans.

In this chapter, I describe the results of a detailed study on submarine fans in the JDB. Several high-quality 3-D seismic data sets, supplemented by digital 2-D seismic-reflection profiles and well data, were used. The data set provides coverage from canyons incised onto the shelf to lobes deposited on the basin floor. This paper has two primary objectives. The first is to determine the location, architecture, and evolution of Paleocene to Early Eocene submarine fans in the JDB. The second is to evaluate the origin of mounds in the basin by: a) examining their three dimensional architecture; b) evaluating the location of mounds relative to other fan elements (e.g. incised channels) and physiographic features (e.g. shelf-break, slope, basin floor), and c) using key results from previous studies in the North Sea. This study also draws comparisons with modern fans off Eastern Corsica, and to a lesser extent in the Santa Monica Basin off California (Hueneme-Mugu and Dume fans), interpreted with Huntec DTS reflection profiles. Results from high-resolution studies of modern fans provide valuable information about sand body dimensions and distribution in small sandy fans that help to evaluate the origin of mounds in deeply buried systems.

This study is a natural progression from the lithostratigraphic work presented in Chapter 3 (Deptuck et al., 2003a), and the regional work presented in Chapter 4 (which provides context for submarine fans in the basin).

5.1.3 Jeanne d'Arc Basin data set

The JDB data set consists of four 3-D seismic surveys covering an 1800 km² area, a regional grid of migrated 60-fold digital 2-D seismic-reflection profiles (with a line spacing of 2 to 4 km), and 14 wells that provide lithological calibration in regions of fan deposition (Figure 5.3a). 3-D seismic data were provided by Chevron Canada Resources, Mobil Oil Canada (now ExxonMobil), Petro-Canada, Husky Oil, Murphy Oil Company, Mosbacher Operating Ltd., Norsk-Hydro Canada Oil & Gas, and the Hibernia Management and Development Company. The 3-D seismic volumes were collected and processed between 1991 and 1999 with a bin spacing of 25 m x 25 m and a vertical resolution of about 10 m (50 to 60 Hz dominant freq. at average velocity of 2000 m/s).

Digital 2-D seismic data were acquired and processed in 1983 by the ex-Parex Group (CNOPB Project No. 8620-S014-008E), are of good quality in the study interval, and provide regional coverage, but have a lower frequency content than 3-D seismic data (35 to 50 Hz dominant frequency). Additional seismic coverage was provided by paper copies of inlines from a quasi-3-D seismic survey (spaced 125 m apart - one-fifth the conventional spacing), collected in 1986 by GSI (CNOPB Project No. 8624-G005-011P). This data set was particularly useful for the coverage it provided over the northern parts of the Mara fan complex (discussed in a later section), but was not used to generate time-structure and time-thickness maps.

Age control was derived primarily from palynology interpretations done by Rob Fensome and Graham Williams at the Geological Survey of Canada on Avondale A-46, South Mara C-13, Mara M-54, and Terra Nova K-18. Limited biostratigraphic resolution, combined with the lack of core data from lower Paleogene fan intervals necessarily places the emphasis of this study on seismic stratigraphy, with relative ages determined using onlap relationships and regionally correlated seismic markers. To some extent, correlation between existing wells and 3-D seismic data enable prediction of lithofacies where no well control is available.

5.2 Early Paleogene submarine fan complexes

Mapping of regional physiographic features like the shelf-break, slope, and base-of-slope, and their changing position through time, indicates that most mounds developed in a submarine setting, on the lower slope and basin floor of the confined passive-margin rift basin. Physiographic features combined with deeper-water marine biota in strata above, within, and below the mounds, strongly suggests a submarine fan depositional setting. Indirect evidence based on the height of the shelf-break above the base-of-slope, combined with upper bathyal paleoenvironment interpretations from Thomas (1994, 1995), suggests that water depths did not exceed 500 m near the base-of-slope, perhaps deepening to as much as 800 or 1000 m in basinal areas to the north and east (toward the Adolphus salt diapirs - see Chapter 4).

Danian to lower Ypresian mounded seismic facies are primarily observed in three regions in the basin (Figures 5.3a, 5.4). Each has been correlated to an evolving system

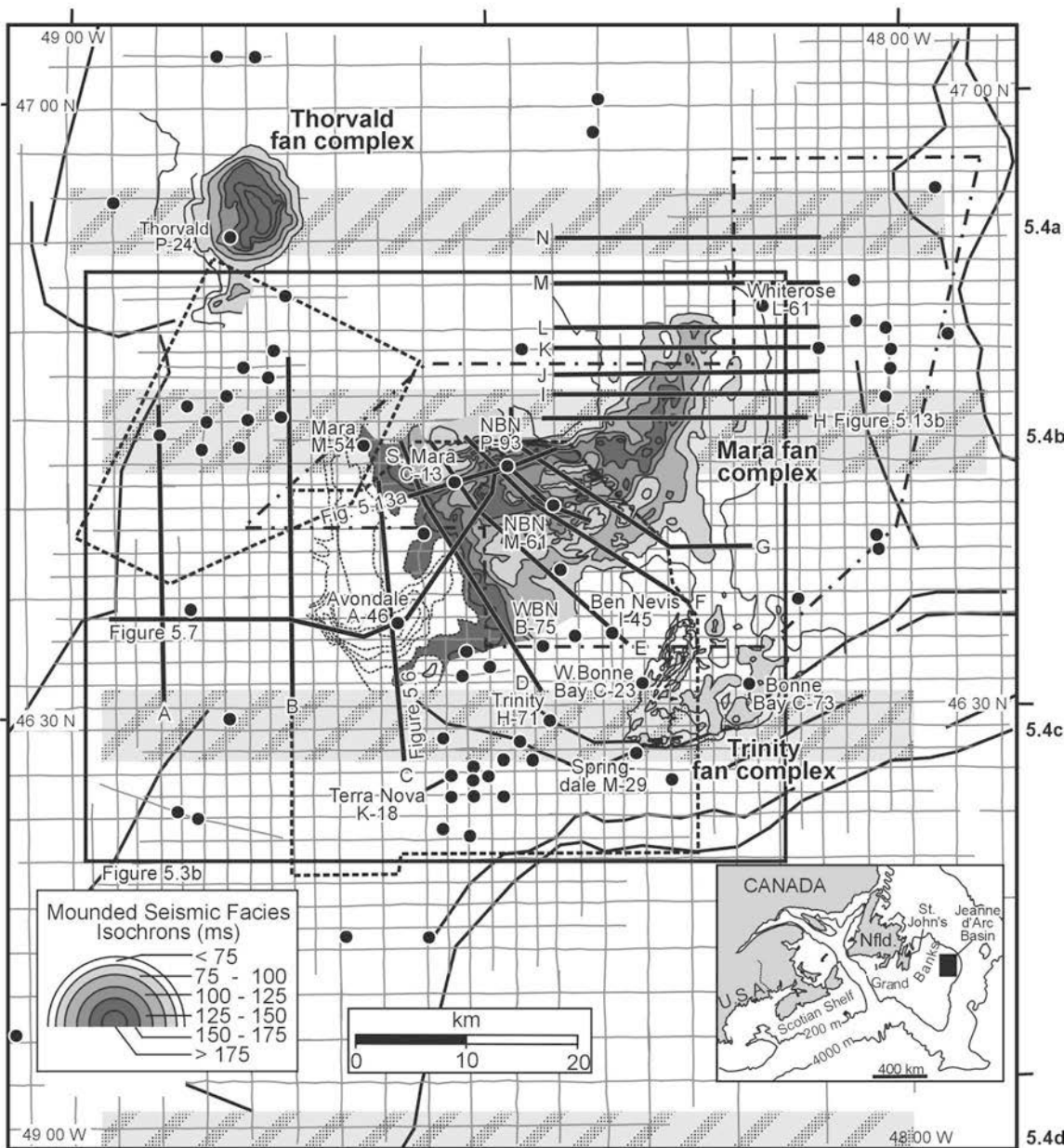


Figure 5.3. a) Basemap of the Jeanne d'Arc Basin showing location of 2-D and 3-D seismic data. Also shown are three time-thickness maps of the mounded seismic facies recognized in the basin. Each time-thickness map represents the total thickness of mounded seismic facies within each submarine fan complex, including both Paleocene and lowermost Eocene strata. Contour interval is 25 ms. From northwest to southeast they are named the Thorvald, Mara, and Trinity complexes. Well locations are shown as black dots. Wells that penetrate the mounded seismic facies or other parts of each fan complex are labeled. The west to east bands of slanted stipple show the approximate areas represented in Figures 5.4 a (furthest north) to 5.4d (furthest south). **NBN** North Ben Nevis, **WBN** West Ben Nevis.

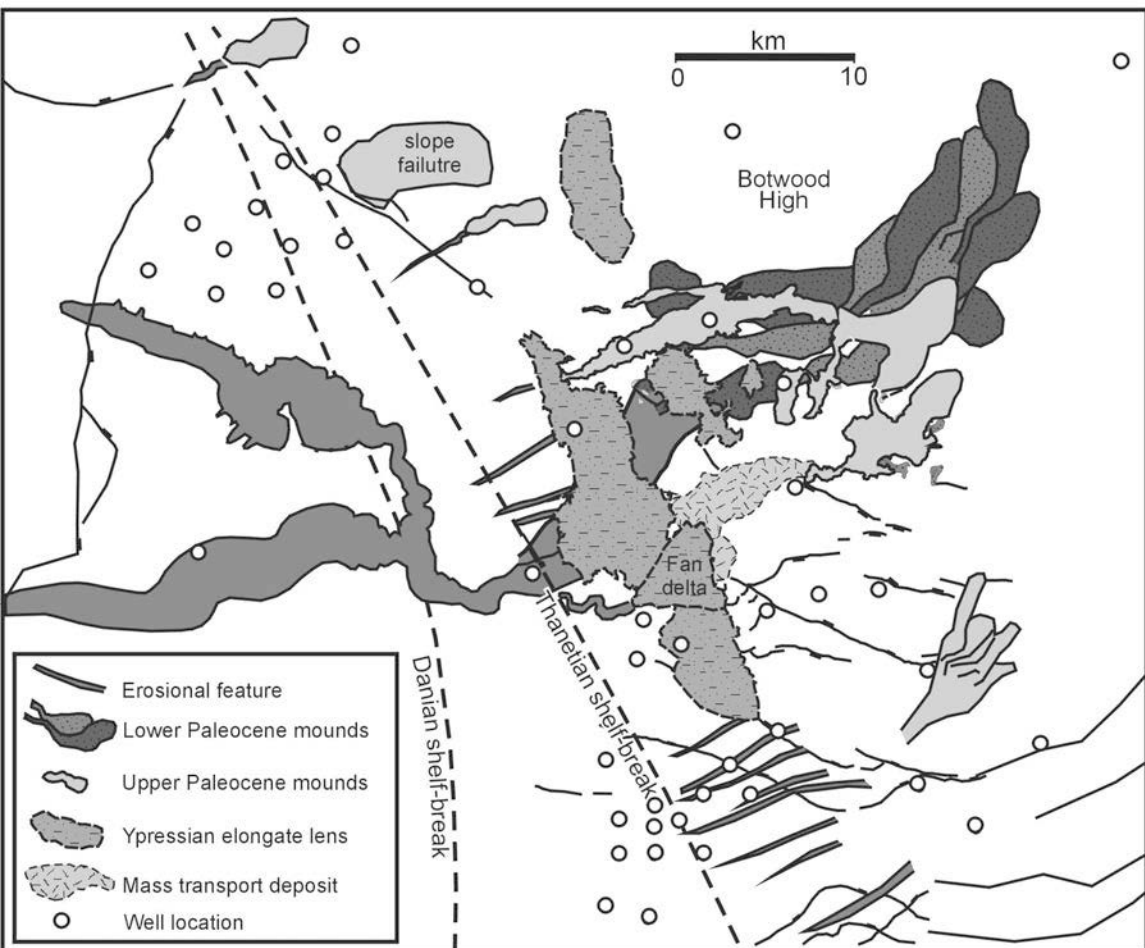


Figure 5.3. b) Basemap showing location of Paleocene to earliest Ypresian mounds and erosional features mapped in this study. See Figure 5.3a for location and text for details.

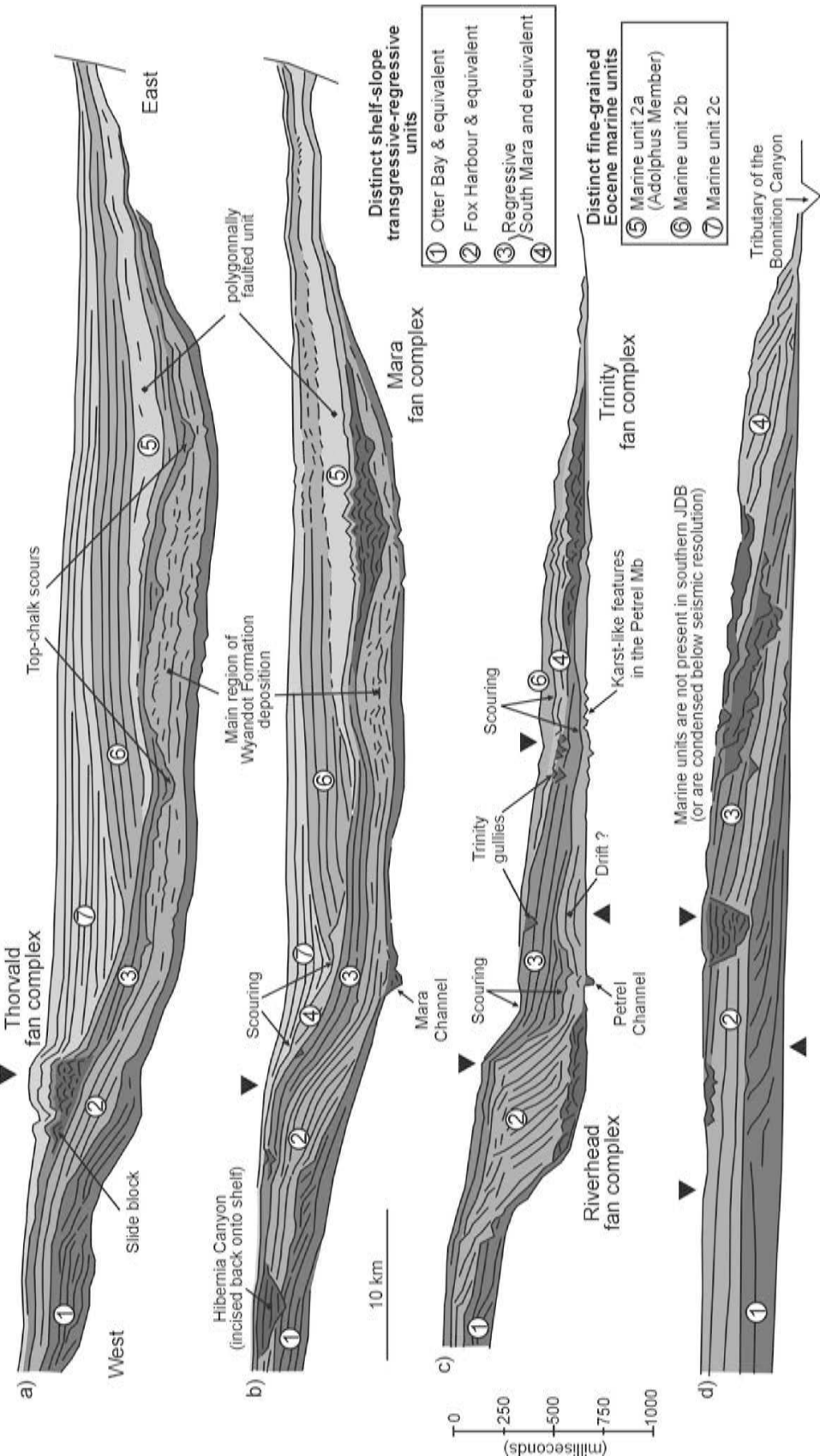


Figure 5.4 Schematic cartoons summarizing stratal architecture from seismic-reflection profiles along four west to east transects across the basin, ordered from north (a) to south (d). Each traverse summarizes observations from several profiles. Regions from which profiles were taken is shown in Figure 5.3. Note that flattening was carried out to restore shelf units to roughly horizontal, and the effects from regional up-arching have been removed. Black triangles point in the direction of relative subsidence/uplift observed on seismic profiles in the subsurface present day.

of erosional conduits (canyons, channels, gullies, slump scarps) that formed on the shelf and slope as the margin advanced, transporting sediment eastward, toward the basin floor (Figure 5.3b). Detailed examination of the mounds in each complex indicates that they are composed of multiple stacked three-dimensional bodies, with variable cross-sectional and planform geometries. Well data indicate that mounds are sand-prone, comprising either the Avondale or South Mara members of the Banquereau Formation (see Deptuck et al., 2003a). Together, the erosional conduits and mounded seismic facies define three fan complexes (*sensu* Mutti and Normark, 1987, 1991), herein named Thorvald (85 km²), Mara (910 km²), and Trinity (150 km²). Of these, the Mara fan complex has the best data coverage, and hence has been studied in the most detail.

5.3 Mara fan complex

The Mara fan complex is located in the central part of the JDB (Figures 5.3a, b, 5.5). It has an axial length of 56 km (from shelf-break to the termination of distal mounds) and a maximum width of about 20 km, narrowing significantly to the north and east. It covers an area of approximately 910 km², and consists of a number of fan elements including erosional features like canyons, gullies, and channels, and stacked mounded to lens-shaped depositional features that accumulated over a period of 10 to 12 m.y. (Danian to early Ypresian). Both 2-D and 3-D seismic data were used to dissect the Mara fan complex, and both regional and local seismic markers (e.g. T1, T10, T15, T20, etc. - Figures 5.6, 5.7), correlated to wells, were used to subdivide it into Danian to Selandian, Thanetian to early Ypresian, and Ypresian growth stages (equivalent to “fan systems” of Mutti and Normark, 1987, 1991).

5.3.1 Early to Middle Paleocene (Danian to Selandian) (T1 to T10)

The Early Paleocene marks a period of shelf and slope erosion in the JDB. Sediment was transported through erosional conduits more than 50 km into the basin (relative to the shelf-break, along main feeder channel), where seismic facies have a prominently mounded character. The slope was generally very steep, locally reaching between 5 and 8 degrees (e.g. immediately south of the Mara fan-valley - discussed in a later section). The system shows an overall down-fan decrease in erosional relief with a

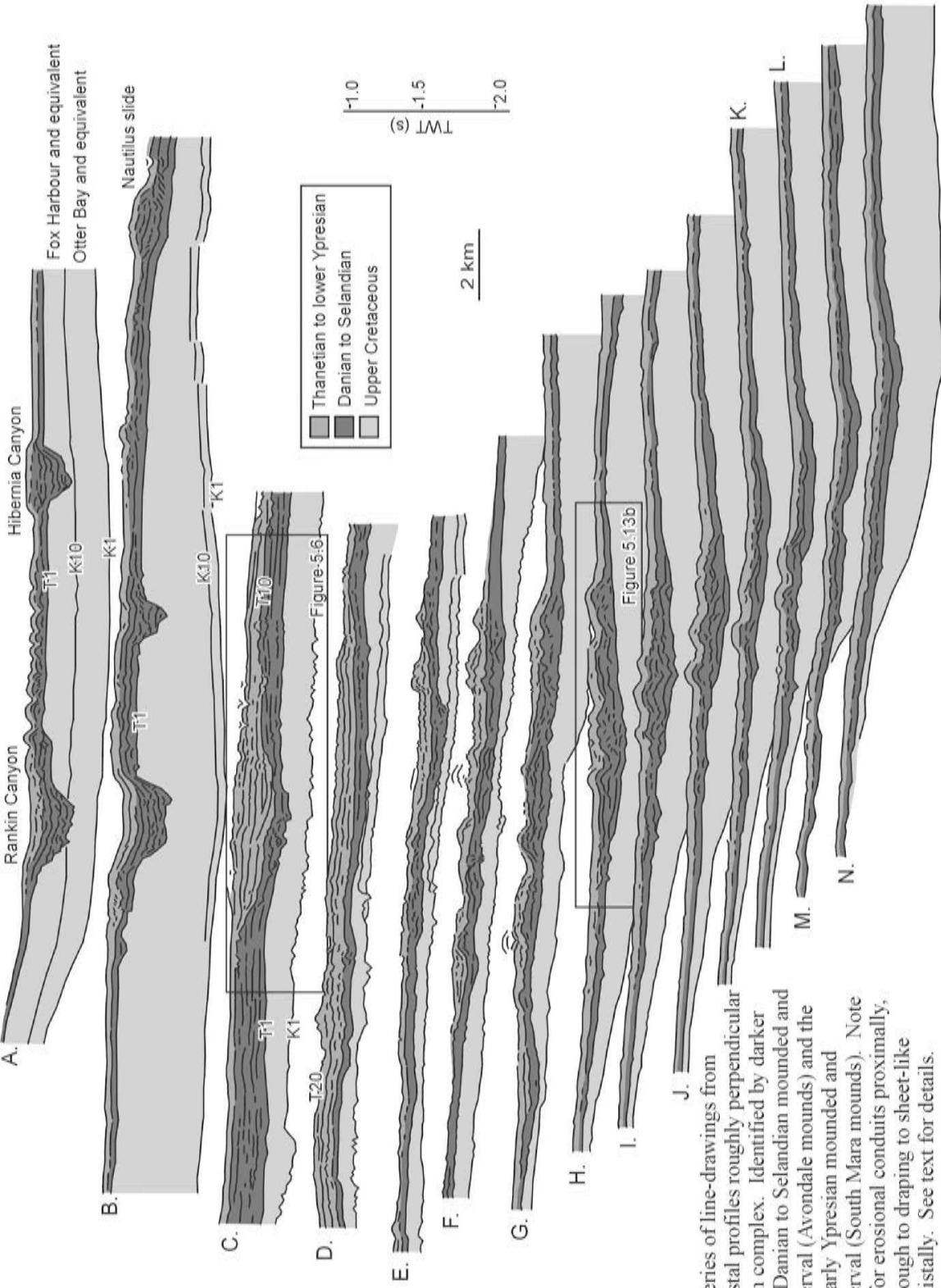


Figure 5.5. Series of line-drawings from proximal to distal profiles roughly perpendicular to the Mara fan complex. Identified by darker shading is the Danian to Selandian mounded and equivalent interval (Avondale mounds) and the Thanetian to early Ypresian mounded and equivalent interval (South Mara mounds). Note the transition for erosional conduits proximally, to mounds, through to draping to sheet-like architectures distally. See text for details.

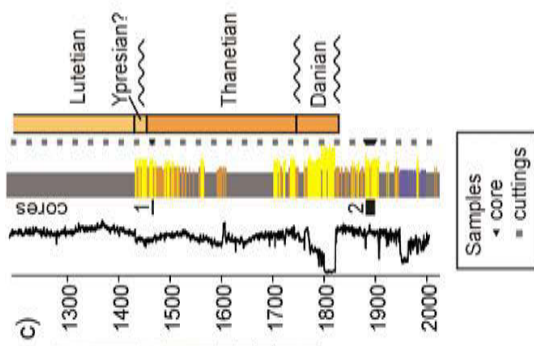
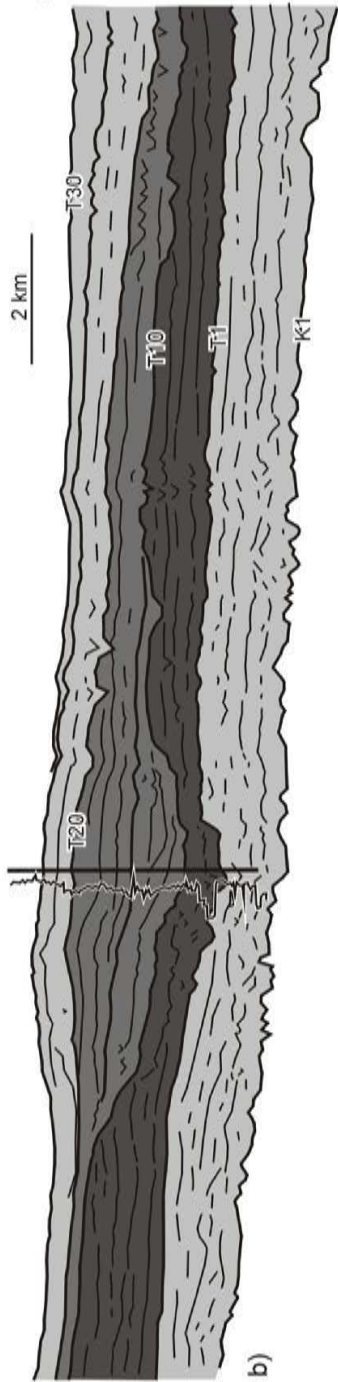
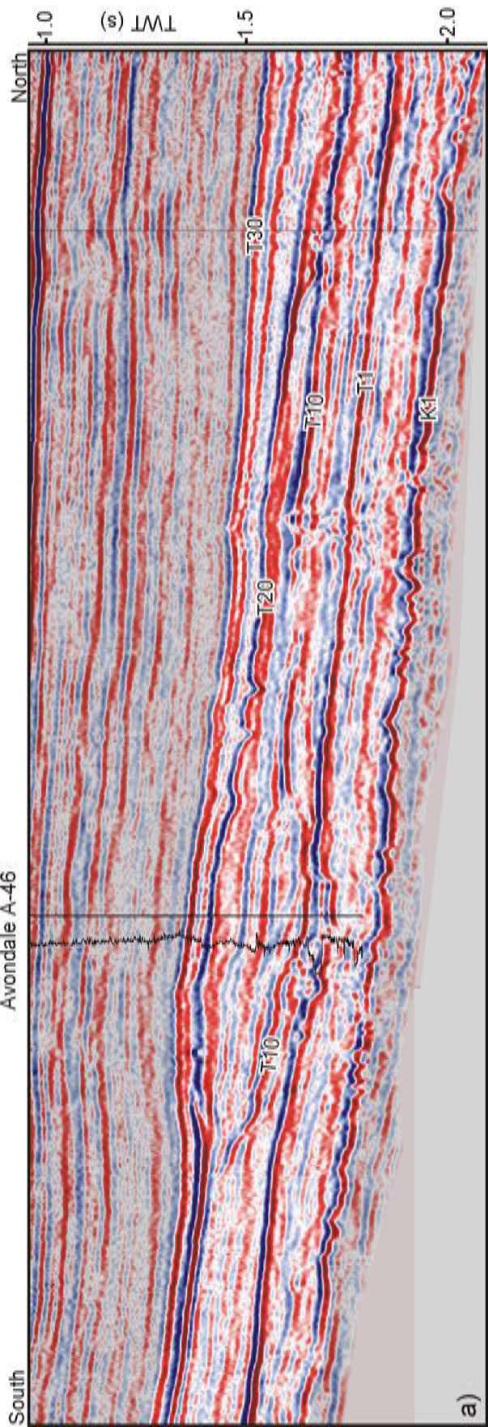


Figure 5.6. a) 3-D seismic profile and b) line drawing through Avondale A-46, across the most expanded Paleocene section in the basin. Note the erosion at both the T1 (Mara fan-valley) and T10 (Avondale Canyon) seismic markers, as well as smaller gullying between the T10 and T20 markers. Location shown in Figures 5.5 and 5.3. c) Lithologic plot of Avondale A-46 with gamma ray log. Age interpretations are from palynology (modified from Fensome, 1996, through personal communication with Rob Fensome and Graham Williams, 2003).

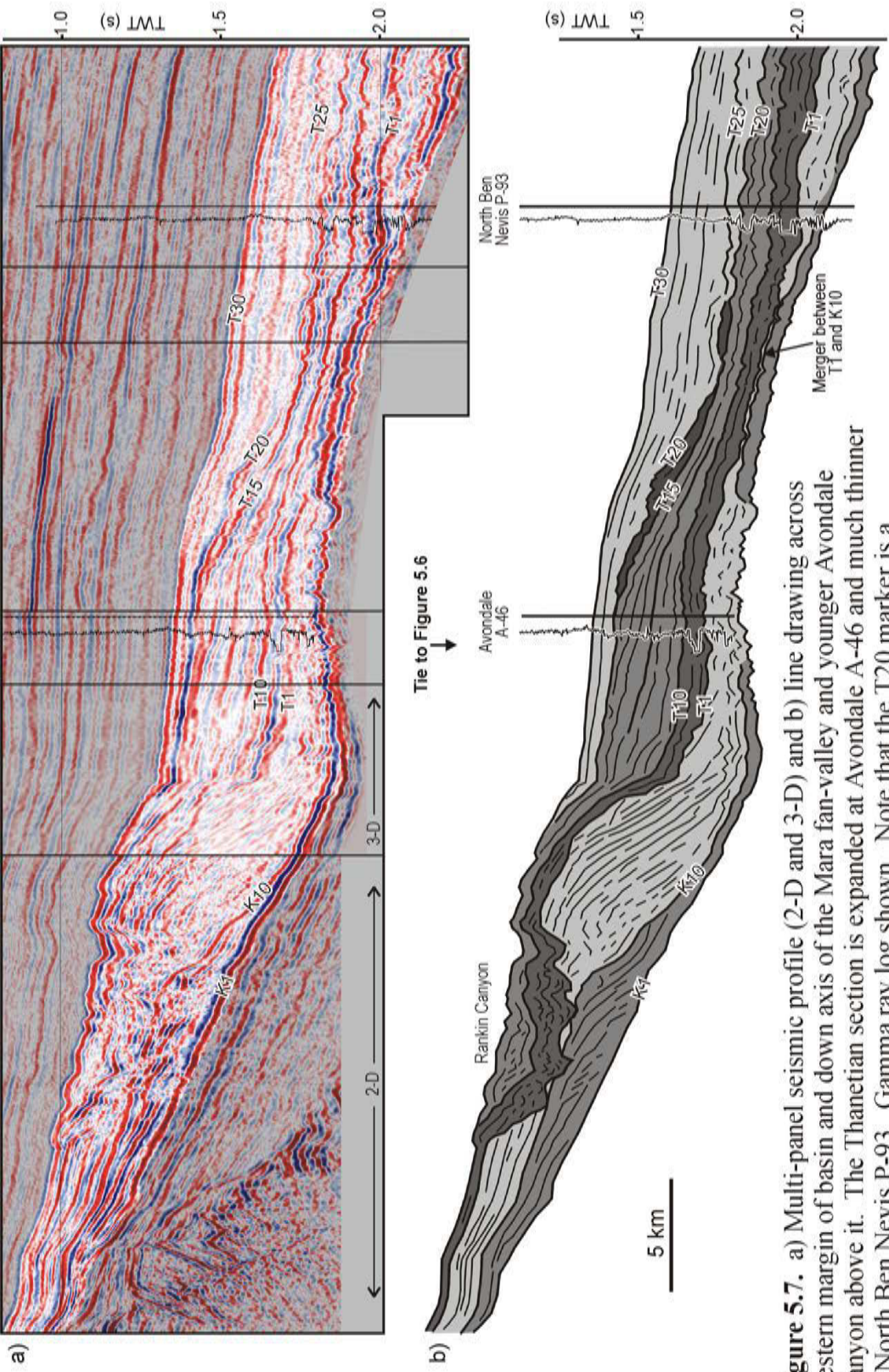


Figure 5.7. a) Multi-panel seismic profile (2-D and 3-D) and b) line drawing across western margin of basin and down axis of the Mara fan-valley and younger Avondale Canyon above it. The Thanetian section is expanded at Avondale A-46 and much thinner at North Ben Nevis P-93. Gamma ray log shown. Note that the T20 marker is a composite surface. See text for details, and Figure 5.3 for location.

corresponding increase in mounded seismic facies, eventually passing distally and laterally into strata with a more sheet-like geometry. Sands deposited on the basin floor during the Early Paleocene correspond to the Avondale Member of the Banquereau Formation, deposited above the T1 seismic marker and below the semi-regional T10 seismic marker (Figures 5.6, 5.7).

The Early Paleocene Mara fan system corresponds well to the early models presented by Normark (1978) and Walker (1978), with proximal canyon erosion (in this case two canyons that merge on the slope), passing down-system into a fan-valley (primary feeder channel), which in turn transitions into mounds at its termination (“suprafan” lobes, sensu Normark, 1978). The mounds, in turn, pass distally and laterally into thin, continuous deposits of the lower fan and basin plain.

Hibernia and Rankin canyons

The Hibernia and Rankin canyons incise the prominent latest Cretaceous prograding shelf and slope along the western margin of the basin (Figures 5.7, 5.8). The canyons truncate the T1 seismic marker and underlying Upper Cretaceous strata, locally cutting as deeply as the K10 marker that defines the top of the Otter Bay Member of the Dawson Canyon Formation (Figure 5.7 - see also Chapter 3). 3-D seismic coverage over the 17 km long Hibernia Canyon indicate a width that ranges from about 1 to 1.5 km on the shelf to about 5 km near the shelf-break, and a range in depth from 150 to 220 m. The head of the canyon is located above the Bonavista Platform, west of the Murre fault. East of the Murre fault, the canyon has a V-shaped cross-sectional geometry (Figure 5.5, profile A). Several erosional notches on the canyon walls (150 to 300 m wide and 200 to 1000 m long) indicate that sediment also entered the canyon laterally, either through canyon wall slumping, perhaps in response to sediment transported along the shelf in littoral drift cells, or through fluvial incision (Figures 3.14, 5.9a).

Where the canyon is narrowest (11 km long segment on the shelf), a low-sinuosity (sinuosity of 1.08) curvilinear erosional thalweg channel is recognized at its erosive base (Figure 5.9b), which, at least during the final stages of incision (prior to the first period of fill), appears to have been stationary (i.e. vertical incision but no significant lateral migration). The Hibernia Canyon is widest near the shelf-break defined by the T1

Figure 5.8. Perspective view of the T1 marker in the JDB, as viewed from the east. Note prominent canyons eroding the shelf and slope along the western margin (top). Inset shows close-up of the Mara fan-valley at the T1 marker, mapped from 3-D seismic data.

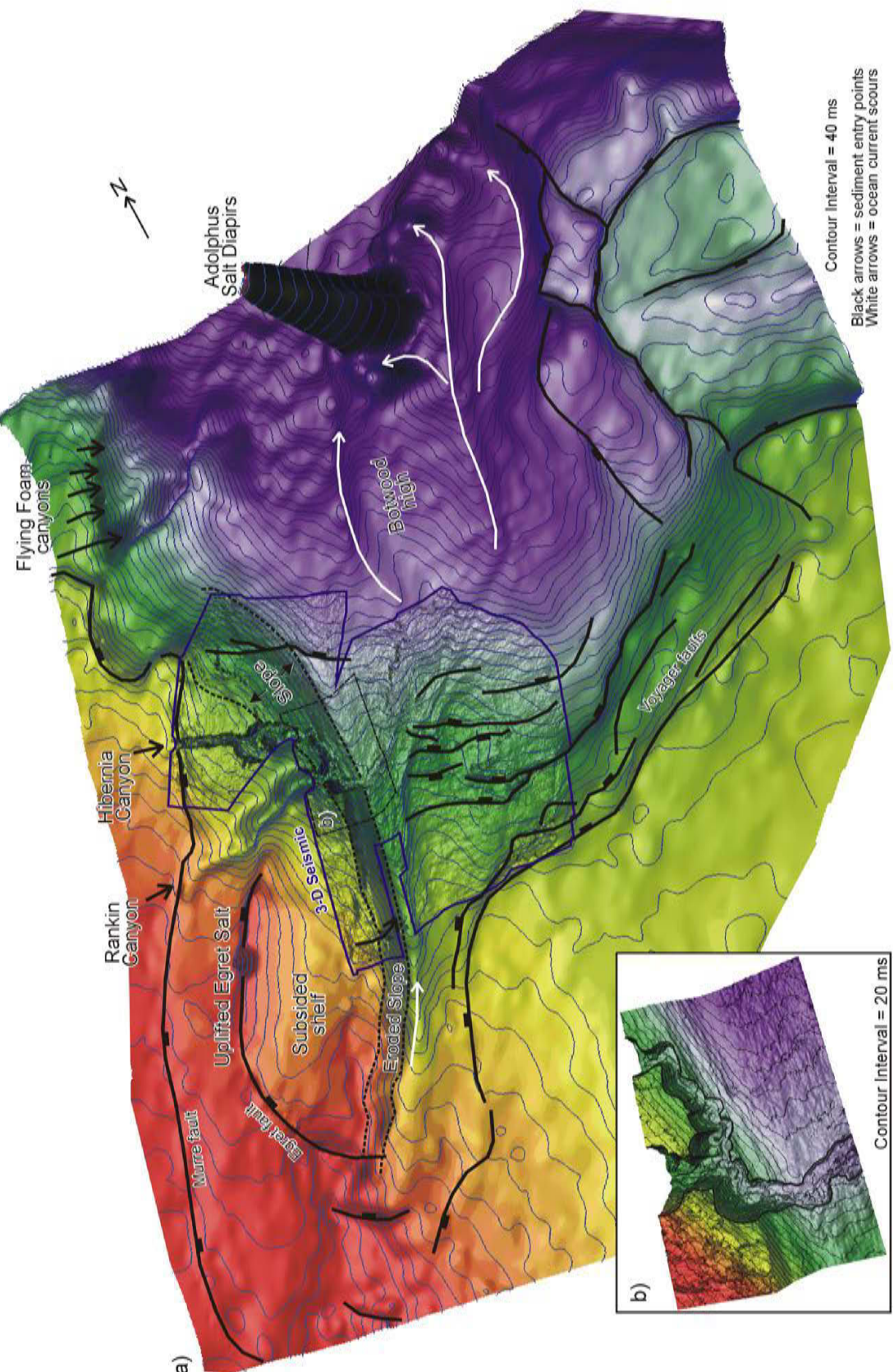


Figure 5.8. Continued (see previous page for caption)

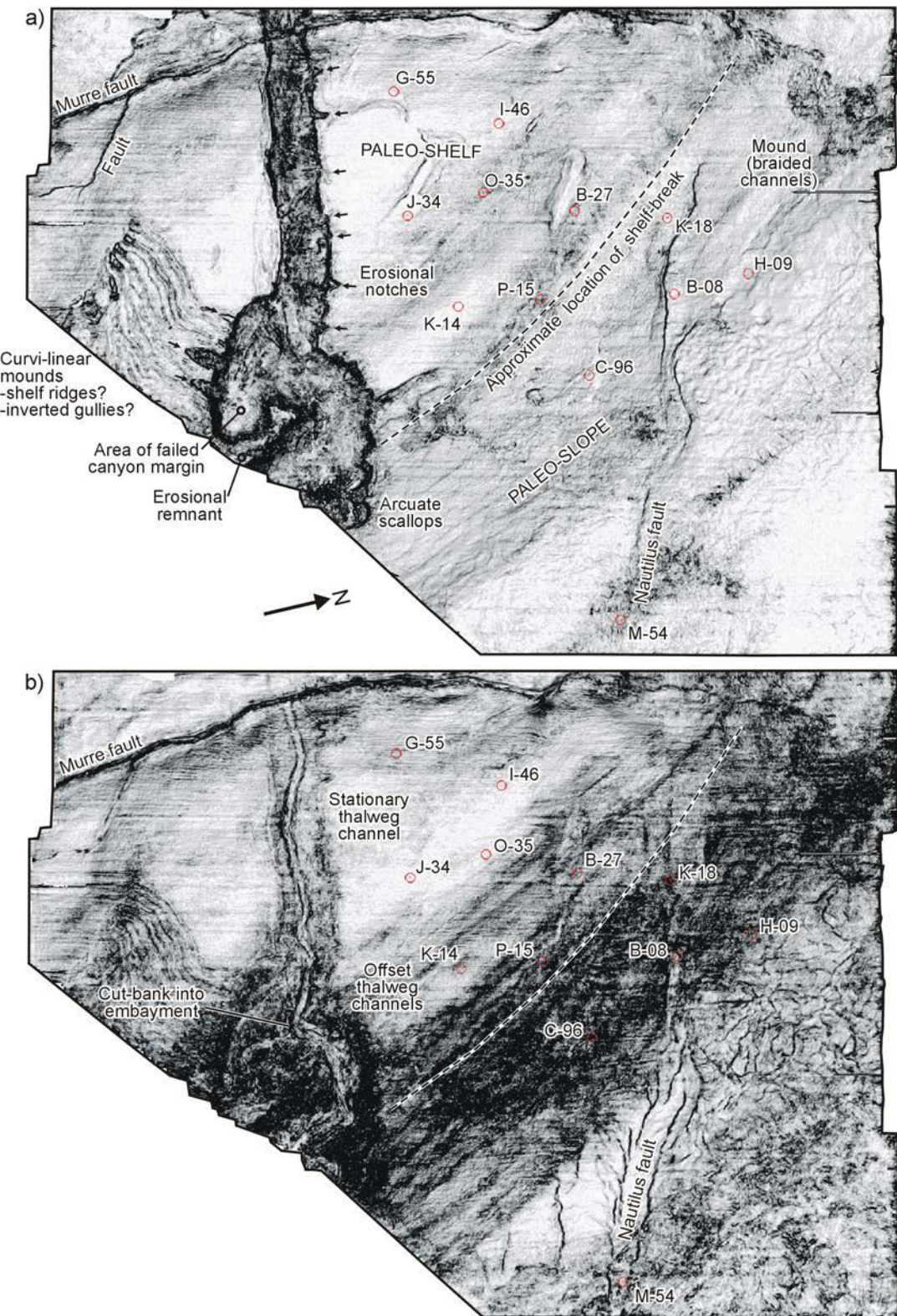


Figure 5.9. Horizon slices at a) the T1 marker and b) 128 ms below T1 marker (mapped horizontally above canyon-fill, not along erosive base as in Figure 3.14) showing planform character near the brim of the canyon (a) and near its erosive base (b).

marker. The increased canyon width coincides with the first canyon reach where several erosive, laterally offset thalweg channels are observed (Figure 5.9b). Thalweg channel migration and undercutting of the canyon margin, causing slumping near the unstable shelf-break, probably accounts for the increased canyon width in this reach.

The Rankin Canyon, south of the Hibernia Canyon, appears to have been diverted around the uplifted Egret salt structure, suggesting that the salt structure formed a positive relief feature during canyon erosion (Figure 5.8). The Egret salt structure is overlapped by Early to Middle Eocene (Ypresian to Lutetian) strata, providing an upper constraint on salt movement.

Mara fan-valley

Just east of the shelf-break, the margins of the Hibernia Canyon have a scalloped appearance and thalweg channels show an increase in sinuosity (sinuosity is the ratio of the straight line distance to the along channel distance). On the upper slope, the Hibernia Canyon makes an abrupt 70 degree turn toward the south where it passes into a much narrower 1 to 1.8 km wide erosional slope channel, referred to herein as the Mara fan-valley. In the absence of faults in the immediate area, differential subsidence of the thickest Upper Cretaceous strata just south of the Rankin Canyon (see restored section in Figure 5.4c, and time-thickness map in Figure 4.8b), causing local southward tilting of the western margin, is considered the most likely mechanism responsible for the southward turn in the fan-valley. Active salt withdrawal at the Egret salt structure, west of the thickest Upper Cretaceous strata, combined with scissor motion along the Egret fault further south still, appears to have accommodated structural sagging (Figure 5.8).

The floor of the fan-valley is erosive and consists of several 280 to 400 m wide thalweg channels that are much more sinuous (sinuosity of 1.4 to 1.6) than the fan-valley itself (Figures 5.8, 5.10). Successive thalweg channels erode one another, in some cases preserving older channel segments as a result of incision and bypass. Several meander bends are cut-off and terraced above the deepest thalweg channel (Figure 5.10). The coincidence between the increased sinuosity of thalweg channels and the increase in prevalence of scallops along the margins of the fan-valley suggests a genetic relationship.

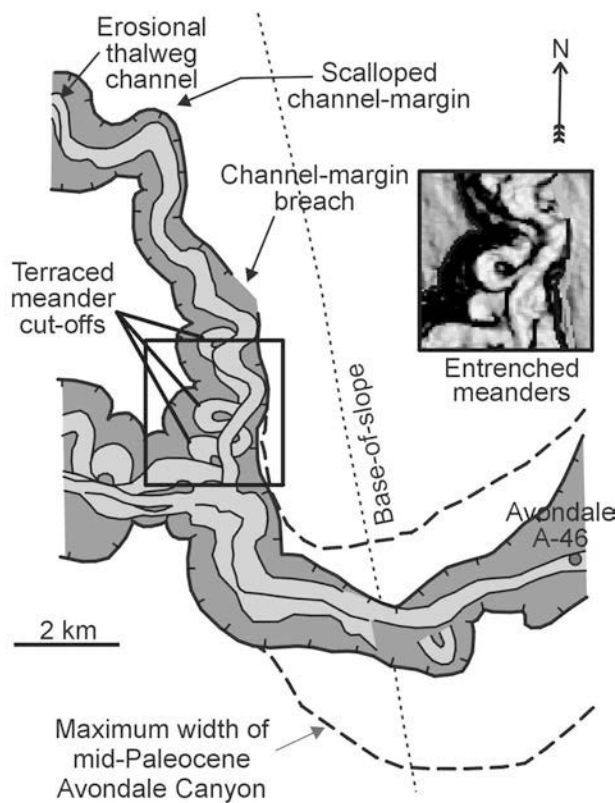
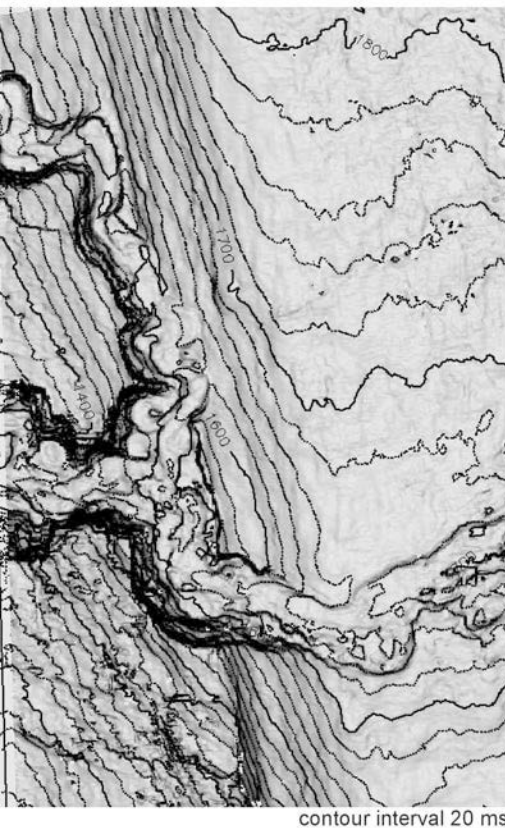


Figure 5.10. a) Contoured dip map and b) line drawing of the T1 marker showing the Mara fan-valley and sinuous thalweg channels at its erosive base.

The thalweg channels appear to have undercut the margins of the fan-valley, causing arcuate slump scarps.

Further south, the Mara fan-valley intercepts the broader (2 to 3 km wide), east-trending Rankin Canyon (Figures 5.8, 5.10). About 1 km south of where the two valleys merge, the Mara fan-valley makes another abrupt turn to the east, perpendicular to a steeper portion of the slope, with an abrupt straightening of thalweg channels (sinuosity of 1.06). On the basin floor, the fan-valley has a “left hook” planform geometry, which in this case appears to be caused by basin structure (i.e. northward tilt towards the Adolphus salt diapirs), and not in response to the formation of a high right-hand levee (facing down-channel) due to Coriolis effect, as has been proposed for many systems (see Menard, 1955). The small dimensions of the Mara fan-valley, combined with limited seismic resolution and compaction, however, may mask the presence of levees, so the Coriolis effect cannot be completely ruled-out.

The erosion base of the Mara fan-valley was mapped for more than 25 km northeast of the base-of-slope, where it erodes muddy deposits of the Upper Cretaceous Dawson Canyon Formation and locally Coniacian or younger chalk deposits (e.g. where the T1 marker merges with the K10 marker in Figure 5.7). Other than one terraced meander bend near the base-of-slope, sinuous thalwegs are not well imaged northeast of the Avondale A-46 well (Figure 5.10). Instead, multiple, shallow-relief and relatively straight, cross-cutting channels define the path of the Mara fan-valley (Figures 5.11, 5.12). In this way, the T1 marker does not define a single period of channel development; rather it shows the cumulative erosive effects of channels that shifted position over a period of time in response to avulsions.

Avondale A-46 penetrated the axis of the Mara fan-valley, about 8 km east of the shelf-break and 4 km east of the base-of-slope (Figures 5.6, 5.10, 5.11). The well is the type section for the sand-prone Avondale Member of the Banquereau Formation (see Chapter 3), which at this location was clearly deposited in a submarine channel, above the T1 seismic marker. Biostratigraphic data indicate the sands accumulated in the Danian (Figure 5.6, Fensome, 1996a).

Fan-valley deposits have been influenced by both faulting and later erosion. Minor normal faults locally offset the fill, but these do not appear to have influenced its

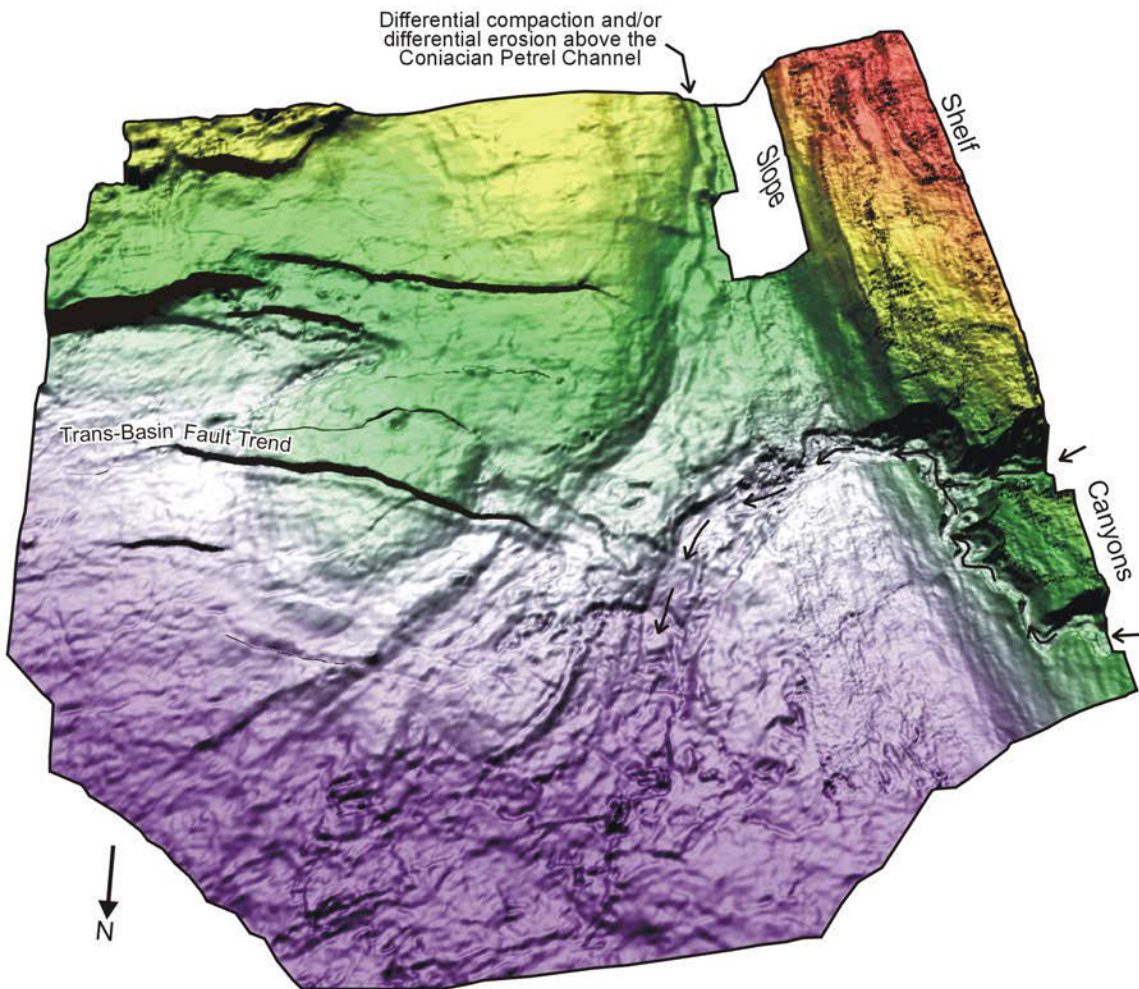


Figure 5.11. Shaded perspective view of the T1 seismic marker (time-structure map - viewed from the north). The surface was interpreted from 3-D seismic data and was gridded with a 40 m grid spacing. A single light source from the south creates the shadows that highlight the Trans-Basin Fault Trend and the erosional features along the western basin margin (right-hand side). Note the differential compaction above the Petrel Channel which underlies this surface. It is possible that ocean currents, which scoured the slope region, accentuated its positive relief through differential erosion between cemented channel sands and surrounding shale, rather than differential compaction.

orientation, so are interpreted as post-depositional features (but they may influence sandstone connectivity). The proximal, upper parts of the Mara fan-valley were eroded by a broad, overlying canyon, herein referred to as the Avondale Canyon. Its base is the T10 seismic marker, and erosion along this surface may in part account for the lack of evidence for overbank deposits flanking the Mara fan-valley.

Avondale mounds

The Mara fan-valley leads to a complicated region consisting of mounded seismic facies that cover an area of 150 km² (Figure 5.12). A profile across the western basin margin and down the axis of the Mara fan-valley shows the transition from channel deposits at Avondale A-46 to mounded seismic facies at North Ben Nevis P-93, 18 km away (Figure 5.7). A time-thickness map between the T1 and T10 seismic markers from both 2-D and 3-D seismic data shows the distribution of mounds (Figure 5.12). The mounds reach a maximum thickness of 140 ms, which at an average interval velocity of 3000 m/s (based on the more proximal North Ben Nevis and Avondale wells) yields a thickness on the order of 210 m. As mentioned above, the T10 marker defines the base of the younger Avondale Canyon, that erodes underlying deposits. The amount of erosion that took place at the T10 marker is illustrated in Figure 5.6, a profile roughly perpendicular to the Mara fan-valley, where Lower to Middle Paleocene slope deposits were eroded. Canyon relief, however, diminishes abruptly to the northeast, and does not extend to the mounded region, and hence the mounds appear to have been unaffected by subsequent canyon erosion.

The entire mounded interval consists of a complicated arrangement of steep- to broad-sided mounds, locally amalgamated on seismic profiles, making them difficult to interpret. The overall distribution of the mounds was strongly influenced by the Botwood High (Figure 5.12), an older positive bathymetric feature formed, at least in part, as a consequence of north-trending erosional scouring on either side of the Botwood G-89 well, just prior to fan deposition in the Danian (see Chapter 4). The Botwood High appears to have formed a prominent bathymetric obstacle that deflected sediment gravity flows to the east. The structurally higher eastern margin of the basin provided additional

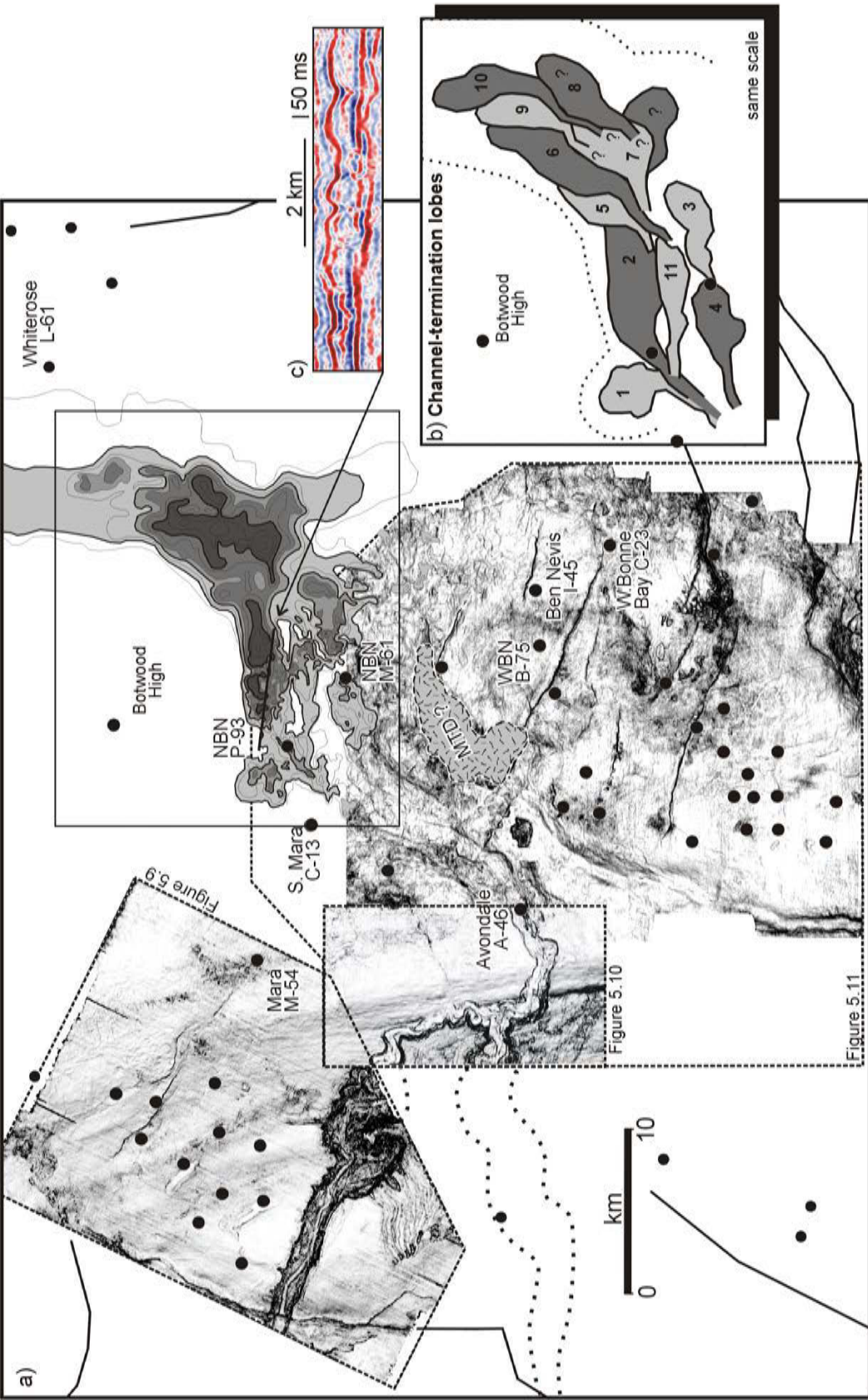


Figure 5.12. a) Basemap of the JDB showing a time-thickness map of the Avondale mounds (T1 to T10) above a mosaic of horizon coherence-slices showing Early Paleocene feeder systems. b) Highly schematic cartoon showing the stacking architecture of individual lobes. c) Profile across Avondale Mound 2. Note minor incision into the top of the mound interpreted and distributary channels. MTD = mass transport deposit.

lateral confinement for the mounds, guiding deposits into the elongate scoured depression on the northeastern basin floor.

Several sub-circular regions of increased travel-time (on the T1 to T10 time-thickness map) provide clues about the planform geometry of individual mounds. On some seismic profiles, individual mounds are separated by surfaces of onlap, downlap or erosion, allowing reconstruction of the temporal relationships between mounds, at least locally (Figure 5.12b). Some mounds are stacked in a shingled manner, adjacent to and above the previous mound (e.g. Figure 5.13b). The mounded interval consists of eleven or more separate mounds. Five of these (labeled 1-4, and 11) were mapped, at least in part, using 3-D seismic data, so the degree of confidence in their location and relative timing is high. The remaining mounds shown in Figure 5.12 were mapped using 2-D seismic profiles of lesser quality, or paper copies of the quasi-3-D seismic survey, so the level of confidence in their temporal relationships, and to a lesser extent their outlines, is lower. A tighter line spacing is needed to map these mounds with greater confidence. Nevertheless, profiles perpendicular to the mounds do show the development of distinct, stacked mounds (e.g. Figures 5.5, 5.13b).

Individual mounds are estimated to cover areas ranging from 11 to 40 km². **Avondale mounds 1, 2, and 3** are stacked progressively to the east, presumably in response to progressive channel-mouth avulsions in the same direction (Figure 5.12b). **Avondale Mound 4** was deposited in a more proximal position, just west of mound 3. Avondale mound 2 extends beyond the limits of 3-D seismic data, and covers an area of about 30 km². Relatively sinuous, small erosive channels erode the upper surface of the mound near the eastern limit of 3-D seismic coverage, and perhaps represent erosive distributary channels (Figure 5.12c). **Avondale Mound 11** has an erosive base that truncates mounds 2, 3 and 4. It is presumed to have formed the conduit for more distal mounds as the proximal mounds were bypassed.

North Ben Nevis P-93 penetrated the proximal part of Avondale Mound 2 and North Ben Nevis M-61 penetrated the distal part of Avondale Mound 4 or the proximal feeder channel of Avondale Mound 3. Both wells penetrated more than 60 m of medium to coarse-grained sandstones that generate a blocky gamma ray response (e.g. Figures 5.7, 5.13). No wells penetrate the thickest mounded region further north. South Mara C-

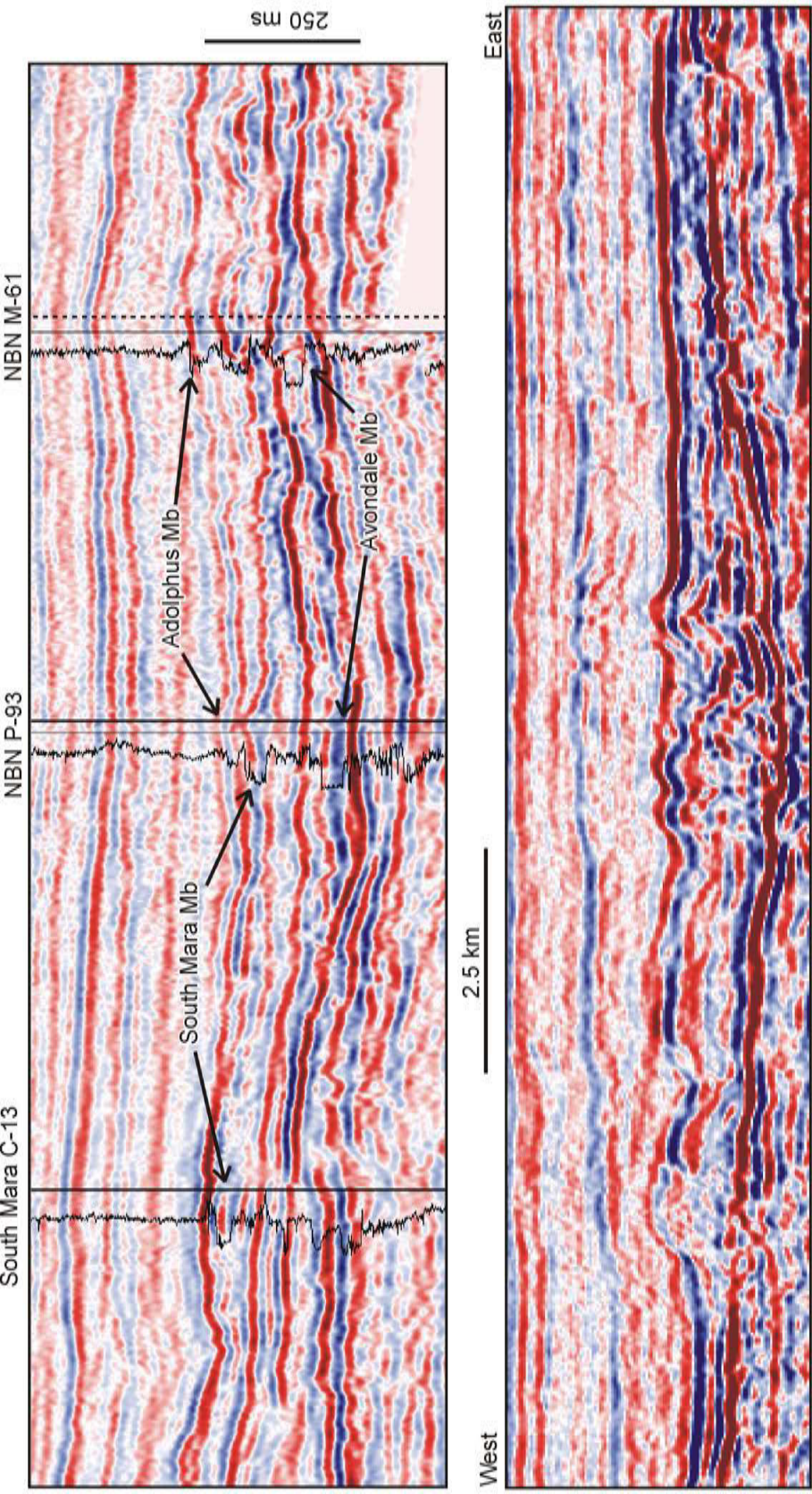


Figure 5.13 a) Multipanel display through South Mara C-13, North Ben Nevis P-93, and North Ben Nevis M-61. Gamma ray curve shown. b) West to East 2-D seismic profile across mounded region on Mara fan complex. Note the laterally offset stacking of prominent mounds. See Figure 5.12 for location. NBN North Ben Nevis

13, located 5 km west of North Ben Nevis P-93, penetrated sub-parallel seismic facies consisting of Danian to Selandian fine-grained sediment on the lower slope, but no sands. Other wells, like Ben Nevis I-45 and West Ben Nevis B-75 penetrate predominantly muddy strata south of the mounded seismic facies.

Basin plain

The bathymetric influence imposed by the Botwood High and the structurally higher eastern basin margin continued to the north, beyond the distal limit of mounded seismic facies. Here, seismic-reflection profiles indicate sheeted to draping deposits (Figure 5.5m, n). Lateral confinement caused deposits to thicken toward the axis of the underlying, north-trending erosional scour at the T1 marker (Figures 5.5, 5.12).

Whiterose L-61 penetrated thinned, seismically continuous deposits 6 km east of the region of mounded seismic facies. The well penetrated fine-grained sandstone and shale, believed to represent a basin plain depositional setting.

5.3.2 Late Paleocene (Thanetian) to earliest Eocene (early Ypresian) (T10 to T15)

The latter part of the Paleocene marks a time of change for fan systems in the JDB. By the end of the Selandian, a new gentler slope (2 to 4 degrees) had formed in front of the steep earliest Danian slope. This slope was later eroded by the Avondale Canyon toward the end of the Selandian, depositing muddy strata on the basin floor, and subsequently filled during the Thanetian (Figure 5.6, Avondale A-46 - R. Fensome, pers. comm., 2003). Sandy fan deposition was renewed in the late Thanetian to earliest Ypresian, and similar to earlier fan systems, it is characterized by mounds with a range of planform and cross-sectional geometries (Figure 5.14). Unlike earlier fans, however, no major erosive canyons are recognized in the study area, and despite the eastward advance of the shelf and slope system, mounded seismic facies formed in more proximal locations than previous Early Paleocene mounds. The feeder system consisted of small, ephemeral gullies incised into the relatively low-gradient slope (Figures 5.14, 5.15), or linear, narrow mounds interpreted as compaction-inverted channels (Figures 5.16, 5.17 - discussed later).

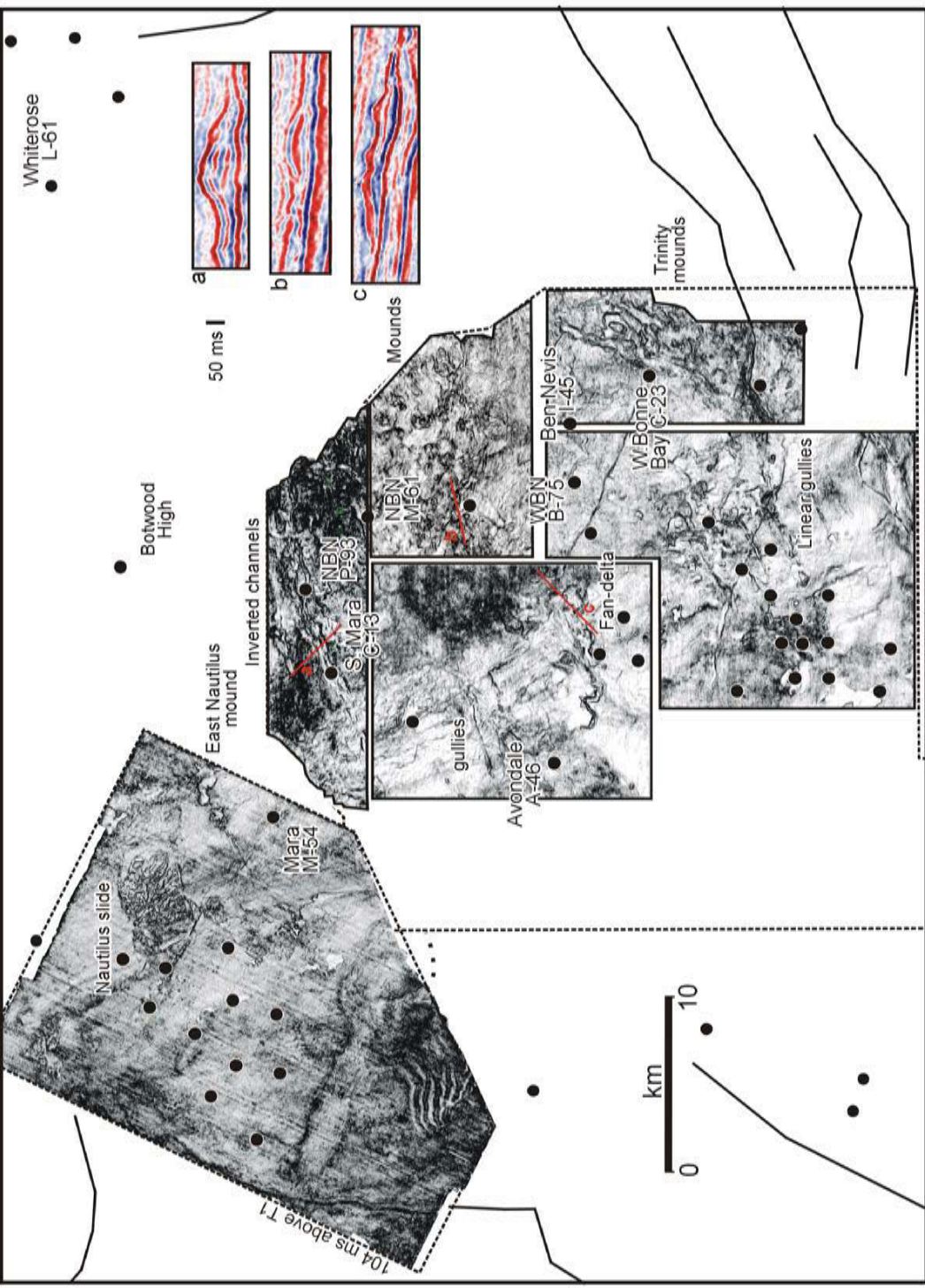


Figure 5.14. Basemap of the JDB showing a mosaic of horizon slices at different levels above the T1 seismic marker, illustrating different erosion features (gullies) and mounded regions in the basin, associated with the South Mara mounds. See text for details.

Fans deposited during the Thanetian to earliest Ypresian do not fit well into the early models proposed by Normark (1970, 1978) and Walker (1978), but do correspond well to the multiple-source sand/mud-rich to sand-rich systems identified by Reading and Richards (1994).

Avondale Canyon

As discussed above, the T10 marker defines the base of the broad (up to 4.5 km wide), erosive Avondale Canyon, incised into fine-grained sediment of the Early to Middle Paleocene slope (Figure 5.6). It has a maximum relief of 200 m that diminished to the northeast over a distance of 18 km. The head of the canyon is located on the upper slope, directly outboard of the Hibernia and Rankin canyons (which were largely filled in at this time), and does not extend back onto the shelf. Erosion appears to have been short-lived, and no significant channel or sandy fan systems developed at its mouth. In fact, the deposits associated with the canyon are challenging to identify. A region of mud-prone, discontinuous, low-amplitude, hummocky to chaotic deposits, covering an area of 100 km², has been identified at the mouth of the canyon, directly above the T10 marker (Figure 5.13a, below the South Mara Member sandstone unit in North Ben Nevis P-93; area of coverage shown in Figure 5.16). These deposits may represent mud-prone mass transport deposits associated with the slope failure (s) that led to canyon formation. The slope appears to have been prone to failure at this time, as a 3 to 4.1 km wide and 8.3 km long slope failure of similar age is recognized 19 km to the north, covering an area of 34 km² (Figure 5.15). In addition, slide blocks and a failure scarp are recognized further north still, near the Thorvald fan complex.

Canyon erosion was followed by a period of high sedimentation rates localized within the canyon. As much as 200 m of mud-prone sediment filled the canyon, generating a significantly expanded Thanetian interval (Avondale A-46 - Fensome, pers. comm., 2003). Elsewhere, the Thanetian section is commonly highly condensed (e.g. 15 m thick at Terra Nova K-18 - Williams, 2002; see also Figure 5.6, adjacent to Avondale Canyon). As the canyon filled, progradational seismic facies advanced above the proximal reaches of the Danian Mara fan-valley (Figure 5.7). At least two cycles of regression and transgression are recorded in the gamma ray log at Avondale A-46.

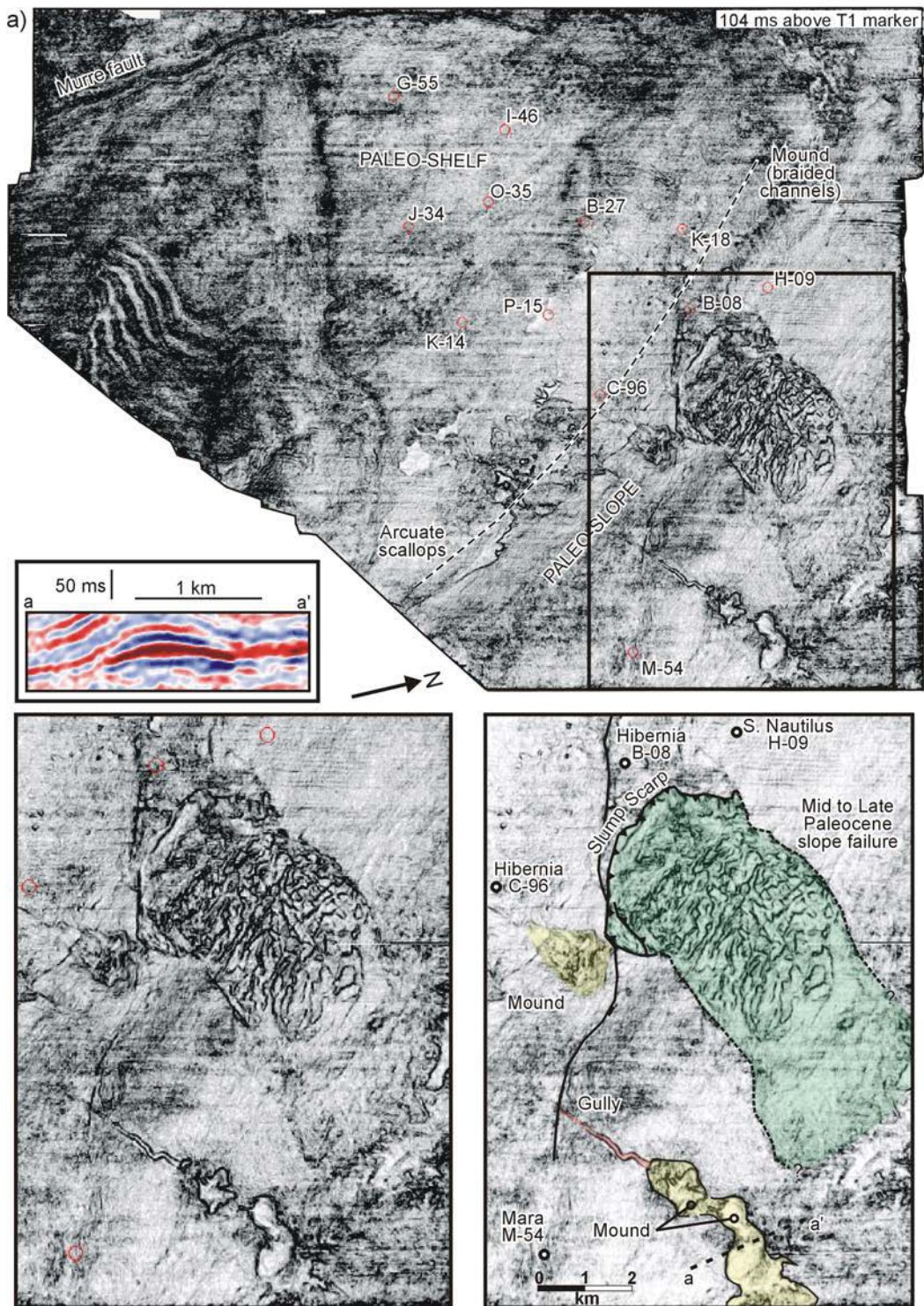


Figure 5.15. Horizon slice 104 ms above the T1 marker (mapped horizontally above canyon-fill) crossing Upper Paleocene deposits on the shelf and slope. Note the small slope gully (orange) with a mounded deposit at its mouth, interpreted to be a small, proximal lobe (yellow), similar to the Pineto gully and lobe off Eastern Corsica. Green shows aerial coverage of the Nautilus slope failure. Seismic profile across East Nautilus mound shown (a to a').

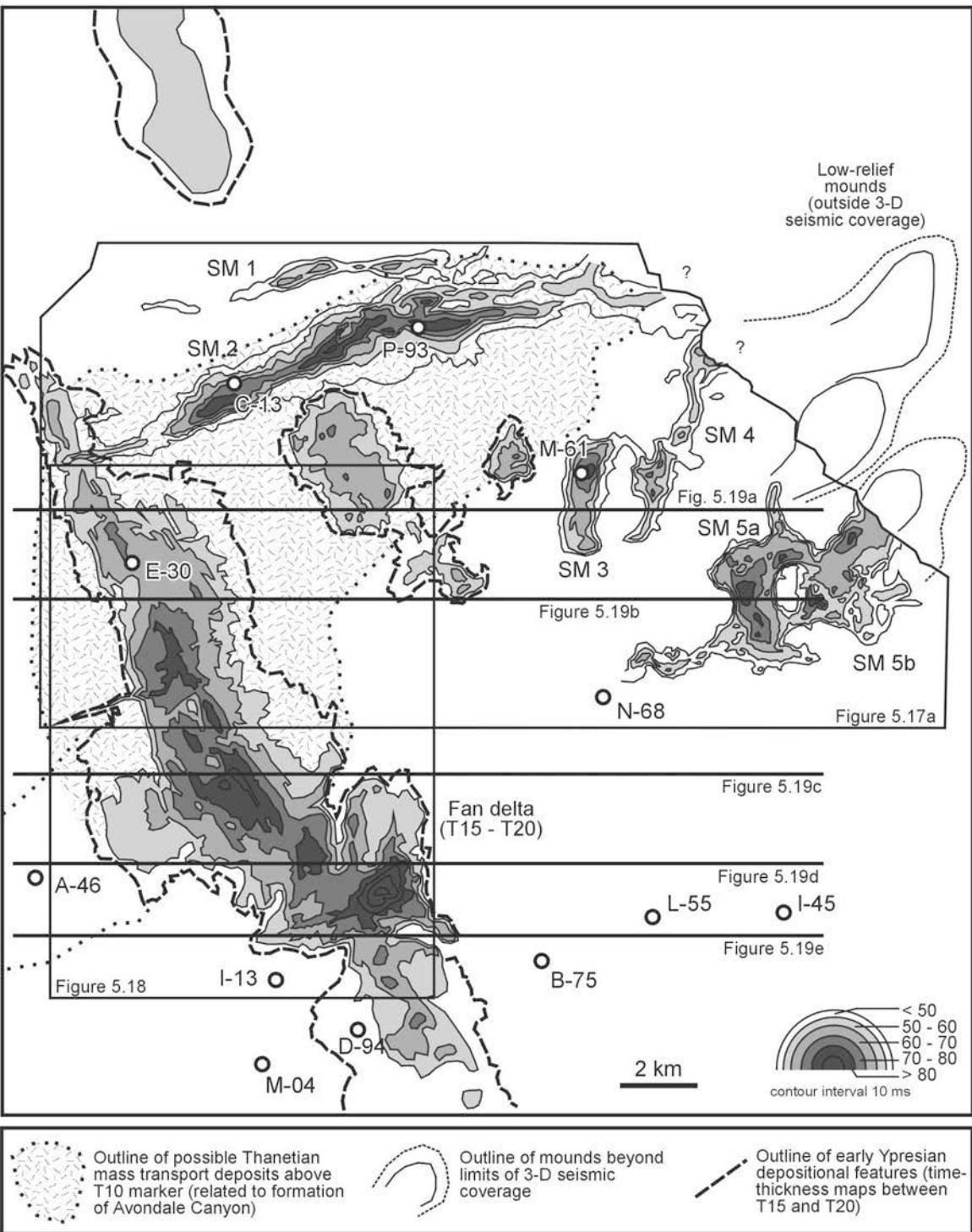


Figure 5.16. Time-thickness map of South Mara mounds between the T10 and T15/T20 seismic markers. SM = South Mara mound. The younger depositional features between the T15 and T20 markers are outlined with the bold dashed line and correspond to elongated northwest trending deposits believed to have been influenced by ocean current circulation during or after deposition. See text for details.

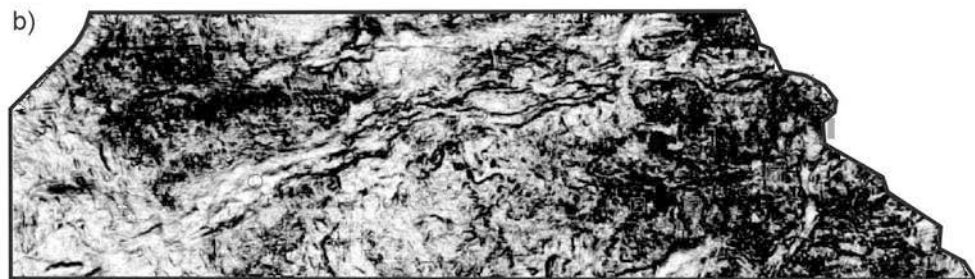
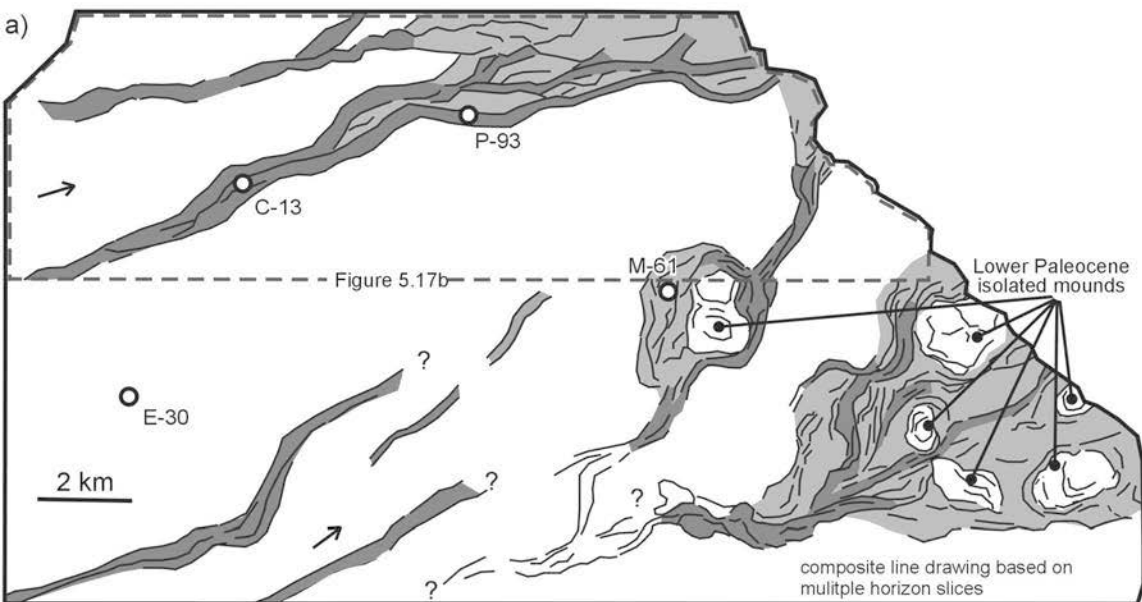


Figure 5.17. a) Line drawing schematic of South Mara mounds and gullies from a series of 3-D coherence horizon-slices. b) Coherence horizon slice through South Mara mounds 1 and 2, showing linear curvi-linear channels.

Slope gullies

Small, linear, V-shaped erosive gullies are recognized along the late Thanetian to earliest Ypresian slope, both in the Mara fan region and further south, on the slope flanking the Trinity fan complex (Figure 5.14). They incise seismic reflections that correlate above the fill of the Avondale Canyon, and therefore post-date its fill. The gullies show up well on coherence slices (Figures 5.14, 5.15), and are typically less than 150 m wide, straight, and range from 2.5 km (East Nautilus) to 10 km in length (on the North Trinity slope). Incision depths are estimated to be less than 40 m and their heads are located near the latest Paleocene shelf break, but typically do not extend back onto the shelf (Figure 5.14). A relatively straight line connecting the heads of the slope gullies marks approximately the location of the latest Paleocene shelf-break. Over time, the shelf-break shifted eastward of the earliest Danian shelf-break. This shift took place more rapidly near Terra Nova than it did further north near Hibernia, and hence there was a change in the shelf-break orientation.

No major canyons were identified in the Mara fan complex during this time period, and only one erosional feature that could be classified as a small canyon is recognized on the slope south of Terra Nova, west of the Trinity fan complex. Therefore, the multi-gullied character of the feeder systems in the late Thanetian to earliest Ypresian was markedly different from the Danian, when large erosive canyons were prevalent.

South Mara mounds

Late Thanetian to earliest Ypresian submarine fans consist of a network of commonly isolated mounds mapped above the T10 marker and below the T15 marker (which is locally coincident with the T20 composite marker) (Figure 5.16). Their distribution corresponds closely to the distribution of the “blocky” South Mara Member of the Banquereau Formation, penetrated in wells on the slope and basin floor (Deptuck et al., 2003a). They are herein referred to as the South Mara mounds. In contrast to the earlier fan growth stage, most mounds do not extend far out onto the basin floor. The aerial coverage of individual mounds varies significantly, from less than 4 km² to over 20 km². Some mounds are narrow, elongate, and generate linear time-thickness patterns (e.g. South Mara mounds 1 and 2). Other mounds are sub-circular or pod-shaped, and are

found at the mouth of linear slope gullies (e.g. East Nautilus mound 1 and Trinity mounds - see Figure 5.14).

South Mara mound 2 covers an area of 23 km², has a length of 16 km, and a width that ranges from 0.6 km proximally to 2.2 km distally (average of 1.3 km). Both the South Mara C-13 and North Ben Nevis P-93 wells penetrate South Mara mound 2 (Figures 5.13a, 5.16, 5.17). Each contains 30 to 40 m of fine to medium grained sandstone. **South Mara mounds 1 and 4** have a similar elongate geometry, but are narrower (< 500 m wide), shorter (less than 6 km long in the 3-D coverage area), and less continuous. Coherence horizon-slices through mounds 1, 2, and 4 reveal several narrow channel paths (Figure 5.17b). Within South Mara mound 2, several laterally offset channels are recognized within the same mound. The channels branch and increase in offset towards the northeast, where the mound widens and thins. The stacked channels appear to have been predominantly depositional in character, as little erosion is recognized at the base of mound 2. Proximally, the mound transitions into a V-shaped gully near the shelf-break. At the distal end of mounds 2 and 4, a low-relief mound is recognized just outside the limits of 3-D seismic coverage, mapped using paper copies of inlines from the quasi-3-D seismic survey. It is not clear whether the mound, outlined in Figure 5.14, represents a lobe formed at the termination of linear mounds 2 or 4, or both.

South Mara mound 3 (Figure 5.16) and the **East Nautilus mound** (Figure 5.15) form very small, pod-shaped deposits that produce a single, highly coherent, high-amplitude reflection in cross-section. The East Nautilus mound is located on the slope, outboard a short curvilinear gully (2.5 km long, extending from the shelf-break). It is narrow (1.2 km wide) and has a length of 4.7 km, covering an area of 4.76 km². South Mara mound 3 is 1.1 km wide, 3.2 km long, and covers an area of 4.5 km². Neither mound is penetrated by a well, but based on their positive relief are inferred to be sand-rich.

South Mara mound 5 is located on the proximal basin floor. It covers an area of 18 km² and consists of two sub-circular mounds located above a region of small, isolated Early to Middle Paleocene mounds (SM 5a and 5b - Figures 5.16, 5.19b). The isolated mounds may represent injection or soft-sediment deformation features formed during deposition of South Mara mound 5. Coherence data show that channels are present

within the mound (Figure 5.17). The feeder channel for South Mara mound 5 is difficult to map. A string of minor dislocated mounds is recognized leading toward the mound, and may be analogous to the “string of pearls” geometry for channels described by Timbrell (1993) for the Balder Formation in the North Sea. Timbrell (1993) interpreted the discontinuous mound geometry of such channels to originate from compaction of discontinuous sands deposited abruptly at sharp meander bends in response to flow stripping (see Piper and Normark, 1983).

Several nested, elongated “finger-like” mounds are also recognized in the Trinity fan complex to the south. They are located at the termination of several slope gullies (Figure 5.14). The mouth of one of the slope gullies adjacent to the Trinity fan complex has been penetrated by the North Trinity H-71 well. It sampled coarse-grained sands to conglomerates.

5.3.3 *Early Eocene (Ypresian) (T15 to T25)*

After most of the South Mara mounds were deposited, an elongated deposit formed parallel to the western margin of the basin, adjacent to the earliest Ypresian shelf-break (defined at the T15 marker) and above some of the slope gullies (Figures 5.16, 5.18). In cross section, this deposit is a lens that varies in internal character from progradational (Figure 5.19c) to discontinuous and hummocky (Figure 5.19d). The base of the lens is defined by the gullied T15 marker. The top of the lens is defined by the T20 marker, which is heavily scoured (Figures 5.19, 5.19). The scours trend parallel to the slope, in places exposing the topsets of clinofolds within the NW trending lens (e.g. Figure 5.19c), locally eroding the margins of the lens and leaving an erosional remnant (e.g. Figures 5.19a, e). Time-structure maps of the T20 surface show well-developed lineations that correspond to erosionally truncated reflections within the lens or the sharp margins of the scours (Figures 5.18a). Amplitude extractions at the T20 surface show a similar NW trend (Figure 5.18c).

Other than one isolated, very small (2 km²) sub-circular mound, deposits on the slope and basin floor adjacent to the NW trending lens formed low-angle lenses with similar long-axis orientations as the elongated deposit described above (e.g. Figure 5.16). These features are interpreted to have been strongly influenced by shelf currents that

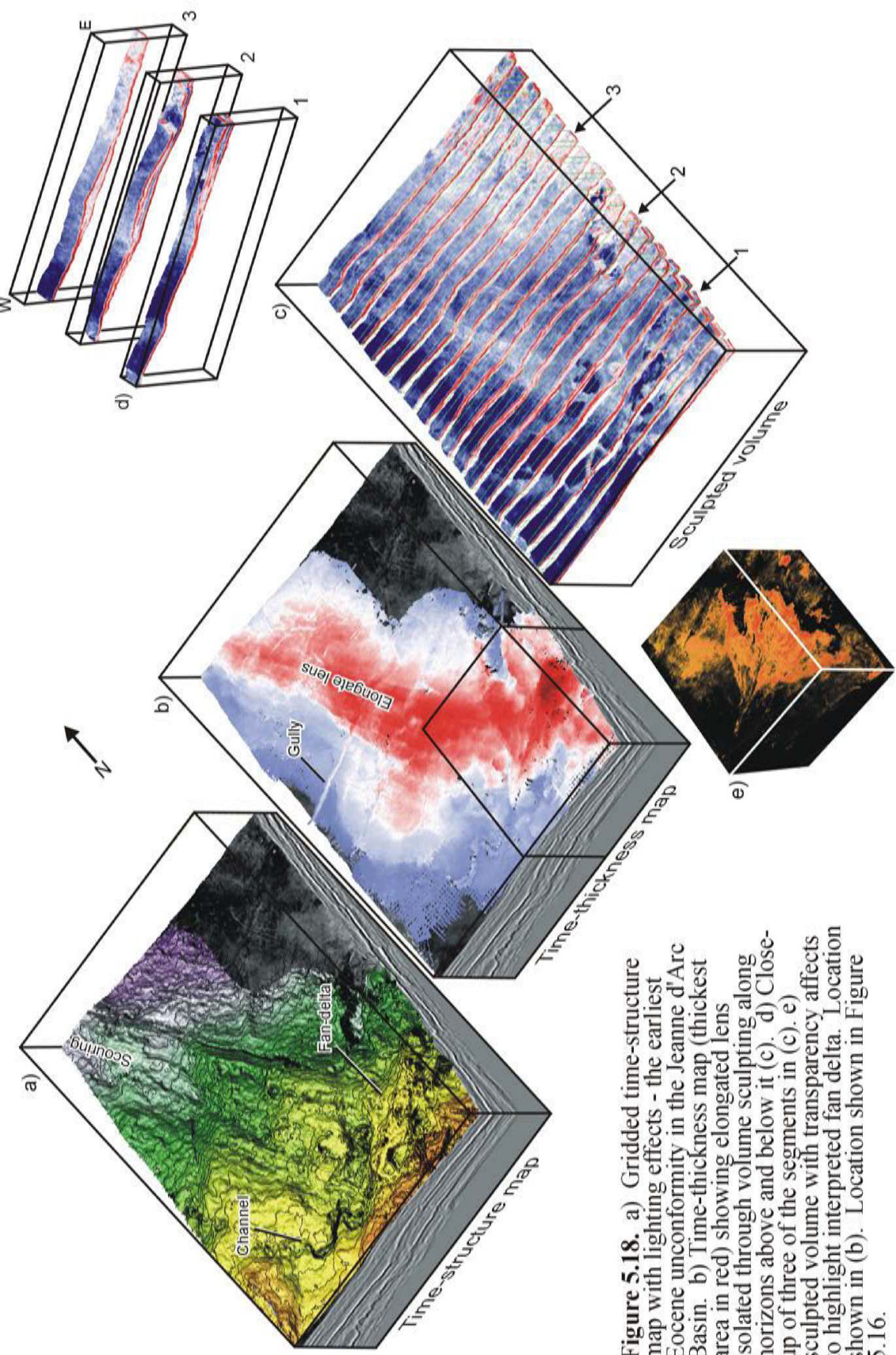


Figure 5.18. a) Gridded time-structure map with lighting effects - the earliest Eocene unconformity in the Jeanne d'Arc Basin. b) Time-thickness map (thickest area in red) showing elongated lens isolated through volume sculpting along horizons above and below it (c). d) Close-up of three of the segments in (c). e) Sculpted volume with transparency affects to highlight interpreted fan delta. Location shown in (b). Location shown in Figure 5.16.

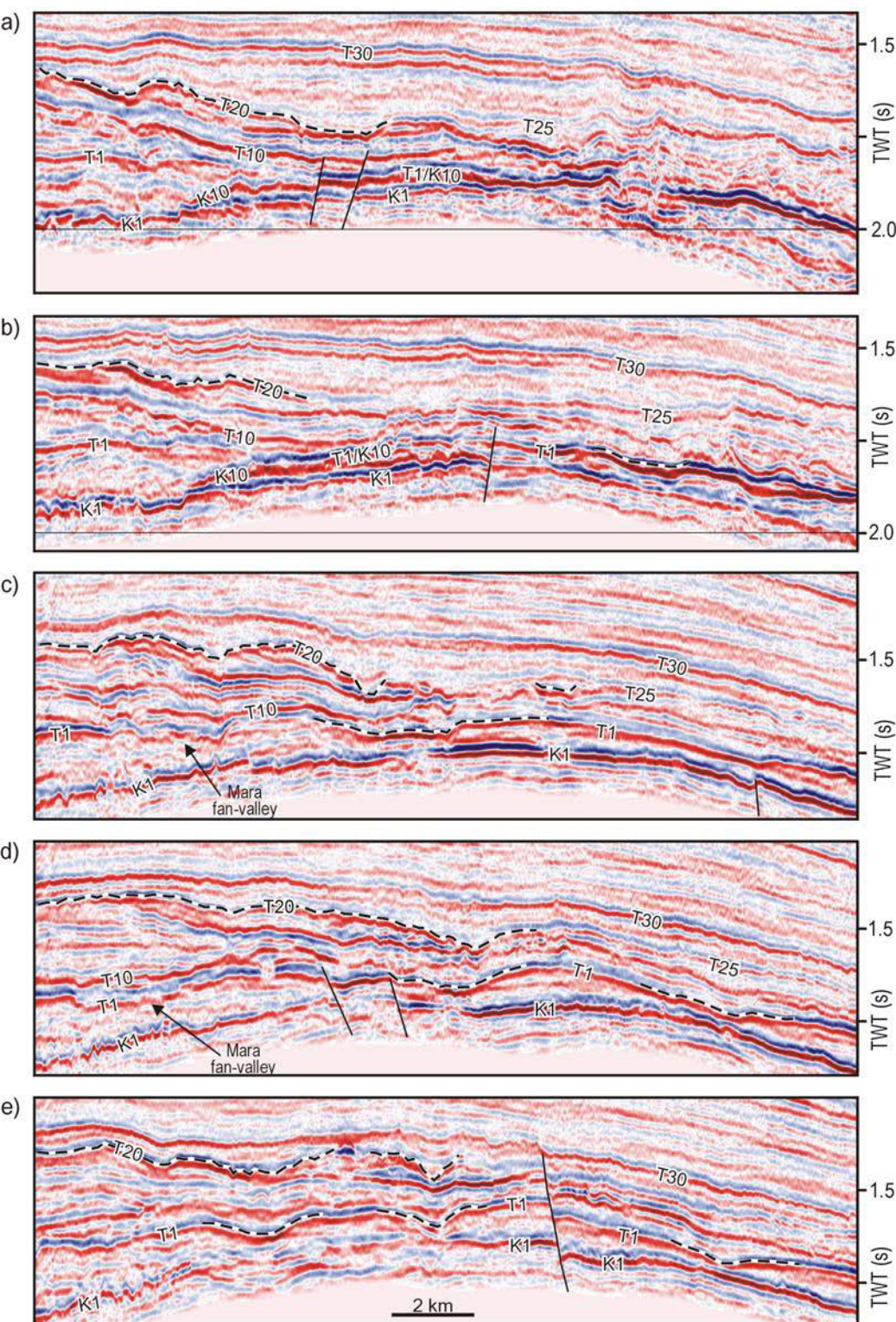


Figure 5.19. Series of 3-D seismic-reflection profiles showing general uparching along the axis of the basin of the occurrence of prominent scours at the T1 and T20 seismic markers (dashed line). The scours trend north, parallel to the axis of the basin, and are interpreted to form from ocean currents. Scouring from ocean currents appears to have been most prevalent at the base (T1) and top (T20) of the study interval. See Figure 5.16 for location.

widely scoured the region and influence sediment dispersal patterns in the early Ypresian, resulting in the formation of elongated deposits.

Fan delta

In Figure 5.18e, the interval between the T15 and T20 markers has been isolated by removing the 3-D seismic data above and below these surfaces. Transparency added to this interval highlights its fan-shaped geometry. The lens-shaped deposit widens from less than 1 km to greater than 5 km over a distance of 6 km. It covers an area of 18 km² (Figure 5.16). The internal braided character of this feature is also evident, suggesting that this feature is a braided depositional lobe. A single narrow V-shaped feeder channel leads into the deposit from the west. The feeder channel is 7 km long, is erosive and has a sinuosity of 1.4. The position of this deposit on the upper slope, adjacent to the T15 shelf-break, suggest that it is a delta or a subaqueous fan-delta, and not a submarine fan.

5.4 Insight from modern fans off the eastern margin of Corsica

Several small, sand-prone submarine fans are located off the eastern margin of Corsica (Stanley et al., 1980; Bellaiche et al., 1994; Gervais et al., in press). Sand body dimensions, stacking architecture, and distribution were studied in detail and used to enhance interpretations in the JDB. The fans off Eastern Corsica, therefore, are used as modern analogues for early Paleogene submarine fans in the JDB. An ideal modern analogue is one that has a similar architectural style (configuration of architectural elements) as the ancient system, has elements that are dimensionally and lithologically similar, and has undergone a similar long-term and short-term depositional history. Finally, there must be some advantage gained by using the modern analogue, for example improved resolution. Modern analogues that fit all of these criteria rarely exist, but insight can still be gained from systems that fit some of these criteria.

Although the hinterland of East Corsica is probably more mountainous than the Bonavista Platform (west of the JDB) was in the Danian, and long-term sedimentation rates are higher than they were in the JDB (> 20 cm per 1000 years over the last 5 m.y. - Stanley et al., 1980), the similarity in basin size and structure, water depths, sediment grade, and dimensions of submarine fan systems (see Figure 5.2b), suggests that the fans

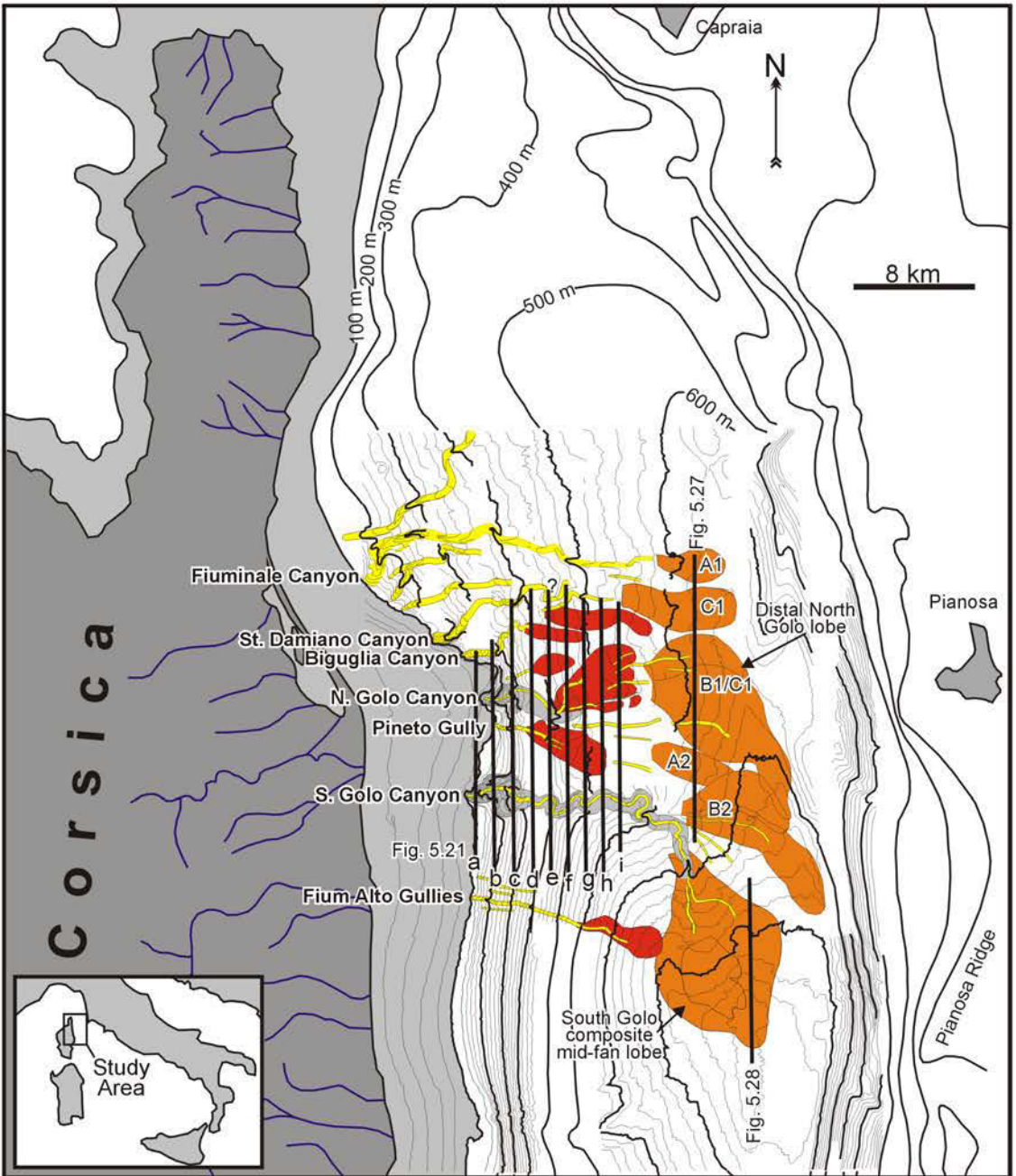


Figure 5.20. Basemap showing submarine fans mapped from Hunttec DTS profiles off Eastern Corsica. Figure locations indicated. Orange = channel-termination lobes (CTLs); Red = proximal-inefficient lobes (PILs); Yellow = channels or gullies. Isobath contours are from a combination of Stanley et al. (1980), Bellaiche et al. (1994), and Pichevin (2000)

off Eastern Corsica are appropriate geometric analogues for the early Paleogene fans in the JDB. Ultra-high resolution Hunttec DTS profiles from the Eastern Corsica fans provide bed-scale details about the dimensions, geometry, and distribution of channels and lobes, and hence provide significantly improved definition of architectural elements than is possible in the JDB.

5.4.1 Regional setting

The island of Corsica, with a maximum topographic relief of 2700 m, is located in the western Mediterranean Sea, just west of Italy (Figure 5.20). Its eastern margin consists of several small fluvial systems that drain its rugged topography and transport sediment towards a continental shelf that varies in width from 5 km to 25 km (Bellaiche et al. 1994). The study area is located off the northeastern margin of Corsica, where the shelf width ranges from 6 km in the south (near the Fium Alto fan - discussed later) to a maximum of 10 km directly outboard the Golo River, to less than 5 km wide further north still (Figure 5.20). The Golo River is the largest river flanking the study area, and was the most important supplier of sediment during the Quaternary (Bellaiche et al., 1994).

The offshore region of Eastern Corsica is characterized by an elongate north-south depression (approximately 150 km long and 42.5 km wide) referred to by Stanley et al. (1980) as the Corsican Trough. The trough deepens and widens to the south-southwest where it reaches a maximum water depth of 900 m in a region termed the Golo Basin, an isolated 11 km wide and 22 km long depression defined approximately by the 850 m isobath (Stanley et al. 1980). The slope along the western margin of the Corsican Trough has a maximum gradient of about 3 degrees (Stanley et al., 1980; Bellaiche et al., 1994). The eastern limit of the Corsican Trough is the shelf-break of the wide Tuscany Shelf (on which the Islands of Capraia and Pianosa are located) and the Pianosa Ridge further south (Figure 5.20). The slope along the eastern margin is steeper (3.5 to 7.5 degrees) than the western margin (Stanley et al., 1980).

A series of small submarine fan systems developed on the western slope and floor of the Corsican Trough during the Pliocene and Quaternary (Stanley et al., 1980, Bellaiche et al., 1994). The submarine fans are connected to the slope by a network of

gullies and canyons that incise the shelf-break in about 120 m of water (Bellaiche et al., 1994).

5.4.2 *Data set*

A total of 1300 line kilometers of Hunttec deep-tow seismic-reflection (DTS) profiles, with a vertical resolution of about 0.5 m, were collected above fans along the eastern margin of Corsica in 1998. Seventeen strike lines, spaced every 1.3 km (roughly parallel to the slope), extend across the shelf, slope, and basin floor. Six dip lines were also available, with an average spacing of 10 km. The seismic-reflection profiles cover an area of about 1240 km². The Hunttec fish was towed at a depth of approximately 120 m with a firing rate ranging from 600 to 1050 ms and a survey speed of about 4 knots (+/- 0.5 knots) or 7.2 km/hour (Corfan 98 Cruise Report). Digital data were filtered to include frequencies between 900 to 7000 Hz, with analogue copies of profiles collected at a quarter-second sweep (250 ms). Tracklines were positioned using GPS, and are accurate to within 30 m. Digital segy files stored on tapes were extracted and corrected for delay offsets using a segy editor. Hunttec lines were then loaded into Geoquest IESX (seismic interpretation package - see Chapter 2).

Additional paper copies of sparker profiles collected over the same fan reaches as the Hunttec DTS profiles were extracted from a Ph.D. thesis by Gervais (2002). Sparker data provide deeper penetration (to about 200 m), but are lower in resolution (200 - 800 Hz - 2-3 m vertical resolution - Gervais et al., in press), and provide a less distinct acoustic response to changing lithology. These profiles were particularly useful for coverage over lobes that were thicker than the penetration of the Hunttec DTS data (about 50 m in sandy sections).

5.4.3 *General fan architecture*

Three fan systems were identified on the eastern margin of Corsica by Bellaiche et al. (1994). From north to south they were termed the Golo, Tavignavo, and Fiume Orbo fan systems. More recent studies on the Golo fan system identified several submarine fans that, from south to north, were named Fium Alto, South Golo, Pineto, North Golo, Biguglia, St. Damiano, and Fiuminale (Pichevain, 2000; Gervais, 2002 -

Figure 5.20). Fan architecture is highly variable over short distances along the margin and in proximal versus distal settings. A series of line drawings from Hunttec DTS profiles, roughly parallel to outer shelf and slope, illustrate the spatial variability of submarine fans along the margin (Figure 5.21a to i).

The outer shelf and upper slope are characterized by several progradational deltas and well-stratified, relatively continuous, mud-prone slope deposits (where Hunttec penetration is excellent - Figure 5.2c, d). Two canyons (North and South Golo - each generally less than 2.5 km wide) truncate outer shelf and slope deposits, and extend back onto the outer shelf. The canyons pass into leveed fan-valleys starting near profile f for South Golo and profile c for North Golo (Figure 5.20). Within the fan-valleys are channel deposits characterized by high-backscatter chaotic Hunttec facies, and lower amplitude, well stratified facies forming stepped depositional “terraces” (e.g. Figure 5.21e, f for South Golo, Figure 5.21 c, d for North Golo). They are interpreted to correspond to inner levees formed adjacent to under-fit and sinuous thalweg channels (see Pichevin, 2000 and Chapter 6 for a more detailed discussion).

In addition to canyons, the upper slope is cut by small V-shaped gullies (e.g. Fium Alto and Pineto gullies - Figures 5.20, 5.21c, d - Gervais et al., in press). Adjacent to the North Golo channel-levee system, several small sandy lobes were deposited at the mouths of these gullies (e.g. Pineto, Marana) or at the mouths of slightly larger erosive channels near the base-of-slope (e.g. recent North Golo and Biguglia lobes - Figure 5.21e, f, g). The most recent North Golo lobe was deposited above and adjacent to the North Golo channel-levee system, filling its remaining relief (Figure 5.23), and the Pineto lobe was deposited above its southern levee, pinching out abruptly down-slope (Figure 5.22 - see also Pichevin, 2000; Gervais, 2002). Erosive channels, like the St. Damiano and Fiuminale, locally eroded the small lobes (e.g. proximal Biguglia lobe, eroded by the St. Damiano channel - Figure 5.24), presumably as larger, more erosive gravity flows transported sediment to the middle fan. Some erosive channels are draped by hemipelagic mud, indicating an extended period of inactivity, whereas others appear to have been recently active, with little or no drape (e.g. the St. Damiano channel - Figure 5.24). In general, the dimensions of the proximal lobes diminish significantly by profile

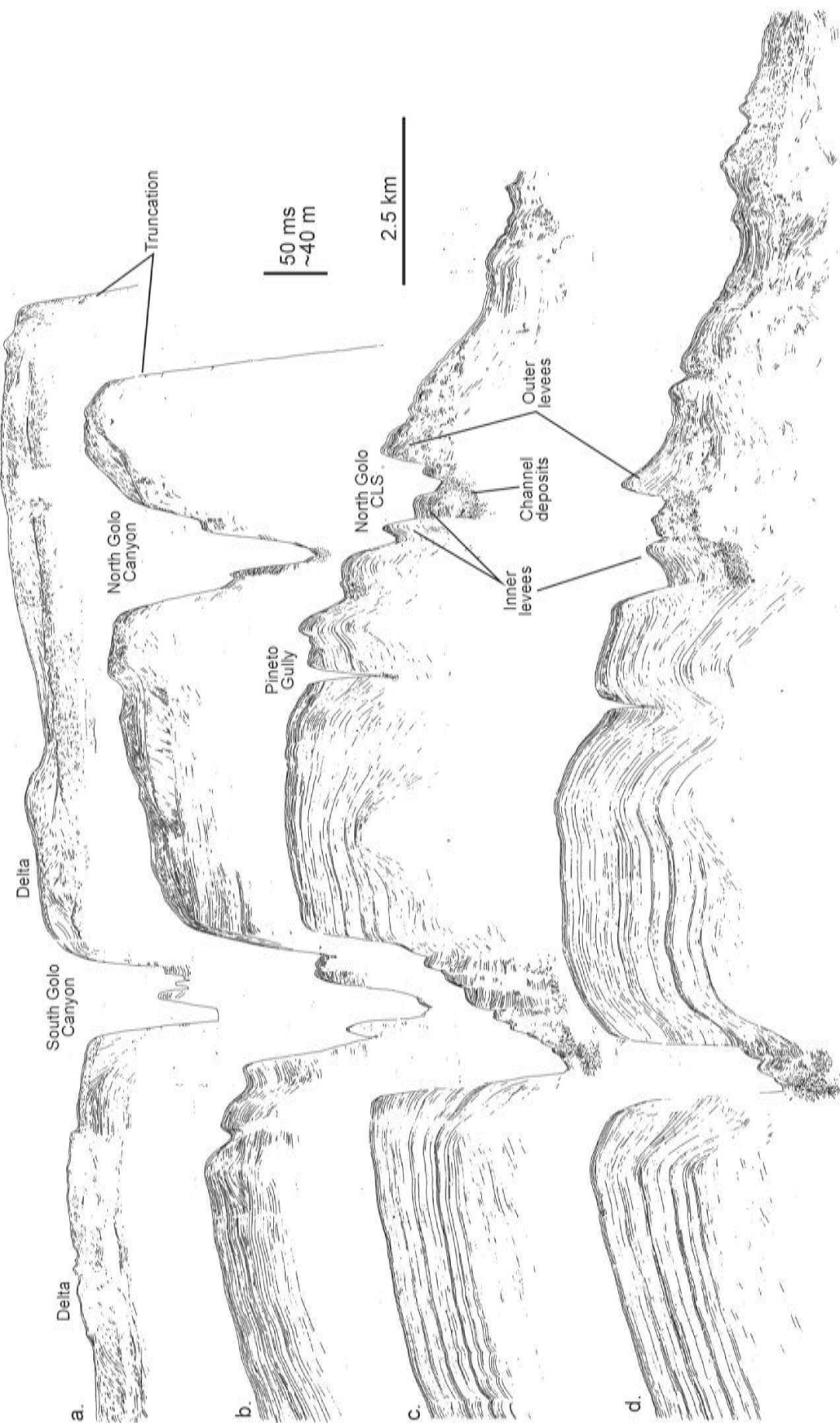


Figure 5.21. Series of line drawings (a to d) from Huntet DTS profiles across the outer shelf and slope, East Corsica. See Figure 5.20 for location and text for details. CLS = channel-levee system.

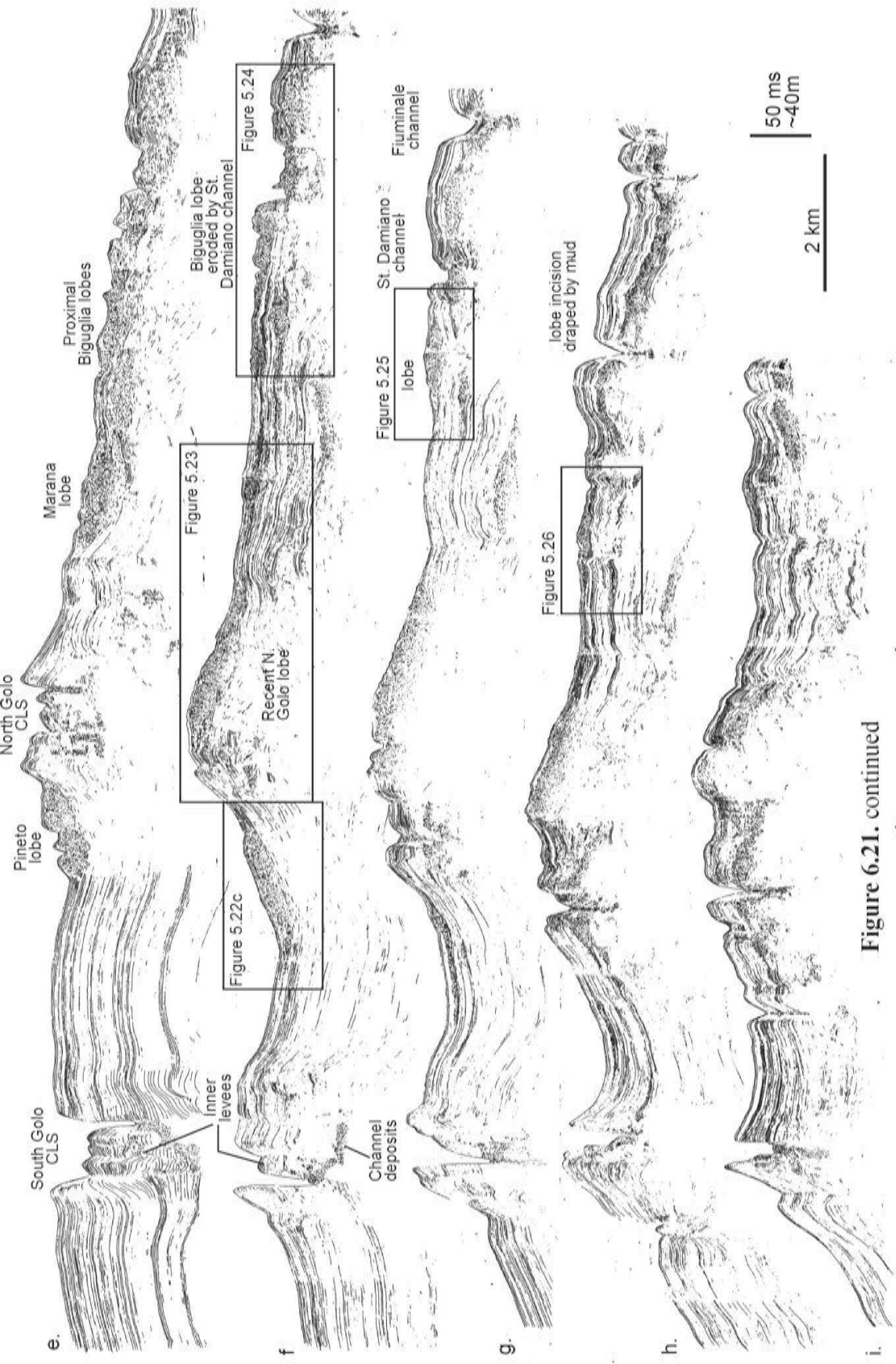


Figure 6.21. continued

i, near the transition from the upper fan to the middle fan (relative to the North and South Golo fans -compare Figures 5.24, 5.25, and 5.26).

At the termination of the North and South Golo channel-levee systems, and other narrower erosive channels further north, several large, stacked mid-fan lobes are recognized on the basin floor (Gervais, 2002; Gervais et al., in press) (Figures 5.27, 5.28). These large lobes, described in more detail below, pass distally, and to a lesser extent laterally, into lobe-fringe deposits characterized by continuous, mixed-amplitude seismic facies that eventually pass into acoustically transparent to poorly stratified deposits of the basin plain.

5.4.4 East Corsica lobes - potential mound forming elements?

Two end-member populations of lobes are recognized in the fans off East Corsica. The first are small lobes located in proximal settings on the slope or near the base-of-slope, and are fed by relatively ephemeral slope gullies or erosive channels that extend onto the proximal basin floor. These lobes are referred to as “**proximal-inefficient lobes**” (or **PILs** for short) in this study. The second end-member population of lobes are large mid-fan lobes deposited on the basin floor, and fed by well-developed fan-valleys (Gervais, 2002). These lobes are referred to as “**channel-termination lobes**” (or **CTLs** for short) in this study (following the terminology of Piper et al., 1999). It should be noted, however, that the term refers to the termination of the main feeder channel, and not necessarily the smaller-scale distributary channels that may extend onto, and erode, CTLs. Several intermediate lobes, that share some of the characteristics of both end-members are also recognized, particularly in the northern parts of the study area.

Proximal-inefficient lobes (PILs)

PILs are small, sub-circular to elongated deposits on the slope or near the base-of-slope, rarely extending more than 10 km into the basin (from the shelf-break). They commonly form at the termination of small, linear to curvi-linear slope incisions, or at the termination of erosive channels on the proximal basin floor. They reach a maximum.

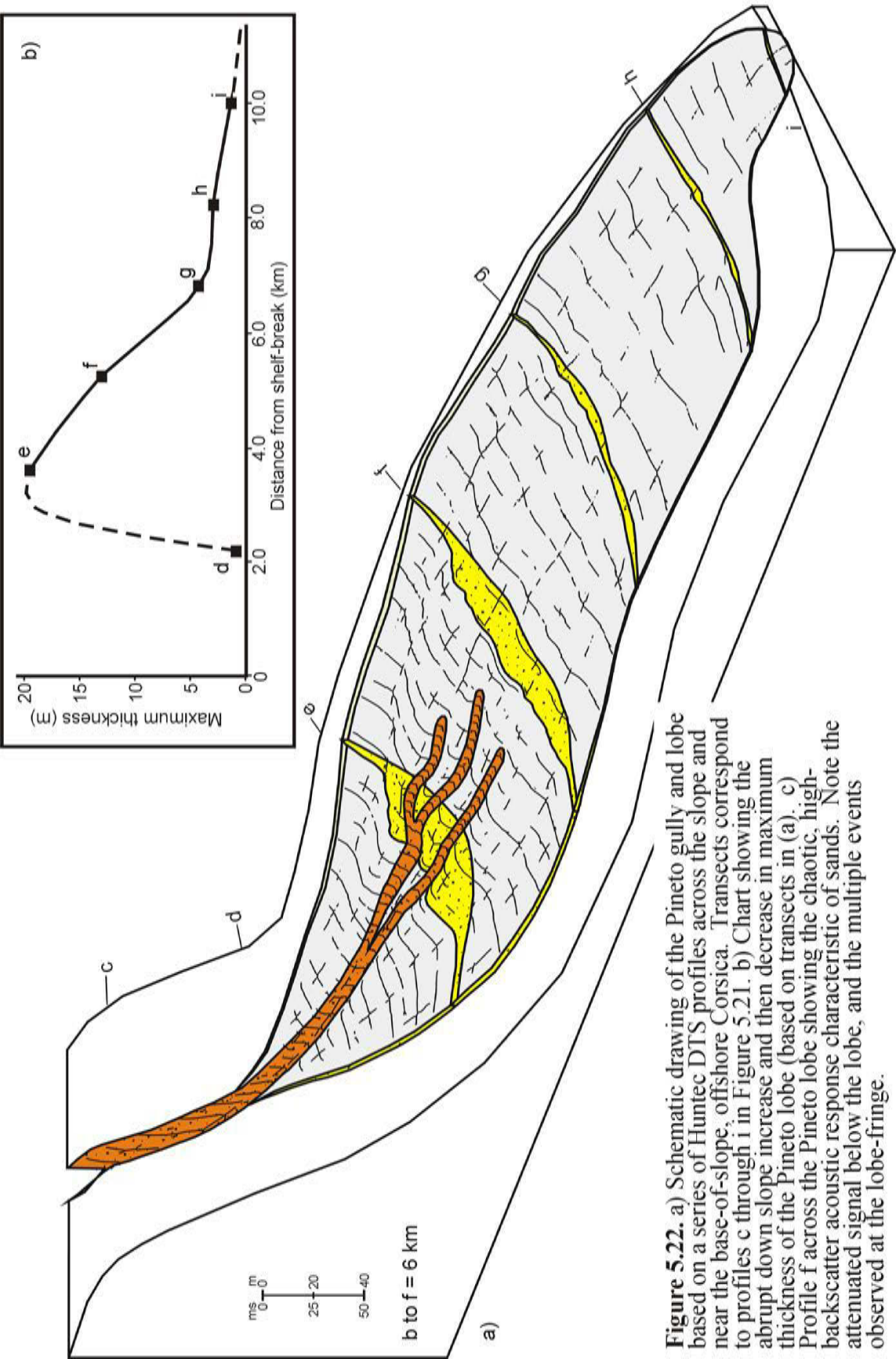


Figure 5.22. a) Schematic drawing of the Pineto gully and lobe based on a series of Hunttec DTS profiles across the slope and near the base-of-slope, offshore Corsica. Transsects correspond to profiles c through i in Figure 5.21. b) Chart showing the abrupt down slope increase and then decrease in maximum thickness of the Pineto lobe (based on transects in (a). c) Profile f across the Pineto lobe showing the chaotic, high-backscatter acoustic response characteristic of sands. Note the attenuated signal below the lobe, and the multiple events observed at the lobe-fringe.

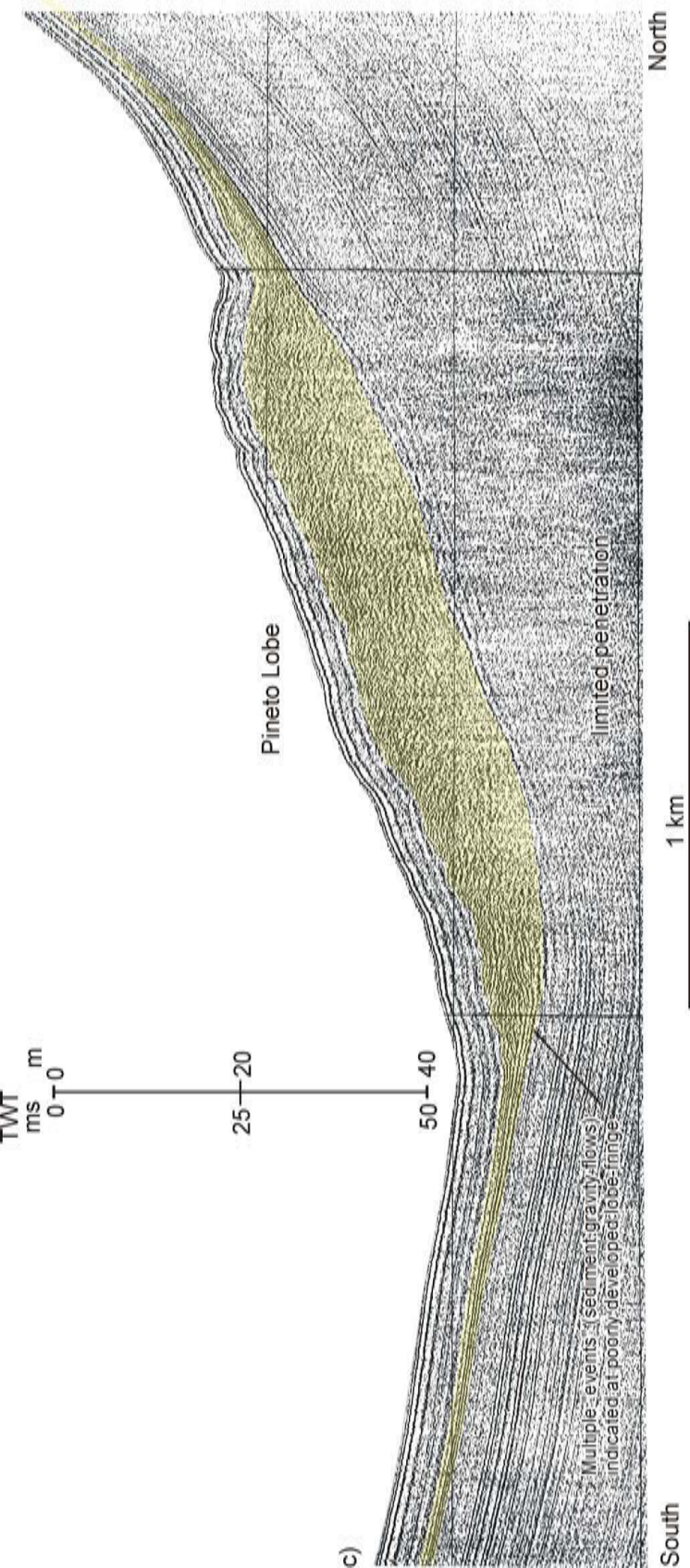


Figure 5.22 c) Continued (see previous page for caption)

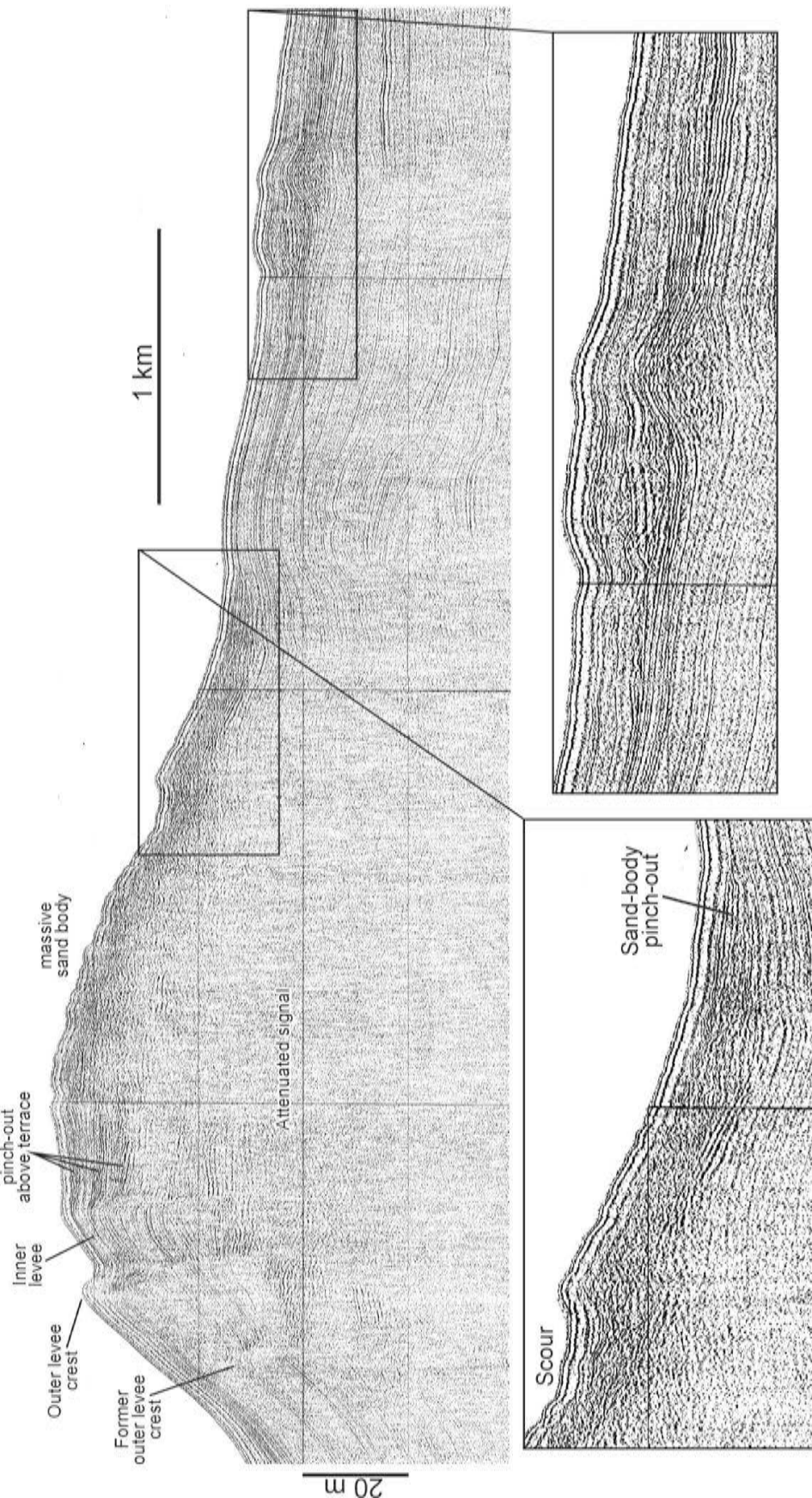


Figure 5.23. Huntect DTS profile across the proximal North Golo lobe that fills the last remaining relief of the North Golo channel-levee system. See Figure 5.21f for location.

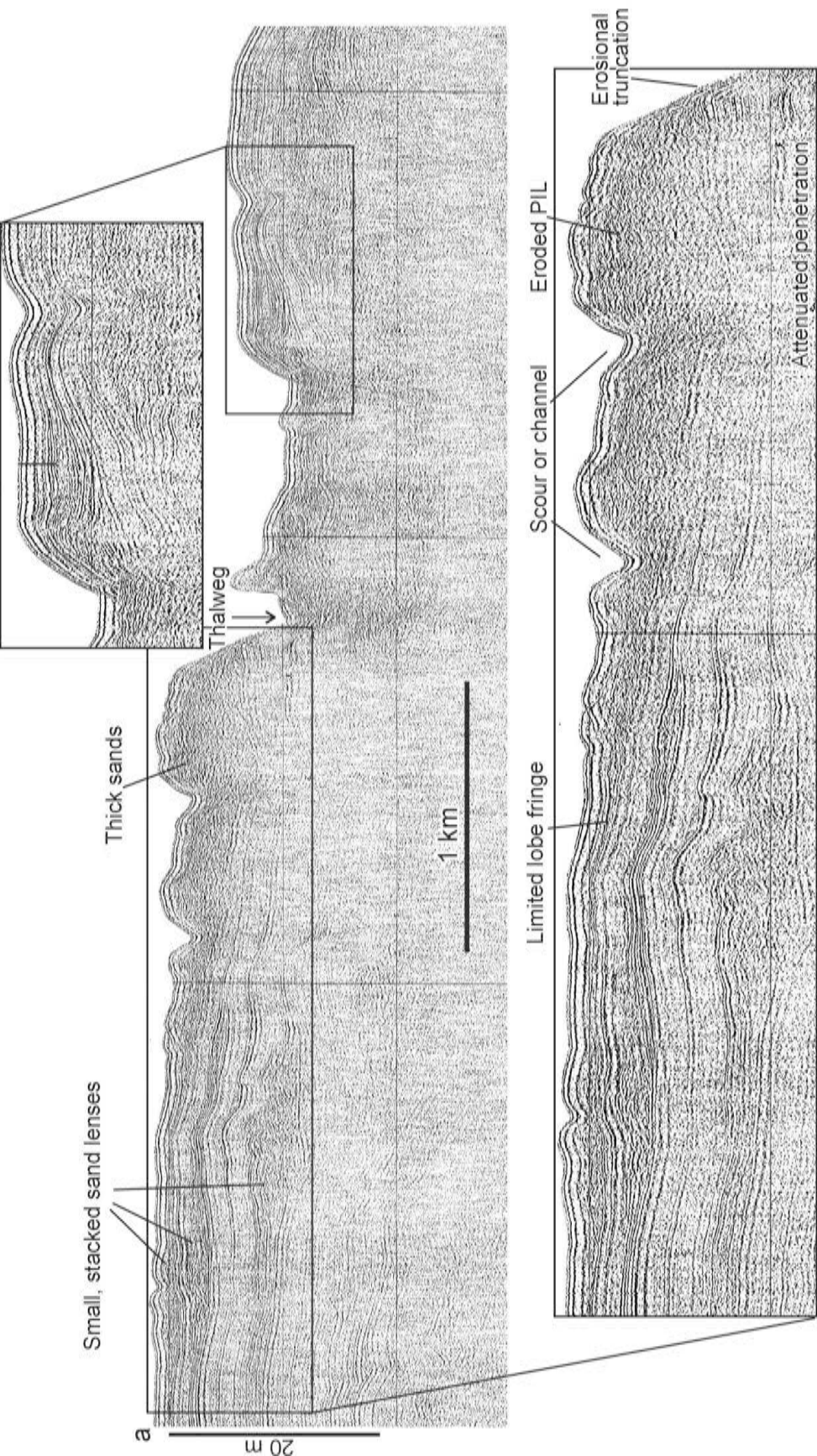


Figure 5.24. Huntect DTS profile across one of the proximal Biguglia lobes, eroded by the St. Damiano channel. See Figure 5.21 for location.

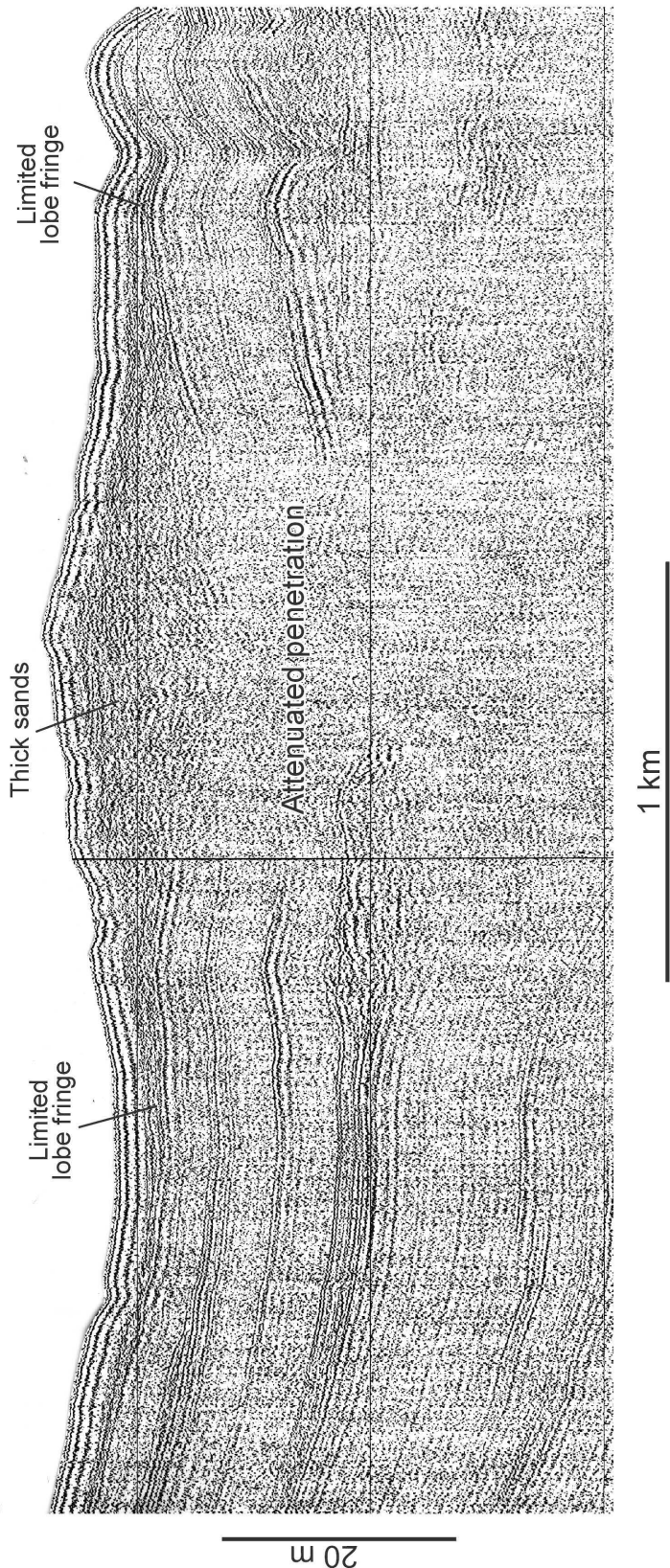


Figure 5.25. Huntec DTS profiles across Biguglia lobe, just updip from Figure 5.26. Note the chaotic high backscatter seismic facies and the attenuated signal below this sandy, proximal-inefficient lobe.

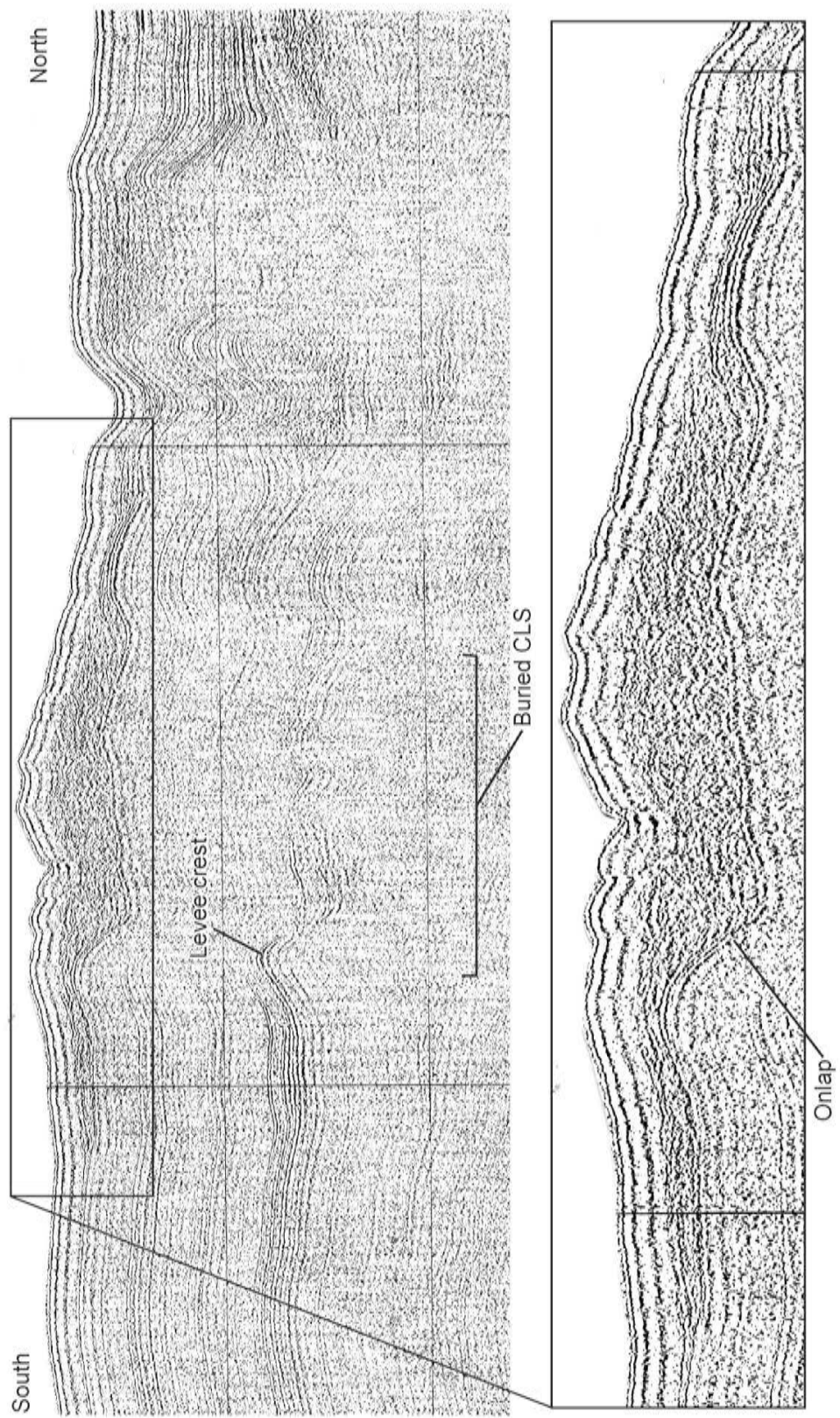


Figure 5.26. Huntec DTS profile across the distal end of the proximal Biguglia lobe. Note that sands were deposited within a depression, filling the remnant relief above an abandoned and draped channel. See Figure 5.21h for location. CLS = channel-levee system

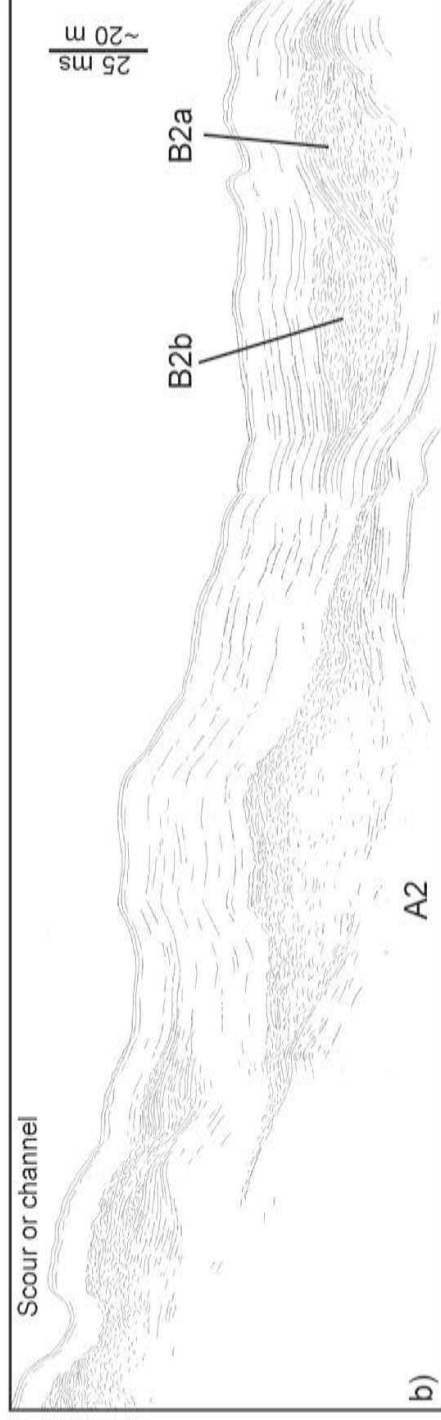
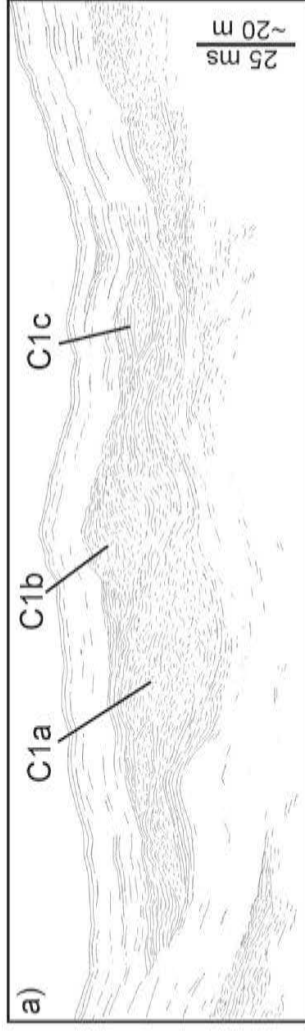
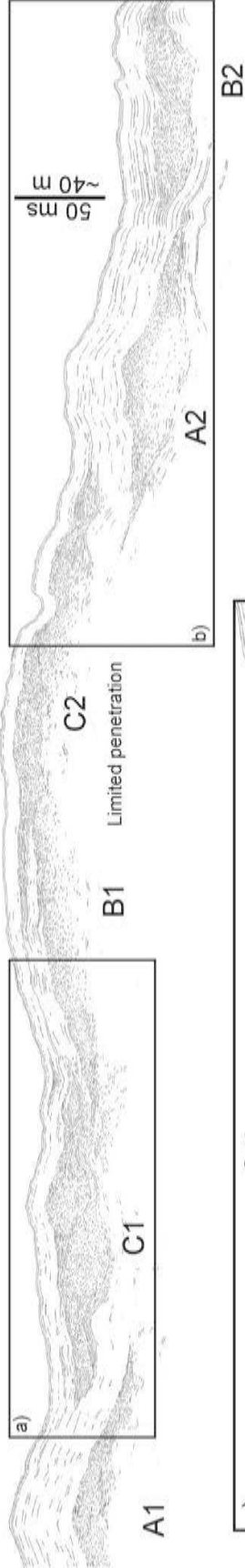


Figure 5.27. Line drawing from a Huntect DTS profile across several stacked channel-termination lobes (CTLs) on the floor of the Corsican trough. Figure and lobe location shown on Figure 5.20. a) and b) are close-up views.

Figure 5.28. a) Line drawing from a Hunttec DTS profile down the length axis of the South Golo composite mid-fan lobe. Note that the profile does not cross its thickest part. The drawing illustrates the transition from chaotic-stratified acoustic facies (right) to well stratified, mixed-amplitude facies (middle region), and eventually to low amplitude, poorly stratified facies (far left). This transition corresponds to the change from massive sands deposited near the channel-mouth, to interbedded mud and sand deposits of the lobe-fringe, to fine-grained hemipelagic deposits of the basin plain. b) and c) show progressive close-ups views. Location shown on Figure 5.20.

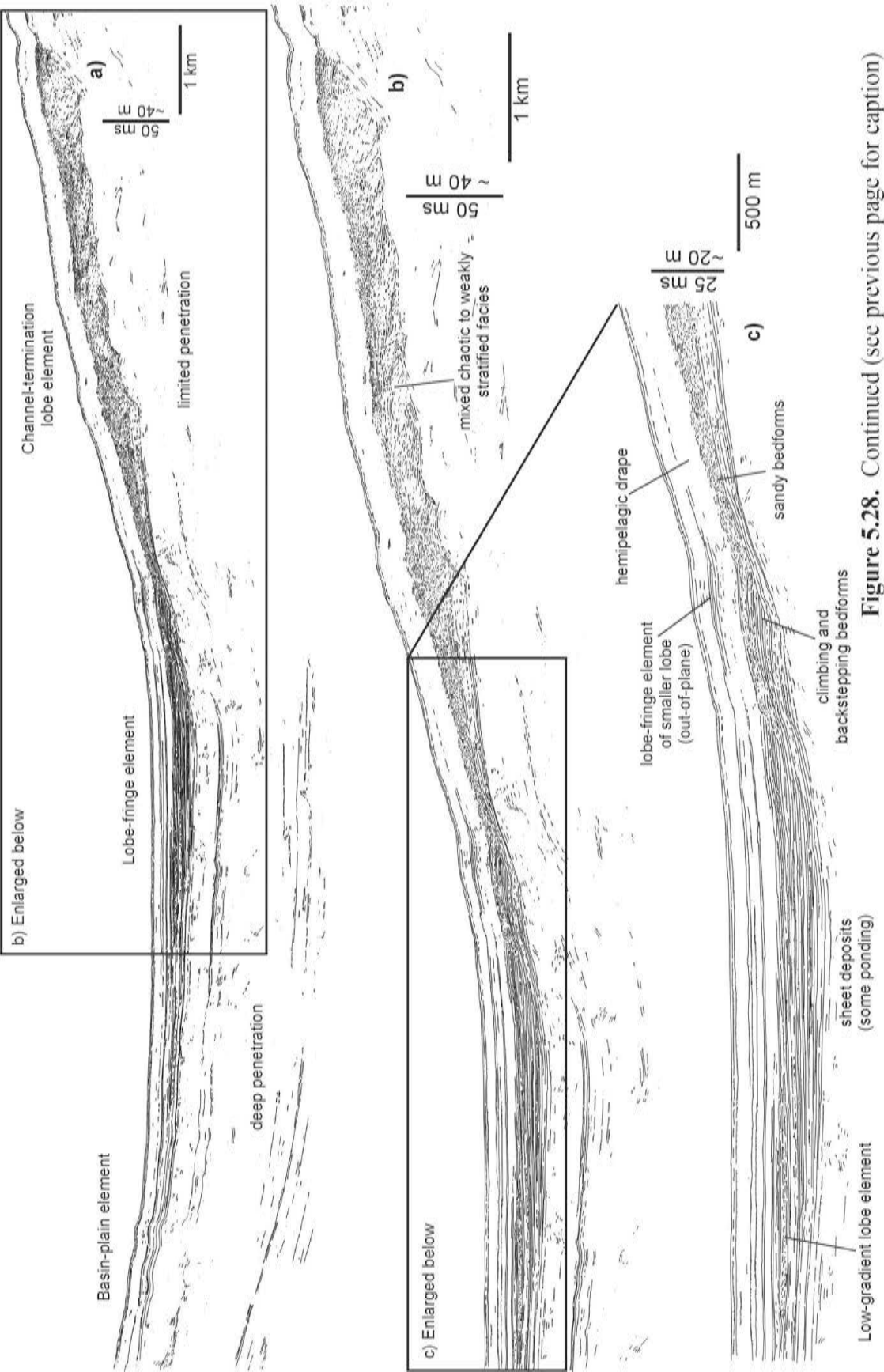


Figure 5.28. Continued (see previous page for caption)

thickness between 9 and 20 m near the mouth of the erosional conduit, typically between 3 and 6 km from the shelf-break, and decreasing abruptly in thickness down-slope (i.e. they form wedges on dip profiles). They are characterized by chaotic, high-backscatter Huntect seismic facies, an acoustic response that is typical of massive sands (Piper et al., 1999). The abrupt attenuation of the acoustic pulse below PILs is additional evidence for their sandy character (e.g. Figures 5.22c, 5.23, 5.24, 5.25).

The Pineto lobe is considered the type example for PILs off East Corsica (Figures 5.22). It covers an area of about 7 km², with its thickest parts (> 5 m) covering an area of about 4.5 km². It reaches a maximum thickness of 20 m near the mouth of the Pineto gully, 2.5 km from the shelf-break, abruptly decreasing in thickness down-slope (Figure 5.22b). Though the Pineto lobe is roughly 8 km long, its rapidly decreasing thickness results in a wedge-shaped deposit (along dip - Figure 5.22b), with very thin accumulations beyond the first 4 km from the gully mouth. At least two or three separate flows can be identified within the lobe-fringe, but cannot be distinguished in the main body of the lobe, where coarse-grained deposits are inferred to be amalgamated (Figure 5.22c).

Limited development of lobe-fringe deposits, and no equivalent basin plain deposits, and a lack of levees flanking the gully, imply that the Pineto lobe was supplied by a clean, sandy sediment source, lacking fines. The lack of levees on the Pineto gully also suggests that flows were fairly thin (less than 30 m thick, the depth of the gully), and the rapid sediment thinning rate with distance implies abrupt deposition from fairly high-concentration flows (i.e. sand transport in sediment gravity flows was inefficient). The Pineto lobe, and other PILs, are therefore inferred to develop from the failure of sandy mouth bars near the shelf-break or the failure of well-sorting sands transported by shelf-currents (see also Normark and Piper, 1991; Normark et al., 1998; Piper et al., 1999; Gervais et al., in press). PILs can also be deposited from relatively clean sandy flows triggered during flushing of the canyon head (a process described for the Scripps Canyon by Mastbergen and Van den Berg, 2003). The proximal North Golo lobe, deposited above and adjacent to the North Golo channel-levee system, may have formed from such a process (Figure 5.23). Increased confinement during passage through channel-levee systems in some cases results in longer transport distances than would be possible outside

a confining channel. Hyperpycnal flows are not considered to be an important source of sediment for PILs because such flows are commonly well-mixed, resulting in longer transport distances (i.e. more efficient flows) and thicker flows. Hyperpycnal flows are also inferred to deposit muddy levees that flank the main feeder channels (Piper et al., 1999), and/or deposit lobes with well-developed lobe-fringe deposits (in cases where the muddy dilute suspension cloud is not strongly segregated from the high concentration, coarser-grained bedload by overbank processes). Neither of these features are observed on most of the proximal lobes. Therefore, PILs may be most common during times of less frequent hyperpycnal flows or in areas with limited direct linkage to fluvial systems (e.g. systems fed by littoral drift cells, or times of higher sea level)

Additional examples of PILs include the Marana lobe and several proximal Biguglia lobes in the northern study area (Figures 5.20, 5.21e-g, 5.24, 5.25), and the small Dume fan identified by Normark et al. (1998) and Piper et al. (1999) along the margin of the Santa Monica Basin, offshore California. Dume fan consists of several stacked rapidly thinning wedges of high-backscatter, chaotic Huntect seismic facies, interpreted as massive sands and referred to as “high-gradient lobes” by Piper et al. (1999). The massive sands were pre-sorted on the shelf by littoral drift cells, prior to triggering of sediment gravity flows, and are not believed to have originated from direct fluvial input (Normark et al., 1998; Piper et al., 1999).

Channel-termination lobes (CTLs)

At the other end of the spectrum are CTLs located at the mouths of major, relatively stable and commonly leveed, feeder channels, in a mid-fan position. Several compensationally stacked (offset stacked) CTLs are recognized on the floor of the Corsican Trough, at the mouths of the North and South Golo channel-levee systems, as well as smaller, more erosive channels further north (Figure 5.20, 5.27). These mid-fan lobes are much larger than PILs, are deposited in more distal settings, and are typically characterized by chaotic, high-backscatter acoustic facies that pass distally, and to a lesser extent laterally, into stratified-chaotic to well-stratified, continuous, mixed-amplitude seismic facies.

Like the more proximal lobes, the chaotic facies are interpreted as thick sand-prone intervals associated with rapid deposition at the termination of channels. Scours or smaller-scale channels are sometimes recognized within the chaotic facies (e.g. Figure 5.27, lobes C1 and C2 - see also Gervais, 2002). The stratified-chaotic facies are common adjacent to the thickest parts of lobes, and are interpreted as proximal lobe-fringe deposits. The continuous, well-stratified, mixed-amplitude facies are best developed at the distal ends of major lobes, interpreted as distal lobe-fringe deposits consisting of interbedded muds and graded turbidities. The distal lobe-fringe eventually passes into low-amplitude, mud-prone deposits of the basin plain (e.g. Figure 5.27). Some ponding of distal lobe-fringe deposits is observed at the distal end of the South Golo composite mid-fan lobe (mapped extensively by Gervais, 2002). In terms of area, lobe-fringe deposits commonly make up about 40 % of the total lobe area. For example, the South Golo composite mid-fan lobe covers an area of about 90 km², including the lobe-fringe. In contrast, the chaotic to stratified-chaotic high-backscatter facies cover an area of about 55 km².

Individual CTLs in the Corsican Trough cover areas ranging from 10 to 30 km² and are commonly greater than 30 m thick, to as much as 60 m thick. They commonly decrease in thickness abruptly perpendicular to their length-axis. For example, CTL A2 (Figure 5.27) decreases from 28 m thick at its crest, to less than 5 m thick at its flank, over a distance of 1.5 km (with an original depositional relief of about 1 degree). Compaction of finer-grained lobe-fringe deposits in a deeply buried system would enhance this affect (perhaps increasing the depositional dip to about 1.5 to 2.0 degrees depending on the abruptness of the shale transition). The proximal to distal decrease in thickness is commonly less abrupt. For example, a profile down the easternmost lobe of the South Golo composite mid-fan lobe (Figure 5.28), decreases from 25 m thick to less than 5 m thick over a distance of about 6 km. The profile in Figure 5.28 does not cross the thickest part of the easternmost South Golo lobe. Using lower frequency sparker data, Gervais (2002) showed this lobe to have a maximum thickness of about 50 m near the mouth of the South Golo channel-levee system.

The relative age of individual CTLs can be determined by examining the thickness of hemi-pelagic deposits above them. For example, in Figure 5.27 CTLs A1

and A2 are draped by about 25 m of low-amplitude, stratified seismic facies, interpreted as muddy drape. Lobes B1 and B2 are younger, covered by about 14 m of drape, and C1 and C2 are younger still, draped by less than 8 m of mud drape. Stacking of several CTLs within a confined area may produce a composite mid-fan lobe. Lobe B2 actually consists of two lobes that diverge downdip (labeled B2a and B2b), and lobe C1 can be further subdivided in lobes C1a, C1b, and C1c (Figure 5.27). Similarly, the South Golo lobe described in detail by Gervais (2002) and Gervais et al. (in press), is a composite mid-fan lobe consisting of several smaller, more elongated, compensationally stacked CTLs (as many as 6 according to Gervais, 2002) that produce an overall radial “lobe” geometry. In the case of the South Golo lobe, confinement within the Golo Basin (a bathymetric depression defined by the 850 m isobath), combined with a relatively stable channel-mouth for an extended period of time, led to both vertical and lateral stacking of successive CTLs (Gervais et al., in press).

The transition from chaotic, high-backscatter to well-stratified lobe-fringe deposits implies that many flows had a mixed-load, with the coarser fraction deposited near the mouth of the main feeder channel, and finer-grained deposits (remaining after overbank processes removed some fines and deposited them on levees) continuing towards the lobe-fringe and into the basin plain. Flows with a mixed composition can originate either from direct river input during floods (hyperpycnal flows - Mulder and Syvitski, 1995) or could be generated by canyon head slumps of mixed mud and sand facies (triggered by seismicity, canyon head flushing, rip-currents, etc. - Normark and Piper, 1991).

5.5 Discussion

5.5.1 Origin of mounds in the Jeanne d'Arc Basin

Study of the East Corsica fans demonstrates a range of erosional and erosional-depositional conduits, and a range in the dimensions and distribution of lobes at their termination. At least three elements with dimensions sufficient to generate mounds after compaction and burial are recognized in submarine fans off East Corsica: a) channel-termination lobes (CTLs) deposited at the mouths of major fan-valleys; b) proximal-inefficient lobes (PILs) deposited at the termination of relatively ephemeral slope gullies

or small erosive channels on the proximal basin floor; and c) leveed fan-valleys or sand-filled channels incised into muddy slope deposits. Study of these elements provides insight into the origin of mounds in the JDB.

Both the original depositional geometry of fan elements and post-depositional processes like compaction appear to be important for generating mounded seismic facies. Compaction can significantly modify the original depositional geometry of submarine fan elements. For example, coarse-grained channel deposits flanked by muddy levees, or incised into muddy slope facies, may become inverted after burial in response to differential compaction between coarse-grained and fine-grained sediment. The result is a channel expressed as a positive relief convex-upward linear mound (Veeken, 1997). Similarly, compaction of finer-grained lobe-fringe deposits can enhance the relief of lobes at the termination of major feeder channels.

Compacted channel-termination lobes

The location of the Avondale mounds at the termination of the Mara fan-valley, on the distal basin floor (Figure 5.12), suggests that they may consist of a series of stacked CTLs. Looking at Figure 5.27, it is not hard to see how compaction and burial of stacked CTLs off East Corsica could produce a complex arrangement of mounded seismic facies similar to that observed in the JDB (e.g. Figure 5.5, profiles F to L). In some locations, CTLs off East Corsica can stack both laterally and vertically, particularly where there is some confinement from adjacent basement highs. In the JDB, lateral confinement was provided by the Central Ridge to the east and the Botwood High to the west. Similar to the Avondale mounds, the Ypresian Frigg field in the Viking Graben in the North Sea contains elongated to sub-circular mounds interpreted as channeled lobes by McGovney and Radovich (1985). In addition, the late Thanetian Balder field south of the Frigg fan consists of mounded deposits that were interpreted by Sarg and Skjold (1982) as prograded and channelized lobes consisting of 20 to 60 m thick massive sands deposited downfan from a leveed valley. Therefore, CTLs off East Corsica may be good analogues for some fans in both the JDB and the North Sea.

In addition to similarities in distribution (i.e. on the basin floor, at the termination of major feeder channels), scaled comparisons between individual Avondale mounds in

the JDB and CTLs from East Corsica show similarities in dimensions. The North Ben Nevis P-93 and M-61 wells through the proximal Avondale mounds penetrated 61 and 55 m of continuous sandstone, respectively, suggesting a compacted thickness for mounds on the order of 50 to 60 m. The flanks of individual Avondale mounds typically have a final maximum compacted gradient that ranges from 1.5 to 3.0 degrees. In comparison, CTLs off East Corsica are typically 30 m to 50 m thick at their apex (without compaction, therefore slightly thinner than mounds in the JDB), near the mouth of the main feeder channel, thinning to less than 5 m at the lobe-fringe over a distance of about 1.5 km to 2 km. In this case, the lobe flanks have an original depositional dip of about 1.0 to 1.5 degrees. With increased burial depths of CTLs off East Corsica, differential compaction between thick sand at the lobe-apex and thinner sand, silt, and mud in the lobe-fringe should result in an increase in the gradient of the lobe flank. The exact nature of the change in lobe geometry depends largely on the lithological transition from the lobe-apex to the lobe-fringe over distances of 1 to 2 km. Assuming that the finer-grained lobe-fringe shows a 60% reduction in thickness due to compaction, and the lobe-apex shows only a 20% reduction in thickness, the flanks of individual compacted CTLs off East Corsica could have dips that approach 1.5 to 2.0 degrees, comparable to at least some of the mounds in the JDB.

With compaction, CTLs off East Corsica are prone to generate elongated mounds (i.e. sands decrease in thickness more abruptly perpendicular to the lobe length-axis than they do along the length-axis), with the thickest, most sand-prone parts of most CTLs ranging in width from 2 to 5 km. Many of the mounds in the JDB are also somewhat elongated, but range from broad features (2 to 5 km across) to narrow elongated features (less than 2 km across) that appear to be too narrow to be CTLs. Instead, some of the mounds are interpreted as compaction-inverted channels (see below), stacked together with CTLs (shown in Figure 5.12).

Local erosion of proximal lobes by channels that fed more distal lobes is recognized in areas covered by 3-D seismic data in the JDB. Similarly, erosion of more proximal lobes by channels that supplied sediment to more distal lobes is recognized off East Corsica (e.g. Figure 5.24), substantially increasing the abruptness with which lobes “pinch out” in proximal settings. In more distal settings, narrow elongated mounds have

little erosion at their base and may represent more depositional channels. The combination of compacted CTLs stacked together with compaction-inverted channels, and local erosion between lobes, is inferred to be responsible for the rather complex mounded seismic facies shown on profiles G through L in Figure 5.5.

Compacted proximal-inefficient lobes

In contrast to the Avondale mounds, most of the South Mara mounds are smaller and more proximal, or narrow and elongated. The smaller, isolated pod-shaped mounds in the JDB resemble the isolated proximal-inefficient lobes (PILs) off East Corsica. Scaled comparison between the East Nautilus mound and the Pineto lobe, for example, show remarkable similarities, including the length of the gully (about 2.5 km), aerial extent of the lobe and mound, and their physiographic location on the lower slope (e.g. Figures 5.15, 5.20, 5.22). The East Nautilus mound, therefore, is interpreted as a deeply buried PIL. Other South Mara mounds, like mounds 3, 5a and 5b (Figure 5.16) may represent hybrids between the PIL and CTL end-members.

PILs like the Pineto lobe show rather abrupt pinchout both perpendicular to the lobe length-axis and parallel to it, decreasing from 20 m thick to less than 5 m thick over a down-slope distance of about 2 km (see Figure 5.22b) and a cross-slope distance of less than 1 km. In contrast to CTLs, however, compaction of PILs like the Pineto lobe is unlikely to increase the gradient between the lobe-apex and the lobe-flank because lobe-fringe deposits are poorly developed. However, the relief of the lobe should increase relative to the surrounding mud-prone slope deposits due to differential compaction. Such lobes encased in muddy slope deposits should be detectable using conventional industry seismic reflection data, though limitations in industry seismic resolution may prevent determining their thickness without well data.

Compaction-inverted channels

As discussed above, some mounds appear to be too narrow and long to represent lobes. Such elements are recognized within the Avondale mounds, but are most easily mapped within the South Mara mounds, where 3-D seismic coverage is available. The length to width ratio of South Mara mounds 1, 2, and 4 is greater than 10 (as compared to

3 to 5 for most lobes off East Corsica and other mounds in the JDB). Combined with 3-D seismic evidence for nested channels within the elongated mounds (as discussed in an earlier section), they are interpreted as compaction-inverted channels.

Compaction-inversion of channels is accomplished in one of two ways. The first involves differential compaction between muddy levees (more prone to compact) and sandy channel deposits (less prone to compact). This scenario is inferred to be more important for channels that are predominantly depositional, with little or no erosion at their base (as appears to be the case for most of the elongated South Mara mounds). The second involves differential compaction between muddy slope deposits and sandy channel deposits that fill an erosional incision. The relief of the sandy channel deposits increases only in a relative sense, compared to the more compactable surrounding shale. This scenario is restricted to channels with significant erosion at their base. Some channels may be flanked by levees and also have an erosion base (e.g. see Chapter 6), in which case both methods of compaction-inversion may be important.

Similar to some of the South Mara mounds, elongated, finger-like mounds are also recognized in the North Sea. For example, the Alba field is characterized by a 9 km long, elongate mound consisting of uniform sands believed to have been deposited by high-density turbidity currents that filled a linear, erosive channel (Newton and Flanagan, 1993 - see Figure 5.2b for scaled comparison). Jennette et al. (2000) also recognized several elongate mounds in the Ypresian Tay Formation in the Central Graben of the North Sea, and interpreted them as deposits of sandy debris flows (*sensu* Shanmugam, 1996) or as compaction inverted channels. Little to no sandstone is found outside the axes of the linear mounds (Jennette et al., 2000), suggesting confined deposition either between muddy levees or within an erosive channel. In terms of dimensions and geometry, the elongate South Mara mounds compare well to linear mounds identified in the North Sea (see Figure 5.2b) and hence are interpreted to have a similar origin.

5.5.2 Reservoir potential of PILs and CTLs

PILs probably contain continuous massive sands with few baffles or barriers to impede hydrocarbon flow. They commonly form isolated sand bodies within muddy slope deposits, and hence if the feeder gully is mud-filled, they probably form

compartmentalized deposits with good potential for updip seal. Their isolation, combined with their relatively small size, however, makes them less attractive targets and may present problems for hydrocarbon migration into them.

CTLs are bigger targets, contain thicker sands, but may also contain baffles or barriers to fluid flow, particularly in cases of stacked CTLs are separated by hemi-pelagic drape. Some stacked CTLs off East Corsica, however, are separated by only a very thin (less than 2 m) shale drape. The South Golo composite mid-fan lobe, for example, contains several stacked bodies in close proximity to one another that attain a cumulative thickness of about 60 m. Minimal shale drape between successive lobes suggests that there were only short pauses in active lobe sedimentation between periods of lobe-switching (i.e. insufficient periods of time for significant shale drapes to accumulate). The North Golo composite mid-fan lobe (B1 and C2 - Figure 5.27) shows significant erosion between successive lobes, suggesting that even if some lobes were blanketed by shale, the shale may be eroded as the adjacent lobe is deposited, producing a thicker, amalgamated sand body. Post-depositional deformation, like sand injection, could also reduce the effects of baffles and barriers to flow by increasing sand body connectivity (Lonergan et al., 2000).

The Avondale mounds in the JDB are interpreted to consist of a combination of vertically and laterally-offset stacked CTLs, and channels, which in some cases erode underlying lobes as they feed more distal ones. Smaller-scale erosion at the top of Avondale mound 2 (see seismic profile in Figure 5.12) may be similar to the scour or distributary channel observed in CTL C2 of the North Golo fan (Figure 5.27) and on several other lobes off East Corsica. These features are commonly mud-filled. The gross thickness of sandstone in the Avondale mounds is expected to increase to the north where the mounds become more prominent and where no wells are available. Likewise, the thickness of shale (lobe-fringe deposits and shale drape) between stacked sandy lobes is also expected to increase.

Updip seal could be a problem for CTLs because they are commonly fed by channels containing sand-rich deposits. In some cases, erosive channels are mud-filled and an updip seal is possible. For CTLs fed by channels with significant coarse-grained fill, however, it is not clear how an updip seal can be achieved without a structural

control. Combined depositional and compaction relief of CTLs may be an important trapping mechanism in some areas (as observed in several fans in the North Sea, e.g. Frigg fan).

5.5.3 *Why does submarine fan style change in the JDB?*

There was a fundamental change in the types and size of fans deposited in the basin during the Early Paleocene versus the latest Paleocene to earliest Eocene (Figure 5.3b). Despite the advance of the early Paleogene shelf and slope, the basin saw a retreat or backstepping of fans through time, from large amalgamated fans characterized by aurally extensive mounds deposited on the distal basin floor in the Early Paleocene (Avondale mounds), to smaller, isolated mounds deposited on the lower slope and basin floor in the latest Paleocene (South Mara mounds). The fans retreated even further in the earliest Ypresian as only a very proximal fan delta was deposited on the upper slope, prior to the termination of fan deposition altogether.

What accounts for the observed change in fan style in the basin? Because the submarine fans were deposited over a period of 10 to 12 m.y., it is unlikely that the change in fan style reflects specific changes in sea level position. Hence, the changes in fan style cannot be related directly to the lowstand fan models proposed by Mitchum (1985), Posamentier and Vail (1988), and Posamentier (1991), where canyons are incised and basin floor fans are deposited during rapid sea level fall, and channel-levee systems and slope fans are deposited when the rate of sea level fall decreases towards the maximum lowstand and into the subsequent transgression. Instead, the change in fan character probably reflects other processes, like an evolving sediment source region. Climatic changes (drier versus wetter), a shift in the position of river systems, denudation of the sediment source region (reducing the amount of sediment shed into the basin), or changes in the prevalence of shelf transport processes, could all alter the sediment delivery to the margin. These in turn could result in variations in the character of sediment gravity flows through time, reflected in the types of fans deposited in the basin. Some periods of fan deposition may have been triggered by global eustatic sea level falls (e.g. Haq et al., 1987), but fluctuations in third-order sea level position alone cannot account for the change in fan style.

Regional studies indicate that there was a southward shift in the location of fluvial systems sometime after the latest Cretaceous but before the end of the Paleocene (Deptuck et al., 2003a). The change in submarine fan style could therefore reflect the amount of direct fluvial input into the system. Early Paleocene fans were fed by canyons that extended several kilometers back onto the shelf. Hence, they would have provided good linkage to both littoral drift cells (perhaps more important during highstands - see Normark et al., 1998) and rivers transporting sediment directly into the canyon heads during floods. Slumping during canyon formation probably also played an important role in supplying sediment to the Avondale mounds. Based on the sedimentary characteristics of the Fox Harbour member and equivalent Bay Bulls member strata that preceded canyon erosion (see Chapter 3), sediment gravity flows triggered either by direct river input or slumps probably had a mixed composition of sand and mud, and hence sand transport in such flows would have been efficient, capable of reaching the far out into the basin (where the Avondale mounds were deposited).

In contrast, by the Middle to Late Paleocene, fluvial systems had shifted south of Terra Nova (where the most prominent progradation is observed), and hence, coupled with an apparent second-order eustatic sea level rise (Haq et al., 1987), the potential for direct fluvial input was reduced. Instead, increased evidence for shelf scouring at this time (e.g. Figure 5.19) suggests that sediment transported in littoral drift cells was more important than direct fluvial input in the late Thanetian (at least north of Terra Nova).

5.6 Summary of key points

1. The JDB contains submarine fans that were deposited in the Danian to early Ypresian. Mounded seismic facies, associated with the submarine fans, are recognized in three primary locations in the basin, each comprising a fan complex (Thorvald, Mara, and Trinity fan complexes). Each fan complex consists of stacked mounds of varying dimensions and geometry. The most extensive mounding is found in the Mara fan complex.
2. A proximal to distal transition from erosional dominated architectural elements to depositional architectural elements is recognized in the basin. Erosional conduits are

typically located in more proximal fan settings (i.e. the slope, sometimes extending back onto the shelf) and may or may not contain fill that produces positive relief after compaction. Depositional elements are typically found at the mouths of erosional elements and can have an elongated or sub-circular planform geometry. Like the mounds in the North Sea, mounds in the JDB typically contain thick sands that produce a “blocky” gamma ray response where penetrated by wells.

3. In the Early Paleocene, large canyons eroded the shelf and slope and funneled sands out to the basin floor. The slope was steep and was entirely bypassed by sediment gravity flows. The largest, most extensive mounds developed at this time (the Avondale mounds) and are believed to be dominated by stacked channel-termination lobes (CTLs), like those described for submarine fans off Eastern Corsica. The prominent canyons that extend across the shelf, provided a direct link to fluvial systems. Both hyperpycnal flows and slumping during canyon formation, are believed to have been the dominant triggering mechanisms for sediment-gravity flows.

4. In the Thanetian to earliest Ypresian, sediment was supplied to mounds by smaller gullies. The slope was more gradual and some mounds accumulated in very proximal settings, above the slope or just beyond the base-of-slope. Incisions on the slope commonly pass down-slope into positive relief, convex-upward mounds with a pod-shaped to linear planform geometry, interpreted to correspond to proximal-inefficient lobes (PILs), like those identified in proximal settings off Eastern Corsica, or compaction-inverted channels. Increased evidence for shelf transport (elongated depositional bodies parallel to the margin) and scouring (with a similar orientation as the depositional bodies) may indicate that winnowed sources of sediment, transported by shelf currents, ultimately supplied sediment to late Thanetian to Ypresian gullies that fed the small submarine fans.

5. There appears to be a spectrum of lobe types in the JDB as well as modern analogues, ranging from proximal fan-deltas, deposited near the shelf-break, to proximal-inefficient lobes (PILs), deposited on the slope or near the base-of-slope, to channel-termination

lobes (CTLs), deposited well out on the basin floor. The spectrum reflects flow efficiency, which in turn probably reflects grain population, gradients, and the degree of channel confinement. The most proximal lobes off eastern Corsica (like Pineto) have the most limited lobe-fringe deposits, and pinch-out abruptly down system, probably indicating very sand-rich flows with rapid sediment fallout rates from high-concentration flows (either sandy debris flows or high-density turbidity currents). Lobes deposited in more distal settings have better developed finer-grained fringe deposits, suggesting that such flows are commonly more mud-rich. Other anecdotal evidence like the presence of levees flanking the fan-valley, and inner levees developed within the fan-valley, support this interpretation.

CHAPTER 6 - INSIGHT INTO CHANNEL-BELT ARCHITECTURE AND EVOLUTION FROM MUCH LARGER SYSTEMS

6.1 Introduction

Submarine channels flanked by levees have been recognized as important components of deep water systems since the early work of Normark (1970, 1978) and Walker (1978) and many others. Channel-levee systems dominate the upper fan architecture of most large- and medium-sized submarine fans, including the Mississippi (Bouma et al., 1985), Amazon (Damuth and Flood, 1985), Indus (McHargue and Webb, 1986; Kolla and Coumes, 1987), Bengal (Emmel and Curray, 1985), Zaire (Droz et al., 1996), Toyama (Nakajima et al., 1998), and Rhone (Bellaiche et al., 1984), and also many smaller fans like Hueneme (Piper et al., 1999) and Golo (Bellaiche et al., 1994). They act as conduits through which clastic sediment is transported into the deep sea, and they provide confining and sorting mechanisms that allow sand to reach the basin plain. Channel-levee systems also form important repositories for coarse-grained sediment deposited along channel-axes (Bouma et al., 1985; Manley et al., 1997) and for fine-grained sands and silts deposited on levees (Hiscott et al., 1997; Piper and Deptuck, 1997). For these reasons, the architecture and evolution of channel-levee systems are of interest to the petroleum industry.

Studies on channel-levee architecture in the shallow and deep subsurface are sometimes hindered by problems related to poor data-quality [e.g. problems imaging channel-axis deposits due to sideswipe (Flood, 1987) and diffraction from channel walls in single-channel or poorly migrated data] or insufficient channel-levee thickness to reveal detailed internal architecture (as is the case for the early Paleogene submarine channels in the Jeanne d'Arc Basin). These issues hamper the study of channel evolution and in particular make it difficult to assess how submarine channels migrate through time and the importance of point bars and inner levees. Resolving these issues is important for developing improved reservoir models that better predict baffles and barriers to fluid flow.

This chapter focuses on two locations - the Arabian Sea and the Niger Delta slope - where high-quality industry seismic data cover the proximal reaches of several large

channel-levee systems (i.e. immediately outboard of the canyon mouth). A vertical seismic resolution of 6 to 7 m, combined with the large size of the channel-levee systems, provide a unique opportunity to study their evolution and architecture. A detailed 3-D seismic morphological study of one channel-levee system on the Niger Delta slope provides details about the evolution of channel-axis deposits and inner levees that have not previously been recognized.

A channel-levee system (abbreviated to **CLS**) is defined as a single channel-belt, bordered by outer levees. A channel-levee complex (abbreviated to **CLC**) is defined as a series of stacked channel-levee systems that are fed by the same canyon. Incision of a new canyon, therefore, results in the deposition of a new CLC, and is a first order control on fan architecture. A similar convention was used in studies of the Amazon Fan (e.g. Damuth and Flood, 1985). The term “**HARs**” is used in this study to describe high amplitude seismic reflections located within the channel-belt. HARs are believed to correspond to coarser-grained lithologies associated with the fill of aggrading or laterally migrating channel-axes (e.g. Damuth et al., 1983; Kastens and Shor, 1985). Core calibration from the Mississippi and Amazon fans confirms the coarser-grained nature of HARs (Bouma et al., 1985; Manley et al., 1997). As will be discussed, some high amplitude reflections within the channel-belt correspond to deposits above terraces that are not directly related to channel-axis deposits. The term **channel-axis deposit** is used in this study to describe deposits on the floor of the channel, near its axis but not exclusively along the thalweg. Channel-axis deposits are commonly wider than the true axis or thalweg of the system, but show a similar planform geometry.

6.2 Indus Fan - Arabian Sea

The Indus Fan is a large, river-fed submarine fan (Kenyon et al., 1995), second in size only to the Bengal Fan on the opposite side of India. It was deposited in a predominantly unconfined setting on the continental slope, rise, and basin floor, covering much of the Arabian Sea. The entire fan extends over an area of $1.1 \times 10^5 \text{ km}^2$ with greater than 9 km of sediment accumulating near the toe-of-slope (Kolla and Coumes, 1987; Clift et al., 2001). Fan sedimentation is estimated to have begun at the end of the

Oligocene or beginning of the Miocene, during Himalayan uplift (Kolla and Coumes, 1987; McHargue and Webb, 1986; Clift et al., 2001).

The upper Indus Fan, both past and present, consists of some of the largest CLSs observed. They have been studied by several authors using a variety of data types, ranging from multichannel industry seismic data to 3.5 kHz single channel seismic data and shallow piston cores (e.g. Naini and Kolla, 1982; McHargue and Webb, 1986; Kolla and Coumes, 1987; Droz and Bellaiche, 1991; McHargue, 1991). Three canyon incisions have been reported on the shelf and slope, including the modern Indus Canyon and two ancestral canyons located further west. Outboard of these canyons, much of the upper 3 km of strata consists of stacked CLCs, each consisting of two or more CLSs. A total of 14 CLSs were mapped in this study and several others were identified in the deeper section on isolated profiles (Figure 6.2). These systems have been divided into 4 CLC's, each fed by a distinct canyon incised into the shelf and slope. Of these, CLC C has been studied in the most detail and will be the focus of the remaining section on Indus Fan.

6.2.1 *Seismic data set*

Just west of the modern Indus Canyon, 2042 line kilometers of excellent quality 2-D seismic data from two different vintages (1999 and 1977- reprocessed in 1999) were used. The data set covers an area similar to that studied by McHargue and Webb (1986), but with a tighter grid spacing (Figure 6.1). The 1999 data set is 120-fold, with frequency roll-off at near 80 Hz (approximately a 6 m vertical resolution). The reprocessed 1977 data set, combined with the 1999 data set, yield a grid spacing ranging from 2.5 to about 8 km. Coverage extends from the shelf in less than 100 m of water to near the base-of-slope at present-day water depths of 1700 m (Figure 6.1). These data provide detailed information about the distribution and architecture of CLSs to subsurface depths of more than 3 km.

6.2.2 *Channel-levee complex C*

CLC C is the largest in the study area and has the best seismic coverage (Figure 6.1). It is draped by 250 - 300 m of strata consisting of continuous and parallel seismic facies. CLC C consists of three CLSs (C1, C2, and C3 - Figures 6.1, 6.2) that stack both

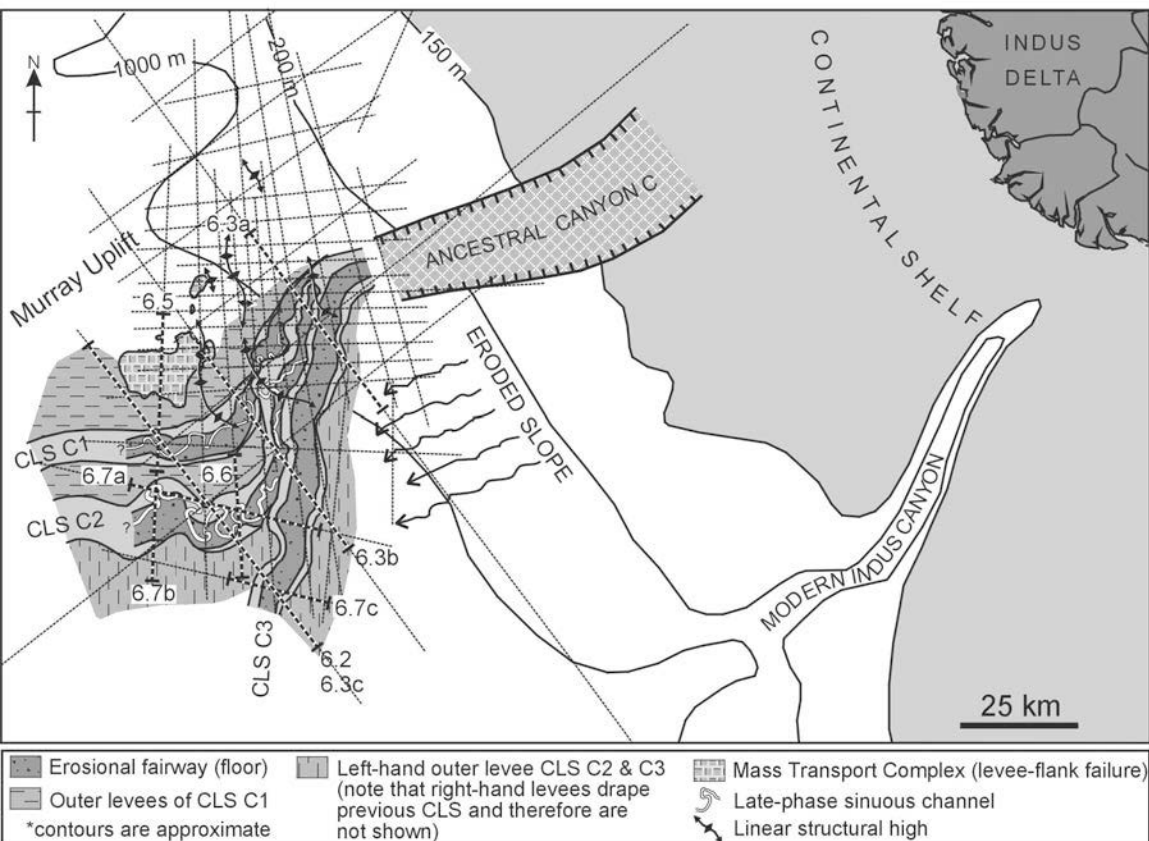


Figure 6.1. Indus upper fan with location of 2-D seismic data, channel-levee systems (CLSs) C1, C2, and C3, and figure locations. Also shown is the planform geometry of two distinctive narrow HARs discussed in text.

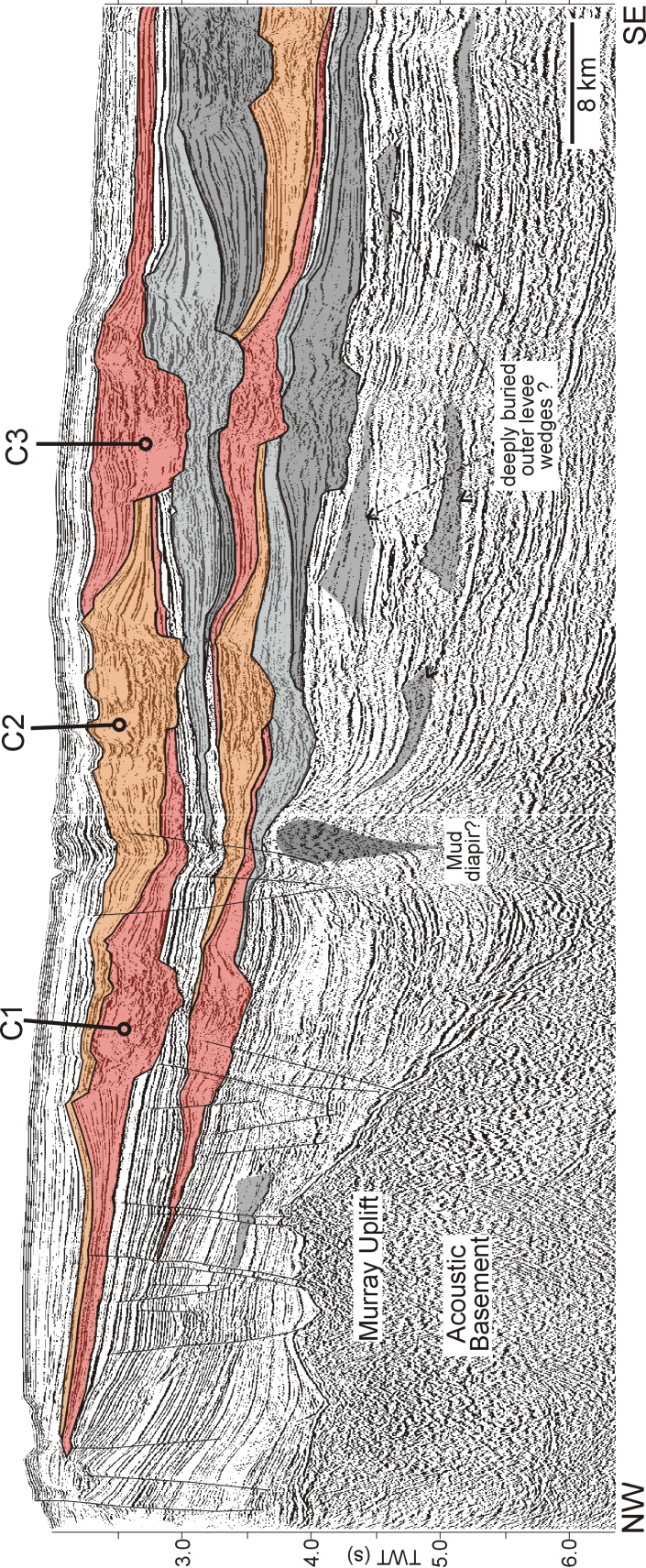


Figure 6.2. Regional profile located roughly perpendicular to orientation of several stacked channel systems on the upper Indus Fan. A total of 13 CLSs are shown on this profile, and several other poorly imaged partial systems are shown underlying them. The alternating orange/red and greyscale shades represent different channel-levee complexes, each consisting of two or more channel-levee systems. Each complex is sourced by a distinct canyon on the shelf and slope, with the shingled/compensational stacking of different systems accomplished by upper fan avulsions (see discussion for details).

laterally and vertically to produce a maximum composite thickness of 950 ms (twt). Assuming an interval velocity of 2100 m/s (extrapolated from Kolla and Coumes, 1987), this would yield a maximum thickness of about 1000 m. The stacking pattern of C1, C2, and C3 produces an overall fan-shaped planform geometry extending from the mouth of ancestral canyon C. The width of the complex increases from about 30 km near the canyon mouth to greater than 80 km near the distal limits of the study area (where the CLSs are laterally offset from one another - Figure 6.1). CLS C1 was deposited furthest west, and each successive system (C2 and C3) was deposited further east.

CLC C has been studied previously by McHargue and Webb (1986 - their canyon-channel system C, Ca, Cb) and Kolla and Coumes (1987 - their canyon 2 and channels 2a, 2b, 2c) using a sparser grid of data. Their results were particularly useful for confirming some of the interpretations and the location of the feeder canyon (ancestral canyon C), most of which lies just outside the study area. Tighter line spacing and improved data quality allows me to build on their work and to draw important comparisons with CLSs in other settings (e.g. Niger Delta slope).

Precise age control for CLC C is not available. Onlap relationships, however, indicate that the complex postdates the Early Miocene uplift of the Murray Ridge (Figure 6.1), a structural high located along the northern margin of the study area (see also Clift et al., 2001 and references therein). Both Kolla and Coumes (1987) and Clift et al. (2001) used well data from the shelf for additional age control. Kolla and Coumes (1987) inferred that the complex (their canyon 2) was active in the Pliocene, whereas jump ties to seismic profiles from Clift et al. (2001) suggest the complex was active in the Late Miocene, therefore providing only a rough estimate of its age (Late Miocene and/or Pliocene).

Channel-levee system stacking architecture

Just outboard of the canyon mouth, the outer levees of C1, C2, and C3 stack vertically to form a large compound levee (up to 850 ms thick) on the northwestern side of the complex (Figures 6.3a, b). In contrast, conjugate levees on the southeastern side of the system were removed by erosion during the development of each successive system. The axis of the complex near the canyon mouth consists of several sharply defined

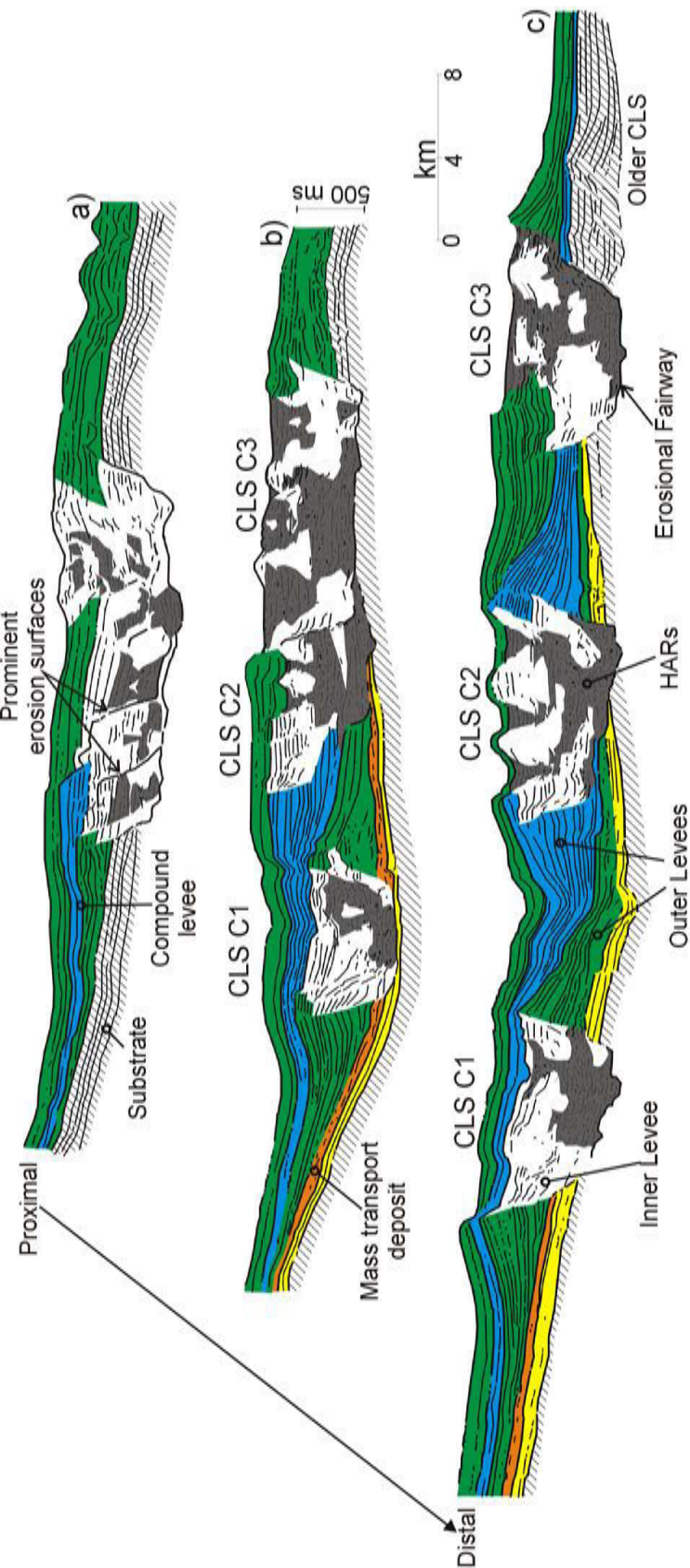


Figure 6.3. Three traverses roughly perpendicular to CLC C showing the distribution of different seismic facies representing outer levees (blue and green), inner levees (white), HARs (dark grey), mass transport deposits (orange), and sheet-like deposits at base of complex (canyon initiation deposits - yellow) are dominated by erosion. The western levee associated with CLS C1 is preserved whereas the eastern levee has been eroded by CLS C2. Similarly, the western levee of CLS C2 is preserved, whereas its eastern levee is eroded away by CLS C3. Note that the western levees of CLSs C1, C2, and C3 stack to form a large compound levee on the western margin of the complex. b) shows a remnant of eastern levee of CLS C1, and c) shows all three systems, each with both an eastern and western levee. The offset-stacking/compensation-stacking of the CLSs results from the positive relief created by the previous system, which diverts successive systems. See figure 6.1 for location.

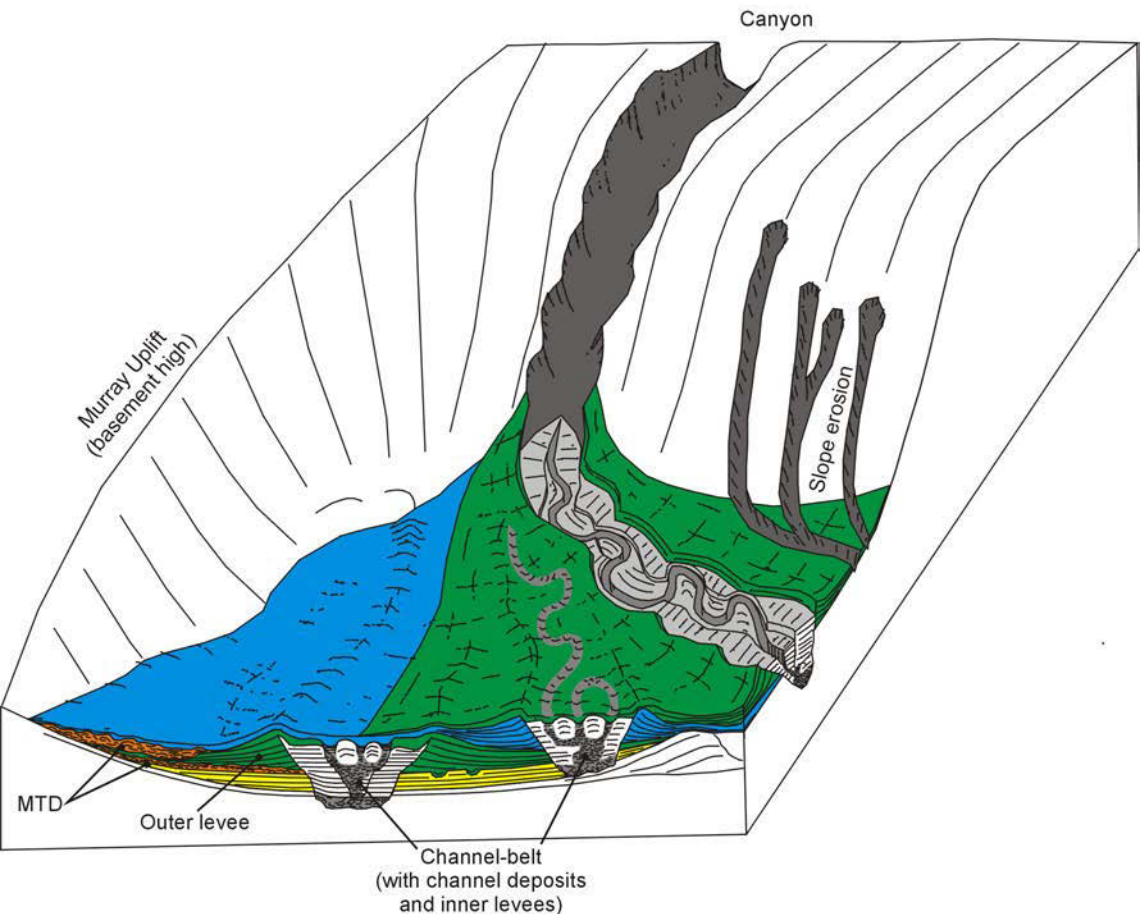


Figure 6.4. Block diagram illustrating the three dimensional relationship between CLSs C1, C2, and C3 on the Indus Fan. Note the compensated stacking architecture developed after two separate upper fan avulsions near the canyon mouth. MTD = mass transport deposit

erosive surfaces, separated by intervals consisting of high amplitude, predominantly chaotic reflections, and low amplitude, predominantly continuous reflections that onlap the erosive surfaces (Figure 6.3a).

With increasing distance from the canyon mouth, C1, C2 and C3 diverge and the southeastern levees of each system are increasingly preserved (Figures 6.3c, 6.4). Here, they show a laterally offset **compensated** stacking geometry with the northwestern levee of each successive system onlapping the southeastern levee of the previous system. The shift from a dominantly erosive character to increasingly depositional character corresponds well to the pattern reported by McHargue and Webb (1986) who described a change from the degradational zone in the erosive canyon, to the transition zone represented by a leveed channel with an erosive base. This pattern, however, is altered locally where the erosive bases of CLSs erode bathymetric higher areas, locally increasing their degradational character.

6.2.3 Architecture of individual channel-levee systems

CLSs C1, C2, and C3 each have a maximum thickness of about 750 ms (twt), a width of about 30 km and a distance of roughly 8 - 10 km between the outer levee crests. Several common architectural elements are recognized in each system. The elements most pertinent to the channel-belt and most easily recognized on 2-D seismic data include the erosional fairway (defines the base of the channel-belt), outer levees (provide additional lateral confinement for the channel-belt), inner levees, and channel-axis deposits (expressed as HARs).

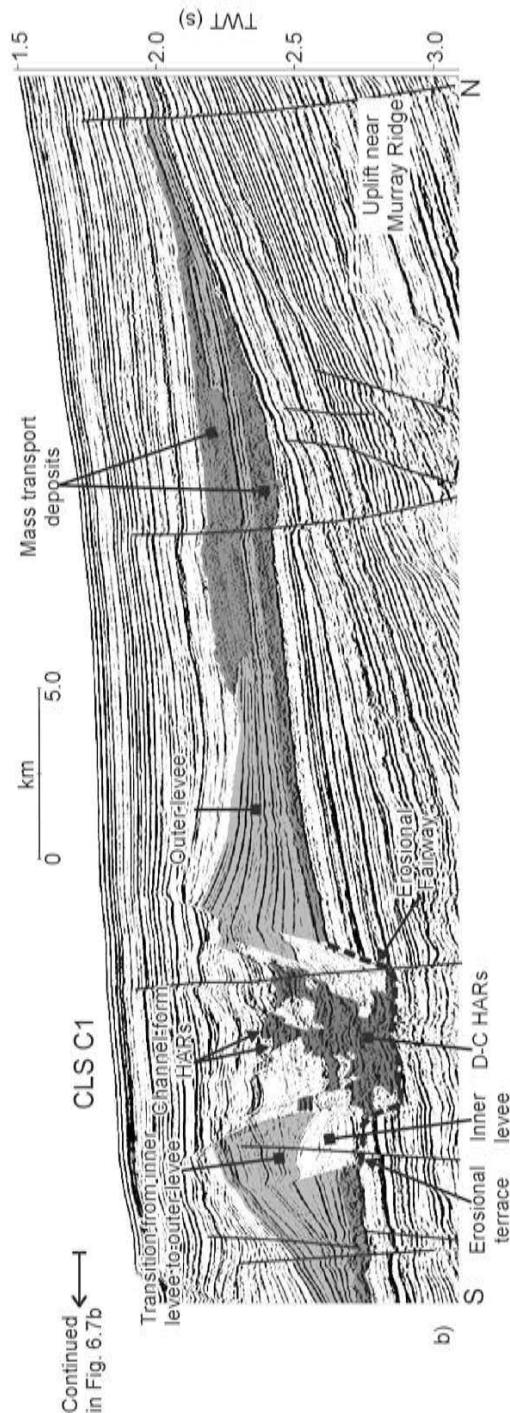
Erosional fairway element

The erosional fairway element is a canyon-like incision flanked by wedge-shaped outer levees, typically found on the middle to lower slope (Figures 6.5 - 6.7). The up-dip limit of the erosional fairway (i.e. the canyon mouth) is defined as the position along the canyon where outer levees are first recognized. Its distal limit is defined where erosion is no longer recognized at the base of the system.

The erosional fairway element in systems C1, C2, and C3 ranges in depth from less than 200 m to over 600 m and in width from approximately 5 km to 8 km.



a)



b)

Figure 6.5. a) Uninterpreted and b) interpreted seismic profile across CLS C1 showing the first-order architectural elements (erosional fairway, inner levees, outer levees, and various types of HARS corresponding to channel deposits). Note the sharp contacts between inner and outer levees. Profile location and the inferred planform geometry of the narrow channel-form (near top of HARS) are shown in Figure 6.1.

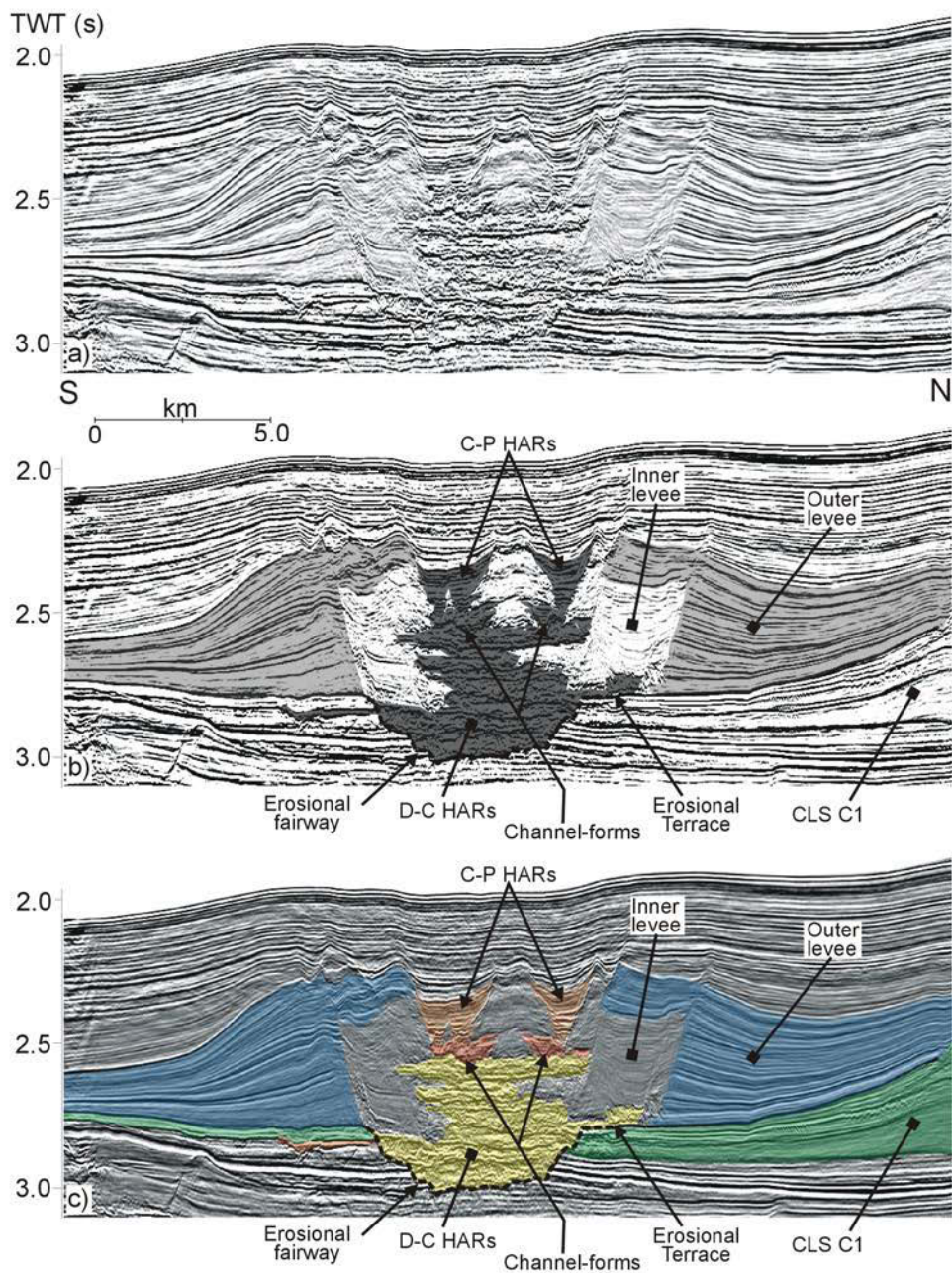


Figure 6.6. a) Uninterpreted and interpreted b) black and white and c) colour seismic profile across CLS C2 showing the principal architectural components identified in CLSs in this study. Note the sharp contact between the roughly symmetrical outer levees and the channel-belt (consisting of inner levees and HARs). Note also the prominent erosive base (erosional fairway) and that the HARs are wider near the base of the system and narrower at the top. Figure 6.1 shows location and the planform geometry of the narrow C-P HARs at the top of the system. Other profiles crossing the same C-P HARs are shown in Figures 6.7 a and b.

Figure 6.7. a) Interpreted seismic profile traversing perpendicular to CLS C3, and roughly down the axis of CLS C2, showing a complicated “cactus-like” HARs, and the repetitive crossings of the same sinuous narrow C-P HARs (inferred planform geometry shown in Figure 6.1). Note the sharp erosive contact between CLSs C2 and C3. CLS C3 probably experienced several periods of re-incision. b) Interpreted seismic profile oblique to CLS C2, showing multiple phases of inner levee growth developed opposite a prominent cut-bank. Much of the outer levee has been eroded at the cut-bank. c) Interpreted seismic profile across CLS C3 showing a rather complex channel-belt architecture. Note the transition from confined inner levees, to unconfined inner levees, and eventually to outer levees as the system aggraded and eventually healed over the prominent incision at the base of the system. Note also the continuous high amplitude reflections within, and near the base of, the inner levees on both the left and right side of the channel-belt (interpreted as a sandy deposits within the inner levees). See Figure 6.1 for locations.

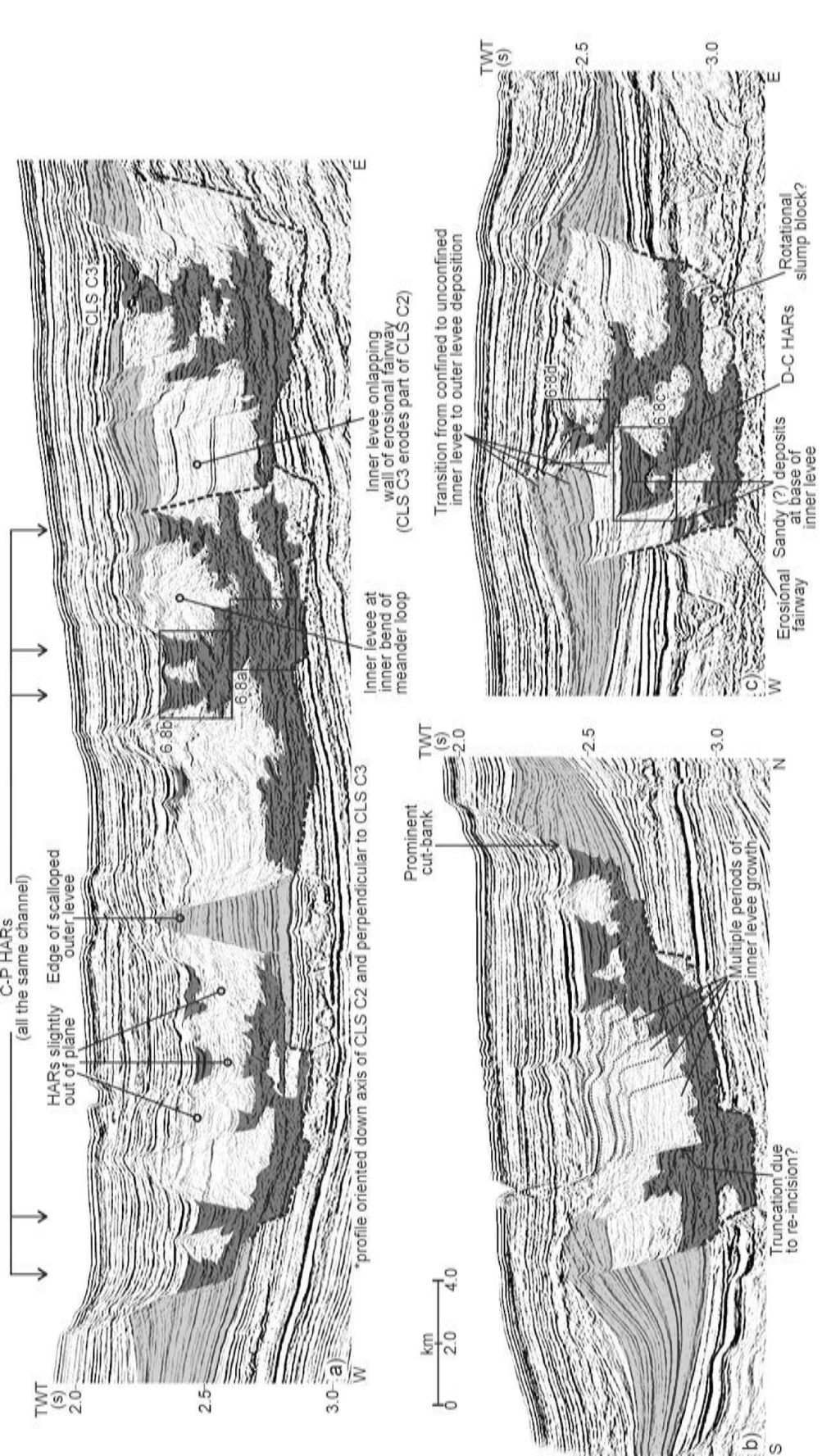


Figure 6.7. (see previous page for caption)

Generally, the deepest incision is observed nearest the canyon mouth or where the erosional fairway cuts through positive bathymetric features on the sea floor (e.g. where CLS C3 erodes through an older CLS - Figure 6.7c). In contrast, shallowest incision is observed within structural sags and distally (i.e. furthest away from the canyon mouth).

Deposits within erosional fairways range from high amplitude facies associated with channel-axis deposits, to lower amplitude facies associated with chaotic mass transport deposits, rotational slump blocks, and inner levees.

Outer levee element

The most common and diagnostic elements on the Indus Fan are outer levees (Figures 6.5 - 6.7), believed to form from the overbanking of predominantly fine-grained sediment during the passage of turbidity currents (Naini and Kolla, 1982). Their original external depositional geometry is wedge-shaped, converging away from the erosional fairway axis. They reach a maximum thickness of over 500 m at the crest, and thin to less than 100 m on the flank, over distances of around 10 km.

Seismic reflections within outer levees are almost always continuous, but can range from low to high amplitude. Individual seismic reflections show an increase in dip as outer levees aggrade. Near the southern edge of the study area, where outer levees are best developed, they show an increase in maximum dip from less than 2° (at their base) to greater than 5° (at the top). Seismic reflections within outer levees may also show internally developed downlap and apparent toplap surfaces.

Near the canyon mouth, only the right-hand outer levees (facing down channel) are preserved. At a distance of 5 km outboard of the canyon mouth, the right-hand levee of CLS C1 has a width of about 2 km and a thickness of less than 300 ms (twt) at the levee crest. At a distance of 20 km down-slope from the canyon mouth, the right-hand outer levee of CLS C1 reaches a maximum thickness of 550 ms (twt) and a width of approximately 10 km. The outer levee plateaus at this thickness over the following 20 km down system, to the distal edge of the data-set. At distances greater than 25 km from the canyon-mouth, the conjugate left-hand outer levees are also preserved, with comparable dimensions.

Inner levee element

Von Rad and Tahir (1997) noted the occurrence of muddy bench-like depositional “terraces” within the modern Indus Canyon, at several stepped levels above the channel floor, ranging from 80 to 360 m. Hubscher et al. (1997) recognized similar features on the Bengal Fan and referred to them as inner levees. Similar “terrace” forming features are also recognized in many of the buried systems of the Indus Fan, and were referred to by McHargue (1991) as overbank deposits from thalweg channels. Most of these features are interpreted as inner levees, following the terminology of Hubscher et al. (1997). They are interpreted to form from both depositional processes (i.e. vertical aggradation of inner levee deposits resulting from the overbanking of under-fit channels) and erosional processes (i.e. sculpting of inner levees along channel margins).

Inner levees are common and easily recognized on the upper Indus Fan, where they form quadrilateral shapes like squares, rectangles or parallelograms in vertically exaggerated seismic cross-sections (e.g. Figures 6.5 - 6.7). They may also form irregular shapes, particularly on traverses crossing the inside bend of meander loops (e.g. Figure 6.7a) and wedge-shaped geometries, particularly in areas of reduced confinement. They are typically less than 3 km wide on the Indus Fan, and usually cannot be mapped with confidence for down-channel distances greater than 6 km. Inner levee elements are commonly bordered by sharply defined erosive surfaces that are generally inclined at less than 25 degrees. Erosive interfaces are observed between inner levees and outer levees, between different periods of inner levee growth, and also at boundaries between inner levees and channel-axis deposits, particularly at cut-banks.

Channel and channel-fill elements (HARs)

Channel and channel-fill elements (Mutti and Normark, 1991) are found primarily between the crests of outer levees. Since the channels in CLSs C1, C2, and C3 are no longer active, seismic data record the deposits that accumulated on the channel floor (near its axis) during channel aggradation and migration. McHargue and Webb (1986) described the multi-channel reflection seismic character of “channel-axis” deposits in CLSs C1, C2, and C3 as high amplitude and discontinuous (H-D). In this study, the H-D seismic facies of McHargue and Webb (1986) are broken down into three distinct high

amplitude reflection (HAR) seismic facies types: D-C HARs, C-P HARs, and channel-form HARs.

D-C HARs are the most common of the three, consisting of intervals of discontinuous and chaotic seismic reflections, locally containing continuous reflections that look like broad scours (e.g. Figures 6.6, 6.8a). In cross-section, D-C HARs vary in width from less than 1 km to greater than 5 km, and are commonly wider near the base of the system, within the erosional fairway, than the top. McHargue (1991) interpreted these high amplitude, largely discontinuous seismic facies as coarse-grained thalweg deposits from laterally migrating channels that underwent little vertical aggradation. He reasoned that such deposits could have formed from braided channels. D-C HARs located stratigraphically higher up in the CLSs tend to be narrower and are bordered by prominent inner levees. Such deposits probably originated from the vertical aggradation of sinuous channels (McHargue, 1991). For the most part, the deposits forming D-C HARs do not preserve the original cross-sectional geometry of the channels inferred to have formed them.

In contrast, **channel-form HARs** (channel-forms, for short) consist of isolated or stacked U- to V-shaped reflections (e.g. Figures 6.8b - f). Each channel-form is defined by a single continuous to discontinuous high amplitude reflection, inferred to originate from the impedance contrast between deposits below the erosive floor and walls of the channel, and the deposits that partially filled the channel. Channel-forms are therefore interpreted as partially filled second-order incisions, located within the first-order incision of the erosional fairway. Channel-form geometry may be symmetrical or skewed towards the direction of channel migration. Some channel-forms are capped by a single horizontal to sub-horizontal high amplitude reflection. On some profiles, only partial channel-forms are preserved where they are eroded by an overlying or adjacent one. Channel-forms that stack adjacent to one another may form a series of shingled events inclined in the direction of channel migration. The inclined events are interpreted to correspond to the remnants of channel-forms preserved after several periods of cut-and-fill, the result of abrupt channel migrations (e.g. Figure 6.8b). Channel-forms that stack vertically may also incise one another (e.g. Figure 6.8d). Successive channel-forms will aggrade if the amount of incision between channel-forms is less than the thickness of

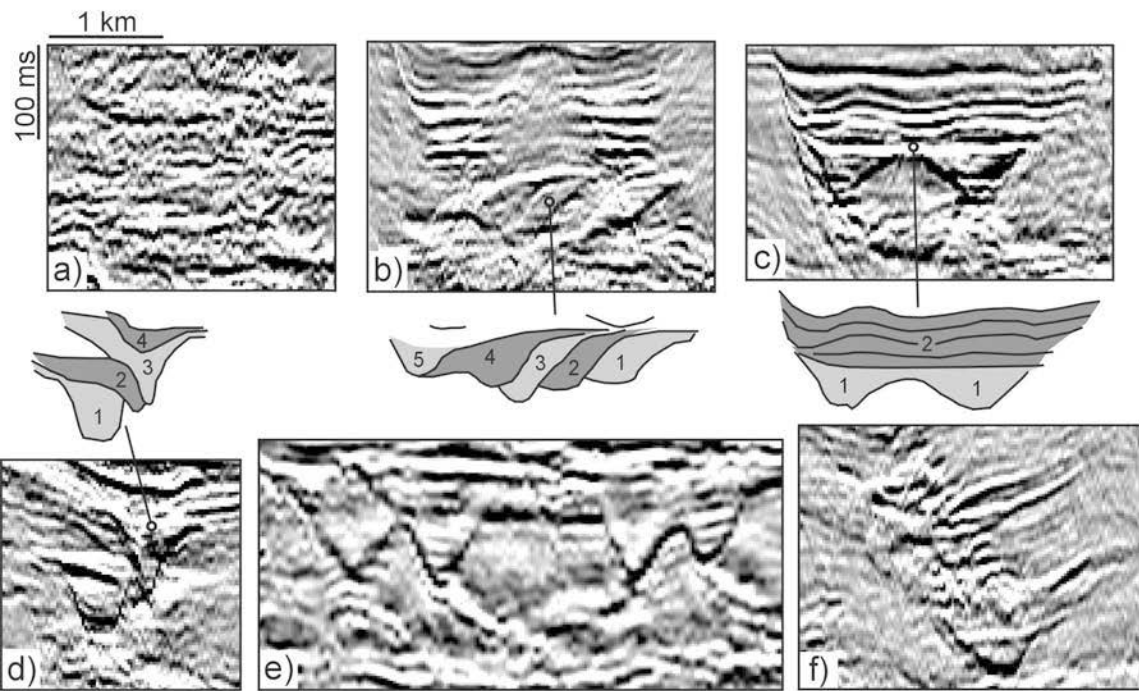


Figure 6.8. Seismic profiles illustrating different characteristics of HARs on Indus Fan. a) Discontinuous to chaotic (D-C) HARs from CLS C2. b) Profile from CLS C2 showing D-C HARs (at base) passing up-section into laterally migrating cut-and-fill channel-forms (middle), that in turn pass up-section into two limbs of the same narrow continuous and parallel (C-P) HARs (at top). The interval in the middle of the profile consists of at least five separate, partially preserved channel-forms that developed as the channel migrated left through alternating periods of cut-and-fill (line drawing below). Note the inclined events representing 2nd order erosion surfaces that separate each period of cut-and-fill (1 to 5). No vertical aggradation is observed because the amount of incision between, is approximately equivalent to the amount of deposition within, each channel-form. c) Profile from CLS C3 showing D-C HARs (base) passing up-section into a channel-form (crossed twice - 1). The channel-form was abandoned and draped by parallel continuous reflections (2), interpreted to be sand-prone deposits within a meander cut-off or above an erosional terrace. These deposits pass up-section into an inner levee (shown in Figure 6.7c). d) Four stacked channel-forms separated by 2nd order erosive surfaces. In this case the amount of incision between channel-forms is less than the amount of deposition within each channel-form, resulting in overall aggradation. Location shown in Figure 4. e) Profile through CLS C2, crossing the same isolated channel-form four times, indicating that it has a sinuous planform geometry. f) Profile through a hybrid of narrow aggradational D-C and channel-form HARs from a smaller CLS that underlies CLS C1. The HARs in this example are flanked directly by outer levees, rather than inner levees, because the system lacks an erosive base. See text for details.

sediment that accumulates within each second-order incision. Some inclined events may also be generated from point-bar like deposits that result from gradual channel migration (see Abreu et al., in press), although they are not widely recognized in this study area.

In CLC C, channel-form HARs are most common in stratigraphically higher positions within each CLS. For example, an isolated channel-form is observed near the top of CLS C1. Based on repeated crossings on single linear seismic profiles (as many as four – Figure 6.8e), it is inferred to have a sinuous planform geometry (shown in Figure 6.1). Aside from the tentative recognition of concordant, transparent or chaotic stratal patterns within each channel-form, a more detailed understanding of channel-form fill would require higher resolution seismic and/or core data.

C-P HARs, consisting of intervals of continuous and parallel (to sub-parallel) seismic reflections, are fairly rare within channel-belts in the study area. In CLS C2, vertical profiles cross individual limbs of the distinctive C-P HARs several times (e.g. Figures 6.6, 6.7a,b, 6.8b), suggesting a sinuous planform geometry (shown in Figure 6.1). Each “limb” consists of a number of stacked continuous horizons that resemble very shallow relief (flat-lying) channel-forms, interpreted as channel-floor deposits (Figure 6.8b). No lateral offset is observed between successive reflections, suggesting that little lateral migration occurred during aggradation. The successive widening of reflections, combined with the lack of lateral migration, suggests that the C-P HARs in this example developed during the gradual abandonment of the system, as the remaining channel-relief was filled.

Commonly, the deposits from migrating and aggrading channels produce a hybrid of D-C, C-P, and channel-form HARs. Obviously, distinguishing between the 3 different HAR facies types requires well processed seismic data, and at higher seismic frequencies (i.e. greater than 80 Hz), more facies types will be recognized (including different stratal fill patterns within individual channel-forms).

Mass transport deposits

Two mass transport deposit elements are recognized within CLC C (Figure 6.5). The first is located at the base of CLS C1. It consists of variable amplitude, discontinuous seismic reflections that sometimes show a hyperbolic or hummocky

reflection character. The second mass transport deposit is located above the right-hand northwestern outer levee of CLS C2. It has a similar acoustic character as the first mass transport deposit, but consists of lower amplitude seismic events, and has an erosive base. An updip failure scarp on the right-hand outer levee of CLS C1 is believed to be the source for the second mass transport deposit located down-system, stratigraphically between the outer levees of CLSs C1 and C2. The scarp truncates several reflections on the flank of the outer levee.

6.2.4 Temporal relationship between inner and outer levees

Two end-member possibilities are proposed to explain the temporal relationship between inner levees, outer levees, and HARs on the Indus Fan. The first end-member possibility (end-member Model A) is that inner and outer levees were deposited relatively contemporaneously. Inner levee deposition is either from smaller muddy flows or from the tail-end (waning stages) of larger flows. The distinctly transparent, low amplitude character of the inner levees on CLS C1 and C2 suggests that they consist of a fairly uniform lithology lacking impedance contrasts (muds?). In contrast, the well-stratified outer levees are interpreted to consist of interbedded fine-grained turbidite muds, silts, and rare sands that produce moderate impedance contrasts.

Contemporaneous inner and outer levee deposition is accomplished in one of two ways. Either there is an alternation of large and small flows, resulting in contributions to the outer and inner levees during the passage of each respectively, or individual flows contribute sediment to both the inner and outer levees at the same time, but from different parts of the flow. It is difficult to imagine how the passage of alternating large and small flows would result in an acoustically transparent inner levee, therefore the latter mechanism is preferred for Model A. In this case, Model A would only work if mixed sediment (mud, silt, fine-grained sands) in the thicker and more turbulent head and body of the flow were preferentially deposited on the outer levees, whereas the muddy sediment in the thinner, less turbulent tail of the flow were preferentially deposited on the inner levees.

The second end-member possibility (end-member Model B) is that outer levees were deposited during an initial bypass phase corresponding to the incision of the

erosional fairway and continuing during the accumulation of broader HARs near the base of the CLS. This phase probably represents a time where the largest, most erosive flows traveled down the channel. The progressive widening of conjugate outer levee crests may be due to a gradual increase in flow size (and hence the walls are erosional), or perhaps represents an “angle of repose” for a given rheology of the outer levee wall during a period of channel undercutting. In either case, slumps from the outer levee walls might be expected to contribute to the broader HARs near the base of the system during this period. In this model (B) deposition of the inner levees represents an “**under-fit**”, confined stage, after the bathymetric expression of the channel was already established by earlier flows.

During the under-fit stage, HARs are narrower and inner levees are deposited, onlapping and stabilizing the erosional fairway or outer levee walls. Inner levees in this model are presumed to originate from smaller turbidity currents confined between the outer levee walls. The difference in acoustic character between the inner and outer levees according to end-member model B, then, is the temporal differences in the types of flows transmitted through the channel (i.e. their size, composition, and perhaps initiation mechanisms). During the early incision phase, flows passing through the channel are inferred to have been larger, more erosive, and compositionally mixed, whereas flows passing through the channel during the “under-fit” stage are inferred to be smaller and less erosive. This model has significant implications for temporal changes in the character of lobe deposits at the mouth of the channel as the channel-belt evolves, and may be linked to sea level history. Results from Benin-major, described next, clearly support end-member Model B.

Data from the proximal Indus Fan provide useful two-dimensional information about the architecture of large CLSs in upper fan settings, but questions still remain about the three dimensional character of HARs and other elements, as well as their temporal evolution. Detailed 3-D seismic investigations were used to study the cross-sectional and planform architecture and evolution of the Benin-major CLS, located on the western Niger Delta slope. The Benin-major CLS has a similar architecture as the systems

described above and therefore provides new insight into observations made from 2-D seismic data.

6.3 Benin-major CLS

The Niger Delta is located along the western margin of Africa in the Gulf of Guinea. It covers an area of about 75 000 km² and consists of a prominent regressive clastic wedge supplied by the modern Niger River and its ancestral counterparts (Doust and Omatsola, 1989). The second study area is located on a relatively undeformed portion of the western Niger Delta slope, between water depths of 850 and 1900 m (Figure 6.9). The Benin-major CLS, named here because of its up-dip proximity to the modern Benin River (as identified by Allen, 1964), is located within the upper 500 ms of strata in the study area (Figures 6.9 - 6.11). The precise age of the system is uncertain, but given its shallow burial depth, it is believed to have been active in the Pleistocene.

6.3.1 Data and methodology

A large 3-D seismic volume, located on the mid-slope of the western Niger Delta, covers an area of 1250 km² (25 x 50 km). Bin spacing is 25 x 12.5 m and frequency roll-off is near 65 Hz (approximately a 7 m vertical resolution). The 3-D seismic volume captures a 54 km long segment of the Benin-major CLS. The data also encompass a much smaller, slightly older CLS, herein named the Benin-minor CLS. The most detailed study was carried out on a smaller subset of the 3-D seismic survey covering an area of 360 km² and a 23 km long segment of the Benin-major CLS, between 850 and 1400 m of water (Figure 6.9).

Both amplitude and dissemblance 3-D seismic volumes were used to interpret the Benin-major CLS. Because the slope has a dip of about 1°, the modern sea floor was used as a datum for flattening and to generate horizon-slices. In the detailed study area, the Benin-major CLS has little remaining bathymetric expression and the sea floor marker is relatively flat lying (Figures 6.9, 6.10b). To eliminate local irregularities, a smoothing filter was applied to the horizon. Mapping of individual stacked channel-forms within the detailed study area confirms that their thalwegs are roughly parallel to the modern sea floor. Therefore, when the sea floor horizon is used to generate horizon-

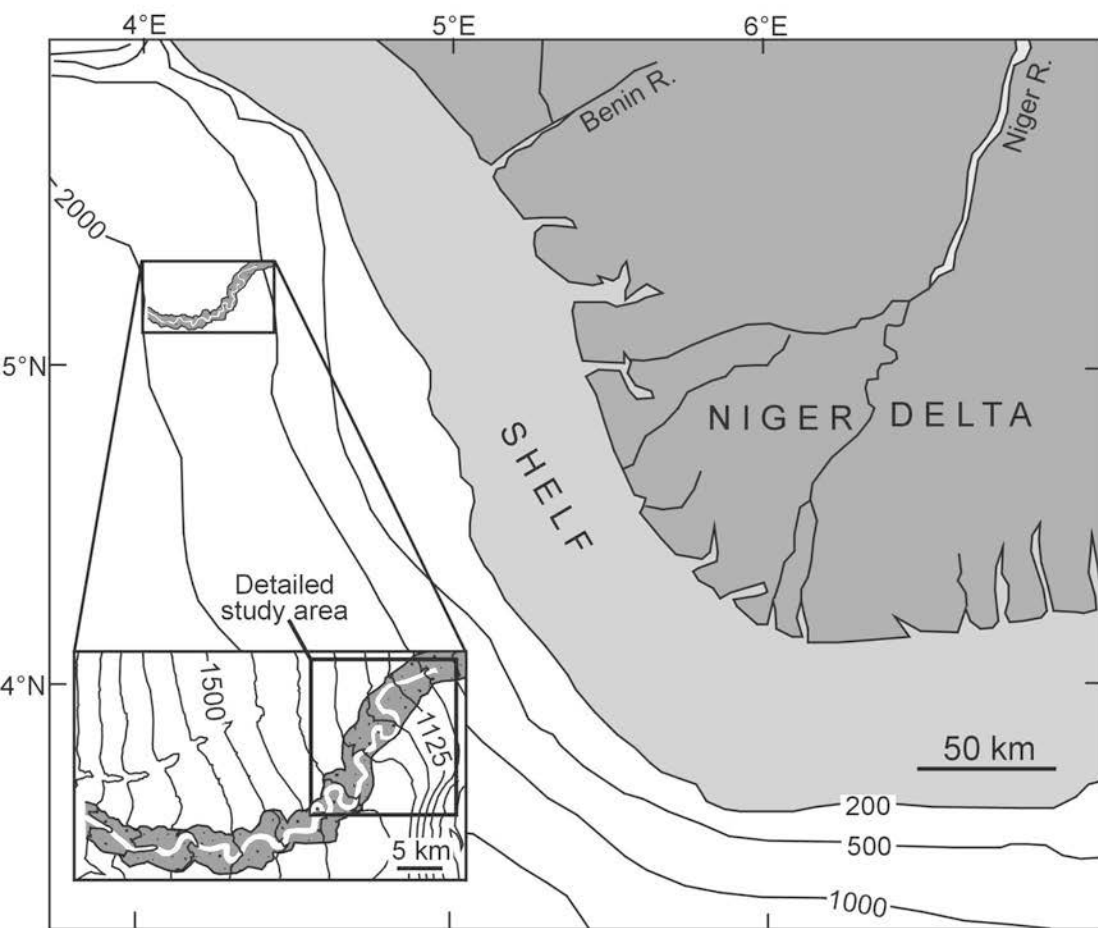


Figure 6.9 Regional location map of Niger Delta, and the Benin-majors channel-belt located on the western slope (inset shows close-up). Dark shaded zones represent locations dominated by inner levees and HARS. The sinuous white channel represents the final channel position prior to the abandonment of the system. The location of the smaller 3-D seismic sub-set (the detailed study area) is shown in the inset. Isobath contours are in meters.

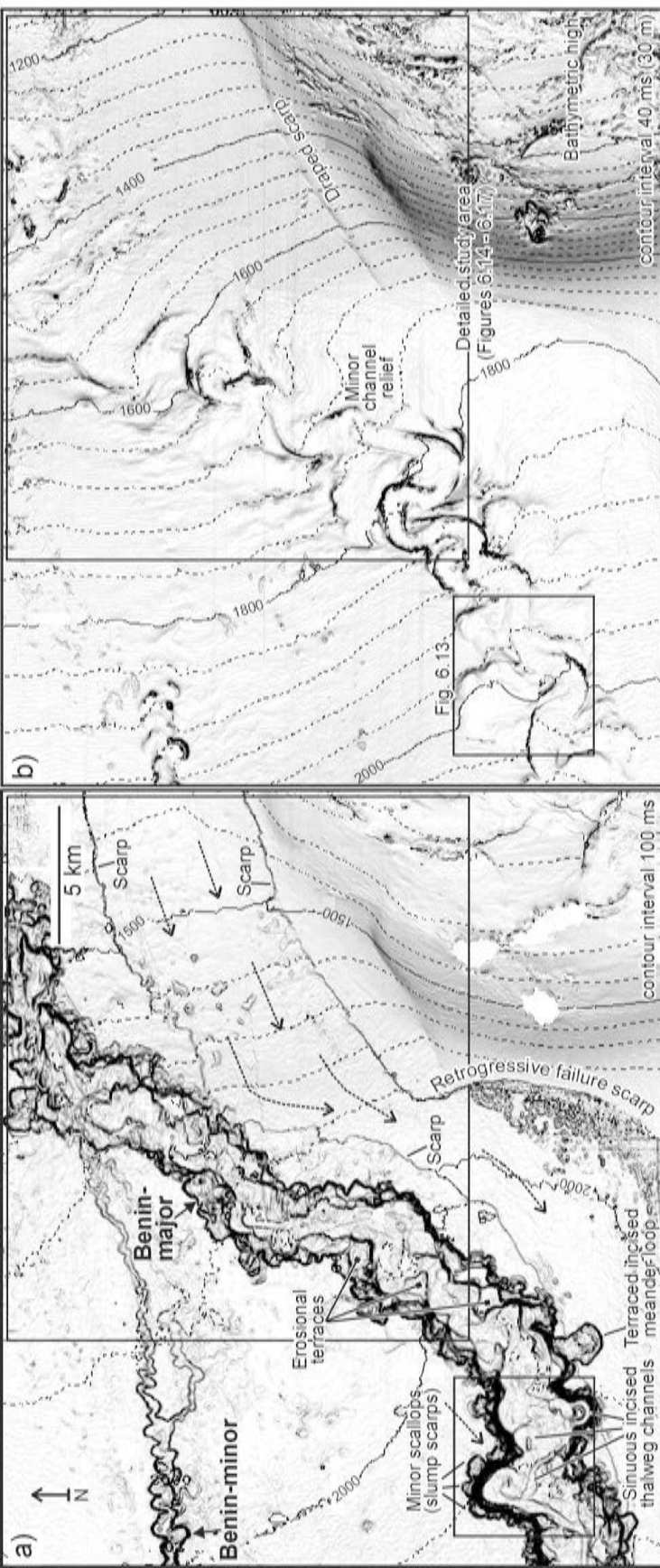


Figure 6.10. a) Contoured dip map from the erosive base of the Benin-major CLS, mapped along the base of the outer levees that flank the system. The surface represents a period of significant slope instability. The failure scarps define a corridor through which mass transport deposits passed. Dashed arrows indicate the orientation of linear scours believed to be related to the passage of mass transport deposits. Note the much smaller Benin-minor CLS (to the northwest) that incises the same surface that displays the failure scarps and linear scours. b) Contoured dip map of the sea floor showing the modern day expression of the abandoned Benin-major CLS and surrounding area. Note that the failure scarps and the Benin-major CLS have little remaining relief. A single, sinuous channel is present along the axis of the Benin-major CLS.

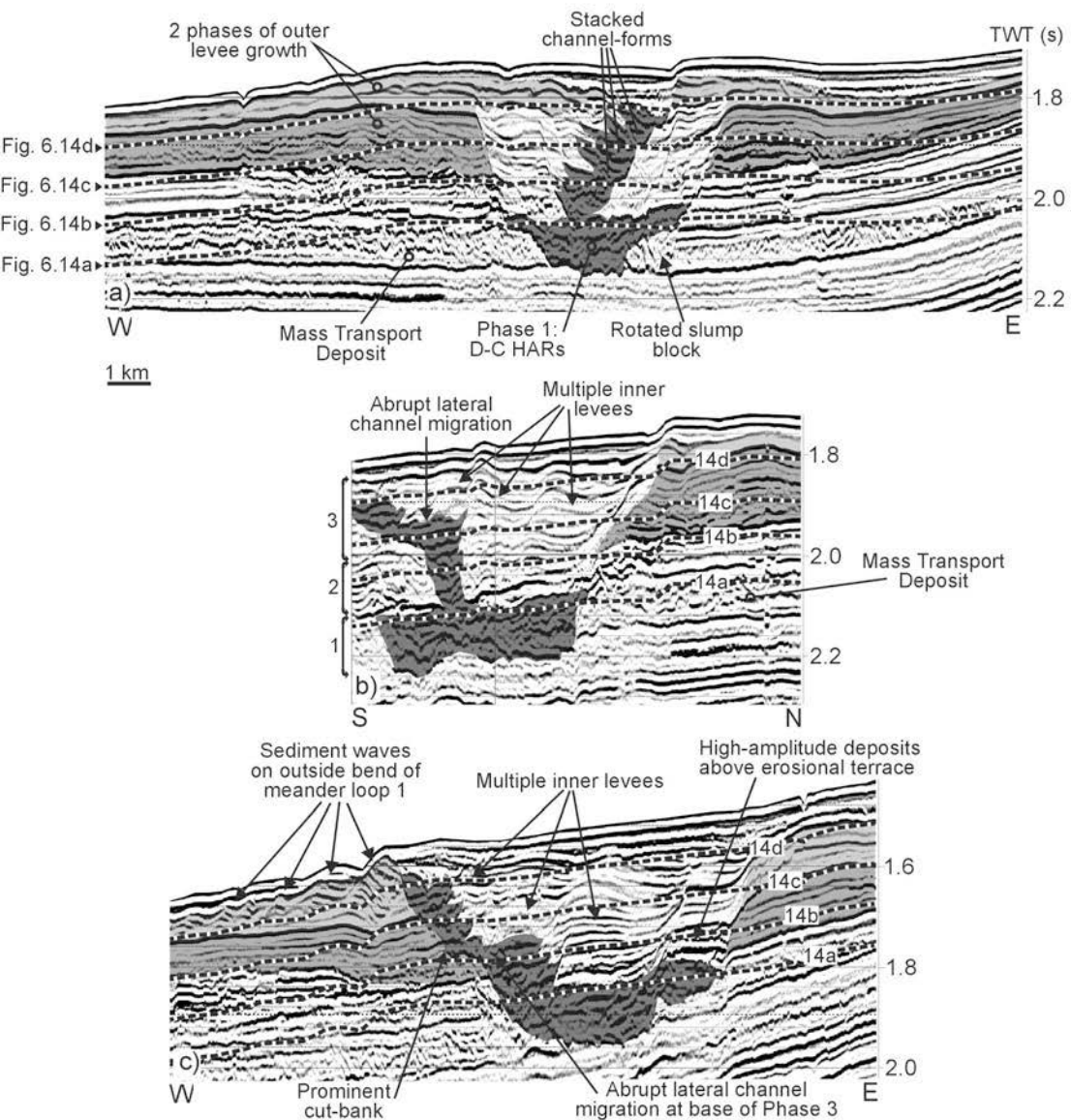


Figure 6.11. Interpreted seismic profiles across Benin-major. a) Profile roughly perpendicular to the axis of the erosional fairway, showing wide D-C HARs near the base of the system, and narrow HARs bordered by inner levees above. Narrow HARs migrates gently to the east (right) creating a cut-bank and a sharp transition between the channel deposits and inner levees. On the opposite side, an inter-fingering of channel deposits and inner levees is observed. Two phases of outer levee growth are recognized. b) Interpreted profile perpendicular to the direction of meander loop 3, showing an increase in HAR width corresponding to an increase in lateral channel migration between 1920 and 1980 ms (middle of phase 3). Multiple phases of inner levee growth are recognized opposite the cut-bank. c) Interpreted profile across migrating channel segment at meander loop 1, showing multiple phases of inner levee growth and a period of abrupt channel migration (base of phase 3). Rapid migration of this meander loop, therefore takes place at a deeper level than in the loop shown in figure 6.11b. Locations shown in Figure 6.15.

slices, it crosses roughly the same stratigraphic position within each stacked channel-form.

6.3.2 *General channel-levee architecture*

The Benin-major CLS has a maximum thickness of 450 ms (about 350 m - at the channel-axis), and a distance of 3.0 - 4.5 km between outer levee crests. It is therefore about half the width and thickness of the CLSs described earlier for the Indus Fan. Similar to the CLSs on the Indus Fan, it consists of an erosional fairway at its base, and is bordered by outer levees. These elements confine the channel-belt comprised of inner levees, HARs (both wide and narrow), coherent rotated slump blocks, and incoherent slump masses (Figure 6.11). The erosional fairway is about 170 m deep in the detailed study area, reaching 295 m deep near the western limit of the 3-D seismic volume (west of the detailed study area).

Outer levees have a maximum thickness of about 200 m and consist of continuous moderate to low amplitude seismic reflections that converge away from the channel-axis. They are similar to, but less steep than, the outer levees on the Indus Fan. A prominent, high amplitude seismic marker, mapped across both the eastern and western outer levees, separates it into a lower unit and an upper unit (Figure 6.11a). The lower outer levee consists of dominantly continuous seismic events. The upper outer levee contains some discontinuous seismic events and has locally developed sediment waves that are most prominent near the outer bend of meander loops 1 and 3, where flow stripping is inferred to have been an important process (e.g. Figure 6.11c; see Piper and Normark, 1983; Normark et al., 2003).

The margins of the erosional fairway and outer levee crests are erosionally scalloped, as are the boundaries between successive periods of inner levee growth. A wide zone of D-C HARs is located just above the erosional fairway, near the base of the system, passing abruptly up-section into a narrower hybrid of D-C HARs and stacked channel-forms.

6.3.3 *Evolution of the channel-belt*

In the detailed study area (Figure 6.10), the Benin-major CLS shows an evolution that can be divided into a period of incision followed by a three-phase fill history. Each fill phase is defined on the basis of planform channel geometry, channel-stacking architecture, and the nature of overbank deposits.

Incision

Prior to vertical incision of the Benin-major erosional fairway, erosional and depositional features associated with slope instability dominated the study area (Figure 6.12a). Two parallel scarps, each about 20 m high, define a corridor through which slides passed over a failure plane (Figure 6.10a). An arcuate shaped retrogressive failure scarp is observed west of the bathymetric high located at the southeastern corner of Figure 6.10a. Incoherent deposits accumulated above the failure plane at the base of the scarp. In most other areas, the failure plane appears to have been largely bypassed by mass wasted material. Several linear scours, some extending for greater than 10 km, are observed on the floor of the failure plane. Nissen et al. (1999) interpreted these scours as glide tracks related to the passage of slide blocks. Posamentier et al. (2000) provided an alternate explanation, interpreting similar features offshore eastern Kalimantan (Indonesia) as grooves that developed at the erosive base of large mass transport deposits. Both interpretations are consistent with a period of mass wasting.

In the northwestern corner of Figure 6.10a, two small leveed tributaries join the Benin-minor CLS. This much smaller system has a prominent erosive base that incises the same stratigraphic level as the failure scarps. The development of Benin-minor terminated during, or shortly after, prominent vertical incision of the Benin-major erosional fairway. The fairway erodes through a combination of parallel-bedded, in places polygonally faulted, strata inferred to correspond to mud-prone slope sediment, and chaotic units corresponding to mass transport deposits (Figure 6.11).

A dip map (draped by time-structure contours) of the erosional fairway at Benin-major reveals several important elements (Figure 6.10a). The base of the erosional fairway consists of several cross-cutting, incised channels up to 350 m wide. They have a sinuous planform geometry, in some cases with sharp meander bends. One incised

meander loop is terraced about 160 m above the thalweg of the erosional fairway, suggesting that channels had a sinuous planform geometry even during the earlier stages of incision (Figure 6.10a). Several relatively horizontal erosional terraces, ranging in height from 20 to 100 m above the thalweg, are also observed on the floor of the erosional fairway.

Scallops of various dimensions characterize the margins of the erosional fairway. The largest scallops probably originated from direct cut-bank erosion from incised sinuous channels at the base of the erosional fairway. Prominent incised meander bends on the floors of two large scallops in Figure 6.13a support this interpretation. Some large and small scallops also originated from slumps that left behind curved slump scars. Rotational slump blocks, forming crescent-shaped inclined or flat benches, are observed adjacent to some scallops. Most are inferred to have formed during vertical incision (and hence destabilization) of the erosional fairway (see Friedmann, 2000; Pirmez et al., 2000; Mayall and Stewart, 2000).

Fill - Phase 1

The interval directly above the floor of the erosional fairway is complex. It consists of a wide zone of D-C HARs with an overall tabular geometry, but also contains patches of low amplitude seismic facies, locally developed continuous high amplitude reflections, and intact to semi-intact rotated slump blocks (Figures 6.11, 6.12c, 6.14a, 6.15).

In some areas, D-C HARs are located directly above the erosive base of the fairway; in other areas they are located above transparent to chaotic units interpreted as mass transport deposits (Figure 6.13d). Horizon-slices indicate that D-C HARs consist of discontinuous remnants of sinuous channels that are largely confined within the deepest parts of the erosional fairway (Figures 6.14a, 6.16a). A single channel cannot be mapped down the length of the system. The discontinuous channel remnants are inferred to originate from the self-cannibalizing nature of laterally migrating channels with limited vertical aggradation. Cross-sections indicate that periods of cut-and-fill were common within the phase 1 fill, sometimes resulting in the development of erosional terraces. Continuous very high amplitude seismic reflections and/or low amplitude inner levee

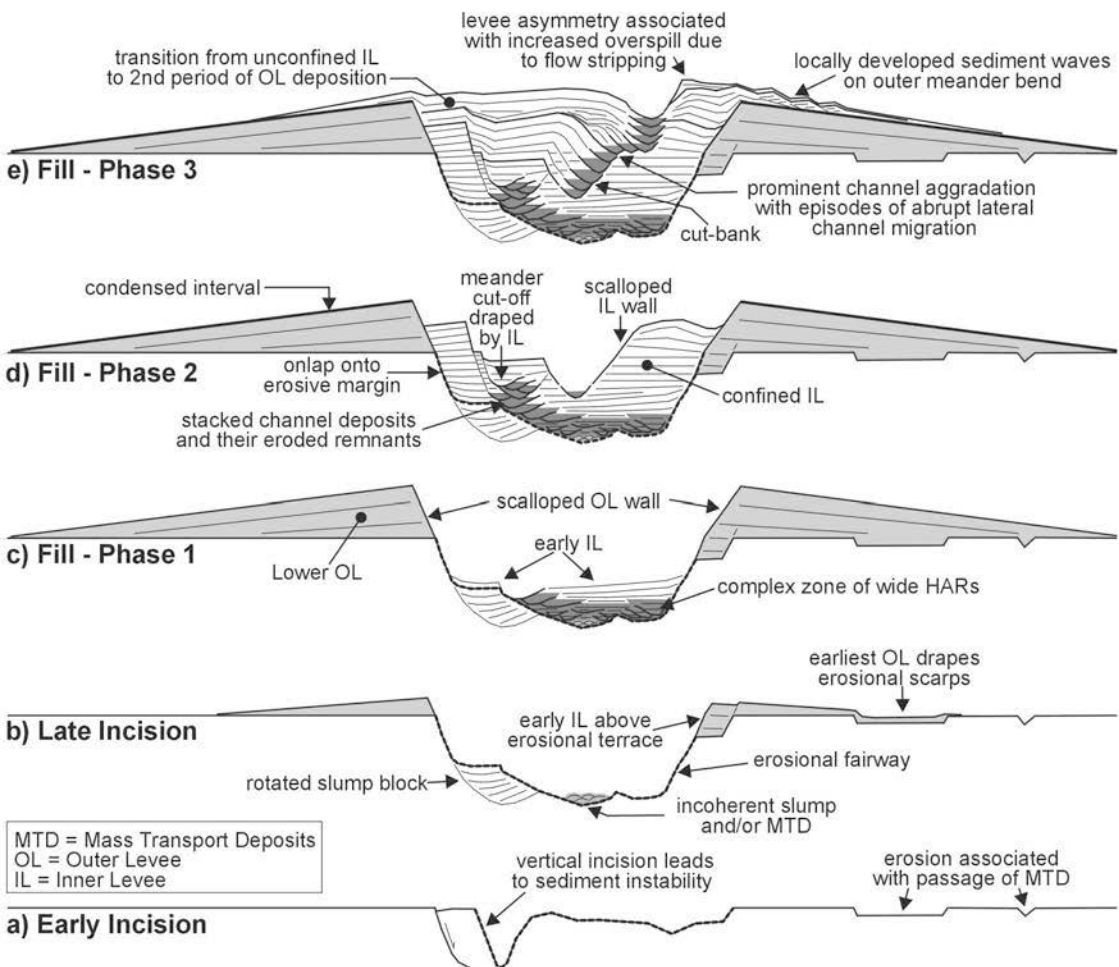


Figure 6.12. Generalized schematic drawing showing the incision (a-b) and three-phase fill history (c-e) of the Benin-major channel-levee system. See text for details.

deposits overlie some erosional terraces (e.g. Figure 6.13). Patches of low amplitude seismic facies within the phase 1 fill may be the remnants of mass transport deposits, dissected during periods of channel re-incision, or the remnants of early inner levees. Such mud-prone deposits act as baffles to the flow of hydrocarbons, and are therefore an important consideration when assessing the reservoir performance of the phase 1 fill.

Fill - Phase 2

Phase 2 is characterized by a period of prominent vertical inner levee aggradation that outpaced channel floor aggradation. The base of phase 2 is defined by the first (deepest) channel that can be mapped down the entire 23 km long segment within the detailed study area (Figures 6.12d, 6.16a). During phase 2, the planform channel geometry exhibits a tortuous sinuosity (average of 1.63, and a range of 1.47 to 1.80 - calculated by dividing the along channel distance by the straight-line distance), with immature meander loops that have a short radius of curvature and short wavelengths (Figures 6.16a). Phase 2 HARs are narrower than phase 1 HARs, and consist of a combination of stacked channel-forms and D-C HARs. Along some channel segments, eroded remnants of channel-forms are observed where they have been incised by an adjacent or overlying one.

Horizon-slices through phase 2 channel-axis deposits show sporadic changes in the number of channel bends and in sinuosity. These changes can be abrupt, the result of meander cut-offs, or subtle, the result of slight changes in the thalweg path, with some channel reaches shifting from slightly sinuous to straight, and vice versa (Figure 6.16). Two meander cut-offs are observed, each results in a decrease in the number of channel bends and a corresponding decrease in sinuosity (Figures 6.14b, 6.16b). Both cut-offs were later draped by inner levees (e.g. Figure 6.14c).

The most pronounced inner levees appear to have developed during phase 2. Inner levee “terraces” were at a maximum height above the channel thalweg, overlapping and to some extent stabilizing, the scalloped margins of the erosional fairway. Sharp, erosive channel walls were located on one or both sides of the narrow channel-axis. In some areas, minor scallops along the channel walls are interpreted as slump scarps formed when sediment from the inner levees failed into the channel-axis. In other

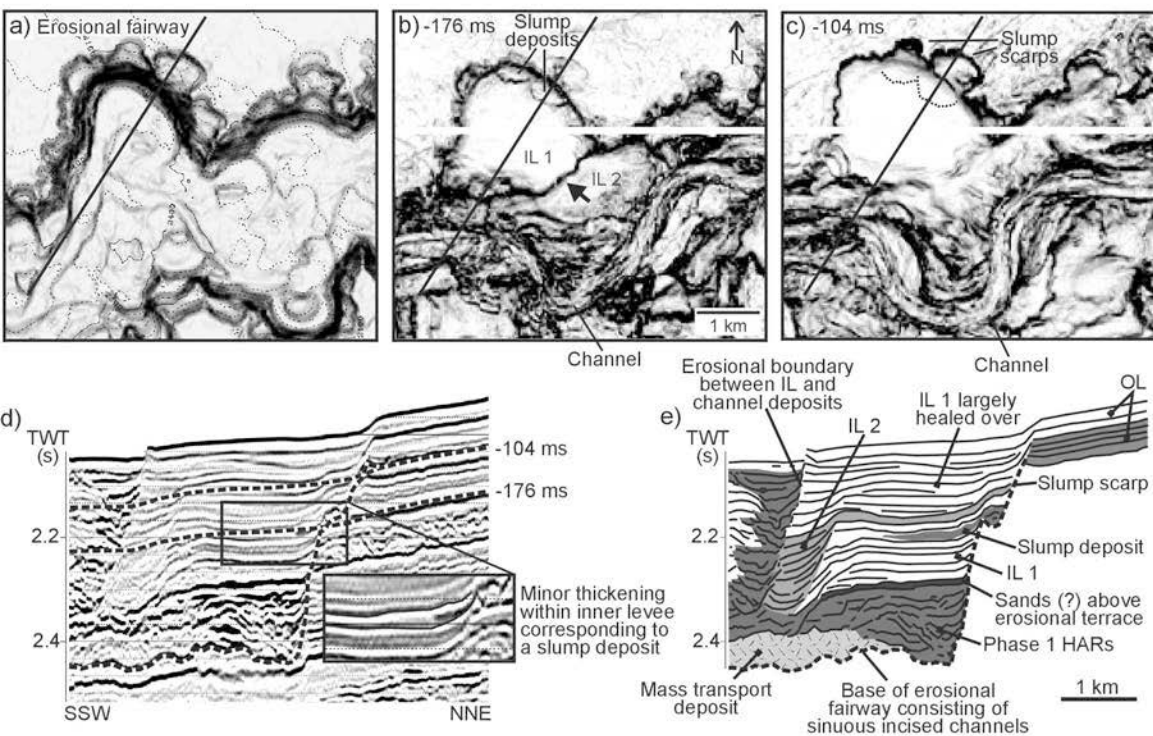


Figure 6.13. a) Dip map of the base of incision of the erosional fairway at Benin-major. Note the two incised meander loops located at the base of the prominent scallops. The large arcuate scallops are interpreted to have formed from cut-bank erosion (probably accompanied by slumping) associated with the incised sinuous channel. The smaller scallops are interpreted as slump scarps that developed sometime after the initial incision of the erosional fairway. b) Dissemblance horizon-slice at 176 ms below the sea floor showing potential slump deposits within inner levee 1 (IL 1), suggesting that the smaller-scale scallops developed after inner levee deposition had begun. c) Dissemblance horizon slice at 104 ms below the sea floor crossing channel and inner levee deposits, and also crossing the smaller-scale scallops. d) Seismic profile and corresponding line drawing (e) across the northern margins of the system. Two major periods of inner levee growth are recognized as well as a slight thickening within IL 1, corresponding to the interpreted slump deposit associated with the smaller-scale scallop (also crossed by the profile). The boundary between the first and second inner levees is sharply defined in (b) (arrow), whereas it is barely discernible in (c) where the horizon slice no longer crosses the boundary between two inner levees. Location shown in Figure 6.10.

locations, minor scallops along the margins of the erosional fairway developed as sediment was shed from the outer levee and erosional fairway walls and accumulated above inner levee “terraces” (e.g. Figures 6.10a, 6.13). In Figure 6.13, for example, two minor scallops are observed along the margin of the system. A subtle thickening within the adjacent inner levee (Figure 6.13d) is interpreted as the corresponding slump deposit (Figure 6.13e).

The cross-sectional and planform geometry of the system during phase 2 is inferred to have resembled that of the modern “empty” terraced upper fan channel-belts on the Zaire (Droz et al., 1996) and Indus fans (Von Rad and Tahir, 1997).

Transition - Phase 2 to Phase 3

The planform channel geometry established in phase 2 transforms abruptly into a much different channel planform geometry by phase 3. The transition from phase 2 to phase 3 is abrupt, marked by a decrease in the number of channel bends. The planform geometry evolves rapidly from a tortuous geometry with 18 channel bends (at 224 ms below sea floor), to a much straighter geometry with 11 channel bends (at 192 ms below sea floor - Figure 6.16b). Planform channel re-adjustments create a “rope-like” fabric on dissemblance slices.

Although the overall sinuosity decreased as the channel-axis straightened, several meander loops maintained their form during the transition to phase 3 (e.g. loops 1, 2, 3 and 4 - Figure 6.15). In fact, loops 1 and 2 show an abrupt increase in their radius of curvature, with a corresponding abrupt shift in the channel position at the bend, opposite to the trend observed elsewhere (Figure 6.15). The period of accelerated channel migration is expressed in cross section as a localized lateral offset in the HARs (Figure 6.11c).

Fill - Phase 3

In comparison to phases 1 and 2, the overall channel floor aggradation rate increased during phase 3 (relative to the inner levee aggradation rate). Phase 3 begins at 192 ms below the sea floor, with an abrupt increase from 11 to 14 channel bends in the lowermost 24 ms, above which the system shows a consistent number of channel bends

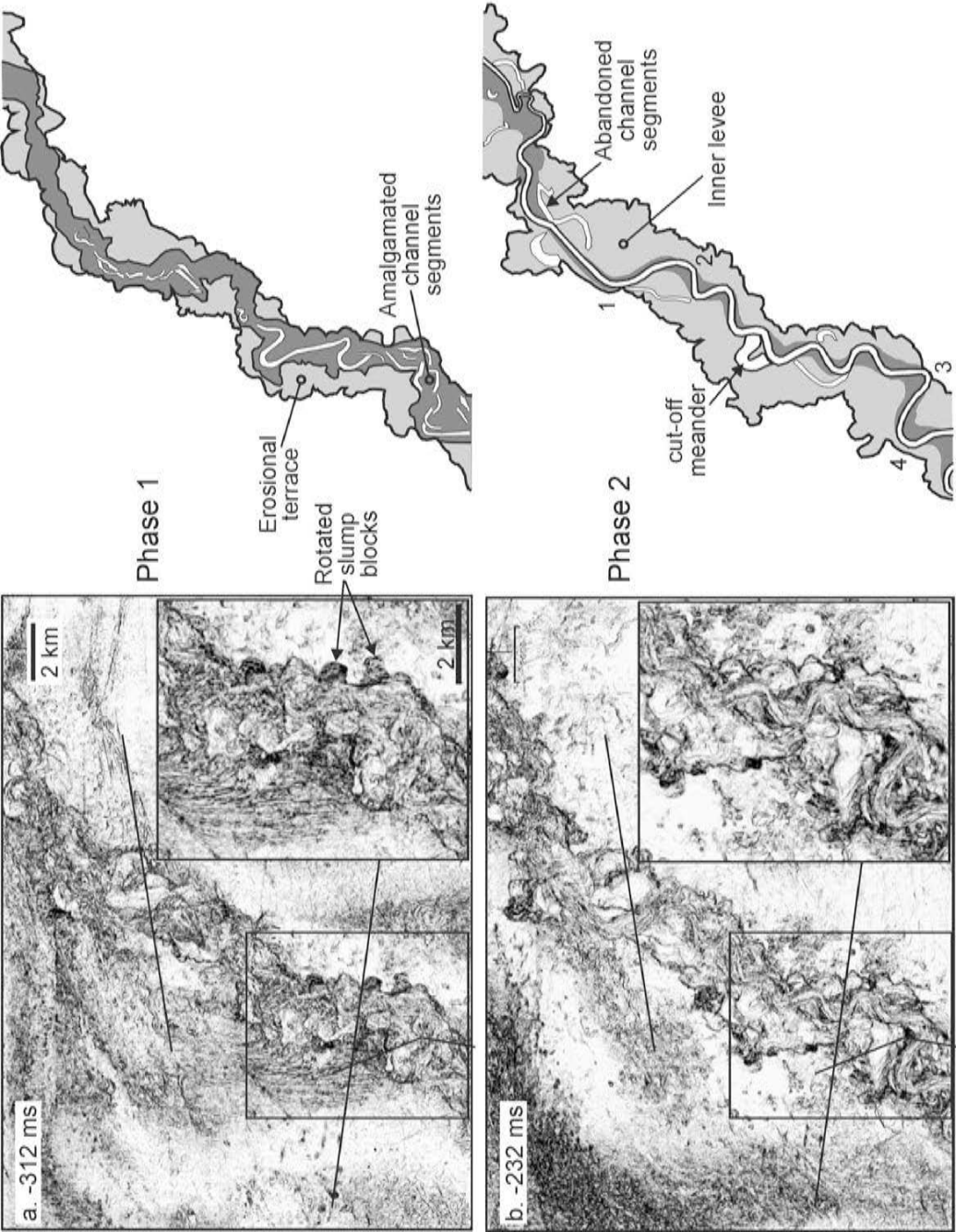
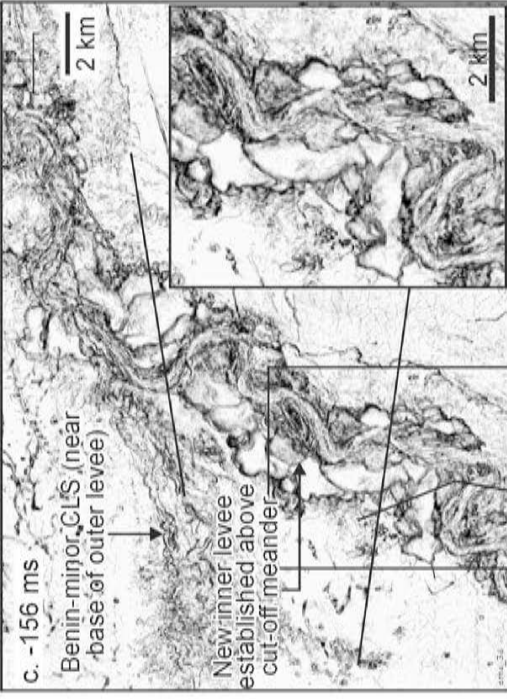
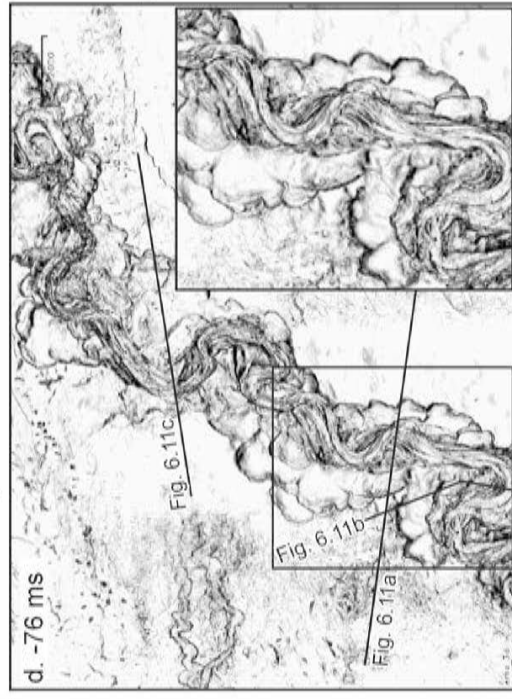
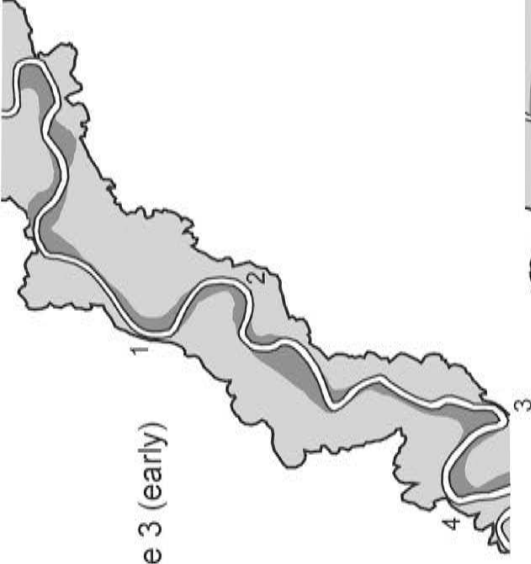


Figure 6.14. (see next page for caption)



Phase 3 (early)



Phase 3 (late)

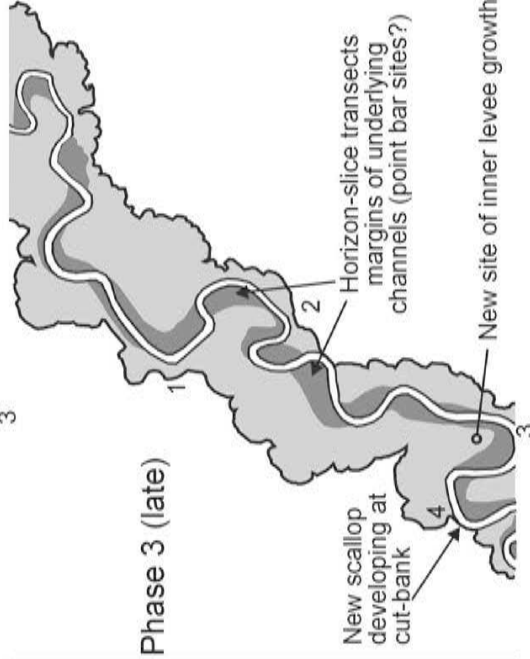


Figure 6.14. Series of uninterpreted dissemblance horizon-slices, flattened on the seafloor with corresponding line drawings at a) 312 ms (phase 1), b) 232 ms (phase 2), c) 156 ms (phase 3), and d) 76 ms (phase 3) below the sea floor. See text for details.

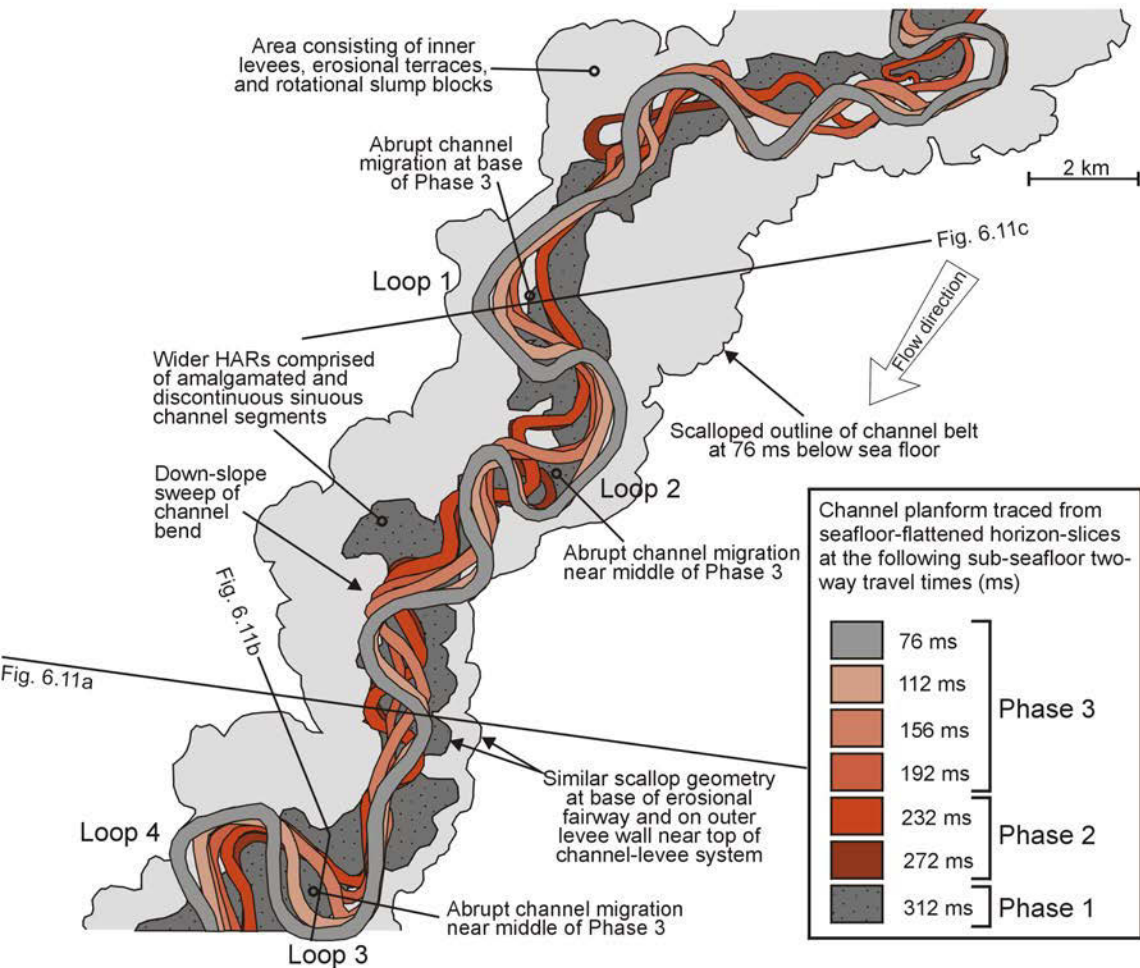


Figure 6.15. Drawing showing the planform geometry of the stacked channel-axis deposits (HARs) every 36 to 40 ms below the sea floor (from seafloor-flattened dissemblance slices). Note the overall down-channel migration and the abrupt jumps at some meander loops where abrupt channel-migration has taken place. Channel-axis deposits aggrade and migrate within the scalloped confines of the erosional fairway, where inner levees flank the phase 2 and phase 3 channel deposits.

(14) through its remaining history. Although the number of channel bends remains constant, the planform geometry of the stacked channel-forms evolves during aggradation (Figures 6.12e, 6.16a). Phase 3 is characterized by narrow channel-forms that stack near vertically, locally showing abrupt lateral offset (migration) and incision between channel-forms. Successive channel-forms commonly migrate both in the down-channel (sweep) and cross-channel (swing) direction, with only one meander loop showing a component of up-dip migration (loop 4 - Figure 6.15).

There is a consistent increase in sinuosity through time, from 1.65 at the base of phase 3 to a maximum of 2.07 near the top (average 1.9). Near the middle of phase 3, a period of accelerated meander growth rate occurred (similar to the transition from phase 2 to 3 in loops 1 and 2). This is particularly evident at meander loops 2 and 3, which show a dramatic increase in the radius of curvature as the channel-axis migrated laterally, eroding rapidly into the cut-bank (Figure 6.15). A vertical profile perpendicular to the direction of channel migration on meander loop 3 shows an increase in the width of the HARs, and multiple phases of inner levee growth opposite to the cut-bank, occupying former channel positions (Figure 6.11b). On dissemblance horizon-slices, older channel positions (now occupied by inner levees) are observed on the inside bend of meander loop 3 (Figures 6.14d, 6.17). It is unclear whether this inner bend formed as a result of lateral accretion (similar to the Lateral Accretion Packages described by Abreu et al., in press), or whether the inner bend formed as a result of multiple periods of cut-and-fill, with channels migrating into a cut-bank (e.g. as in Figure 6.8b). The limitations of seismic resolution in this case preclude distinguishing between the two.

The average sinuosity increased at a slower rate (relative to aggradation) near the top of phase 3, and eventually decreased as the system was abandoned (Figure 6.16b). Because channel floor deposits aggraded at a faster rate than the inner or outer levees, there was a progressive decrease in channel relief during phase 3. The final channel had very little relief, and thus if a particularly large flow had traversed the channel, it probably would not have been contained between the levee crests, and may have led to an avulsion. The final abandonment of the Benin-major CLS occurred when a mass transport deposit, originating from the east, was deposited above the southeastern upper outer levee. The mass transport deposit has a maximum thickness of about 60 m, and

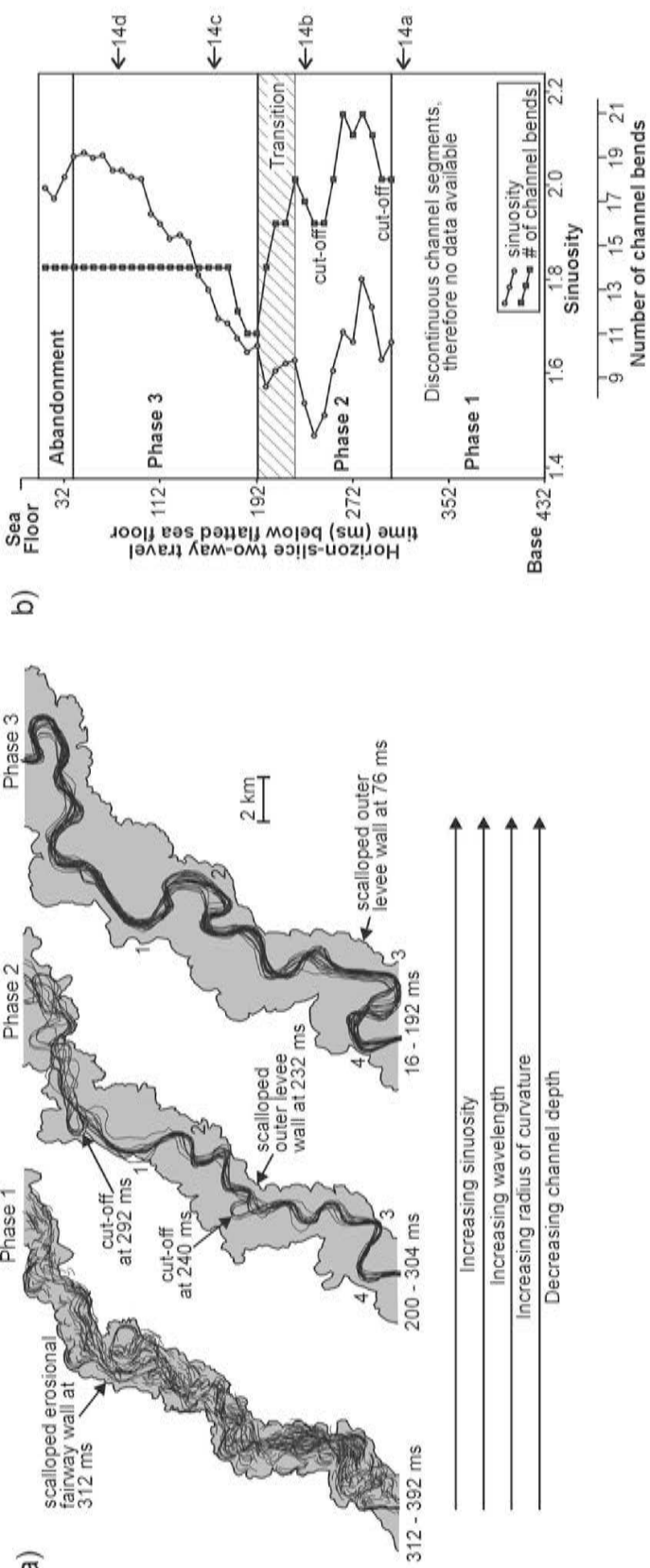


Figure 6.16. a) Channel-centerline plots every 8 ms showing three phases of channel deposit evolution at Benin-major. Phase 1 corresponds to the wide zone of HARs deposited within the erosional fairway and is inferred to consist of amalgamated channel segments and slump deposits (originating from failures along the erosional fairway and/or outer levee walls). Channel paths show little vertical aggradation and are self-cannibalizing with significant lateral migration, resulting in a tabular zone of HARs. Phase 2 corresponds to channel geometries displaying a tortuous sinuosity, with immature meander loops that have a short radius of curvature and wavelength. The number of meander bends and sinuosity change sporadically due to subtle changes in the thalweg path and meander cut-offs. The transition from phase 2 to phase 3 occurs abruptly as the channel goes through a period of straightening. Phase 3 begins when the channel-planform geometry has stabilized, with a consistent number of meander bends and an overall increase in sinuosity, from about 1.65 to 2.07. Phase 3 channel deposits show a progressive increase in meander wavelength, radius of curvature, and channel-floor aggradation rates (relative to inner levees), and ends when the system is abandoned. b) Chart showing vertical trends in the number of channel bends and sinuosity, from the base of Benin-major to the modern sea floor. Note the meander cut-offs corresponding to decreases in sinuosity in phase 2 and the abrupt decrease in the number of channel bends during the transition to phase 3. The location of horizon slices in Figure 6.14 are shown on the left.

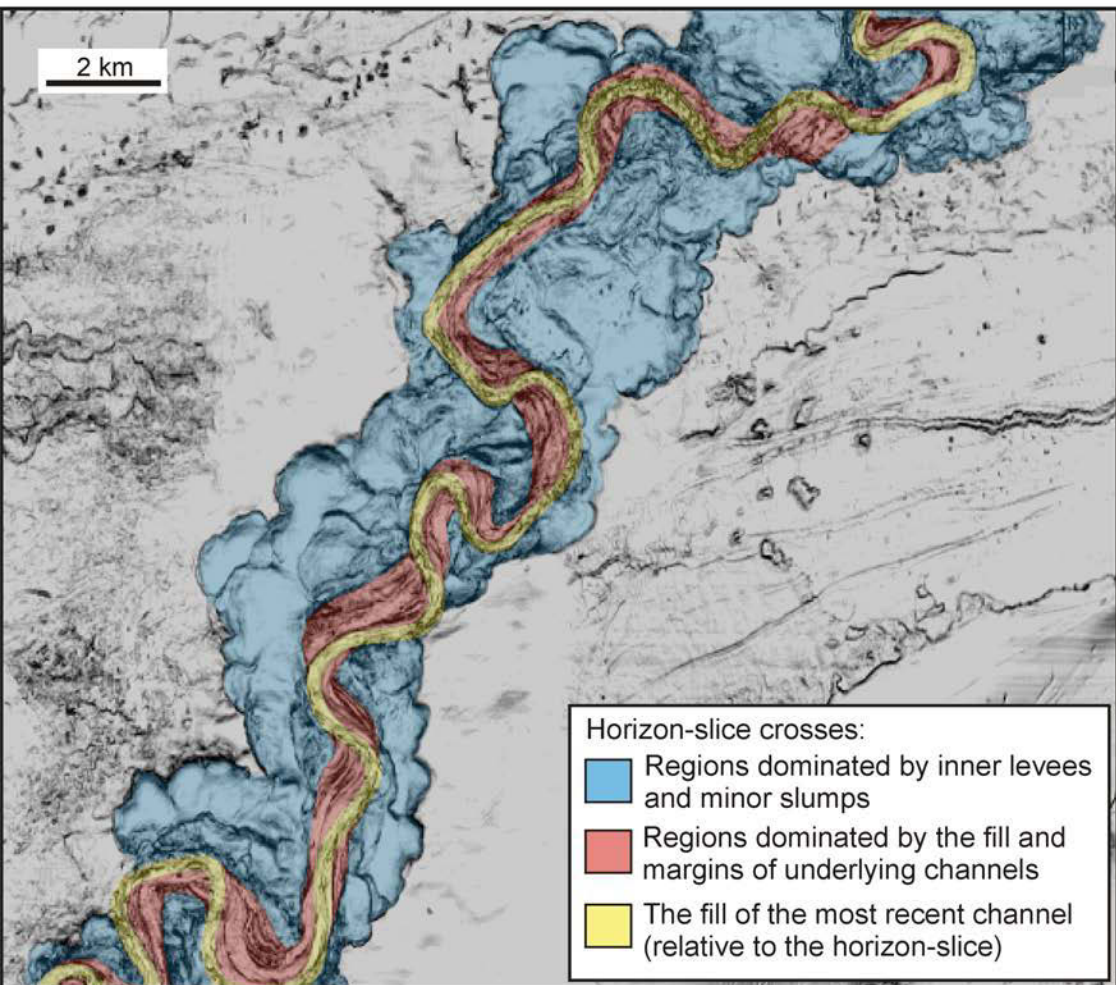


Figure 6.17. Dissemblance horizon-slice at 76 ms below the flattened sea floor horizon. The horizon-slice crosses the stacked channel-forms that occupied the system during phase 3 (yellow and red) as well as inner levee dominated facies that developed during phases 2 and 3 (blue).

appears to have plugged the remaining depositional relief of the youngest channel in the detailed study area (which prior to the mass transport deposit had a depth between 50 and 75 m).

6.3.4 Outer levee deposition

The erosional scarps, linear scours, and the Benin-minor CLS, were all draped by the lower outer levees of Benin-major. Determining the precise timing for the start of outer levee deposition, however, is difficult. Three lines of evidence help to constrain it. First, some scallops observed along the margins of the erosional fairway (e.g. at -312 ms in Figure 6.14a) have the same geometry as much shallower scallops developed along the margins of the lower outer levee walls (e.g. at -76 ms in Figure 6.14d). The same scallop geometry, extending from the incision near the base of the erosional fairway, up to near the top of the lower outer levee walls, implies that outer levee deposition began during the incision of the erosional fairway or the phase 1 fill (Figure 6.15). Second, inner levees associated with the phase 2 fill, onlap the outer levee walls, requiring the outer levees to have formed earlier. Third, on some profiles outer levees drape erosional terraces along the margins of the erosional fairway, implying that the outer levees developed sometime after the earliest incision (e.g. the terraced meander loop in Figure 6.10a is draped by outer levee deposits). The lower outer levees, therefore, appear to have been deposited sometime after the start of vertical incision, but before the phase 2 fill (Figures 6.12b, c).

6.4 Discussion

6.4.1 Upper fan avulsions

Upper fan avulsions are an important control on the architecture of the Indus Fan, and result in an abrupt lateral shift in the canyon mouth position and the deposition of a new CLS adjacent to the old one. At the base of CLC are tabular to sheet-like deposits of variable seismic amplitudes, which have been dissected by the erosional fairways of overlying CLSs. These deposits onlap bathymetric highs (like previous CLSs) and are inferred to have accumulated abruptly during the initial erosion of the canyon (Figure

6.18a). A mass transport deposit also accumulated prior to the development of CLS C1 (Figure 6.18a).

Prior to the first upper fan avulsion, CLS C1 probably consisted of prominent levees on both sides of the erosional fairway and channel-belt (Figure 6.18b). The first upper fan avulsion took place on the eastern side of the complex and resulted in the removal of the eastern levee and some of the channel-belt, whereas the western levee of C1 was preserved (Figures 6.3a, 6.18c). Similarly, the eastern levee of C2 was removed by erosion during the second upper fan avulsion that eventually led to the deposition of C3, whereas the eastern levee draped the remnants of C1 and C2 (Figures 6.3a, 6.18e). The only eastern outer levee that is well recognized near the canyon mouth in CLC C is the one associated with C3, which developed just prior to the abandonment of the complex (Figure 6.3a).

On the upper fan, the stacking architecture of CLSs depends strongly on whether successive avulsions take place on the same side of the complex each time, or whether avulsions occur more randomly, on both sides. All of the complexes in the study area, including C, avulse in a single direction only, either towards or away from the Murray Ridge (e.g. away from the ridge in CLC C - Figure 6.18). In contrast, the most recent complex on the Amazon Fan has undergone upper fan avulsions in both directions and at more variable water depths (Pirmez, 1994). The precise control for this difference is unclear.

In CLC C the process of repeated avulsions on one side of the complex led to the formation of a highly asymmetric compound levee on its western side (Figures 6.3a, b), effectively fortified the western margin of the complex and prevented subsequent systems from avulsing in that direction. Therefore, successive systems are prone to continue avulsing in the same direction until a new canyon is eroded elsewhere on the shelf and slope. Upper fan avulsions have a profound impact on overall fan architecture. They result in the erosion of a significant proportion of the previous system and the subsequent deposition of an entirely new system, adjacent to the old one. The trigger for upper fan avulsions is unclear, but is inferred to be related to the channel-belt aggradation history, perhaps combined with additional more regional controls like eustasy, climate or tectonism (each of which may alter sediment supply).

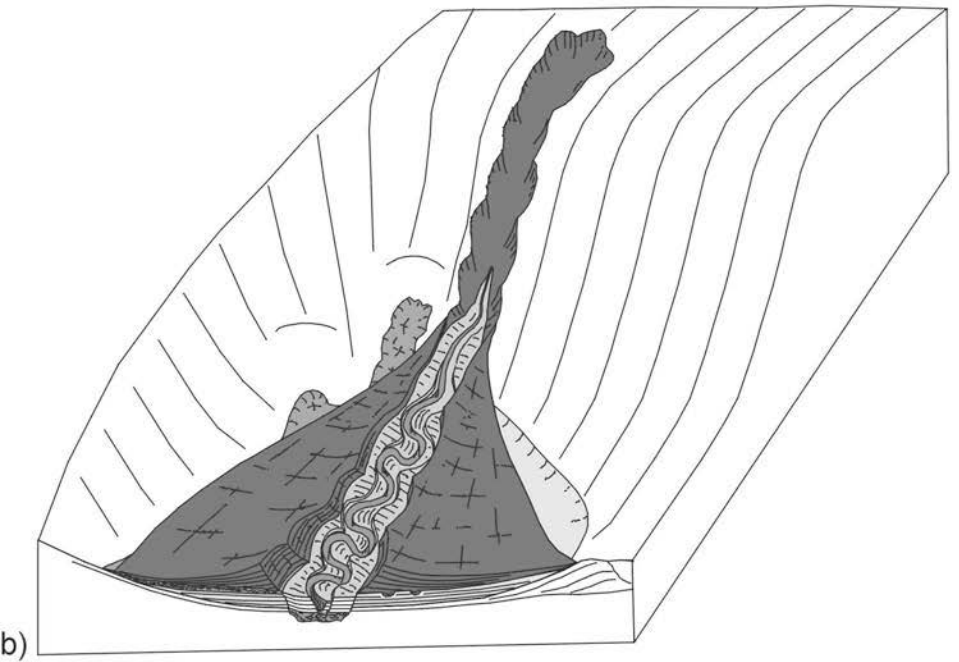
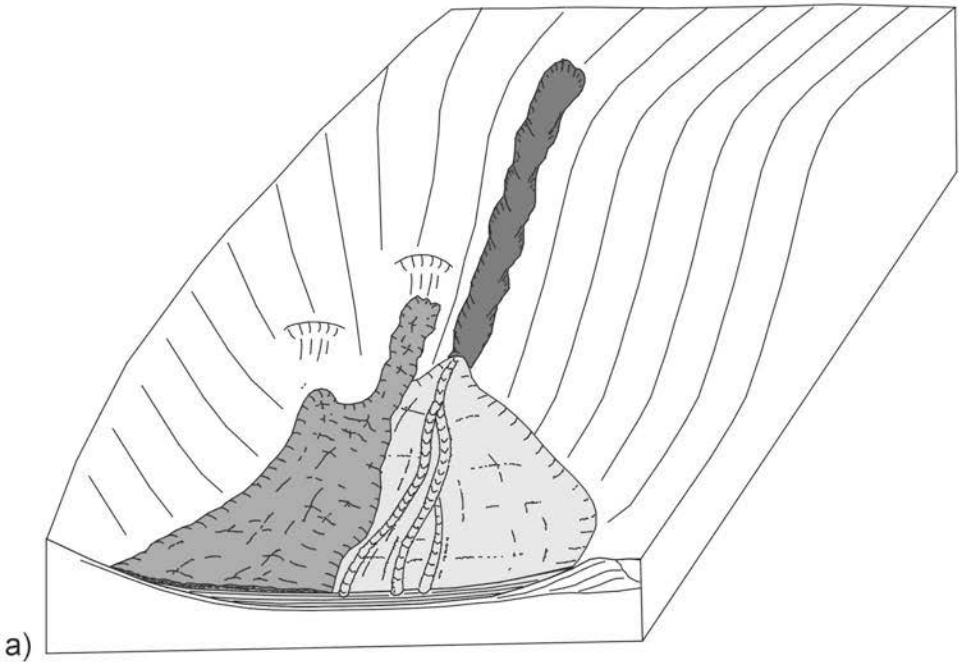


Figure 6.18. (see 6.18e for caption)

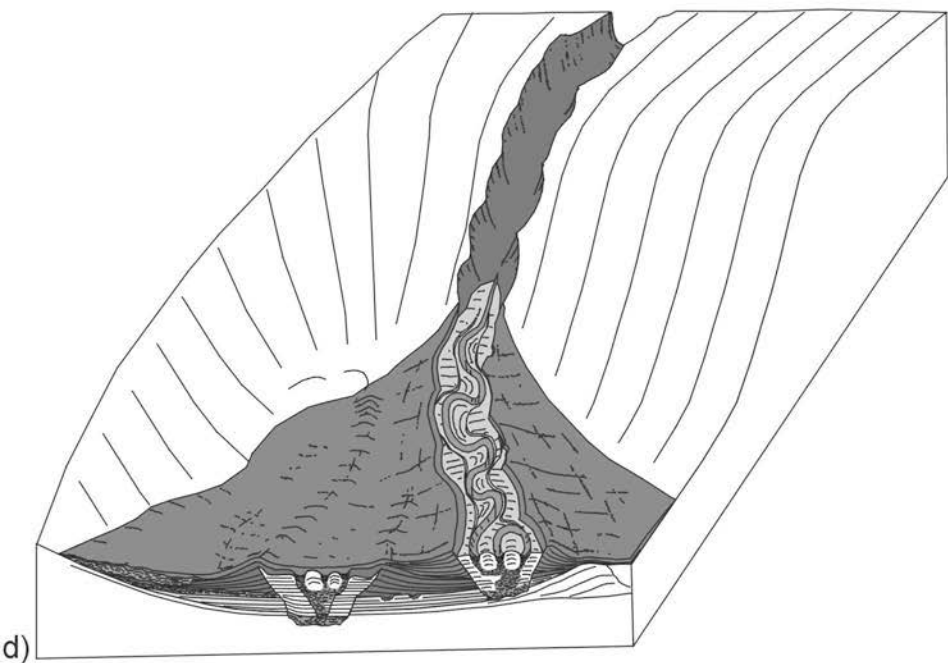
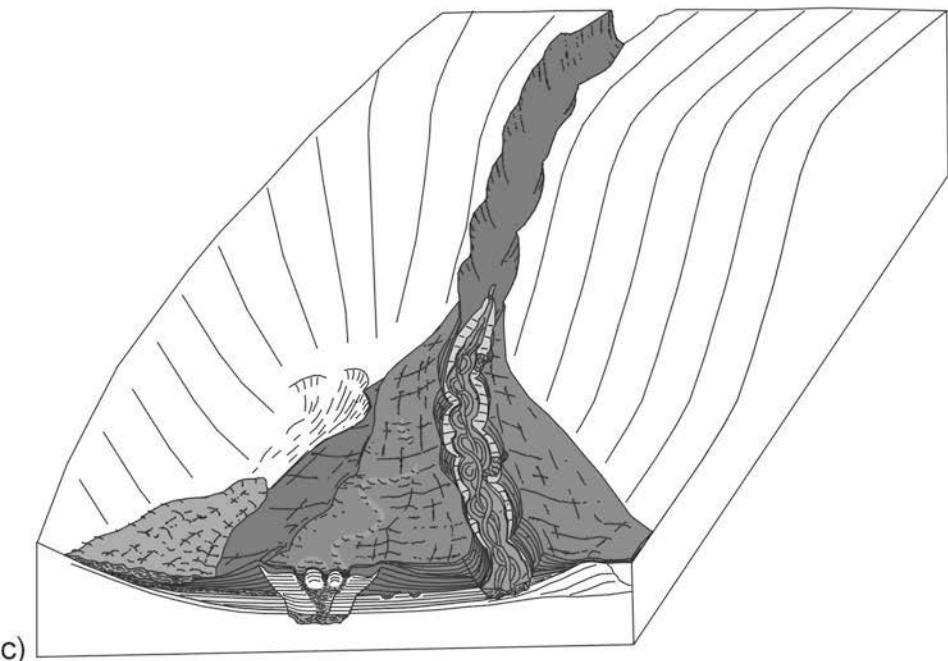


Figure 6.18. continued (see next page for caption)

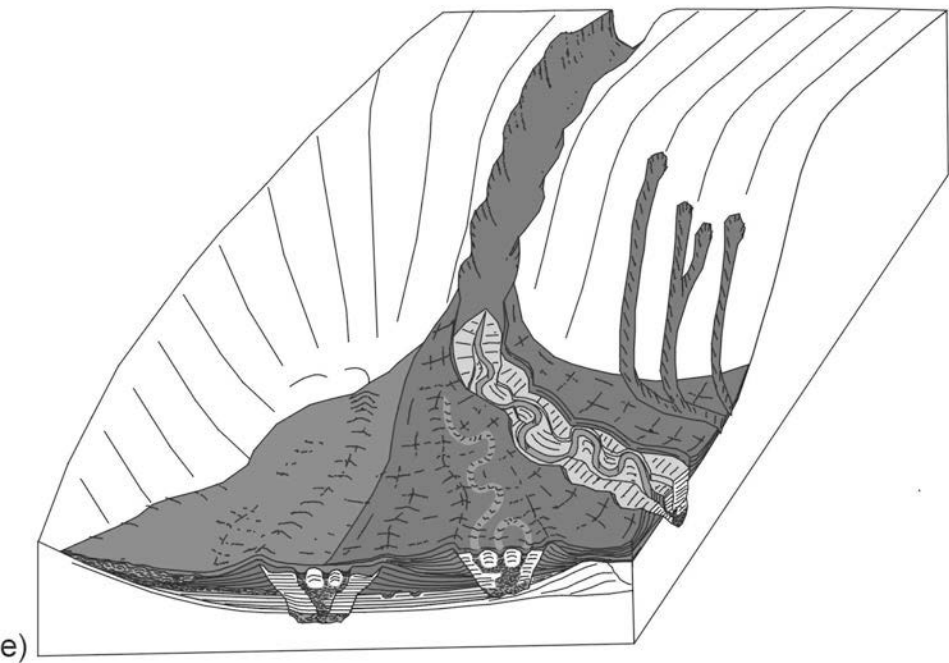


Figure 6.18. Series of block diagrams illustrating the initiation of a new channel-levee complex and two subsequent upper fan avulsions. See text for details.

An upper fan avulsion could be triggered by a flow that is out of equilibrium with the aggraded channel-belt (e.g. during the passage of an abnormally large or erosive flow). The outer levee walls may not contain such a flow, resulting in an avulsion. Observations from CLS C1 lend credence to this interpretation. Inner levees and HARs within the proximal parts of CLS C1 appear to have aggraded to the level of the outer levee crests, prior to the first avulsion. In contrast, at the southern limits of the data-set, the channel-belt failed to aggrade to the level of the outer levee crests, prior to the first avulsion. This observation suggests that the channel-belt aggraded more rapidly near the canyon mouth than it did distally, providing a mechanism for “plugging” the canyon mouth and promoting an upper fan avulsion.

Similar observations are made at Benin-major, off West Africa, where the system filled completely in the up-dip direction (through inner levee and channel aggradation, and a late mass transport deposit), whilst the system had significant relief in the down-dip direction. With the exception of the switch from Benin-minor to the much larger Benin-major CLS, however, there is no evidence for upper fan avulsions in the Benin study area. The lack of upper fan avulsions could reflect a number of processes, including smaller volume flows, shorter duration link between the canyon head and the fluvial system, greater sediment stability, and/or less tectonism. Of these, the most important may be the duration of time the canyon head remains connected to the fluvial system. In the case of Indus Fan, the canyons extend all the way back onto the shelf, therefore increasing their potential to link into shelf fluvial systems and/or sediment transported by shelf currents. In contrast, most canyon heads off the western Niger Delta slope begin at the shelf break and therefore the fluvial connection is less secure during times of higher sea level.

6.4.2 *Origin of “terrace” forming elements*

An inspection of the literature indicates that terrace-like features are recognized in a wide range of CLSs, including those within large fans like Zaire (Droz et al., 1996; Vittori et al., 2000), Indus (Von Rad and Tahir, 1997), Bengal (Hubscher et al., 1997), Toyama (Nakajima et al., 1998), and Laurentian (D. Piper, pers comm. 2002), medium-sized fans like Rhone (Bellaiche et al., 1984; Torres et al. 1997) and Monterey (Gardner

et al., 1996), and smaller fans like Hueneme (Piper et al., 1999), La Jolla (Shepard and Buffington, 1968; Normark, 1970), North and South Golo (Pichevin, 2000), and Einstein (Hackbarth and Shew, 1994; C. Winker, pers comm. 2001).

Interpretations for the origin of terraces vary widely, from levee margin growth faults (Clark and Pickering, 1996a), slumped levee material (Hackbarth and Shew, 1994) and rotated slump blocks (originating from channel walls - Shepard and Buffington, 1968; Shepard and Emery, 1973; Kenyon et al., 1995; Friedmann, 2000), to depositional terraces (Von Rad and Tahir, 1997), channel-bank deposits (McHargue and Webb, 1986; Kolla and Coumes, 1987), confined or underfit inner levees (Hubscher et al., 1997; Torres et al., 1997; Piper et al., 1999), to rejuvenation features resulting from channel entrenchment into flat-lying strata (i.e. erosional terraces - Normark, 1970, 1978; O'Connell et al., 1995).

Three different types of terrace-forming elements are recognized in the channel-belts examined in this study: rotated/subsided slump blocks, erosional terraces, and inner levees. The relative importance of each terrace-type varies from one system to another, and during different periods in the evolution of each system.

Several intact and semi-intact **slump blocks** are recognized locally along the margins of the erosional fairways at Benin-major and Indus Fan (Figures 6.7c, 6.11a, 6.14a). In some cases they contain seismic markers that can be correlated to undeformed strata adjacent to the system. Most slump blocks developed during the incision of the erosional fairway, or during its early fill history, when its margins were most unstable. Slump block movement is accommodated both by rotation along listric fault planes and subsidence into underlying poorly consolidated strata. At Benin-major, slump blocks are commonly sculpted along their channel-ward-exposed surfaces by channels associated with the phase 1 HARs.

Purely **erosional terraces** are also recognized locally along the margins of erosional fairways in both study areas (e.g. Figures 6.5, 6.6). Many erosional terraces formed during the incision of the erosional fairway. They form flat benches consisting internally of strata deposited prior to the incision of the erosional fairway. At Benin-major, erosional terraces are also recognized within the phase 1 deposits where they are

associated with rejuvenated incision, and in phase 2 deposits where they are associated with meander loop cut-offs (e.g. Figure 6.14b).

Both slump blocks and erosional terraces (remnants and cut-offs) commonly become sites of prominent inner levee deposition (e.g. Figures 6.5, 6.6, 6.12c-d, 6.17). **Inner levees**, which also develop independent of pre-existing terrace relief, are commonly found adjacent to narrow HARs and onlap the outer levee and erosional fairway walls. At least three periods of inner levee growth are recognized in both study areas (e.g. Figures 6.7b, 6.11b, c). They are best preserved opposite major cut-banks, where the channel-axis has consistently migrated away from one channel wall and towards another. For example, as the channel-axis migrated towards the outer levees in Figures 6.7b (CLS C2) and 6.11c (Benin-major), several phases of inner levee growth occupied former channel positions opposite the prominent cut-bank. Each successive period of inner levee growth onlaps and/or drapes the previous one, creating a “stepped” channel margin profile. Multiple inner levee “steps” may aggrade at different levels above the channel floor at the same time, and probably at different rates. The inner levee closest to the channel-axis appear to aggrade at the fastest rate.

Inner levee terraces merge with outer levee crests when the rate of inner levee growth exceeds that of the outer levees, leading eventually to the “healing” of the terrace relief. At Benin-major, deposition resumed above the lower outer levee once the inner levees aggraded near the level of the lower outer levee crests. As this occurred, the confined inner levees evolved into unconfined inner levees and eventually back into outer levees. The result was a shift in the outer levee crests towards the axis of the under-fit channel (e.g. Figure 6.11a, see also Skene, 1998).

Cross-sectional profiles in both study areas show that between 45 and 60% of the channel-belt consists of inner levees.

6.4.3 *Lithological composition of inner levees*

The acoustic character of inner levees in both study areas ranges from low amplitude and almost transparent, to moderate amplitude and well stratified. Their acoustic character can be in striking contrast to adjacent outer levees (e.g. Figure 6.6), suggesting that they are compositionally different. The near-transparent character of

some inner levees implies a uniform lithological composition. Shallow piston cores obtained from inner levees on other fans indicate that they are mud-prone (e.g. Von Rad and Tahir, 1997; Hubscher et al., 1997), but these studies only sampled the uppermost parts of inner levees.

High amplitude reflections, resembling C-P HARs, are observed locally within inner levees (e.g. Figure 6.7c) or above other elevated regions of the channel-belt (e.g. erosional terraces or meander cut-offs - Figures 6.8c, 6.13d). These high amplitude reflections are interpreted as sand-prone pod-like deposits, although the mechanism for their formation is poorly understood. Clark and Pickering (1996a) inferred that sandy deposits could form above channel terraces or benches as a result of hydraulic jumps (thickening and increase in turbulence due to water entrainment, commonly at sharp decreases in gradient) within the through-channel turbidity current. Piper et al. (1999) documented sandy deposits, forming beds a few metres thick, interbedded with muddy inner levee sediment in the Hueneme fan valley (CLS), in the Santa Monica Basin, offshore California. In addition, cores from Site 934 on Amazon Fan (ODP Leg 155) demonstrate that an inner levee, deposited above a meander cut-off on the most recently active Amazon Channel, consists of thick muddy turbidites (up to 30 cm thick - Piper and Deptuck, 1997) interbedded with fine-grained sands. Inner levees may also contain slump deposits shed from the outer levee or erosional fairway walls, as observed in Figure 6.13.

Too few inner levees, however, have been calibrated with cores, and consequently there is considerable uncertainty about their composition and whether there are systematic changes in lithology from bottom to top or from one system to another. There is also uncertainty whether different types of inner levees (e.g. those formed as a result of under-fit confined flows versus those developed above meander cut-offs) are compositionally different. Whether inner levees are mud-dominated, or contain significant sandy intervals, has important implications for potential reservoir communication with adjacent sinuous channels, and therefore warrants further study.

6.4.4 *HARs - Indus Fan and Benin-major*

HARs show significant variability in width, acoustic character and vertical stacking patterns in both study areas. Variations in width can be real, or can reflect the orientation of the seismic profile relative to the orientation of the channel-axis. Since the orientation of the channel-axis can evolve through time, a single vertical seismic profile may show apparent variations in width that do not necessarily reflect changes in the channel width through time. In addition, the ratio of channel aggradation to channel migration may also influence the horizontal extent of HARs. Narrow channels that stack vertically will produce narrow HARs; narrow channels that stack adjacent to one another (i.e. laterally), with little vertical aggradation, will produce wider HARs.

On the Indus Fan, stacked HARs can be as much as 800 m thick and show a complex “multi-limb” or “branching-cactus” aggradational pattern in cross-section (e.g. Figures 6.5 - 6.7). In the Benin-major CLS, the cross-sectional character of HARs is less complex than on the Indus Fan. The base of the system consists of a wider zone of HARs (confined within the erosional fairway) that passes up-section into one or more “limbs” of narrow HARs (the number of “limbs” depends on whether a meander loop or a straight channel segment is crossed). In general, the CLSs in both study areas contain HARs that are wider near the base (within the erosional fairway) than they are near the top.

Cross-sectional profiles in both study areas show that between 40 and 55 % of the channel-belt consists of HARs. The fill of the basal erosional fairway, on the other hand, may consist of greater than 75% HARs, with the remainder consisting of transparent seismic facies interpreted as early inner levees and/or muddy slump deposits shed from channel walls.

6.4.5 *Relationship between channel migration and inner levee deposition*

The aggradation of channel deposits at Benin-major records both down-channel and cross-channel migrations (see also Posamentier et al., 2000; Abreu et al., in press). The Benin-major CLS demonstrates that some channels adjust their planform geometry periodically, perhaps in response to changes in the equilibrium profile or flow character (e.g. size, composition). In addition, different parts of the same channel may evolve in different ways contemporaneously. A single meander loop can undergo a period of rapid

lateral migration at the same time that other segments of the same channel show little migration (see also Kolla et al., 2001).

The history of inner levee deposition is intimately linked to the evolution of channels. On horizon slices (both amplitude and dissemblance), major periods of inner levee growth are separated by sharp boundaries (e.g. Figure 6.13b) that are sometimes erosionally scalloped (e.g. Figures 6.14c, 6.17). The development of distinct boundaries between inner levees implies that the channel-axis migrated in discrete pulses, eroding into the cut-bank, and creating space for a new inner levee to develop. The scalloped margin of the inner levee is preserved as it is overlapped and draped by the adjacent, younger inner levee (Figures 6.11b, c). After a period of rapid channel migration and new inner levee growth, channel position is inferred to be relatively stable, characterized by vertical channel-fill and inner levee aggradation, with gradual, rather than abrupt, lateral channel migration.

The trigger for abrupt lateral channel migrations is poorly understood. Kolla et al. (2001) postulated that periods of discrete channel migrations were the result of stronger, surge-type flows, whereas periods of gradual channel migration and vertical aggradation were the result of steady-type flows. At least two mechanisms can promote the rapid lateral migration of channels. Episodic failure of the outer bend of a meander loop (via a slump) can promote a rapid lateral shift in the channel by removing the confining channel wall. Such failures could be triggered by the undercutting of the channel wall at a cut-bank during the passage of surge- or steady-type flows, or even by tectonism, unrelated to the passage of a flow.

Abrupt deposition of a debris plug could also promote rapid channel migration by changing the gradient profile along the channel. On a straight channel segment, the channel may respond by incising the plug to re-establish an equilibrium gradient profile. On a meander bend, however, the plug may promote accelerated cut-bank erosion, leading to a period of rapid channel migration, or may promote erosion at the neck of a meander loop resulting in a cut-off. A contorted slump deposit at Site 934 on the Amazon Fan, for example, is believed to have triggered a meander cut-off on the most recently active channel (Flood et al., 1995). The slump may have partially filled the channel, causing flows to divert around it and across the narrow meander neck. The

alternative hypothesis is that the emplacement of an underlying 18 m thick sand unit may have plugged the channel, in turn causing undercutting of the channel banks, leading to the failure of the levee margin (Flood et al., 1995).

6.4.6 *Why does sinuosity increase through time?*

The observation that sinuosity increases through time has been documented in this study and by others (e.g. Peakall et al. 2000, Kolla et al., 2001). The general trend of increasing sinuosity is interpreted in this study as an autocyclic response caused by a combination of 1) the increase in channel width with increasing channel height (an obvious relationship unless the channels walls are perpendicular to the channel floor), and 2) the alternation of periods of second order incision (defining a channel-form) and periods of vertical fill within the incision (higher-order stratal fill within second order incisions - Figure 6.19a).

The result of these two observations is illustrated in Figure 6.19b. Because channel width increases with channel height, a period of vertical fill within a channel-form must also result in an increase in channel-floor width (assuming roughly flat-lying beds that onlap the walls of the incision). The greater the vertical fill, the wider the channel floor becomes (so long as the channel is V- or U-shaped in cross-section), and the less each subsequent flow will tend to the original thalweg of the underlying second-order incision. Following the period of depositional flows and channel-form fill, the passage of one or more erosive, bypassing flows (now out of equilibrium with the channel due to the period of fill), results in incision into underlying deposits. Whether incision is centered above the channel-form fill, or skewed to one side, dictates the abruptness of channel migration. On relatively straight channel segments, incision will take place near the center of the channel-floor or randomly, and hence thalweg position may not change significantly (and may be unpredictable). In contrast, on a meander bend, the basal parts of an erosive flow passing through the channel will hug the outer wall of the bend due to centrifugal force, and hence incision will be skewed in this direction. Because the channel-floor has widened, the thalweg *must* shift as the flow hugs the outer wall. Unless channel erosion causes a meander cut-off, the *only* alternate

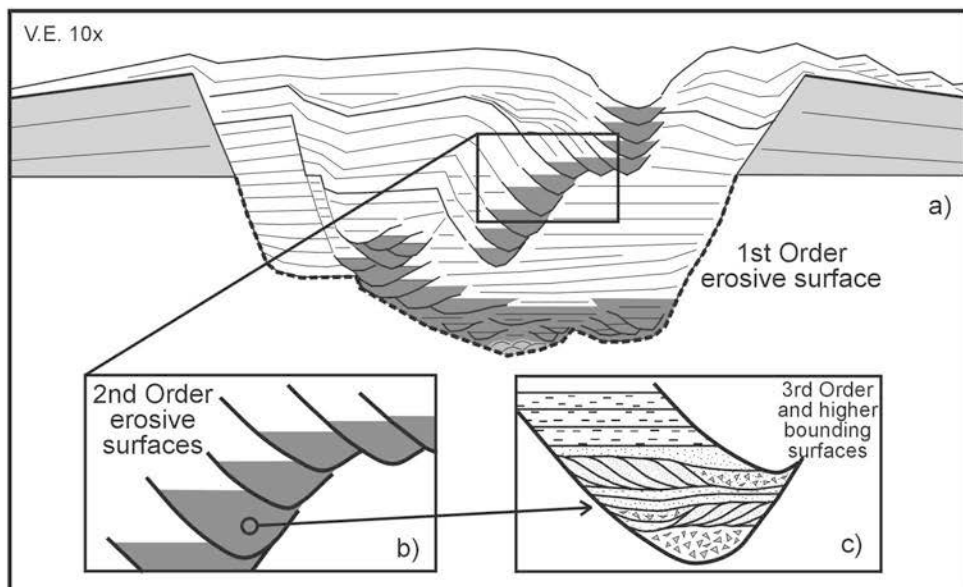


Figure 6.19. Scales of observation in deep-water systems. a) First order erosive surfaces can commonly be identified in conventional 3-D seismic of ancient buried fan systems (like the Paleocene fans in the Jeanne d'Arc Basin). b) Second order surfaces can typically be identified from convention 3-D seismic data if the channel system is large enough (e.g. Benin-major), but such detail cannot be seen in small deeply buried ancient systems. c) Third order and higher detail can typically only be detected in ultra-high resolution, shallow penetrating seismic data like Huntec DTS reflection profiles for modern systems or in outcrop studies of ancient systems.

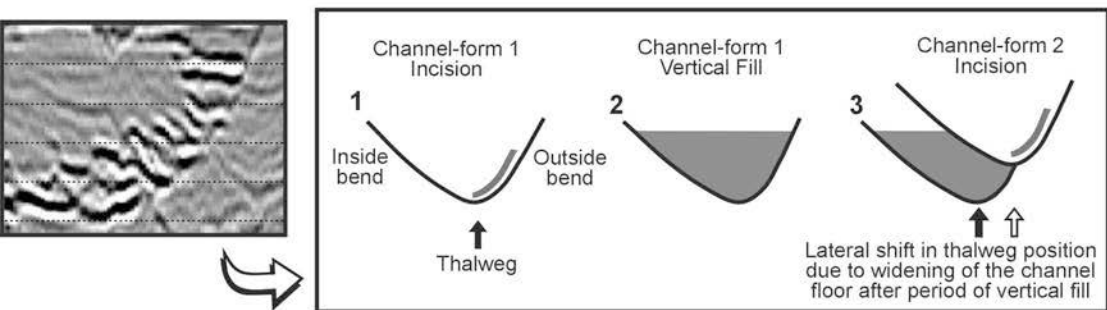
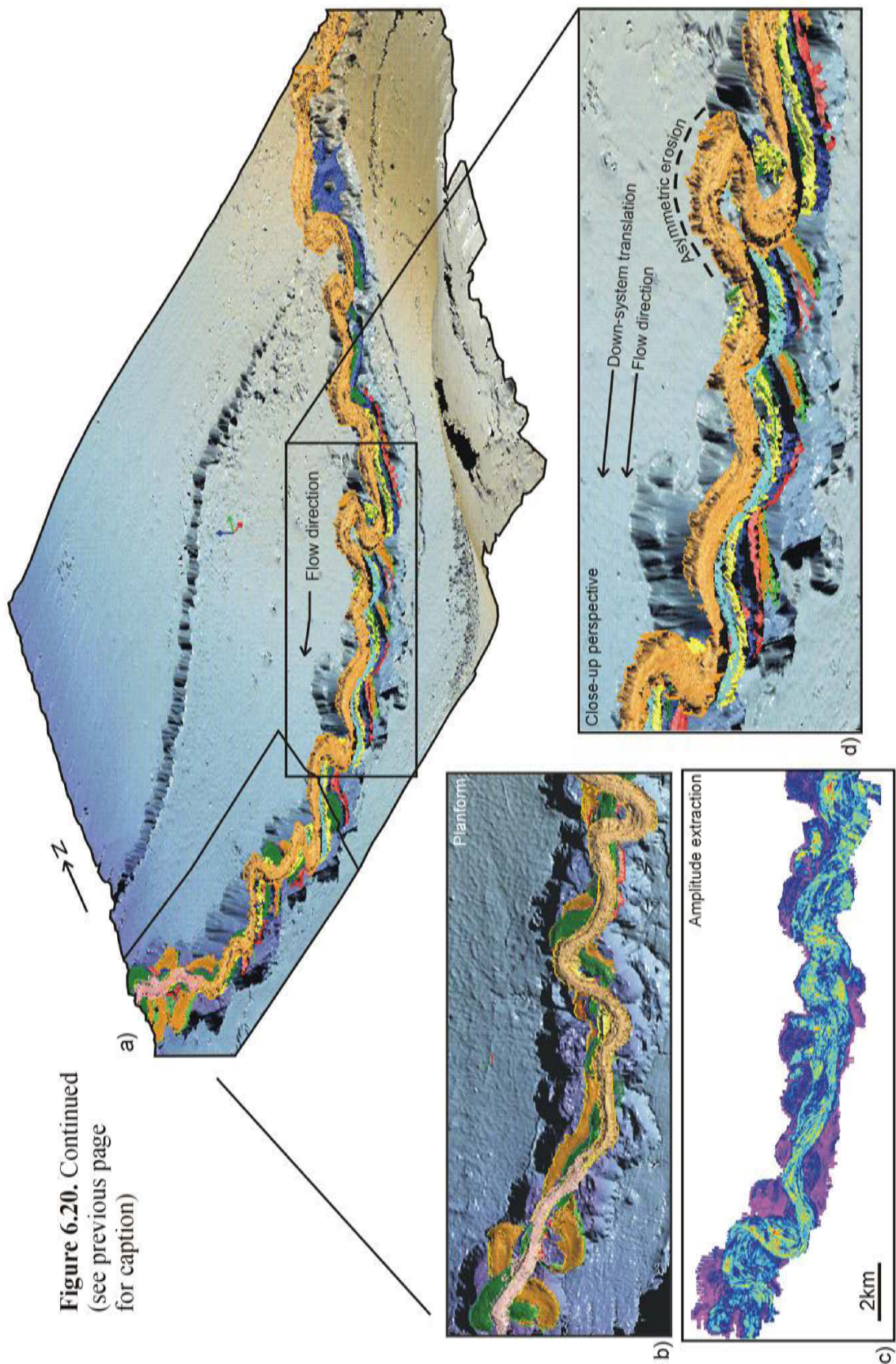


Figure 6.19. d) Schematic model illustrating how abrupt or punctuated lateral channel migration is accomplished. Alternating periods of channel-form fill and incision result in abrupt shifts in the channel position and a stepwise increase in sinuosity through time. The amount of offset from one channel-form to the next depends largely on the amount of fill within the underlying channel-form.

Figure 6.20. a) Perspective view from the southeast of the Benin-major erosional fairway and several stacked channel-forms mapped within the channel-belt. b) Planview close-up of late-stage channel-forms showing abrupt channel-straightening and the development of three meander cut-offs in cause by local uplift and the up-dip migration of a knickpoint. Channel-straightening occurred near the base of Phase 3. c) Amplitude extraction from an 80 ms window near the base of the system (equivalent to Phase 1 and 2 channels) showing the sinuous character of stacked channel-forms prior to the channel-straightening shown in (b). Purple and blue are low amplitudes. Green, yellow, and red are high amplitudes. d) Close-up perspective view of stacked channels showing down-system translation and cross-channel stepwise migration of successive channel-forms.



response is a shift in the thalweg position that will result in an increase in sinuosity (Figure 6.19b).

Hence, alternating periods of channel-form fill and incision result in abrupt shifts in the channel position and a stepwise increase in sinuosity through time. The amount of offset from one channel-form to the next depends largely on the amount of fill within the underlying channel-form. The more fill, the greater the offset. In an extreme case, an extended period of vertical fill could actually smooth over the original thalweg geometry to the extent that the planform geometry of a subsequent second-order incision could bear little resemblance to the underlying channel-form. What causes sinuosity to develop in the first place is not certain, but as soon as even a slight sinuosity evolves, the autocyclic controls described above will take over, and the system will develop a higher sinuosity through time (assuming no external, allocyclic controls modify the response).

Not only do channels shift laterally through time, but they also migrate down-slope (Figures 6.20, 6.21), implying that erosion is both focused on the outer walls of meander bends, and on the down-dip portion of the bend (i.e. erosion is asymmetric, with an increased tendency to erode in the down-dip direction). The result is a stepwise down-system translation in the channel position (as observed in Figure 6.20d). Interestingly, the crests of inner levees appear to migrate up-dip, in a similar manner to sediment waves (opposite to the direction of stepwise channel shifts).

As will be discussed below, changes in the equilibrium profile, perhaps due to local uplift, can result in channel straightening rather than an increase in sinuosity. The channel straightening in Figure 6.20b (distal part of the channel-belt) was in response to uplift of an underlying structure which locally increased the channel-gradient, resulting in a up-dip migrating knickpoint and the formation of three abrupt cut-offs. In contrast, the same channels up-dip show a progressive increase in sinuosity and a down-system translation of the channel planform (as described earlier - Figure 6.20b). Hence in this example, the up-dip portion of the channel-belt responded in an autocyclic manner, whereas contemporaneous channels down-dip responded to external (allocyclic) controls (i.e. uplift).

Sinuosity can also increase gradually during the fill of individual channel-forms, through progressive cut-bank erosion and point bar accretion, in a manner similar to

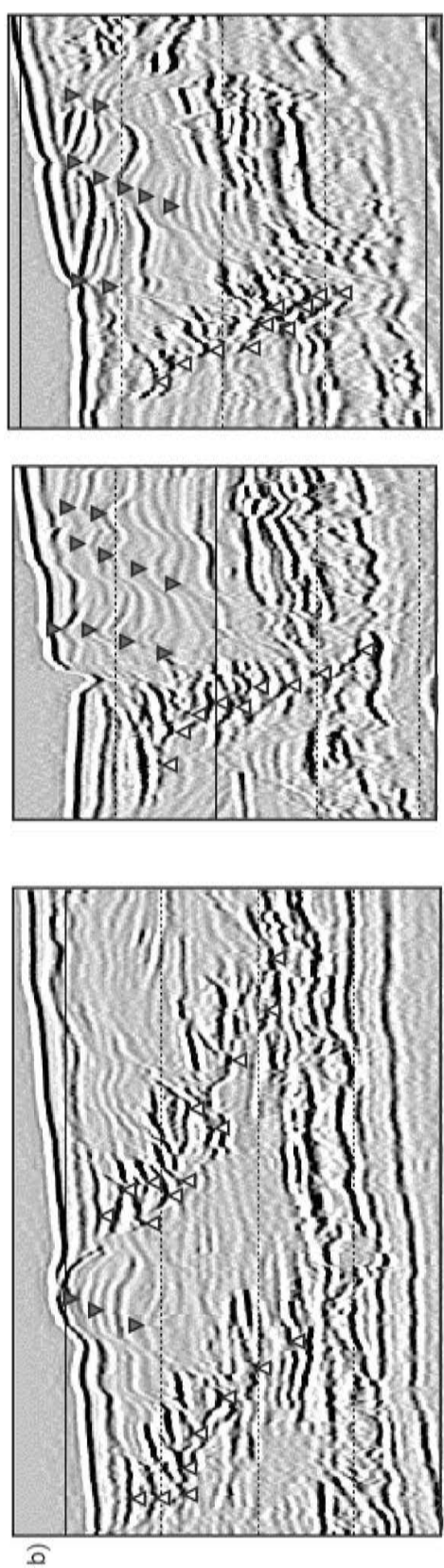
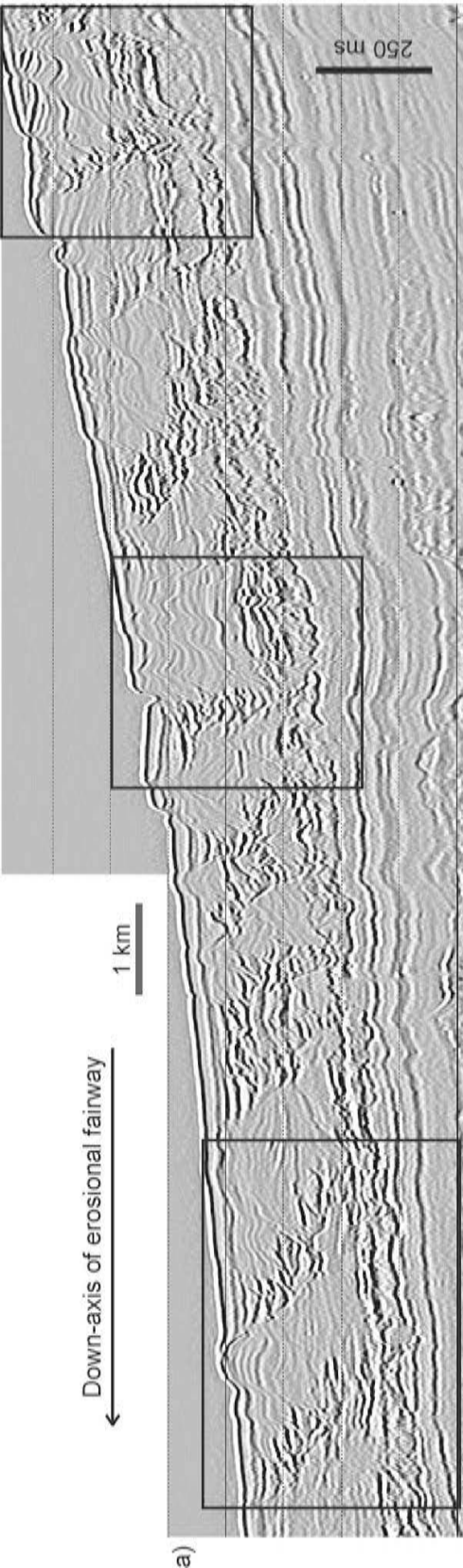


Figure 6.21. a) Seismic profile down the axis of the Benin-major CLS showing stepwise down-system translation in successive channel-forms. b) Close-up views showing down-system stacking of channel-forms (white triangles) and up-dip migration of inner levee crests (black triangles).

fluvial systems and documented in submarine channels by Abreu et al. (in press). However, this mechanism is considered an inefficient means of meander bend growth.

6.4.7 *Scaled comparisons with other systems*

Regardless of whether a CLS is isolated (as in Benin-major) or whether several systems stack adjacent to one another (as in CLC C on Indus Fan), individual CLSs in both study areas are characterized by a basal erosional fairway flanked by outer levees, containing under-fit channels flanked by inner levees. Similar architectural styles are repeated at multiple scales in upper fan CLSs around the world, including several other systems on the Niger Delta slope (e.g. Benin-minor) and in the Arabian Sea (e.g. modern Indus Fan), as well as CLSs on the modern Zaire (offshore Angola), Bengal (offshore India and Bangladesh) and Rhone (Mediterranean Sea) fans (Figure 6.22). At least two CLSs in the eastern Gulf of Mexico also show similar architectural styles; they include the very small Einstein CLS (Hackbarth and Shew, 1994) and the larger Joshua CLS (Posamentier, in press). All of these systems are floored by erosional fairways with incision ranging from a few tens to a few hundreds of metres, and are bordered by outer levees that vary significantly in thickness (at their crest – from one system to another). Together they confine channel-belts that vary over an order of magnitude in width, from 1 km (e.g. Benin-minor) to greater than 10 km (e.g. modern Indus - see Figure 6.22). The channel-belts commonly contain sinuous channels that vary in width from less than 100 m to greater than 1 km, and show strong evidence for inner levee development with heights above the channel-floor ranging from less than 20 m to greater than 360 m.

Similar architectural styles are also recognized in some systems that have much shorter length-scales, that feed small fan systems deposited in relatively confined basins, like Hueneme (offshore California - Piper et al., 1999) and South Golo (offshore eastern Corsica - Pichevin, 2000; Gervais, 2002). Similar architectural styles are also inferred for the Mara fan-valley in the Jeanne d'Arc Basin (early Paleogene, eastern Canada - Deptuck, 2000), but the deep burial depth and small dimensions of the system preclude imaging inner levees, though prominent sinuous thalweg channels are observed (see Chapter 5). Figure 6.23 shows a scaled comparison between the erosive bases (erosional fairways) of the Benin-major, Benin-minor, and the 65 Ma Mara fan-valley in the Jeanne

Figure 6.22. a) Scaled comparison of three cross-sections through channel-levee systems, showing the range of dimensions from small systems like Einstein (Gulf of Mexico), to very large systems like CLS C2 on the Indus Fan. All three examples consist of the same types and similar configurations of architectural elements (erosional fairway, inner levees, outer levees, channel-axis deposits), with significant variability in scale. b) Scaled comparison of selected channel-belt planforms, from small systems like South Golo (offshore east Corsican margin) and Einstein (Gulf of Mexico), to large systems like the modern Indus, Zaire, Amazon and Rhone. Only the upper fan portions of the channel-belts are shown, although in most cases data exist down-slope (e.g. Zaire). It is noteworthy that the planform channel-axis geometry shown for the modern Indus, Zaire, Rhone, Amazon, and South Golo represent the modern erosive channel-thalweg within an unfilled CLS, whereas the planform channel geometry shown for Indus CLSs C1, C2 and the Benin-major CLS represents the final channel position prior to the abandonment of each system, mapped from HARs (channel deposits). c) The approximate locations for systems shown is (b). d) Simplified schematic diagram of a CLS showing the length and extent of coverage of each channel-belt shown in (b), relative to the entire length of the system. Note that nearly the entire length of S. Golo, Mara, and Rhone are shown, whereas only the upper fan reaches of Indus, Zaire, Amazon, Benin, and Einstein are shown.

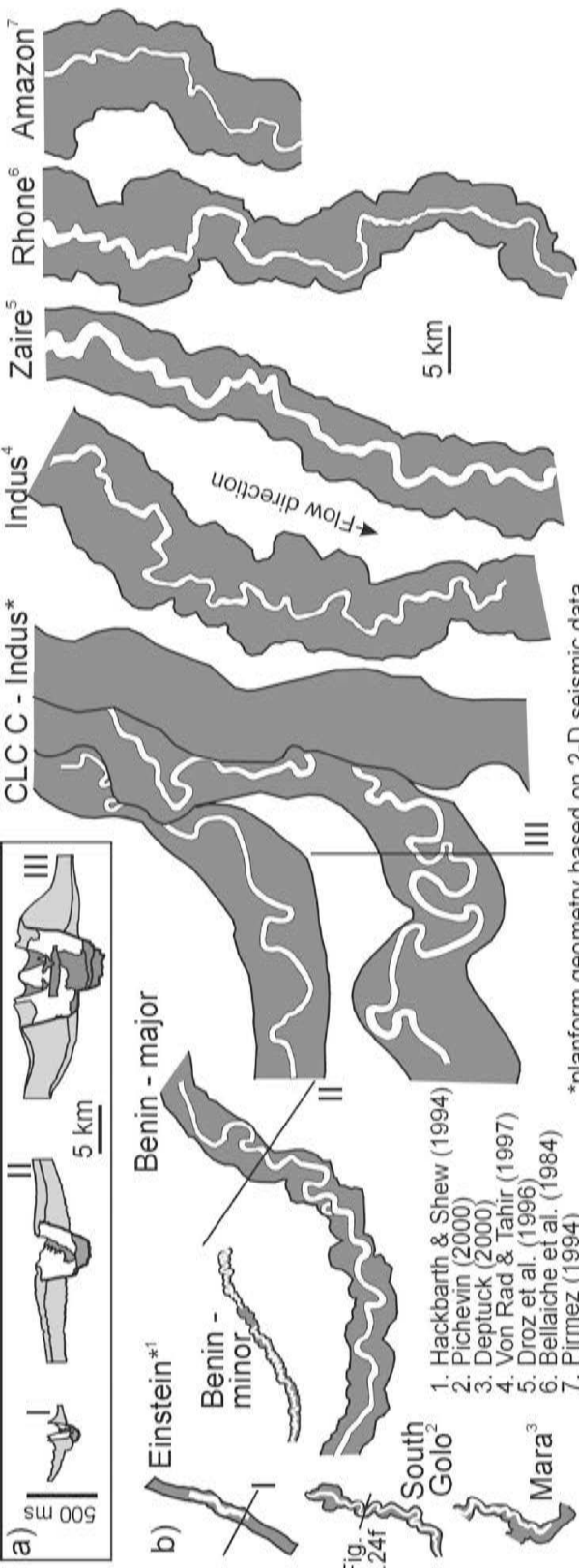


Fig. 6.24f

1. Hackbarth & Shew (1994)
2. Pichevin (2000)
3. Deptuck (2000)
4. Von Rad & Tahir (1997)
5. Droz et al. (1996)
6. Bellaiche et al. (1984)
7. Pirmez (1994)

*planform geometry based on 2-D seismic data

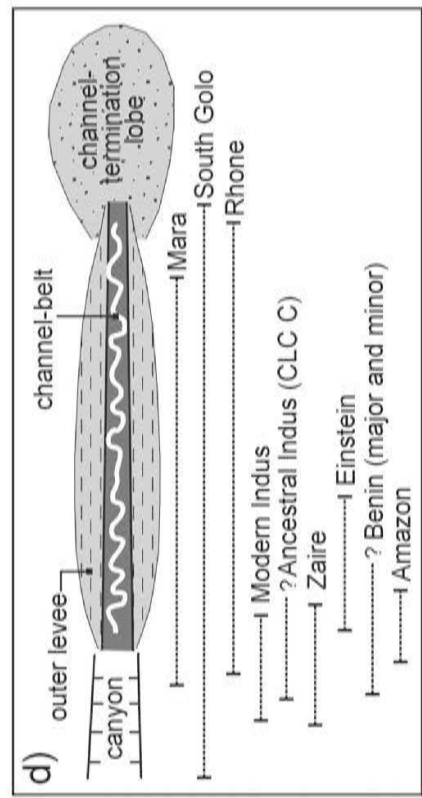
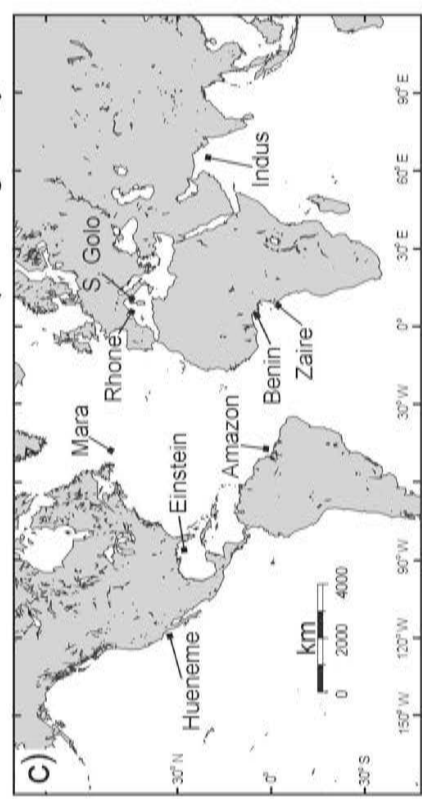


Figure 6.22. Continued (see previous page for caption)

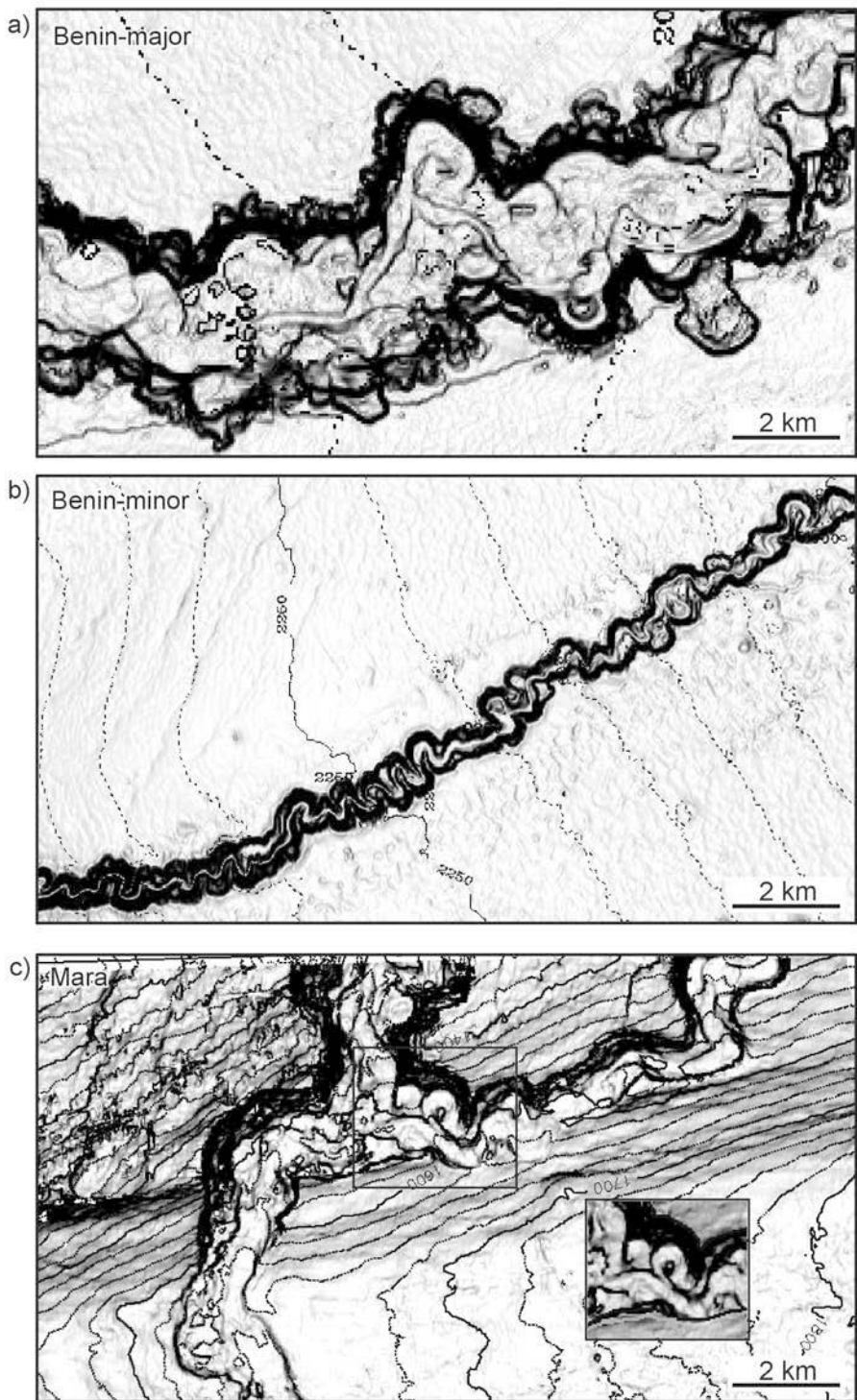


Figure 6.23. Dip map attribute scaled comparisons of entrenched meandering channels at the erosive base of a) Benin-major and b) Benin-minor, West Africa, and c) the Mara fan-valley, Jeanne d'Arc Basin, offshore Newfoundland. Note the similar scalloped character along the erosive walls in each system. The principal difference between the Mara fan-valley and the two Benin systems appears to be their length-scale.

Figure 6.24. Line drawing scaled comparisons of HARs from a) CLS C2 (Indus Fan), b) Benin-major (Niger Delta slope), c) a deeper CLS located below CLS C1 (Indus Fan), d) South Golo CLS (offshore eastern Corsica), and e) a line drawing of the “Solitary” channel (SE Spain - drawing based on photo mosaic in Figure 6.20). Note that the HARs to the left of the arrows are shown at 7 times vertical exaggeration, whereas the HARs to the right are shown with no vertical exaggeration (a more useful scale for making outcrop comparisons). Note also the wide range of dimensions exhibited for channel-deposits in different systems. Some very small systems like South Golo show similarities in architectural style to much larger systems. A line drawing transect through the proximal South Golo CLS (f), shows strong evidence for inner levee development and aggradational channel deposits. Scaled comparisons to the “Solitary” channel indicate that the two systems are fairly comparable in size and setting (< 900 m deep narrow trough-shaped basin flanked by mountainous terrain). These observations raise questions about whether systems like the “Solitary” channel contain inner levees and how to recognize them in outcrops. It may be very difficult to distinguish between periods of passive fill and inner levee deposits. Orange shows wider zones of HARs and yellow shows narrower zones of HARs. Blue shows outer levee and slope deposits for the South Golo CLS.

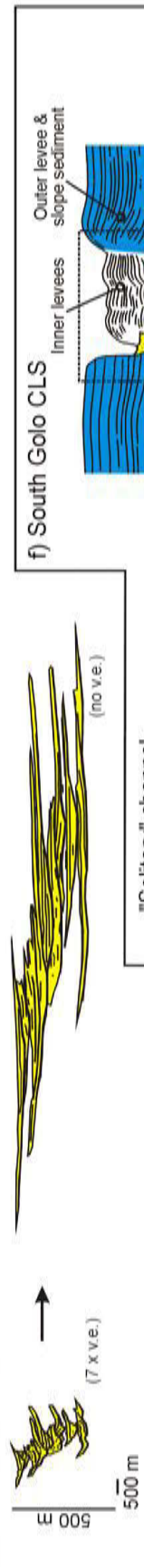
a) Indus - CLS C2 (Fig. 3)



b) Benin-major (Fig. 6.11a)



c) Indus (Fig. 6.8f)



d) South Golo (see Fig. 6.24f)



e) "Solitary" channel (Fig. 6.25)

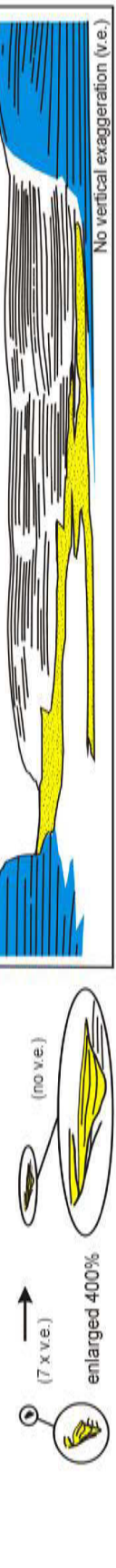


Figure 6.24. Continued (see previous page for caption)

Figure 6.25. a) Uninterpreted and b) interpreted photo mosaic of the “Solitary” channel, in SE Spain (Site 2 of Cronin, 1995). A first-order erosive surface is identified along the left-hand margin. Two second-order erosive surfaces are also shown, each defining the base of major channel units inferred to be similar to “channel-forms” described for Benin-major. Channel-form 2 of the “Solitary” channel is the only one exposed along both of its margins. It incises channel-form 1 and has a maximum thickness of 25 m and a width of 150 m. Channel-form 2 consists of coarse-grained to conglomeratic deposits, containing mud rip-up clasts and cobbles that are overlain by coarse-grained sandy turbidites and intervals of finer-grained sediment (Cronin, 1995; Haughton, 2000; Pickering et al., 2001). Sandstone bodies within second-order incisions display onlap, convergence, and lateral accretion, and may be separated by third-order erosive surfaces.



Figure 6.25. Continued (see previous page for caption)

d'Arc Basin. Note the entrenched sinuous thalweg channels at the base of each of these systems, and the scalloped external geometry of the fairways.

The South Golo CLS has similar width and length-scale dimensions as the Mara fan-valley in the Jeanne d'Arc Basin. It was mapped using ultra-high frequency Hunttec DTS seismic data (< 1 m vertical resolution). The system formed off the mountainous eastern margin of Corsica, along the edge of a narrow (25 km wide) and relatively shallow (< 900 m deep) trough-shaped basin. The South Golo CLS is much smaller and shorter than Benin-major (a mapped length of about 18 km - Figure 6.22a), but shows the same architectural elements with configurations similar to the much larger systems described earlier in this chapter. Although data quality is not sufficient to identify individual channel-forms, a channel-belt consisting of HARs and inner levees is well imaged (see also Pichevin, 2000; Gervais, 2002). In Figure 6.24f, the channel-axis deposits (expressed as HARs) were generated from a sinuous channel that migrated to the left during aggradation, creating a prominent cut-bank and multiple periods of inner levee growth opposite the cut-bank. The most significant difference between the South Golo system and Benin-major appears to be their length-scale.

The recognition of similar architectural elements, in systems that vary significantly in size and setting, suggests that common channelized flow processes exist at different scales. There also appear to be general evolutionary trends in many upper fan CLSs that lead to common architectural configurations (wider erosional incision filled with narrow sinuous channels flanked by inner levees).

6.4.8 Linking seismic- and outcrop-scale observations

Relating the architectural styles described above to outcrops can be challenging. This is due largely to differences in resolution between outcrop and seismic data, and limited well control to bridge the resolution gap. In addition, outcrops are rarely laterally extensive enough to allow for a broad-scale perspective or vertically extensive enough to expose the base and top of most CLSs (a problem that is also encountered in high resolution seismic studies). Perhaps the most important consideration is aspect ratio. The CLSs imaged on seismic data in this study are typically shown (and interpreted) at a minimum of 7 x vertical exaggeration. Viewing these systems at a 1:1 vertical to

horizontal scale reveals how challenging it can be to identify, for example, vertical aggradation of channels on outcrops, particularly in large systems (e.g. Figure 6.24). Consider the 500 m x 500 m box drawn above the Benin-major CLS in Figure 6.24b. If this box represented the extent of outcrop exposure, it is unlikely that the entire succession would be interpreted as the same aggradational system, and even less likely that the unit between the lower orange and upper yellow channel deposits would be interpreted as inner levee deposits.

The “Solitary” channel, located in southeastern Spain (Tabernas-Sorbas Basin), has been studied in detail by several workers (the reader is directed to Kleverlaan, 1989; Cronin, 1995; Haughton, 2000; and Pickering et al. 2001 for detailed descriptions) and is used here in an attempt to link seismic and outcrop-scale observations. The “Solitary” channel has an erosive base that incises slope mudstones and marlstones (Figure 6.25). The incision represents a first-order erosive surface interpreted to have a near-linear planform geometry (Haughton, 2000), and is inferred to be analogous to the erosional fairway at Benin-major. At least three second-order erosive surfaces, each defining a major channel unit (“channel-form”), stack in an offset multi-storey fashion within the first-order incision (see Haughton, 2000, his figure 3 inset). These second-order incisions are inferred to be analogous to U- or V-shaped channel-form HARs at Benin-major.

Haughton (2000) suggested that the first-order incision developed during a period of slope bypass, whereas the second-order incisions were caused by episodic flushing of the erosional conduit as it filled. Episodic flushing resulted in abrupt lateral shifts in the second-order channel position (abrupt migrations) followed by a period of fill within each second-order incision, with sandstone bodies displaying onlap, convergence, and lateral accretion. These observations are consistent with the channel-form stacking architecture observed during phases 2 and 3 at Benin-major, where aggradation and migration commonly occur via alternating periods of second-order incision and channel fill. Where the amount of channel fill is greater than the amount of vertical incision, the net effect is channel-form aggradation (with lateral migration accomplished by variable amounts of cut-bank erosion and the process described in section 6.4.6). Lateral accretion stratal architectures tend to develop within the second-order incisions at the “Solitary” channel, suggesting that gradual channel migrations occur between episodes of abrupt migrations.

The same may be true for other seismic examples, but limited resolution in most cases precludes resolving the fill of individual channel-forms.

The dimensions, length-scale, and setting (10 km wide structurally active E-W trending trough-shaped basin - Haughton, 2000) of the “Solitary” channel are fairly compatible with the small, modern South Golo CLS (Figures 6.24d - f). The off-set stacking of the two second-order incisions (each defining a “channel-form”) creates a cut-bank on the left margin of the “Solitary” channel (Figure 6.25), while the opposite channel margin grades laterally into shale with thin interbeds of siltstone and sandstone. Were these finer-grained interbedded strata deposited as passive fill (i.e. background sedimentation) as suggested by Haughton (2000) and Pickering et al. (2001), or could some of these deposits represent inner levee facies, as observed in the South Golo CLS (Figure 6.24f)? Inner levees also form important elements in several other small, active-margin fans, including La Jolla and Hueneme (both off California), and therefore they may be more common in such systems than previously thought. Clearly, the distinction between inner levee and passive fill deposits has important implications for interpreting the evolution of channel systems exposed in outcrops, and in particular for drawing time-lines through the channel fill. What criteria to use to distinguish between the two in outcrops, however, is not yet clear.

6.4.9 *General changes in flow character through time – Benin-major*

What causes a system to evolve from a wide erosional fairway bordered by outer levees, to a narrow confined channel bordered by inner levees, ultimately reflects changes in gravity flow character through time. Channel-levee geometry at Benin-major is used here to infer general changes in flow character through its development (Figure 6.26).

The incision of the erosional fairway suggests that gravity flows were most erosive during its early history. Erosion began initially during the passage of mass transport deposits, eventually leading to vertical incision of the erosional fairway (see also Coleman et al., 1983). Clark and Pickering (1996a), Hubscher et al. (1997), Friedmann (2000), Badalini et al. (2000), Mayall and Stewart (2000), and Kolla et al. (2001) have also reported erosion at the base of other systems. In contrast to other studies, however, sinuous, cross-cutting erosional channels are preserved on the floor of

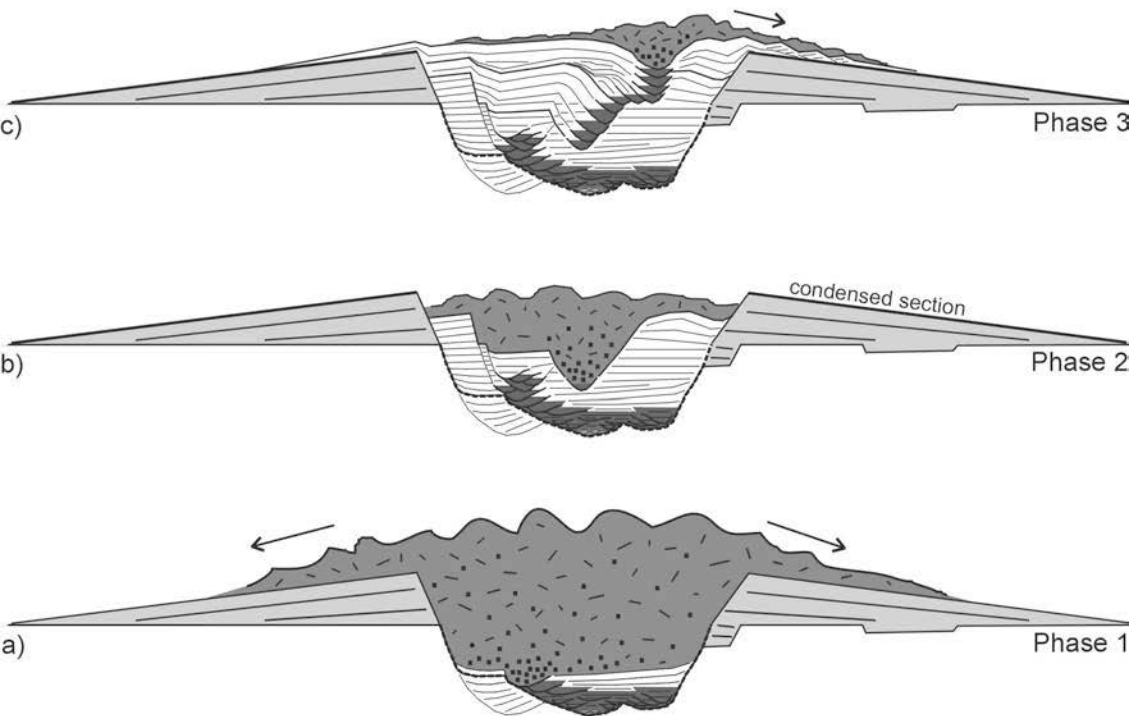


Figure 6.26. Schematic illustration showing the change in cross-sectional geometry of the Benin-major CLS during a) Phase 1, b) Phase 2, and c) Phase 3. Schematic shows the inferred cross-section character through the head of a sediment-gravity flow as it passes through the system. The progressive decrease in flow thickness for the average flow is based on observed decreases in the height of levee crests (outer for Phase 1 and inner for Phases 2 and 3) above the channel floor.

the erosional fairway at Benin-major. This implies that the basal portion of flows traveled down sinuous paths as they erosionally deepened, and largely bypassed, the fairway floor. It also indicates that sinuous channels can be highly erosive. During the phase 1 fill, the apparent synchronous deposition of the lower outer levees indicates that flows must have been thick enough to overbank the erosional fairway margins. Using the height difference between the lower outer levee crests and the thalweg of the erosional fairway, a lower limit ranging from 200 to 350 m would have been required for flows to overbank the outer levee crests during the earliest fill history (Figure 6.26a). Any sediment accumulation within the erosional fairway would reduce this predicted value.

In contrast to phase 1, the development of inner levees during phases 2 and 3 caused a reduction in channel cross-sectional area, a proxy for the size of throughput turbidity currents (Pirmez, 1994). The high amplitude seismic reflection that defines the top of the lower outer levee is interpreted as a condensed interval that marks the change from large, erosive flows (phase 1), to smaller, under-fit flows that rarely overbanked the outer levee crests (phase 2). Reflections near the base of many inner levees are inclined towards the channel-axis or are flat lying, and terminate abruptly as onlap onto the erosional fairway or outer levee walls (e.g. Figure 6.7c). These inner levees are inferred to be from flows that were completely confined between the outer levee crests. In contrast, as the channel floor aggraded (particularly during phase 3), reflections near the tops of some inner levees are inclined away from the channel-axis, and sometimes form wedge-shaped geometries characteristic of less confined flows. Reflections within these inner levees can sometimes be correlated out onto the outer levees (e.g. Figures 6.7c, 6.11), indicating that flows once again overbanked the lower outer levee crests. These observations indicate a transition from confined flows during early inner levee deposition, to flows that were not completely contained within the conduit later on, after a period of channel and inner levee aggradation (Figures 6.26b, c).

Approximations of through-channel flow thickness during fill phases 2 and 3 can be made in areas where inner levee horizons can be correlated into equivalent channel-form horizons (i.e. where there is continuity between inner levee and channel-floor deposits, typically on the inside bend of meanders). The maximum height of inner levee markers above the channel thalweg yields a minimum approximate flow thickness on the

order of 120 to 150 m during phase 2 (Figure 6.26b), decreasing to 50 to 75 m just prior to the abandonment of the system (Figure 6.26c). The estimated decrease in flow thickness between fill phases 1 through 3, combined with the decrease in cross-sectional area, are consistent with McHargue (1991) who predicted a decrease in flow volume during the evolution of CLSs on the Indus Fan.

Although much thinner (80 m thick) than the CLSs described in this paper, the most recently active CLS on the Bengal Fan is characterized by a 14 km wide erosional channel flanked by outer levees, which narrows to a less than 1 km wide channel bordered by inner levees (Hubscher et al., 1997). Using ^{14}C dates from shallow piston cores, Weber et al. (1997) interpreted outer levee growth to have ceased at the end of the last glacial maximum, whereas inner levee growth occurred later, during rising sea level in the Holocene. Based on this information, it is reasonable to infer that the erosive base of the system developed during the falling stage of sea level, when sediment supply to the shelf break and slope instability were probably the greatest. The under-fit narrower channels flanked by inner levees, then, would correspond to periods of reduced sediment supply during rising sea level (Hubscher et al., 1997).

Understanding the cause for the apparent decrease in gravity flow size and erosiveness in the Benin-major CLS, however, is hindered because of the lack of core data and age control. There is uncertainty about whether Benin-major evolved through a single cycle or multiple cycles of sea level fluctuation. Its evolution may reflect a combination of changing sea level position and evolving sediment source characteristics (sediment supply, grain size, proximity to the canyon head, etc.), which may or may not be intimately related. These variables, in turn, are believed to have caused changes in gravity flow character through time (including flow composition, size, erosiveness, frequency, and perhaps triggering mechanisms - Piper and Normark, 2001). The precise nature of these changes, and their impact on channel-levee architecture, are still being investigated.

6.4.10 Architectural variability

Although similar configurations of architectural elements are observed at multiple scales, the detailed geometry of individual elements and their geology can vary from one

system to another, or even within different reaches of the same system. Variations include the thickness and inclination of outer levees, the presence or absence of sediment waves, the depth of incision of the erosional fairway, and the planform geometry and grain-size characteristics of channel deposits. Architectural element variability probably reflects some of the controls described by Piper and Normark (2001), including the volume, grain-size, and dominant triggering mechanisms for flows, and the interaction of those flows with pre-existing channel and basin/sea floor morphology (gradients, bathymetric obstacles, etc.).

The geometry of one architectural element may have a strong impact on the geometry of another architectural element or suite of elements. As a result, intimate architectural relationships may be observed between some elements. For example, where the depth of incision of the erosional fairway is large, the thickness of contemporaneous outer levees (at the levee crest) tends to be small, and vice-versa (Deptuck et al., 2003b). This apparent inverse relationship probably reflects the ability of through-channel turbidity currents to overbank the margins of the erosional fairway. Down-slope variations in the depth of the erosional fairway are recognized along CLSs off west Africa and in the Arabian Sea, with local increases observed where the fairways cross pre-existing bathymetric highs. In some systems, the erosional fairway may be too deeply incised to allow flows to overbank (in which case I would call the incision a canyon). Such systems may only develop outer levees after a period of deposition within the erosional fairway. Consequently, the timing for the start of outer levee deposition may vary from one system to another.

A deeply incised erosional fairway may also promote the development of inner levees, by increasing the potential for confinement (and thus under-fitting) of flows. In contrast, systems that lack erosion at their base, or have a very shallow erosional fairway, may develop confined inner levees only after periods of abrupt lateral channel migration or above meander cut-offs. Aggradational channel deposits in such systems may be flanked directly by outer levees (e.g. Figure 6.8f), and their bases may be characterized by sheet or channeled-sheet deposits, rather than an erosional fairway (“HARPs” - an architectural style that is believed to be more common in middle to lower fan settings).

The amount of incision at the base of a CLS, early in its history, therefore has a significant impact on its final architecture.

The evolutionary trends shown for the Benin-major CLS, if assumed to be “normal” (i.e. using it as a baseline for comparison), can be perturbed by events like upper fan avulsions that can terminate the evolution of the system down-dip of the avulsion site (in effect freezing it). Alternatively, a large mass transport complex, deposited within an erosional fairway, could smooth over the confinement (i.e. fill the erosional fairway) that may have otherwise lead to the development of inner levees. A similar result could be accomplished by an extended period of muddy slope deposition within the proximal reaches of an erosional fairway.

Complex architectural styles can be generated if a system enters into an under-fit phase with deposition of inner levees and narrow aggradational channels, and then switches back to a highly erosive phase. Such a scenario may explain the more complicated architecture observed in CLSs C2 and C3 on the Indus Fan (e.g. Figure 6.7). The evolution of CLSs can also be perturbed by active structural deformation at the sea floor. Such deformation can trigger rotational slump blocks along the unstable margins of the system, which could plug the channel-axis and disturb channel development. Localized regions of uplift along a system may result in local changes in channel stacking pattern and planform geometry, by disturbing the gradient profile and promoting local incision, channel-straightening, and/or the formation of meander cut-offs (e.g. Deptuck et al., 2003b - Figure 6.20b). The opposite effect may be observed in areas of structural sagging. Therefore, local variations in architecture within a given system should be expected, and can be caused by changes in the local bathymetry (either pre-existing or the result of active deformation like a rising salt or mud diapir).

When comparing one CLS to another, some apparent variations in architecture may also reflect the stage in the “normal” evolution the system is in. I have demonstrated that the planform and cross-sectional channel geometry at Benin-major evolves through time. The modern slope off West Africa is crossed by several CLSs of various dimensions and in various “stages” of fill. Some systems are empty erosional conduits (e.g. similar to phase 1 at Benin-major - Figure 6.10a), others contain deep narrow channels flanked by inner levees (e.g. similar to phase 2 at Benin-major), and still others

are nearly entirely filled, with little remaining relief (e.g. similar to the modern sea floor expression of Benin-major - Figure 6.10b). Comparisons between the final cross-sectional and planform channel geometry at Benin-major (late phase 3 - low channel-margin relief, well developed sinuosity), to the modern “empty” Zaire or Indus CLSs (with channel floors as much as 400 m below levee crests), for example, may not be meaningful. Instead, a better comparison may be made with phase 2 at Benin-major, when the system had a similar cross-sectional geometry (albeit smaller) as the upper fan CLSs on the modern Zaire and Indus fans.

Finally, the architectural styles described in this chapter are from the upper fan reaches of CLSs. Down-fan changes in style are expected (e.g. a decrease in erosional fairway depth and inner levee height; a transition from incision to sheet-like deposition at the base of CLSs, etc.), but have not yet been investigated in detail.

6.5 Summary of key points

- 1) Several common architectural elements are recognized in upper fan settings, just outboard the canyon mouth in CLSs C1, C2, and C3 of Indus Fan, and the Benin-major CLS on the western Niger Delta slope. These elements include outer levees, inner levees, erosional fairways, channel-axis deposits, slump blocks, and mass transport deposits.
- 2) Vertical, sub-vertical, and lateral stacking patterns of sinuous and/or meandering channel-axis deposits create a range of narrow and wide zones of HARs that vary in acoustic character from discontinuous-chaotic (D-C HARs), to continuous-parallel (C-P HARs), or can appear as isolated channel-forms filled with variable seismic facies. HAR width is controlled by the original width of the channel and the ratio between vertical aggradation and lateral migration of the channel floor. Wide HARs, therefore, either originate from wide channels or from narrow channels that have migrated significantly laterally, with little vertical aggradation. The latter are believed to share the most similarities with fluvial meander-belts, including the development of point bars.
- 3) Pulses of rapid channel migration can occur within short channel segments, at any point in the channels aggradational history. They result in local widening of the HARs,

the development of prominent cut-banks, and the deposition of a new inner levee opposite the cut-bank. Inner levees are primary architectural elements in many CLSs. Their intimate relationship with channel-axis deposits provides insight into how channels migrate and aggrade through time. Onlapping by inner levees also helps to stabilize the margins of the erosional fairway as it fills.

4) The early history of the Benin-major CLS is characterized by incision of the erosional fairway. The initial development of outer levees in this system appears to be synchronous with the late incision of the erosional fairway or its early fill history (phase 1). Three phases of channel-deposit evolution are recognized within the erosional fairway. Phase 1 is characterized by a wide unit of D-C HARs that consist of several cross-cutting and amalgamated sinuous channel segments deposited within the erosional fairway. Slumps from the outer levee or erosional fairway walls may be most abundant in this interval. Phase 2 is characterized by narrower D-C and/or stacked channel-form HARs with tortuous sinuosities, bordered by highly aggradational inner levees. Phase 3 is characterized by narrow D-C and/or stacked channel-forms, with well developed meander loops bordered by inner levees. Phase 3 channel floor deposits aggraded at a faster rate than either the inner or outer levees, resulting in a progressive reduction in channel relief prior to abandonment.

5) The similarities in first-order architectural elements in upper fan settings in a wide range of CLSs suggest that similar channelized flow processes exist at different scales. Although the evolution presented for the Benin-major CLS is not intended to be a general model, similar architectural element configurations are repeated in several CLSs around the world, suggesting that common evolutionary trends do exist. Many CLSs experience an early incisional history inferred to result from the passage of large, erosive flows. The same systems commonly experience a later period of channel-belt aggradation characterized by narrow channels flanked by confined inner levees, inferred to result from the passage of smaller, under-fit flows. The cause of the switch from dominantly erosive to dominantly depositional is not well understood, but probably reflects a combination of sea level position and evolving sediment source characteristics. An

important control on the final architecture of many CLSs appears to be the amount of incision, if any, that takes place early in its history.

CHAPTER 7 - CONTRIBUTIONS AND FUTURE WORK

7.1 Lithostratigraphy and basin evolution

In chapter 3 I subdivided and formalized the Upper Cretaceous and Tertiary stratigraphic succession in the JDB, while attempting to honour past definitions, both formal and informal. The lithostratigraphic framework provides a concise set of definitions for stratigraphic units in the basin that should help prevent some of the confusion in the interval that has existed in past studies. These definitions allow for meaningful comparisons to be made between the JDB and surrounding areas that will help to evaluate regional versus local controls on depositional systems. Chapter 3 demonstrates the contrasting early Paleogene depositional styles in the JDB proper versus the southern JDB. In the JDB proper, subsidence provided accommodation that allowed submarine fans to accumulate, and slowed the advance of the shelf along the edge of a depression. In the southern JDB the lack of subsidence generated a margin that was characterized by progradational stratal architectures, accompanied by a rapid advance of the shelf-break towards the Carson Basin, where space was available for fans to accumulate.

In Chapter 4, I provide a more regional perspective on the evolution of the JDB and its relationship to surrounding regions such as Orphan Basin and Flemish Pass. I propose a four-stage regional framework describing the post-rift history of the JDB that differs significantly from classic passive-margin models traditionally characterized by a seaward-thickening passive-margin wedge. In the JDB, a period of confinement preceded the formation of a seaward-thickening passive-margin wedge. During stage 1 (Late Cretaceous to earliest Eocene), progradational units built out from the west into a confined basin, with submarine fans deposited seaward in water depths that probably did not exceed 600 m. During stage 2 (Early to Middle Eocene), thick fully marine shales were deposited in deep water above stage 1 deposits. At the onset of stage 2, basin-margin progradation and submarine fan deposition terminated abruptly, suggesting that relative sea level rose to flood the basin margins. By the end of stage 2, marine shale filled in much of the remaining relief of the JDB, and the Central Ridge (the basement high that defines the eastern margin of the JDB during stages 1 and 2) no longer played

an important role in controlling sediment distribution. Strata loaded onto the unconfined margin during stage 3 (late Middle Eocene to Miocene) caused regional tilting and a northward plunge along the axis of the JDB, and the corresponding deposition of a northeastward-thickening wedge of mud-dominated sediment (the proto-Grand Banks). In contrast to stage 3, which was dominated by shelf and slope aggradation in the study area, stage 4 (latest Miocene to recent) marks an abrupt change to slope progradation, with deposition focused primarily in the Flemish Pass area, east of the Grand Banks. Stage 4 experienced a significant increase in sedimentation rates related to the onset of glaciation in the region.

The complex post-rift history of the JDB reflects its proximity to several rift-drift margins and the extended period of rifting that took place in the region. Transform motion along the Charlie Gibbs Fracture Zone, and renewed periods of plate separation north and south of it (e.g. during the opening of the Labrador Sea), is inferred to have strongly influenced the broad-scale evolution of the JDB. This thesis improves the understanding of the post-rift geologic history of the JDB, but the nature of the relationship between sediment influx from the west, basin subsidence to the north, lack of subsidence to the south, and regional-scale plate tectonics is not yet entirely clear.

The abrupt change in the sediment transport direction at the onset of stage 1 indicates a shift in sediment source regions, from just south of the JDB in the Early to mid Cretaceous, to west of the basin in the Late Cretaceous. The shift resulted in the influx of Upper Cretaceous to lowermost Eocene coarse clastics, starting in the Coniacian, peaking in the late Campanian, and abruptly diminishing by the Ypresian. The period of confinement, accompanied by an influx of clastics from the west, was important because it led to the deposition of submarine fans in the basin that are potential hydrocarbon targets. The western source is inferred to be linked to renewed plate separation just north or south of the Charlie Gibbs Fracture Zone, in response to a break-up unconformity during final separation of the Orphan Knoll and Porcupine Bank (84 Ma - Verhoef and Srivastava, 1989) or southern Labrador from western Greenland (68 Ma - Srivastava, 1978; or 61 Ma - Chalmers and Laurson, 1995).

The recognition of bottom current indicators (e.g. scours, drifts, sediment waves) in this study provides insight into ocean circulation during the latest Cretaceous and

Tertiary. The results suggest that ocean surface currents periodically swept through the JDB starting at the end of the Cretaceous and continuing until the basin filled in the Bartonian. After the Bartonian, ocean current indicators are recognized only in the Flemish Pass, presumably because currents were diverted to the east by the proto-Grand Banks shelf. Near the K-T boundary, elongated scours are believed to have formed as the proto-Gulf Stream passed through the basin, in a similar way that it scoured the Florida (Dillon and Popenoe, 1988) and Scotian (A. MacRae, pers. comm., 2003) margins. The occurrence of stage 3 current indicators in Flemish Pass, at water depths exceeding 1000 m, suggests that deeper thermohaline currents were more important, but the direction from which they came (north or south) is not known. During stage 4 the south-flowing Western Boundary Undercurrent was the most important deep thermohaline current (Kennard et al., 1990) in the study area, and stage 3 current indicators may have formed from a precursor to this current.

Presumably sea level fluctuations influenced the location of surface currents passing through the JDB. If the initiation of canyon erosion and fan deposition in the Early Paleocene reflects a lowstand in relative sea level, then it could also explain why ocean current scouring, which had been prevalent during the latest Cretaceous to earliest Paleocene, appears to have stopped (or significantly diminished) at the onset of fan deposition (i.e. scours are observed at the base of the fans, but not within fan deposits). Exposure of the proto-Grand Banks shelf during lowstands would have periodically diverted surface currents toward the Flemish Pass, in a similar way that the Charleston Bump along the Florida margin diverted the Gulf Stream to the east during Paleogene lowstands (Pinet and Popenoe, 1985). The two periods of most prominent basin scouring - in the latest Cretaceous or earliest Paleocene and again in the Ypresian - indicate that ocean current intensity fluctuated through time. The challenge is to understand what caused this fluctuation (sea level position? climate?). Is there a link between ocean current circulation and deposition of the "low gamma ray", commonly siliceous, Tilton and Adolphus members of the Banquereau Formation (both of which drape the unconformities generated by periods of intensified circulation)? Periods of less intense wind-driven surface currents could have promoted upwelling of nutrient-rich waters

around the basin margins, rather than scouring the basin floor, resulting in blooms of siliceous microplankton. Indeed, many large-scale questions remain unanswered.

7.2 Early Paleogene submarine fans and modern analogues

Near-basin-wide coverage of recently acquired 3-D seismic data, combined with vintage 2-D seismic and well data, afforded new opportunities to study the architecture and evolution of Paleocene to early Ypresian submarine fans in the JDB. Three potential sequence boundaries were identified, one near the base of the Danian, one in the Selandian, and the third near the top of the Thanetian. The characteristics of the submarine fans associated with each sequence boundary vary significantly. The early Danian sequence boundary is associated with erosion of large canyons incised into the shelf and slope and prominent mounded sand-prone deposits on the distal basin floor (the Avondale mounds). The Selandian sequence boundary is associated with erosion of a broad canyon into fine-grained Danian to Selandian slope deposits and with muddy deposits lacking significant seismically-defined mounds on the basin floor. The latest Thanetian sequence boundary is associated with several small, linear to curvilinear slope gullies and isolated sand-prone mounded fans deposited on the lower slope and basin floor (the South Mara mounds).

There is no obvious relationship between the change in submarine fan character in the JDB and eustatic sea level fluctuations. The change in fan style occurs over a period of 10 to 12 m.y., an interval apparently containing as many as 7 third-order sequences (Haq et al., 1987). Limitations in biostratigraphic control prevent assigning specific ages to the unconformities, so it is unclear which, if any, of the 7 or so global sequence boundaries identified by Haq et al. (1987) are equivalent to the three sequence boundaries identified in the study interval. Nonetheless, if the sequence boundaries in the JDB are assumed to have formed from lowering of relative sea level, the substantial long-term changes in fan style suggest that controls other than relative sea level fluctuations are responsible for altering submarine fan style in the basin. Falling sea level may trigger fan deposition, but changes in the sediment source character and the dominant types of sediment gravity flows probably account for the long-term changes in fan architecture (see also Piper and Normark, 2001).

Using sequence stratigraphic models for submarine fans (Posamentier and Vail, 1988; Posamentier, 1991), only the early Danian unconformity and associated “lowstand systems tract” can be tentatively separated into a “basin floor fan”, characterized by mounded deposits on the basin floor, supplied by erosive canyons incised on the shelf and slope during a rapid sea level fall, and a “lowstand wedge”, characterized by siliceous to shaly Danian to Selandian slope deposits, forming as the rate of relative sea level fall decreased and canyons were back-filled. There is no evidence, however, for slope fans or channel-levee systems within the apparent lowstand wedge. The “lowstand systems tracts” associated with the other two unconformities show little correspondence to sequence stratigraphic models for submarine fans, which could reflect limitations in seismic resolution, or alternatively could indicate that such models have limited applicability in the JDB.

Studying the temporal and spatial changes in architectural elements appears to be a useful approach, particularly if interpretations are guided by modern analogues. There appears to be a spectrum of lobe types in the JDB, ranging from channel-termination lobes (CTLs) deposited well out onto the basin floor, to proximal-inefficient lobes (PILs) deposited on the slope or near the base-of-slope, to an even more proximal fan-delta deposited near the shelf-break. The spectrum reflects flow efficiency, which in turn reflects grain population, gradients, triggering mechanism, and the degree of channel confinement. The Avondale mounds in the JDB are dominated by CTLs, which are more prone to form outboard major canyons, perhaps during periods of lowered sea level. The South Mara mounds are dominated by PILs, inverted channels, and hybrid lobes (intermediate between CTLs and PILs), which are preferentially deposited in proximal settings outboard slope gullies.

Small, sand-prone submarine fans off East Corsica provide insight into the types of flows responsible for both CTLs and PILs. PILs off East Corsica (like Pineto) have the most limited lobe-fringe deposits, and pinch-out abruptly down system, probably indicating very sand-rich flows with rapid sediment fallout rates from high-concentration flows (either sandy debris flows or high-density turbidity currents). CTLs, deposited in more distal settings, have well developed finer-grained lobe-fringe deposits and are

commonly supplied by leveed fan-valleys, suggesting sediment gravity flows with a mixed sand and mud load.

7.3 Submarine channel-belt architecture and evolution

In Chapter 6, I presented results from detailed examination of submarine channels-belts from several locations around the world, but principally from West Africa and in the Arabian Sea, where channel-levee systems are very large and allow detailed examination with relatively low-resolution tools (conventional 2-D and 3-D multichannel seismic data). The results provide information about how submarine channels evolve through time, and the nature of meander growth in such systems. Vertical, sub-vertical, and lateral stacking patterns of sinuous and/or meandering channels create seismic facies that range from narrow to wide zones of HARs (high amplitude reflections). Multiple phases of inner levee growth are commonly observed adjacent to HARs, each intimately linked to the channel migration and aggradation history. The recognition and understanding of inner levees provided by this study is an important step forward for understanding the behaviour of submarine channels as they evolve through time.

The recognition of similar first-order architectural elements in channel-levee systems that vary significantly in scale suggests that similar channelized flow processes exist at different scales (see Skene et al., 2002). Many channel-levee systems experience an early incisional history inferred to result from the passage of large, erosive flows. The same systems commonly experience a later period of channel-belt aggradation characterized by narrow channels flanked by confined inner levees, inferred to result from the passage of smaller, under-fit flows. The cause of the switch from dominantly erosive to dominantly depositional is not well understood, but is interpreted to reflect sea level position (at least in part).

Existing sequence stratigraphic models for submarine fans predict that canyons are incised when the rate of sea level fall is at a maximum, and channel-levee systems are deposited later as the rate of sea level fall decreases towards the maximum lowstand and into the subsequent transgression (e.g. Mitchum, 1985; Posamentier and Vail, 1988; Posamentier, 1991). Many workers agree that submarine fan growth and canyon erosion are accelerated during lowstands, but significant disagreement exists regarding the

temporal relationship between canyon erosion, formation of overbank deposits, and deposition of lobes (e.g. see also Kolla and Macurda, 1988; Flood and Piper, 1997). This study demonstrates that outer levees are contemporaneous with the incision or earliest fill history of the erosional fairway, inferred to form in response to an abrupt fall in relative sea level. In contrast, the under-fit channels flanked by inner levees are inferred to form during periods of slowed relative sea level fall and the subsequent sea level rise, a significant departure from traditional sequence stratigraphic models for submarine fans.

7.4 Suggestions for future research

1) Most of the members defined in this study would be considered formations in the North Sea and elsewhere, and the current formations are too all encompassing. Serious consideration should therefore be given to upgrading the formation-level stratigraphic units in the JDB to groups, and the member-level stratigraphic units to formations. Because the Banquereau and Dawson Canyon formations were originally defined for the Scotian Shelf, it requires that these units be upgraded there initially, which is beyond the scope of this study. I would propose keeping the Wyandot as a formation-level stratigraphic unit, as it does not warrant group status (in many areas it is thinner than the Petrel Member in the JDB). Upgrading the nomenclature would result in the definition of two groups: the Dawson Canyon Group and the Banquereau Group. The Dawson Canyon Group would be subdivided into the Petrel, Otter Bay, Red Island, Fox Harbour, Bay Bulls, and Wyandot formations in the JDB, and other units that are yet to be formally defined on the Scotian Shelf. Correspondingly, the Banquereau Group would be subdivided into the Avondale, Tilton, South Mara, Botwood, and Thorvald formations. The issue concerning the placement of the boundary between the Dawson Canyon and Banquereau formations, in the JDB versus the Scotian Shelf, can be resolved at the same time that the stratigraphic units are formally upgraded.

2) Provenance studies for the Upper Cretaceous and lower Paleogene progradational strata may be useful for determining their origin (eroded Lower to Upper Carboniferous? Precambrian? rocks). Specific basement terranes may have petrographically distinct mineralogy (e.g. Carboniferous St. Anthony Basin, Avalon, Gander, Humber, Dunnage,

etc.) that may help to determine the extent of the drainage system (i.e. how far landward did it extend). In addition, a more detailed assessment of the maturity of grains would help to constrain transport distance.

3) More work is needed to understand the Late Cretaceous and Paleogene oceanography in the JDB. Clearly there is evidence for ocean circulation of some sort, and anecdotal evidence points to a proto-Gulf Stream, at least at the end of the Cretaceous and earliest Paleogene. More substantial evidence, however, is needed to understand the origin of surface currents. The possibility that erosion near the K-T boundary originated from tidal currents or even in response to a tsunami from the 65 Ma bolide impact, can not be completely ruled out based on the results from this study. To understand the source of surface currents, a more detailed paleoenvironmental assessment of warm versus cold water species is needed. A new IODP core site off Newfoundland may help to evaluate the origin of currents, particularly deeper thermohaline currents.

4) Generation of synthetic seismic models, using the dimensions and stacking architecture of lobes (both proximal-inefficient lobes and channel-termination lobes) would be useful for demonstrating their similarity to mounds in the JDB and North Sea. Such models could use velocity and density information from buried fan intervals in both the JDB and North Sea and lobe dimensions could be modified to mimic compaction of lobe-fringe deposits and shale drapes (e.g. a 50% decrease in shale drape thickness relative to massive sands, etc.).

5) A more detailed study on the controls of channel-levee architecture is needed. Do these systems develop during a single sea level cycle, with incision of the erosional fairway during the falling stage and filling with inner levees and channels during the rising phase? What is the impact on lobe development during the incision of the erosional fairway versus deposition of inner levees? Presumably inner levee deposition corresponds to a reduction in the amount of sediment reaching the channel mouth. Coring and better age calibration is needed in this regard. The most practical locations to investigate the relationship between sea level position, erosional fairway incision, inner

levee deposition, and lobe deposition are small fans where correlation of key markers from prograding deltas on the shelf into fan succession on the basin floor is possible. Such an approach holds great promise for understanding the relationship between sea level position and fan deposition, and may help to resolve the controversy about submarine fan deposition within a sequence stratigraphic framework.

REFERENCES

- Abreu, V. and Haddad, G. A. (1998). Glacioeustatic fluctuations: the mechanism linking stable isotope events and sequence stratigraphy from the Early Oligocene to Middle Miocene, *in* P.C. de Graciansky, J. Hardenbol, T. Jacquin, and P. R. Vail (eds), Mesozoic and Cenozoic sequence stratigraphy of European basins, Society of Economic Paleontologists and Mineralogists (SEPM), Special Publication 60.
- Abreu, V., Sullivan, M., Mohrig, D., and Pirmez, C. (in press). Architectural analysis of sinuous, erosionally confined channels: the under-appreciated deepwater channel type, *Marine and Petroleum Geology*.
- Agrawal, A., Williamson, M. A., Coflin, K. C., Dickie, K., Shimeld, J., McAlpine, K. D., Altheim, B., Thomas, F. J., Semper, T., and Pascucci, V. (1995). Sequence stratigraphic analysis of the Late Cretaceous-Palaeogene formations in the Jeanne d'Arc Basin, offshore eastern Canada, *in* J. S. Bell, Bird, T. D., Hillier, T. L., and P. L. Greener (eds.), Proceedings of the oil and gas forum 1995, Geological Survey of Canada Open File 3058, 241-245.
- Allen, J. R. L. (1964). The Nigerian continental margin: bottom sediments, submarine morphology and geological evolution, *Marine Geology*, 1, 289-332.
- Amoco Canada Petroleum Ltd. and Imperial Oil Ltd. (1973a). Regional geology of the Grand Banks, *Bulletin of Canadian Petroleum Geology*, 21, 479- 503.
- Amoco Canada Petroleum Ltd. and Imperial Oil Ltd. (1973b). Well history report, Gull F-72, Report available at the Canada-Newfoundland Offshore Petroleum Board (C-NOPB), fifth floor, TD Place, 140 Water Street, St. John's Newfoundland.
- Arthur, K. R., Cole, D. R., Henderson, G. G. L., and Kushnir, D. W. (1982). Geology of the Hibernia discovery, *in* M. T. Halbouty (ed.), The deliberate search for the subtle trap: AAPG Memoir 32, 181-196.
- Badalini, G., Kneller, B., and Winker, C. D. (2000). Architecture and processes in the late Pleistocene Brazos-Trinity turbidite system, Gulf of Mexico continental slope, *in* P. Weimer, R. M. Slatt, J. Coleman, N. C. Rosen, H. Nelson, A. H. Bouma, M. J. Styzen, and D. T. Lawrence (eds.), Deep-water reservoirs of the world: GCSSEPM Foundation 20th Annual Research Conference, 16-34.
- Bagnold, R. A. (1962). Auto-suspension criteria of transported sediment: turbidity currents, *Royal Society of London Proceedings, Series A*, 265, 315-319.
- Balkwill, H. R. (1987). Labrador Basin: structural and stratigraphic style, *in* C. Beaumont and A. J. Tankard (eds.) Sedimentary basins and basin-forming mechanisms, Canadian Society of Petroleum Geologists, Memoir 12, 17-43.

Bally, A. W. (1983). Atlantic-type margins, *in* A. W. Bally, A. B. Watts, J. A. Grow, W. Manspeizer, B. Bernouli, C. Schreiber, and J. M. Hunt (eds.), *Geology of passive continental margins: History, structure and sedimentologic record (with an emphasis on the Atlantic margin)*, Education course note series #19, 1-47.

Barnes, N. E. and Normark, W. R. (1985). Diagnostic parameters for comparing modern submarine fans and ancient turbidite systems, *in* A. H. Bouma, W. R. Normark, and N. E. Barnes (eds.), *Submarine fans and related turbidite systems*, New York: Springer-Verlag, 13-14, and wall chart.

Barron, E. J. and Peterson, W. H. (1991). The Cenozoic ocean circulation based on ocean General Circulation Model results, *Palaeogeography, Palaeoclimatology, Palaeoecology*, 83, 1-28.

Bellaiche, G., Droz, L., Coutellier, V., Berthon, J.-L., Orsolini, P., Ravenne, C., Aloisi, J.-C., Got, H. and Monaco, A. (1984). Detailed morphology, structure and main growth pattern of the Rhone deep-sea fan, *Marine Geology*, 55, 181-193.

Bellaiche, G., Droz, L., Gaullier, V., and Pautot, G. (1994). Small submarine fans on the eastern margin of Corsica: Sedimentary significance and tectonic implications, *Marine Geology*, 117, 177-185.

Berggren, W. A. and Hollister, C. D. (1974). Paleogeography, Paleobiogeography, and the history of circulation in the Atlantic Ocean, *in* W. W. Hay (ed.) *Studies in paleo-oceanography*, SEPM Special Publication No. 20, Tulsa, Oklahoma, 126-186.

Berggren, W. A., Kent, D. V., Swisher, C. C., and Aubrey, M.-P. (1995). A revised Cenozoic geochronology and chronostratigraphy, *in* W. A. Berggren, D. V. Kent, M.-P. Aubrey, and J. Hardenbol (eds.), *Geochronology time scales and global stratigraphic correlation: Society of Sedimentary Geology, Special Publication no. 54*, 95-126.

Boudreau, R. R., Meehan, P. J., Wishart, H. A., and Harding, S. C. (1986). Mesozoic stratigraphy of the Jeanne d'Arc Basin (abs.), *in* Program and Abstracts, Canadian Society of Petroleum Geologists Convention, Calgary, Alberta, June 1-4, 1986, 28

Bouma, A. H., 1962, *Sedimentology of some flysch deposits: a graphic approach to facies interpretation*, Amsterdam, Elsevier Publishing Company, 168 p.

Bouma, A. H., and Coleman, J. M., DSDP Leg 96 Shipboard Scientists (1985). Mississippi fan: Leg 96 program and principal results, *in* A. H. Bouma, W. R. Normark, and N. E. Barnes (eds.), *Submarine fans and related turbidite systems*, New York: Springer-Verlag, 247-252.

Brown, A. R. (1996). *Interpretation of three-dimensional seismic data*, Fourth Edition, AAPG Memoir 42, 416 p.

Bujak, J. P. and Brinkhuis, H. (1998). Global warming and dinocyst changes across the Paleocene/Eocene Epoch boundary, *in* M. -P. Aubry et al. (eds.), Late Paleocene-early Eocene biotic and climatic events in the marine and terrestrial records, Columbia University Press, New York, 277-295.

Bralower, T. J., Paull, C. K., and Leckie, R. M. (1998). The Cretaceous - Tertiary boundary cocktail: Chicxulub impact triggers margin collapse and extensive sediment gravity flows, *Geology*, 26, 331-334.

Canada-Newfoundland Offshore Petroleum Board (C-NOPB) (1998). Schedule of wells, Newfoundland offshore area, Saint John's Newfoundland, November, 1999.

Carter, L. and Schafer, C. T. (1983). Interaction of the Western Boundary Undercurrent with the continental margin off Newfoundland, *Sedimentology*, 30, 751-768.

Chalmers, J. A. and Laursen, K. H. (1995). Labrador Sea: the extent of continental and oceanic crust and the timing of the onset of seafloor spreading, *Marine and Petroleum Geology*, 12, 205-217.

Chalmers, J. A., Pulvertaft, T. C. R., Christiansen, F. G., Larsen, H. C., Laursen, K. H., and Ottesen, T. G. (1993). The southern West Greenland continental margin: rifting history, basin development, and petroleum potential, *in* J. R. Parker (ed), *Petroleum Geology of Northwest Europe: Proceedings of the 4th Conference*, The Geological Society, London, 915-931.

Chalmers, J. A., Dahl-Jensen, T., Bate, K. J., and Whittaker, R. (1995). Geology and petroleum prospectivity of the region offshore southern West Greenland - a summary, *Rapp. Gronlands geol. Unders*, 165, 13-21.

Clark, J.D., Kenyon, N.H. and Pickering, K.T. (1992). Quantitative analysis of the geometry of submarine channels: Implications for the classification of submarine fans. *Geology*, 20, 633-636.

Clark, J. D. and Pickering, K. T. (1996a). Architectural elements and growth patterns of submarine channels: application to hydrocarbon exploration. *AAPG Bulletin*, 80, 194-221.

Clark, J.D. and Pickering, K.T. (1996b). *Submarine Channels: Processes and Architecture*. London: Vallis Press, 232 pp.

Clausen, O. R. and Huuse, M. (1999). Topography of the top chalk surface on – and offshore Denmark, *Marine and Petroleum Geology*, 16, 677-691.

Clift, P.D., Shimizu, N., Layne, G.D., Blusztajn, J.S., Gaedicke, C., Schlüter, H.-U., Clark, M.K., and Amjad, S. (2001). Development of the Indus Fan and its significance

for the erosional history of the Western Himalaya and Karakoram, *Geological Society of America Bulletin*, 114, 1039–1051.

Cloetingh, S. (1988). Intraplate stresses: a tectonic cause for third-order cycles in apparent sea level? in C. K. Wilgus, B. S. Hastings, C. G. Kendall, H. W. Posamentier, C. A. Roos, and J. C. Van Wagoner (eds), *Sea-level changes: an integrated approach*, SEPM Special Publication no. 42, 19-30.

Coleman, J. M., Prior, D. B., and Lindsay, J. F. (1983). Deltaic influences on shelfedge instability processes, in D. J. Stanley and G. T. Moore (eds.), *The shelfbreak: Critical interface on continental margins*, SEPM Special Publication, Tulsa, 33, 121-137.

Cronin, B. T. (1995). Structurally-controlled deep sea channel courses: examples from the Miocene of southeast Spain and the Alboran Sea, southwest Mediterranean, in A. J. Hartley and D. J. Prosser (eds.), *Characterization of deep marine clastic systems*, Geological Society Special Publication, 94, 115-135

Dam, G. and Sonderholm, M. (1994). Lowstand slope channels of the Itilli succession (Maastrichtian - Lower Paleocene), Nuussuaq, West Greenland, *Sedimentary Geology*, 94, 49-71.

Dam, G. and Sonderholm, M. (1998). Sedimentological evolution of a fault-controlled early Paleocene incised-valley system, Nuussuaq Basin, West Greenland, in *Relative role of eustasy, climate and tectonism in continental rocks*, SEPM Special Publication No. 59, 109-121.

Damuth, J. E., and Flood, R. D. (1985). Amazon Fan, Atlantic Ocean, in A. H. Bouma, W. R. Normark, and N. E. Barnes (eds.), *Submarine fans and related turbidite systems*, New York: Springer-Verlag, 97-106.

Damuth, J. E., Kowsmann, R. O., Flood, R. D., Belderson, R. H., and Gorini, M. A. (1983). Age relationships of distributary channels on Amazon deep-sea fan: Implications for fan growth pattern, *Geology*, 11, 470-473.

Deptuck, M. E. (1998). Characterization and interpretation of Upper Cretaceous to Eocene erosional features and submarine fans of the Jeanne d'Arc Basin, offshore Newfoundland, B.Sc. Honours Thesis, Saint Mary's University, Halifax, Nova Scotia, 120 p.

Deptuck, M. E. (2000). The Mara turbidite fan system in the Jeanne d'Arc Basin: Architecture, evolution, and modern analogues, in *Conference CD with Extended Abstracts*, GeoCanada 2000, Calgary, Alberta, May 28 – June 2 2000, Abstract number 679.

Deptuck, M. E., MacRae, R. A., Shimeld, J. W., Williams, G., and Fensome, R. (2003a). Revised Upper Cretaceous and lower Paleogene lithostratigraphy and depositional history

of the Jeanne d'Arc Basin, offshore Newfoundland, Canada, *AAPG Bulletin*, 87, 1459-1483.

Deptuck, M. E. and Piper, D. J. W. (2003). Paleocene and Eocene "North Sea-like" submarine fans in the Jeanne d'Arc Basin, offshore Newfoundland, Eastern Canada, *in* Program with Abstracts, AAPG Annual Meeting, Salt Lake City, Utah, May 11 - 14.

Deptuck, M. E., Steffens, G. S., and Pirmez, C. (2003b). Detailed anatomy and evolution of a West African channel-levee system: response to changing bathymetry and gravity flow processes. *in* Program with Abstracts, AAPG Annual Meeting, Salt Lake City, Utah, May 11 - 14.

Deptuck, M. E., Steffens, G. S., Barton, M., and Pirmez, C. (in press). Architecture and evolution of upper fan channel-belts on the Niger Delta slope and in the Arabian Sea, *in* E. Mutti, G. Steffens, C. Pirmez, and M. Orlando (eds.), *Turbidites: Models and Problems*, Special Issue: Marine and Petroleum Geology.

de Silva, N. (1993). Sequence stratigraphy and hydrocarbon potential of Cenomanian-Eocene interval, Jeanne d'Arc Basin, offshore Newfoundland, *The Leading Edge*, 12, 694-697.

de Voogd, B., Keen, C. E., and Kay, W. A. (1990). Fault reactivation during Mesozoic extension in eastern offshore Canada, *Tectonophysics*, 173, 567-580.

Dillon, W. P., and Popenoe, P. (1988). The Blake Plateau Basin and Carolina Trough, *in* R. E. Sheridan and J. A. Grow (eds.), *The Atlantic Continental Margin*, U.S. Geological Society of America, *The Geology of North America*, I-2, 291-327.

Doust, H., and Omatsola, E. (1989). Niger Delta, *in* Edwards, J. D., and P.A. Santogrossi (eds.), *Divergent/passive margin basins*, AAPG Memoir 48, 201-238.

Doeven, P. H. (1983). Cretaceous nannofossil stratigraphy and paleoecology of the Canadian Atlantic margin, *Geological Survey of Canada, Bulletin* 356, 1 - 57

Driscoll, N. W., Hogg, J. R., Christie-Blick, N., and Karner, G. D. (1995). Extensional tectonics in the Jeanne d'Arc Basin, offshore Newfoundland: implications for the timing of break-up between Grand Banks and Iberia, *in* R. A. Scrutton, M. S. Stoker, G. B. Shimmield, and A. W. Tudhope (eds.), *The tectonics, sedimentation and palaeoceanography of the North Atlantic region: Geological Society Special Publication* 90, 1 - 28.

Droz, L. and Bellaiche, G. (1991). Seismic facies and geologic evolution of the central portion of the Indus Fan, *in* P. Weimer and M. Link (eds.), *Seismic facies and sedimentary processes of submarine fans and turbidite systems*, New York: Springer-Verlag, 383-402

- Droz, L., Rigaut, F., Cochonat, P., and Tofani, R. (1996). Morphology and recent evolution of the Zaire turbidite systems (Gulf of Guinea), *Geological Society of America Bulletin*, 108, 253-269.
- Duranti, D., Hurst, A., Bell, C., Groves, S., Hanson, R. (2002). Injection and remobilized Eocene sandstone from the Alba Field, UKCS: core and wireline log characteristics, *Petroleum Geoscience*, 8, 99-107.
- Ebdon, C. C., Granger, P. J., Johnson, H. D., and Evans, A. M., Early Tertiary evolution and sequence stratigraphy of the Faeroe-Shetland Basin: implications for hydrocarbon prospectivity, *in* R. A. Scrutton, M. S. Stoker, G. B. Shimmield, and A. W. Tudhope (eds.), *The tectonics, sedimentation and palaeoceanography of the North Atlantic region: Geological Society Special Publication 90*, 51-69.
- Edwards, A., Moir, P. and Coflin, K. (2000), Structure and isopach maps of the Jeanne d'Arc Basin, Grand Banks, Newfoundland, Geological Survey of Canada, Open File 3755.
- Edwards, A., (1990). The western margin of the Jeanne d'Arc Basin, offshore Newfoundland (eastern Canada), *in* B. Pinet and C. Bois (eds.), *The potential of deep seismic profiling for hydrocarbon exploration: Editions Technip, Paris*, 161-173.
- Elder, W. P., Gustason, E. R., and Sageman, B. B. (1994). Correlation of basinal carbonate cycles to nearshore parasequences in the Late Cretaceous Greenhorn seaway, Western Interior, USA, *Geological Society of America Bulletin*, 106, 892-902.
- Emery, D and Myers, K. J. (1996). *Sequence stratigraphy*, Blackwell Science Ltd., Uxbridge, London, 297 p.
- Emmel, F. J., and Curray, J. R. (1985). Bengal Fan, Indian Ocean, *in* A. H. Bouma, W. R. Normark, and N. E. Barnes (eds.), *Submarine fans and related turbidite systems*, New York: Springer-Verlag, 107-112.
- Enachescu, M. E. (1987). The tectonic and structural framework of the northwest Newfoundland continental margin, *in* C. Beaumont and A. J. Tankard (eds.), *Sedimentary basins and basin forming mechanisms*, Canadian Society of Petroleum Geologists, Memoir 12, 117-145.
- Falvey, D. A. (1974). The development of continental margins in plate tectonic theory, *Australian Journal of Petroleum Exploration*, 14, 95 - 106.
- Falvey, D. A. and Middleton, M. F. (1981). Passive continental margins: evidence for a prebreakup deep crustal metamorphic subsidence mechanism, *Oceanologica Acta, SP Geology of Continental Margins Symposium*, 4, 103-114.

- Faugères, J.-P., Stow, D. A. V., Imbert, P., and Viana, A. (1999). Seismic features diagnostic of contourite drifts, *Marine Geology*, 162, 1 - 38.
- Fensome, R. A. (1995). Palynological analysis of the Cenozoic section in Mobil et al. Hibernia B-08 well, Jeanne d'Arc Basin, Grand Banks, Report No. BAS-PAL.3-95RAF, Report available at the Canada-Newfoundland Offshore Petroleum Board (C-NOPB), fifth floor, TD Place, 140 Water Street, St. John's Newfoundland, 4 p.
- Fensome, R. A. (1996a). Palynological analysis of the Cenozoic section in Mobil et al. Avondale A-46 well, Jeanne d'Arc Basin, Grand Banks, Report No. M.RES.G.-PAL.1-96RAF, Report available at the Canada-Newfoundland Offshore Petroleum Board (C-NOPB), fifth floor, TD Place, 140 Water Street, St. John's Newfoundland, 7 p.
- Fensome, R. A. (1996b). Palynological analysis of the Cenozoic section in Mobil et al. South Mara C-13 well, Jeanne d'Arc Basin, Grand Banks, Report No. M.RES.G.-PAL.2-96RAF, Report available at the Canada-Newfoundland Offshore Petroleum Board (C-NOPB), fifth floor, TD Place, 140 Water Street, St. John's Newfoundland, 10 p.
- Fensome, R. A. (1997). Palynological analysis of the Cenozoic section in Mobil et al. Mara M-54 well, Jeanne d'Arc Basin, Grand Banks, Report No. M.RES.G.-PAL.2-97RAF, Report available at the Canada-Newfoundland Offshore Petroleum Board (C-NOPB), fifth floor, TD Place, 140 Water Street, St. John's Newfoundland, 9 p.
- Flood, R. D. (1987). Side echoes from a sinuous fan channel obscure the structure of submarine fan channel levee systems, *Amazon Fan*, *Geo-Marine Letters*, 7, 15-22.
- Flood, R. D., Piper, D. J. W., and Shipboard Scientific Party (1995). Site 934, *in* Flood, R. D., Piper, D. J. W., Klaus, A., et al., *Proceedings of the Ocean Drilling Program, Initial Reports*, 155, 241-271.
- Flood, R. D. and Piper, D. J. W. (1997). Amazon fan sedimentation: the relationship to equatorial climate change, continental denudation, and sea-level fluctuations, *in* R.D. Flood, D.J.W. Piper, A. Klaus, and L.C. Peterson (eds.), *1997 Proceedings of the Ocean Drilling Program, Scientific Results*, 155, 653-675.
- Fowler, M. G. and McAlpine, K. D. (1995). The Egret Member, a prolific Kimmeridgian source rock from offshore eastern Canada, *in* B. J. Katz (ed.), *Petroleum source rocks: Springer - Verlag*, 111-130.
- Friedmann, S. J. (2000). Recent advances in deep-water sedimentology and stratigraphy using conventional and high-resolution 3D seismic data, *in* Conference CD with Extended Abstracts, *GeoCanada 2000*, Calgary, Alberta, May 28 - June 2 2000.
- Friis, N. (1997). A well log and 3D seismic study of the Late Cretaceous to Eocene deposits in the Hibernia area of the Jeanne d'Arc Basin, offshore Newfoundland, Canada, M.Sc. Thesis, Aarhus University, Denmark, 88 p.

- Gadd, S. A. and Scrutton, R. A. (1997). An integrated thermomechanical model for transform continental margin evolution, *Geo-Marine Letters*, 17, 21-30.
- Galloway, W. E. and Hobday, D. K. (1996). Terrigenous clastic depositional systems, Second Edition, Heidelberg, Springer-Verlag, 489 p.
- Garner, J. V., Bohannon, R. G., Field, M. E., and Masson, D. G. (1996). The morphology, processes, and evolution of Monterey Fan: A revisit, *in* J. V. Gardner, M. E., Field, and D. C. Twitchell (eds.), *Geology of the United States' Seafloor: The view from GLORIA*, New York: Cambridge University Press, 193-220
- Gervais, A. (2002). Analyse multi-echelles de la morphologie, de la geometrie et de l'architecture d'un system turbiditique sableux profond (System du Golo, Marge et-Corse, Mer Mediterranee), Ph.D. Thesis, 285 p.
- Gervais, A., Savoye, B., Piper, D. J. W., Mulder, T., Cremer, M., and Pichevin, L. (in press). Present morphology and depositional architecture of a sandy confined submarine system: the Golo turbidite system, *Marine and Petroleum Geology*.
- Goetz, J. F. and Nutt, R. L. (1997). Basic well log interpretation - short-course manual. Oil and Gas Consultants International, Inc., Tulsa Oklahoma.
- Gradstein, F. M. (1981). Micropaleontology of Ezzo Voyager Gabriel C-60, Flemish Pass, Part II, Geological Survey of Canada Internal Report EPGS-PAL, 1-81 FMG, 2 p.
- Gradstein, F. M., and Srivastava, S. P. (1980). Aspects of Cenozoic stratigraphy and paleoceanography of the Labrador Sea and Baffin Bay, *Palaeogeography, Palaeoclimatology, Palaeoecology*, 30, 261-295.
- Gradstein, F. M., Jansa, L. F., Srivastava, S. P., Williamson, M. A., Bonham Carter, G., and Stam, B. (1990). Aspects of North Atlantic paleo-oceanography, *in* M. J. Keen and G. L. Williams (eds.), *Geology of the continental margin of Eastern Canada: Geological Survey of Canada*, 351-389.
- Gradstein, F. M., Agterberg, F. P., Ogg, J. G., Hardenbol, J., Van Veen, P., Thierry, J. and Huang, Z. (1995). A Triassic, Jurassic, and Cretaceous time scale, *in* W. A. Berggren, D. V. Kent, M. P. Aubry, and J. Hardenbol (eds.), *Geochronology time scales and global stratigraphic correlation: Society of Sedimentary Geology, Special Publication* 54, 95-126.
- Grant, A. C. (1975). Structural modes of the western margin of the Labrador Sea, *in* W. J. M. van der Linden and J. A. Wade (eds.), *Offshore geology of Eastern Canada, Geological Survey of Canada, Paper 74-30*, 217-231.

- Grant, A. C. and McAlpine, K. D. (1990). Chapter 6, The continental margin around Newfoundland, *in* M. J. Keen and G. L. Williams (eds.), *Geology of the continental margin of Eastern Canada: Geological Survey of Canada*, 239-292.
- Grant, A. C., Jansa, L. F., McAlpine, K. D., and Edwards, A. (1988). Mesozoic-Cenozoic geology of the eastern margin of the Grand Banks and its relation to Galicia Bank, *in* G. Boillot, E. L. Winterer et al. (eds.), *Proceedings of the Ocean Drilling Program, Scientific Results: College Station, TX*, 103, 787-807.
- Hackbarth, C. J., and Shew, R. D. (1994). Morphology and stratigraphy of a mid-Pleistocene turbidite leveed channel from seismic, core and log data, in Northeastern Gulf of Mexico, *in* *Submarine Fans and Turbidite Systems: GCSSEPM Foundation 15th Annual Research Conference*, 127-133.
- Haq, B. U. (1984). Paleooceanography: A synoptic overview of 200 million years of ocean history, *in* B. U. Haq and J. P. Milliman (ed.), *Marine geology and oceanography of Arabian Sea and Coastal Pakistan*, Van Nostrand Reinhold, New York, NY, 201-231.
- Haq, B. U., Hardenbol, J., and Vail, P. R. (1987). Chronology of fluctuating sea level since the Triassic, *Science*, 235, 1156 – 1167.
- Hardage, B. A. (1985). Vertical seismic profiling - a measurement that transfers geology to geophysics, *in* O. R. Berg and D. G. Woolverton (eds.), *Seismic stratigraphy 2: An integrated approach to hydrocarbon exploration*, AAPG Memoir 39, 13-34.
- Hardy, I. A. (1975). Lithostratigraphy of the Banquereau Formation on the Scotian Shelf, *in* W. J. M van der Linden and J. A. Wade (eds.), *Offshore geology of eastern Canada: Geological Survey of Canada, Paper 74-30*, 163-174.
- Hart, B. S. (1999). Definition of subsurface stratigraphy, structure and rock properties from 3-D seismic data, *Earth-Science Reviews*, 47, 189-218.
- Hart, B. S. (2000). 3-D seismic interpretation: a primer for geologists, *SEPM Short Course No. 48*, 123 p.
- Haughton, P. D. W. (2000). Evolving turbidite systems on a deforming basin floor, Taberna, SE Spain, *Sedimentology*, 47, 497-518.
- Haworth, R. T. and Lefort, J. P. (1979). Geophysical evidence for the extent of the Avalon zone in Atlantic Canada, *Canadian Journal of Earth Sciences*, 16, 552-567.
- Hay, W.W., DeConto, R., Wold, C.N., Wilson, K.M., Voigt, S., Schulz, M., Wold-Rossby, A., Dullo, W.-C., Ronov, A.B., Balukhovskiy, A.N. and Soeding, E. (1999). Alternative global Cretaceous Paleogeography, *in* E. Barrera and C. Johnson (eds.), *The Evolution of Cretaceous Ocean/Climate Systems*, Geological Society of America Special Paper 332, 1-47.

- Heezen, B. C. and Hollister, C. (1964). Deep-sea current evidence from abyssal sediments, *Marine Geology*, 1, 141-174.
- Henriet, J.-P., De Batist, M., Van Vaerenbergh, W., and Verscheren, M. (1988). Seismic facies and clay tectonic features on the Ypresian clay in southern North Sea, *Bulletin van de Belgische Vereniging voor Geologie*, 97-3/4, 457-472.
- Heritier, F. E., Lossel, P., and Wathne, E. (1979). Frigg field - large submarine fan trap in lower Eocene rocks of North Sea Viking Graben, *AAPG Bulletin*, 63, 1999-2020.
- Hernandez-Molina, J., Llave, E., Somoza, L., Fenandez-Puga, M. C., Maestro, A., Leon, R., Medialdea, T., Barnolas, A., Garcia, M., del Rio, V. D., Fernandez-Salas, L. M., Vazquez, J. T., Lobo, F., Dias, J. M. A., Rodero, J., Gardner, J. (2003). Looking for clues to paleoceanographic imprints: a diagnosis of the Gulf of Cadiz contourite depositional systems, *Geological Society of America*, 31, 19-22.
- Hiscott, R. N., Hall, R. R., and Pirmez, C. (1997). Turbidity-current overspill from the Amazon Channel: texture of the silt/sand load, paleoflow from anisotropy of magnetic susceptibility, and implications for flow processes, *in* R.D. Flood, D.J.W. Piper, A. Klaus, and L.C. Peterson (eds.), 1997 Proceedings of the Ocean Drilling Program, *Scientific Results*, 155, 53-78.
- Hiscott, R. N., Wilson, R. C. L., Harding, S. C., Pujalte, V., Kitson, D. (1990). Contrasts in Early Cretaceous depositional environments of marine sandbodies, Grand Banks – Iberia, *Bulletin of Canadian Petroleum Geology*, 38, 203-214.
- Hollister, C. D. and McCave, I. N. (1984). Sedimentation under deep-sea storms, *Nature*, 309, 220-225.
- Howe, J. A. (1996). Turbidite and contourite sediment waves in the northern Rockall Trough, North Atlantic Ocean, *Sedimentology*, 43, 219-234.
- Hubbard, R. J., Pape, J., and Roberts, D. G. (1985). Depositional sequence mapping to illustrate the evolution of a passive continental margin, *in* O. R. Berg and D. G. Woolverton (eds.), *Seismic stratigraphy 2: An integrated approach to hydrocarbon exploration*, AAPG Memoir 39, 93 - 115.
- Hubscher, C., Spieb, V., Breitzke, M., and Weber, M. E. (1997). The youngest channel-levee system of the Bengal Fan: results from digital sediment echosounder data, *Marine Geology*, 141, 125-145.
- Husky – Bow Valley et al. (1984). Well history report, North Ben Nevis P-93, Report available at the Canada-Newfoundland Offshore Petroleum Board (C-NOPB), fifth floor, TD Place, 140 Water Street, St. John's Newfoundland.

- Jansa, L. F. and Wade, J. A. (1975a). Paleogeography and sedimentation in the Mesozoic and Cenozoic, Southeastern Canada, *in* C. J. Yorath, E. R. Parker, and D. J. Glass (eds.), *Canada's Continental Margins and Offshore Petroleum Exploration: Canadian Society of Petroleum Geologists, Memoir 4*, 79-102.
- Jansa, L. F. and Wade, J. A. (1975b). Geology of the continental margin off Nova Scotia and Newfoundland, *in* W. J. M van der Linden and J. A. Wade (eds.), *Offshore geology of eastern Canada: Geological Survey of Canada, Paper 74-30*, 51-105.
- Jansa, L. F., Enos, P., Tucholke, B. E., Gradstein, F. M., and Sheridan, R. E. (1979) Mesozoic-Cenozoic sedimentary formations of the North American Basin, western North Atlantic, *in* M. Talwani, W. Hay, W. B. F., Ryan (eds.), *Deep drilling in the Atlantic Ocean - continental margins and paleoenvironments*, American Geophysical Union, Maurice Ewing Series, 3, 1-57.
- Jennette, D. C., Garfield, T. R., Mohrig, D. C., Cayley, G. T. (2000). The interaction of shelf accommodation, sediment supply and sea level in controlling the facies, architecture and sequence stacking patterns of the Tay and Forties/Sele basin floor fans, Central North Sea, *in* P. Weimer, R. M. Slatt, J. Coleman, N. C. Rosen, H. Nelson, A. H. Bouma, M. J. Styzen, and D. T. Lawrence (eds.), *Deep-water reservoirs of the world: GCSSEPM Foundation 20th Annual Research Conference*, 402-421.
- Jennsen, A. I., Bergslein, D., Rye-Larsen, M., and Lindholm, R. M. (1993). Origin of complex mound geometry of Paleocene submarine-fan sandstone reservoirs, Balder field, Norway, *in* J. R. Parker (ed.), *Petroleum geology of northwest Europe: Proceedings of the 4th Congress*, The Geological Society of London, 137-143.
- Johnson, D. (1938). Origin of submarine canyon, *Journal of Geomorphology*, 1, 111-129.
- Kastens, K. A., and Shor, A. N. (1985). Depositional processes of a meandering channel on Mississippi fan, *AAPG Bulletin*, 69, 190-202.
- Kearey, P. and Brooks, M. (1991). *An introduction to geophysical exploration*, Second Edition, Blackwell Scientific Publications, Oxford, 254 p.
- Keen, C. E., Boutilier, R., de Voogd, B., Mudford, B. S., and Enachescu, M. E. (1987). Crustal geometry and extensional models for the evolution of the rift basins on the Grand Banks, Eastern Canada: constraints from deep seismic reflection data, *in* C. Beaumont and A. J. Tankard (eds.), *Sedimentary basins and basin-forming mechanisms: Canadian Society of Petroleum Geologists, Memoir 12*, 101-115.
- Keen, C. E., Loncarevic, B. D., Reid, I., Woodside, J., Haworth, R. T., and Williams, H. (1990). Chapter 2: Tectonic and geophysical overview, *in* M. J. Keen and G. L. Williams (eds.), *Geology of the continental margin off eastern Canada: Geological Survey of Canada*, 31-85.

- Keen, C. E., and Beaumont, C. (1990). Chapter 9: Geodynamics of rifted continental margins, *in* M. J. Keen and G. L. Williams (eds.), *Geology of the continental margin off eastern Canada: Geological Survey of Canada*, 391-472.
- Keller, G., MacLeod, N., Lyons, J. B., and Officer, C. B. (1993). Is there evidence for Cretaceous - Tertiary boundary-age deep-water deposits in the Caribbean and Gulf of Mexico?, *Geology*, 21, 776-780.
- Kennard, L., Schafer, C., and Carter, L. (1990). Late Cenozoic evolution of Sackville Spur: a sediment drift on the Newfoundland continental slope, *Canadian Journal of Earth Sciences*, 27, 863-878.
- Kennett, J. (1982). *Marine Geology: Chapter 15*, Prentice-Hall, Eaglewood Cliffs, N.J., p. 505 - 535.
- Kenyon, N.H., Amir, A., and Cramp, A. (1995). Geometry of the younger sediment bodies of the Indus Fan, *in* K. T. Pickering, R. N. Hiscott, N. H. Kenyon, F. Ricci Lucchi, and R. D. A. Smith (eds.), *Atlas of deep water environments: Architectural style in turbidite systems*, London: Chapman and Hall, 89-93
- Kidd, G. D. (1999). *Fundamentals of 3-D seismic interpretation*, The Leading Edge, June, 1999.
- Klaus, A., Norris, R. D., Kroon, D., and Smit, J. (2000). Impact-induced mass wasting at the K-T boundary: Blake Nose, western North Atlantic, *Geology*, 28, 319-322.
- Kleverlaan, K. (1989). Three distinctive feeder-lobe systems within one time slice of the Tortonian Tabernas fan, SE Spain, *Sedimentology*, 36, 25-45.
- Kolla, V. and Coumes, F. (1987). Morphology, internal structure, seismic stratigraphy, and sedimentation of Indus Fan, *AAPG Bulletin*, 71, 650-677.
- Kolla, V., Bourges, Ph., Urruty, J.-M, and Safa, P. (2001). Evolution of deep-water Tertiary sinuous channels offshore Angola (west Africa) and implications for reservoir architecture, *AAPG Bulletin*, 85, 1373-1405.
- Kolla, V. and Macurda, D. B. (1988). Sea-level changes and timing of turbidity current events in deep-sea fan systems, *in* *Sea level changes - An integrated approach*, SEPM Special Publication No. 42, 381-393.
- Komar, P. D. (1985). The hydraulic interpretation of turbidites from their grain sizes and sedimentary structures, *Sedimentology*, 32, 395-407.
- Kuenen, Ph. H. (1958). Sole markings of graded graywacke beds, *Journal of Geology*, 65, 231-258.

- Kulpecz, A. A. and van Geuns, L. C. (1990). Geological modeling of a turbidite reservoir, Forties field, North Sea, in J. H. Barwis, J. G. McPherson, J. R. J. Studlick (eds.), *Sandstone Petroleum Reservoirs*, Springer-Verlag, New York, 489-507.
- Laine, E. P. and Hollister, C. D. (1981). Geological effects of the Gulf Stream on the northern Bermuda Rise, *Marine Geology*, 39, 277-310.
- Lonergan, L., Lee, N., Johnson, H. D., Cartwright, J. A., and Jolly, R. J. G. (2000). Remobilization and injection in deepwater depositional systems: Implications for reservoir architecture and prediction. *in* P. Weimer, R. M. Slatt, J. Coleman, N. C. Rosen, H. Nelson, A. H. Bouma, M. J. Styzen, and D. T. Lawrence (eds.), *Deep-water reservoirs of the world: GCSSEPM Foundation 20th Annual Research Conference*, 515-532.
- Lorenzo, J. M. (1997). Sheared continent-ocean margins: an overview, *Geo-Marine Letters*, 17, 1-3.
- Lorenzo, J. M. and Wessel, P. (1997). Flexure across a continent-ocean fracture zone: the northern Falkland/Malvinas Plateau, South Atlantic, *Geo-Marine Letters*, 17, 110-118.
- Lowe, D. R. (1982). Sediment gravity flows: II. Depositional models with special reference to the deposits of high-density turbidity currents, *Journal of Sedimentary Petrology*, 52, 279-297.
- MacLean, B. C. and Wade, J. A. (1992). Petroleum geology of the continental margin south of the islands of St. Pierre and Miquelon, offshore Eastern Canada, *Bulletin of Canadian Petroleum Geology*, 40, 222-253.
- MacLeod, K. G., Fullagar, P. D., and Huber, B. T. (2003). $^{87}\text{Sr}/^{86}\text{Sr}$ test of the degree of impact-induced slope failure in the Maastrichtian of the western North Atlantic, *Geology*, 31, 311-314.
- MacRae, A., Shimeld, J., and Fensome, R. (2002). Cryptic erosion on the Upper Cretaceous Wyandot Formation, Sable Island area, Scotian Shelf (abstract), *Atlantic Geology*, 38, p. 93.
- Manley, P. L., Pirmez, C., Busch, W., and Cramp, A. (1997). Grain-size characterization of Amazon Fan deposits and comparison to seismic facies units, *in* R.D. Flood, D.J.W. Piper, A. Klaus, and L.C. Peterson (eds.), *1997 Proceedings of the Ocean Drilling Program, Scientific Results*, 155, 35-52.
- Martini, E. (1971). Standard Tertiary and Quaternary calcareous nannoplankton zonation, *in* A. Farinacci (ed.), *Proceedings of the second planktonic conference*, Roma, 1970, *Tecnoscienza*, 739-785.

- Masclé, J., Lohmann, P., and Clift, P. (1997). Development of a passive transform margin: Cote d'Ivoire - Ghana transform margin - ODP Leg 159, Preliminary Results, *Geo-Marine Letters*, 17, 4-11.
- Mastbergen, D. R. and Van Den Berg, J. H. (2003). Breaching in fine sands and the generation of sustained turbidity currents in submarine canyons, *Sedimentology*, 50, 625-637.
- Mayall, M., and Stewart, I. (2000). The architecture of turbidite slope channels, *in* P. Weimer, R. M. Slatt, J. Coleman, N. C. Rosen, H. Nelson, A. H. Bouma, M. J. Stytzen, and D. T. Lawrence (eds.), *Deep-water reservoirs of the world: GCSSEPM Foundation 20th Annual Research Conference*, 578-586.
- McAlpine, K. D. (1990). Mesozoic stratigraphy, sedimentary evolution, and petroleum potential of the Jeanne d'Arc Basin, Grand Banks of Newfoundland, Geological Survey of Canada, Paper 89-17, 1-50.
- McCave, I. N. and Tucholke, B. E. (1986). Deep current-controlled sedimentation in the western North Atlantic, *in* P. R. Vogt and B. E. Tucholke (eds.), *The geology of North American*, Volume M, *The western North Atlantic Regions*, Geological Society of America, 451-468.
- McGovney, J.E., and Radovich, B. J. (1985). Seismic stratigraphy and facies of the Frigg Fan Complex, *in* O. R. Berg and D. G. Woolverton (eds.), *Seismic stratigraphy 2: An integrated approach to hydrocarbon exploration*, AAPG Memoir 39, 139-156.
- McHargue, T. R. (1991). Seismic facies, processes, and evolution of Miocene inner fan channels, Indus Submarine Fan, *in* P. Weimer and M. Link (eds.), *Seismic facies and sedimentary processes of submarine fans and turbidite systems*, New York: Springer-Verlag, 402-413.
- McHargue, T. R. and Webb, J. E. (1986). Internal geometry, seismic facies, and petroleum potential of canyons and inner fan channels of the Indus Submarine Fan, *AAPG Bulletin*, 70, 161-180.
- McIver, N. L. (1972). Cenozoic and Mesozoic Stratigraphy of the Nova Scotia Shelf, *Canadian Journal of Earth Sciences*, 9, 54-70.
- McKenzie, D. (1978). Some remarks on the development of sedimentary basins, *Earth and Planetary Science Letters*, 40, 25-32.
- McWhae, J. R. H., Elie, R., Laughton, K. C., and Gunther, P. R. (1980). Stratigraphy and petroleum prospects of the Labrador Shelf, *Bulletin of Canadian Petroleum Geology*, 28, 460-488.

- Miall, A. D. (1985). Architectural-element analysis: A new method of facies analysis applied to fluvial deposits, *Earth Science Reviews*, 22, 261-308.
- Miall, A. D. (1992). Exxon global cycle chart: an event for every occasion?, *Geology*, 20, 787-790.
- Middleton, G. V., and Hampton, M. A. (1973). Part I - Sediment gravity flows: mechanics of flow and deposition, *in* Middleton and Bouma (eds.) *Turbidites and deep-water sedimentation*, lecture notes for a Short Course sponsored by the Pacific Section of SEPM, Los Angeles, California, 1-38.
- Miller, P. E., D'Eon, G. J., and Bell, J. S. (1988). Mesozoic and Tertiary paleoenvironments of the Labrador Shelf, offshore Eastern Canada, *in* D. P. James and D. A. Leckie (eds.), *Sequences, stratigraphy, sedimentology: Surface and subsurface*, Canadian Society of Petroleum Geologists, Memoir 15, 351-360.
- Mitchell, S. M. Beamish, G. W. J., Wood, M. V., Malacek, S. J., Armentrout, J. A., Damuth, J. E., and Olsen, H. C. (1993). Palaeogene sequence stratigraphic framework of the Faeroe Basin, *in* J. R. Parker (ed.), *Petroleum geology of northwest Europe: Proceedings of the 4th Congress*, The Geological Society of London, 1011-1023.
- Mitchum, R. M., Vail, P. R., and Thompson, S. (1977a). Seismic stratigraphy and global changes of sea level, part 2: The depositional sequence as a basic unit for stratigraphic analysis, *in* C. E. Payton (ed.), *AAPG Memoir 26, Seismic stratigraphy - applications to hydrocarbon exploration*, Tulsa Oklahoma, 53-62.
- Mitchum, R. M., Vail, P. R., and Sangree, J. B. (1977b). Seismic stratigraphy and global changes of sea level, part 6: Stratigraphic interpretation of seismic reflection patterns in depositional sequences, *in* C. E. Payton (ed.), *AAPG Memoir 26, Seismic stratigraphy - applications to hydrocarbon exploration*, Tulsa Oklahoma, 117-133.
- Mitchum, R. M. (1985). Seismic stratigraphic expression of submarine fans, *in* O. R. Berg and D. G. Woolverton (eds.), *AAPG Memoir 39, Seismic stratigraphy II: an integrated approach to hydrocarbon exploration*, Tulsa, Oklahoma, 117-136.
- Mitlehner, A. G. (1996). Palaeoenvironments in the North Sea Basin around the Paleocene-Eocene boundary: evidence from diatoms and other siliceous microfossils, *in* R. W. Know, R. M. Corfield, and R. E. Dunay (eds.), *Correlation of the Early Paleogene in northwest Europe: Geological Society Special Publication 101*, 255-273.
- Mobil et al. (1988). Well history report, Avondale A-46, Report available at the Canada-Newfoundland Offshore Petroleum Board (C-NOPB), fifth floor, TD Place, 140 Water Street, St. John's Newfoundland.

Mobil et al. (1992). Biostratigraphy and paleoecology report for Mobil et al. Botwood G-89. Report available at the Canada-Newfoundland Offshore Petroleum Board (C-NOPB), fifth floor, TD Place, 140 Water Street, St. John's Newfoundland.

Mobil et al. (1992). Well history report, Botwood G-89, Report available at the Canada-Newfoundland Offshore Petroleum Board (C-NOPB), fifth floor, TD Place, 140 Water Street, St. John's Newfoundland.

Mobil Oil Canada (1991). Hibernia 3-D seismic survey, C-NOPB Project No. 8624-M003-036E, 40E, Canada-Newfoundland Offshore Petroleum Board, fifth floor, TD Place, 140 Water Street, St. John's Newfoundland.

Mosher, D. C., LaPierre, A. B., Hughes, J. E., and Gilbert, G. R. (2002). Theoretical comparison of seafloor surface renders from multibeam sonar and 3D seismic exploration data, Offshore Technology Conference, Houston, Texas, May 6-9 2002.

Mosher, D. C. and Simpkin, P. G. (1999). Environmental Marine Geoscience 1. Status and trends of marine high-resolution seismic-reflection profiling: Data acquisition, Geoscience Canada, 26, 174-188.

Mutti, E. (1979). Turbidites et cones sous-marins profonds, in P. Homewood (ed.), Sedimentation detritique (fluviale, littorale et marine), Institut de Geologie, Universite de Frigbourg, Suisse, 353-419.

Mutti, E. (1985a). Turbidite systems and their relations to depositional sequences, in G. G. Zuffa (ed.), Provenance of Arenites, Reidel Publishing Company, 65-93.

Mutti, E. (1985b). Chapter 30 - Hecho turbidite system, Spain, in A. H. Bouma, W. R. Normark, and N. E. Barnes (eds.), Submarine fans and related turbidite systems, New York: Springer-Verlag, 205-208.

Mutti, E. and Normark, W. R. (1987). Comparing examples of modern and ancient turbidite systems: problems and concepts, in J. K. Leggett and G. G. Zuffa (eds.), Marine clastic sedimentology, Graham and Trotman, 1-38.

Mutti, E. and Normark, W. R. (1991). An integrated approach to the study of turbidite systems, in P. Weimer and M.H. Link (eds.), Seismic facies and sedimentary processes of modern and ancient submarine fans, New York: Springer-Verlag, 75-106.

Mutti, E. and Ricci Luchi, F. (1972). Le torbiditi dell' Appennino settentrionale: introduzione all' analisi di facies, Memorie della Societa Geologica Italiana, 11, 161-199.

Nadin, P. A., Kusnir, N. J., and Cheadle, M. J. (1997). Early Tertiary plume uplift of the North Sea and Faeroe-Shetland basins, Earth and Planetary Science Letters, 148, 109-127.

- Naini, B. R. and Kolla, V. (1982). Acoustic character and thickness of sediments of the Indus Fan and the continental margin of western India, *Marine Geology*, 47, 181-195.
- Nakajima, T., Satoh, M., and Okamura, Y. (1998). Channel-levee complexes, terminal deep-sea fan and sediment wave fields associated with the Toyama deep-sea channel system in the Japan Sea, *Marine Geology*, 147, 25-41.
- Newman, M. St. J., Reeder, M. L., Woddruff, A. H. W., and Hatton, I. R. (1993). The geology of the Gryphon oil field, *in* J. R. Parker (ed.), *Petroleum geology of northwest Europe: Proceedings of the 4th Congress*, The Geological Society of London, 123-133.
- Newton, S. K. and Flanagan, K. P. (1993). The Alba field: evolution of the depositional model, *in* J. R. Parker (ed.), *Petroleum geology of northwest Europe: Proceedings of the 4th Congress*, The Geological Society of London, 123-133.
- Nissen, S. E., Haskell, N. L., Steiner, C. T., and Coterill, K. L. (1999). Debris flow outrunner blocks, glide tracks, and pressure ridges identified on the Nigerian continental slope using 3-D seismic coherency, *The Leading Edge*, May 1999, 595-599.
- Normark, W. R. (1970). Growth patterns of deep sea fans, *AAPG Bulletin*, 54, 2170-2195.
- Normark, N. R. (1978). Fan valleys, channels, and depositional lobes on modern submarine fans: characters for recognition of sandy turbidite environments, *AAPG Bulletin*, 62, 912-931.
- Normark, W. R. (1991). Turbidite elements and the obsolescence of the suprafan concept, *Giornale di Geologia*, ser 3, v. 53/2, p. 1-10.
- Normark, W. R., and Gutmacher, C. E. (1985). Delgada fan, Pacific Ocean, *in* A. H. Bouma, W. R. Normark, and N. E. Barnes (eds.), *Submarine fans and related turbidite systems*, New York: Springer-Verlag, 59-64.
- Normark, W. R. and Piper, D. J. W. (1991). Initiation processes and flow evolution of turbidity currents: implications for the depositional record, *in* *From shoreline to abyss*, SEPM Special Publication No. 46, 207-230.
- Normark, W. R., Piper, D. J. W., Posamentier, H., Pirmez, C., and Migeon, S. (2003). Variability in form and growth of sediment waves on turbidite channel levees, *Marine Geology*, 192, 23-58.
- Normark, W. R., Posamentier, H., and Mutti, E. (1993). Turbidite systems: state of the art and future directions, *Reviews of Geophysics*, 31, 91-116.

- Normark, W. R., Piper, D. J. W., and Hiscott, R. N. (1998). Sea level controls on the textural characteristics and depositional architecture of the Hueneme and associated submarine fan systems, Santa Monica Basin, California, *Sedimentology*, 45, 53-70.
- Norris, R. D., Firth, J., Blusztajn, J. S., Ravizza, G. (2000). Mass failure of the North Atlantic margin triggered by the Cretaceous - Paleogene bolide impact, *Geology*, 1119-1122.
- North, F.K., 1985. *Petroleum Geology*. Chapter 12: Well logs. Allen and Unwin Inc., Mass. p. 127-151
- O'Connell, S., McHugh, C., and Ryan, W. B. F. (1995). Unique fan morphology in an entrenched thalweg channel on the Rhone Fan, *in* K. T. Pickering, R. N. Hiscott, N. H. Kenyon, F. Ricci Lucchi, and R. D. A. Smith (eds.), *Atlas of deep water environments: Architectural style in turbidite systems*, London: Chapman and Hall, 80-83
- Owens, B. (1981). Chapter 13, Palynology, its biostratigraphic and environmental potential, *in* *Petroleum geology of the continental shelf of North-West Europe*, Institute of Petroleum, London, 162-168.
- Parker, R. S. (1999). Ancient canyons and fans of the Carson Basin, Grand Banks, offshore Newfoundland, Canada, B.Sc. Honours Thesis, Dalhousie University, Halifax, Nova Scotia, 77 p.
- Paull, C. K. and Dillon, W. P. (1980). Structure, stratigraphy, and geologic history of Florida-Hatteras shelf and inner Blake Plateau, *AAPG Bulletin*, 64, 339-358.
- Peakall, J. McCaffrey, B., and Kneller, B. (2000). A process model for the evolution, morphology, and architecture of sinuous submarine channels, *Journal of Sedimentary Research*, 70, 434-448.
- Pe-Piper, G., Piper, D. J. W., Keen, M. J., and McMillan, N. J. (1990). Igneous rocks of the continental margin, *in* M. J. Keen and G. L. Williams (eds.), *Geology of the continental margin off eastern Canada: Geological Survey of Canada*, 75-84.
- Petro-Canada (1984). Terra Nova area 3-D seismic survey, C-NOPB Project No. 8624-P28-70E: Canada-Newfoundland Offshore Petroleum Board, fifth floor, TD Place, 140 Water Street, St. John's Newfoundland.
- Pichevin, L. (2000). Etude sédimentaire et sismique d'un éventail turbiditique sableux: le système récent du Golo (Marge Est-Corse), DEA Environnements et Paléoenvironnements Cotiers et Océaniques, Université Bordeaux, 57 p.
- Pickering, K. T., Clark, J. D., Smith, R. D. A., Hiscott, R. N., Ricci Lucchi, F., and Kenyon, N. H. (1995). Architectural element analysis of turbidite systems, and selected topical problems for sand-prone deep-water systems, *in* K. T. Pickering, R. N. Hiscott, N.

- H. Kenyon, F. Ricci Lucchi, and R. D. A. Smith (eds.), Atlas of deep water environments" Architectural style in turbidite systems, Chapman and Hall, London, 1-9.
- Pickering, K. T., Hodgson, D. M., Platzman, E., Clark, J. D., and Stephens, C. (2001). A new type of bedform produced by backfilling processes in a submarine channel, Late Miocene, Tabernas-Sorbas Basin, SE Spain, *Journal of Sedimentary Research*, 71, 692-704.
- Pinet, P. R., Popenoe, P., Nelligan, D. F. (1981). Gulf Stream: reconstruction of Cenozoic flow patterns over the Blake Plateau, *Geology*, 9, 266-270.
- Pinet, P. R. and Popenoe, P. (1985). A scenario of Mesozoic-Cenozoic ocean circulation over the Blake Plateau and its environs, *Geological Society of America Bulletin*, 96, 618-626.
- Piper, D. J. W. (1970). Transport and deposition of Holocene sediment on La Jolla deep sea fan, California, *Marine Geology*, 8, 211-227.
- Piper, D. J. W., and Deptuck, M. E. (1997). Fine-grained turbidites of the Amazon Fan: facies characterization and interpretation. *in* R.D. Flood, D.J.W. Piper, A. Klaus, and L.C. Peterson (eds.), 1997 Proceedings of the Ocean Drilling Program, Scientific Results, 155, 79-108.
- Piper, D. J. W, Hiscott, R.N. and Normark, W.R. (1999). Outcrop-scale acoustic facies analysis and the latest Quaternary development of Hueneme and Dume submarine fans, offshore California, *Sedimentology*, 46, 47-78.
- Piper, D. J. W., Kontopolous, N., Anagnostou, C., Chronis, G., and Pnagos, A. G. (1990). Modern fan deltas in the western Gulf of Corinth, Greece, *Geo-Marine Letters*, 10, 5-12.
- Piper, D. J. W., and Normark, W. R. (1983). Turbidite depositional patterns and flow characteristics, Navy Submarine fan, California Continental Borderlands, *Sedimentology*, 30, 681-694.
- Piper, D. J. W., and Normark, W. R. (1989). Late Cenozoic sea-level changes and the onset of glaciation: impact on continental slope progradation off eastern Canada, *Marine and Petroleum Geology*, 6, 336-347.
- Piper, D. J. W., and Normark, W. R. (2001). Sandy fans - from Amazon to Hueneme and beyond, *AAPG Bulletin*, 85, 1407-1438.
- Piper, D. J. W., Stow, D. A. V., and Normark, W. R. (1985). Laurentian fan, Atlantic Ocean, *in* A. H. Bouma, W. R. Normark, and N. E. Barnes (eds.), Submarine fans and related turbidite systems, New York: Springer-Verlag, 137-142.

- Pirmez, C. (1994). Growth of a submarine meandering channel-levee system on the Amazon Fan, Unpublished Ph.D. Thesis, Columbia University, New York, 587 p.
- Pirmez, C., Beaubouef, R. T., Friedmann, S. J., and Mohrig, D. C. (2000). Equilibrium profiles and baselevel in submarine channel: Examples from Late Pleistocene systems and implications for the architecture of deepwater reservoirs. *in* P. Weimer, R. M. Slatt, J. Coleman, N. C. Rosen, H. Nelson, A. H. Bouma, M. J. Styzen, and D. T. Lawrence (eds.), *Deep-water reservoirs of the world: GCSSEPM Foundation 20th Annual Research Conference*, 782-805.
- Poag, C. W. (1992). U.S. middle Atlantic continental rise: provedence, dispersal, and deposition of Jurassic to Quaternary sediments, *in* C. W. Poag and P. C. de Graciansky (eds.) *Geologic evolution of Atlantic continental rises*, Van Nostrand Reinhold, New York, 101-156.
- Posamentier, H. W. and Vail, P. R. (1988). Eustatic controls on clastic deposition II - sequence and systems tract models, *in* *Sea level changes - An integrated approach*, SEPM Special Publication No. 42, 125-154.
- Posamentier, H. W. (1991). Chapter 6 - Models for submarine-fan deposition within a sequence-stratigraphic framework, *in* P. Weimer and M.H. Link (eds.), *Seismic facies and sedimentary processes of modern and ancient submarine fans*, New York: Springer-Verlag, 127-136.
- Posamentier, H. W., Meizarwin, Wisman, P. S., and Plawman, T. (2000). Deep water depositional systems – Ultra-deep Makassar Strait, Indonesia, *in* P. Weimer, R. M. Slatt, J. Coleman, N. C. Rosen, H. Nelson, A. H. Bouma, M. J. Styzen, and D. T. Lawrence (eds.), *Deep-water reservoirs of the world: GCSSEPM Foundation 20th Annual Research Conference*, 806-816.
- Posamentier, H. W. (in press). Depositional elements associated with a basin floor channel-levee complex: case study from the Gulf of Mexico, *Marine and Petroleum Geology*.
- Postma, G., Nemeč, W., and Kleinspehn, K. L. (1988). Large floating clasts in turbidites: a mechanism for their emplacement, *Sedimentary Geology*, 58, 47-61.
- Purvis, K., Kao, J., Flanagan, K., Henderson, J., Duranti, D. (2002). Complex reservoir geometries in a deep water clastic sequence, Gryphon field, UKCS: injection structures, geological modelling, and reservoir simulation, *Marine and Petroleum Geology*, 19, 161-179.
- Reading, H. G. and Richards, M. (1994). Turbidite systems in deep-water basin margins classified by grain size and feeder system, *AAPG Bulletin*, 78, 792-822.

Ricci Lucchi, F. (1985). Chapter 9: Crati fan, *in* A. H. Bouma, W. R. Normark, and N. E. Barnes (eds.), *Submarine fans and related turbidite systems*, New York: Springer-Verlag, 59-64.

Rider, M. H. (1991). *The Geological Interpretation of Well Logs*. Revised edition. Whittles Publishing, Caithness, 175 p.

Roest, W. R. and Srivastava, S. P. (1989). Sea-floor spreading in the Labrador Sea: A new reconstruction, *Geology*, 17, 1000-1003.

Roksandic, M. M. (1978). Seismic facies analysis concepts, *in* M. M. Roksandic (ed.), *Seismic facies analysis concepts*, *Geophysical prospecting*, 26, 383-398.

Roksandic, M. M. (1985). Stratification and reflections, *First Break*, 3, 9-16.

Royden, L. and Keen, C. E. (1980). Rifting process and thermal evolution of the continental margin of Eastern Canada determined from subsidence curves, *Earth and Planetary Science Letters*, 51, 343-361.

Sangree, J. B. and Widmier, J. M. (1977). Seismic stratigraphy and global changes of sea level, part 9: Seismic interpretation of clastic depositional facies, *in* C. E. Payton (ed.), *AAPG Memoir 26, Seismic stratigraphy - applications to hydrocarbon exploration*, Tulsa Oklahoma, 165-184.

Sangree, J. B. and Widmier, J. M. (1979). Interpretation of depositional facies from seismic data, *Geophysics*, 44, 131-160.

Sarg, J. F., and Skjold, L. J. (1982). Stratigraphic traps in Paleocene sands in the Balder area, North Sea, *AAPG Memoir 32*, 197-206.

Schlische, R.W. (1993). Anatomy and evolution of the Triassic-Jurassic continental rift system, Eastern North America, *Tectonics*, 12, 1026-1042.

Shanmugam, G. (1996). High-density turbidity currents: are they sandy debris flows?, *Journal of Sedimentary Research*, 66, 2-10.

Shanmugam, G. and Moiola, R. J. (1988). Submarine fans: Characteristics, models, classification, and reservoir potential, *Earth Science Reviews*, 24, 383-428.

Shanmugam, G. and Moiola, R. J. (1991). Types of submarine fan lobes: models and implications, *AAPG Bulletin*, 75, 156-179.

Shanmugam, G. Bloch, R. B., Mitchell, S. M., Beamish, G. W. J., Hodgkinson, R. J., Damuth, J. E., Staume, T., Syvertsen, S. E., and Shields, K. E. (1995). Basin-floor fans in the North Sea: sequence stratigraphic models vs. sedimentary facies, 79, 477-512.

- Shannon, P. M. (1992). Early Tertiary submarine fan deposits in the Porcupine Basin, offshore Ireland, in J. Parnell (ed.), *Basins on the Atlantic Seaboard: Petroleum geology, sedimentology, and basin evolution*, Geological Society Special Publication No 62, 351-373.
- Shepard, F. P. and Buffington, E. C. (1968). La Jolla Submarine fan-valley, *Marine Geology*, 6, 107-143.
- Shepard, F. P., Dill, R. F., and Von Rad, U. (1969). Physiography and sedimentary processes of La Jolla submarine fan and fan-valley, California, *AAPG Bulletin*, 53, 390-420.
- Shepard, F. P., and Emery, K. O. (1973). Congo submarine canyon and fan valley, *AAPG Bulletin*, 57, 1679-1691.
- Sheriff, R. E. (1985). Aspects of seismic resolution. *in* O. R. Berg and D. G. Woolverton (eds.), *Seismic stratigraphy II*, AAPG Memoir 39, 1-10.
- Sheriff, R. E. (1989). *Geophysical Methods*. Chapter 26: Borehole measurements. Prentice Hall, p. 530-542.
- Sheriff, R. E. and Geldart, L. P. (1995). *Exploration seismology*, second edition, Chapter 6, Cambridge University Press, New York, 145-189.
- Shimeld, J. W., MacRae, R. A., and Wielens, B. W. (2000). Sequence stratigraphy and hydrocarbon potential of regional Upper Cretaceous limestone units, offshore Eastern Canada (abs.), Conference CD with Extended Abstracts, GeoCanada 2000, Calgary, Alberta, May 28 – June 2 2000, Abstract number 784.
- Sinclair, I. K. (1987). Evolution of Mesozoic-Cenozoic sedimentary basins in the Grand Banks area of Newfoundland and comparison to other North Atlantic basins, Canada-Newfoundland offshore Petroleum Board Report GL-CNOPB-87-1, 60 p. Report available from Canada-Newfoundland Offshore Petroleum Board, fifth floor, TD Place, 140 Water Street, St. John's Newfoundland.
- Sinclair, I. K. (1988). Evolution of Mesozoic-Cenozoic sedimentary basins in the Grand Banks area of Newfoundland and comparison with Falvey's (1974) rift model, *Bulletin of Canadian Petroleum Geology*, 36, 255-273.
- Sinclair, I. K., McAlpine, K. D., Sherwin, D. F., and McMillan, N. J. (1992). Part 1: Geological Framework, *in* Petroleum resources of the Jeanne d'Arc Basin and environs, Grand Banks, Newfoundland, Geological Survey of Canada paper 92-8, 1-38.
- Sinclair, I. K. (1993). Tectonism: the dominant factor in mid-Cretaceous deposition in the Jeanne d'Arc Basin, Grand Banks, *Marine and Petroleum Geology*, 10, 530-549.

Sinclair, I. K. (1995). Sequence stratigraphic response to Aptian-Albian rifting in conjugate margin basins: a comparison of the Jeanne d'Arc Basin, offshore Newfoundland, and the Porcupine Basin, offshore Ireland, *in* R. A. Scrutton, M. S. Stoker, G. B. Shimmield, and A. W. Tudhope (eds.), *The tectonics, sedimentation and palaeoceanography of the North Atlantic region: Geological Society Special Publication 90*, 29-49.

Skene, K. I. (1998). Architecture of submarine channel levees, Unpublished Ph.D. Thesis, Dalhousie University, Halifax, Nova Scotia, 362 p.

Skene, K. I., Piper, D. J. W., and Hill, P. S. (2002). Quantitative analysis of variations in depositional sequence thickness from submarine channel levees, *Sedimentology*, 49, 1411-1430.

Smith, R. and Moller, N. (in press). Sedimentology and reservoir modelling of the giant Ormen Lange field, mid Norway, *Marine and Petroleum Geology*.

Sohn, Y. K. (1997). On traction-carpet sedimentation, *Journal of Sedimentary Research*, 67, 502-509.

Soquip/Parex Group (1983). Geophysical survey over the Jeanne d'Arc Basin, C-NOPB Project No. 8620-S14-8E: Paper copies of survey available at the Canada-Newfoundland Offshore Petroleum Board (C-NOPB), fifth floor, TD Place, 140 Water Street, St. John's Newfoundland.

Srivastava, S. P. (1978). Evolution of the Labrador Sea and its bearing on the early evolution of the North Atlantic, *Geophysical Journal of the Royal Astronomical Society*, 52, 313-357.

Srivastava, S. P. and Tapscott, C. R. (1986). Chapter 23 - Plate kinematics of the North Atlantic, *in* P. R. Vogt, B. E. Tucholke (eds.), *The Geology of North America, Volume M, The Western North Atlantic Region: Geological Society of America*, 379-404.

Srivastava, S. P., Roest, W. R., Kovacs, L. C., Oakey, G., Levesque, S., Verhoef, J., and Macnab, R. (1990). Motion of Iberia since the Late Jurassic: results from detailed aeromagnetic measurements in the Newfoundland Basin, *Tectonophysics*, 184, 229-260.

Swift, J. H., Switzer, R. W., and Turnbull, W. F. (1974). The Cretaceous Petrel limestone of the Grand Banks, Newfoundland, *in* C. J. Yorath, E. R. Parker, and D. J. Glass (eds.), *Canada's continental margins and offshore petroleum exploration: Canadian Society of Petroleum Geologists, Memoir 4*, 181-194.

Tankard, A. J., and Welsink, H. J. (1987). Extensional tectonics and stratigraphy of Hibernia oil field, Grand Banks, Newfoundland, *AAPG Bulletin*, 71, 1210-1232.

- Tankard, A. J., Welsink, H. J., and Jenkins, W. A. M. (1989). Structural styles and stratigraphy of the Jeanne d'Arc Basin, Grand Banks of Newfoundland, *in* A. J. Tankard and H. R. Balkwill (eds.), *Extensional tectonics and stratigraphy of the North Atlantic margins*, AAPG Memoir 46, 266-282.
- Taylor, G. C., Best, M. E., Campbell, G. R., Hea, J. P., Henao, D., and Procter, R. M. (1992). Part 2: Hydrocarbon potential, *in* *Petroleum resources of the Jeanne d'Arc Basin and environs, Grand Banks, Newfoundland*, Geological Survey of Canada paper 92-8, 39-46.
- Thomas, F. C. (1991). Paleocology of Late Eocene-Oligocene foraminiferal assemblages in a two-well transect across the North-East Newfoundland shelf, *Journal of Micropalaeontology*, 10, 57-67.
- Thomas, F. C. (1994). Preliminary Cenozoic micropalaeontological biostratigraphy of 16 wells, Jeanne d'Arc Basin, Grand Banks of Newfoundland, Geological Survey of Canada Open File 2799, 54 p.
- Thomas, F. C. (1995). A Paleogene radiolarian event of the South Mara unit, Banquereau Formation, Jeanne d'Arc Basin, offshore Newfoundland, and its implications, *in* *Current research 1995-E: Geological Survey of Canada*, 211-220.
- Timbrell, G. (1993). Sandstone architecture of the Balder Formation depositional system, UK Quadrant 9 and adjacent areas, *in* J. R. Parker (ed.), *Petroleum geology of northwest Europe: Proceedings of the 4th Congress*, The Geological Society of London, 107-121.
- Torres, J., Droz, L., Savoye, B., Terentieva, E., Cochonat, P., Kenyon, N. H., and Canals, M. (1997). Deep-sea avulsion and morphosedimentary evolution of the Rhone Fan Valley and Neofan during the Late Quaternary (north-western Mediterranean Sea), *Sedimentology*, 44, 457-477.
- Tucholke, B. E. and Mountain, G. S. (1979). Seismic stratigraphy, lithostratigraphy, and paleosedimentation patterns in the North American Basin, *in* M. Talwani, W. Hay, W. B. F., Ryan (eds.), *Deep drilling in the Atlantic Ocean - continental margins and paleoenvironments*, American Geophysical Union, Maurice Ewing series, 3, 59-86.
- Tucholke, B. E. and Mountain, G. S. (1986). Tertiary paleoceanography of the western North Atlantic Ocean, *in* P. R. Vogt, B. E. Tucholke (eds.), *The Geology of North America, Volume M, The Western North Atlantic Region: Geological Society of America*, 631-650.
- Vagnes, E. (1997). Uplift at thermo-mechanically coupled ocean-continent transforms: modeled at the Senja Fracture Zone, southwestern Barents Shelf, *Geo-Marine Letters*, 17, 100-109.

- Van der Zwaan, G. J., Jorissen, F. J., and De Stigter, H. C. (1990). The depth-dependency of planktonic/benthic foraminiferal ratios: constraints and applications, *Marine Geology*, 95, 1-16.
- Van der Zwaan, G. J., Duijnste, I. A. P., den Dulk, M., Ernst, S. R., Jannink, N. T., and Kouwenhoven, T. J. (1999). Benthic foraminifers: proxies or problems? A review of paleocological concepts, *Earth-Science Reviews*, 46, 213 - 236.
- Vaneste, K., Henriot, J.-P., Posewang, J., and Theilen, F. (1995). Seismic stratigraphy of the Bill Bailey and Lousy Bank area: implications for subsidence history, in R. A., Scrutton, M. S. Stoker, G. B. Shimmield, and A. W. Tudhope (eds.), *The Tectonics, Sedimentation, and Palaeoceanography of the North Atlantic Region*, Geological Society Special Publication N. 90, p. 125-139.
- Van Hinte, J. E. (1978). Geohistory analysis - application of micropaleontology in exploration geology, *AAPG Bulletin*, 62, 201-222.
- Veeken, P. C. H. (1997). Cenozoic fill of the North Sea Basin (UK sector 56-62N), a seismic stratigraphic study with emphasis on Paleogene massflow deposits, *Geologie en Mijnbouw*, 75, 317-340.
- Verhoef, J. and Srivastava, S. P. (1989). Chapter 9 - Correlation of sedimentary basins across the North Atlantic as obtained from gravity and magnetic data, and its relation to the early evolution of the North Atlantic, in A. J. Tankard and H. R. Balkwill (eds.), *Extensional tectonics and stratigraphy of the North Atlantic margins*, AAPG Memoir 46, 131-147.
- Vittori, J., Morash, A., Savoye, B., Marsset, T., Lopez, M., Droz, L., and Cremer, M. (2000). The Quaternary Congo deep-sea fan: preliminary results on reservoir complexity in turbiditic systems using 2D high resolution seismic and multibeam data, in P. Weimer, R. M. Slatt, J. Coleman, N. C. Rosen, H. Nelson, A. H. Bouma, M. J. Styzen, and D. T. Lawrence (eds.), *Deep-water reservoirs of the world: GCSSEPM Foundation 20th Annual Research Conference*, 1045-1058.
- Von Rad, U. and Tahir, M. (1997). Late Quaternary sedimentation on the outer Indus shelf and slope (Pakistan), evidence from high-resolution seismic data and coring, *Marine Geology*, 138, 193-236.
- Walker, R. G. (1978). Deep-water sandstone facies and ancient submarine fans: models for exploration for stratigraphic traps, *AAPG Bulletin*, 62, 932-966.
- Walker, R. G. (1990). Facies modeling and sequence stratigraphy, *Journal of Sedimentary Petrology*, 60, 777-786.

- Weber, M. E., Wiedicke, M. H., Kudrass, H. R., Hubscher, C., and Erlenkeuser, H. (1997). Active growth of the Bengal Fan during sea-level rise and highstand, *Geology*, 25, 315-318.
- Welsink, H. J., Srivastava, S. P., and Tankard, A. J. (1989). Basin architecture of the Newfoundland continental margin and its relation to ocean crust fabric during extension, *in* A. J. Tankard and H. R. Balkwill (eds.), *Extensional tectonics and stratigraphy of the North Atlantic margins*, AAPG Memoir 46, 197-213.
- Williams, G. L., Fyffe, L. R., Wardle, R. J., Colman-Sadd, S. P., and Boehner, R. C. (1985). *Lexicon of Canadian stratigraphy, volume VI, Atlantic region*, Canadian Society of Petroleum Geologists, Calgary, Canada.
- Williams, G. L. (2002). Palynological analysis Petro-Canada et al. Terra Nova K-18 well, Jeanne d'Arc Basin, Grand Banks of Newfoundland, Report No. M.R.G.-PAL.8-2002GLW, Report available at the Canada-Newfoundland Offshore Petroleum Board (C-NOPB), fifth floor, TD Place, 140 Water Street, St. John's Newfoundland, 18 p.
- Williamson M. A., Shimeld, J., Dickie, K., Fensome, R., Pascucci, V., Coflin, K., Prior, D. B. (1996). Preliminary 3-D reconstruction of a paleo-sedimentary system offshore Newfoundland, eastern Canada, Gulf Coast Society and SEPM Foundation 17th Annual Research Conference, 341-351.
- White, R. S. (1989). Initiation of the Iceland Plume and opening of the North Atlantic, *in* A. J. Tankard and H. R. Balkwill (eds.), *Extensional tectonics and stratigraphy of the North Atlantic margins*, AAPG Memoir 46, 149-154.
- White, R. S. and Lovell, B. (1997). Measuring the pulse of a plume with the sedimentary record, *Nature*, 387, 888-891.
- Yilmaz, O. (1987). *Seismic data processing*, Society of Exploration Geophysicists, Tulsa, Oklahoma, 526 p.
- Ziegler, P. A. (1988). Evolution of the Arctic-North Atlantic and the western Tethys, AAPG Memoir 43, 198 p.
- Ziegler, P. A. (1989). Evolution of the North Atlantic - an overview, *in* A. J. Tankard and H. R. Balkwill (eds.), *Extensional tectonics and stratigraphy of the North Atlantic margins*, AAPG Memoir 46, 111-129.

Appendix I

a) Principle biostratigraphic control

Adolphus D-50

1983 DOEVEN, P.

GSC BULLETIN 356

2659.68	2659.68	TERTIARY	NANNOFOSS
2667.61	2667.61	LATE MAASTRICHTIAN	NANNOFOSS
2682.24	2682.24	MIDDLE-LATE MAASTRICHTIAN	NANNOFOSS
2697.48	2743.20	EARLY-MIDDLE MAASTRICHTIAN	NANNOFOSS
2756.61	2788.31	L CAMPANIAN-E MAASTRICHTIAN	NANNOFOSS
2802.94	2802.94	MIDDLE-LATE CAMPANIAN	NANNOFOSS
2816.35	2816.35	EARLY-MIDDLE CAMPANIAN	NANNOFOSS
2828.85	2880.36	EARLY CAMPANIAN	NANNOFOSS
2897.12	2948.64	LATE SANTONIAN	NANNOFOSS
2973.02	3048.00	CONIACIAN-E SANTONIAN	NANNOFOSS
3057.14	3057.14	CONIACIAN	NANNOFOSS
3077.57	3088.54	LATE TURONIAN	NANNOFOSS
3107.74	3107.74	EARLY TURONIAN	NANNOFOSS
3112.01	3129.08	LATE CENOMANIAN	NANNOFOSS

Avondale A-46

1996 FENSOME, R.A.

M.RES.G.-PAL-01-96RAF

630.00	630.00	L EOCENE OR E OLIGOCENE (PRIABONIAN OR BASAL RUPELIAN)	PALYNOLOGY
650.00	780.00	LATE EOCENE (PRIABONIAN)	PALYNOLOGY
800.00	990.00	MIDDLE EOCENE (BARTONIAN)	PALYNOLOGY
1010.00	1410.00	MIDDLE EOCENE (LUTETIAN)	PALYNOLOGY
1430.00	1620.00	EARLY EOCENE (YPRESIAN)	PALYNOLOGY
1620.00	1640.00	(PROBABLE UNCONFORMITY)	PALYNOLOGY
1640.00	1740.00	LATE PALEOCENE (THANETIAN)	PALYNOLOGY
1760.00	1800.00	EARLY PALEOCENE (DANIAN)	PALYNOLOGY
1800.00	1820.00	(PROBABLE UNCONFORMITY)	PALYNOLOGY
1820.00	1890.00	LATE CRETACEOUS (CAMPANIAN OR OLDER)	PALYNOLOGY

Cormorant N-83

1979 WILLIAMS, G.L.

GSC PAPER 78-24

265.18	329.18	EARLY OLIGOCENE	PALYNOLOGY
377.95	384.05	LATE EOCENE	PALYNOLOGY
384.05	402.34	EARLY EOCENE	PALYNOLOGY
402.34	466.34	EARLY PALEOCENE	PALYNOLOGY
475.49	484.63	CAMPANIAN	PALYNOLOGY

493.78 640.08	SANTONIAN	PALYNOLOGY
658.37 667.51	CONIACIAN	PALYNOLOGY
771.14 777.24	TURONIAN	PALYNOLOGY

Hibernia B-08**1995 FENSOME, R.A.****BAS-PAL-03-95RAF**

540.00 780.00	EARLY OLIGOCENE (RUPELIAN)	PALYNOLOGY
780.00 1210.00	LATE EOCENE (PRIABONIAN)	PALYNOLOGY
1210.00 1225.00	MIDDLE EOCENE (BARTONIAN)	PALYNOLOGY
1225.00 1565.00	MIDDLE EOCENE (LUTETIAN)	PALYNOLOGY
1565.00 1565.00	(UNCONFORMITY)	PALYNOLOGY
1565.00 1640.00	LATE PALEOCENE (EARLY THANETIAN)	PALYNOLOGY
1640.00 1742.00	EARLY PALEOCENE (DANIAN)	PALYNOLOGY
1742.00 1742.00	(UNCONFORMITY)	PALYNOLOGY

Mara M-54**1997 FENSOME, R.A.****M.RES.G.-PAL-02-97RAF**

490.00 820.00	EARLY OLIGOCENE (RUPELIAN)	PALYNOLOGY
820.00 1060.00	LATE EOCENE (PRIABONIAN)	PALYNOLOGY
1060.00 1540.00	MIDDLE EOCENE (BARTONIAN)	PALYNOLOGY
1540.00 1755.00	MIDDLE EOCENE (LUTETIAN)	PALYNOLOGY
1755.00 1755.00	(POSSIBLE UNCONFORMITY)	PALYNOLOGY
1755.00 1905.00	EARLY EOCENE (YPRESIAN)	PALYNOLOGY
1905.00 2025.00	PALEOCENE (THANETIAN)	PALYNOLOGY
2025.00 2085.00	PALEOCENE (DANIAN)	PALYNOLOGY
2050.00 2050.00	(UNCONFORMITY)	PALYNOLOGY
2085.00 2265.00	LATE CRETACEOUS (E CAMPANIAN)	PALYNOLOGY
2265.00 2325.00	LATE CRETACEOUS (SANTONIAN)	PALYNOLOGY

South Mara C-13**1996 FENSOME, R.A.****M.RES.G.-PAL-02-96RAF**

800.00 950.00	LATE EOCENE (PRIABONIAN)	PALYNOLOGY
950.00 1500.00	MIDDLE EOCENE (BARTONIAN)	PALYNOLOGY
1500.00 1500.00	(POSSIBLE UNCONFORMITY)	PALYNOLOGY
1500.00 1755.00	MIDDLE EOCENE (EARLY LUTETIAN)	PALYNOLOGY
1755.00 1755.00	(PROBABLE UNCONFORMITY)	PALYNOLOGY
1755.00 1900.00	EARLY EOCENE (YPRESIAN)	PALYNOLOGY
1900.00 1900.00	(POSSIBLE UNCONFORMITY)	PALYNOLOGY
1900.00 2010.00	PALEOCENE (THANETIAN)	PALYNOLOGY
2010.00 2050.00	PALEOCENE (DANIAN)	PALYNOLOGY
2050.00 2050.00	(UNCONFORMITY)	PALYNOLOGY

2075.00		LATE CRETACEOUS (CAMPANIAN OR OLDER)	
			PALYNOLOGY
Terra Nova K-18			
2002 WILLIAMS, G.L.			
M.R.G. - PAL.9-2002GLW			
677.00	610.00	EARLY RUPELIAN	PALYNOLOGY
842.00	700.00	PRIABONIAN	PALYNOLOGY
939.00	950.00	BARTONIAN	PALYNOLOGY
1055.00	970.00	LUTETIAN	PALYNOLOGY
1100.00	1060.00	YPRESIAN	PALYNOLOGY
1125.00	1110.00	THANETIAN	PALYNOLOGY
1169.00	1120.00	SELANDIAN	PALYNOLOGY
1280.00	1190.00	DANIAN	PALYNOLOGY
1309.00	1286.00	EARLY CAMPANIAN	PALYNOLOGY
1460.00	1338.00	TURONIAN - CONIACIAN	PALYNOLOGY

b) Supplemental biostratigraphic control

Adolphus D-50

1982 BUJAK, J.P.

EPGS-PAL-06-82JPB

347.47 384.05	LATE MIOCENE	PALYNOLOGY
402.34 466.34	MIDDLE MIOCENE	PALYNOLOGY
484.63 777.24	EARLY MIOCENE	PALYNOLOGY
795.53 859.54	LATE-MIDDLE OLIGOCENE	PALYNOLOGY
877.82 1143.00	EARLY OLIGOCENE	PALYNOLOGY
1325.88 1975.10	LATE EOCENE	PALYNOLOGY
1993.39 2386.58	MIDDLE EOCENE	PALYNOLOGY
2407.92 2599.94	EARLY EOCENE	PALYNOLOGY
2621.28 2660.90	LATE PALEOCENE	PALYNOLOGY
2682.24 2782.82	MAASTRICHTIAN	PALYNOLOGY
2804.16 2813.30	LATE-MIDDLE CAMPANIAN	PALYNOLOGY
2837.69 2880.36	EARLY CAMPANIAN	PALYNOLOGY
2895.60 3026.66	SANTONIAN	PALYNOLOGY
3048.00 3077.57	CONIACIAN	PALYNOLOGY
3078.48 3087.62	TURONIAN	PALYNOLOGY
3112.01 3297.94	CENOMANIAN	PALYNOLOGY

Ben Nevis I-45

1991 ASSOCIATED BIOSTRATIGRAPHIC CONSULTANTS

PALYNOLOGY OF 15 WELLS IN THE JEANNE D'ARC BASIN

1620.00 1705.00	L PALEOCENE TO E EOCENE	PALYNOLOGY
1705.00 1770.00	EARLY PALEOCENE	PALYNOLOGY
1770.00 1770.00	(UNCONFORMITY)	PALYNOLOGY
1770.00 1810.00	EARLY SANTONIAN	PALYNOLOGY
1810.00 1890.00	CONIACIAN	PALYNOLOGY
1890.00 1890.00	(UNCONFORMITY)	PALYNOLOGY
1890.00 1955.00	EARLY TURONIAN	PALYNOLOGY
1955.00 1955.00	(UNCONFORMITY)	PALYNOLOGY
1955.00 2025.00	EARLY CENOMANIAN	PALYNOLOGY

Ben Nevis I-45

1987 BUJAK DAVIES GROUP

PALYNOLOGICAL ANALYSIS REPORT

550.00 770.00	EARLY OLIGOCENE	PALYNOLOGY
790.00 920.00	LATE EOCENE	PALYNOLOGY
940.00 1130.00	MIDDLE EOCENE (POSSIBLE)	PALYNOLOGY
1150.00 1490.00	MIDDLE EOCENE	PALYNOLOGY
1510.00 1610.00	EARLY EOCENE	PALYNOLOGY
1630.00 1760.00	EARLY PALEOCENE	PALYNOLOGY
1780.00 1790.00	SANTONIAN	PALYNOLOGY
1810.00 1910.00	TURONIAN	PALYNOLOGY

1930.00 2020.00 LATE CENOMANIAN PALYNOLOGY

Botwood G-89

1992 MOBIL E&P SERVICES INC.

WELL HISTORY REPORT & LOGS

1500.00 1800.00	EOCENE-OLIGOCENE ?	MICRO/PALY
1800.00 2000.00	EOCENE	MICRO/PALY
2000.00 2120.00	PALEOCENE-E EOCENE	MICRO/PALY
2120.00 2265.00	EARLY PALEOCENE	MICRO/PALY
2265.00 2265.00	(UNCONFORMITY)	MICRO/PALY
2265.00 2280.00	EARLY TO MIDDLE MAASTRICHTIAN	MICRO/PALY
2280.00 2330.00	EARLY MAASTRICHTIAN	MICRO/PALY
2330.00 2550.00	CAMPANIAN	MICRO/PALY
2550.00 2660.00	SANTONIAN-CAMPANIAN	MICRO/PALY
2660.00 2775.00	CONIACIAN-SANTONIAN	MICRO/PALY
2775.00 2800.00	CONIACIAN ?	MICRO/PALY
2800.00 2880.00	TURONIAN	MICRO/PALY
2880.00 2880.00	(UNCONFORMITY ?)	MICRO/PALY
2880.00 2980.00	LATE CENOMANIAN	MICRO/PALY

1500.00 1800.00	EOCENE-OLIGOCENE ?	MICROPALEO
1800.00 2020.00	EOCENE	MICROPALEO
2020.00 2180.00	PALEOCENE-E EOCENE	MICROPALEO
2180.00 2260.00	PALEOCENE	MICROPALEO
2260.00 2260.00	(UNCONFORMITY)	MICROPALEO
2260.00 2280.00	EARLY TO MIDDLE MAASTRICHTIAN	MICROPALEO
2280.00 2320.00	EARLY MAASTRICHTIAN	MICROPALEO
2320.00 2490.00	CAMPANIAN	MICROPALEO
2490.00 2550.00	SANTONIAN ?-CAMPANIAN	MICROPALEO
2550.00 2660.00	SANTONIAN	MICROPALEO
2660.00 2780.00	CONIACIAN-SANTONIAN	MICROPALEO
2780.00 2800.00	CONIACIAN	MICROPALEO
2800.00 2820.00	TURONIAN	MICROPALEO
2820.00 2840.00	MID ? TURONIAN	MICROPALEO
2840.00 2880.00	EARLY ? TURONIAN	MICROPALEO
2880.00 2880.00	(UNCONFORMITY ?)	MICROPALEO
2880.00 2980.00	LATE CENOMANIAN	MICROPALEO

2000.00 2120.00	PALEOCENE	NANNO
2120.00 2265.00	EARLY PALEOCENE	NANNO
2265.00 2330.00	EARLY MAASTRICHTIAN	NANNO
2330.00 2615.00	LATE CAMPANIAN	NANNO
2615.00 2630.00	EARLY CAMPANIAN	NANNO
2630.00 2690.00	SANTONIAN ?	NANNO
2690.00 2775.00	SANTONIAN	NANNO
2775.00 2890.00	LATE TURONIAN	NANNO

2890.00	2890.00	(UNCONFORMITY ?)	NANNO
2890.00	3030.00	CENOMANIAN	NANNO

Dominion O-23**1989 BUJAK DAVIES GROUP****PALYNOLOGICAL ANALYSIS REPORT**

365.76	530.35	PLIOCENE	PALYNOLOGY
530.35	557.78	LATE MIOCENE	PALYNOLOGY
557.78	841.25	MIDDLE MIOCENE	PALYNOLOGY
841.25	1005.84	EARLY MIOCENE	PALYNOLOGY
1005.84	1252.73	EARLY OLIGOCENE	PALYNOLOGY
1252.73	1938.53	LATE EOCENE	PALYNOLOGY
1938.53	2551.18	MIDDLE EOCENE	PALYNOLOGY
2551.18	3069.34	EARLY EOCENE (POSSIBLE)	PALYNOLOGY
3069.34	3194.30	LATE PALEOCENE (POSSIBLE)	PALYNOLOGY
3194.30	3224.78	VALANGINIAN	PALYNOLOGY

Gabriel C-60**1981 GRADSTEIN, F.M.****EPGS-PAL-01-81FMG**

1605.00	1770.00	PLIOCENE-PLEISTOCENE	MICROPALEO
1770.00	1970.00	EARLY MIOCENE	MICROPALEO
2000.00	2030.00	EARLY OLIGOCENE	MICROPALEO
2060.00	2430.00	LATE EOCENE	MICROPALEO
2430.00	2450.00	(M EOCENE HIATUS)	MICROPALEO
2450.00	2490.00	(LATE PART OF) E EOCENE	MICROPALEO
2490.00	2510.00	(L MAASTRICHTIAN-E EOCENE HIATUS)	MICROPALEO
2510.00	2520.00	L CAMPANIAN-E MAASTRICHTIAN	MICROPALEO
2520.00	2540.00	(ALBIAN-E CAMPANIAN HIATUS)	MICROPALEO

Hebron I-13**1987 BUJAK DAVIES GROUP****PALYNOLOGICAL ANALYSIS REPORT**

390.00	580.00	EARLY OLIGOCENE	PALYNOLOGY
600.00	760.00	LATE EOCENE	PALYNOLOGY
780.00	1000.00	MIDDLE EOCENE	PALYNOLOGY
1020.00	1150.00	EARLY EOCENE (POSSIBLE)	PALYNOLOGY
1170.00	1360.00	EARLY EOCENE	PALYNOLOGY
1380.00	1505.00	EARLY PALEOCENE	PALYNOLOGY
1505.00	1515.00	MAASTRICHTIAN	PALYNOLOGY
1535.00	1570.00	SANTONIAN-CAMPANIAN	PALYNOLOGY
1590.00	1600.00	CONIACIAN	PALYNOLOGY
1620.00	1630.00	LATE TURONIAN	PALYNOLOGY
1650.00	1660.00	EARLY TURONIAN	PALYNOLOGY
1680.00	1690.00	LATE CENOMANIAN	PALYNOLOGY

North Ben Nevis P-93**1987 BUJAK DAVIES GROUP****GSC OPEN FILE REPORT #1875**

915.00 1070.00	EARLY OLIGOCENE	PALYNOLOGY
1090.00 1400.00	LATE EOCENE	PALYNOLOGY
1415.00 1655.00	MIDDLE EOCENE	PALYNOLOGY
1695.00 1975.00	EARLY EOCENE	PALYNOLOGY
1995.00 2035.00	LATE PALEOCENE	PALYNOLOGY
2055.00 2155.00	EARLY PALEOCENE	PALYNOLOGY
2180.00 2190.00	MAASTRICHTIAN	PALYNOLOGY
2210.00 2280.00	CAMPANIAN	PALYNOLOGY
2300.00 2310.00	EARLY-LATE TURONIAN	PALYNOLOGY
2330.00 2490.00	EARLY-LATE CENOMANIAN	PALYNOLOGY

North Trinity H-71**1991 ASSOCIATED BIOSTRATIGRAPHIC CONSULTANTS****PALYNOLOGY OF 15 WELLS IN THE JEANNE D'ARC BASIN**

1400.00 1405.00	L PALEOCENE TO E EOCENE	PALYNOLOGY
1405.00 1523.00	EARLY PALEOCENE	PALYNOLOGY
1523.00 1523.00	(UNCONFORMITY)	PALYNOLOGY
1523.00 1543.00	(NOT EXAMINED)	PALYNOLOGY
1543.00 1543.00	(UNCONFORMITY)	PALYNOLOGY
1543.00 1625.00	CONIACIAN TO SANTONIAN	PALYNOLOGY
1625.00 1670.10	CONIACIAN	PALYNOLOGY
1670.10 1670.10	(UNCONFORMITY)	PALYNOLOGY
1670.10 1695.00	EARLY TURONIAN	PALYNOLOGY
1695.00 1785.00	CENOMANIAN	PALYNOLOGY

Springdale M-29**1989 NOVA/HUSKY RESEARCH CORP LTD****WELL HISTORY REPORT & LOGS**

1100.00 1425.00	L PALEOCENE & EOCENE	PALYNOLOGY
1425.00 1500.00	CENOMANIAN, TURONIAN, ? SANTONIAN & CAMPANIAN	PALYNOLOGY

Thorvald P-24**1992 CHEVRON CANADA RESOURCES****BIOSTRATIGRAPHY REPORT**

570.00 853.00	OLIGOCENE	MICROPALEO
853.00 1020.00	EARLY OLIGOCENE	MICROPALEO
1020.00 1480.00	LATE EOCENE	MICROPALEO
1480.00 1730.00	MIDDLE ? EOCENE	MICROPALEO
1730.00 1819.00	EARLY EOCENE	MICROPALEO
1819.00 2033.00	PALEOCENE	MICROPALEO
2033.00 2050.00	DANIAN	MICROPALEO
2050.00 2250.00	SANTONIAN	MICROPALEO
2250.00 2480.00	CONIACIAN	MICROPALEO

2480.00 2700.00	TURONIAN	MICROPALEO
2700.00 2960.00	CENOMANIAN	MICROPALEO

Vojager J-18**1987 BUJAK DAVIES GROUP****GSC OPEN FILE REPORT #1882**

780.00 790.00	EARLY OLIGOCENE (PROBABLE)	PALYNOLOGY
810.00 940.00	EARLY OLIGOCENE	PALYNOLOGY
960.00 1240.00	LATE EOCENE	PALYNOLOGY
1260.00 1270.00	EARLY EOCENE (POSSIBLE)	PALYNOLOGY
1290.00 1330.00	EARLY EOCENE	PALYNOLOGY
1350.00 1420.00	EARLY PALEOCENE	PALYNOLOGY
1440.00 1510.00	ALBIAN (POSSIBLE)	PALYNOLOGY

West Ben Nevis B-75**1985 PETRO-CANADA INC****BIOSTRATIGRAPHY REPORT**

720.00 820.00	OLIGOCENE	MICRO/PALY
820.00 1160.00	EOCENE	MICRO/PALY
1160.00 1410.00	EARLY EOCENE	MICRO/PALY
1410.00 1540.00	PALEOCENE	MICRO/PALY
1540.00 1560.00	CAMPANIAN-MAASTRICHTIAN	MICRO/PALY
1560.00 1660.00	SANTONIAN	MICRO/PALY
1660.00 1850.00	CENOMANIAN-TURONIAN ?	MICRO/PALY

Whiterose L-61**1989 BUJAK DAVIES GROUP****PALYNOLOGICAL ANALYSIS REPORT**

770.00 1350.00	EARLY OLIGOCENE	PALYNOLOGY
1350.00 1780.00	LATE EOCENE	PALYNOLOGY
1780.00 2110.00	MIDDLE EOCENE	PALYNOLOGY
2110.00 2460.00	EARLY EOCENE	PALYNOLOGY
2460.00 2490.00	LATE PALEOCENE	PALYNOLOGY
2490.00 2580.00	EARLY PALEOCENE	PALYNOLOGY
2580.00 2610.00	MAASTRICHTIAN	PALYNOLOGY
2610.00 2670.00	CONIACIAN OR OLDER TO CAMP.	PALYNOLOGY
2670.00 2765.00	APTIAN OR OLDER	PALYNOLOGY

Appendix II

a) Formal definition of the Adolphus Member of the Banquereau Formation

Whiterose L-61 is designated the type section for the Adolphus Member (237 m thick, between 2310 to 2547 m), where it consists of brown to grey siltstone and shale, and is Early Eocene in age. Here the member contains shell fragments, plant remains, scattered glauconite, and iron stained fragments. Adolphus D-50 (2596 - 2636 m) is designated the reference section, where the member was logged as bedded cherts (Figure 3.6). North Ben Nevis P-93 (1882 - 1907 m) and Botwood G-89 (2148 - 2185 m) penetrate the member near its western limit, where it is much thinner (25 m and 37 m thick, respectively). The caliper logs at Botwood G-89 and Whiterose L-61 indicate that the Adolphus Member, like the Tilton Member, is well indurated. Though not labeled, this unit corresponds to the low gamma ray interval near the top of North Ben Nevis P-93, North Ben Nevis M-61, and Whiterose L-61 in Figure 3.4 (Chapter 3).

In most wells, the Adolphus Member is bracketed above and below by dark grey, high gamma ray shale to claystone markers. Its lower boundary varies from gradational to sharp. Its upper boundary is usually very sharp, corresponding to an abrupt increase in the gamma ray log. To the west, the Adolphus Member thins above the Botwood High, a pod-shaped erosional remnant consisting of pelagic carbonates of the Wyandot Formation. To the south and east, it thins against the southern flank of the basin, and pinches out just north of the Terra Nova wells.

The origin for the low gamma ray response of the Adolphus Member is uncertain, but could be related to reduced sediment input into the basin after the abrupt termination of submarine fan deposition. Reduced terrigenous sediment input could result in the enrichment in siliceous microfossils (similar to the interpretation of the Tilton Member - Deptuck et al., 2003a). Lower Eocene sediments enriched in siliceous components, some forming cherts, have been reported by Tucholke and Mountain (1979) in the Sohm Abyssal Plains where sedimentation rates were as low as 0.1 cm/1000 years (Gradstein et al., 1990). Alternatively, perhaps winnowing from ocean currents produced clean siltstones with little clay content.

On seismic reflection profiles, the Adolphus Member corresponds closely to marine unit 2a (Figure 4.10a), consisting of an elongated seismic package that contains many small-scale faults, and thins above the Botwood High. The abundant small-scale faults that cut the unit may indicate that the Adolphus Member has a brittle lithological character.

b) Formal definition of the Thorvald Member of the Banquereau Formation

Thorvald P-24 (659 - 855 m) is designated the type section for the Thorvald Member, where it consists of a lower and an upper sand within a 196 m muddy section. The upper sand is 27 m thick and shows an upward coarsening character with upward decreasing gamma ray values. The lower sand is 22 m thick and shows both upward coarsening and fining characteristics. The sands are light brown, medium to well sorted, subangular to subrounded, and contain quartz pebbles, plant remains, and rare chert fragments. Biostratigraphic interpretations at Thorvald P-24 indicate an Oligocene age (Chevron Canada Resources, 1992).

The sands are widely distributed across much of the central JDB, though because they are located in the shallow interval, they were not always carefully logged (in which case I relied on their well log character for their identification). The Thorvald Member is best developed near Hibernia but can be correlated as far north as Flying Foam L-23 and as far south as Egret K-36. The lower sand at Thorvald P-24 can be most widely correlated, reaching a thickness of 45 m at Hibernia C-96 and Hibernia B-27. Its lower boundary ranges from gradational to sharp, and its upper boundary is commonly sharp. The sands pinch out or shale out towards the east. For example, no Thorvald Member sands were penetrated at either of the North Ben Nevis wells, 22 km east of Hibernia. The member is Lower to Middle Oligocene in most of the Hibernia wells (Graham Williams, pers. comm., 2003).

The Thorvald Member generates a slow sonic velocity in most wells, attributed to the unconsolidated nature of the sands. The gamma ray character is typical for that of sand, and locally shows both upward increasing and upward decreasing values interpreted to indicate transgressive and regressive sands. The Thorvald Member also produces a seismic response, in the form of one or two higher amplitude, continuous seismic reflection that decrease in amplitude to the east (interpreted to correspond to the eastward thinning of the member).

Appendix III

Selected Lithology samples from cuttings and sidewall cores

Appendix III - lithology samples

Fine to very fine grained
green glauconitic sand
South Mara Member
Port au Port J-97 - 685 m
(sidewall core)



Poorly sorted very fine sand
with medium grained quartz
grains
Otter Bay Member
(equivalent)
Port au Port J-97 - 910 m
(sidewall core sample)



Medium to coarse grained
sand
Otter Bay Member
Cormorant N-83 - 642- 645 m
(cuttings sample)



Chalk - pink hue
Petrel Member
Cormorant N-83 - 772-781 m
(cuttings sample)



Fine to coarse grained sand rich in carbonaceous plant material and coal flakes. Also a scaphopod shell found (mollusc)
 Fox Harbour Member ?
 Cormorant N-83 - 1320 ft
 (approx. 400 m)
 (cuttings sample)



Dark grey chert and siliceous siltstone fragments (conchoidal fracture)
 Tilton Member
 Mara E-30 - 1900 m
 (cuttings sample)



Appendix IV

Copyright Permission from AAPG for Deptuck et al. (2003a)